

2135

P. 340

NEDO-10958-A  
Class I  
January 1977

**GENERAL ELECTRIC BWR THERMAL ANALYSIS BASIS (GETAB):  
DATA, CORRELATION AND DESIGN APPLICATION**

*S. Levy*

Approved:

S. Levy, General Manager  
BWR Systems Department

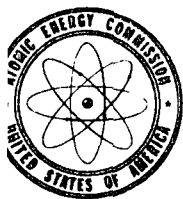
BOILING WATER REACTOR PROJECTS DEPARTMENT • GENERAL ELECTRIC COMPANY  
SAN JOSE, CALIFORNIA 95125



### **DISCLAIMER OF RESPONSIBILITY**

*This report was prepared as an account of research and development work performed by General Electric Company. It is being made available by General Electric Company without consideration in the interest of promoting the spread of technical knowledge. Neither General Electric Company nor the individual author:*

- A. Makes any warranty or representation, expressed or implied, with respect to the accuracy, completeness, or usefulness of the information contained in this report, or that the use of any information disclosed in this report may not infringe privately owned rights; or*
- B. Assumes any responsibility for liability or damage which may result from the use of any information disclosed in this report.*



UNITED STATES  
ATOMIC ENERGY COMMISSION

WASHINGTON, D.C. 20545

OCT 24 1974

Mr. Ivan Stuart, Manager  
Safety and Licensing  
Nuclear Energy Division  
General Electric Company  
175 Curtner Avenue  
San Jose, California 95114

RECEIVE

OCT 24 1974

I. E. STUART

Dear Mr. Stuart:

The Regulatory staff has completed its review of the General Electric Company proprietary topical report NEDE-10958, "General Electric BWR Thermal Analysis Basis (GETAB): Data, Correlation and Design Application". Enclosure 1 is the Regulatory staff's evaluation of this report.

As a result of our review, we have concluded that the above report provides an acceptable boiling transition correlation and an acceptable method of thermal analysis of GE BWR 8x8 and 7x7 fuel assemblies.

As such, NEDE-10958 is acceptable for reference on license applications and requests for changes in licenses when used to support the thermal hydraulic design and operating limits of GE BWR 8x8 or 7x7 fuel assemblies.

The staff does not intend to repeat its review of NEDE-10958 when it appears as a reference in a particular license application or in a request for a change in a license except to assure that the operating and safety limits based on NEDE-10958 are applicable to the specific plant involved.

Should Regulatory criteria or regulations change such that our conclusions concerning NEDE-10958 are invalidated, you will be notified and be given the opportunity to revise and resubmit your topical report for review, should you so desire.

Enclosure 2 is a summary of our evaluation. In accordance with established procedure, it is requested that General Electric issue revised versions of NEDE-10958 (proprietary) and NEDO-10958 (non-proprietary version) to include the AEC acceptance letter and the summary of our evaluation (Enclosure 2).

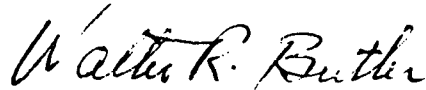
Mr. Ivan Stuart, Manager

- 2 -

003 3 1974

If you have any questions concerning our evaluation of NEDE-10958, please contact us.

Sincerely,



Walter R. Butler, Chief  
Light Water Reactors Branch 1-2  
Directorate of Licensing

Enclosures:

1. Evaluation of NEDE-10958
2. Summary of evaluation of NEDE-10958.

cc: Mr. L. Gifford  
General Electric Company  
4720 Montgomery Lane, Suite 1107  
Bethesda, Maryland 20014

ENCLOSURE 1

REVIEW AND EVALUATION OF GETAB  
(General Electric Thermal Analysis Basis)  
FOR BWRs

By

Technical Review

Directorate of Licensing

United States Atomic Energy Commission

September 1974

## TABLE OF CONTENTS

1. INTRODUCTION
  2. ANALYTICAL
    - A. Critical Heat Flux Correlations
      - a. Methods
      - b. GEXL
      - c. Data Basis for GEXL
    - B. Subchannel Analysis Method
    - C. Data Comparison
      - a. Comparison of ATLAS Data with Hench-Levy Correlation
      - b. Comparison of Hench-Levy and GEXL for Rod Bundle Power
      - c. Comparison of ATLAS Data with GEXL
    - D. Evaluation
  3. EXPERIMENTAL
    - A. The ATLAS Heat Transfer Facility
      - a. The Loop
      - b. Test Sections
      - c. Test Procedures
    - B. Comparison of ATLAS Data with Columbia University Data
    - C. Evaluation
  4. GETAB APPLICATION
  5. STAFF FINDINGS AND CONCLUSIONS
- REFERENCES

## 1. INTRODUCTION

During anticipated abnormal operating transients in a boiling water reactor, a criterion of no fuel rod damage is applied. Historically, the thermo-hydraulic conditions resulting in a departure from nucleate boiling have been used to mark the beginning of the region where fuel damage could occur. Although it is recognized that a departure from nucleate boiling would not necessarily result in damage to BWR fuel rods, the critical heat flux at which boiling transition is calculated to occur has been adopted as a convenient limit.

Since 1966 this limit for BWR fuel assemblies has been based on the Hench-Levy correlation<sup>(1)</sup> which was formulated as a lower limit line to the existing rod bundle critical heat flux data. To allow sufficient margin for uncertainties, the steady state operating conditions of General Electric Company reactors were limited such that during anticipated abnormal transients the calculated heat flux was always less than the lower limit critical heat flux line. That is, during transients, the critical heat flux ratio was always greater than unity.

Based on recent extensive critical heat flux data obtained with full size, full power rod bundles in the ATLAS test loop, the General Electric Company has developed a new method of critical heat flux correlation. With this General Electric Critical Quality ( $X_c$ )- Boiling Length Correlation, (GEXL)<sup>(2,3)</sup> critical power, the fuel assembly power at which boiling transition is expected to occur, is based on the correlation of the critical quality and boiling length. The basic form of GEXL is identical to the

well verified CISE (Italy) correlation. In contrast to the Hench-Levy correlation, which is a lower limit line to the data, the GEXL correlation is a best fit to the ATLAS data. GE proposes to determine thermal limits using a new thermal design method, the General Electric Thermal Analysis Basis (GETAB)<sup>(2,3)</sup> which incorporates the GEXL correlation. The uncertainties associated with the GEXL correlation and the reactor steady state operating parameters are combined statistically. The steady state operating conditions are to be limited such that during anticipated abnormal transients, more than 99.9% of the fuel rods in the core are expected not to experience boiling transition. That is, during transients, the minimum critical power ratio is to be greater than a value determined by the magnitude of these uncertainties. A typical value is 1.05.

This report presents the results of our review of the GEXL correlation and the GETAB method. We have reviewed the GEXL correlation and its basis including the experimental data and analytical methods used to determine the correlation. We have also reviewed the experimental methods used to obtain the data, including the design and operation of the ATLAS test loop. Finally we reviewed the application of the correlation to the design and operation of boiling water reactors. As discussed at the end of this report, based on this review we conclude that the GEXL correlation and a statistical application of the correlation, similar to the proposed GETAB method, are acceptable.



## 2. ANALYTICAL

### A. Critical Heat Flux Correlations

#### a. Methods

Several methods, as described by Keays, et al<sup>(4)</sup> have been proposed for the prediction of heat input for, and the position of, critical heat flux in non-uniformly heated tubes. These prediction methods have the following features:

- (a) In the "Average Heat Flux" concept the critical heat flux is assumed to be correlated thus:

$$\phi_c = f (G, D, P, \Delta H_{in}, L), \quad (1)$$

where L is the total heated length,  $\Delta H_{in}$  is the inlet subcooling; G is mass velocity, D is the equivalent diameter, P is the pressure, and  $\phi_c$  is the average heat flux. Inspection of these parameters show that the critical power is assumed to be independent of the form of the heat flux spatial distribution. Although this method does not permit the prediction of the critical heat flux location, it is simple and has been shown, by Lee<sup>(5)</sup>, to give predictions within 10% of experimental data for tubes with large L/D ratios and moderate peak-to-average heat flux form factors.

- (b) In the "Local Conditions" concept the expression for critical heat flux is:

$$\phi_c = f (G, D, P, X_c) \quad (2)$$

This method assumes that the critical heat flux location will occur at a local heat flux,  $\phi_c$ , and a local steam quality,  $X_c$ , irrespective of the axial heat flux distribution. Examples of

this type of correlation are those of Thompson and Macbeth<sup>(6)</sup>, Tong (W-3)<sup>(7)</sup>, and Gellerstedt, et al, (B&W-2)<sup>(8)</sup>. However, the need for a correction to the predicted uniform critical heat flux, for the case of non-uniform axial heat flux, is described in Reference 9 for the W-3 correlation<sup>(8)</sup>, and in Reference 10 for the B&W-2 correlation<sup>(9)</sup>. The Hench-Levy correlation<sup>(1)</sup>, for use in BWR rod bundles, is similar in form to equation 2.

$$\phi_c = f (G, P, X_{CB}) \quad (3)$$

where  $\phi_c$  is local critical heat flux, and  $X_{CB}$  is the bundle average critical steam quality. The equivalent diameter does not appear as the correlation is applicable only to GE BWR rod bundles. Since 1966, the Hench-Levy correlation, in the form of a lower limit line to the then existing rod bundle data, has served as the basis for predicting the thermal margin in BWRs.

- (c) In the "Boiling Length" concept the critical quality is correlated in the following form:

$$x_c = f (G, P, D, L_B), \quad (4)$$

where  $x_c$  is the steam quality at dryout conditions and  $L_B$  is the length over which boiling takes place. Examples of this type of correlation are those of Bertolotti, et al<sup>(11)</sup>, and Hewitt<sup>(12)</sup>. The "boiling length" type of correlation has the demonstrated advantage of being able to correlate critical heat flux data for both uniform axial heat flux as well as non-uniform

axial heat flux. Since the axial (and radial) heat flux distribution in a BWR fuel bundle is not uniform, the correlation of Bertoletti et al<sup>(11)</sup> was chosen as the basis for the new GE correlation called GEXL (General Electric Critical Quality  $X_c$  - Boiling Length). As used for GE rod bundles, GEXL relates the bundle average critical quality,  $X_{CB}$ , to boiling length.

A recent comparison of the correlations described above (excluding GEXL), and adaptations of some of the methods to use with rod bundles, to BWR rod bundle critical heat flux data is described by Guarino, et al.<sup>(13)</sup> The compared data comprised 785 points and included uniform heat flux, radially non-uniform heat flux, and axially non-uniform heat flux.

b. GEXL

The GEXL correlation is a variation of the critical quality vs boiling length correlation of Bertoletti, et al<sup>(11)</sup> which was based on single tube data, but was shown to apply, with good success, to a large amount of rod bundle critical heat flux data.<sup>(11)</sup> Subsequently, the similar ( $X_c$  vs  $L_B$ ) correlation of Hewitt, et al,<sup>(14)</sup> for single uniformly heated tubes, was applied to rod bundles by Marinelli and Pastori<sup>(15)</sup> on the basis of ascribing the flow rate attending each rod to that which exists within a zero shear interface between rods (the CISE criterion).

The GEXL correlation is of the form:

$$X_{CB} = f(G, D, P, L_B, L, R)$$

where the terms are as previously defined,  $L$  is the heated length, and  $R$  is a weighting factor which characterizes the local rod-to-rod peaking pattern with respect to the most limiting rod. In addition,  $R$  is dependent on lattice dimensions (7x7 or 8x8) and grid spacer configuration. Since  $R$ , in effect, accounts for the flow and enthalpy distribution within the bundle, it can be interpreted as being the bundle average analog of subchannel analysis.

The form of the CISE correlation<sup>(11)</sup> is:

$$X_c = \frac{a L_B}{b + L_B} \quad \text{where } a = f(P, G) \\ b = f(P, G, D)$$

where  $L_B$  is defined as the heated length over which the steam quality is greater than zero. The form of the GEXL correlation is similar to that of CISE; however, in GEXL,  $L_B$  is defined as the distance from the initiation of bulk boiling to the boiling transition point.\*

An example of the ability of the critical quality - boiling length CISE correlation,<sup>(11)</sup> which is the basis for GEXL, to bring critical heat data for various axial heat flux distributions into a single curve is shown in Figure 1. These data, for 1000 psia steam, from Keays, et al,<sup>(4)</sup> include the following heat flux distributions:

---

\*Keays, et al<sup>(4)</sup> use  $L_B$  as defined in GEXL, whereas Hewitt, et al<sup>(14)</sup> use  $L_B$  as defined by Bertolotti, et al<sup>(11)</sup>. However, this difference is not important as long as the particular definition is consistently applied.

uniform, exponential decrease, and symmetrical chopped cosine. Figure 2, from Reference 2, the report under review, shows the identical results for Freon-114 wherein critical heat flux data for uniform, cosine, half cosine, inlet peak, and outlet peak heat flux distributions as well represented by a single critical quality-boiling length curve.

c. Data Basis for GEXL

The GEXL correlations (7x7, 8x8) are based on experimental data which cover the following ranges:

Pressure: 800 to 1400 psia

Mass Flux:  $0.1 \times 10^6$  to  $1.25 \times 10^6$  lb/hr sq. ft.

Inlet Subcooling: 0 to 100 Btu/lb

Local Peaking: 1.61 corner to 1.47 interior

Axial Profile: Uniform

Cosine (1.39 max. to avg. at 72 in. from inlet)

Inlet Peak (1.60 max. to avg. at 51 in. from inlet)

Outlet Peak (1.60 max. to avg. at 93 in. from inlet)

Double Hump (1.46 and 1.38 max. to avg. at 51 and  
108 in. from inlet)

Lattice: 7x7 and 8x8

Rod Bundles: 16, 49, 64 rods

Heated Lengths: 6 ft, 12 ft, 12-1/3 ft

The GEXL correlations are based on data of which the overwhelming portion were obtained in the ATLAS loop and the remainder in the Columbia University test loop. The data used for GEXL are:

<u>Lattice</u>	<u>No. of Rods</u>	<u>Axial Profile</u>	<u>Heated Length</u>	<u>No. of Points</u>
7 x 7	16	Uniform	6 ft*	84*
	16	Cosine	12 ft	223
	49	Cosine	12 ft	127
8 x 8	16	Cosine	12-1/3 ft	211
	64	Cosine	12-1/3 ft	1058

\*Columbia University data.

From the above, it can be seen that the GEXL correlations (7x7 and 8x8) are based on 1803 data points of which 1285 were obtained with full size (49 and 64 rods), full length (12 ft and 12-1/3 ft) rod bundles. Except for 84 points which were obtained with a uniform axial heat flux, the data were obtained with a cosine heat flux distribution.

After development of the correlations they were compared to additional data which represent the whole range of parameters. The data used for comparison are:

<u>Lattice</u>	<u>No. of Rods</u>	<u>Axial Profile</u>	<u>No. of Points*</u>
7 x 7	16	Uniform	456
	16	Cosine	121
	49	Cosine	470
	16	Inlet Peak	484

<u>Lattice</u>	<u>No. or Rods</u>	<u>Axial Profile</u>	<u>No. of Points*</u>
	16	Outlet Peak	477
	49	Outlet Peak	32
	16	Double Hump	434
8 x 8	16	Cosine	131

\*Includes 220 points from the Freon loop

Inspection of these comparisons shows that the 7x7 GEXL correlation, which was based on uniform and cosine axial profiles, accurately predicts the whole range of data.

While the formulation of the GEXL correlations (7x7 and 8x8) relied very heavily (1269 out of 1803 points) on data taken with the 8x8 lattice, only a small fraction (131 out of 2605 points) of the data used to check the GEXL correlations were for the 8x8 lattice. In addition, about half of these confirming data for the 8x8 lattice, were for Freon and all were for a cosine heat flux distribution. GE is performing additional tests with 8x8 lattices and non-uniform axial profiles. These additional tests will include profiles with a peak toward the outlet. Inlet peaked profiles may also be included. Although these tests can provide additional confirmation of the 8x8 GEXL correlation predictive capability, they are not required for two reasons. First, the 7x7 GEXL correlation, which was based solely on data from uniform and cosine axial heat flux profiles tests,

accurately predicts boiling transition for the other tested profiles. There is no reason to believe that the 8x8 GEXL correlation would not perform similarly. Second, in the application of GEXL, the standard deviation of the uncertainty in the 8x8 GEXL correlation will be increased to account for the less complete data base. The standard deviation of 2700 experimental critical power ratios (ECPR) about the 7x7 GEXL correlation is 3.6%. The standard deviation of 1299 ECPR about the 8x8 GEXL is 2.8%. In applying the 8x8 GEXL to the determination of BWR thermal limits, the standard deviation will be increased to at least 3.4%, which is the square root of the sum of the variance of the 8x8 experimental results and the variance of the means of the 7x7 data for each flux shape.



## B. Subchannel Analysis Method

The subchannel analysis methods used to develop and complement the GEXL correlation have been reviewed and evaluated by our PNL consultant. (16) This evaluation indicates that the primary General Electric subchannel analysis model has a reasonable basis. The basic formulations and computations of the model are typical of subchannel analyses available in the open literature; however, formulations of the exchange mechanisms between subchannels contain some unique features. The inclusion of the particular formulations of the turbulent mixing and void drift exchange models is one of the most significant aspects in the GE subchannel analysis formulation and is the primary reason that the GE model does a good job of predicting subchannel flow and enthalpy data for simulations of BWR rod bundles.

As part of its subchannel analysis package, GE has included a subchannel critical power correlation which correlates GE rod bundle data with subchannel parameters of mass velocity, quality and boiling length determined by the subchannel analysis. It is important to note that tube and annulus correlations were not directly used in the subchannel correlation, but instead were merely used to establish the important parameters for correlation of the boiling transition data for rod bundles. The complete subchannel analysis method correlates the experimental data within +6%. Because of its subchannel nature, the subchannel analysis method is a valuable tool for use in parametric design studies of BWR fuel bundles. Thus, GE has two methods which each correlate the GE data well, namely, the subchannel analysis method and the bundle average GEXL method.

However, it does not logically follow that since the two empirical methods provide comparable critical power results that any one of the individual factors in either of the correlations can be justified on that basis alone. Each function must stand on its own merits in conjunction with the empirical or semi-empirical correlating scheme of which it is a part. Consequently, the arguments associated with the justification of the bundle average R factor via the subchannel critical power results are not only circular in nature, since both critical power correlations are based on the same rod bundle data, but are unnecessary since the GEXL correlation stands on its own merits as a method of predicting critical bundle power.

C. Data Comparison

a. Comparison of ATLAS Data with Hench-Levy Correlation

As the Hench-Levy correlation<sup>(1)</sup> presently forms the basis for predicting thermal limits for BWRs, this correlation was independently compared, by our ANC consultant,<sup>(17)</sup> to the rod bundle boiling transition data obtained in the ATLAS test loop. The comparison, consisting of 5868 data points, showed that, except for the case of uniform axial and radial heat flux distribution, the Hench-Levy correlation, which is a lower limit line, is not conservative.\* That is, the experimental critical heat fluxes are generally less than those predicted by the correlation.

Figure 3, from Reference 17, shows critical bundle power as a function of inlet subcooling with mass velocity as a parameter. The consistency shown by these data is typical of that obtained in the ATLAS test loop.

\*This argument as to "conservative" does not embrace the use of Hench-Levy i.e., the present requirement that MCHFR using Hench-Levy be greater than 1.9 during steady state operation.

A comparison between measured and predicted critical heat flux (Hench-Levy) for uniform axial and radial heat flux distribution, is shown in Figure 4.<sup>(17)</sup> It can be seen that almost all of the measured heat fluxes are greater than the predictions thus showing that, for these conditions, the Hench-Levy correlation is conservative. This result is not too surprising as the experimental basis for establishing the Hench-Levy correlation was primarily comprised of uniform axial and radial heat flux rod bundle data. However, as shown in the following two figures, the greater the departure from uniform axial and radial heat flux distribution, the greater becomes the disparity between the Hench-Levy correlation and measured critical heat fluxes, with Hench-Levy being the higher.

Figure 5,<sup>(17)</sup> which compares critical heat flux for uniform axial heat flux and non-uniform radial peaking to predictions, shows that about one-half of the data points are less than the Hench-Levy prediction. When corner peaking is combined with non-uniform axial heat flux distributions (cosine, inlet peak, outlet peak, double hump), the comparison in Figure 6<sup>(17)</sup> results. Here it is seen that, for the vast majority of data points, the Hench-Levy predictions substantially exceed the measured critical heat fluxes. Thus, it can be concluded that, for rod bundle heat flux distributions and heated lengths which correspond to those found in a GE BWR (non-uniform axial heat flux with corner peaking, 12 ft. heated length) the Hench-Levy correlation does not provide a lower limit line.

Two possible reasons why the Hench-Levy correlation does not provide a lower limit line to the ATLAS data which were obtained with reactor fuel assembly-like rod bundles are:

- 1) The approximately 700 critical heat flux data points for 4 and 9 rod bundles, which form the basis for the Hensch-Levy correlation, were obtained with uniform axial heat flux with some data obtained with corner peaking or interior rod peaking. As shown in Figure 7, from Reference 4, the critical heat flux, for a single tube, is substantially greater with uniform axial heat flux than with a cosine heat flux distribution.
- 2) For a 19 rod bundle, using 1000 psia steam, Matzner et al<sup>(18)</sup> demonstrated that, over the heated length range of 1-1/2 ft. to 9 ft., the bundle average critical heat flux increases as heated length decreases. At a given steam quality, a pressure of 1000 psia, and a mass velocity of  $1 \times 10^6$  lb/hr, sq. ft., a decrease in the heated length from 9 ft. to 5 ft. increases the critical heat flux by about 40%.

Since the heated lengths of the 4 and 9 rod bundle critical heat flux data which formed the basis for the Hensch-Levy correlation varied from 3 to 5 feet, it follows that these data provided greater critical heat flux than would have been obtained had the heated length been more representative of actual fuel rods; i.e., 12 ft.

From the above considerations, it can be concluded that the critical heat flux data used to develop the Hensch-Levy correlation were high with the result that the correlation is not a lower limit line when applied to data obtained in long (12 ft.) rod bundles with non-uniform axial and radial heat flux profiles.

b. Comparison of Hensch-Levy and GEXL for Rod Bundle Power

It was previously shown that, for non-uniform axial and radial heat flux distributions, the critical heat flux predicted by the Hensch-Levy correlation generally was substantially greater than that measured. Since GEXL is a close representation of the experimental boiling transition data, it might be anticipated that, on a bundle power basis, Hensch-Levy will provide higher values than GEXL. That is the case shown below.

Figures 8 and 9 show critical power, for a 7 x 7 rod bundle, as a function of inlet subcooling, for mass velocities of  $.5 \times 10^6$  and  $1 \times 10^6$  lb/hr-sq.-ft., respectively. The two upper curves in Figure 8 represent the Hensch-Levy correlation and GEXL, respectively, along with experimental data. It is seen that the Hensch-Levy correlation predicts about 5 percent greater power than GEXL or the data. The two lower curves represent the operating curves for each of the correlations; Hensch-Levy is based on critical heat flux divided by 1.9 whereas GEXL is, in a typical case, based on critical bundle power divided by 1.2.\* Note that, with respect to the operating curves, GEXL permits higher power than Hensch-Levy at low inlet subcoolings while the converse holds true at high inlet subcoolings. At a mass velocity of  $1 \times 10^6$  lb/hr sq. ft., as shown in Figure 9, both the Hensch-Levy correlation and its operating curve are always higher than the respective GEXL curves.

c. Comparison of ATLAS Data with GEXL

Our ANC consultant,<sup>(19)</sup> independently compared all of the ATLAS data, consisting of 5868 data points, to the GEXL correlation (February 1974 version). The ANC comparison has basically substantiated the claim by GE that

---

\*As discussed in Section 4, use of the arithmetic mean, rather than the geometric mean, in the statistical analysis, will increase the required CPR from 1.20 to 1.24. This would correspondingly lower the GEXL operating curves on both Figure 8 and 9.

the GEXL correlation fits the ATLAS data with a standard deviation of 3.5%, the value quoted prior to the second data submittal. ANC has determined the standard deviation to be 3.7% based on the data from all 69 assemblies and the February 1974 version of the GEXL correlation.

No significant error trends in the correlation are observed with respect to the input variables (pressure, mass flux, axial power shape, radial power shape, inlet subcooling, quality). While small systematic differences between assemblies are shown, these differences are not associated with any particular phenomenon.

The variation of the ratio of the difference between the measured and calculated power to calculated power with axial flux shape is shown in Figure 10. When compared to the uniform and cosine power shapes which formed the basis for the 7 x 7 and 8 x 8 GEXL correlations, the inlet peak shape is seen to be slightly conservative while the outlet peak and double hump shapes are slightly non-conservative. The same relative positions among the various axial power shapes is shown, in terms of predicted to measured power, on p. 5-5 of Reference 3. However, it should be noted that these comparisons are applicable only to the 7 x 7 lattice as data with inlet peak, outlet peak, and double hump axial shapes have not, as yet, been obtained with the 8 x 8 lattice.

General Electric has limited the application of the GEXL correlation to conditions where the inlet subcooling is 100 Btu/lb or less. However, as no trend with respect to inlet subcooling is observed over the entire range of subcooling, this restriction does not appear to be necessary.

The sensitivity of the 7 x 7 and 8 x 8 GEXL correlations to pressure, mass flux, and R factor was evaluated. This parameter study has shown that at a particular combination of conditions it is possible to predict negative critical quality at positive values of boiling length. As shown in Figure 11, this inconsistency occurs at the higher pressures ( $P > 1200$  psia), at higher mass fluxes ( $G > 1 \times 10^6$  lb/hr sq. ft.), and at high values of R factor ( $R > 1.2$ ). The consequences of such a condition are that it is impossible to obtain a convergence of the GEXL critical quality-boiling length curve and the energy balance quality-boiling length curve. This problem occurs only at short boiling lengths where boiling transition does not occur for BWR conditions. If required, it may be possible to achieve a solution by ignoring the first 15-20 inches of boiling length. Only four ATLAS data points had conditions where a negative quality was predicted by GEXL. For two of these points, a reasonable solution was obtained by ignoring the first 20 inches of boiling length. For the other two points, convergence was obtained, but the results were unsatisfactory. Another anomaly in the behavior of GEXL was observed at a high R factor ( $R = 1.25$ ) where at 800 and 1400 psia, the curve for  $G = 1 \times 10^6$  lb/hr sq. ft. crosses the curves for  $G = .75 \times 10^6$  and  $G = 1.25 \times 10^6$  lb/hr sq. ft. However, the difference between the two highest mass flux curves is very small over the entire boiling length range.

Unmodified, the GEXL correlation fails to predict accurately the location of boiling transition. To correct this, GE has formulated a location predictor correction to modify the GEXL correlation for use in the prediction of the boiling transition location. An error trend with respect to boiling

length is observed in Figure 12 where the location residual is plotted vs. boiling length. This figure shows that at shorter boiling lengths, the correlation, using the location predictor correction, generally predicts the location downstream of the measured position while, at the longer boiling length, the correlation generally predicts the location upstream of the measured position. The shorter boiling lengths are characteristic of the inlet peaked axial profile. Figure 13 shows the location residual vs. axial power shape. Generally, the scatter for the prediction of location is greater than for the prediction of power.

While this review shows that the GEXL correlation does a good job of predicting the critical power for the ATLAS data, it must be borne in mind that the correlation is completely empirical and no attempt has been made by General Electric to make phenomenological explanations or justifications for any of the terms in the correlation. Consequently, the correlation should be used only for heat transfer predictions which are within the range of the thermal-hydraulic conditions from which it was derived.

#### D. Evaluation

In view of the fact that the Hench-Levy correlation does not, as originally thought, provide a lower limit line to the recent (ATLAS) critical heat flux data which were obtained in rod bundles which closely simulate reactor fuel assemblies, it is reasonable to ask: "What assurance is there that the new correlation, GEXL, will not be found to be inadequate, with regard to the prediction of fuel assembly thermal margin, at some future date?" This question can be answered by the following:



While fairly extensive, the data used to develop the Hench-Levy correlation were obtained from rod bundles which did not duplicate the number of rods, the axial and radial heat flux profile, or the heated length of reactor fuel assemblies. However, test operating conditions (flow rate, pressure, inlet temperature) did duplicate reactor conditions.

In contrast, GEXL is based on more than four thousand boiling transition data points, many of which were obtained from full size, full length, rod bundles with a wide range of axial and radial heat flux profiles. Furthermore, the spacer grids used in critical heat flux tests were very similar to those used in a fuel assembly, and in addition, had the same axial spacing. A wide range of operating conditions (flow rate, pressure, inlet temperature) duplicating those of reactor conditions were used in performing the tests. Since the test sections (49 and 64 rods) are, except for the method of heating, virtually duplicates of fuel assemblies when the axial heat flux distribution of the test and fuel assembly coincide, the ATLAS test data can be considered to be in the nature of calibration.

Based on the above evidence, there is high assurance that the ATLAS test assemblies and tests duplicate the thermal performance of fuel assemblies. From this, it follows that the GEXL correlations (7 x 7 and 8 x 8), which are based on ATLAS data, can be expected to faithfully mirror the thermal performance of BWR fuel assemblies for conditions which fall within the prescribed limits of the correlations. Based on the very detailed, independent evaluation of GEXL, the Hench-Levy correlation, and the ATLAS data, by our ANC consultant,<sup>(20)</sup> the revelation of some anomalies in the GEXL correlation under certain extreme conditions, does not seriously flaw

GEXL or its utility as a prediction method. In total, the ATLAS data - GEXL correlation combination provides a distinct improvement over the presently used Hench-Levy method.

### 3. EXPERIMENTAL

#### A. The Atlas Heat Transfer Facility

The GEXL boiling-transition correlation is based on data measured in the ATLAS heat transfer facility. ATLAS was constructed by the General Electric Company for the purpose of doing steady-state and transient thermal-hydraulic tests of full scale electrically heated rod bundles which simulate reactor fuel.

In preparation for this review, a team of four AEC Regulatory staff members and consultants visited San Jose, the site of ATLAS, to witness boiling transition tests and discuss the operation of the loop with members of the ATLAS operations staff. The following discussion is based on information obtained at that time, together with a written description of ATLAS provided by GE and is directed at areas relating to accuracy and reliability of the ATLAS test results. More details on ATLAS can be found in a letter, dated July 31, 1973, from J. A. Hinds to Dr. J. M. Hendrie. (20)

##### a. The Loop

ATLAS is an all stainless-steel loop designed to operate with water at wide ranges of conditions up to the following maxima:

2250 psig system pressure

655<sup>0</sup>F system temperature

1000 gpm test section flow

17.2 MW test section power

It can therefore be used for the full range of steady state testing appropriate to boiling (and pressurized) water reactors. Furthermore, power, flow, and pressure controls are available to simulate a wide variety of transient and accident conditions.

The power supply consists of four silicon controlled rectifier units each comprised of 96 SCR cells balanced in impedance to equally share the load. Voltage to the test section is controlled manually by operator adjustment of a 0-10v demand signal to a feedback control system. This control system alters the firing phase at the gates of all SCR cells so as to reduce the error between the demand and output voltage to within  $\pm 1/4\%$ . For transient tests there is provision for automatically following a programmed power history with a time constant of less than 10 ms.

The AC ripple component of the rectified voltage is 5 to 6v compared to a full power voltage of 180v. The contribution of this ripple to the test section power varies from 0.5% at full power to 1% at 30% full power and is accounted for by a compensated, Hall-effect wattmeter. The output of this wattmeter is displayed as a digital reading in kilowatts and is available to the data acquisition and control systems. Calibrated DC shunts are also used to calculate the test section power. They measure the current from each SCR unit and the resultant calculated power agrees with the wattmeter measurement within  $\pm 1\%$ .

Redundant measurements are also made of other parameters which affect boiling transition:

- test section inlet temperature is measured to  $\pm 1^{\circ}\text{F}$  by an RTD and checked by three Chromel-constantan thermocouples
- test section pressure is measured to  $\pm 5$  psi by a Heise gauge and the pressure drop by the differential pressure transducer.

- test section flow is measured to  $\pm 1\%$  by both a turbine flowmeter and an orifice/servomanometer

b. Test Sections

The test sections consist of a number of heater rods arranged in an array identical to that of the nuclear fuel being simulated and held by grid spacers of the appropriate design and location. The heater array is housed within a flow channel which accurately simulates the fuel channel wall.

In the tests to date, heat has been generated ohmically in the heater wall. The axial distribution of the heat flux is, therefore, dependent on the local wall thickness which is determined by drawing the tube over a variable mandrel. Boiling transition is detected by electrically insulated, ungrounded Chromelconstantan thermocouples with Inconel sheaths silver soldered to the inner surface of the heater wall. For axially uniform power distributions boiling transition is known to occur at the downstream end of the test section, in general, so there is no problem in locating the thermocouples at the correct axial location. For non-uniform cases however, boiling transition occurs over a range of axial locations, usually between 0.7 and 0.9 times the channel length. Therefore, in these cases, GE installs a larger number of thermocouples, selecting a variety of axial locations based on their experience with non-uniform test sections. Once tests begin on a particular test section, it soon becomes apparent where boiling transition tends to occur and thermocouples in this region are monitored preferentially. The error associated with this detection procedure is minimal for two reasons:

- considerable experience has shown that boiling transition is initiated just upstream of a spacer grid on one of the higher powered rods, and thermocouples were attached accordingly.
- if, in spite of the GE experience, boiling transition occurs between two planes of thermocouples, only a minimal power increase (1 to 2% according to experience) will cause the boiling transition zone to advance to the thermocouple plane.

Test sections geometries in ATLAS have included 4 x 4 and 7 x 7 heater bundles arranged in the 7 x 7 reactor fuel assembly array and 8 x 8 bundles arranged in the 8 x 8 fuel assembly array, in each case using the appropriate heater diameter and length.

The grid spacers of the heater bundles were spaced at the same axial intervals as fuel bundle spacers. Except for overall dimensions, in the case of the 16 rod bundles, and the design of the lantern spring the bundle spacer materials and dimensions are the same as the fuel assembly spacers. Stiffer springs were provided for the test bundles in order to resist the magnetic forces present in the tests. Based on comparative tests with 8 x 8 bundles in the Freon loop, GE stated that the critical power in the bundles with unmodified spacers was equal to or greater than in the bundles with the stiffer springs.

The axial flux shapes tested are those shown in Figure 14. They were chosen to represent the widest range of shapes anticipated during the core life. Considering the wide range of peaking factors included in the ATLAS program the tests appear to simulate as closely as possible the geometry and power distributions expected to occur in BWR fuel.

c. Test Procedures

The following procedure is used to measure boiling transition at steady state conditions. The inlet temperature, flow and pressure are selected and held constant by the loop operators. Errors between the selected and measured values signal alarms which the operators may cancel by correcting these parameters. The test section power is slowly increased by operator manual adjustments while the operators continually monitor the operating conditions and the strip-chart records of the thermocouple signals intended to indicate boiling transition. The onset of boiling transition is identified by an increase in heater temperature of about 25<sup>0</sup>F. At this point, all thermocouple signals are checked on a Metrascope to assure that no thermocouple which is not connected to the strip-chart recorder is indicating boiling transition, and the operators signal the on-line computer to record all the pertinent data. The engineering data required to assess the result and to proceed to the next run are pointed out, the subcooling is changed to a new value and the next run done in the same manner, until the desired range of subcoolings is covered. The flow rate is then changed and the procedure repeated.

For transient tests, the flow rate is varied by timer circuits which actuate an air-operated flow control valve and the power is varied by a programmed function generator. The raw data, including heater thermocouple signals, can be sampled as often as 50 times per second and recorded on magnetic tape for subsequent processing.

### B. Comparison of ATLAS Data with Columbia University Data

As evidence of the accuracy of the ATLAS loop results, GE repeated a test series run earlier in the Columbia University Heat Transfer Facility. A comparison of the two sets of results is shown in Figures 15 through 19. Estimates of the percentage difference between curves drawn through each set of data, shown in the lower right hand corner as  $\Delta$  lie between -5% (the ATLAS data are lower) and +3% (the ATLAS data are higher). In view of the scatter which typifies boiling transition test data, the Columbia University and ATLAS loops agree remarkably well.

### C. Evaluation

In general, the ATLAS Heat Transfer Facility compares favorably with any facility in the world constructed for steady-state and transient boiling transition tests. Furthermore, it incorporates special features:

- automatic alarm system to ensure required test conditions are closely met
- specially designed controls and data acquisition system to facilitate transient tests
- highest test section power of any loop

which make ATLAS superior to other facilities and ensure a valuable source of data useful in the safe design of BWRs.

#### 4. GETAB APPLICATION

General Electric proposes to establish design and operational thermal limits based on the GEXL correlation. These limits were previously based on the Hensch-Levy correlation. The GEXL correlation is based on a larger amount of more representative data than the Hensch-Levy correlation. The GEXL correlation is a best-fit of the data while the Hensch-Levy correlation is a lower limit of the data.

GE proposes to state the thermal limit in terms of the critical power ratio (CPR) which is not only a consequence of the form of the new GEXL correlation, but is also more representative of the available thermal margin. Previously, the thermal limit was stated in terms of the critical heat flux ratio (CHFR), which is not directly related to the thermal margin. The use of CPR rather than CHFR as a thermal limit more clearly defines the thermal margin available.

GE also proposes to combine the effect of the uncertainties in the GEXL correlation with the uncertainties in the reactor operating variables in determining the thermal limits. Previously, only nominal values of the operating variables were used in determining heat flux relative to the CHF limit line. Although statistical analyses have been applied to the previous CHF thermal limit in order to evaluate the effect of uncertainties in the operating variables, the direct incorporation of uncertainties in the proposed CPR thermal limit assures that uncertainties are considered during design and operation of the reactor.

GE proposes that transients caused by single operator error or equipment malfunction shall be limited such that considering uncertainties



in defining the core operating state, more than 99.9% of the fuel rods would be expected to avoid boiling transition. The application of this design basis to the determination of steady state operating limits is in two steps.

First, a statistical model is used to calculate the minimum critical power ratio (MCPR) for which less than 0.1% of the rods are expected to experience boiling transition. Second, a transient model is used to calculate the change in CPR resulting from transients. The steady-state operating limit is determined as the sum of the largest change in CPR due to any of the transients considered and the MCPR at which less than 0.1% of the rods are expected to experience boiling transition. The transient model (NEDO-10802)<sup>(21)</sup> is the same model previously used in calculating the Hench-Levy CHF limit, and is not a subject of this review. The staff is reviewing this subject separately. The statistical procedure uses a computer program which calculates the CPR of the bundles in the core assuming a given power distribution and values of the operating variables. Using the calculated values of CPR, the probability of boiling transition occurring is summed for all rods in the core. Successive trials using random variations in the operating variables are performed until the mean and standard deviation of the probability of boiling transition occurring in the core is found.

The probability of boiling transition occurring is calculated based on the standard deviation of the ATLAS data relative to the GEXL correlation assuming a normal distribution. Because only tests with a symmetrical cosine axial profile are included in the 8 x 8 data, the magnitude of the uncertainty in the 8 x 8 GEXL correlation

is increased to be comparable to the larger variability of the 7 x 7 data which included four other axial profiles. GE originally used the anti-log of the mean of the logarithm of the number of rods expected to experience boiling transition, in the determination of the CPR limit. The use of this geometric mean reduces the uncertainty interval. The procedure has been modified, by GE, <sup>(22)</sup> to use the arithmetic mean. This resulted in an increase in the MCPR for which less than 0.1% of the rods are expected to experience boiling transition.

The random variations in operating variables are based on estimates of the uncertainties in each variable. <sup>(23, 24)</sup> A review and evaluation of these variables has shown that the variables which contribute significantly to the overall uncertainty have been considered. The estimated value of these uncertainties and the basis for the value depend on the specific design and equipment of each reactor and will be evaluated for each reactor at the time Technical Specifications are issued.

The proposed design basis appears at first to be a departure from the intent of the previous basis. The intent of the previous basis was that boiling transition would not reasonably be expected to occur on any rod in the core when at the thermal limit (i.e., the worst fuel assembly had a calculated MCHFR of unity). Under the proposed basis for core-wide transients, 0.1% of the rods in the core would be expected to experience boiling transition at the thermal limit (e.g., a MCPR of 1.05 on the worst assembly in a typical reactor). However, the proposed limit includes

uncertainties in the reactor operating variables and the previous limit does not. If uncertainties in operating variables are not considered, there is a 95% confidence that with a CPR of 1.05 there is a 95% probability that boiling transition does not occur in the worst bundle. Therefore, a MCPR of 1.05 is roughly equivalent to a MCHFR of unity and both design bases provide similar assurance that boiling transition would not occur following core wide transients.

However, for local transients, the proposed design basis is a departure from the previous basis. Previously, the calculated MCHFR in any assembly was limited to unity and no rods were expected to experience boiling transition. Under the proposed basis, all of the rods in a fuel assembly could be expected to experience a boiling transition without violating the proposed basis, since all of the rods in one bundle comprise only approximately 0.1% of the rods in a core. For example, if a MCPR of 0.95 were calculated for the worst fuel assembly, that is, boiling transition would be predicted to occur, the proposed basis would not be violated. Therefore, the proposed design basis provides less thermal margin following a localized transient than the previous basis.

We conclude that the proposed design basis (i.e. more than 99.9% of the fuel rods in the core would be expected to avoid a boiling transition caused by single operator errors or equipment malfunctions) is acceptable when applied to core-wide transients such as a turbine-trip or pump-coastdown transient. We also conclude that the method used to calculate the MCPR thermal limit is an acceptable method by which power distribution

and uncertainties in the GEXL correlation and the reactor operating parameters can be included in the determination of whether the design basis is met. However, we conclude that applying the proposed design basis to local transients such as control rod withdrawal, is inappropriate. Therefore, we require that the MCPR thermal limit determined for core wide transients also be used as the MCPR thermal limit for local transients.

## 5. STAFF FINDINGS AND CONCLUSIONS

The Staff has reviewed the General Electric Thermal Analysis Basis and its application to reactor design and operation. Included in the review were the GEXL correlation, which is the basis for GETAB; the analytical methods used to develop this correlation; the experimental results from which the correlation was synthesized; and the experimental methods used to obtain the data.

Based on our review of the design and operation of the ATLAS test facility, the Staff concludes that the steady state and transient tests had accurately controlled and measured test conditions. Comparison among the results of tests conducted on the ATLAS loop and between the results of tests conducted on both the ATLAS and Columbia loops verified reproducibility and lack of bias of the experimental results.

The experimental results were mainly obtained from full size, full length rod bundles which duplicated fuel assemblies in all respects that could significantly affect boiling transition. The tests were performed with a range of test conditions (flow, pressure, temperature and power) and heat flux distributions, both axial and radial, which equaled or exceed those expected to occur in a fuel assembly. Therefore, we conclude that the experimental results represent the thermal performance of GE 8 x 8 and 7 x 7 fuel assemblies.

Based on an independent comparison of the ATLAS data to the GEXL correlation, we conclude that the data can be conservatively treated as normally

distributed about the correlations with a standard deviation of 3.6% and 3.4% for the 7 x 7 and 8 x 8 GEXL respectively. While small systematic differences between assemblies with different power distributions are shown, the correlation is slightly conservative with respect to the most probable distributions, (i.e., inlet peak and symmetrical cosine). Although the correlation has some anomalies at extreme conditions, GEXL can predict within a defined uncertainty the thermal performance of GE 8 x 8 and 7 x 7 fuel assemblies for the expected range of reactor normal steady state operation and abnormal operating transients.

General Design Criterion 10 requires that "acceptable fuel design limits are not exceeded during any condition of normal operation, including the effects of anticipated operational occurrences." We conclude that the proposed design bases (i.e. Transients caused by single operator error or equipment malfunction shall be limited such that considering uncertainties in monitoring the core operating state, more than 99.9% of the fuel rods would be expected to avoid boiling transition) meets the criterion when applied to core - wide transients. However, we require that the MCPR limit derived for core-wide transients also be used as the Safety Limit applicable to local transients such as a control rod withdrawal. We also conclude that the statistical model used to derive the MCPR limit is acceptable.

## REFERENCES

1. J. M. Healzer, J. E. Hench, E. Janssen, and S. Levy, "Design Basis for Critical Heat Flux Condition in Boiling Water Reactors," APED-5186, Class II, 1966.
2. "General Electric BWR Thermal Analysis Basis (GETAB): Data, Correlation and Design Application," NEDO-10958, 73NED9, Class I, November 1973.
3. "General Electric Thermal Analysis Basis; Data, Correlation, and Design Application," NEDE-10958, Supplement 1, Class III, November 1973.
4. R. K. F. Keays, J. C. Ralph, and D. N. Roberts, "Post Burnout Heat Transfer in High Pressure Steam Water Mixtures in a Tube with Cosine Heat Flux Distribution," AERE-R6411 (1971).
5. D. H. Lee, "An Experimental Investigation of Forced Convection Burnout in High Pressure Water, Part 3; Long Tubes with Uniform and Non-uniform Axial Heating," AEEW-R 335 (1965).
6. B. Thompson and R. V. Macbeth, "Boiling Water Heat Transfer Burnout in Uniformly Heated Round Tubes: A Compilation of World Data with Accurate Correlation," AEEW-R 356 (1964).
7. L. S. Tong, "Prediction of Departure from Nucleate Boiling for an Axially Non-uniform Heat Flux Distribution," J. Nucl. Energy 21 (1967).
8. J. S. Gellerstedt, R. A. Lee, M. J. Oberjohn, R. H. Wilson, and L. J. Stanek, "Correlation of Critical Heat Flux in a Bundle Cooled by Pressurized Water," Two-Phase Flow and Heat Transfer in Rod Bundles, A.S.M.E. New York (1969).
9. L. S. Tong, H. B. Curran, P. S. Larson, and O. G. Smith, "Influence of Axially Non-uniform Heat Flux on DNB," Chem. Eng'g. Prog. Symp. Series, No. 64, Vol. 62 (1966).
10. R. H. Wilson, L. J. Stanek, J. S. Gellerstedt, and R. A. Lee, "Critical Heat Flux in a Nonuniformly Heated Rod Bundle," Two Phase Flow and Heat Transfer in Rod Bundles, A.S.M.E. New York (1969).
11. S. Bertoletti, G. P. Gaspari, C. Lombardi, G. Peterlongo, M. Silvestri, and F. A. Tacconi, "Heat Transfer Crisis with Steam-Water Mixtures," Energia Nucleare, Vol. 12, No. 3, (1965).
12. G. F. Hewitt, "A Method of Representing Burnout Data in Two-Phase Heat Transfer for Uniformly Heated Round Tubes," A.E.R.E.-R4613, (1964).
13. D. Guarino, V. Marinelli, and L. Pastori, "Status of Art in Burnout Predictions for BWR Rod Bundles," Trans. Am. Nucl. Soc., Vol. 17, (1973).

14. G. F. Hewitt, H. A. Kearsy, and J. G. Collier, "Correlation of Critical Heat Flux for the Vertical Flow of Water in Uniformly Heated Channels," AERE-R5590 (1970).
15. V. Marinelli and L. Pastori, "Simple but Accurate Method for Predicting Burn-out in BWR Rod Bundles," Trans. Am. Nucl. Soc., Vol. 16 (1973).
16. A. M. Sutey, "A Preliminary Evaluation of the Subchannel Thermal Hydraulics Analysis Model of GETAB," Pacific Northwest Laboratories, April 1974.
17. Letter: K. G. Condie to L. H. Sullivan, "Review of GE ATLAS Data," March 18, 1974.
18. B. Matzner, J. E. Casterline, E. O. Moeck, and G. A. Wikhammer, "Experimental Critical Heat Flux Measurements Applied to a Boiling Reactor Channel," A.S.M.E. Paper 66-WA/HT-46 (1966).
19. Letter: K. G. Condie to L. H. Sullivan, "Review of GE GEXL Correlation," May 3, 1974.
20. Letter: J. A. Hinds to J. M. Hendrie, "General Electric ATLAS Test Facility," July 31, 1973.
21. R. B. Linford, "Analytical Methods of Plant Transient Evaluations for the General Electric Boiling Water Reactor," NEDO-10802, 73NED29, Class 1, February 1973.
22. Letter: J. A. Hinds to W. R. Butler, "Responses to Additional AEC Questions on the General Electric Topical Reports NEDO-10958 and NEDE-10958, General Electric BWR Thermal Analysis Basis (GETAB): Data, Correlation and Design Application," April 3, 1974.
23. Letter: J. A. Hinds to W. R. Buller, "Responses to the Third Set of AEC Questions on the General Electric Licensing Topical Reports NEDO-10558 and NEDE-10558," General Electric BWR Thermal Analysis Basis (GETAB): Data, Correlation and Design Application," July 24, 1974.
24. J. F. Carew, "Process Computer Performance Evaluation Accuracy" NEDO-20340, 74 NED 32, Class I, June 1974.



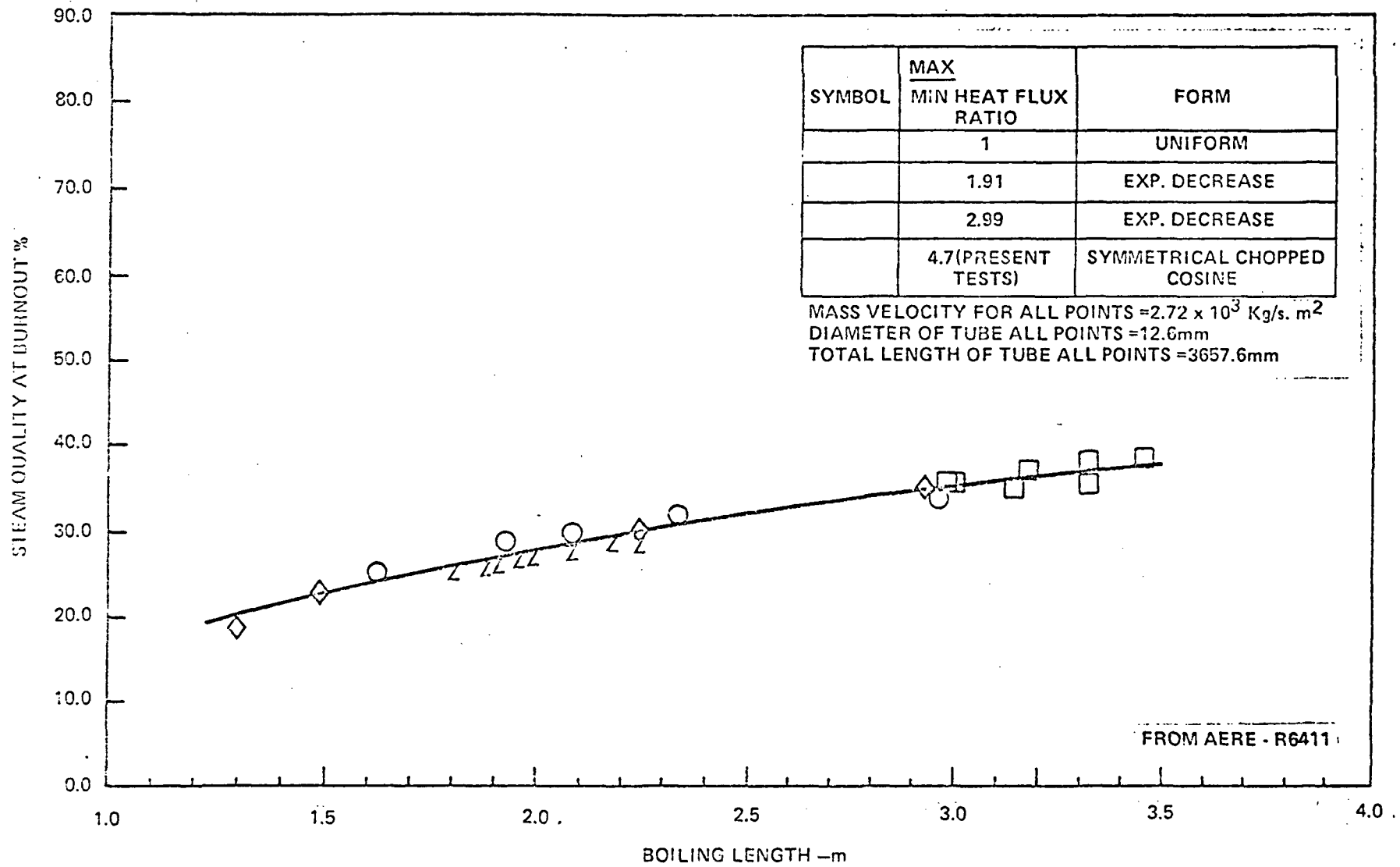


Figure 1 COMPARISON OF BURNOUT CONDITIONS ON A BOILING LENGTH BASIS FOR VARIOUS HEAT FLUX DISTRIBUTIONS

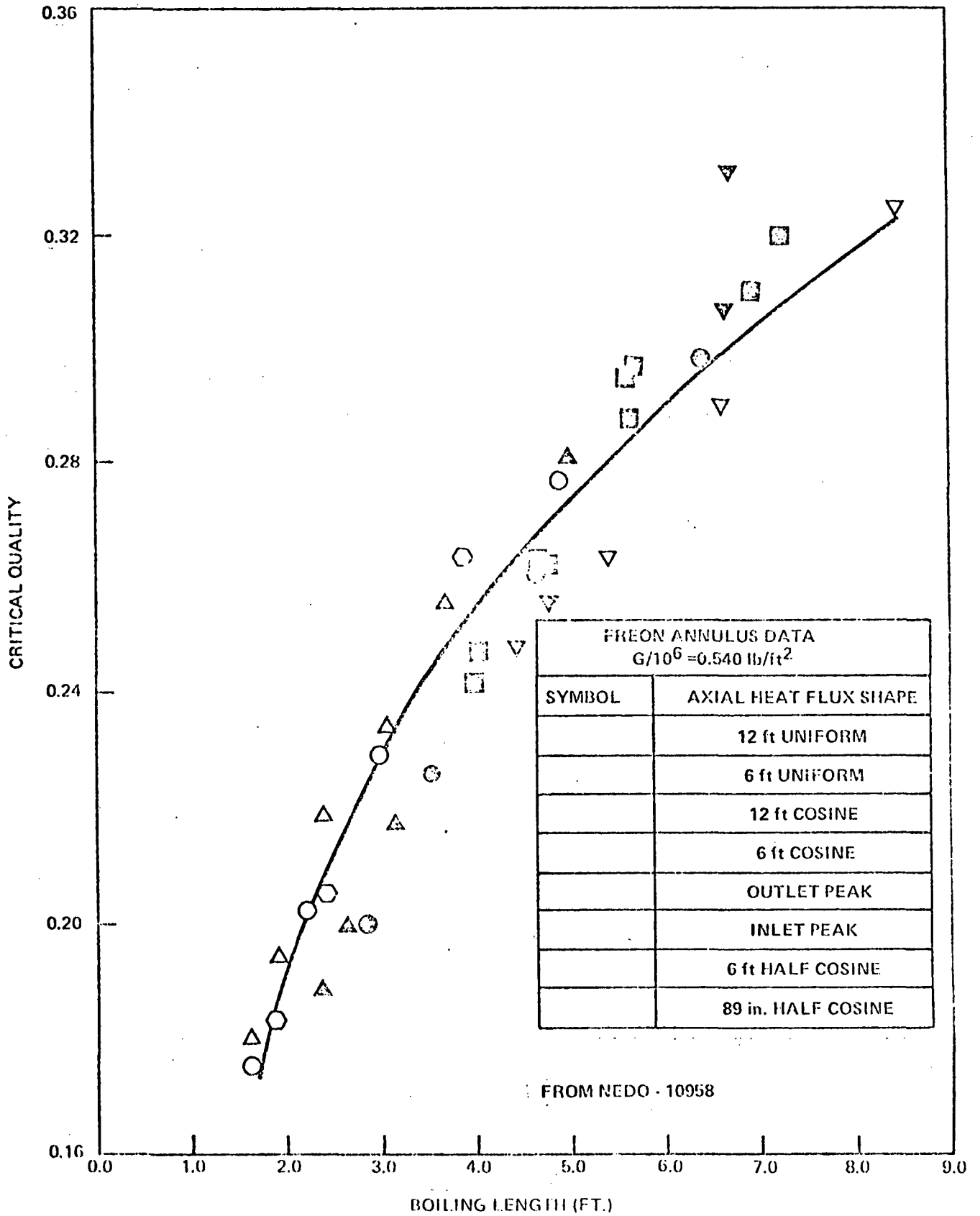


Figure 2 CRITICAL QUALITY VS. BOILING LENGTH, FREON-114 ANNULUS DATA

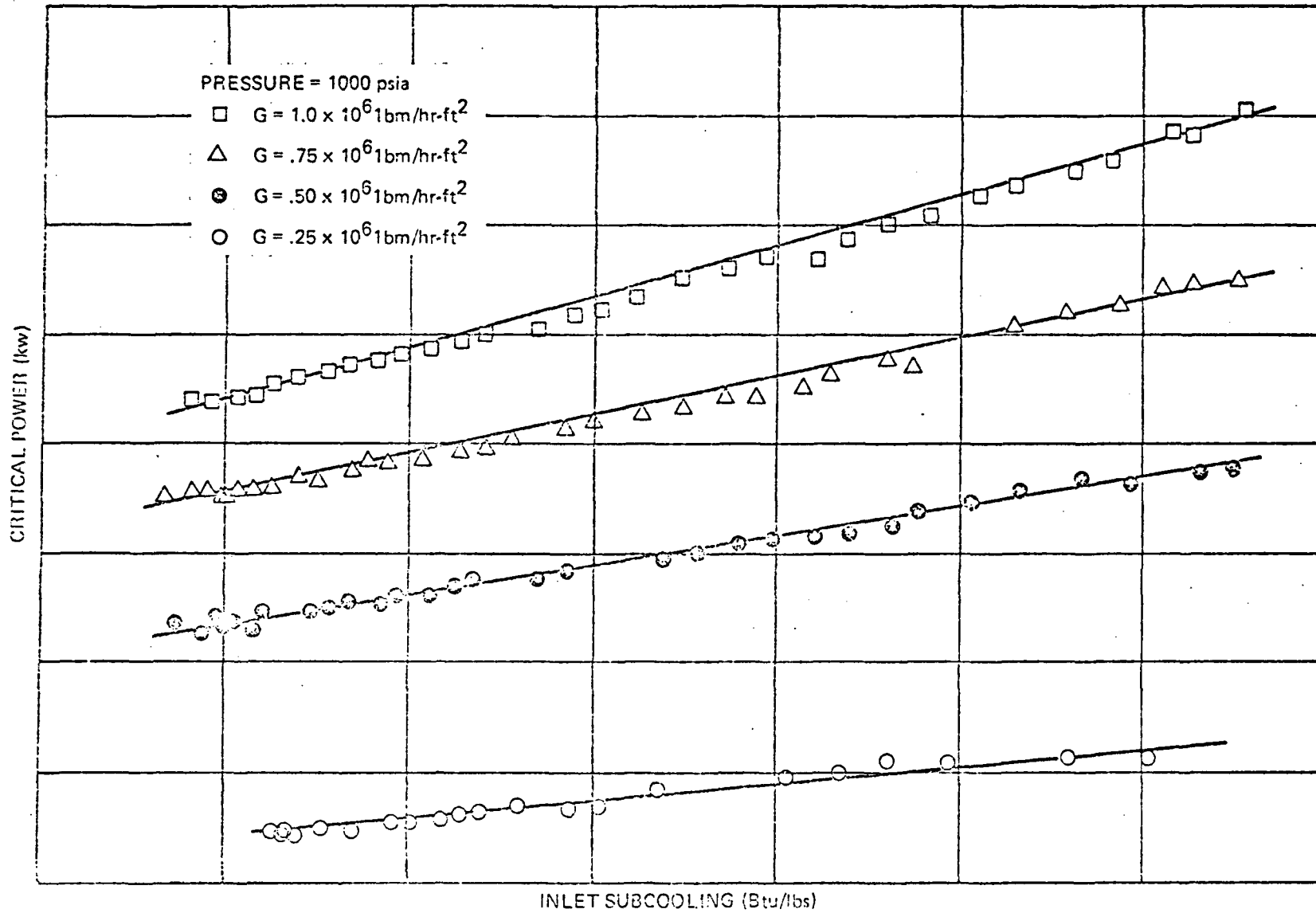


Figure 3 CRITICAL POWER VS. INLET SUBCOOLING FOR ATLAS TEST ASSEMBLY 30B

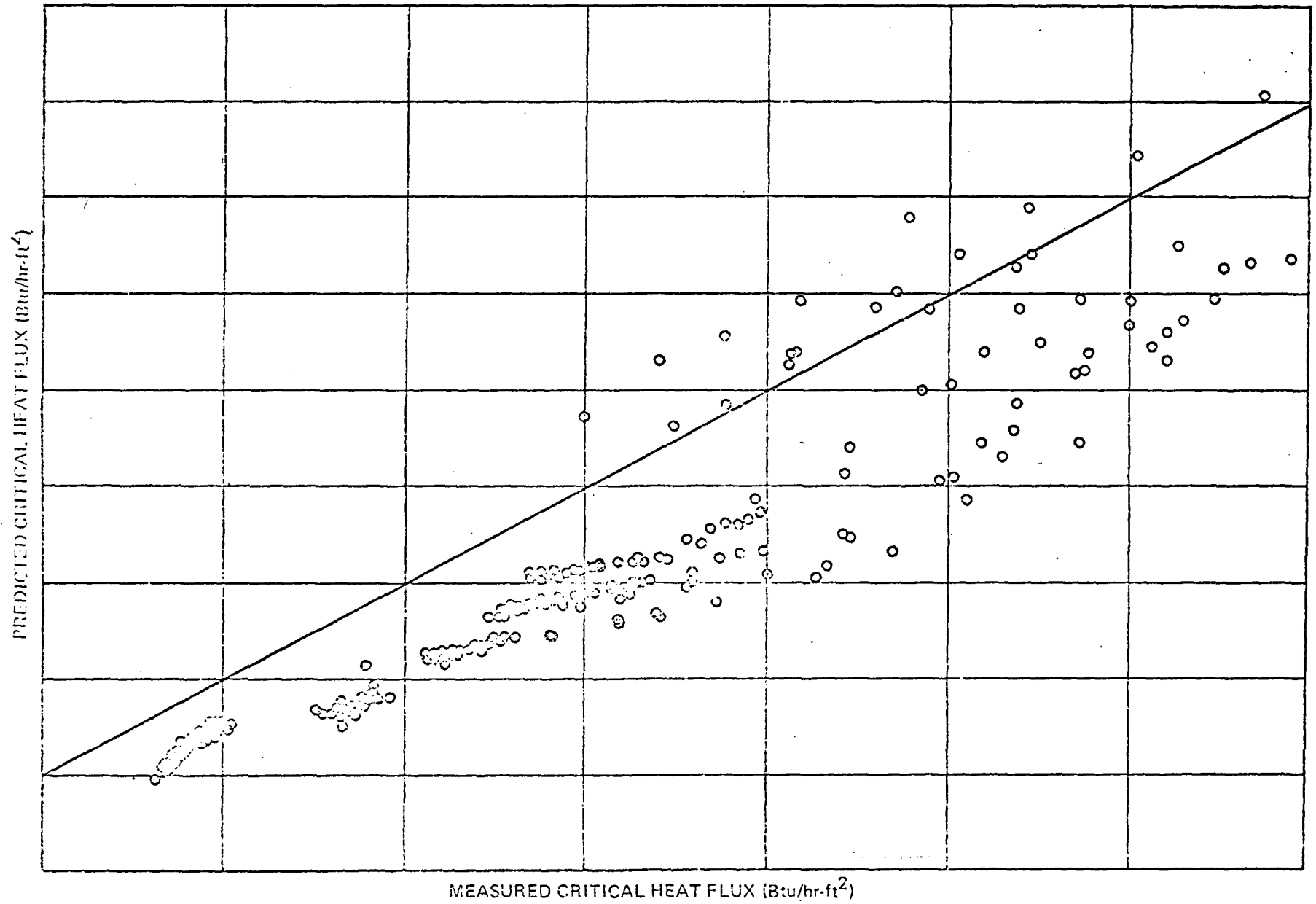


Figure 4 MEASURED VS. PREDICTED CRITICAL HEAT FLUX FOR ATLAS DATA WITH UNIFORM AXIAL AND UNIFORM

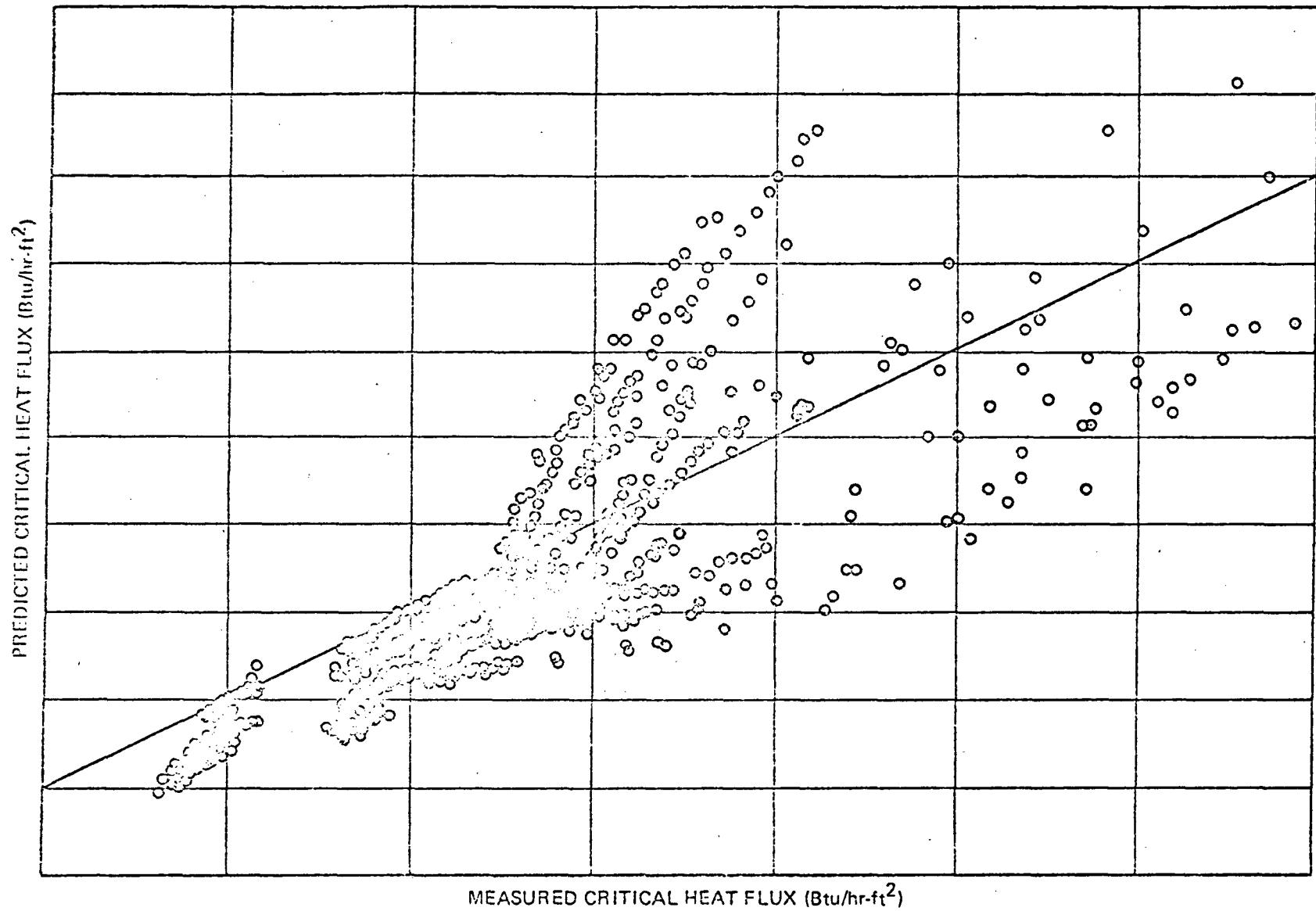


Figure 5 MEASURED VS. PREDICTED CRITICAL HEAT FLUX FOR ATLAS DATA WITH UNIFORM AXIAL POWER PROFILE

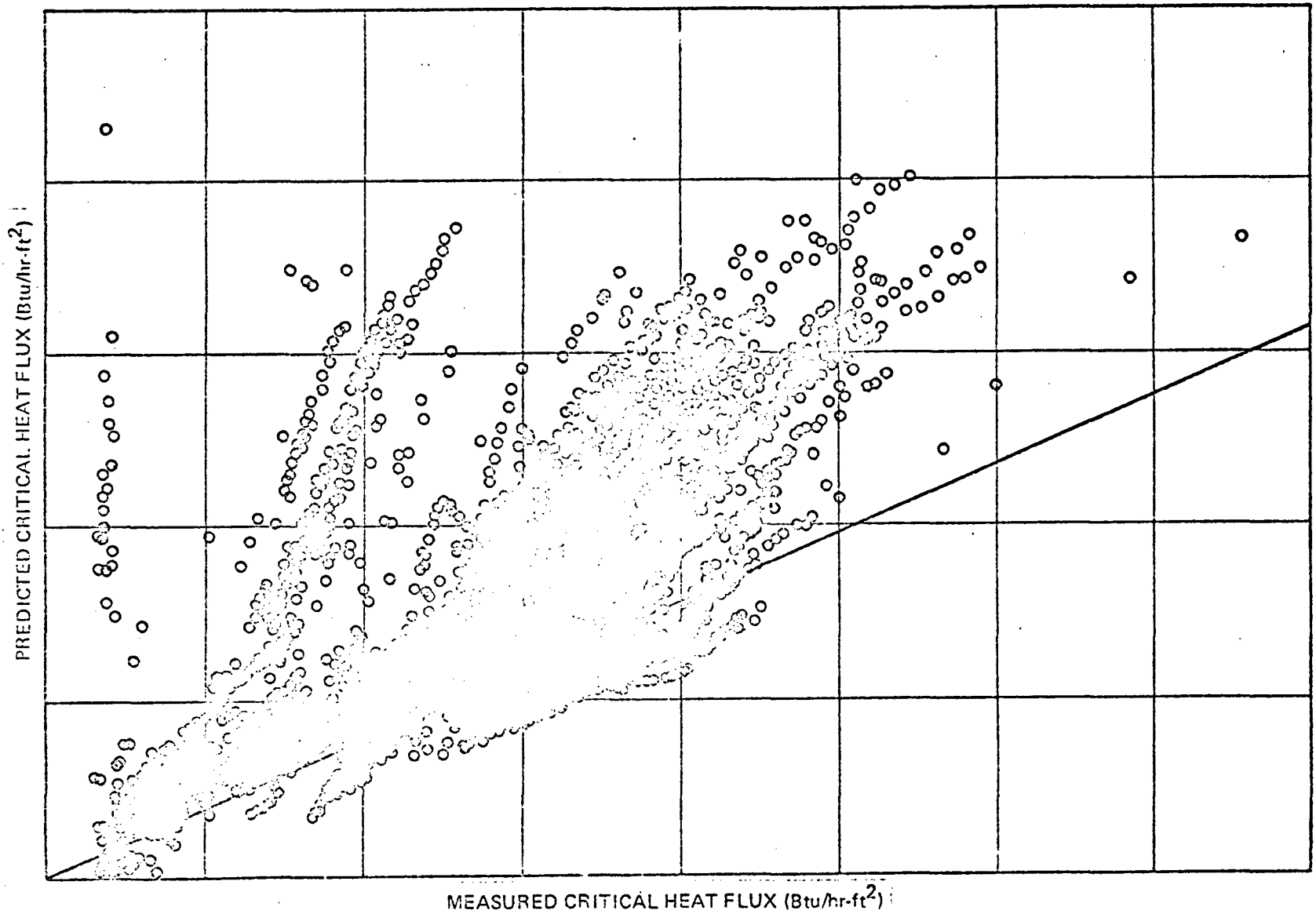


Figure 6 MEASURED VS. PREDICTED CRITICAL HEAT FLUX FOR ATLAS DATA WITH CORNER PEAKED RADIAL POWER PROFILE

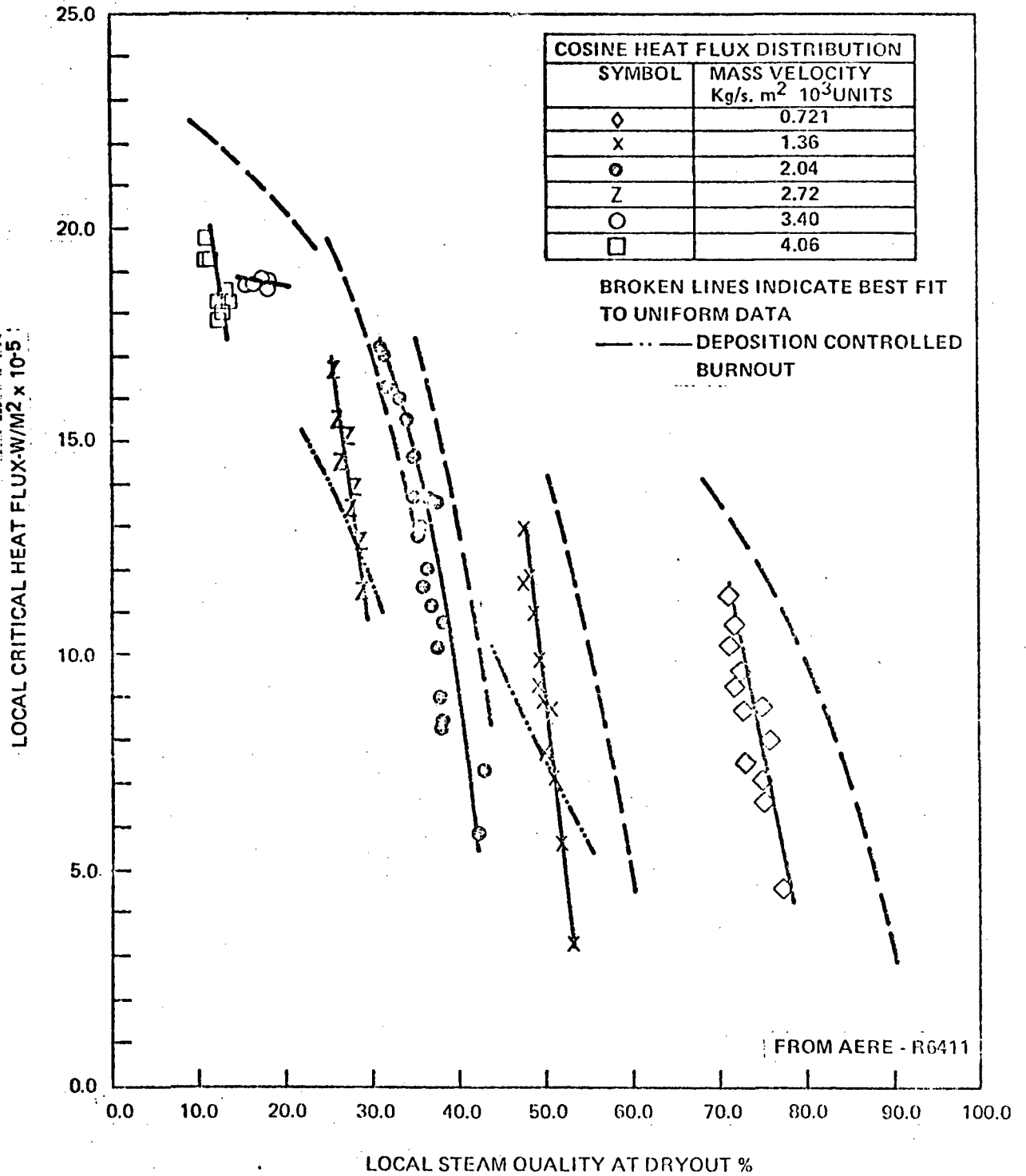


Figure 7 COMPARISON OF BURNOUT CONDITIONS ON A LOCAL CONDITIONS BASIS FOR UNIFORM AND COSINE HEAT FLUX DISTRIBUTIONS

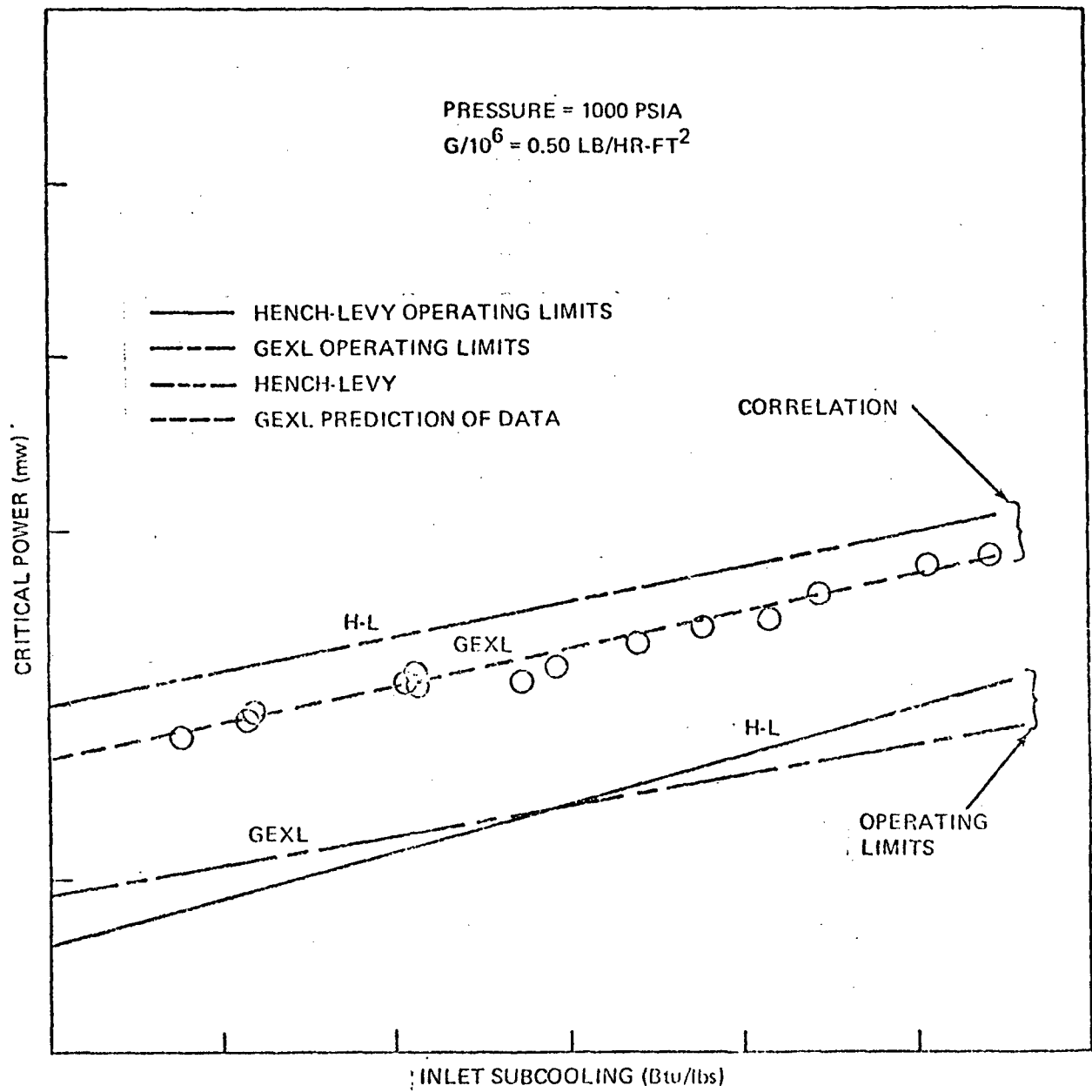


Figure 8 COMPARISON OF HENCH-LEVY AND GEXL WITH 49 ROD ATLAS DATA  
 (1.23 CORNER PEAKING, COSINE)



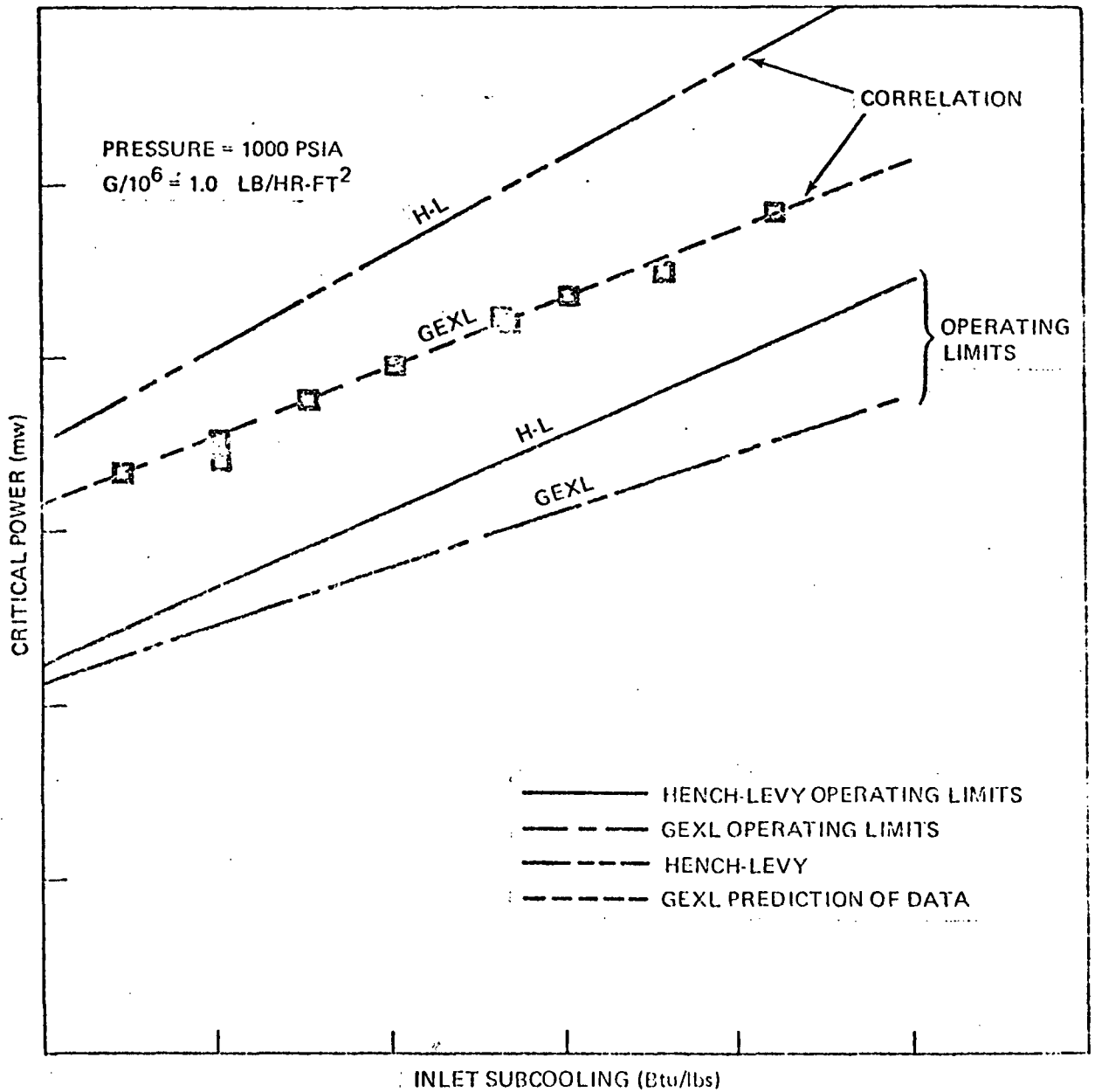


Figure 9 COMPARISON OF HENCH-LEVY AND GEXL WITH 49 ROD ATLAS DATA (1.23 CORNER PEAKING, COSINE)

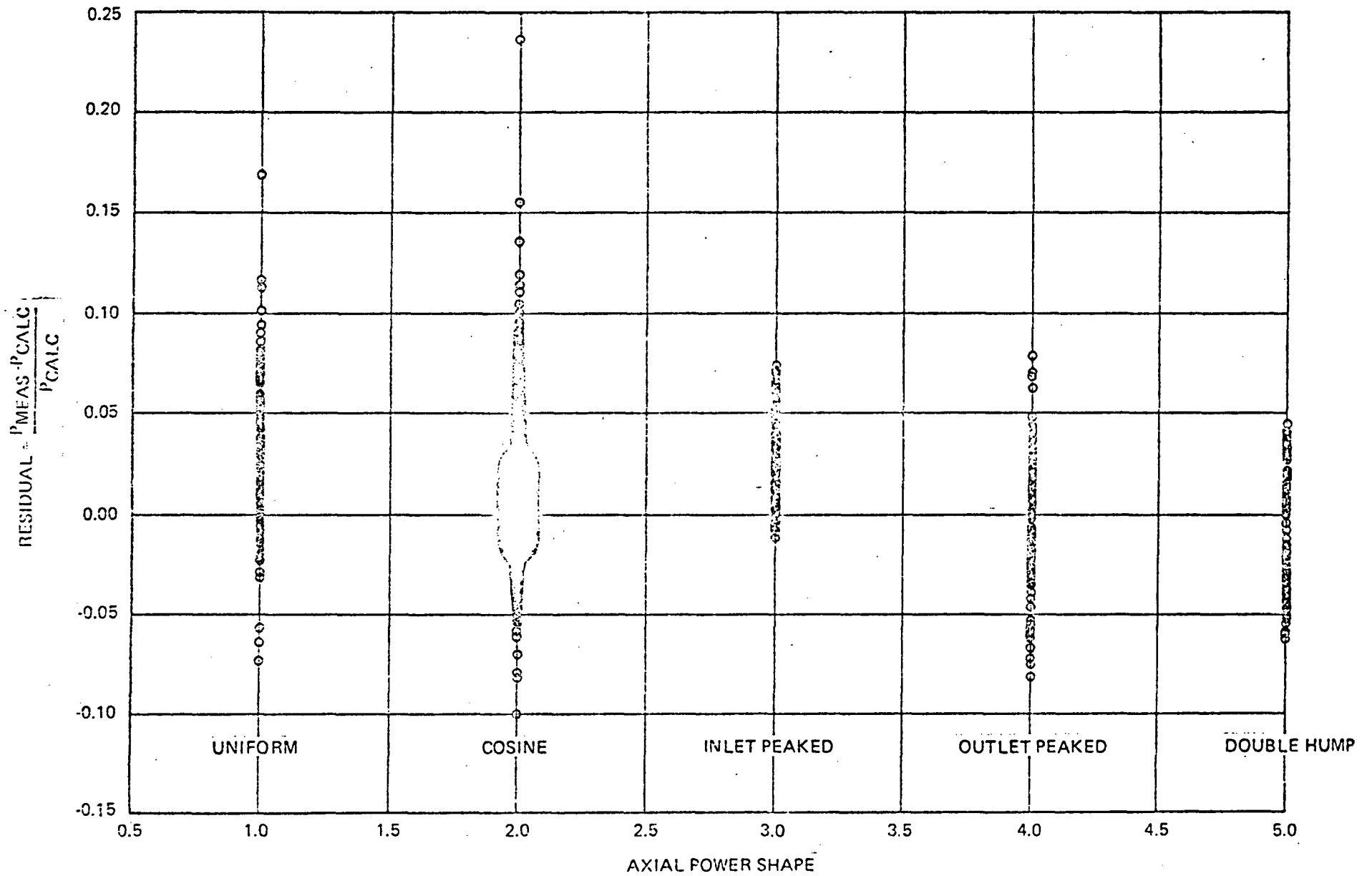


Figure 10 RESIDUAL VS. AXIAL POWER SHAPE FOR GEXL CORRELATION OF ATLAS DATA

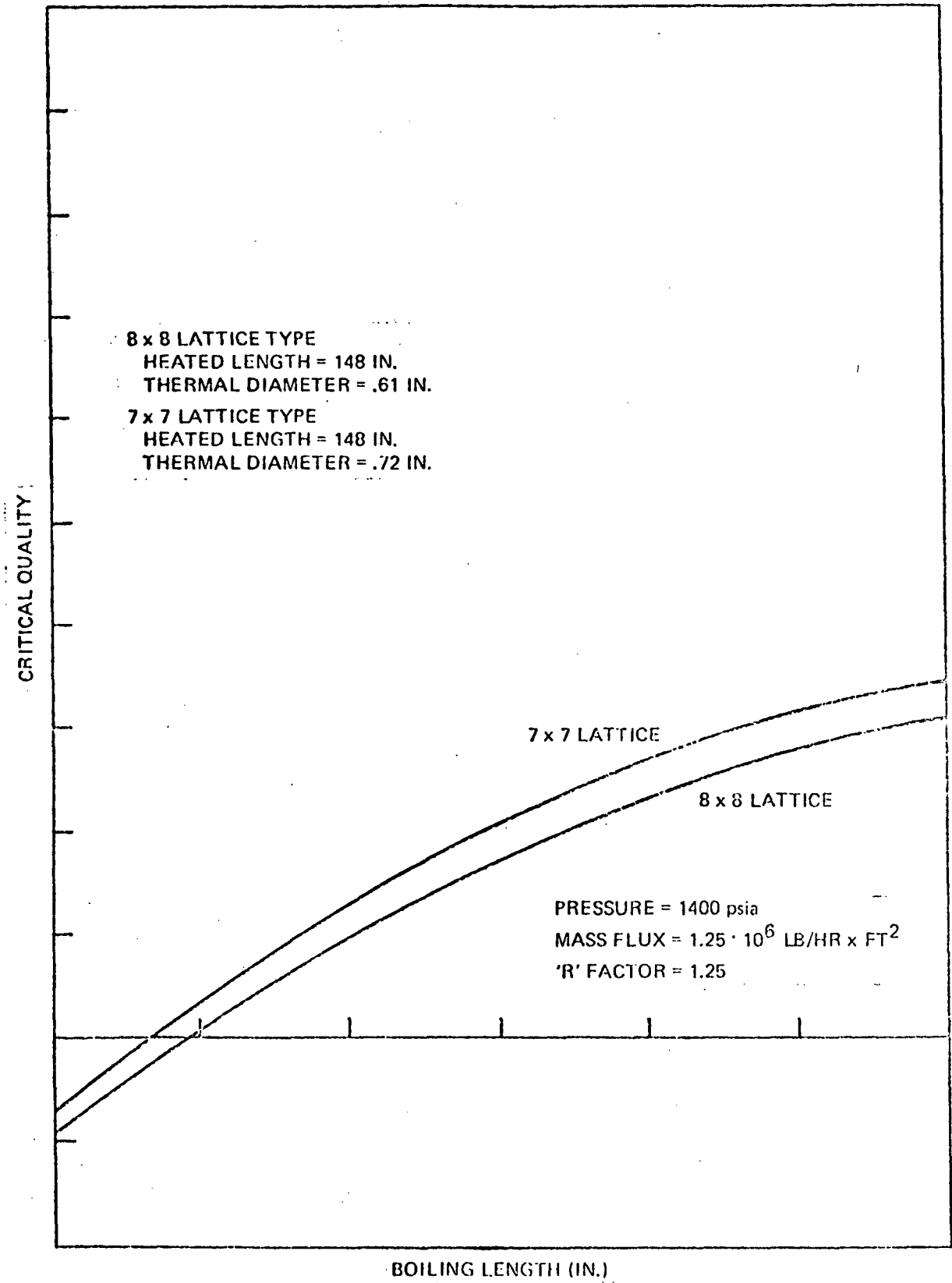


Figure 11 EFFECT OF LATTICE TYPE FOR GEXL CORRELATION

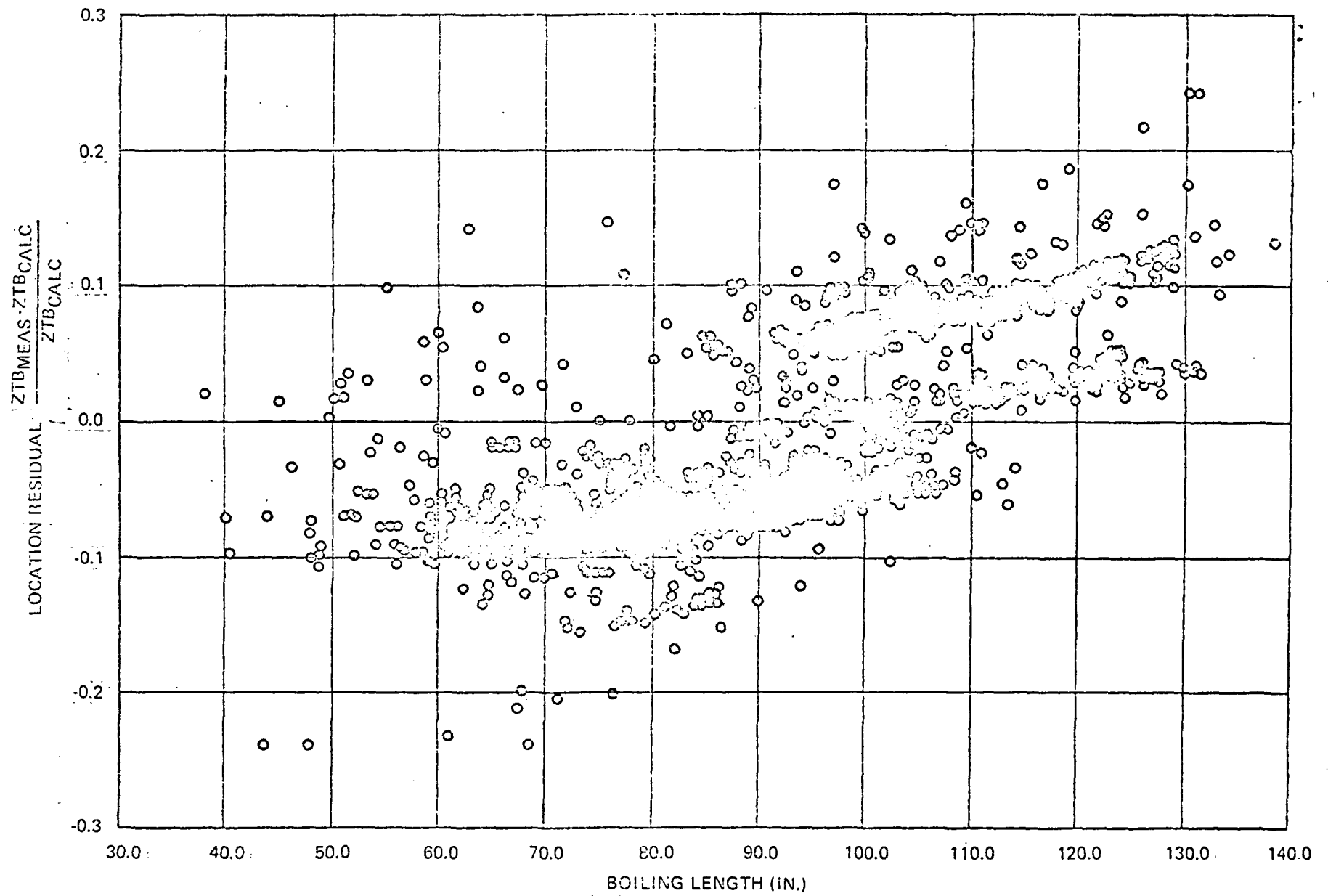


Figure 12 LOCATION RESIDUAL VS. BOILING LENGTH FOR GEXL CORRELATION OF ATLAS DATA

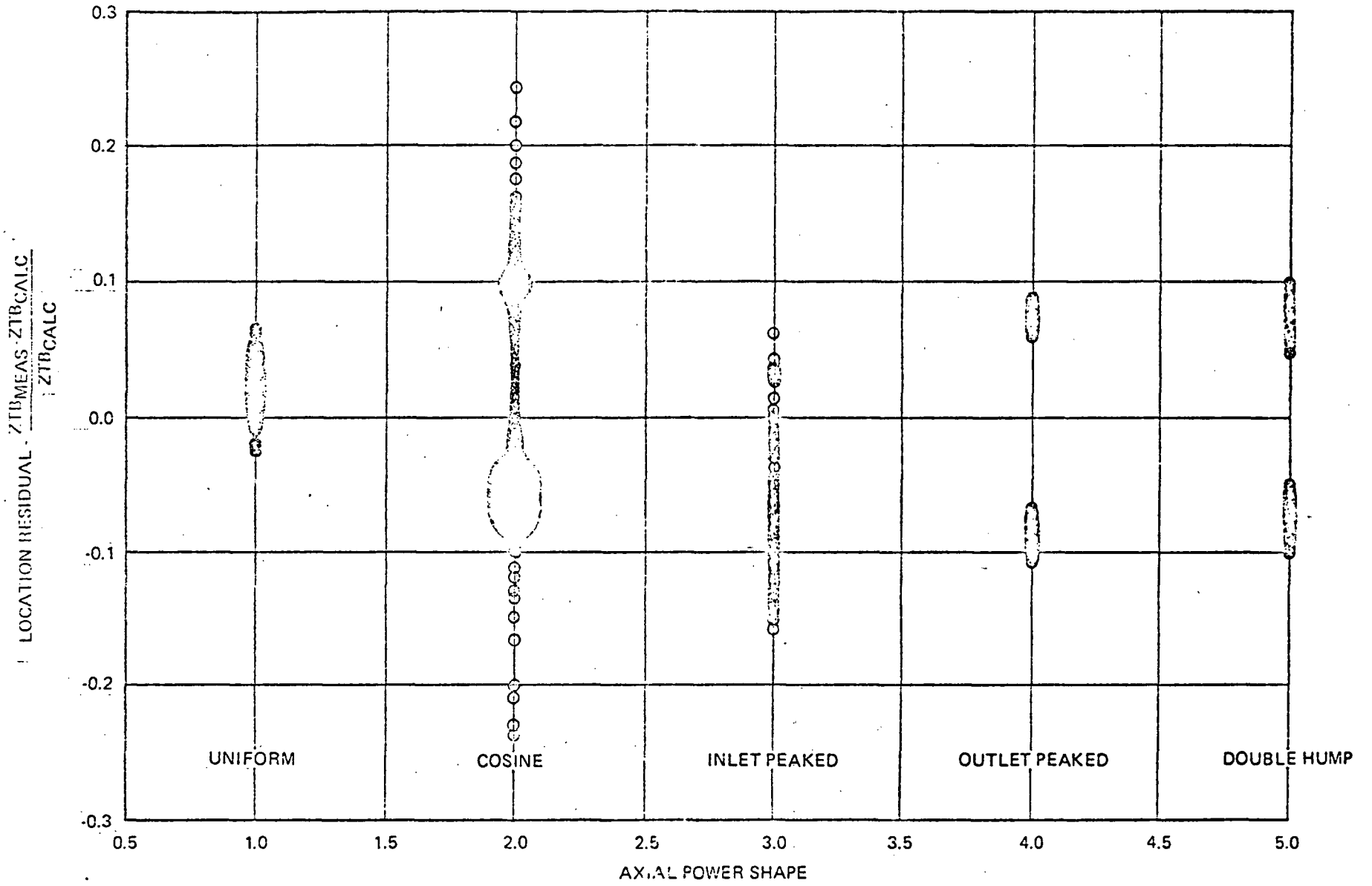


Figure 13 LOCATION RESIDUAL VS. AXIAL POWER SHAPE FOR GEXL CORRELATION OF ATLAS DATA

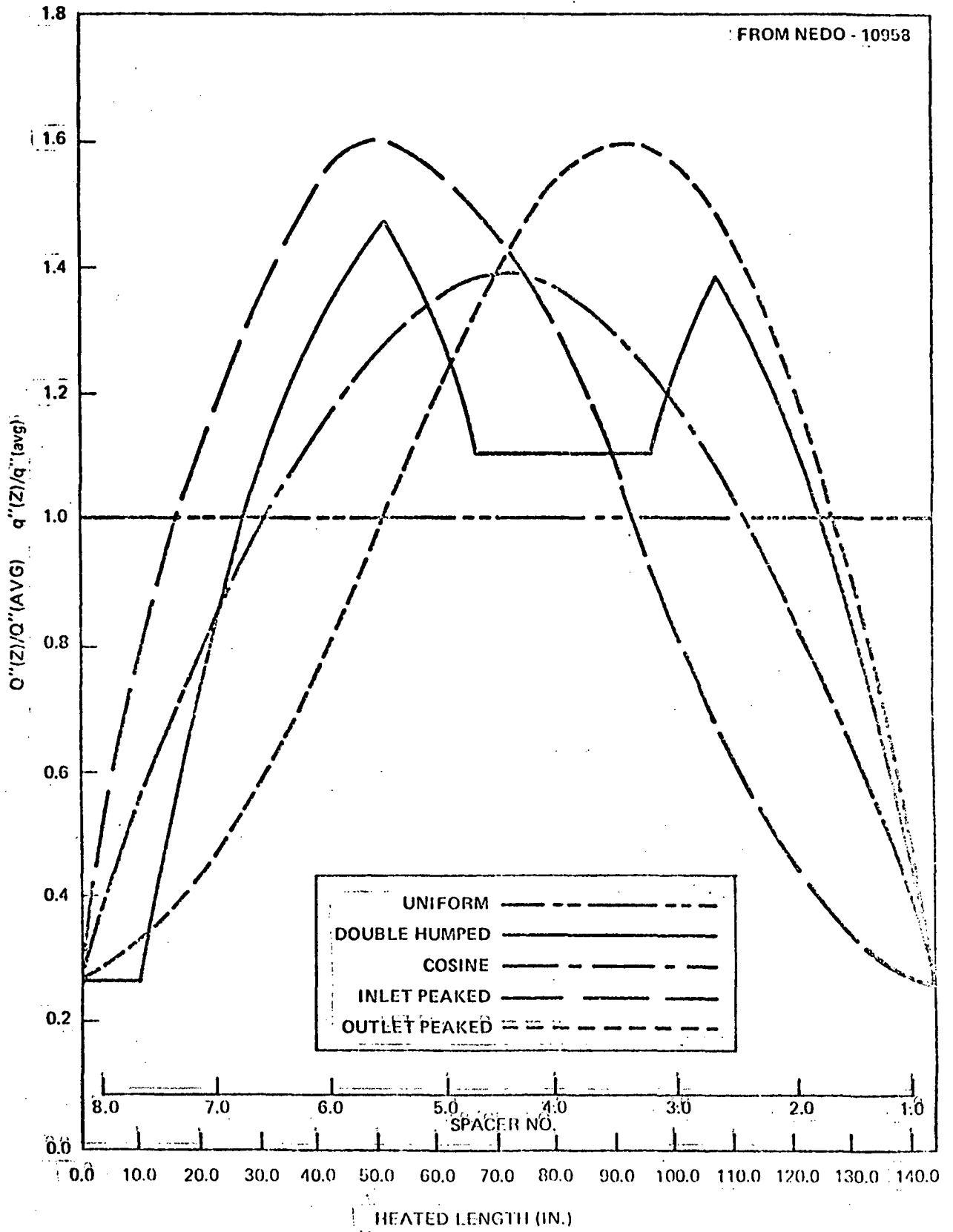


Figure 14 AXIAL FLUX SHAPES FOR 7 X 7 LATTICE

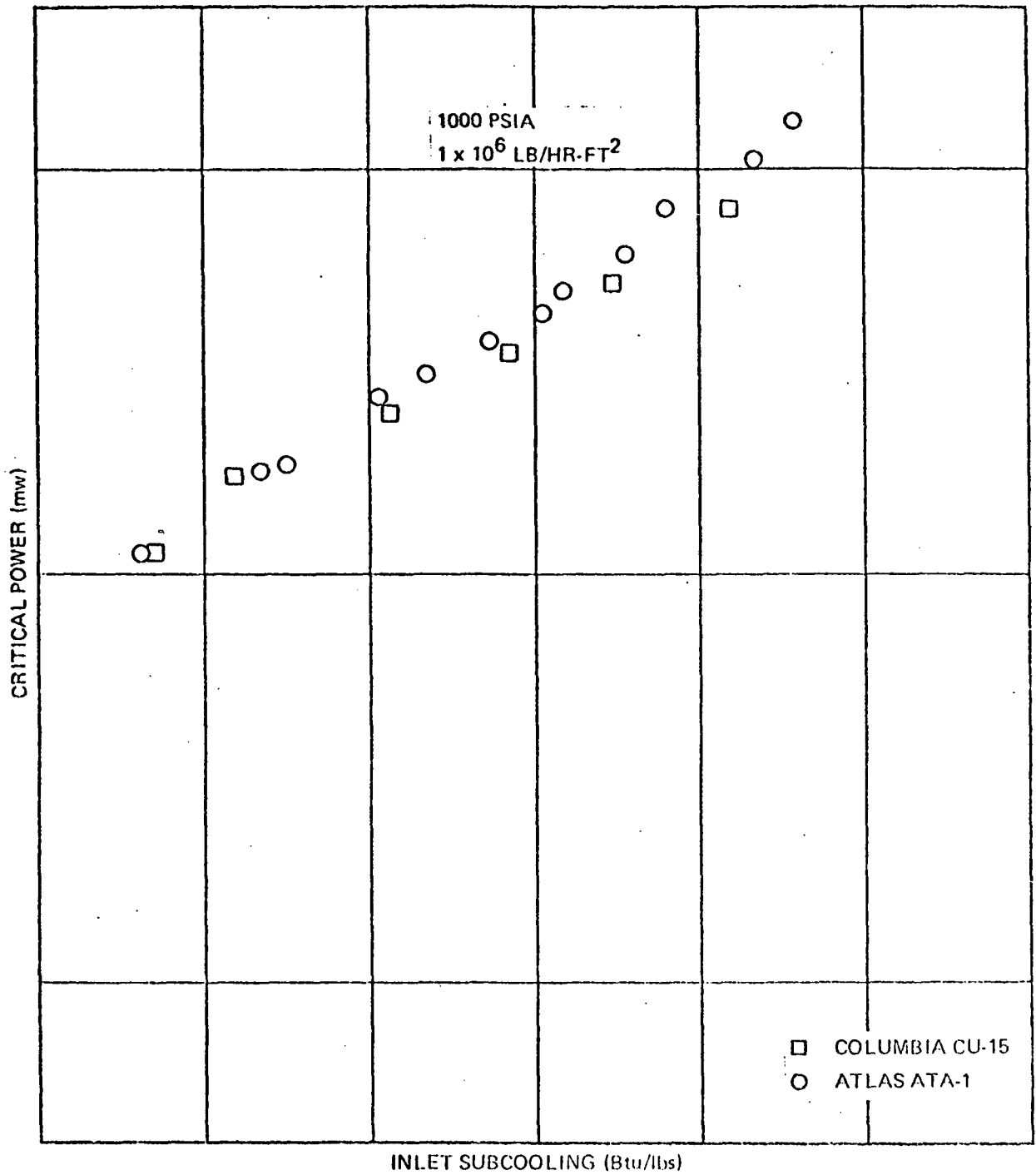


Figure 15 ATLAS VS. COLUMBIA DATA

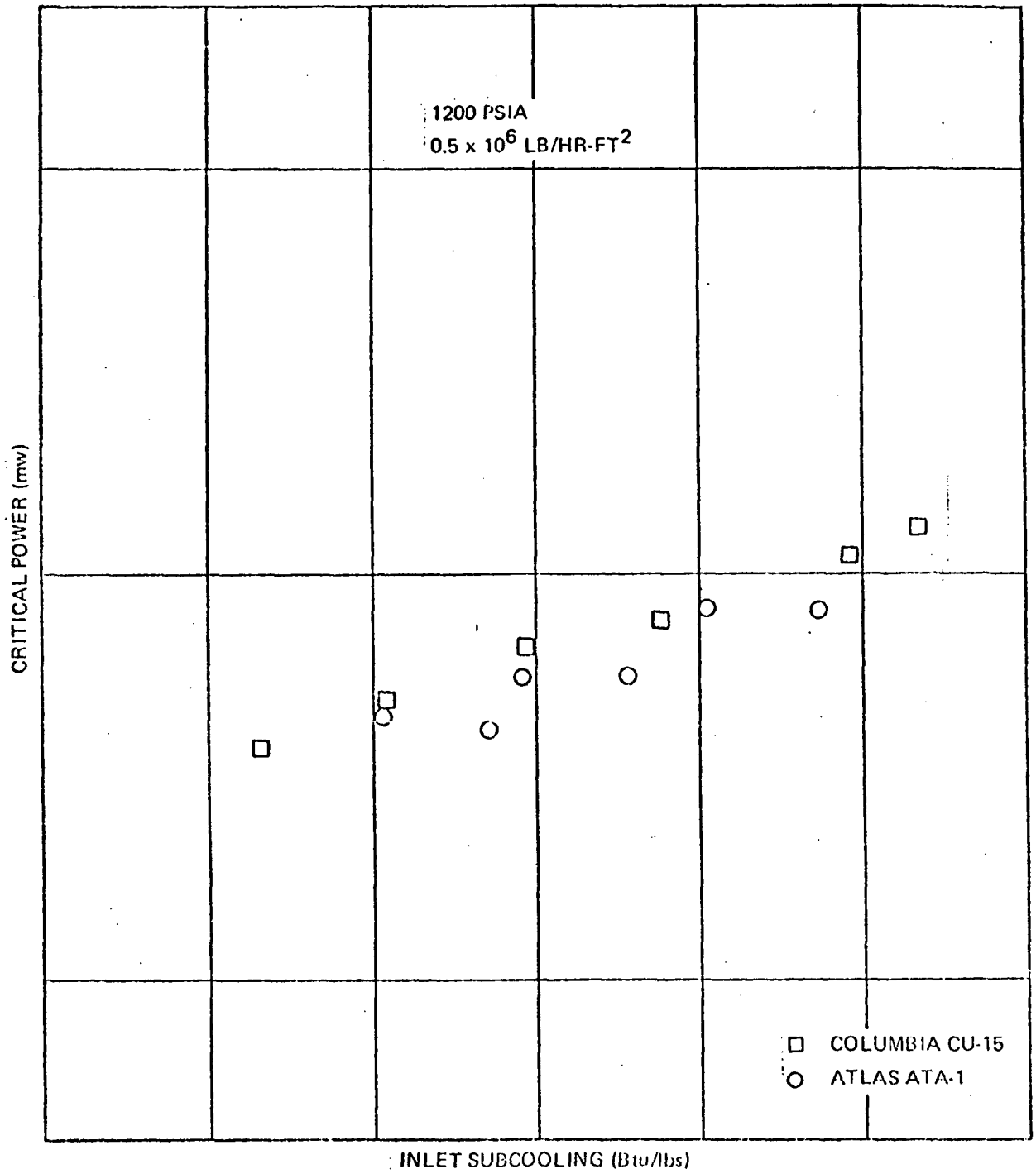


Figure 16 ATLAS VS. COLUMBIA DATA



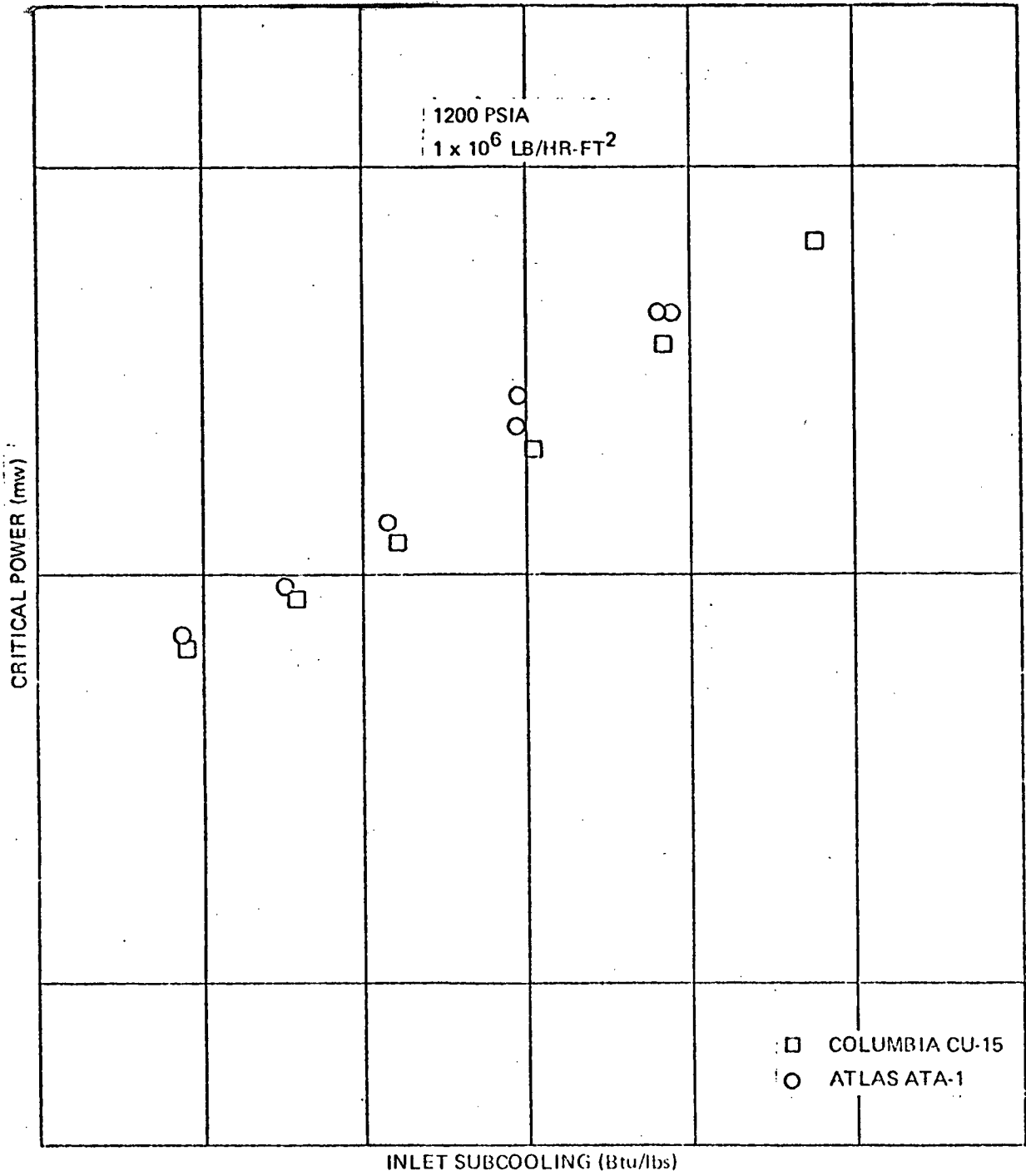


Figure 17 ATLAS VS: COLUMBIA DATA

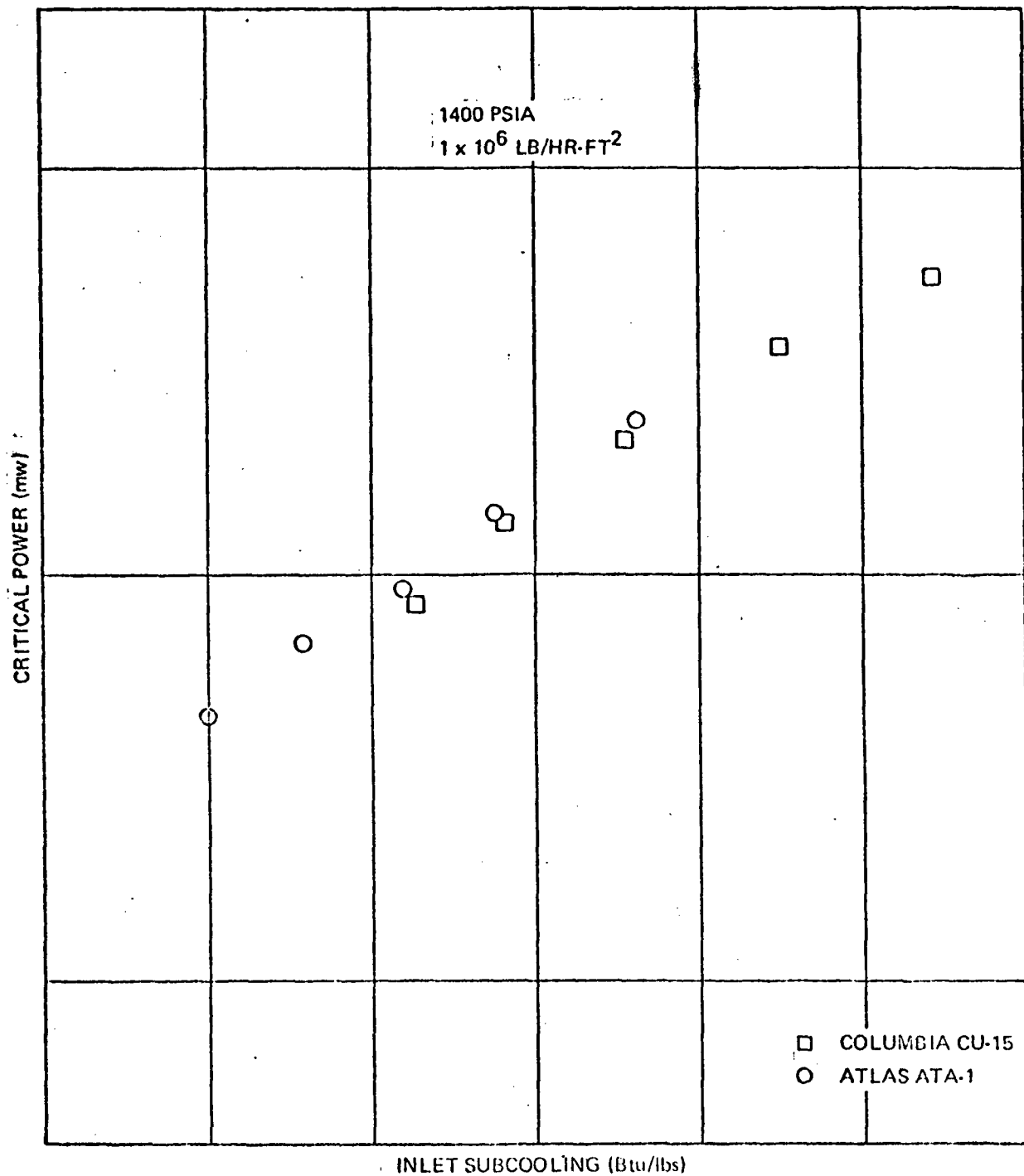


Figure 18 ATLAS VS. COLUMBIA DATA

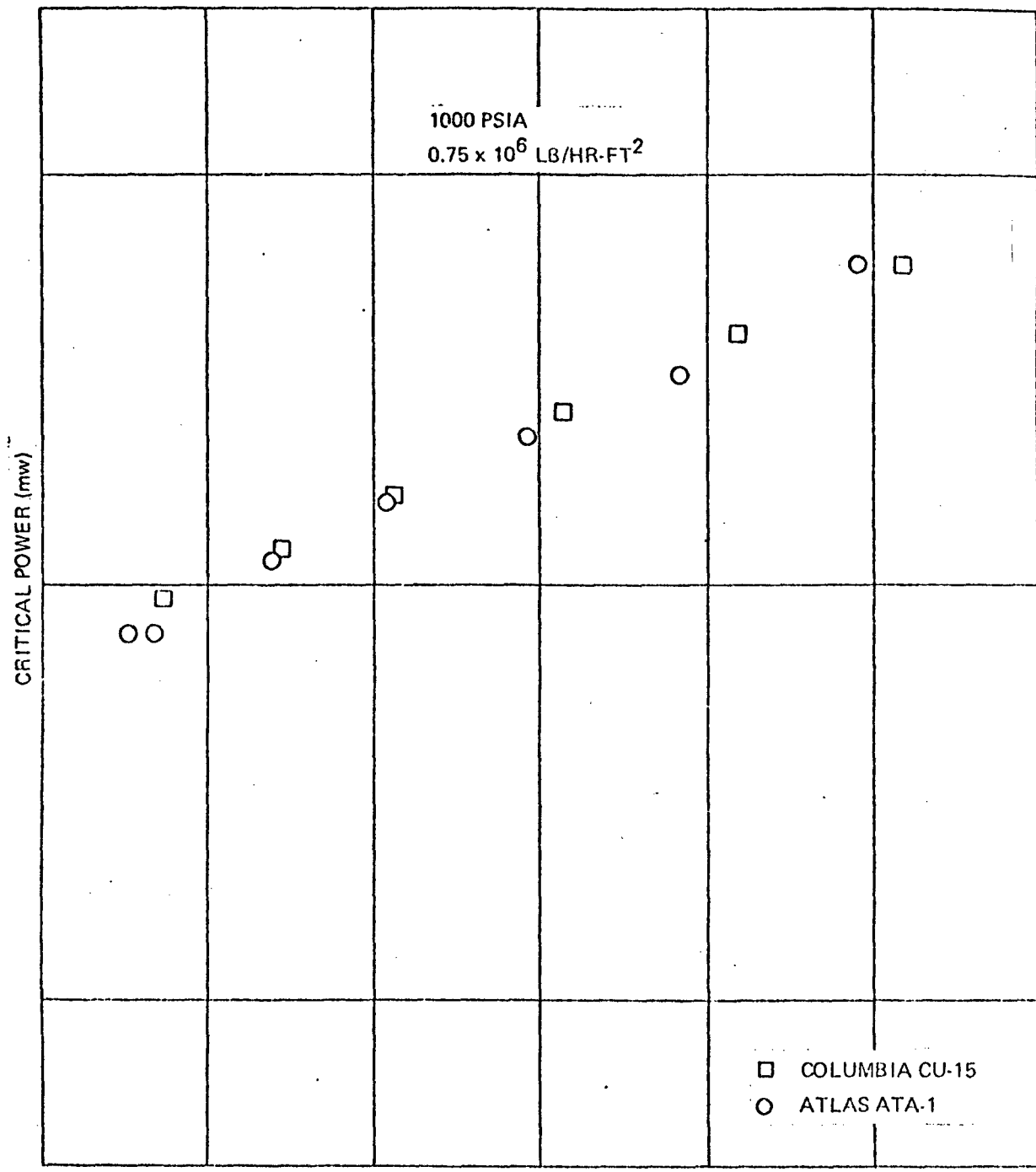


Figure 19 ATLAS VS COLUMBIA DATA

ENCLOSURE 2

SUMMARY OF TOPICAL REPORT EVALUATION

Report No.: NEDE-10958 (Proprietary); NEDO-10958 (Non-Proprietary Version)

Report Title: General Electric BWR Thermal Analysis Basis (GETAB): Data, Correlation and Design Operation

Report Date: November 1973

Originating Organization: General Electric Company

Reviewed By: Reactor Systems Branch  
Directorate of Licensing  
U. S. Atomic Energy Commission

## SUMMARY OF TOPICAL REPORT

During anticipated abnormal operating transients in a boiling water reactor, a criterion of no fuel rod damage is applied. Historically, the thermal hydraulic conditions resulting in a departure from nucleate boiling have been used to mark the beginning of the region where fuel damage could occur. Although it is recognized that a departure from nucleate boiling would not necessarily result in damage to BWR fuel rods, the critical heat flux at which boiling transition is calculated to occur has been adopted as a convenient limit.

Since 1966 this limit for BWR fuel assemblies has been based on the Hench-Levy correlation which was formulated as a lower limit line to the existing rod bundle critical heat flux data. To allow sufficient margin for uncertainties, the steady state operating conditions of General Electric Company reactors were limited such that during anticipated abnormal transients, the calculated heat flux was always less than the lower limit critical heat flux versus local quality. That is, during transients, the critical heat flux ratio was always greater than unity.

Based on recent extensive critical heat flux data obtained with full size, full power rod bundles in the ATLAS test loop, the General Electric Company has developed a new method of critical heat flux correlation. With this General Electric Critical Quality ( $X_c$ )- Boiling Length Correlation, (GEXL) critical power, the fuel assembly power at which boiling transition is expected to occur, is based on the correlation

of the critical quality and boiling length. In contrast to the Hench-Levy correlation, which is a lower limit line to the data, the GEXL correlation is a best fit to the ATLAS test data. This topical report and supplementary information describe the design and operation of the ATLAS facility. The report also provides the critical heat flux correlation, the steady state and transient data on which the correlation is based, and the statistical analysis of the correlation.

A new thermal design method, the General Electric Thermal Analysis Basis (GETAB) which incorporates the GEXL correlation, is also described in the report. The uncertainties associated with the GEXL correlation and the reactor steady state operating parameters are combined statistically. The steady state operating conditions are to be limited such that during anticipated abnormal transients, more than 99.9% of the fuel rods in the core are expected not to experience boiling transition. That is, during transients, the minimum critical power ratio (MCPR) is to be greater than a value determined by the magnitude of these uncertainties. A typical value is 1.05.

SUMMARY OF REGULATORY STAFF EVALUATION

The Staff reviewed the General Electric Thermal Analysis Basis and its application to reactor design and operation. The details of this review are presented in the Staff report "Review and Evaluation of GETAB for BWR's" dated September 1974. Included in the review were the GEXL correlation, which is the basis for GETAB; the analytical methods used to develop this correlation; the experimental results from which the correlation was synthesized; and the experimental methods used to obtain the data.

Based on our review of the design and operation of the ATLAS test facility, the Staff concludes that the steady state and transient tests had accurately controlled and measured test conditions. Comparison among the results of tests conducted on the ATLAS loop and between the results of tests conducted on both the ATLAS and Columbia loops verified reproducibility and lack of bias of the experimental results.

The experimental results were mainly obtained from full size, full length rod bundles which duplicated fuel assemblies in all respects that could significantly affect boiling transition. The tests were performed with a range of test conditions (flow, pressure, temperature and power) and heat flux distributions, both axial and radial, which equaled or exceed those expected to occur in a fuel assembly. Therefore, we conclude that the experimental results represent the thermal performance of GE 8 x 8 and 7 x 7 fuel assemblies.

Based on an independent comparison of the ATLAS data to the GEXL correlation, we conclude that the data can be conservatively treated as normally distributed about the correlations with a standard deviation of 3.6% and 3.4% for the 7 x 7 and 8 x 8 GEXL respectively. While small systematic differences between assemblies with different power distributions are shown, the correlation is slightly conservative with respect to the most probable distributions, (i.e., inlet peak and symmetrical cosine). Although the correlation has some anomalies at extreme conditions, GEXL can predict within a defined uncertainty the thermal performance of GE 8 x 8 and 7 x 7 fuel assemblies for the expected range of reactor normal steady state operation and abnormal operating transients.

General Design Criterion 10 requires that "acceptable fuel design limits are not exceeded during any condition of normal operation, including the effects of anticipated operational occurrences." We conclude that the proposed design bases (i.e. Transients caused by single operator error or equipment malfunction shall be limited such that considering uncertainties in monitoring the core operating state, more than 99.9% of the fuel rods would be expected to avoid boiling transition) meets the criterion when applied to core -- wide transients. However, we require that the MCPR limit derived for core-wide transients also be used as the Safety Limit applicable to local transients such as a control rod withdrawal. We also conclude that the statistical model used to derive the MCPR limit is acceptable.



REGULATORY POSITION

As a result of our review, we have concluded that NEDE-10958 provides an acceptable boiling transition correlation and an acceptable method of thermal analysis of GE BWR 8 x 8 and 7 x 7 fuel assemblies. NEDE-10958 is acceptable for reference in license applications and requests for changes in licenses when used to support the thermal and hydraulic design and operating limits of GE BWR 8 x 8 and 7 x 7 fuel assemblies. As stated previously, the staff requires that the MCPR limit derived for core-wide transients also be used as the safety limit applicable to local transients such as control rod withdrawal.

## ACKNOWLEDGMENT

The following individuals contributed to this document:

E. C. Eckert, J. Gonzalez, E. Janssen, H. T. Kim, R. T. Lahey, D. Liffengren, B. Matzner, C. L. Miller, D. Radcliffe, J. C. Rawlings, A. E. Rogers, and B. S. Shiralkar.

**TABLE OF CONTENTS**

**1. INTRODUCTION . . . . . 1-1**

    1.1 General . . . . . 1-1

    1.2 Terminology . . . . . 1-1

    1.3 List of Symbols . . . . . 1-1

**2. SUMMARY AND CONCLUSIONS . . . . . 2-1**

**3. BACKGROUND . . . . . 3-1**

    3.1 Limit Line Approach . . . . . 3-1

    3.2 Alternates to the Limit Line Approach . . . . . 3-1

**4. CRITICAL POWER DATA BASE . . . . . 4-1**

    4.1 Historical Review . . . . . 4-1

    4.2 Experimental Objectives . . . . . 4-1

    4.3 Steady-State Data . . . . . 4-1

    4.4 Boiling Transition Testing Procedure: Steady-State . . . . . 4-2

    4.5 Salient Features of the Steady-State Data . . . . . 4-2

    4.6 Transient Data . . . . . 4-3

    4.7 Experimental Procedure: Transient . . . . . 4-4

    4.8 Salient Features of the Transient Data . . . . . 4-4

**5. NEW CORRELATION . . . . . 5-1**

    5.1 Form of the GEXL Correlation . . . . . 5-1

    5.2 Prediction Capabilities: Steady-State . . . . . 5-1

    5.3 Prediction Capabilities: Transient (7 x 7 Lattice) . . . . . 5-3

    5.4 Prediction Capabilities: Transient (8 x 8 Lattice) . . . . . 5-6

**6. APPLICATION TO BWR DESIGN . . . . . 6-1**

    6.1 Introduction . . . . . 6-1

    6.2 Critical Power Ratio (CPR) . . . . . 6-1

    6.3 Statistical Basis for Establishing Design and Operational Thermal Limits . . . . . 6-2

    6.4 Technical Specifications Safety Limit . . . . . 6-5

    6.5 Procedures for Design Evaluations . . . . . 6-6

**REFERENCES . . . . . R-1**

**APPENDICES**

**I. RELATIONSHIPS FOR MAPPING ERROR BAND FROM  
     $X_C - L_B$  PLANE TO  $KW_C$  vs  $-\Delta h_S$  PLANE . . . . . I-1**

**II. TABLES OF CRITICAL POWER TEST CONDITIONS AND  
    PREDICTION CAPABILITIES . . . . . II-1**

**III. AXIAL PROFILES AND LOCAL PEAKING PATTERNS . . . . . III-1**

**IV. STATISTICAL ROD BOILING TRANSITION ANALYSIS . . . . . IV-1**

**V. EFFECT OF AXIAL POWER SHAPE AND R FACTOR ON MCPR REQUIREMENT . . . . . V-1**

**VI. EFFECT OF AXIAL POWER SHAPE ON LOCA . . . . . VI-1**

## LIST OF ILLUSTRATIONS

Figure	Title	Page
1-1	Summary of Boiling Transition Test Data to October 1973 . . . . .	1-3
3-1	Hench-Levy Limit Line, 1000 psia, $G = 1 \times 10^6$ lb/hr ft <sup>2</sup> . . . . .	3-5
3-2	Heat Flux vs. Quality at Location of Boiling Transition, B&W 0.45 in. dia. Round Tube Data, 6-ft Heated Length, Various Axial Profiles, $P = 1000$ psia, $G = 1.5 \times 10^6$ lb/h-ft <sup>2</sup> . . . . .	3-6
3-3	Critical Quality vs. Boiling Length, B&W Round Tube Data . . . . .	3-7
3-4	Heat Flux vs. Quality at Location of Boiling Transition, Freon 114 Annulus Data, $D_1 = 0.563$ in., $D_2 = 0.875$ in., 6- and 12-ft Heated Length, Various Axial Profiles, $P = 123$ psia, $G = 0.54 \times 10^6$ lb/h-ft <sup>2</sup> . . . . .	3-8
3-5	Critical Quality vs. Boiling Length, Freon-114 Annulus Data . . . . .	3-9
3-6	Critical Quality vs. Boiling Length, British <sup>(10)</sup> 12.6 mm dia. Round Tube Data, 3.66m Heated Length, Various Axial Profiles, $G = 2.72 \times 10^3$ kg/sec-m <sup>2</sup> . . . . .	3-10
3-7	Correlation Curve and Heat Balance Curves for Freon 114 Annulus with Inlet Peak Profile, Showing Typical Iterations in the Prediction of Critical Power ( $P = 123$ psia, $G = 0.66 \times 10^6$ lb/h-ft <sup>2</sup> , 14.8 Btu/lb (Subcooling) . . . . .	3-11
3-8	Error Band in kW vs. $\Delta h_s$ Plane Corresponding to an Error Band of $\pm 0.01$ in $X_c$ vs. LB Plane (12-ft Cosine, $G = 0.66 \times 10^6$ lb/h-ft <sup>2</sup> ) . . . . .	3-12
4-1	Critical Power vs. Inlet Subcooling, Atlas Test Assembly No. 14, 16-Rod x 12-ft Cosine, Uniform Local Peaking, 1000 psia, Various Flow Rates . . . . .	4-5
4-2	Critical Power (Normalized with Respect to Value for Columbia Test Assembly No. 15 at $G = 1 \times 10^6$ lb/h-ft <sup>2</sup> , $\Delta h_s = 20$ Btu/lb vs. Inlet Subcooling . . . . .	4-6
4-3	Critical Power vs. Flow Rate (cross plot of Figure 8 Data) . . . . .	4-7
4-4	Critical Power (Normalized with Respect to Value at 1000 psia) vs. Pressure, Four Atlas Test Assemblies, $\Delta h_s = 20$ Btu/lb, $G = 0.5 \times 10^6$ and $1.0 \times 10^6$ lb/h-ft <sup>2</sup> . . . . .	4-8
4-5	Critical Power Per Unit Mass Rate (Normalized with Respect to Value for Uniform Local Peaking) vs. Corner Rod Peaking, $P = 1000$ psia, $\Delta h_s = 20$ Btu/lb, $G = 0.5 \times 10^6$ and $1.0 \times 10^6$ lb/hr-ft <sup>2</sup> . . . . .	4-9
4-6	Critical Power (Normalized with Respect to Value for Symmetrical Cosine Axial Profile at $\Delta h_s = 20$ Btu/lb) versus Inlet Subcooling, Various Axial Profiles, 1.23/1.26 3-Rod Corner Peaking, 1000 psia, $G = 1 \times 10^6$ lb/h-ft <sup>2</sup> . . . . .	4-10
4-7	Effect on Critical Power of Rod-to-Wall Clearance in Hot Corner, for Bundles with Corner Rod Peaking . . . . .	4-11
4-8	Definition of Transient Times . . . . .	4-12
4-9	Flow Decay at Constant Power (Atlas Test Assembly No. 14, Run No. 101) . . . . .	4-13
4-10	Flow On/Off/On at Constant Power (Run No. 138) . . . . .	4-14
4-11	Flow On/Off/On at Constant Power (Run No. 139) . . . . .	4-15
4-12	Simultaneous Flow and Power Decay (Run No. 200) . . . . .	4-16
4-13	Simulated Loss-of-Coolant Accident (Run No. 248) . . . . .	4-17
5-1	Nine- and 16-Rod Critical Quality versus Boiling Length, 1000 psi . . . . .	5-7
5-2	Predicted vs. Measured Critical Power, Columbia 7x7 Lattice 16-Rod Test Assemblies, 6-ft Uniform Axial Profile, Various Local Peaking Patterns, $800 \leq P \leq 1400$ psia, $0.25 \leq G/10^6 \leq 1.25$ lb/h-ft <sup>2</sup> , $\Delta h_s \leq 100$ Btu/lb (84 points) . . . . .	5-8
5-3	Predicted vs. Measured Critical Power, Atlas 7x7 Lattice 16-Rod Test Assemblies, Various 12-ft Nonuniform Axial Profiles, Various Local Peaking Patterns, $800 \leq P \leq 1400$ psia, $0.25 \leq G/10^6 \leq 1.25$ lb/h-ft <sup>2</sup> , $\Delta h_s \leq 100$ Btu/lb (2136 points) . . . . .	5-9
5-4	Predicted vs. Measured Critical Power, Atlas 7x7 Lattice 49-Rod Test Assemblies, 12-ft Cosine Profile, Various Local Peaking Patterns, $800 \leq P \leq 1200$ psia, $0.25 \leq G/10^6 \leq 1.25$ lb/h-ft <sup>2</sup> , $\Delta h_s \leq 100$ Btu/lb (403 points) . . . . .	5-10
5-5	Predicted versus Measured Critical Power, Atlas 8x8 Lattice 16-Rod Test Assemblies, 12-1/3-ft Cosine Profile, Various Local Peaking Patterns, $800 \leq P \leq 1400$ psia, $0.25 \leq G/10^6 \leq 1.25$ lb/h-ft <sup>2</sup> , $\Delta h_s \leq 100$ Btu/lb (266 points) . . . . .	5-11

**LIST OF ILLUSTRATIONS (Continued)**

Figure	Title	Page
5-6	Predicted versus Measured Critical Power, Atlas 8x8 Lattice 64 Rod Test Assemblies, 12-1/2-ft Cosine Profile, Various Local Peaking Patterns, $800 \leq P \leq 1400$ psia, $0.25 \leq G/10^6 \leq 1.25$ lb/h-ft <sup>2</sup> , $\Delta h_s \leq 100$ Btu/lb (426 points) . . . . .	5-12
5-7	Histogram, Frequency vs ECPR, for 7x7 Lattice 16- and 49-Rod Test Assemblies, (2700 Points) (Mean = 0.9885, Standard Deviation = 0.0360) . . . . .	5-13
5-8	Histogram, Frequency vs ECPR, for 8x8 Lattice, 16- and 64-Rod Test Assemblies (692 points) . . . . .	5-14
5-9	Predicted vs Measured Critical Power, Early 4-Rod and 9-Rod Test Assemblies, Uniform Axial Flux Profile, Various Heated Lengths, $600 \leq P \leq 1400$ psia, $0.20 \leq G/10^6 \leq 1.50$ lb/h-ft <sup>2</sup> $\Delta h_s \leq 200$ Btu/lb . . . . .	5-15
5-10	Predicted vs Measured Critical Power, 7x7 Lattice, 16-Rod x 144-in. Heated Length Freon Data, Uniform Local Peaking . . . . .	5-16
5-11	Predicted vs Measured Critical Power, 7x7 Lattice, 49-Rod x 144-in. Heated Length Freon Data, Uniform Local Peaking . . . . .	5-17
5-12	Freon 16-Rod Test Assembly 8x8 Lattice, 30 Points . . . . .	5-18
5-13	Freon 64-Rod Test Assembly, 8x8 Lattice, 46 Points . . . . .	5-19
5-14	Predicted and Measured Critical Powers (Normalized with Respect to Measured Value for Symmetrical Cosine Axial Profile at $\Delta h_s = 20$ Btu/lb) vs. Inlet Subcooling, Various Axial Profiles, 1.23/1.26 3-Rod Corner Peaking, 1000 psia, $G = 1 \times 10^6$ lb/h-ft <sup>2</sup> . . . . .	5-20
5-15	Calculated Transient Critical Power Ratio and Measured Heater Rod Cladding Temperature Vs Time . . . . .	5-21
5-16	Calculated Transient Critical Power Ratio and Measured Heater Rod Cladding Temperature Vs Time . . . . .	5-22
5-17	Calculated Transient Critical Power Ratio and Measured Heater Rod Cladding Temperature Vs Time . . . . .	5-23
5-18	Axial Penetration of Boiling Transition Vs Time . . . . .	5-24
5-19	Axial Penetration of Boiling Transition Vs Time . . . . .	5-25
5-20	Axial Penetration of Boiling Transition Vs Time . . . . .	5-26
5-21	Calculated Time versus Measured Time to Initial Boiling Transition . . . . .	5-27
5-22	Boiling Transition Axial Penetration Calculated Vs Measured . . . . .	5-28
5-23	Calculated Transient Critical Power Ratio and Measured Heater Rod Cladding Temperature vs Time . . . . .	5-29
5-24	Calculated Transient Critical Power Ratio and Measured Heater Rod Cladding Temperature Vs Time . . . . .	5-30
5-25	Calculated Minimum Critical Power Ratio and Measured Heater Rod Cladding Temperature Vs Time . . . . .	5-31
5-26	Axial Penetration of Boiling Transition Vs Time . . . . .	5-32
5-27	Axial Penetration of Boiling Transition Vs Time . . . . .	5-33
5-28	Axial Penetration of Boiling Transition Vs Time . . . . .	5-34
5-29	Calculated Time Vs Measured Time to Initial Boiling Transition . . . . .	5-35
5-30	Boiling Transition Axial Penetration – Calculated Versus Measured . . . . .	5-36
5-31	Calculated Transient Critical Power Ratio and Measured Heater Rod Cladding Temperature Vs Time . . . . .	5-37
5-32	Calculated Transient Critical Power Ratio and Measured Heater Rod Cladding Temperature Vs Time . . . . .	5-38
5-33	Calculated Transient Critical Power Ratio and Measured Heater Rod Cladding Temperature Vs Time . . . . .	5-39
5-34	Axial Penetration of Boiling Transition Vs Time . . . . .	5-30

LIST OF ILLUSTRATIONS (Continued)

Figure	Title	Page
5-35	Axial Penetration of Boiling Transition Vs Time . . . . .	5-41
5-36	Axial Penetration of Boiling Transition Vs Time . . . . .	5-42
5-37	Calculated Time Vs Measured Time to Initial Boiling Transition . . . . .	5-43
5-38	Boiling Transition Axial Penetration Calculated Vs Measured . . . . .	5-44
5-39	Calculated Transient Critical Power Ratio and Measured Heater Rod Cladding Temperature Vs Time . . . . .	5-45
5-40	Calculated Transient Critical Power Ratio and Measured Heater Rod Cladding Temperature Vs Time . . . . .	5-46
5-41	Calculated Transient Critical Power Ratio and Measured Heater Rod Cladding Temperature Vs Time . . . . .	5-47
5-42	Axial Penetration of Boiling Transition Versus Time . . . . .	5-48
5-43	Axial Penetration of Boiling Transition Versus Time . . . . .	5-49
5-44	Axial Penetration of Boiling Transition Versus Time . . . . .	5-50
5-45	Calculated Time Vs Measured Time to Initial Boiling Transition . . . . .	5-51
5-46	Boiling Transition Axial Penetration, Calculated Vs Measured . . . . .	5-52
5-47	Calculated Transient Critical Power Ratio and Measured Heater Rod Cladding Temperature Vs Time . . . . .	5-53
5-48	Calculated Transient Critical Power Ratio and Measured Heater Rod Cladding Temperature Vs Time . . . . .	5-54
5-49	Calculated Transient Critical Power Ratio and Measured Heater Rod Cladding Temperature Vs Time . . . . .	5-55
5-50	Axial Penetration of Boiling Transition Vs Time . . . . .	5-56
5-51	Axial Penetration of Boiling Transition Vs Time . . . . .	5-57
5-52	Axial Penetration of Boiling Transition Versus Time . . . . .	5-58
5-53	Calculated Time Vs Measured Time to Initial Boiling Transition . . . . .	5-59
5-54	Boiling Transition Axial Penetration Calculated Vs Measured . . . . .	5-60
5-55	Calculated Time versus Measured Time to Initial Boiling Transition . . . . .	5-61
5-56	Calculated Transient Critical Power Ratio and Measured Heater Rod Cladding Temperature versus Time . . . . .	5-62
5-57	Calculated Transient Critical Power Ratio and Measured Heater Rod Cladding Temperature versus Time . . . . .	5-63
5-58	Calculated Transient Critical Power Ratio and Measured Heater Rod Cladding Temperature versus Time . . . . .	5-64
5-59	Axial Penetration of Boiling Transition versus Time . . . . .	5-65
5-60	Axial Penetration of Boiling Transition versus Time . . . . .	5-66
5-61	Axial Penetration of Boiling Transition versus Time . . . . .	5-67
5-62	Calculated Time versus Measured Time to Initial Boiling Transition . . . . .	5-68
5-63	Calculated versus Measured Boiling Transition Axial Penetration . . . . .	5-69
5-64	Calculated Transient Critical Power Ratio and Measured Heater Rod Cladding Temperature versus Time . . . . .	5-70
5-65	Calculated Transient Critical Power Ratio and Measured Heater Rod Cladding Temperature versus Time . . . . .	5-71
5-66	Calculated Transient Critical Power Ratio and Measured Heater Rod Cladding Temperature versus Time . . . . .	5-72
5-67	Axial Penetration of Boiling Transition versus Time . . . . .	5-73

LIST OF ILLUSTRATIONS (Continued)

Figure	Title	Page
5-68	Axial Penetration of Boiling Transition versus Time . . . . .	5-74
5-69	Axial Penetration of Boiling Transition versus Time . . . . .	5-75
5-70	Calculated Time versus Measured Time to Initial Boiling Transition . . . . .	5-76
5-71	Boiling Transition Axial Penetration Calculated versus Measured . . . . .	5-77
5-72	Calculated Time versus Measured Time to Initial Boiling Transition . . . . .	5-78
6-1	Graphical Illustration of CPR . . . . .	6-12
6-2	Normalized R Vs Bundle-Average Exposure, Typical Single Enrichment Assembly of BWR-4 Series . . . . .	6-13
6-3	Critical Power Ratio Margins . . . . .	6-14
6-4	Typical Results of 30 Trials . . . . .	6-15
6-5	Core Pressure versus Time (DBA) . . . . .	6-16
6-6	Normalized Core Inlet Flow versus Time (DBA) . . . . .	6-17
6-7	Minimum Critical Heat Flux Ratio and Minimum Critical Power Ratio versus Time (DBA) . . . . .	6-18
6-8	Heat Transfer Coefficient versus Time After Design Basis Accident (Hench-Levy) . . . . .	6-19
6-9	Heat Transfer Coefficient versus Time After Design Basis Accident (GEXL) . . . . .	6-20
6-10	Peak Cladding Temperature Vs Time After Design Basis Accident (IAC Models) . . . . .	6-21
6-11	Minimum Critical Heat Flux Ratio and Minimum Critical Power Ratio Versus Time (Outside Steam Line Break) Typical BWR/4 . . . . .	6-22
6-12	Minimum Critical Heat Flux Ratio and Minimum Critical Power Ratio versus Time (DBA) . . . . .	6-23
III-1	Axial Flux Shapes for 7x7 Lattice . . . . .	III-1
IV-1	Variation of R Factor for A Bundle (7x7) . . . . .	IV-8
IV-2	Fuel Assembly Relative Powers (One Quadrant of a 764 Assembly Core). . . . .	IV-9
IV-3	Frequency of Assembly Relative Powers . . . . .	IV-10
V-1	Effects of Axial Peak Location on Required MCPR Design P/A = 1.4 (Transient Limit MCPR = 1.04) . . . . .	V-2
VI-1	Minimum Critical Power Ratio versus Time (DBA) . . . . .	VI-6
VI-2	Peak Cladding Temperature versus Time After Design Basis Accident . . . . .	VI-6
VI-3a	Axial Power Shape . . . . .	VI-7
VI-3b	Axial Power Shape . . . . .	VI-7
VI-3c	Axial Power Shape . . . . .	VI-8

LIST OF TABLES

Table	Title	Page
6-1	Transient Change in MCPR . . . . .	6-4
6-2	Typical DBA – BWR/4 7x7 Fuel . . . . .	6-10
6-3	Typical BWR/4 Design Basis LOCA (18.5 kW/ft Peak LHGR) . . . . .	6-11
II-1	Nine-Rod Critical Power Test Conditions, 1.7 MP Loop . . . . .	II-2
II-2	Sixteen-Rod Critical Power Test Conditions, Columbia University . . . . .	II-3
II-3	Sixteen, Forty-Nine, and Sixty-Four Rod Critical Power Test Conditions, Atlas Loop . . . . .	II-3
II-4	One, Sixteen, Forty-five, and Sixty-four Rod Critical Power Test Conditions, Freon Loop . . . . .	II-7
II-5	Transient Test Conditions . . . . .	II-15
II-6	Assembly 14 . . . . .	II-17
II-7	Assembly 27C . . . . .	II-18
II-8	Assembly 28D . . . . .	II-19
II-9	Assembly 29D . . . . .	II-20
II-10	Assembly 25A . . . . .	II-21
II-11	Assembly 32B . . . . .	II-22
II-12	Assembly 35C . . . . .	II-23
IV-1	Description of Uncertainties . . . . .	IV-2
IV-2	Manufacturing Induced Uncertainties . . . . .	IV-4
IV-3	Axial Power Distributions (Node Power/Assembly Average Node Power) . . . . .	IV-7
VI-1	Typical Design Basis Accident – BWR/4 (7x7 Fuel) . . . . .	VI-1
VI-2	Calculated Boiling Transition (Base Case) – Design Basis Accident . . . . .	VI-1
VI-3	Axial Power Shape Investigation Parametric Analysis Design Basis Accident – BWR/4 (7x7 Fuel) . . . . .	VI-2
VI-4	Results – Parametric Analysis, R=1.098, G=1x10 <sup>6</sup> lb/h-ft <sup>2</sup> . . . . .	VI-3
VI-5	Effect of R Factor (Axial Peak = 1.5) . . . . .	VI-4
VI-6	Parametric Study – Upper Node APLHGR (Design Basis Accident – BWR/4 – 7x7 Fuel) . . . . .	VI-5



## 1. INTRODUCTION

### 1.1 GENERAL

Since the introduction of the Hench-Levy Design Limit Lines in 1966,<sup>1</sup> General Electric has continued to perform an extensive boiling transition test program, and there have been numerous and extensive advancements in both experimental and analytical methods of investigating and correlating the occurrence of transition boiling. Figure 1-1 graphically illustrates the expansion of the BWR data base that has taken place. Improvements in technology now allow accurate full-scale prototypic simulation of reactor fuel assemblies operating under conditions duplicating those in actual reactor designs. The data obtained provide a direct demonstration giving complete assurance of boiling water reactor (BWR) heat transfer performance. These advancements, the greatly expanded data base, and an improved method of correlating the data provide the impetus for introducing a new boiling heat transfer design basis.

The objective of this report is to present the new design basis in its entirety, including the boiling transition correlation, the data base, the prediction capabilities, and the application to BWR thermal design.

### 1.2 TERMINOLOGY

The authors have attempted to adhere to consistent terminology in order to improve the clarity of this presentation. Definitions of some of the terms are given here so that their relationship can more easily be grasped by the reader.

The physical phenomenon being discussed is the *onset of transition boiling* and this phenomenon is referred to in this report as the *boiling transition*.<sup>\*</sup> The objective is to minimize the frequency of occurrence of this phenomenon during reactor operation. Conditions which produce a boiling transition are determined experimentally. The data points (conditions producing transition boiling) employed as a basis for the limits of APED 5286<sup>1</sup> were critical heat flux (CHF) as a function of critical quality. Data used to develop the new correlation are critical quality as a function of the critical boiling length.

The physical phenomenon is represented by an analytical *correlation* of the data. This presentation describes the development of the *General Electric Critical Quality ( $X_c$ ) – Boiling Length Correlation – GEXL*. GEXL is used in the design and operation of BWRs to establish appropriate thermal margins and to assess appropriate operating transient and accident conditions. That assembly power which causes some point in the assembly to experience a boiling transition is called the *critical power*. The ratio of the critical power to the bundle power at the reactor condition of interest is defined as the *critical power ratio (CPR)* and used as the new figure of merit for expressing BWR thermal margin. The net result is characterized as *GETAB*, the *General Electrical Thermal Analysis Basis*.

### 1.3 LIST OF SYMBOLS

- A = Cross-sectional flow area
- a, b = Terms in CISE boiling length correlation
- C = Term in Tong F factor which determines the strength of the "memory" effect
- $D_h$  = Hydraulic diameter  $\left( D_h = \frac{4A}{\text{wetted perimeter}} \right)$
- $D_Q$  = Thermal diameter  $\left( D_Q = \frac{4A}{\text{perimeter of rods}} \right)$

<sup>\*</sup>The terminology "boiling transition" is considered to be more descriptive of the onset of transition boiling which actually occurs and is used throughout this document rather than terms such as CHF, DNB or the "boiling crisis."

F	= Tong F factor
G	= Mass flux
$h_{fg}$	= Latent heat of evaporation
L	= Heated length
$L_B$	= Boiling length
P	= Pressure
$P_H$	= Heated perimeter
$q''_{nu}$	= Local critical heat flux value for a nonuniform heat flux profile
$q''_U$	= Equivalent uniform heat flux
R	= Weighted peaking factor used to characterize the local peaking pattern in the vicinity of a given rod
r	= Local (rod) peaking factor
$\hat{W}$	= Power input over the boiling region
$X_C$	= Critical quality
z	= Distance along axial direction
$\sigma$	= Standard deviation
$\Delta h_s$	= Inlet subcooling
$\tau, \tau_1, \tau_2, \tau_3$	= Time period referred to transient tests (Figure 4-7)

#### 1.4 REVISIONS

Lines in the margin indicate inclusions or revisions to the original text. Margin bars accompanied by a number indicate an answer to the associated NRC question documented in Appendix VII.

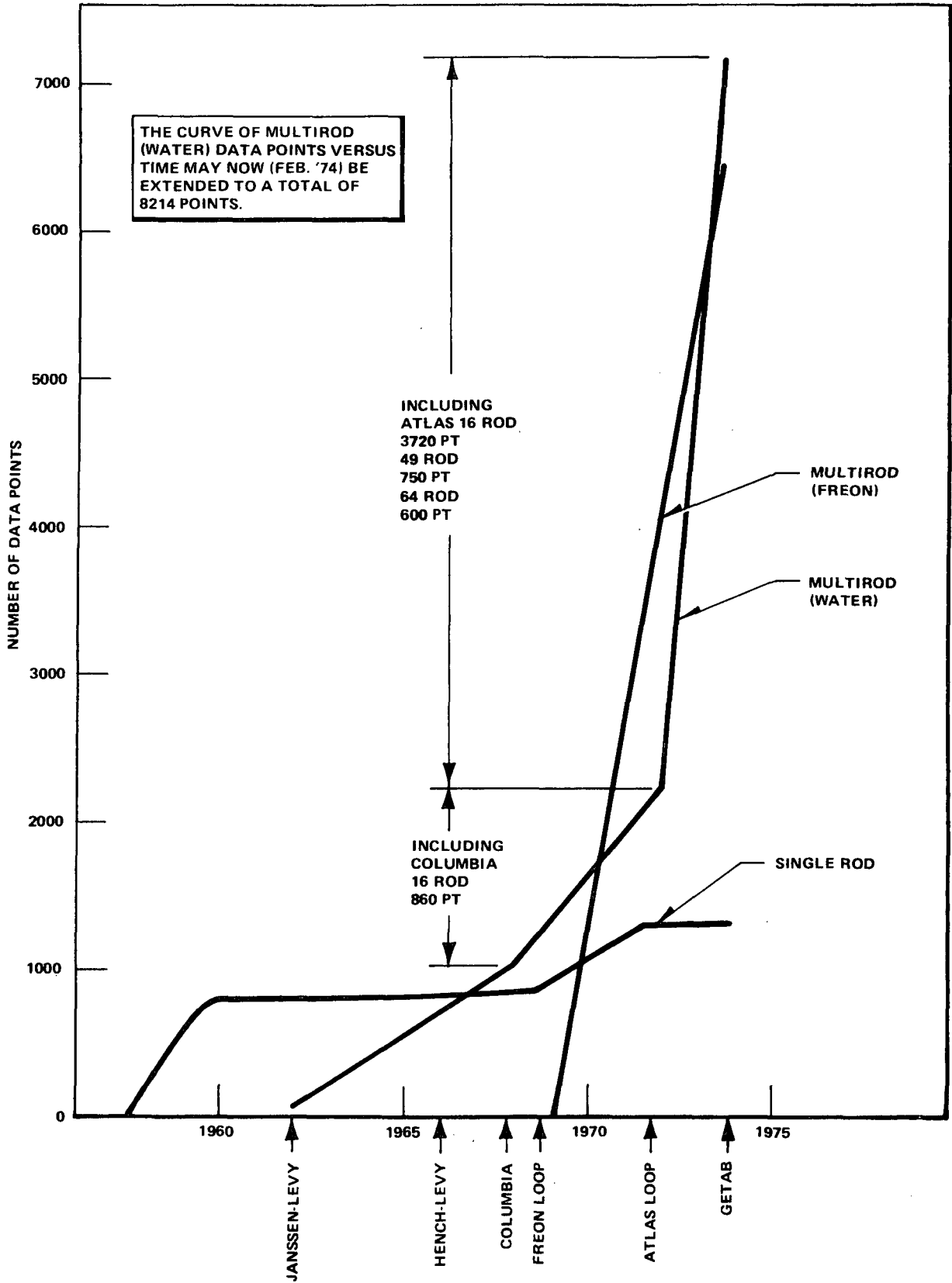


Figure 1-1. Summary of Boiling Transition Test Data To October 1973

## 2. SUMMARY AND CONCLUSIONS

Since the formulation of the 1966 Hench-Levy design basis for use in BWR design, General Electric has continued to perform an extensive boiling transition test program. Over 14,000 data points have been obtained in water and Freon from 16-rod (6-ft and 12-ft heated length), 49-rod (12-ft), and 64-rod (12-1/3-ft) test assemblies having various axial heat flux profiles and rod-to-rod power distributions. Among those, 2100 are water data points obtained from test sections in the ATLAS test facility in San Jose which are full-scale simulations of 7 x 7 and 8 x 8 BWR fuel assemblies.

From this extensive data base, General Electric has developed a new boiling transition correlation (GEXL) for use in BWR core thermal design and operation. This correlation is a best fit to the data in terms of cross-sectional bundle average properties. A critical quality versus boiling length coordinate system which has been used successfully by other researchers<sup>7</sup> was chosen as the best plane for data correlation. As a supplementary design tool, an analytical subchannel model has been developed with which BWR thermal margin can be appraised on a local basis.

In applying the GEXL correlation to core thermal design and operation, the minimum critical power ratio (MCPR) is the new figure of merit for expressing the reactor thermal margin. A statistical analysis showing (with high confidence) that not more than a very small number of rods might possibly experience a boiling transition is the primary analytical basis for establishing required design and operational thermal margins. The statistical basis and the criteria for selection of the required thermal margin have been developed and are applied to determine the MCPR values for various classes of BWR.

Incorporation of the GEXL correlation in the design and use of the statistical analysis to specify the required thermal margin does not affect the analytical procedures regarded as standard components of a core evaluation. Only minor changes to the results of these analyses occur and these are described in this report.

The data provided by the ATLAS facility, presented in detail herein, prove that the resulting GEXL correlation is a much more accurate and valid representation of acceptable heat transfer conditions for BWR fuel assemblies than has thus far been available. In fact, the new correlation includes *all prototypical aspects of reactor performance*. It is, therefore, not necessary to include any added margin in applying the data to represent actual reactor geometry and operating conditions.

As indicated earlier, the GEXL correlation employs different variables from those applied heretofore. It is shown that the establishment of operating limits based on GEXL as described in this report assures that adequate safety margins are maintained. Detailed analyses of specific reactors will be presented separately on each docket.

### 3. BACKGROUND

#### 3.1 LIMIT LINE APPROACH

Thermal-hydraulic design and operating power limits for General Electric BWRs are established to assure that there is an acceptably low probability that boiling transition-induced fuel cladding failure can occur at any point in the core at any time even for the most severe design basis operational transients.

The thermal design basis presently used utilizes a limit line approach to establish the required operating margin. By definition, the limit line is a lower bound in the heat flux versus quality plane for steady-state CHF data. The required operating margin to accommodate transients is obtained by maintaining the heat flux at each point in the reactor core no less than a specified distance below the limit line. The figure of merit expressing the required margin has been the MCHFR (i.e., the minimum value for the most limiting bundle of the ratio of the limit line heat flux to the operating heat flux evaluated at the local bundle average quality under given operating conditions). The established operating limit for the past several years has been  $MCHFR \geq 1.9$ .

The most recent version of the limit line, issued in 1966, is known as the Hensch-Levy Limit Line.<sup>1</sup> The Hensch-Levy line for a system pressure of 1000 psia and mass flux of  $1 \times 10^6$  lb/hr-ft<sup>2</sup> is shown in Figure 3-1.

It has been recognized for some time that use of the local conditions of flux and quality (as given by the limit line) to predict CHF\* has limited applicability. For example, it was noted in the original 1966 submittal describing the Hensch-Levy limit line that under particular conditions with nonuniform axial flux profiles, the measured CHF could be less than that given by the limit line. However, the data available at that time indicated that the heat flux at some other point along the nonuniform axial flux heater rod was higher than the limit line CHF; thus, the occurrence of CHF would have been predicted for these cases, although the actual location of the CHF was not predicted.

Similar limitations of the local conditions approach have been noted in some of the data accumulated over the past several years. The availability of full-scale ATLAS data represents a culmination in this development. The new data (discussed further in Section 4) provide direct verification of the influence of such parameters as axial flux shape and relative rod power distribution, and include full-scale bundle data. This eliminates any need for extrapolation and thus any uncertainty associated with such extrapolations. Now that these data are available, it is appropriate to implement a corresponding improvement in the BWR thermal analysis basis utilizing a new figure of merit. The following discussion summarizes the considerations which led to the choice of a critical quality-boiling length correlation to replace the heat flux-quality limit line concept.

#### 3.2 ALTERNATES TO THE LIMIT LINE APPROACH

Various correlation schemes for predicting the onset of transition boiling have been proposed over the past 25 years.<sup>2,3,4</sup> These schemes are, for the most part, empirical, though a few have considerable analytical content. The majority depend upon the "local conditions hypothesis." Two of the schemes, not tied exclusively to local conditions, have been considered by General Electric as possible methods to replace the limit line: (1) the Tong F-factor method,<sup>5,6</sup> and (2) the Critical Quality versus Boiling Length method.<sup>7,8</sup> These methods usually involve forming a "best fit" to the data rather than using the limit line approach. The two alternate methods have been considered at length,<sup>9</sup> and the following is a brief statement of the considerations.

##### 3.2.1 Tong F-Factor

Tong, et al<sup>5,6</sup> have suggested a method of relating the CHF for a nonuniformly heated test section to that for a uniform axial heat flux. Two general cases have been considered: (1) departure from nucleate boiling (DNB) under subcooled and low quality conditions, and (2) CHF under high-quality (annular flow) conditions. Though the physical principle underlying the analysis is different for the subcooled and the high-quality boiling transition, the resulting relationships are almost identical.

\* This is sometimes referred to as the "local conditions hypothesis."

For subcooled or low-quality boiling, Tong suggested that there is a critical enthalpy rise in the superheated liquid layer next to the heater wall at which the boiling transition occurs, the critical rise being independent of axial flux profile. An analysis was carried out, involving an energy balance on the liquid layer, and an expression was obtained for the CHF for an equivalent uniform profile.

For high-quality annular flow, Smith, Tong, and Rohrer<sup>6</sup> suggested a method involving a mass balance on the liquid film. Assuming a highly simplified model, the equation for the rate of depletion of the liquid film on the heated surface was integrated for uniform and variable heat flux profiles. The condition that the critical film flow rate at the boiling transition point is independent of the heat flux profile was used to derive a relationship for the "equivalent uniform" critical heat flux for the nonuniform flux profile.

Tong defined a factor (now commonly referred to as the Tong F-factor),

$$F \triangleq \frac{q''_u}{q''_{nu}(L_B)} \quad (3-1)$$

where:

$q''_{nu}(L_B)$  = local value of heat flux at the boiling transition location;

$L_B$  = boiling transition location; and

$q''_u$  = equivalent uniform heat flux over a length equal to  $L_B$ .

The expression for F developed by the method of Smith, et al, for high-quality annular flow is:

$$F = \frac{q''_u}{q''_{nu}(L_B)} = \frac{C/D_h}{(1 - e^{-CL_B/D_h}) q''_{nu}(L_B)} \int_0^{L_B} q''_{nu}(Z) e^{-\frac{C}{D_h}(L_B - Z)} dz \quad (3-2)$$

Equation 3-2 is strictly valid only in the annular flow regime and the length  $L_B$  refers to the distance between the inception of the annular flow regime and location of the boiling transition. It is simpler to assume that  $L_B$  is just the equilibrium boiling length, and that is the basis commonly used. Lack of data in different geometries (i.e., different  $D_h$ 's) makes it difficult to determine whether C in Equation 3-2 is independent of the diameter, and whether it is better to correlate C or  $C/D_h$  in terms of burnout parameters. The factor  $e^{-C/D_h(L_B - Z)}$  in the integrand of Equation 3-2 is a weighting factor which determines the degree of influence which upstream values of  $q''_{nu}(Z)$  have on the value of the integral. When C is very large (i.e.,  $C \rightarrow \infty$ ), then only the values at or near  $Z = L_B$  are important and there is said to be no "memory effect" of upstream conditions. On the other hand, as  $C \rightarrow 0$ , the value of the integral approaches the average value of  $q''_{nu}(Z)$  over the length  $L_B$ , and the memory effect is quite strong. It has generally been found that the higher the quality the lower the value of "C" required to correlate the data. In other words, low-quality boiling transition is strongly influenced by local conditions, whereas at high quality it depends primarily on integrated conditions over the boiling length.

The use of the Tong F-factor to calculate critical power is contingent upon having a good correlation for  $q''_u$ :

$$q''_u = f(r, G, L_B) \quad (3-3)$$

where r is the local peaking on the limiting rod. Once  $q''_u$  is accurately known, the nonuniform CHF is, simply,  $q''_{nu}(L_B) = q''_u/F$ . In using this predictive method, an iterative scheme is used, whereby a value for bundle power is assumed, and  $q''$  for the limiting rod and  $L_B$  are determined as functions of Z. F is calculated normally by numerical integration and  $q''_{nu}(L_B)$  is compared with  $q''(Z)$  at every node. If  $q''(Z)$  is everywhere less than  $q''_{nu}(L_B)$ , a higher value for bundle power is assumed, etc. The iteration is continued until at one axial location  $q''(Z)$  is just equal to

$q''_{nu}(L_B)$ , and at all other locations  $q''(Z)$  is less than  $q''_{nu}(L_B)$ . The value of bundle power for this last iteration is the critical power  $P_C$ . The predicted location of CHF is at the axial node for which  $q'' = q''_{nu}(L_B)$ .

### 3.2.2 Critical Quality vs Boiling Length ( $X_C-L_B$ )

Another method is the critical quality versus boiling length approach. These coordinates were suggested by researchers at CISE<sup>7</sup> as being applicable for prediction of the boiling transition point for bulk boiling conditions. The CISE workers were able to correlate the data for a number of widely different axial shapes by correlating in the  $X_C-L_B$  plane. Note that the boiling length is defined here as the distance from the point of initiation of bulk boiling to the boiling transition point, and the critical quality is the quality at the boiling transition point. To illustrate, some Babcock and Wilcox (B&W) round tube data<sup>8</sup> have been plotted on a local basis [i.e., critical heat flux ( $q''_{nu}(L_B)$ ) versus quality ( $X_C$ ) at the boiling transition location], and then on the integral or boiling length basis [i.e., critical quality ( $X_C$ ) versus boiling length to the boiling transition location ( $L_B$ )]. Figure 3-2 shows the results for four different axial profiles plotted on the local basis. The critical heat fluxes for cosine and uniform profiles differ by as much as a factor of three. The same data plotted in the critical quality-boiling length plane (Figure 3-3) correlate much better.

In an effort to gain greater knowledge in this area, a program was undertaken by General Electric to further examine the effects of a nonuniform flux profile. A series of tests were performed in an internally heated annulus with Freon 114 as the working fluid. These are described in Reference 9. Figures 3-4 and 3-5 show some of these data plotted in the local flux-quality and quality-boiling length planes. The correlation of these diverse data in the boiling length plane is quite striking.

To further illustrate the effectiveness of the  $X_C-L_B$  coordinates, AERE data<sup>10</sup> have been plotted in this plane in Figure 3-6. It can be seen that data for four widely different axial shapes are correlated on this basis.

The CISE workers originally proposed a correlation for the critical quality in saturated flow of the form:

$$X_C = \frac{\hat{W}}{GAh_{fg}} = \frac{aL_B}{L_B + b} \tag{3-4}$$

More recent work by them<sup>11</sup> has indicated a quadratic form of the correlation may be preferable.

Figure 3-7 shows typical iterations in the  $X_C$  vs  $L_B$  plane for the critical power. The predicted location of the boiling transition point is the point of tangency between the correlation and the heat balance curve for the critical power.

Overall, the  $X_C$  vs  $L_B$  approach has the merit of correlating, with quite acceptable accuracy, the boiling transition data for various heat flux profiles. Naturally, a more detailed formulation than that given above is required to adequately account for the effects of all the various parameters (e.g., pressure, mass flux, and geometry).

### 3.2.3 Discussion

Either of the two prediction schemes discussed previously can be used to predict the critical power with reasonable accuracy. The drawback of the Tong F-factor method is the difficulty in computation. Except for the simplest flux shapes, numerical integration of an exponential integral becomes necessary. The relative simplicity in the use of the  $X_C$  vs  $L_B$  approach makes it the more practical for BWR application.

It is of interest to note that the  $X_C$  vs  $L_B$  method is equivalent to the Tong F-factor method for the limiting case of  $C = 0$  (i.e., maximum memory effect). For a given pressure, mass flux, and geometry Equations 3-1 and 3-2 can be combined to yield:

$$q''_u = \frac{C/D_h}{(1 - e^{-CL_B/D_h})} \int_0^{L_B} q''_{nu}(Z) e^{-\frac{C}{D_h}(L_B-Z)} dz, \tag{3-5}$$

It may be shown by employing L'Hospital's rule that in the limit, as  $C \rightarrow 0$ ,

$$q''_u = \frac{1}{L_B} \int_0^{L_B} q''(z) dz \quad (3-6)$$

where  $q''_u$  is the equivalent uniform axial critical heat flux for the same boiling length,  $L_B$ . Multiplying both sides of Equation 3-6 by  $P_H L_B / GA h_{fg}$  yields:

$$X_{C(u)} = X_{C(nu)} \quad (3-7)$$

Hence, for a given boiling length, the critical quality is independent of the axial flux shape.

The foregoing discussion gives some insight as to the physical basis for the  $X_C$  vs  $L_B$  approach. Essentially, an integral approach is being utilized. It is clear that, when the flow regime is annular (and thus the onset of transition boiling is one of liquid film dryout), the memory effect is strong and the various values for the heat flux along the boiling length all have essentially equal weighting factors in finally determining the critical power.

One of the considerations when using derived parameters such as critical quality and boiling length is the potential error introduced in the prediction of an independent quantity such as the critical power. In order to examine this question, a transformation from the  $X_C$  vs  $L_B$  plane to a power versus subcooling plane was considered. It is necessary to obtain the error band in the power versus subcooling plane (i.e., the error in power at constant subcooling) corresponding to an error band in the  $X_C$  vs  $L_B$  plane. In general, this will be a function of the flux shape, but an order of magnitude estimate may be obtained for a typical flux shape (e.g., chopped cosine).

The mapping relationships to transfer the error band from the  $X_C$ - $L_B$  plane to the critical power-subcooling plane are developed in an analysis given in Appendix I. The results of this analysis are shown in Figure 3-8. An assumed  $X_C$  error band of  $\pm 0.01$  in the  $X_C$ - $L_B$  plane for the Freon data has been used to predict the error in critical power at given subcoolings for the 12-ft cosine flux. It can be seen that the error in the  $X_C$ - $L_B$  plane is not magnified when predicting critical power at a given subcooling. This is further demonstrated for the case of water data in the response to Question 1-2, Appendix VII.

### 3.2.4 Conclusion

An  $X_C$ - $L_B$  correlation can be used for the prediction of critical power for both nonuniform and uniform axial flux profiles. The precision with which it predicts critical power is of the same order as the precision with which it correlates data in the  $X_C$ - $L_B$  plane. Its relative simplicity makes it preferable to the Tong F-factor approach for the high-quality boiling transition applicable to BWR technology, and its accuracy is at least as good as any other competing scheme.

An  $X_C$ - $L_B$  correlation scheme has therefore been chosen to replace the local conditions approach and constitutes the basis for GEXL\*. It will be described in detail in a later section.

\*See the response to Question 1-1, Appendix VII.



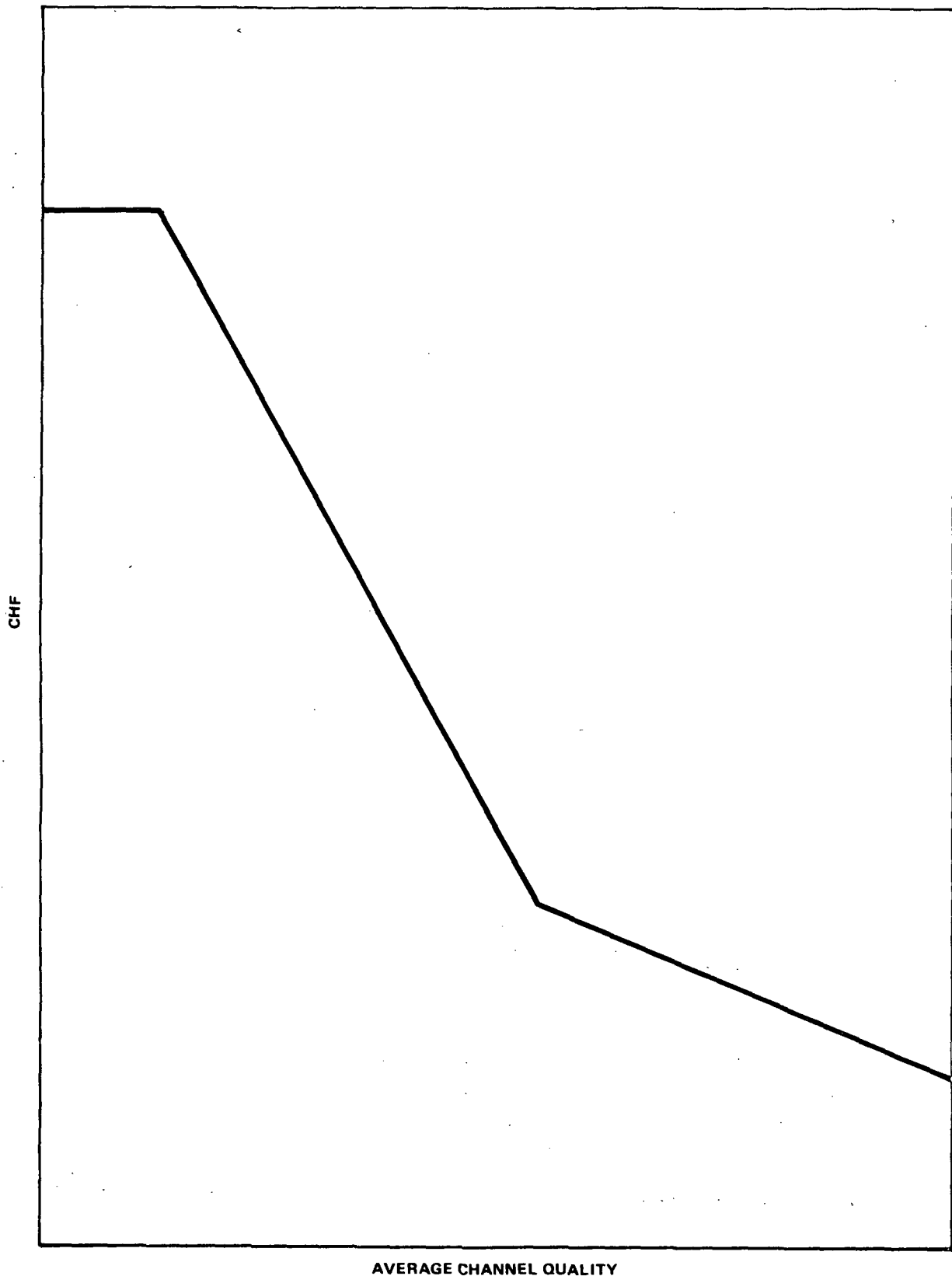


Figure 3-1. Hench-Levy Limit Line, 1000 psia,  $G = 1 \times 10^6$  lb/hr ft<sup>2</sup>

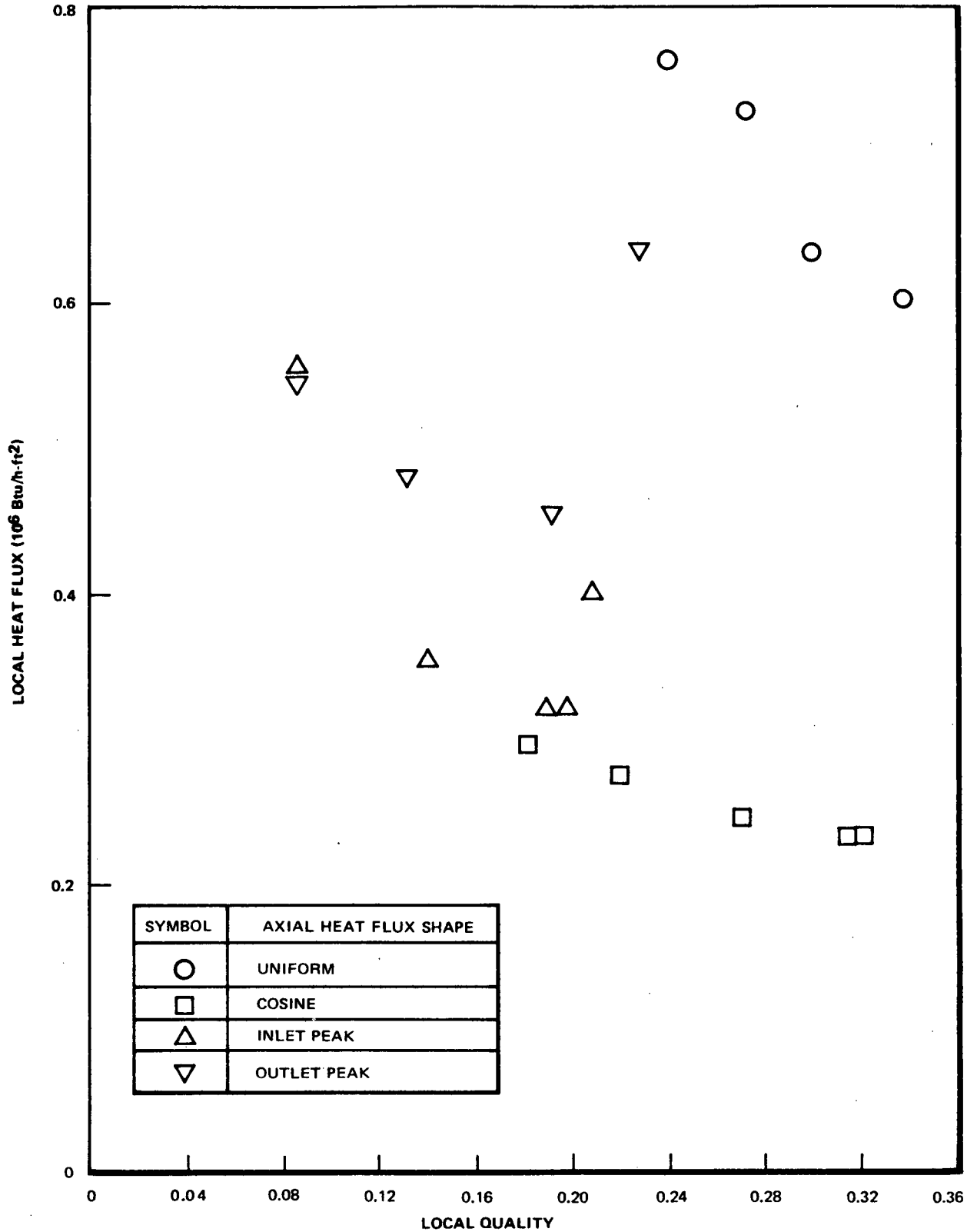


Figure 3-2. Heat Flux vs. Quality at Location of Boiling Transition, B&W 0.45 in. dia. Round Tube Data, 6-ft Heated Length, Various Axial Profiles,  $P = 1000$  psia,  $G = 1.5 \times 10^6$  lb/h-ft<sup>2</sup>

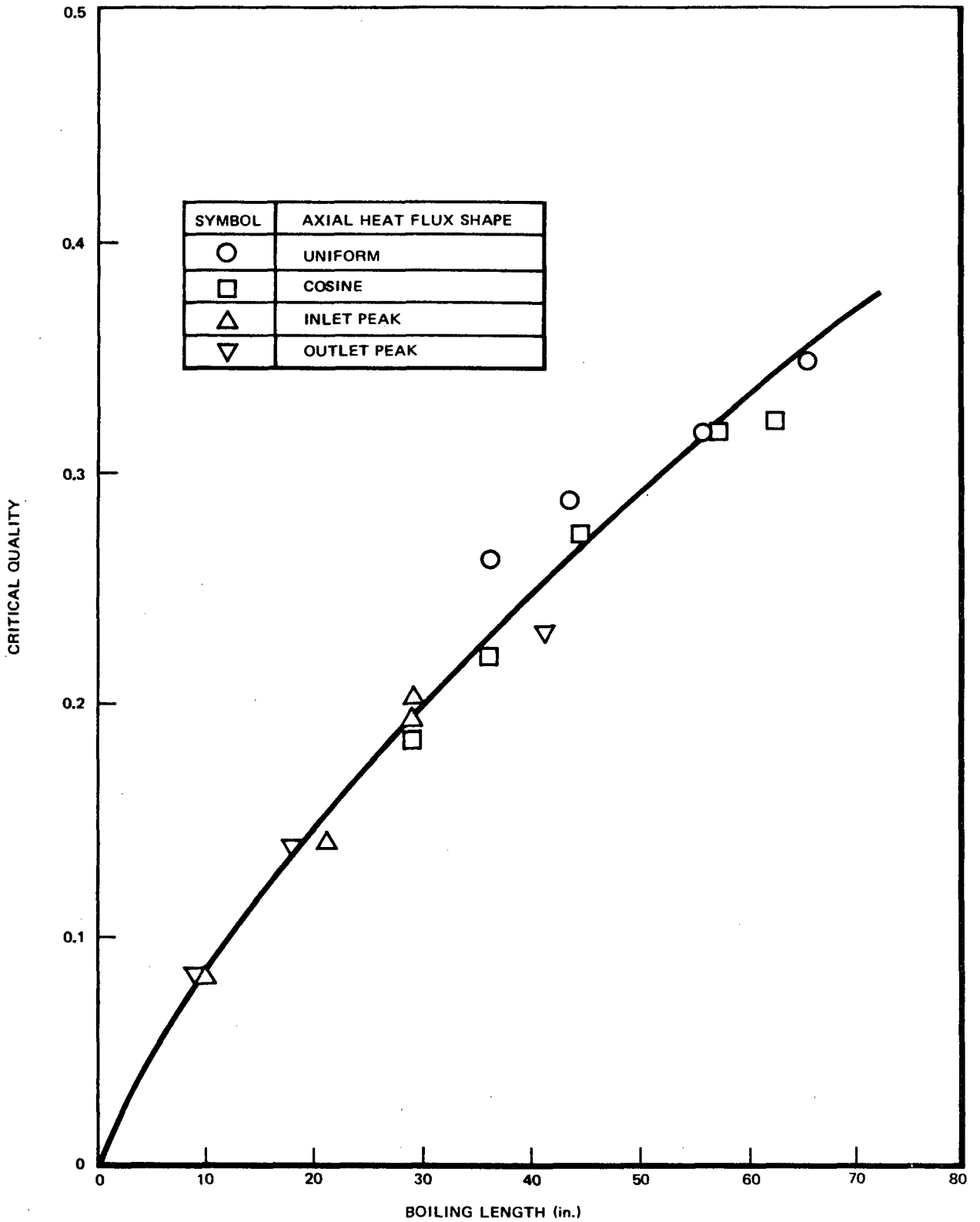


Figure 3-3. Critical Quality vs. Boiling Length, B&W Round Tube Data

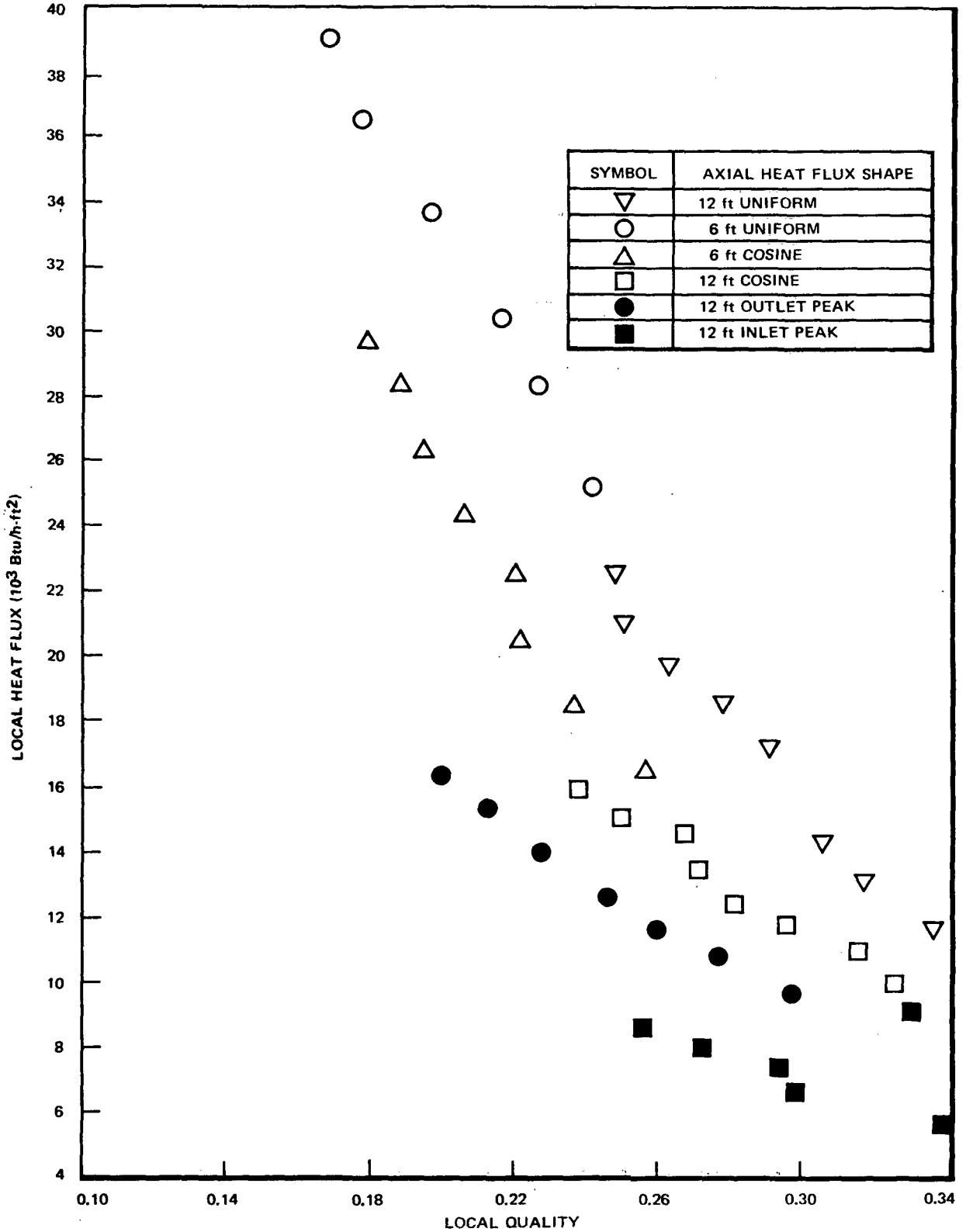


Figure 3-4. Heat Flux vs. Quality at Location of Boiling Transition, Freon 114 Annulus Data,  $D_1 = 0.563$  in.,  $D_2 = 0.875$  in., 6- and 12-ft Heated Length, Various Axial Profiles,  $P = 123$  psia,  $G = 0.54 \times 10^6$  lb/h-ft<sup>2</sup>

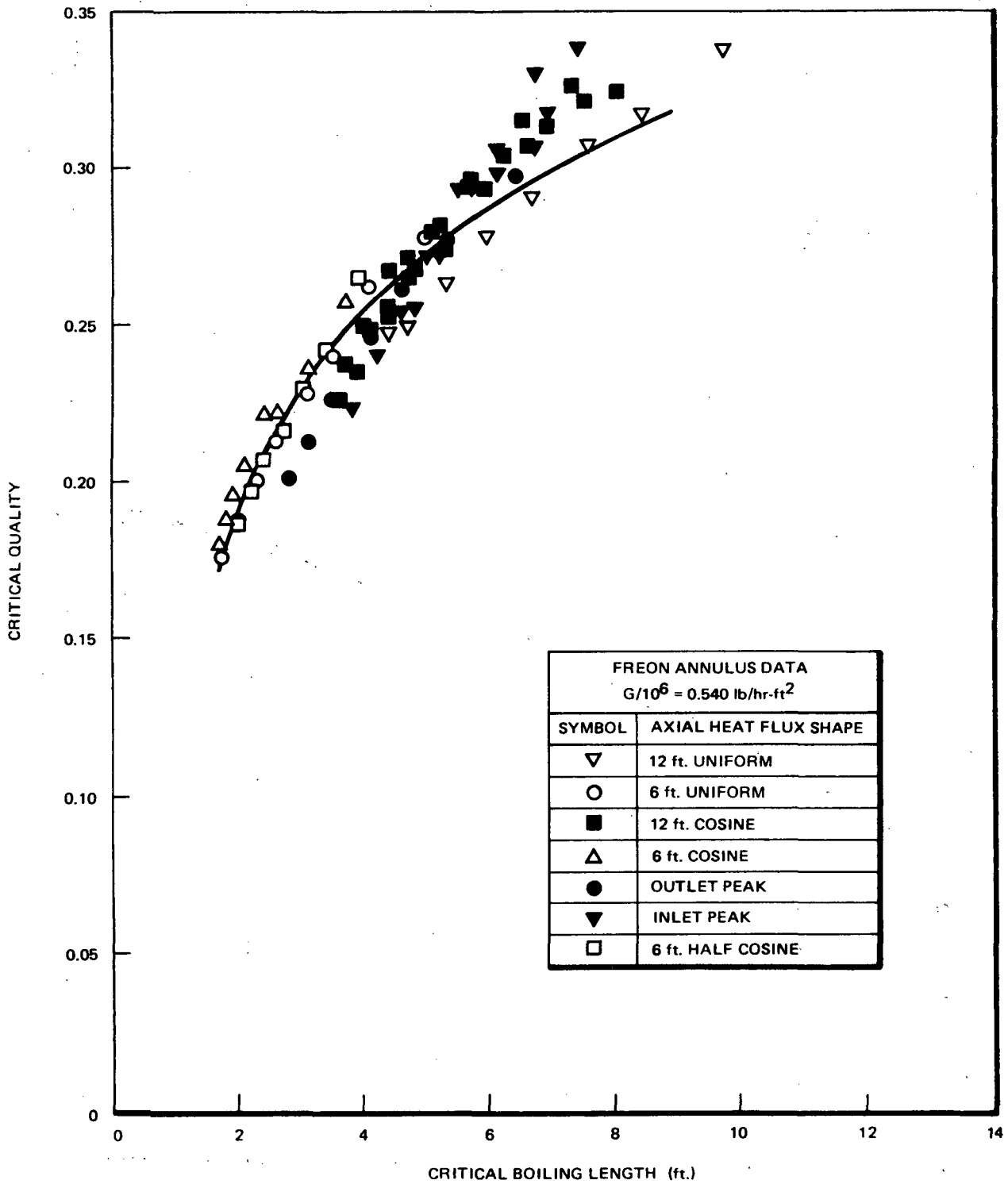


Figure 3-5. Critical Quality vs. Boiling Length, Freon-114 Annulus Data

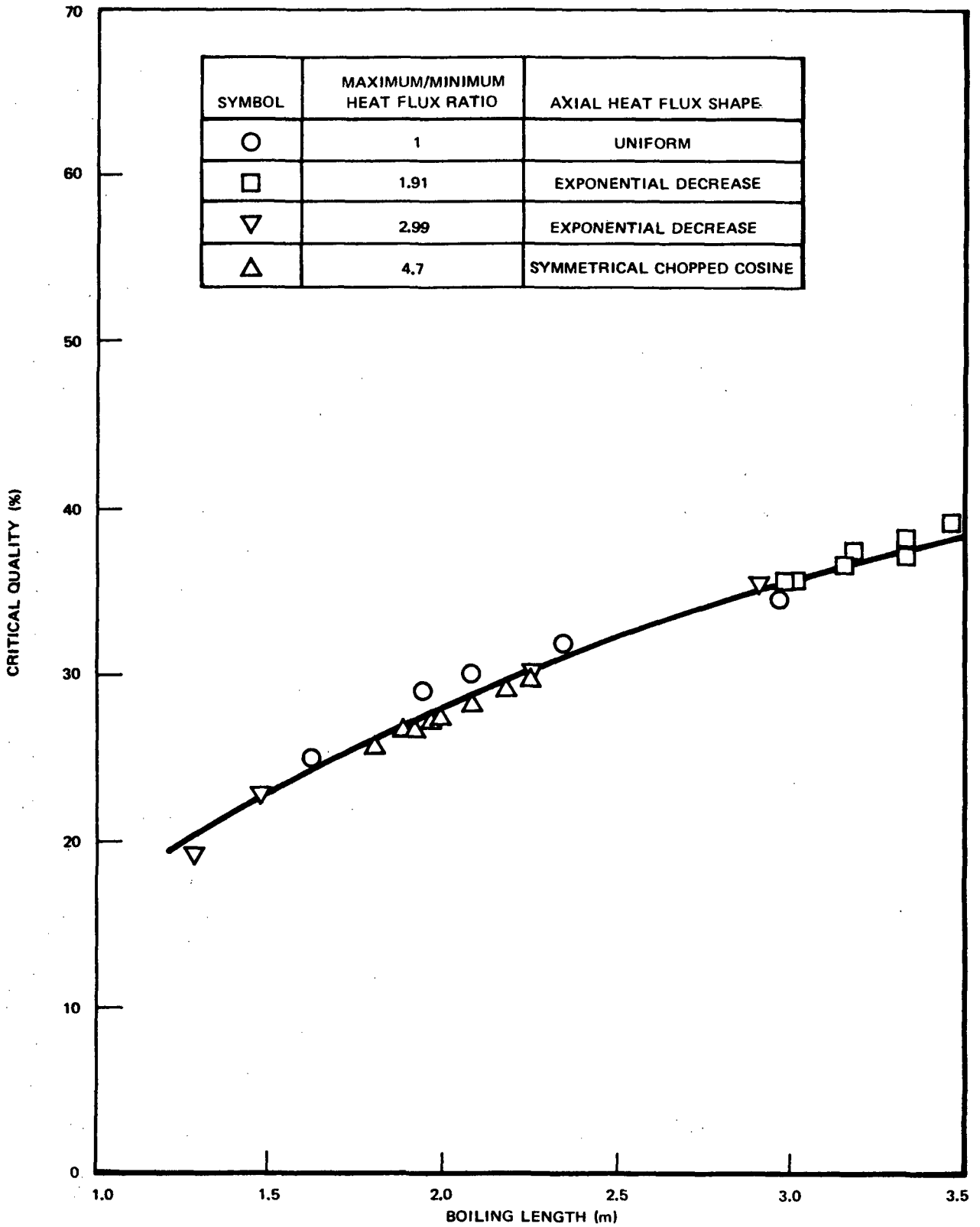


Figure 3-6. Critical Quality vs. Boiling Length, British(10) 12.6 mm dia. Round Tube Data, 3.66m Heated Length, Various Axial Profiles,  $G = 2.72 \times 10^3$  kg/sec-m<sup>2</sup>,  $P = 6895$  KN/m<sup>2</sup>(1000 psia)

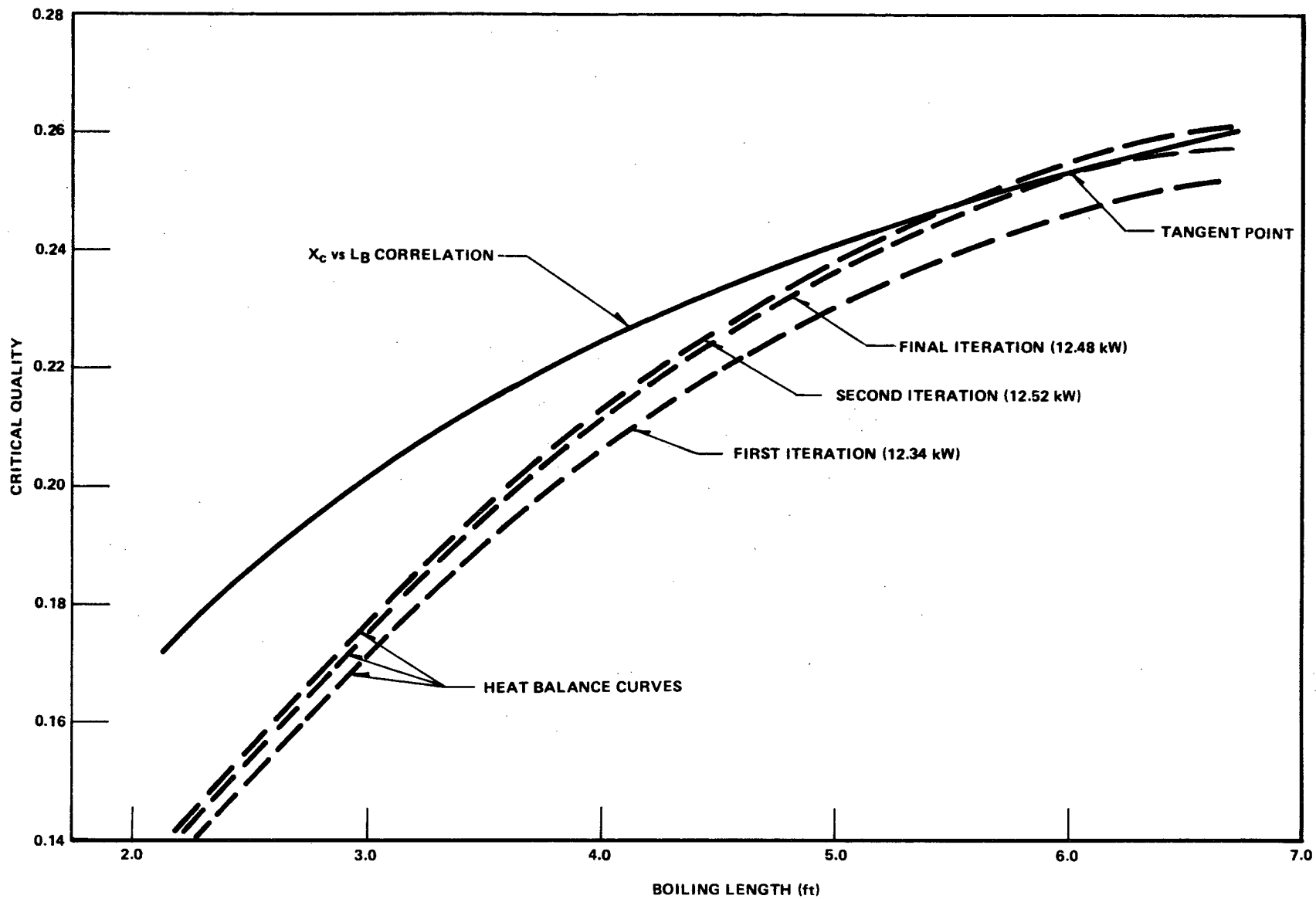


Figure 3-7. Correlation Curve and Heat Balance Curves for Freon 114 Annulus with Inlet Peak Profile, Showing Typical Iterations in the Prediction of Critical Power ( $P = 123$  psia,  $G = 0.66 \times 10^6$  lb/h-ft<sup>2</sup>, 14.8 Btu/lb (Subcooling))

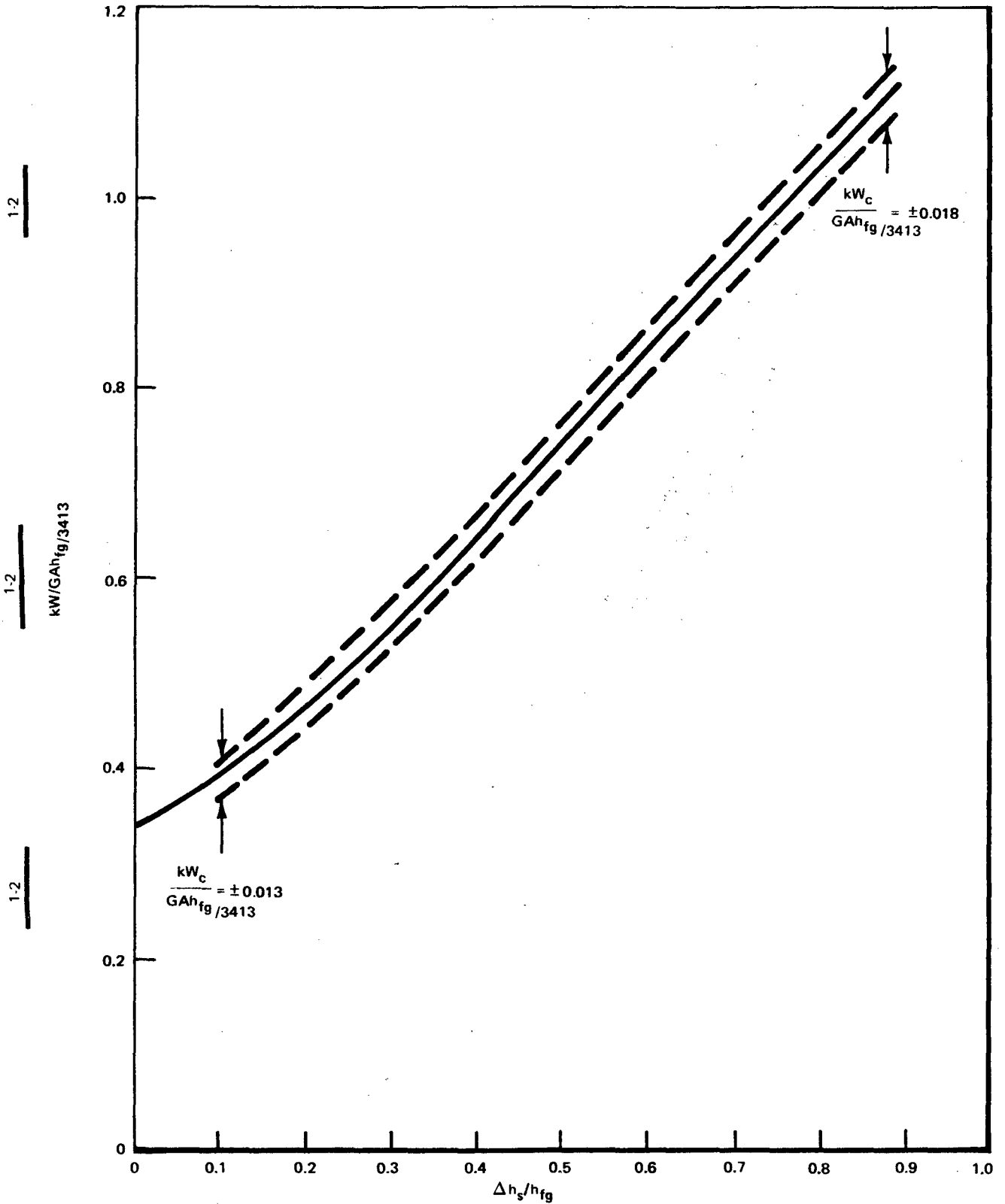


Figure 3-8. Error Band in kW vs.  $\Delta h_s$  Plane Corresponding to an Error Band of  $\pm 0.01$  in  $X_c$  vs.  $L_B$  Plane (12-ft Cosine,  $G = 0.66 \times 10^6$  lb/h-ft<sup>2</sup>)



## 4. CRITICAL POWER DATA BASE

### 4.1 HISTORICAL REVIEW

The first General Electric boiling transition data for BWRs were generated at the San Jose site, starting in 1957, using a single-rod annular test section. This, plus a second single-rod test section which replaced the first in 1960, provided about 700 data points. These points were the experimental basis for the Janssen-Levy limit line, issued in 1962.<sup>12</sup>

After 1962, increased capability permitted extension of testing to 4- and 9-rod bundles. Approximately 700 of these multirod points served as the basis for the Hench-Levy limit line, issued in 1966.<sup>1</sup>

The principal limitation to the acquisition of boiling transition data in even larger bundles was the power supply (1.7 MW). Since 1966, GE has moved along three parallel paths to overcome this limitation: (1) in 1967, and again in 1968, 1969 and 1970, a contract arrangement was made with Columbia University to run tests using 16-rod bundles; (2) in 1969, a Freon loop was completed for the Freon modeling of boiling transition experiments; and (3) in 1969, steps were initiated to procure an 8.6 MW power supply and to build a large water loop, now known as ATLAS.

Because of the low latent heat, a much larger bundle of rods can be tested in Freon than in water, with no increase in site power. Full-size bundles (both 49-rod and 64-rod) are now regularly tested in the Freon loop, which is the largest Freon facility in the world.

ATLAS was specifically designed to handle transients as well as steady-state simulation of reactor conditions. This facility was put into service in 1971. The power supply was recently increased to 17.2 MW to permit testing full-scale 64-rod bundles, making the ATLAS facility the largest and most versatile of its kind in the world. 16-rod, 49-rod and 64-rod bundles are now being tested on a regular basis.

Concurrently with the accumulation of extensive steady-state data, a program for the systematic study of the effects of transients was begun in 1968. Starting with a single-rod test section in early 1968, various kinds of flow, power, and pressure transients were examined. The test program was extended through 1970 to include a 9-rod bundle. Improvements in data acquisition, reduction and storage techniques were incorporated in subsequent data processing under the AEC sponsored Deficient Cooling Program (PA 55). Extensive transient testing was performed under this program in 1971-1972, including 16-rod 12-ft-long bundles in the ATLAS facility. Subsequently (1972-1973), transient data have been acquired in other 16-rod and full-scale 49-rod and 64-rod assemblies with various heater rod peaking configurations.

The history of GE's boiling transition data acquisition program is summarized graphically in Figure 1-1.

### 4.2 EXPERIMENTAL OBJECTIVES

The data since Hench-Levy (1966), referred to previously and shown schematically in Figure 1-1, have all been generated in response to the need to further understand the limits of boiling heat transfer in multi-rod geometries. GE has continually sought to make the conditions under which boiling transition data were generated as representative of reactor conditions as possible. These, as well as other data and analyses in the open literature, have been drawn upon to improve the modeling of reactor geometries, heat flux profiles, and other features of actual reactor conditions including simulated transients. The effect of various parameters has been investigated, so as to more precisely predict the onset of transition boiling.

### 4.3 STEADY-STATE DATA

A great deal of boiling transition data has been generated since 1966. The test conditions under which the data were obtained are listed in Tables II-1 (9-rod water data, obtained in the 1.7 MW loop); II-2 (16-rod water data obtained at Columbia University); II-3 (16-rod, 49-rod and 64-rod water data obtained in the ATLAS loop); and II-4 (1-rod, 16-rod, 49-rod, and 64-rod data obtained in the Freon loop). Axial profiles and individual test assembly local

peaking patterns are described in Appendix III. It is clear that the effect on critical power of many parameters has been investigated in full-scale experiments. The procedures by which the data were obtained and certain salient features of these data are discussed in the following sections.

#### 4.4 BOILING TRANSITION TESTING PROCEDURE: STEADY-STATE

The general test procedures for the ATLAS and Freon loops are quite similar. Each steady-state boiling transition data point is taken by holding pressure, flow rate, and inlet subcooling constant while very slowly increasing test section power until the onset of transition boiling is indicated by a signal from a rod thermocouple. A rod thermocouple signal is considered as indicating a boiling transition condition when about a 25°F rod surface temperature rise is observed on a strip chart recorder.

After the data for each point are recorded, the subcooling is changed to a new value for the next point, until the desired range of subcoolings is covered. The flow rate is then changed and the procedure repeated.

Location of the thermocouples in the test assemblies was selected to assure detection of the first onset of boiling transition during the test. The basis for this selection and the effect of thermocouple location on the measured critical power are discussed in response to Questions 2-9 and 1-9 in Appendix VII.

Because of manufacturing tolerances in the construction of grid spacers and channels, there is generally some clearance between the spacer pad and channel wall. For the purpose of uniformity, shims are used on two sides of each spacer so that spacer pad clearance is zero and bundle/channel clearance is minimum in the corner. Bundle/channel clearance variations have a significant effect upon the size of the corner subchannel: Therefore, the boiling transition is sensitive to this clearance for corner rod limited bundles. Because it is possible for the highest powered corner to sit tightly against the channel in an operating reactor, this most limiting corner condition was used for all tests.\* Variations in the channel clearance have a very small effect upon the conditions in interior regions. Therefore, for interior rod limited bundles the clearance is neither conservative nor nonconservative.

The rod spacers used in the test are slightly different from those used in actual fuel assemblies. These spacers had backup supports added to the spring members to maintain proper clearance under the electromagnetic forces of the tests. The resultant test data have slightly lower values for critical power than would be found in an actual reactor fuel assembly. For additional information, see the response to Question 1-8, Appendix VII.

Typical data thus obtained are shown in Figure 4-1 as critical power versus inlet subcooling for one pressure and various flow rates. The features of these data are typical of all the boiling transition data (both water and Freon) identified in Tables II-1, II-2, II-3, and II-4 (i.e., critical power increases nearly linearly with subcooling and increases with increasing flow).

For the purpose of checking the consistency of ATLAS data with previous Columbia data, the first ATLAS assembly tested (see ATLAS Test assembly No. 1, Table II-3) was a duplicate of two Columbia assemblies (Columbia Test Assembly Nos. 6 and 15). Best-fit lines through the critical power data for both assemblies are plotted in Figure 4-2. The two sets of critical power data are in very good agreement, being generally within 3% of each other.

#### 4.5 SALIENT FEATURES OF THE STEADY-STATE DATA

The Figure 4-1 data have been cross plotted in Figure 4-3 to show how critical power varies with flow rate at two different values of subcooling (20 and 40 Btu/lb) bracketing the range of subcooling likely to be encountered in an operating reactor. The critical power increases continuously with increasing flow rate, steeply at low flows, and more gradually at high flows.

Data for four typical ATLAS test assemblies at various pressures were normalized with respect to 1000 psia data. The results have been plotted in Figure 4-4 to show the effect on critical power of varying the system pressure. Consistent with previous experience in the range 800 to 1400 psia, the critical power varies inversely with system pressure. The relative effect of pressure is about the same for all four assemblies.

\* A departure from this procedure is made only when the object of the experiment is to determine the effect of bundle/channel clearance in the "hot" corner.

The effect of local peaking on critical power is shown in Figure 4-5 for corner rod peaking. In order to compare the local effect of peaking for different size bundles on an equal basis, the critical power per unit of mass flow (normalized with respect to ATLAS Test Assembly No. 4, 7 x 7 lattice 16-rod with uniform local peaking) was plotted versus peaking on the corner (limiting) rod for various test assemblies of both 7 x 7 and 8 x 8 lattices. The more nearly the corner rod power equals the average rod power for the bundle, the higher is the critical power for that particular assembly. Note that the curve for the 8 x 8 lattice lies above the curve for the 7 x 7 lattices.

A similar comparison can be made for side and interior rod peaking. For the 7 x 7 lattice, the critical power with side or interior peaking is much greater (the order of 10% or more) than with corner peaking. On the other hand, for the 8 x 8 lattice, the critical power with interior peaking is less than or equal to the critical power with corner peaking. However, the 8 x 8 lattice performance with interior peaking is approximately the same as the 7 x 7 lattice performance with corner peaking. Effect of the rod bundle geometry of 7 x 7 and 8 x 8 bundles on the critical power is discussed in response to Question 1-7 in Appendix VII.

The relative effect on critical power of various nonuniform axial flux profiles is shown in Figure 4-5. The critical power (normalized with respect to the critical power for the symmetrical cosine profile at an inlet subcooling of 20 Btu/lb) has been plotted versus inlet subcooling for five different axial profiles: (1) symmetrical cosine; (2) inlet peaked; (3) outlet peaked; (4) double hump; and (5) uniform. Figure 4-5 is for 1.23/1.26 corner peaking and  $1 \times 10^6$  lb/hr-ft<sup>2</sup> mass flux, but is representative of other flows and peakings. There is about a 10% spread in critical power associated with the variations in profile represented here. The critical power for the outlet peaked profile is lowest, for the uniform profile is highest; for the other three profiles, critical power falls in between. Obviously the axial flux profile can have an effect on the critical power. The new correlating method described in Section 5 accounts for this effect.

The effect of clearance in the hot corner between the bundle and channel wall is shown in Figure 4-7. As has already been noted, most tests are conducted with this clearance at a minimum. However, special 49-rod tests were run with this clearance at a maximum. The results show a 5 to 10% improvement in critical power.

The effects of rod bowing for the severe case of the limiting corner rod bowed toward the channel wall has been investigated experimentally.<sup>2,3</sup> The results indicated negligible effect of the bow, even for extreme cases. Rod bowing in the interior of the bundle would have less effect upon the local subchannel areas than for the corner condition that was tested. Therefore, interior rod bowing is also expected to have a negligible effect on critical power.

The large amount of boiling transition data described here has provided the basis for the GEXL correlation which will be described in the following section. Not all of the data were used in the synthesis of this correlation. Specifically, the water data points used were limited to those generated in 16-rod, 49-rod, and 64-rod bundles which fall in the range of pressures from 800 to 1400 psia, subcoolings from 0 to 100 Btu/lb, and mass fluxes from  $0.25 \times 10^6$  to  $1.25 \times 10^6$  lb/hr-ft<sup>2</sup>. Columbia data taken with experimental spacer not used in BWRs were excluded, and the ATLAS data with maximum clearance in the hot corner were not used directly but were included in the statistical evaluation, since they represent a possible geometric configuration. Nevertheless, all the water data were useful in some degree in determining the correct trends. As a result, the GEXL correlation predicts the data at flow rates as low as  $0.1 \times 10^6$  lb/hr-ft<sup>2</sup> quite well and is only slightly conservative at flow rates as high as  $1.5 \times 10^6$  lb/hr-ft<sup>2</sup>.

The Freon data points were not used directly in the synthesis of the GEXL correlation. Subsequently, it was found that certain Freon data (i.e., those taken from 16-rod, 49-rod and 64-rod bundles, at the modeling pressure of 123 psia, mass fluxes from  $0.3 \times 10^6$  to  $1.1 \times 10^6$  lb/hr-ft<sup>2</sup>, and uniform local peaking were correlated by GEXL. Nevertheless, most of the Freon Data were useful, to some degree, in establishing correct model relationships, providing insight concerning the effect of various parameters (e.g., spacers) and guidance for instrumenting and running the ATLAS water tests.

In Section 5 the GEXL correlation will be developed and applied to the prediction of critical power for the entire range of parameters of interest to BWRs.

#### 4.6 TRANSIENT DATA

In 1968, tests were performed with a single-rod annular test section to examine the effects of flow and power transients on the onset of transition boiling. A further test program was undertaken in 1970<sup>13</sup> in which both single-rod and nine-rod test sections were used. Reference 13 presents the results of 60 depressurization runs, 22 flow transients and 2 runs combining both variations. The data were analyzed using a steady-state correlation with the instantaneous flow parameters calculated using a single-channel thermal-hydraulic computer code.<sup>14</sup> It was found that the data were generally predicted conservatively.

More extensive transient data was taken during 1971-1972 under the AEC Deficient Cooling Program (PA-55). These data, obtained with single-rod, 9-rod, and 16-rod assemblies, have been tabulated extensively in Reference 15 and are not repeated here. However, a list of the 16-rod test conditions is included in Table II-5. A total of 50 single-rod, 80 9-rod, and 115 16-rod transient tests were made. Predictions of some of these data are given in Section 5.

The latest transient test conditions, run in the ATLAS facility during 1972-73, are listed in Table II-5. The table provides information regarding the type of run, nominal values of the pressure, initial and final mass fluxes, flow decay time, initial power, and inlet temperature. Approximately 130 16-rod and 90 49-rod transients were performed. The four 16-rod bundles tested had different axial flux shapes: chopped cosine, inlet peak, double hump, and outlet peak. The 49-rod data were obtained in full-scale bundles with both local and axial peaking factors representative of reactor operation.

The transients have been grouped under the following headings:

- (1) Flow Decay at Constant Power;
- (2) Flow On/Off/On at Constant Power;
- (3) Power Ramp at Constant Flow;
- (4) Simultaneous Flow and Power Decay; and
- (5) Simulated Loss-of-Coolant Accident (LOCA) Involving Variation in Power, Flow and Pressure.

The first three types of transients were intended as "separate effects" tests, and the fourth type was intended to simulate possible pump trip and seizure transients. The flow decay period ( $\tau$ ) refers to the nominal time for 99% of the flow change. The time intervals,  $\tau_1/\tau_2/\tau_3$ , refer to the initial flow decay period, constant flow period, and the "window" period of zero flow during a loss-of-coolant-accident (LOCA) simulation. These terms are illustrated in Figure 4-8. The rate of decay of power was set to match calculated variations in surface heat flux during reactor transients. Figures 4-9, 4-10, 4-11, 4-12, and 4-13 show typical transient results for the various kinds of runs.

#### 4.7 EXPERIMENTAL PROCEDURE: TRANSIENT

The data acquisition and reduction procedures for the transient tests have been described in detail in References 15, 16, and 17. Briefly, the flow rate was varied using timer circuits to actuate an air-operated flow control valve. The power variation was programmed on a function generator. A high-speed multiplexer capable of sampling 64 input channels at rates up to 15,000 samples per second was used to digitize the various analog inputs. The on-line minicomputer serves as a storage buffer for the digitized signals, which are passed on to the high-speed (45 IPS) magnetic tape. These tapes are processed later at the NED data processing center.

#### 4.8 SALIENT FEATURES OF THE TRANSIENT DATA

Typical data plots, taken from Reference 15, are shown in Figures 4-9 through 4-13. The first thermocouples indicating the onset of transition boiling during transients were generally the same as for the steady-state tests. When transition boiling persists, it may propagate to other locations along the heater rods. The data show that quasi steady-state prediction schemes are quite conservative. That is, the onset of transition boiling occurs under more severe conditions of inlet flow and power than under steady-state conditions. The flow on/off/on tests which were run at constant power and the LOCA simulations show that below a given power no boiling transition occurred for significant periods of time even with no inlet flow of water to the test section, and that at higher power levels the onset of transition boiling did not necessarily occur concurrently with flow stoppage.

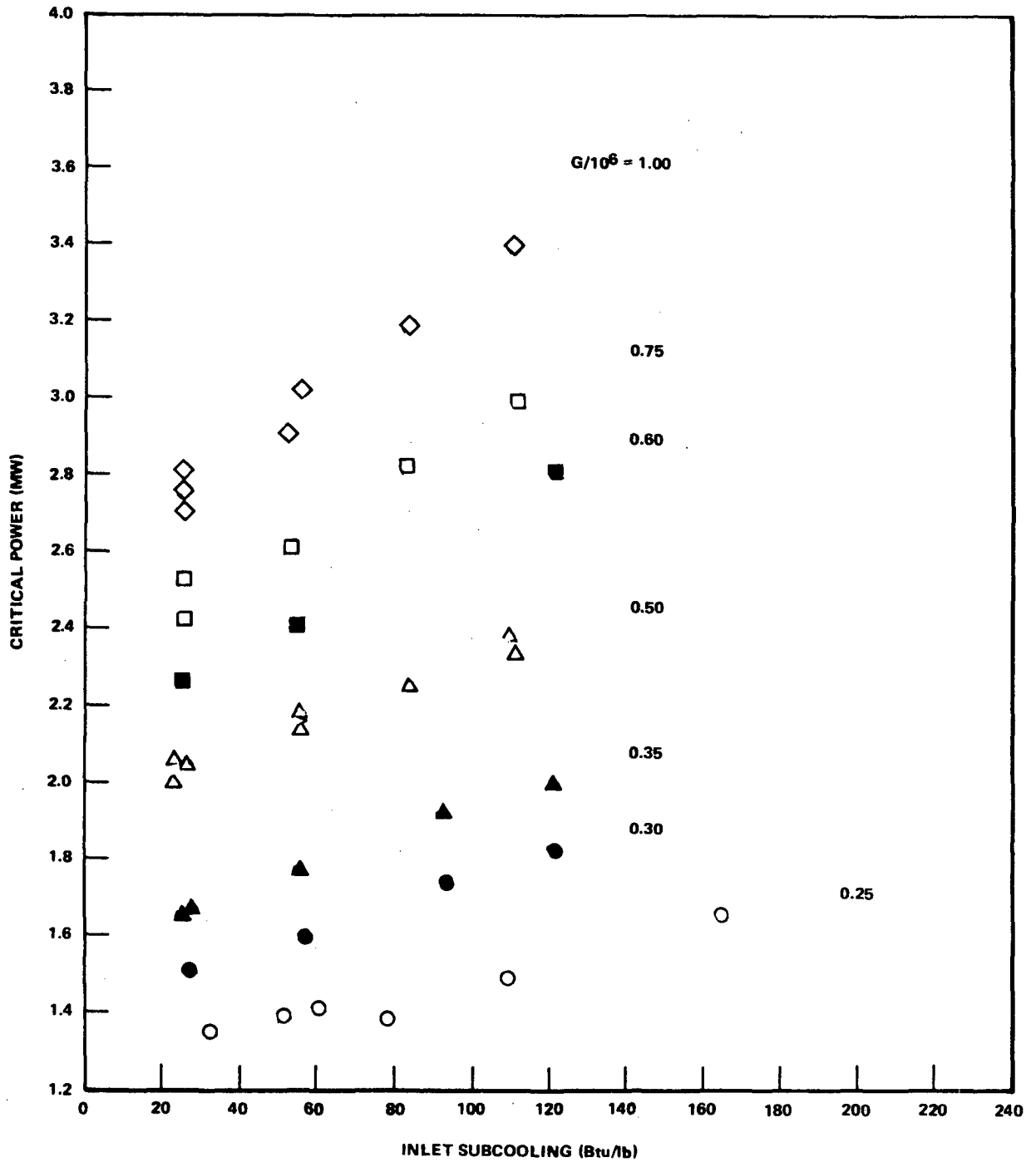


Figure 4-1. Critical Power vs. Inlet Subcooling, Atlas Test Assembly No. 14, 16-Rod x 12-ft Cosine, Uniform Local Peaking, 1000 psia, Various Flow Rates

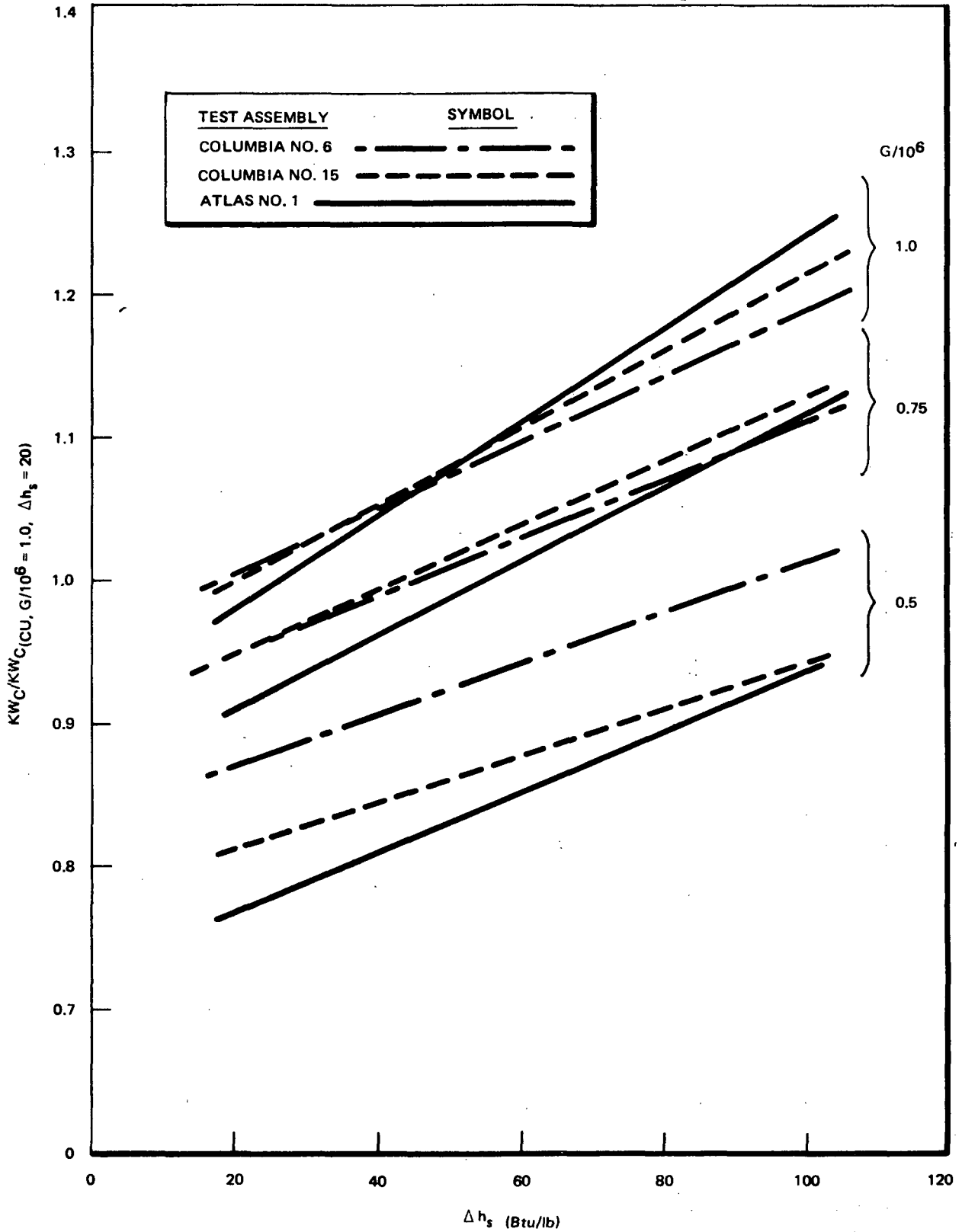


Figure 4-2. Critical Power (Normalized with Respect to Value for Columbia Test Assembly No. 15 at  $G = 1 \times 10^6$  lb/h-ft<sup>2</sup>,  $\Delta h_s = 20$  Btu/lb vs. Inlet Subcooling

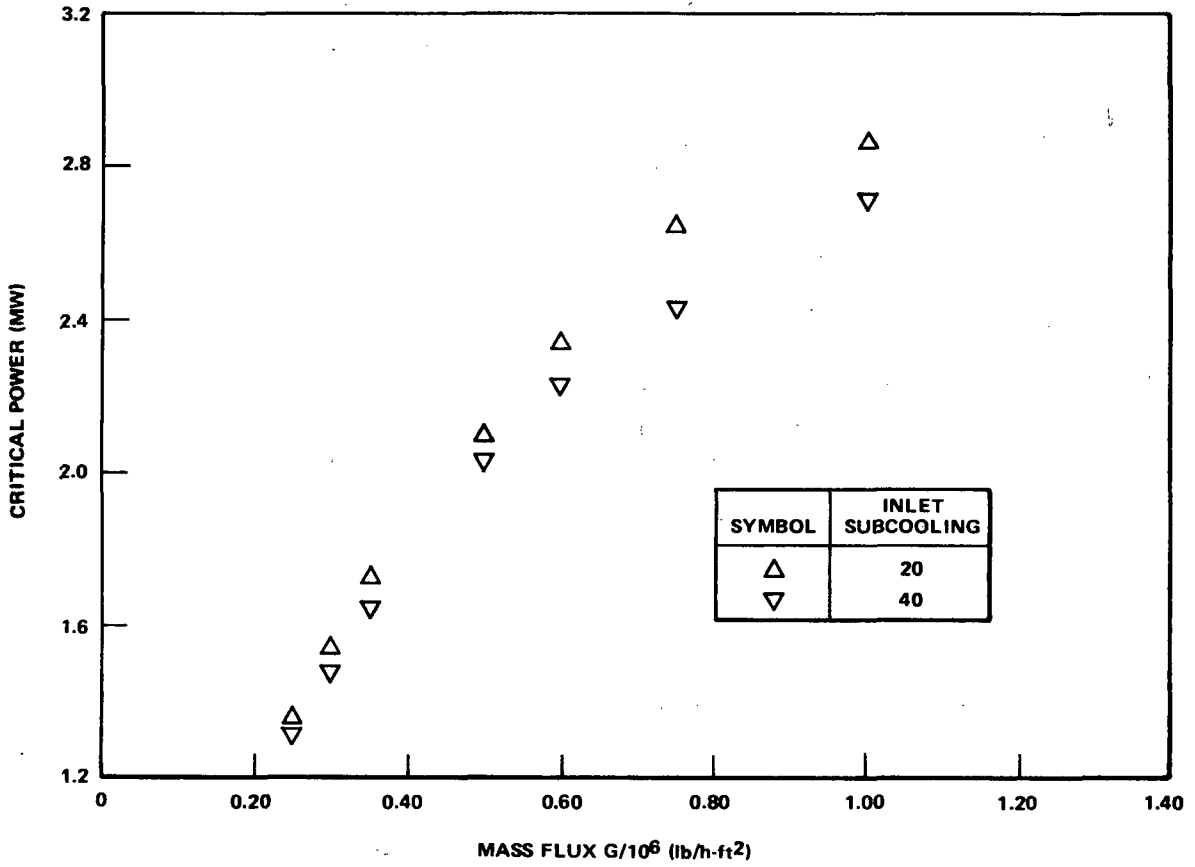


Figure 4-3. Critical Power vs. Flow Rate (cross plot of Figure 4-1 Data)

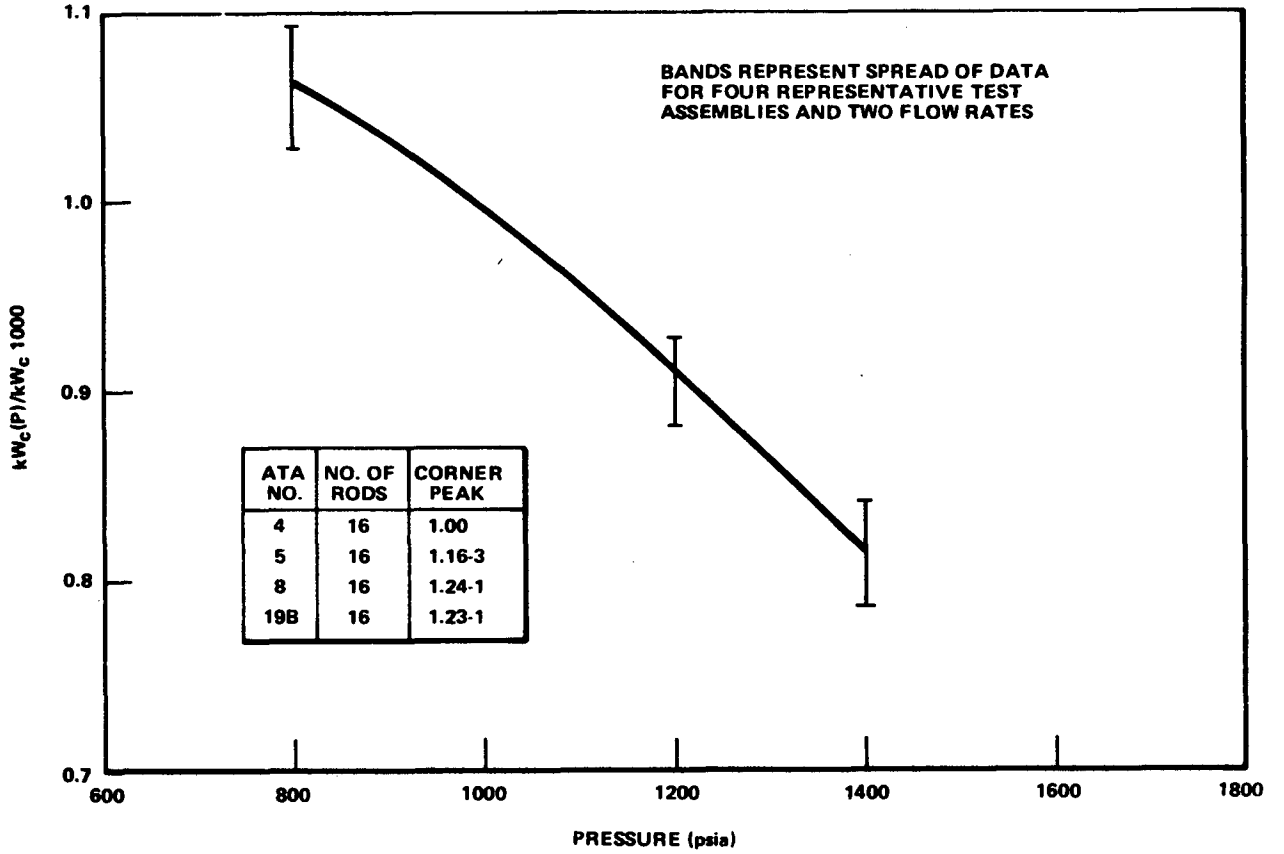


Figure 4-4. Critical Power (Normalized with Respect to Value at 1000 psia) vs. Pressure, Four Atlas Test Assemblies,  $\Delta h_s = 20 \text{ Btu/lb}$ ,  $G = 0.5 \times 10^6$  and  $1.0 \times 10^6 \text{ lb/h-ft}^2$



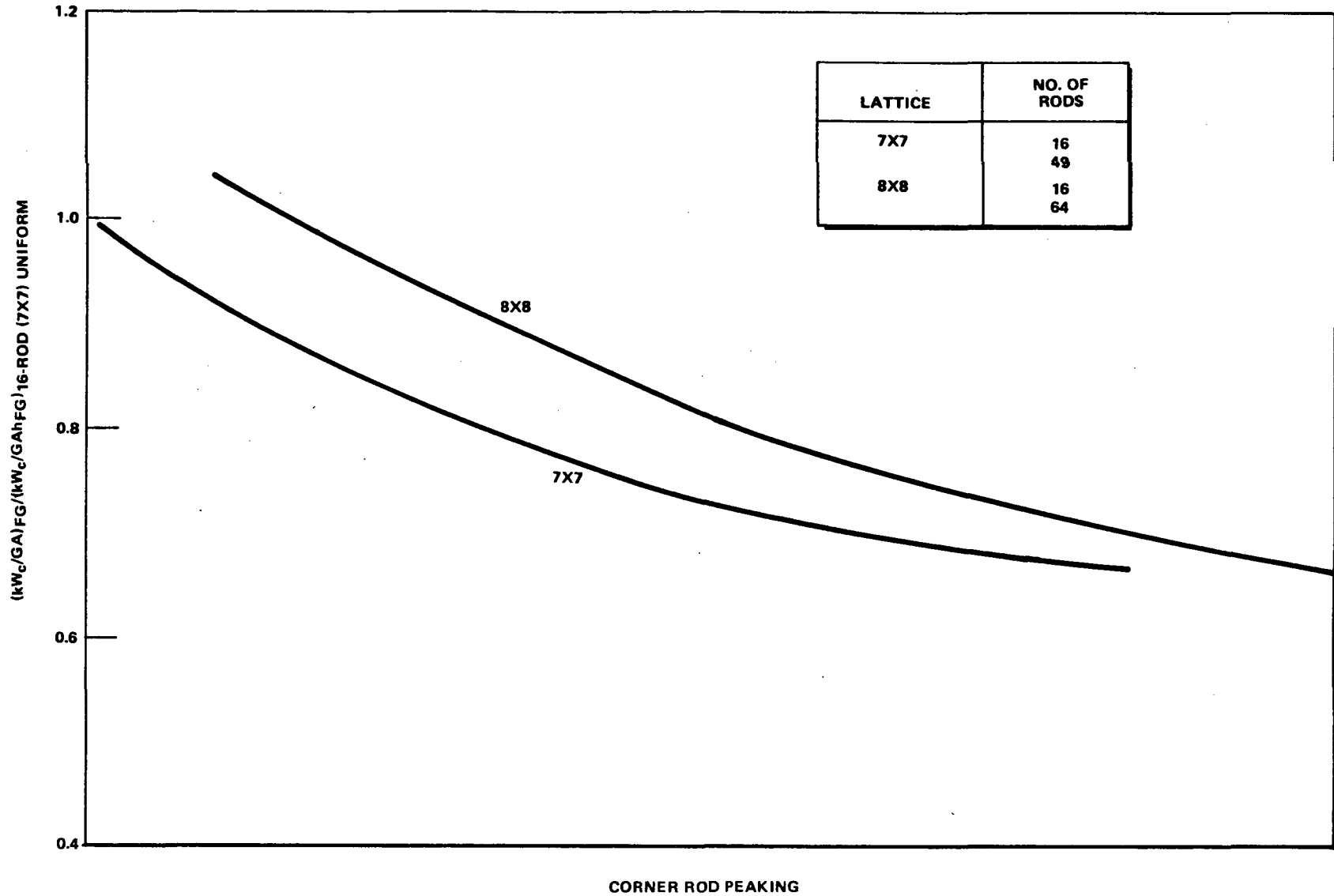


Figure 4-5. Critical Power Per Unit Mass Rate (Normalized with Respect to Value for Uniform Local Peaking) vs. Corner Rod Peaking,  $P = 1000$  psia,  $\Delta h_s = 20$  Btu/lb,  $G = 0.5 \times 10^6$  and  $1.0 \times 10^6$  lb/hr-ft<sup>2</sup>

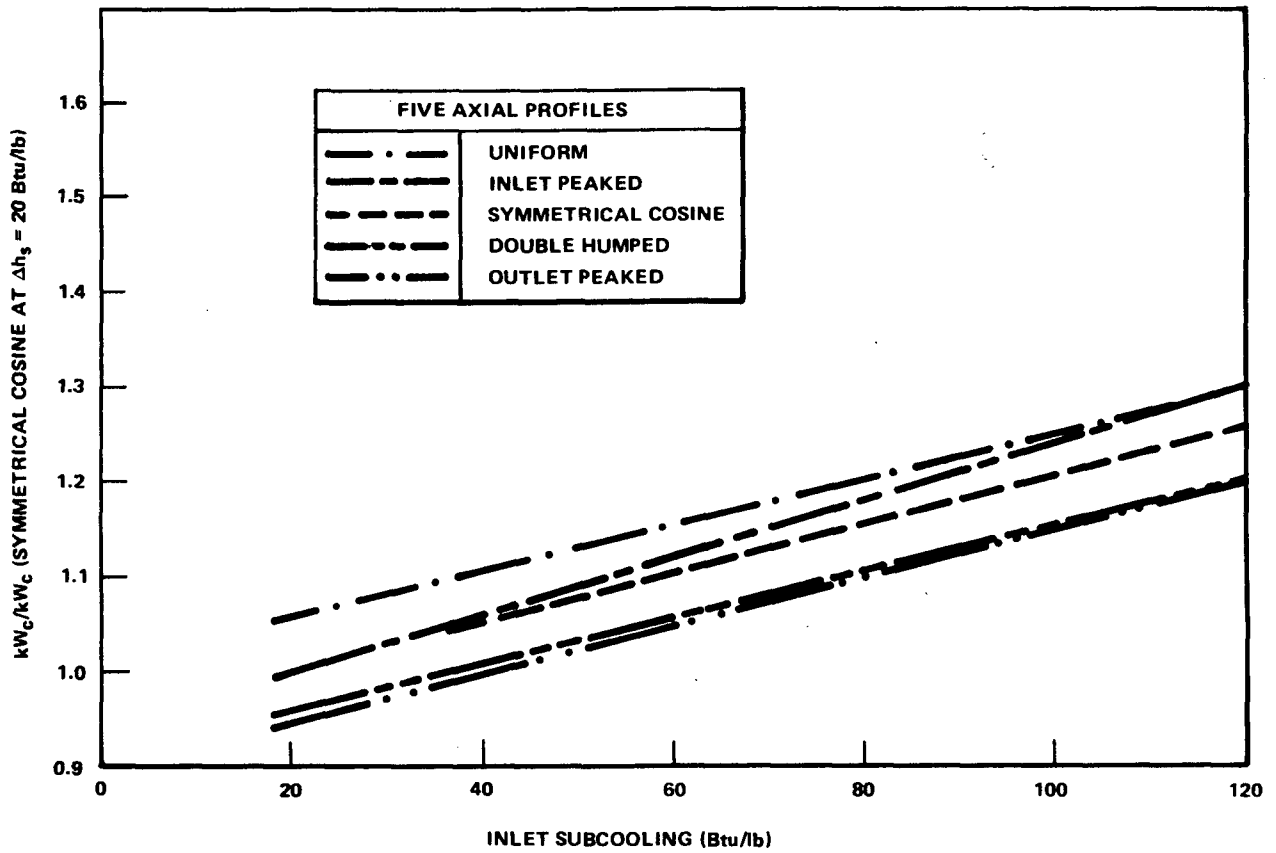


Figure 4-6. Critical Power (Normalized with Respect to Value for Symmetrical Cosine Axial Profile at  $\Delta h_s = 20$  Btu/lb) versus Inlet Subcooling, Various Axial Profiles, 1.23/1.26 3-Rod Corner Peaking, 1000 psia,  $G = 1 \times 10^6$  lb/h-ft<sup>2</sup>

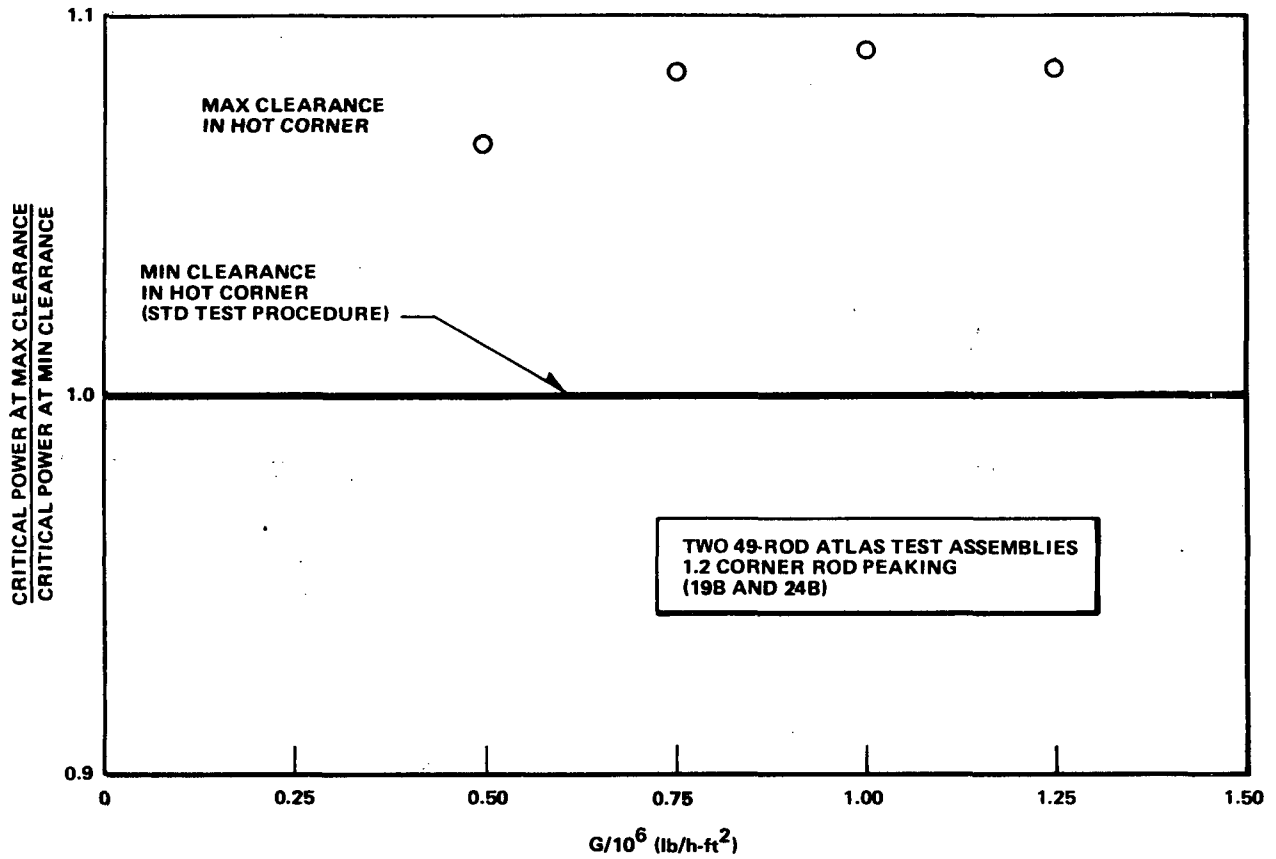


Figure 4-7. Effect on Critical Power of Rod-to-Wall Clearance in Hot Corner, for Bundles with Corner Rod Peaking

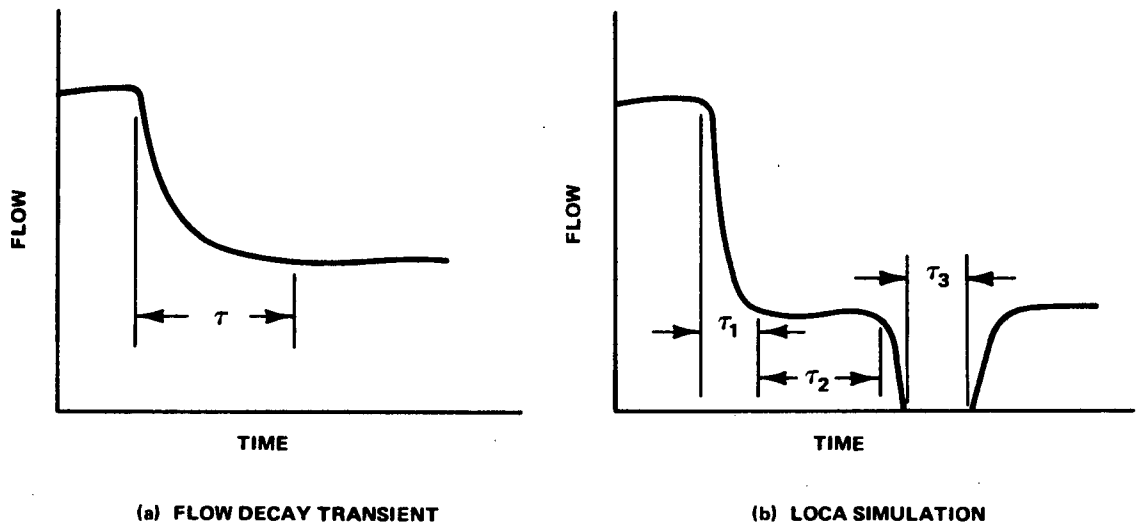


Figure 4-8. Definition of Transient Times

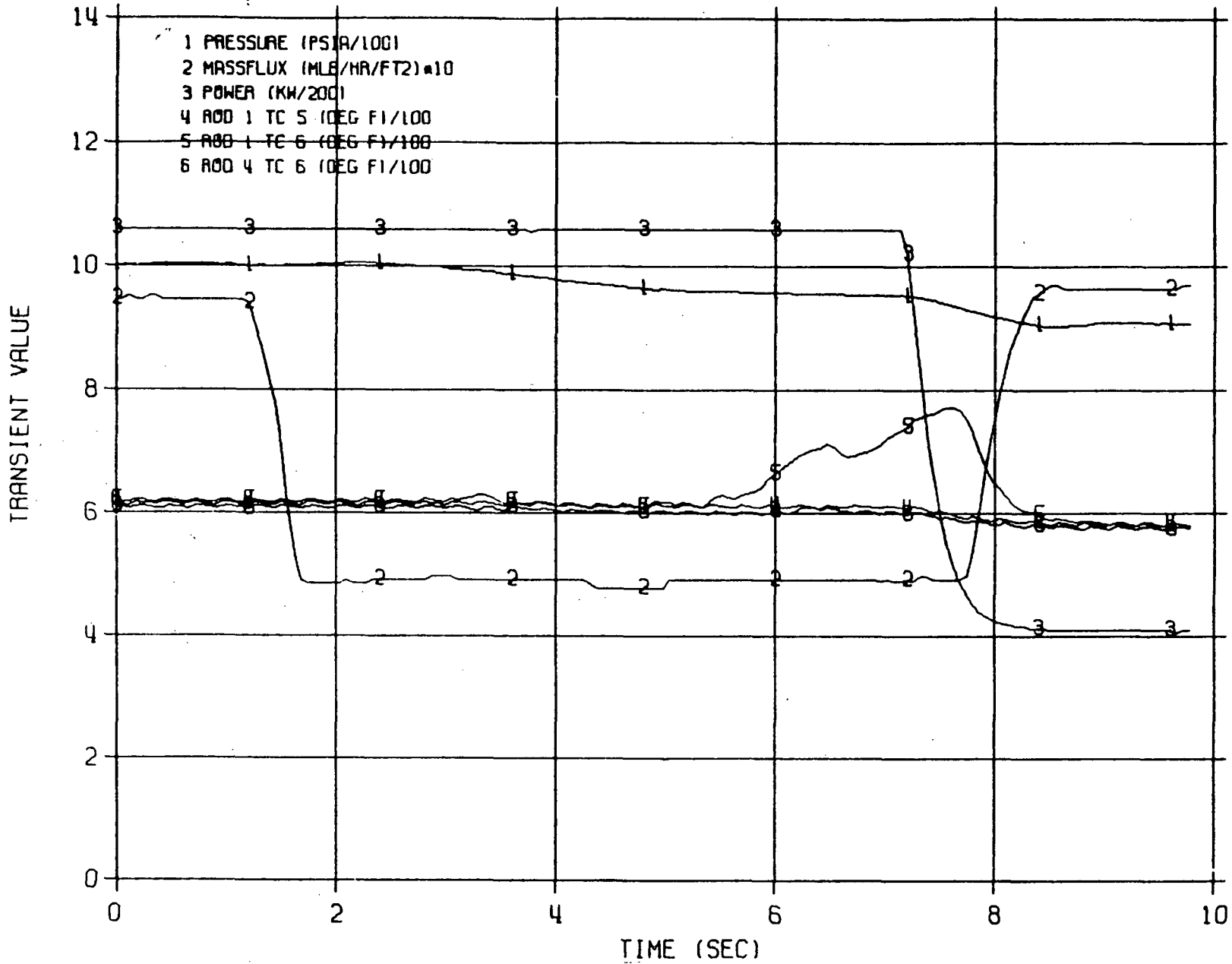


Figure 4-9. Flow Decay at Constant Power (Atlas Test Assembly No. 14, Run No. 101)

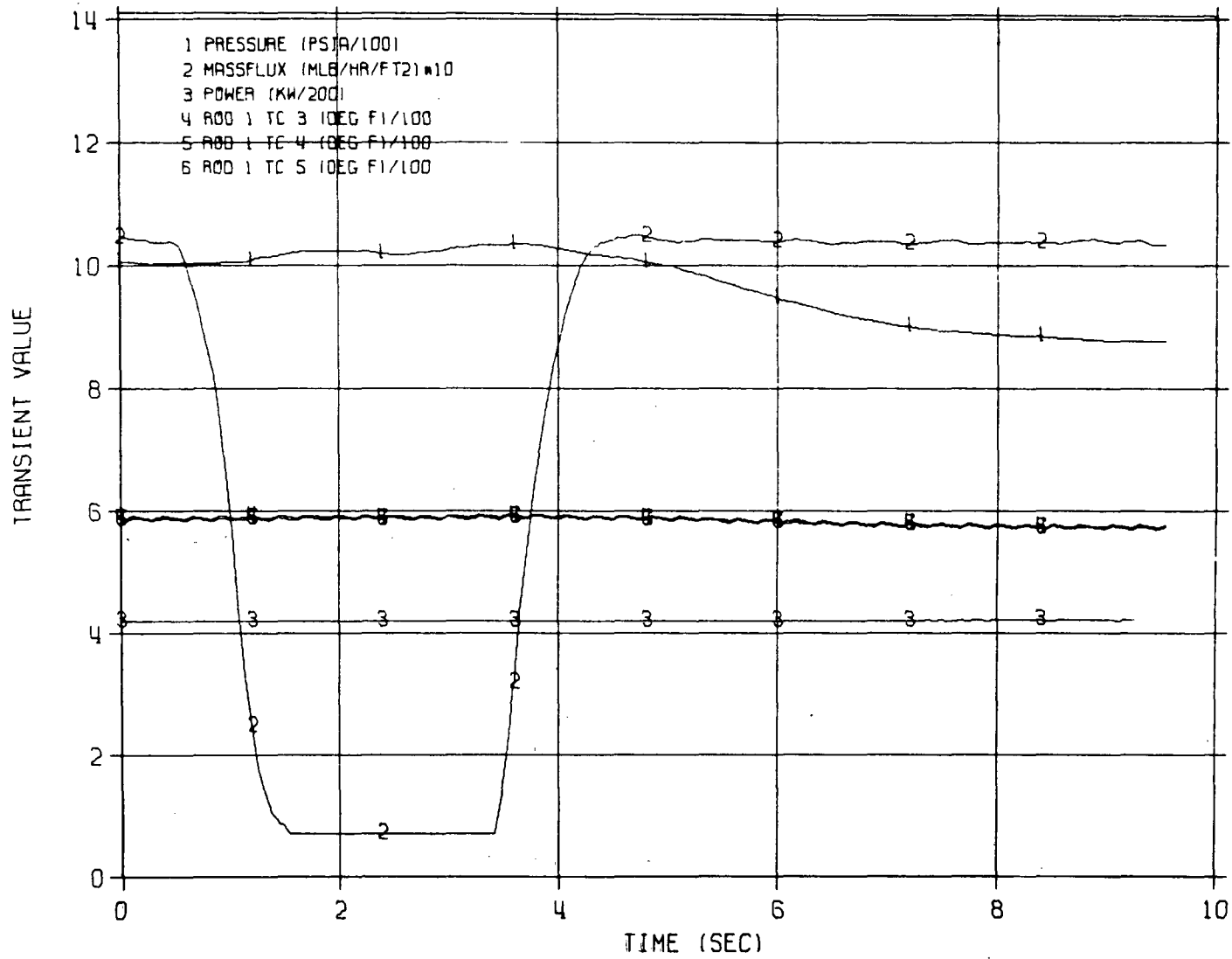


Figure 4-10. Flow On/Off/On at Constant Power (Run No. 138)

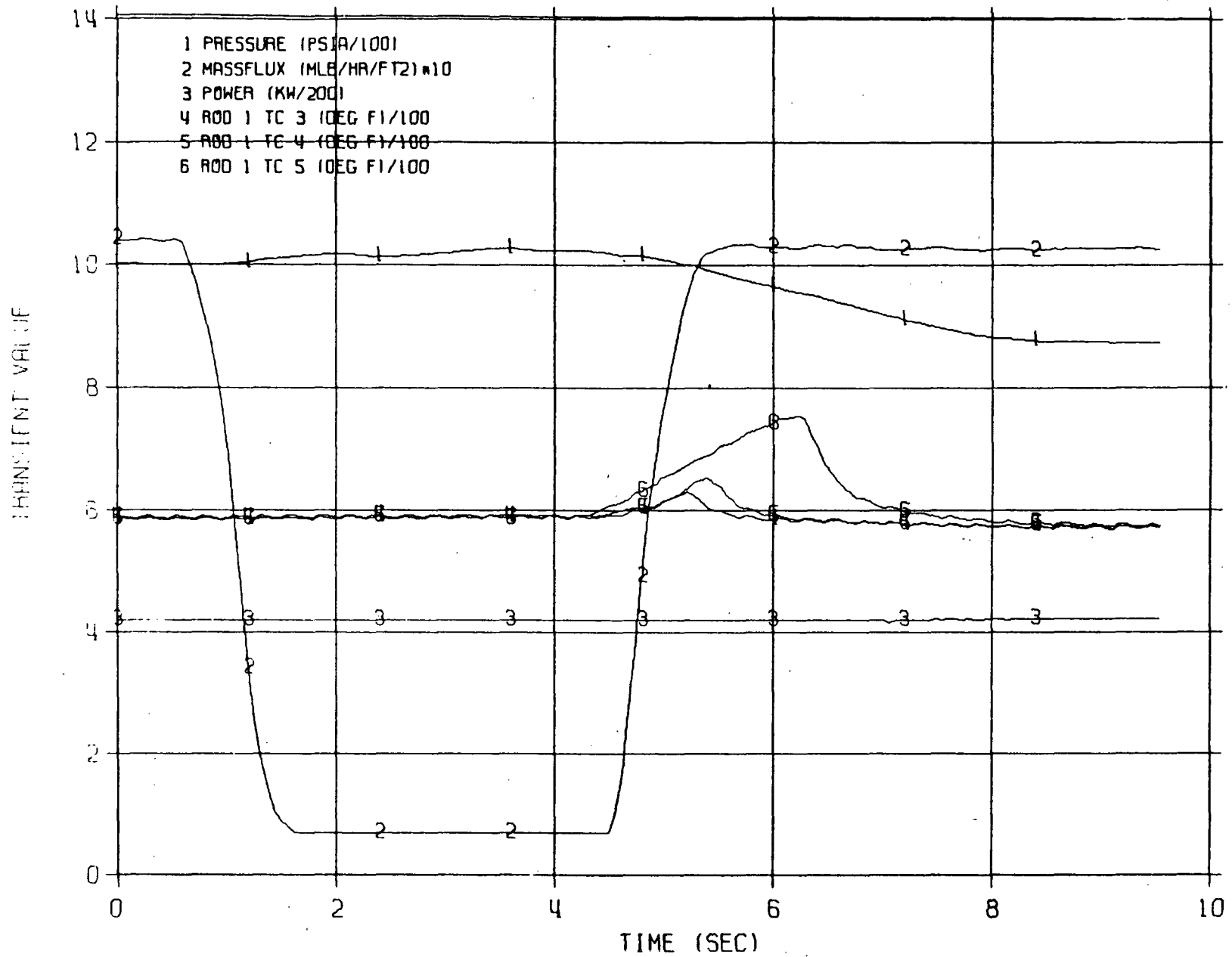


Figure 4-11. Flow On/Off/On at Constant Power (Run No. 139)

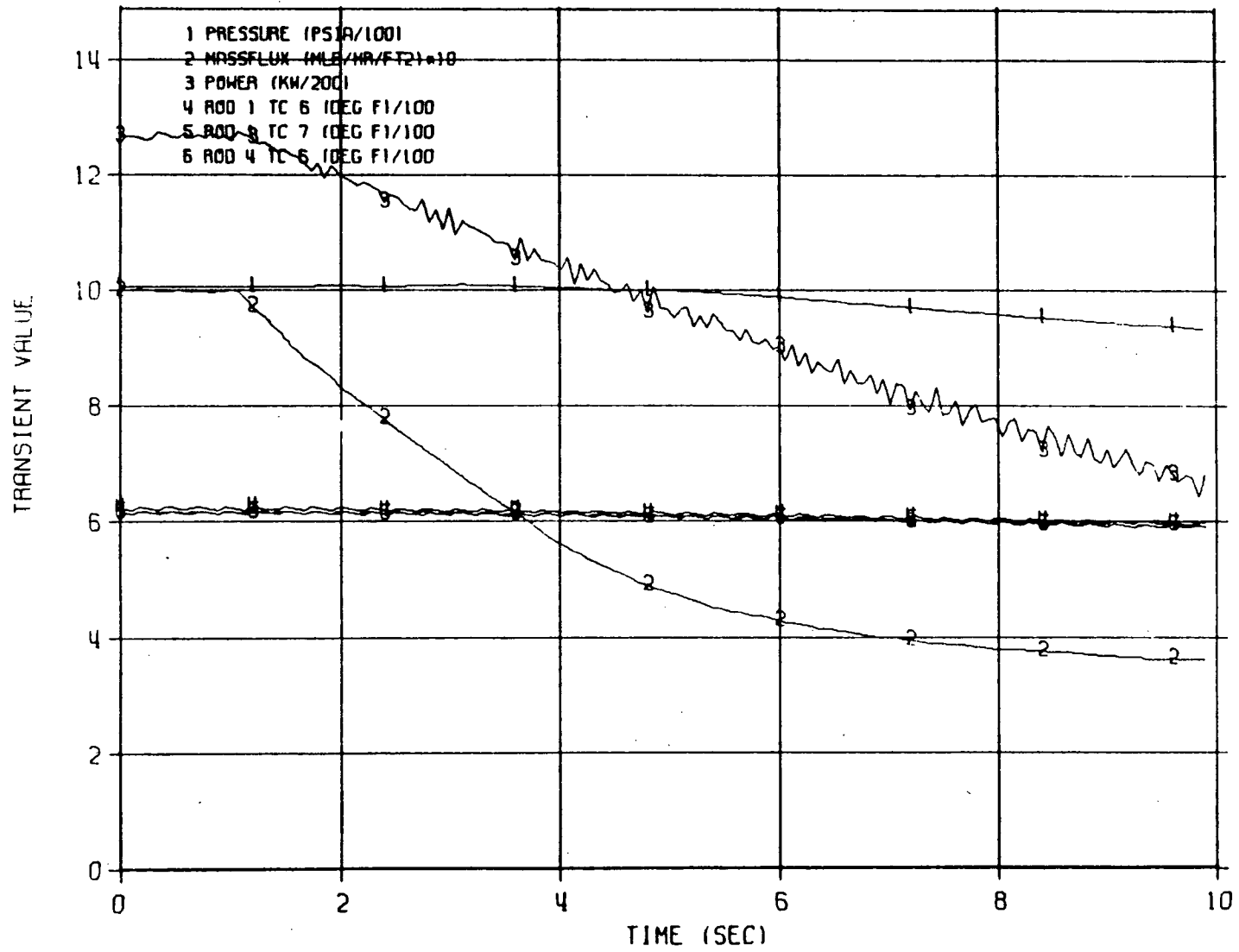


Figure 4-12. Simultaneous Flow and Power Decay (Run No. 200)



4-17/4-18

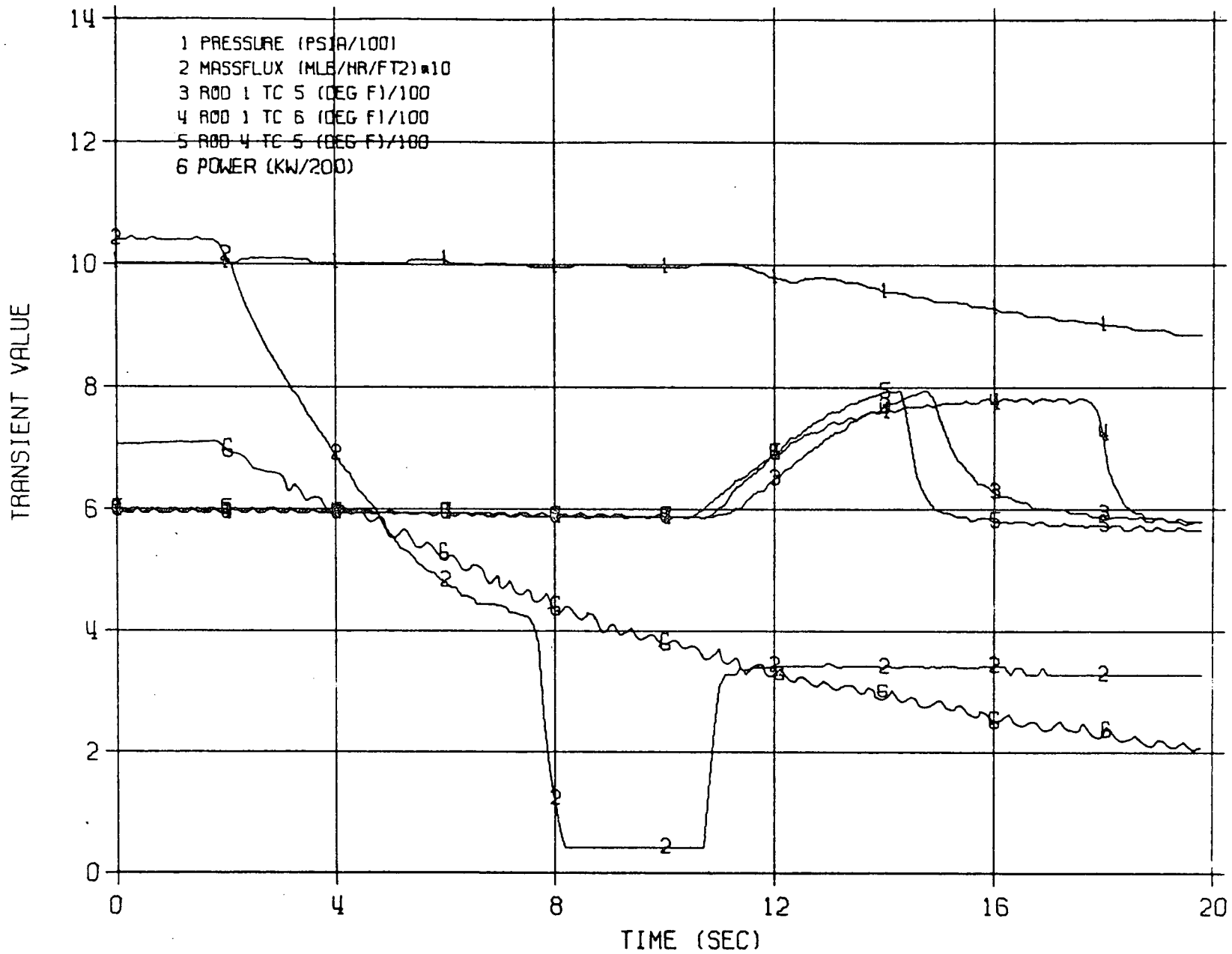


Figure 4-13. Simulated Loss-of-Coolant Accident (Run No. 248)

NEDO-10958-A

## 5. NEW CORRELATION

### 5.1 FORM OF THE GEXL CORRELATION

Critical quality versus boiling length has been chosen by General Electric as the coordinate system for correlating the boiling transition data described in Section 4. As such, it is the essential structure on which the new thermal analysis basis—GETAB is built. It was chosen for the advantages mentioned earlier; namely, that it is relatively independent of axial flux profile, yields good precision, and is fairly simple to apply in both design and operation.

Figure 5-1 is a plot of critical quality versus boiling length for two test assemblies used in the AEC sponsored Deficient Cooling Program.<sup>17</sup> This plot is typical for all the assemblies listed in Tables II-1 through II-4. Note that the points fall into distinct sets, each set for a particular flow rate, with the higher sets corresponding to the lower flows. In each set, making appropriate allowance for slight data scatter, the points form a well-defined curve. In Figure 5-1, the same curves correlate the data for two assemblies. In general, however, the correlating curves are different for each assembly, depending upon lattice dimensions, heated length, thermal diameter, local (i.e., rod to rod) peaking, mass flux, and system pressure.

In the development of the GEXL correlation, much use was made of graphical displays of data in the Quality-Boiling Length plane. The general form was established early and refinements were made as more data were generated, thus better defining the effect of certain parameters. The correlation was tested by (1) graphical comparison with data in the Critical Power-Subcooling plane, and (2) by numerical comparison of predicted critical power with measured critical power at each data point. The ratio of predicted to measured was evaluated, and the mean and standard deviation determined for each test assembly and flow condition. These tests of the correlation provided guidance during the latter stages of its development.

No regression analysis was used in the development of the GEXL 7 x 7 correlation. However, a regression analysis was used in the development of the GEXL 8 x 8. The coefficients were optimized using appropriately weighted data to best represent all the parameters of interest. The resulting correlation was tested as described above.

The correlation, expressed in its most general form, is:

$$X_C = X_C(L_B, D_Q, G, L, P, R) \quad (5-1)$$

where:

$X_C$  = bundle average critical quality;

$L_B$  = boiling length;

$D_Q$  = thermal diameter (i.e., four times the ratio of total flow area to total rod perimeter);

$L$  = heated length;

$P$  = system pressure;

$R$  = a parameter which characterizes the local peaking pattern with respect to the most limiting rod; and

$G$  = mass flux.

The parameter  $R$ , in addition to being a function of the local peaking pattern, is also dependent on lattice dimensions and on the grid spacer configuration. In effect,  $R$  takes into account the details of the flow and enthalpy distribution which are ordinarily only accounted for by a detailed subchannel analysis. Thus,  $R$  can be thought of as the bundle average analog of subchannel analysis. In fact, the expression for  $R$ , which includes weighting factors to apply to the local peaking factors for the rods surrounding the most limiting rod, was developed with the aid of the GE subchannel analysis model.

5.2 PREDICTION CAPABILITIES: STEADY-STATE

The GEXL correlation is based on 16-rod, 49-rod, and 64-rod water data obtained in the ATLAS facilities and on 16-rod data obtained at Columbia University. A direct comparison is made of predicted versus measured critical power for these data in Figures 5-2 through 5-6. These data represent a wide range of conditions over which the correlation is considered to be valid:

- Pressure: 800 to 1400 psia
- Mass Flux:  $0.10 \times 10^6$  to  $1.25 \times 10^6$  lb/hr-ft<sup>2</sup>
- Inlet Subcooling: 0 to 100 BTU/lb
- Local Peaking: 1.61 corner rod to 1.47 interior rod
- Axial Profile: Symmetrical cosine, inlet peak, outlet peak, double hump, and uniform axial

The figures clearly show the excellent agreement between the predictions and data. The predicted values for over 90% of the data are within ±6% of measured. In a similar manner, GEXL has successfully correlated scaled Freon data.

The GEXL correlation was optimized initially for the ATLAS data, and was subsequently optimized for the Columbia data and for early GE data. Subsequently, the statistical analysis has been performed separately for the 7 x 7 lattice (2700 ATLAS data points) and the 8 x 8 lattice (1299 ATLAS data points). These data points cover the range of conditions for which the correlation is considered valid. To facilitate a statistical evaluation of the predictive capability of the GEXL correlation, an Experimental Critical Power Ratio (ECPR) has been identified as,

$$ECPR = \frac{\Delta \text{ Predicted Critical Power}}{\text{Measured Critical Power}}$$

The histograms of this ratio are shown in Figure 5-7 and 5-8, respectively. Figures 5-7 and 5-8 are unimodal, nearly symmetrical, and have decreasing probabilities at greater distances from their means. The modest nonsymmetry present is in the conservative tail. Thus the normal distribution was selected as the single best choice to characterize these distributions. (See the response to Question 2-5c, Appendix VII.) The results of the analysis are summarized in the following table:

	Overall Statistics	
	7 x 7	8 x 8
Lattice Type	7 x 7	8 x 8
Mean ECPR	0.9885 (-1.15%)	0.9848 (-1.52%)
Standard Deviation, $\sigma$	0.0360 (3.60%)	0.0280 (2.80%)

These grand mean differences arise from the procedures used to estimate the coefficients in the prediction equation.\* Resulting critical power predictions by themselves are not unbiased; indeed, they are slightly conservative.

The Columbia University boiling transition data from assemblies with 72 in. heated length, which were not used as a basis for the GEXL optimization, also exhibit good agreement between predicted and measured critical powers as seen in Figure 5-2.

Figure 5-9 shows a comparison of the GE 4-rod and 9-rod data with the GEXL predictions. These data are the basis for the Hench-Levy Limit Lines. As shown, the data from smaller assemblies with heated length ranging from 36 ~ 72 inches are predicted very well by the correlation.

\* A discussion of the effect of the mean differences upon application to plant operations is given in the response to Question 2-3 in Appendix VII.

As previously noted, certain scaled Freon data have been successfully correlated using GEXL. (See answer to Question 1-14b, Appendix VII.) Figures 5-10 through 5-13 show a comparison between predicted versus measured critical power for the scaled Freon data. Agreement is again excellent, and essentially independent of axial flux shape.

The GEXL correlation predicts the same trends with mass flux, pressure, and local peaking as shown by the data of Figures 4-3, 4-4, and 4-5, respectively. It also closely predicts the effect of axial heat flux profile. This can be best seen in a comparison between the measured and predicted critical powers (normalized with respect to measured critical power for the symmetrical cosine bundle at 20 Btu/lb subcooling) shown in Figure 5-14 for four axial profiles.\* In the subcooling range of interest for BWRs (20 to 40 Btu/lb) the prediction is conservative for all four profiles. The prediction for inlet peak is the most conservative, with an ECPR of 0.94 (-6%). The prediction for the uniform profile (not shown) is about the same as for the inlet peak. The predictions for the other three profiles are much closer to measured.

In summary, the GEXL correlation predictions are in excellent agreement with the measured data over a range of conditions that is wider than that encountered in operating BWRs. This has been shown in the plots of Figures 5-2 through 5-6 and further demonstrated by a rigorous statistical evaluation. The correlation correctly predicts the effects of mass flux, pressure, local peaking, and axial profile on critical power and is thus satisfactory for design use.

---

\* Figure 5-14 shows results for 1.23/1.26 corner rod peaking. The results for 1.13/1.16 and 1.4 corner rod peaking are very similar. The original Figure 5-14 was revised; see answer to Question 1-14c.

### 5.3 PREDICTION CAPABILITIES: TRANSIENT (7 x 7 LATTICE)

It has been previously demonstrated that a correlation for the onset of transition boiling based on steady-state data can be used for the prediction of transients, provided that the instantaneous fluid properties are accurately predicted during the transient.<sup>16</sup> This approach is valid for transients that occur in a BWR, where phenomena such as acoustic wave propagation and thermodynamic nonequilibrium are not important. In order to predict the data, the steady-state GEXL correlation was programmed into the GE transient thermal-hydraulics computer code model.<sup>14</sup> This model is a multinode single-channel thermal-hydraulic analytical tool which accounts for the axial variation in power generation. The primary inputs to the model include the bundle dimensions, channel inlet flow versus time, channel pressure versus time, channel inlet enthalpy versus time and the channel power generation versus time and position. As described in Reference 14, the model simultaneously solves partial differential equations which are statements of the mass, energy and momentum conservation laws.

In the analytical evaluation of the experimental data, it is desired to predict the time to reach a boiling transition (i.e., critical quality)\* and the axial location in the bundle where the boiling transition first occurs. In addition, subsequent upstream penetration of the boiling transition is of interest. Therefore, in the comparison of the prediction to the experimental data, the primary criteria are the times and the axial locations of the onset of transition boiling. To date, the transient computer model with the GEXL correlation has been successfully used to analyze several experimental runs from each of five bundles as described in subsequent sections.

#### 5.3.1 Comparison With 16-Rod Test Data

Analytical predictions were made for four separate 12-ft-long electrically heated 16-rod assemblies with 7 x 7 rod configuration and spacing. The primary differences in these four test bundles (described earlier) were as follows:

Assembly Designation	14 (ATLAS)	27C (ATLAS)	28D (ATLAS)	29D (ATLAS)
Axial Power Profile	Chopped Cosine	Inlet Peaked	Double-Humped	Outlet Peaked
Axial Peaking Factor (P/A)	1.39	1.6	1.46	1.6
Local Peaking	Approx. Uniform	1.25 (3-Rod Corner Peaking)	1.26 (3-Rod Corner Peaking)	1.23 (3-Rod Corner Peaking)

The axial profiles and local peaking patterns are shown in Appendix III.

During the tests, it was observed that boiling transition almost always occurred at a location just upstream of one of the spacers. In general, the boiling transition was first observed at either the first or the second spacer before the end of the heated length. In many cases, there was subsequent movement of the boiling transition upstream into the bundle.

#### Assembly 14

A large number of transient tests (115) were completed using 16-rod Assembly 14, which had 1.39 peak-to-average cosine axial heat flux profile. A discussion of these tests and the initial conditions is given in Reference 16.

The analytical predictions in terms of critical power ratio as a function of time are given in Figures 5-15 through 5-17 for several representative cases. Included in the figures is the measured heater rod cladding temperature as a function of time to indicate the time of onset of the transition boiling. The calculated penetration of the boiling transition into the bundle is plotted in Figures 5-18 through 5-20 as a function of time and compared to the experimental data. A complete summary of the runs investigated and a comparison of the prediction capability is included in Table II-6.

A plot of the predicted time versus the experimentally measured time for the initial boiling transition is given in Figure 5-21. Shown in Figure 5-22 is a comparison of the predicted penetration versus the measured penetration of the boiling transition.

\*This condition corresponds to a minimum value of the calculated CPR during the transient being equal to 1.0.

An examination of these predictions indicates that the majority of the tests can be predicted within  $\pm 0.3$  sec for the onset of the transition boiling. Inspection of the run number 203 test data indicates that it is difficult to ascertain the time that a boiling transition occurred since there was initially a small temperature rise followed by a sharp temperature increase approximately 0.5 seconds later. This time uncertainty has been indicated by the two data points with an arrow between them as given on Figure 5-21. The initial location prediction was conservative\* in all cases analyzed.

Subsequent axial penetration of the boiling transition was also conservatively predicted in time and location for all but two runs. Examination of the test data shows that the lack of a strong indication of boiling transition for these two runs results in the prediction of axial penetration within approximately 10 in. (i.e., one half of the distance between spacers). It should be pointed out, however, that this assembly had uniform local peaking, which is not representative of local peaking pattern in nuclear reactor fuel bundles.

Boiling transition was predicted by GEXL on 15 of the 22 transient tests. In four tests the predicted minimum value of CPR during these transients was 1.017 or less, a residual of less than 1.7%. The other three tests which did not result in a calculated boiling transition condition were at low mass flow rates of  $0.6 \times 10^6$  lb/hr-ft<sup>2</sup> with flow decays to about one-half flow. At these flow rates the transient mass flow rate measurement was at the limits of experimental accuracy. Thus, the results must be considered questionable.

### Assembly 27C

Approximately 30 transient tests were completed with assembly 27C. Transition boiling occurred in 19 of these tests. The tests were primarily flow and power transients as described in Section 4. Assembly 27C was a 16-rod assembly with a 1.6 peak-to-average axial heat flux profile with the peak toward the inlet of the bundle. The local peaking configuration was characterized by three corner rods at 1.25. Details of the local peaking pattern and the axial flux shape for this assembly are given in Appendix III.

The analytical predictions for Assembly 27C, in terms of critical power ratio as a function of time, are shown in Figures 5-23 through 5-25 for three representative cases. The transient heater rod cladding temperature is shown in these figures to indicate the time of the onset of transition boiling. The calculated penetration of the boiling transition into the bundle is compared to the measured location for these three cases in Figures 5-26 through 5-28. A summary of the comparison between experiments and the predictions is included in Table II-7. A plot of the predicted time versus the measured time for onset of transition boiling is given in Figure 5-29. Shown in Figure 5-30 is a corresponding comparison of the predicted penetration versus the measured penetration of the boiling transition.

Inspection of the plots indicates that practically all of the tests were predicted conservatively. Only three tests resulted in a larger calculated time, and then by less than 0.15 sec. All 19 tests were predicted conservatively for the location of the boiling transition for both the initial and the deepest axial penetration.

### Assembly 28D

Twenty-seven transient tests were completed with Assembly 28D. A boiling transition occurred in 17 of these tests. These tests included flow and power decays and constant power flow decays. This assembly was a 16-rod electrically heated assembly with a double hump 1.46 peak-to-average axial heat flux profile. The assembly local peaking configuration was characterized by three corner rods at a peaking factor of 1.26. Details of the local peaking pattern and the axial flux shape for the assembly are given in Appendix III.

The analytical predictions for three tests of Assembly 28D in terms of critical power ratio as a function of time are shown in Figures 5-31 through 5-33 for the cases analyzed. The measured heater rod cladding temperatures are given in these figures to indicate the time of the onset of the transition boiling. The calculated penetration of the boiling transition into the assembly is compared to the measured location in Figures 5-34 through 5-36. A complete summary of the experiments analyzed and a comparison of the prediction capability is given in Table II-8. A plot of

---

\* A conservative location predictor from the standpoint of reactor transient analysis is one that predicts the onset of transition boiling at a location with higher heat flux (generally lower in the bundle) than actually occurred.

this predicted time versus the measured time for the onset of the transition boiling is given in Figure 5-37. Shown in Figure 5-38 is a corresponding comparison of the predicted penetration versus the measured penetration of the boiling transition.

Inspection of Figure 5-37 indicates that the correlation is conservative by approximately 0.5 sec for five of the six tests analyzed in the prediction of the time to initial boiling transition. In addition, the comparison given in Figure 5-38 indicates that the penetration of the boiling transition is conservatively evaluated for all of the six tests investigated.

### Assembly 29D

Twenty-six transient tests were completed with Assembly 29D. A boiling transition occurred in 15 of these tests. The tests included flow and power decays and constant power flow decays.

This assembly was a 16-rod electrically heated assembly with a 1.6 peak-to-average axial heat flux profile with the peak toward the outlet of the bundle. The assembly local peaking configuration was characterized by 3 corner rods at a peaking factor of 1.23. Details of the local peaking pattern and the axial flux shape for the assembly are given in Appendix III.

Five representative cases were chosen for analysis. The analytical predictions for three of the tests of Assembly 29D in terms of critical power ratio as a function of time are shown in Figures 5-39 through 5-41. The measured heater rod cladding temperatures are given in these figures to indicate the time of the onset of transition boiling. The calculated penetration of the boiling transition into the assembly is compared to the measured location in Figures 5-42 through 5-44.

A complete summary of the experiments analyzed and a comparison of the prediction capability is given in Table II-9. A plot of this predicted time versus the measured time for the onset of transition boiling is given in Figure 5-45. Shown in Figure 5-46 is a corresponding comparison of the predicted penetration versus the measured penetration of the boiling transition. Inspection of Table II-9 and Figure 5-45 indicate that two of the five tests analyzed resulted in a slightly non-conservative predicted time to boiling transition. Two were predicted almost exactly and one was predicted slightly conservatively.

### 5.3.2 Comparison with 49-Rod Test Data

Analytical predictions of test data using the GEXL correlation have been made for a 12-ft-long electrically heated 49-rod test assembly. The basic dimensions of the assembly were the same as a typical GE-BWR 7 x 7 fuel assembly. This assembly was designated 25A (Atlas Test Assembly No. 25A) and its main features were as follows:

Axial Power Profile	Chopped Cosine
Axial Peaking Factor	1.39
Local Peaking	1.24 (3-rod corner)

The axial flux shape and local peaking pattern used in the test is given in Table II-3.

Of the 59 transient tests conducted with Assembly 25A, 29 tests resulted in transition boiling. A summary of the test is given in Section 4.

The analytical predictions for Assembly 25A in terms of critical power ratio as a function of time are given in Figures 5-47 through 5-49 for several representative cases. The measured heater rod cladding temperature is plotted on the above figures to provide an indication of the time of onset of the boiling transition. The calculated penetration of the transition boiling into the assembly is compared to the measured location in Figures 5-50 through 5-52 for these three cases. A complete summary of the test runs analyzed and a comparison of the prediction capability for Assembly 25A is included in Table II-10. A plot of the predicted time versus the measured time for the onset of the transition boiling is given in Figure 5-53. Shown in Figure 5-54 is a corresponding comparison of the predicted penetration versus the measured penetration of the boiling transition.

The comparison indicates that nearly all of the 49-rod tests were predicted within  $\pm 0.3$  sec for the initiation of the onset of transition boiling. For all cases analyzed, the prediction of the initial penetration of the transition boiling was conservative.

Although the onset of transition boiling was not predicted for all 17 tests analyzed, the discrepancy between measurement and prediction is extremely small. Boiling transition was predicted on 11 of the 17 tests, and on five more tests the predicted minimum critical power ratio (CPR) is 1.009 or less, a residual of less than 1%. In the remaining run, the conditions were on the verge of being in transition boiling condition over a small period of time. It is questionable if these conditions should be classified as onset of transition boiling. However, the predicted minimum CPR was quite close to 1.0 in this case also. Therefore, it is concluded that the transient predictions for Assembly 25A are entirely satisfactory.

### 5.3.3 Conclusions

The overall results of the analysis of the boiling transition tests are given in Tables II-6 through II-10 for the five different assemblies investigated. The onset of transition boiling was predicted in 56 of the 69 tests analyzed. For the remaining 13 tests, a predicted minimum experimental critical power ratio (MECPR) of 1.01 or less was calculated for six tests within 0.5 sec of the measured time of boiling transition. The predicted MECPR was greater than 1.017 in only three of these tests. It should be noted that in many of these tests the onset of boiling transition was marginal with only a very small temperature perturbation. A plot of the predicted time versus the measured time to the boiling transition condition is given in Figure 5-55 for all five of the assemblies analyzed. An examination of the results given in Figure 5-55 and Tables II-6 through II-10 indicates that 38 of the tests were predicted within  $\pm 0.35$  sec of the measured time to the onset of the boiling transition. Of the tests which were not predicted within this range, only two were predicted nonconservatively (late). This may be attributed in one case to an uncertainty in the onset time of boiling transition. In the other case, the error was within 0.5 sec, which is still reasonably good agreement.

Correspondingly, all of the other tests (16 in number) which were not predicted within  $\pm 0.35$  sec of the measured time were predicted even earlier and therefore are conservative.

Because the GEXL correlation is a "best fit" of the steady-state experimental boiling transition data, one might expect the application of this correlation to the transient tests to result in predictions both above and below the measured values. Significantly, however, the results indicate that the use of a transient computer code with the GEXL correlation results in conservative predictions of both the time and the location of the onset of transition boiling. In addition, the axial penetration of the transition boiling into the bundle is conservatively predicted for 54 of the 56 tests in which the onset of the transition boiling was predicted.

In summary, the use of the GEXL correlation in predicting both 16-rod transient tests with inlet, cosine, double-humped, and outlet axial peaking and 49-rod transient tests with cosine axial peaking and uniform and nonuniform local peakings has been shown to produce satisfactory agreement with the experimental data. It is concluded that the technique is fully suitable for transient analysis of BWRs.

## 5.4 PREDICTION CAPABILITIES: TRANSIENT (8 x 8 LATTICE)

It was demonstrated in Subsection 5.3 that the steady-state 7 x 7 GEXL correlation was suitable for the transient analysis of BWR 7 x 7 fuel assemblies. Similarly, the transient computer code model with the 8 x 8 GEXL correlation has been successfully used to analyze several transient runs from each of two 8 x 8 bundles.

### 5.4.1 Comparison with 8 x 8 Bundle Test Data

Analytical predictions were made for two separate 148-in.-long electrically heated 64-rod assemblies. The basic dimensions for each assembly were the same as for a typical GE-BWR 8 x 8 fuel assembly. The main features of these two bundles were as follows:



Assembly Designation	32B	35C
Axial Power Profile	Chopped Cosine	Chopped Cosine
Axial Peaking Factor	1.39	1.39
Local Peaking	1.22 (5-Rod corner peaking)	1.13 (5-Rod corner peaking)
Water Rods (i.e., unheated rod)	1	1

The axial power profiles and local peaking patterns are shown in Appendix III.

During the tests, it was observed that boiling transition almost always occurred at a location just upstream of one of the spacers, either the first or second spacer before the end of the heated length.

#### Assembly 32B

Fifty-six transient tests were completed with Assembly 32B. The tests included flow and power decays, constant power flow decays, constant flow power ramps, and power and flow ramps. In 18 of the 56 tests a boiling transition occurred; seven of the 18 have been analyzed.

The analytical predictions for Assembly 32B in terms of critical power ratio versus time are given in Figures 5-56 through 5-58 for three representative cases, run numbers 133, 145 and 155. These three runs are categorized as follows:

Run Number	Type of Run	Initial Mass Flux (lb/hr-ft <sup>2</sup> )
133	Constant Power, Flow Decay	$1 \times 10^6$
145	Constant Flow, Power Ramp	$1 \times 10^6$
155	Power and Flow Ramp	$0.5 \times 10^6$

The measured heater rod cladding temperature is also plotted as a function of time on Figures 5-56 through 5-58 to provide an indication of the time to the onset of boiling transition.

The calculated penetration of the boiling transition into the assembly for the same three runs is compared to the measured location in Figures 5-59 through 5-61.

A summary of the test runs which were analyzed for Assembly 32B, including a comparison of predicted and measured results is included in Table II-11. A plot of predicted time versus measured time to the onset of transition boiling is given in Figure 5-62. A corresponding comparison of predicted penetration versus measured penetration of the boiling transition is shown in Figure 5-63.

The comparisons indicate that: (1) for five of the seven tests the time to initiation of the onset of transition boiling was predicted within  $\pm 0.35$  sec; (2) the other two tests were predicted even earlier (more conservative); and (3) for all seven cases the predictions of the initial penetration and the maximum penetration of transition boiling were conservative.

#### Assembly 35C

Forty transient tests were completed with Assembly 35C. These tests included flow and power decays, constant power flow decays, constant power flow ramps, and power and flow ramps. In 15 of the 40 runs a boiling transition occurred. Twelve of the fifteen tests have been analyzed.

The analytical predictions for Assembly 35C in terms of critical power ratio versus time are given in Figures 5-64 through 5-66 for three representative cases (run numbers 32, 51 and 56). The three runs are categorized as follows:

Run Number	Type of Run	Initial Mass Flux (lb/hr-ft <sup>2</sup> )
32	Power and Flow Decay	$1 \times 10^6$
51	Constant Power, Flow Decay	$1 \times 10^6$
56	Constant Flow, Power Ramp	$1 \times 10^6$

The measured heater rod cladding temperature is also plotted as a function of time on these figures to provide an indication of the time to onset of boiling transition.

The calculated penetration of transition boiling into the assembly for the same three runs is compared to the measured location in Figures 5-67 through 5-69.

A summary of the test runs which were analyzed for Assembly 35C, including a comparison of predicted and measured results, is given in Table II-12. A plot of predicted time versus measured time to the onset of transition boiling is given in Figure 5-70. A corresponding comparison of predicted versus measured penetration of the boiling transition is shown in Figure 5-71. The comparisons indicate that: (1) for 8 of the 12 runs, boiling transition was predicted; (2) for 7 of the 8 the predicted time to boiling transition was conservative (early) and the one overprediction was less than 0.1 sec late; and (3) for the 8 cases where boiling transition was predicted the predictions of the initial penetration and the maximum penetration of the boiling transition were conservative. For three of the four runs for which the onset of transition boiling was not predicted, the calculated minimum critical power ratio was 1.005 or less. In the remaining analyzed run the calculated minimum critical power ratio was 1.009, a residual of less than 1%.

#### 5.4.2 Conclusions

The results of the analyses of the 8 x 8 experimental tests are given in Tables II-11 and II-12 for the two full 64-rod assemblies investigated. The onset of transition boiling was predicted in 15 of the 19 tests in which it was observed to occur. Of the remaining four tests, a predicted minimum critical power ratio of 1.005 or less was calculated for three tests and 1.009 for the fourth test. All four are well within the scatter of the steady-state GEXL correlation. A plot of predicted versus measured time to a boiling transition condition is given in Figure 5-72 for Assemblies 32B and 35C. An examination of the results of the times to boiling transition indicates that half of the tests were predicted within  $\pm 0.35$  sec. The remainder of the tests were predicted even earlier (i.e., more conservatively).

In addition, the use of the GEXL correlation resulted in the conservative prediction of both the initial and the maximum penetration of boiling transition in each of the two 64-rod assemblies analyzed.

In summary, the use of the GEXL correlation for predicting 64-rod transients has been shown to produce satisfactory agreement with experimental data. It is concluded that the technique is suitable for the transient analysis of 8 x 8 BWR fuel assemblies.

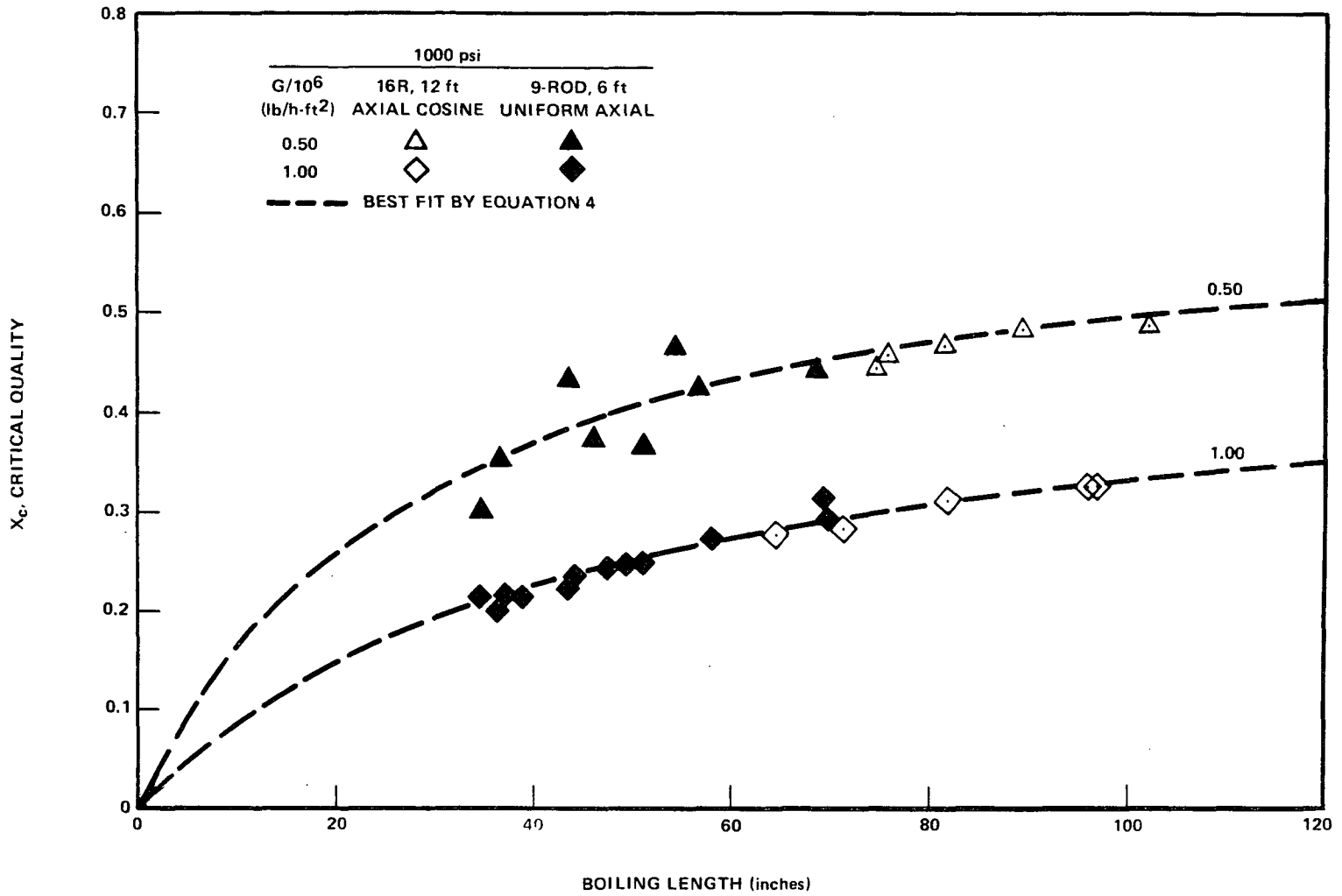


Figure 5-1. Nine- and 16-Rod Critical Quality versus Boiling Length, 1000 psi

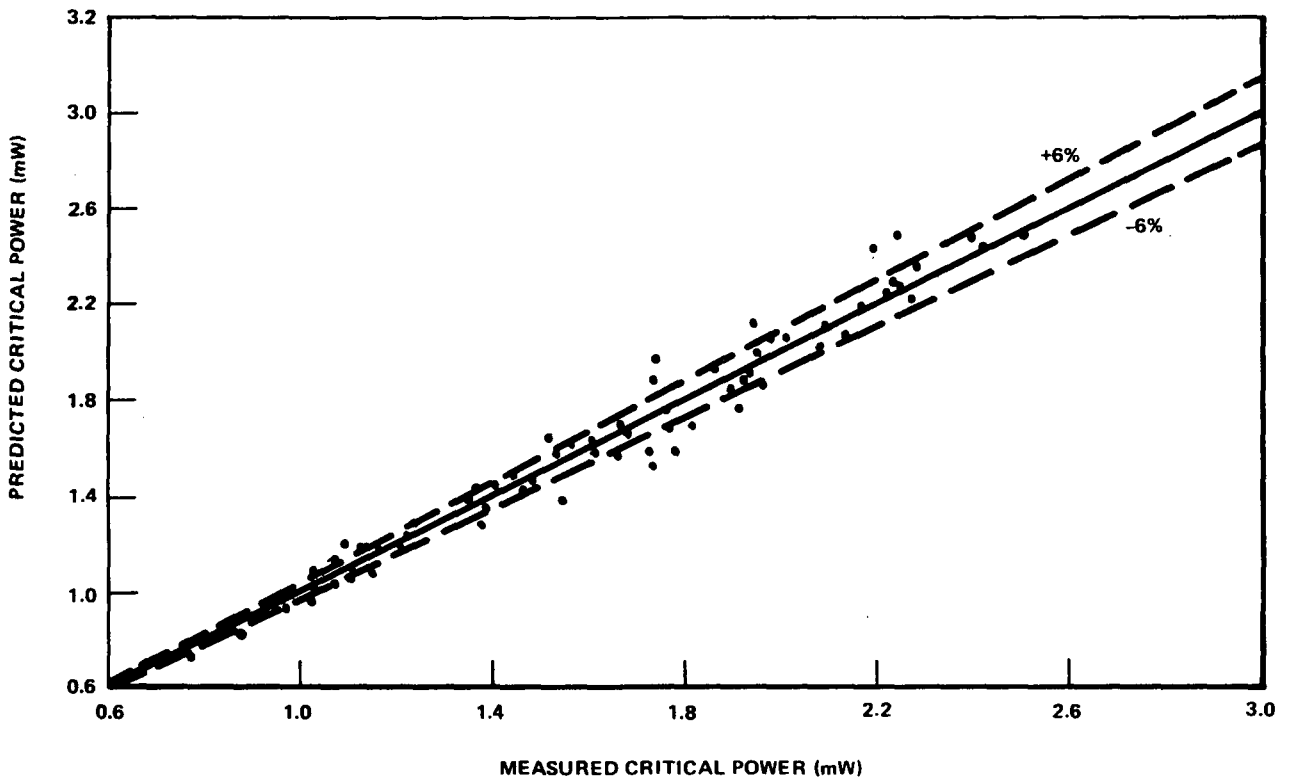
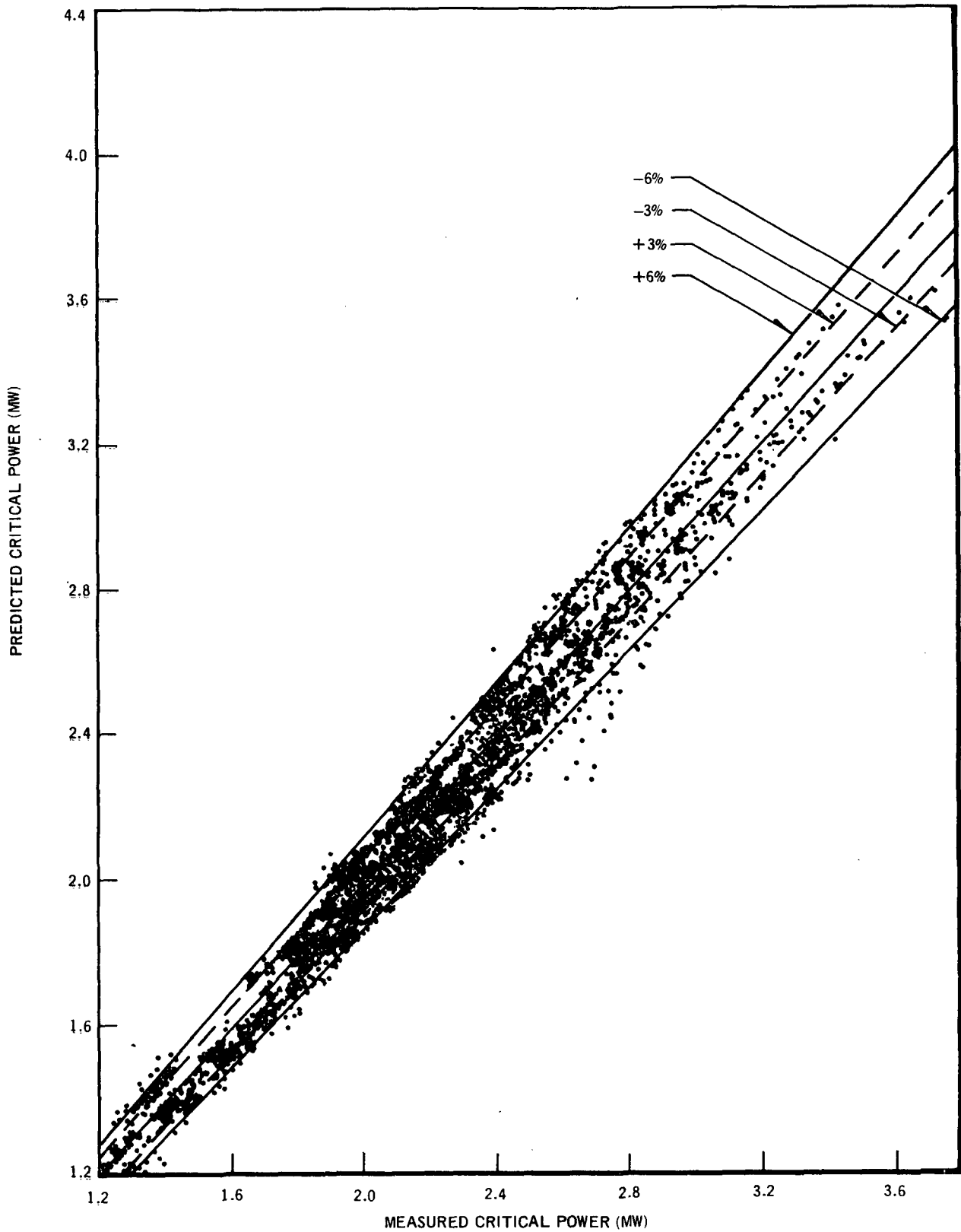


Figure 5-2. Predicted vs. Measured Critical Power, Columbia 7x7 Lattice 16-Rod Test Assemblies, 6-ft Uniform Axial Profile, Various Local Peaking Patterns,  $800 \leq P \leq 1400$  psia,  $0.25 \leq G/10^6 \leq 1.25$  lb/h-ft<sup>2</sup>,  $\Delta h_s \leq 100$  Btu/lb (84 points)



*Figure 5-3. \* Predicted vs. Measured Critical Power, Atlas 7x7 Lattice 16-Rod Test Assemblies, Various 12-ft Nonuniform Axial Profiles, Various Local Peaking Patterns,  $800 \leq P \leq 1400$  psia,  $0.25 \leq G/10^6 \leq 1.25$  lb/h-ft<sup>2</sup>,  $\Delta h_s \leq 100$  Btu/lb (2136 points)*

\*Discussion of the group of data below the -6.0% line is given in the response to Question 1-15, Appendix VII.

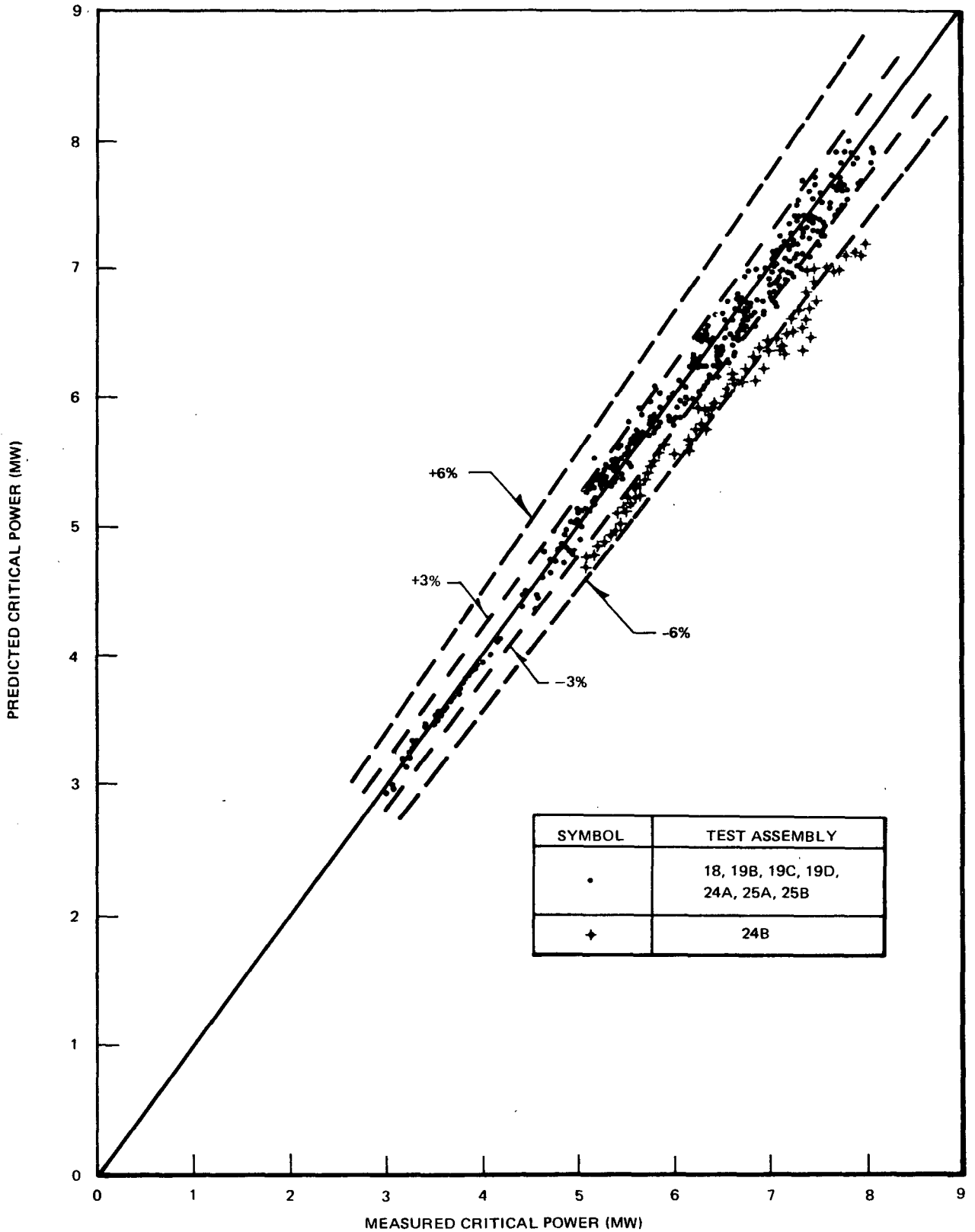


Figure 5-4.\* Predicted vs. Measured Critical Power, Atlas 7x7 Lattice 49-Rod Test Assemblies, 12-ft Cosine Profile, Various Local Peaking Patterns,  $800 \leq P \leq 1200$  psia,  $0.25 \leq G/10^6 \leq 1.25$  lb/h-ft<sup>2</sup>,  $\Delta h_s \leq 100$  Btu/lb (403 points)

\*Discussion of test assembly 24B is given in response to Question 1-10, Appendix VII.

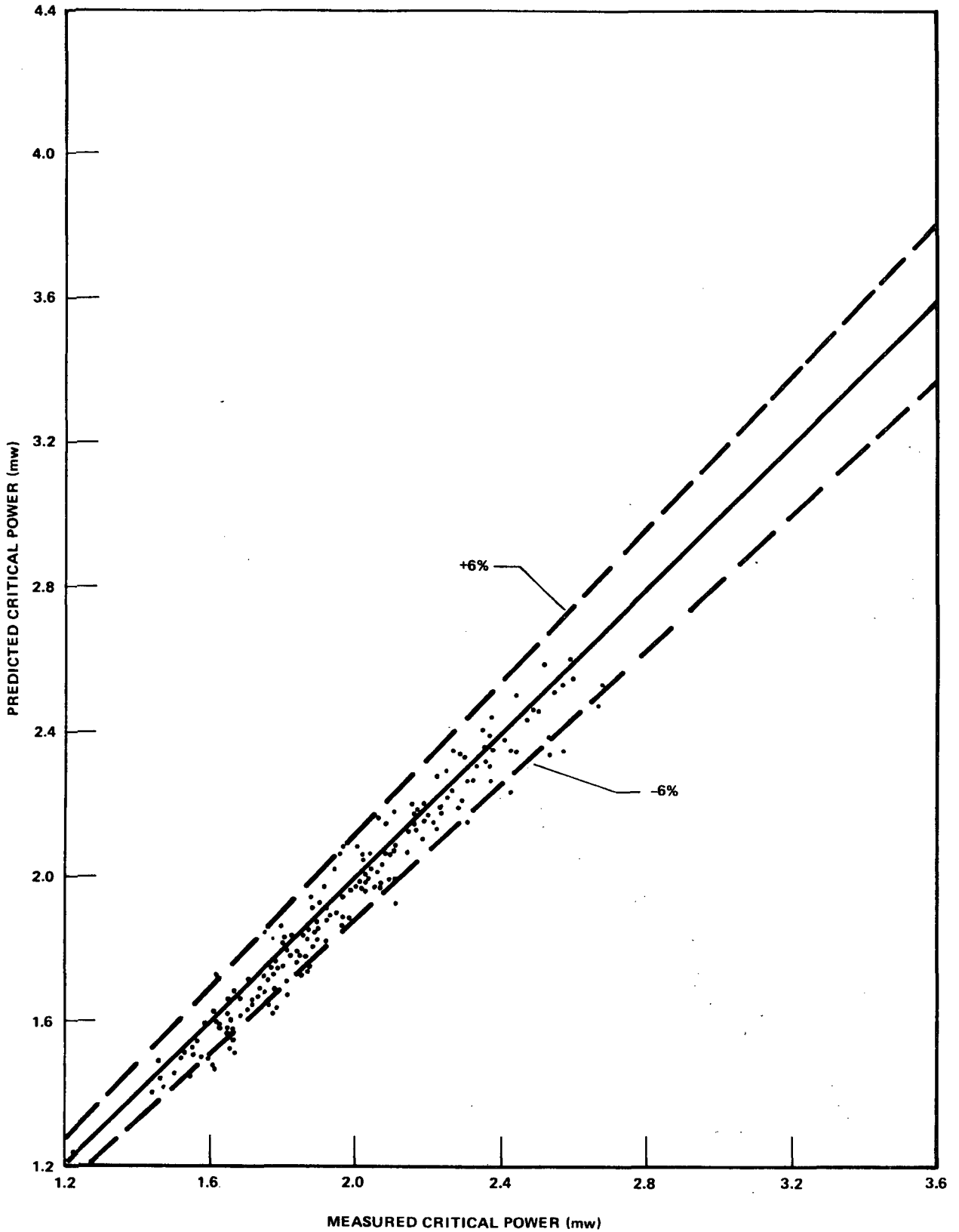


Figure 5-5.\* Predicted versus Measured Critical Power, Atlas 8 X 8 Lattice, 16-Rod Test Assemblies, 12-1/3-ft Cosine Profile, Various Local Peaking Patterns,  $800 \leq P \leq 1400$  psia,  $0.25 \leq G/10^6 \leq 1.25$  lb/h-ft<sup>2</sup>,  $\Delta h_s \leq 100$  Btu/lb (266 points)

\*See answer to Question 1-16, Appendix VII.

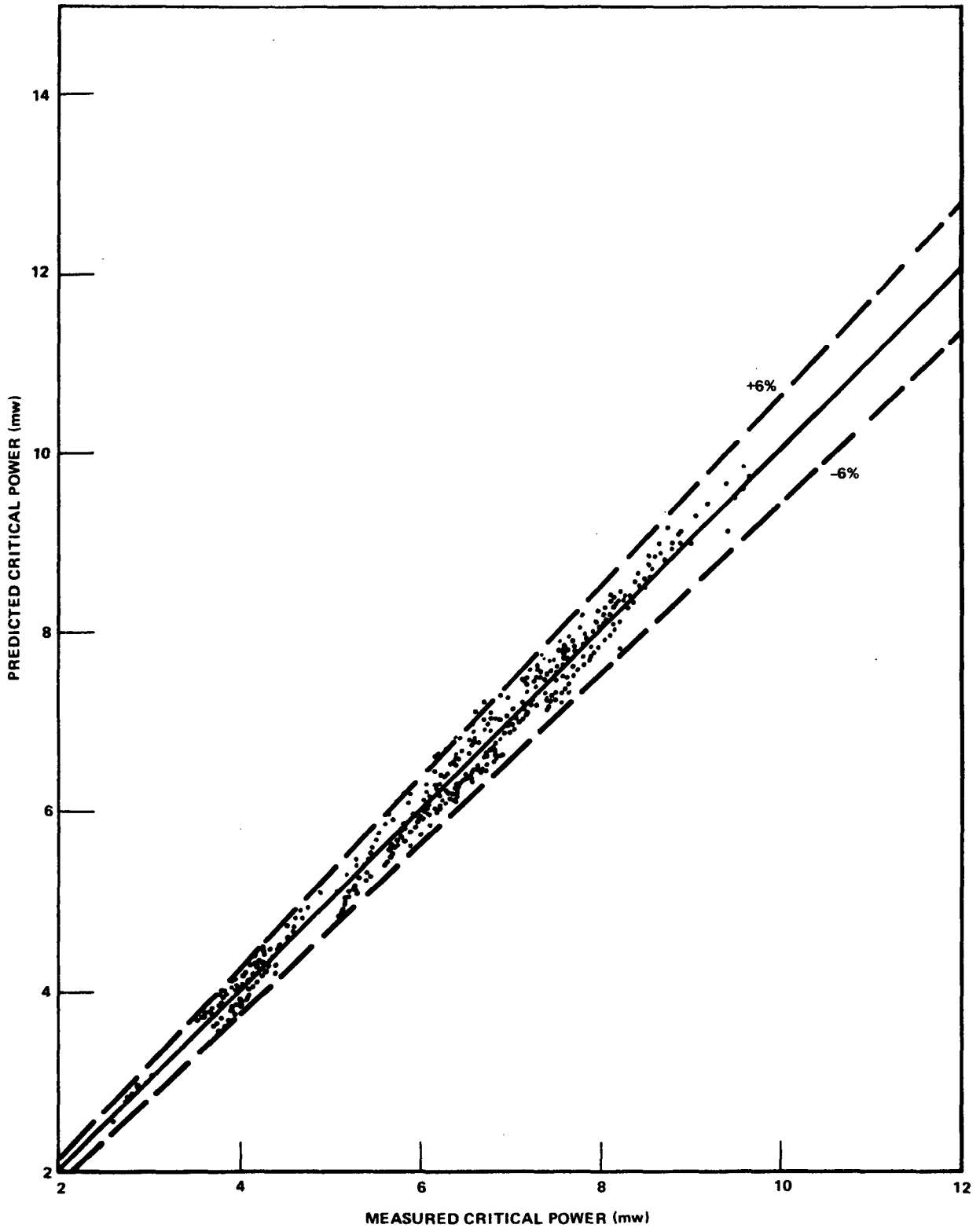


Figure 5-6. Predicted versus Measured Critical Power, Atlas 8 X 8 Lattice 64 Rod Test Assemblies, 12-1/3-ft Cosine Profile, Various Local Peaking Patterns,  $800 \leq P \leq 1400$  psia,  $0.25 \leq G/10^6 \leq 1.25$  lb/h-ft<sup>2</sup>,  $\Delta h_s \leq 100$  Btu/lb (426 points)



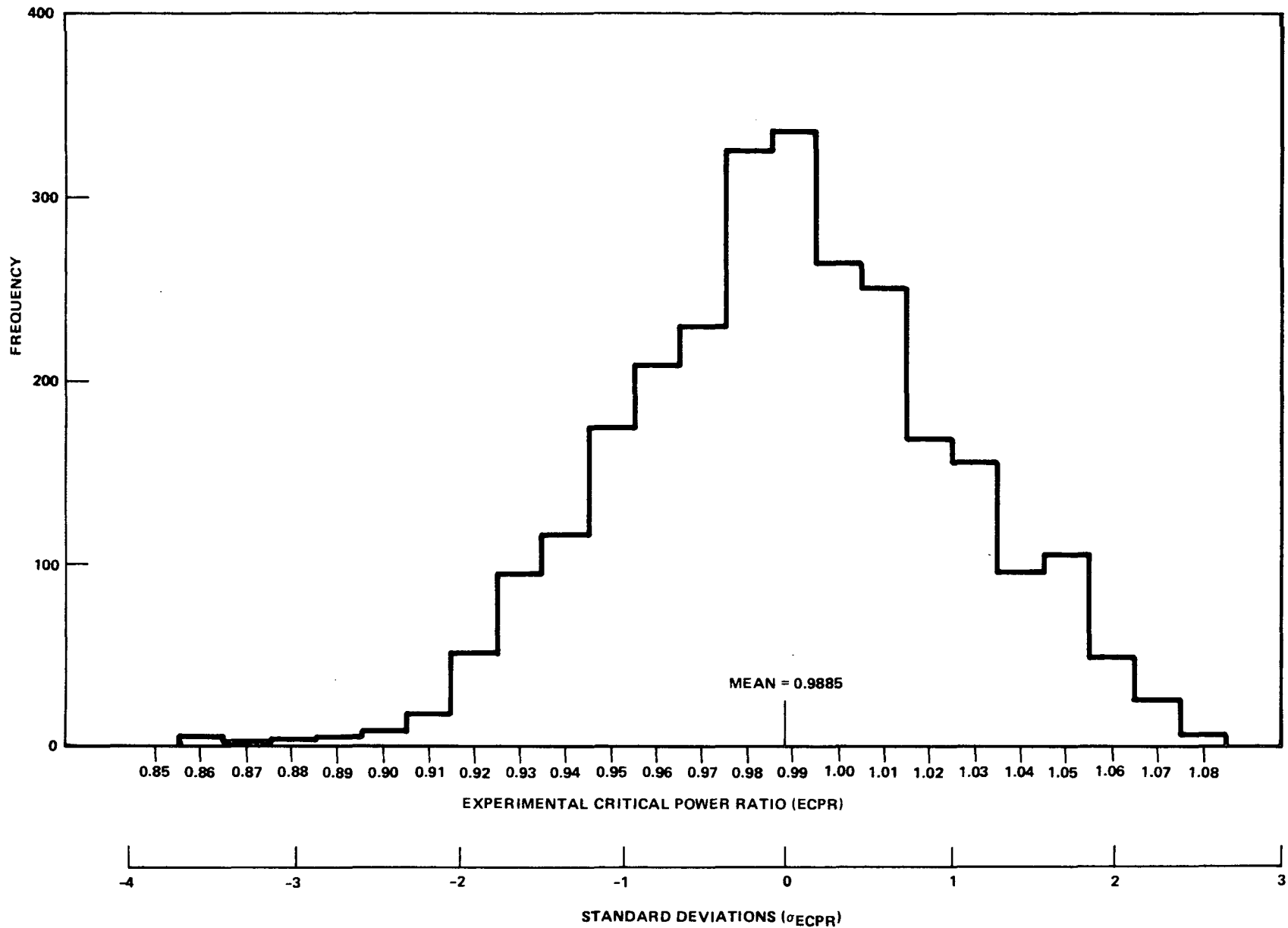


Figure 5-7. Histogram, Frequency vs ECPR, for 7 X 7 Lattice 16- and 49-Rod Test Assemblies (2700 Points)  
(Mean = 0.9885, Standard Deviation = 0.0360)

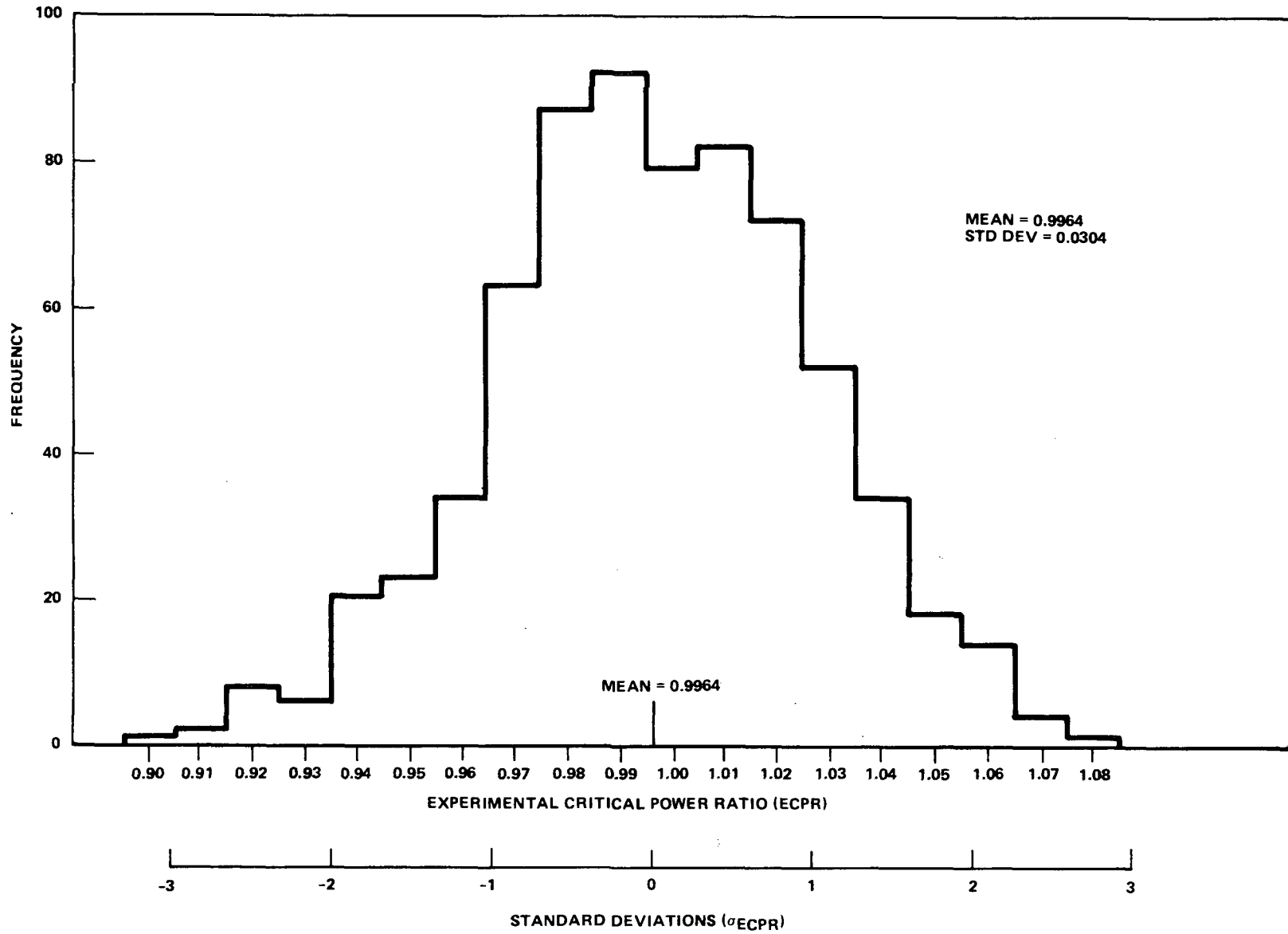


Figure 5-8. Histogram, Frequency vs ECPR, for 8 X 8 Lattice, 16- and 64-Rod Test Assemblies (692 points)

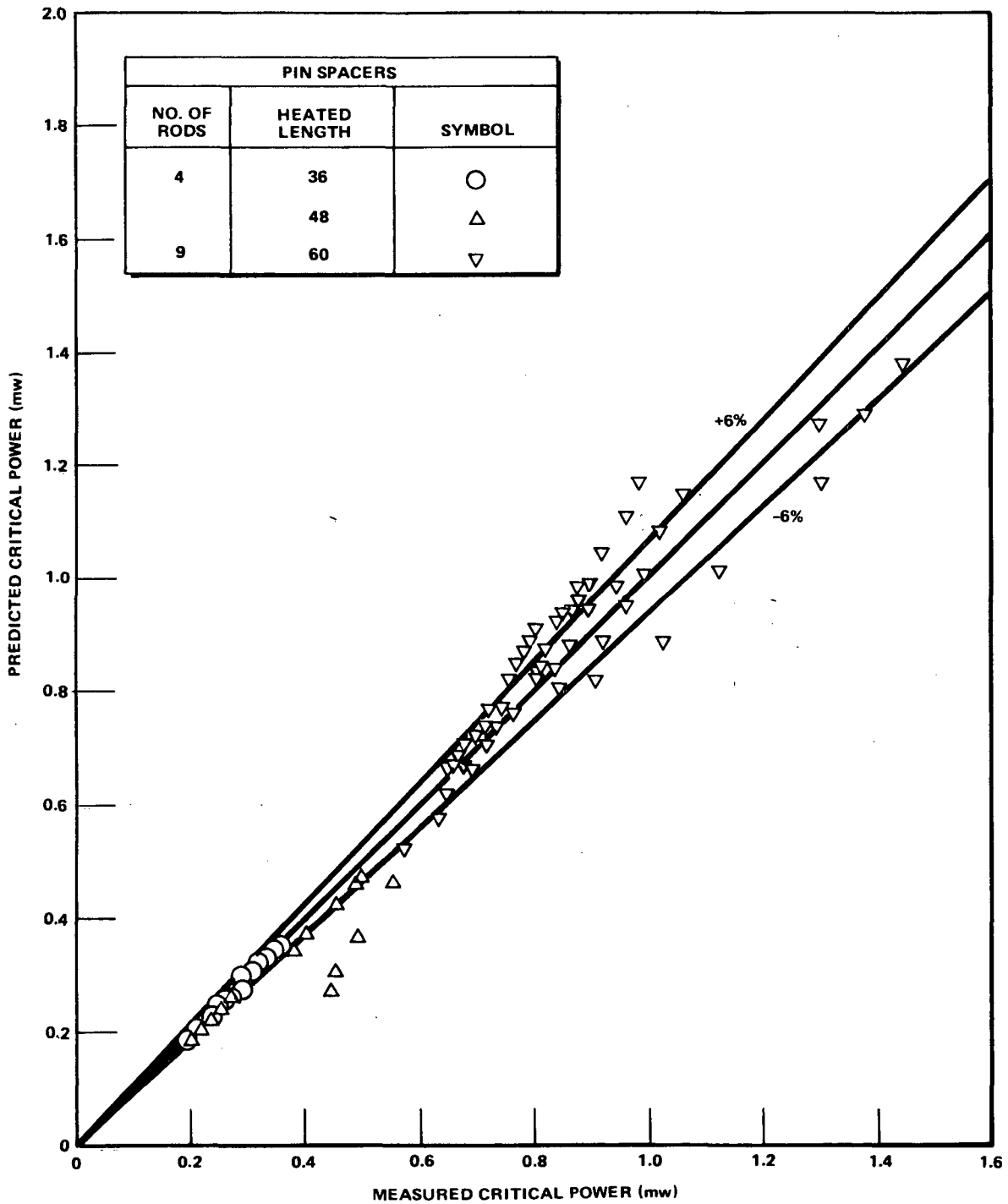


Figure 5-9. Predicted vs Measured Critical Power, Early 4-Rod and 9-Rod Test Assemblies, Uniform Axial Flux Profile, Various Heated Lengths,  $600 \leq P \leq 1400$  psia,  $0.20 \leq G/10^6 \leq 1.50$  lb/h-ft<sup>2</sup>,  $\Delta h_s \leq 200$  Btu/lb

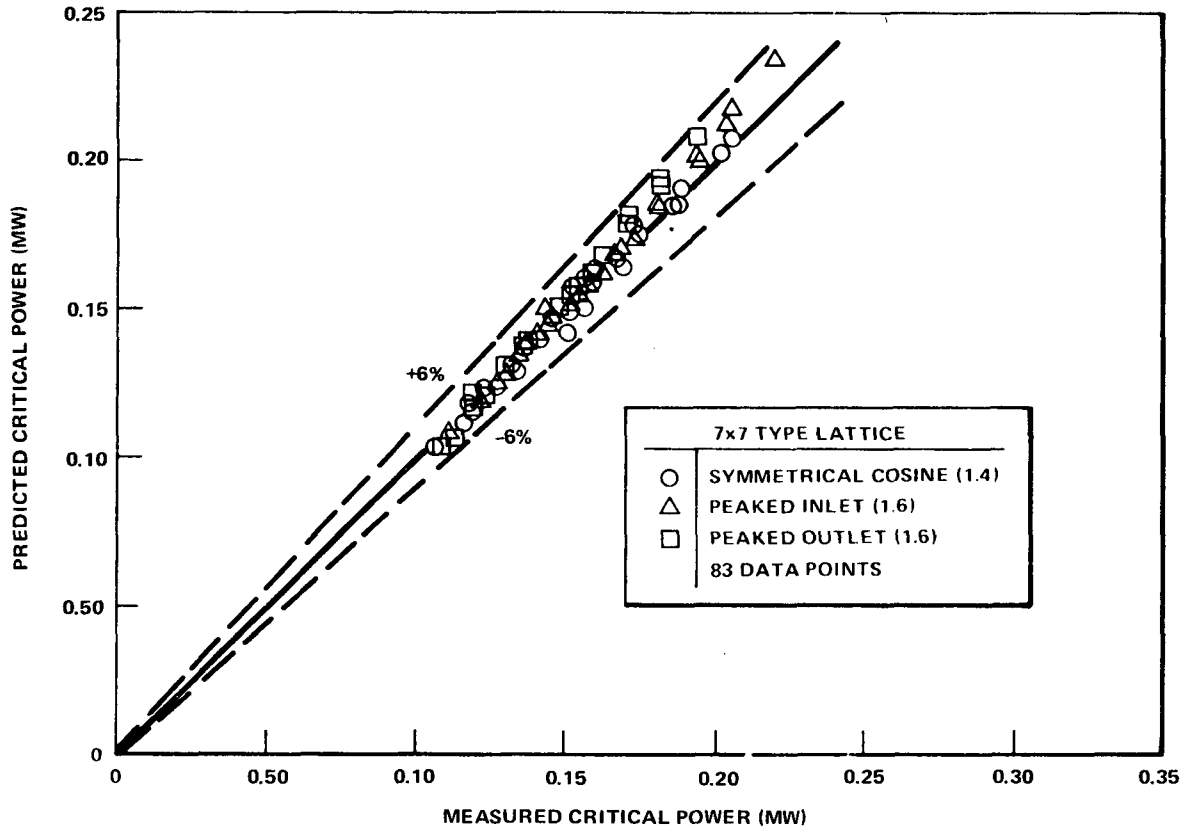


Figure 5-10. Predicted vs Measured Critical Power, 7 X 7 Lattice, 16-Rod X 144-in. Heated Length Freon Data, Uniform Local Peaking

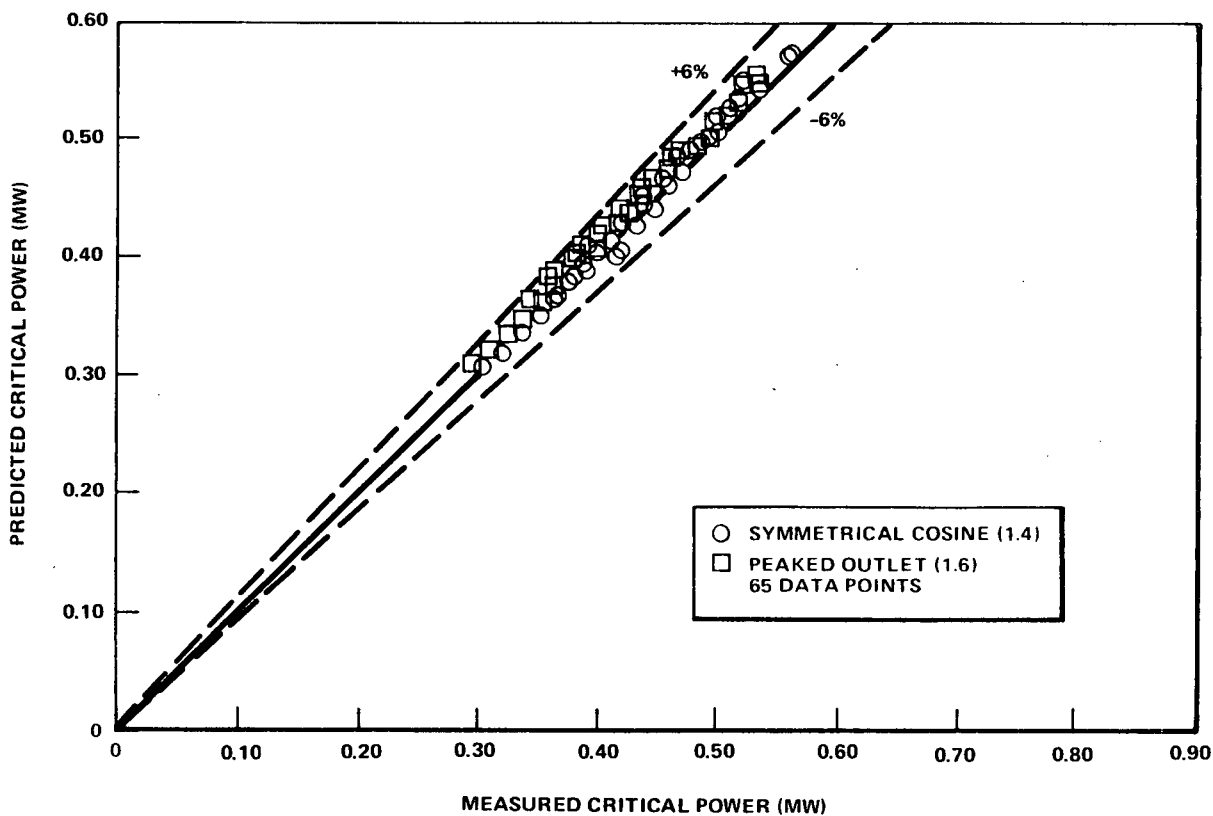


Figure 5-11. Predicted vs Measured Critical Power, 7 X 7 Lattice, 49-Rod X 144-in. Heated Length Freon Data, Uniform Local Peaking

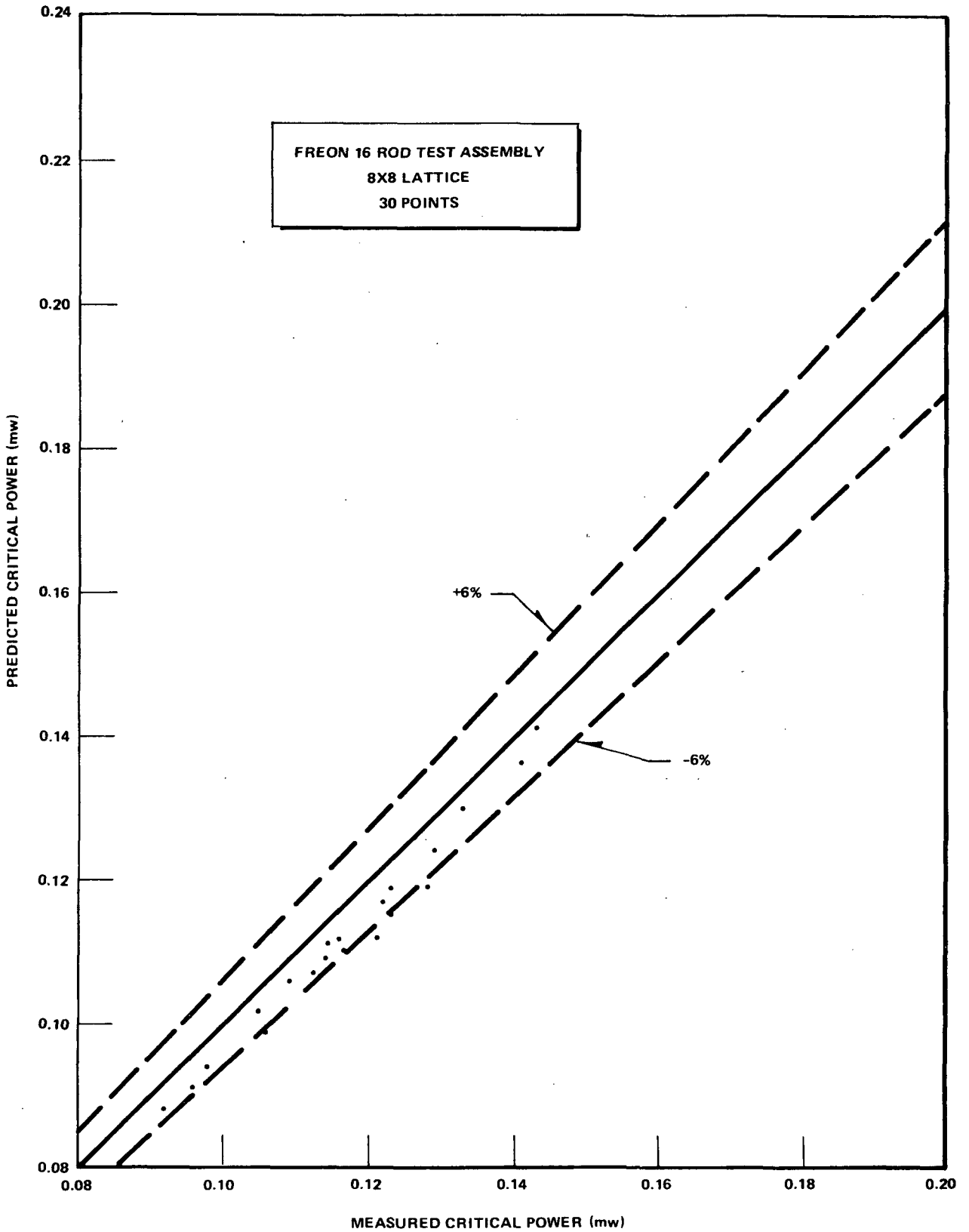


Figure 5-12. Freon 16-Rod Test Assembly, 8 X 8 Lattice, 30 Points

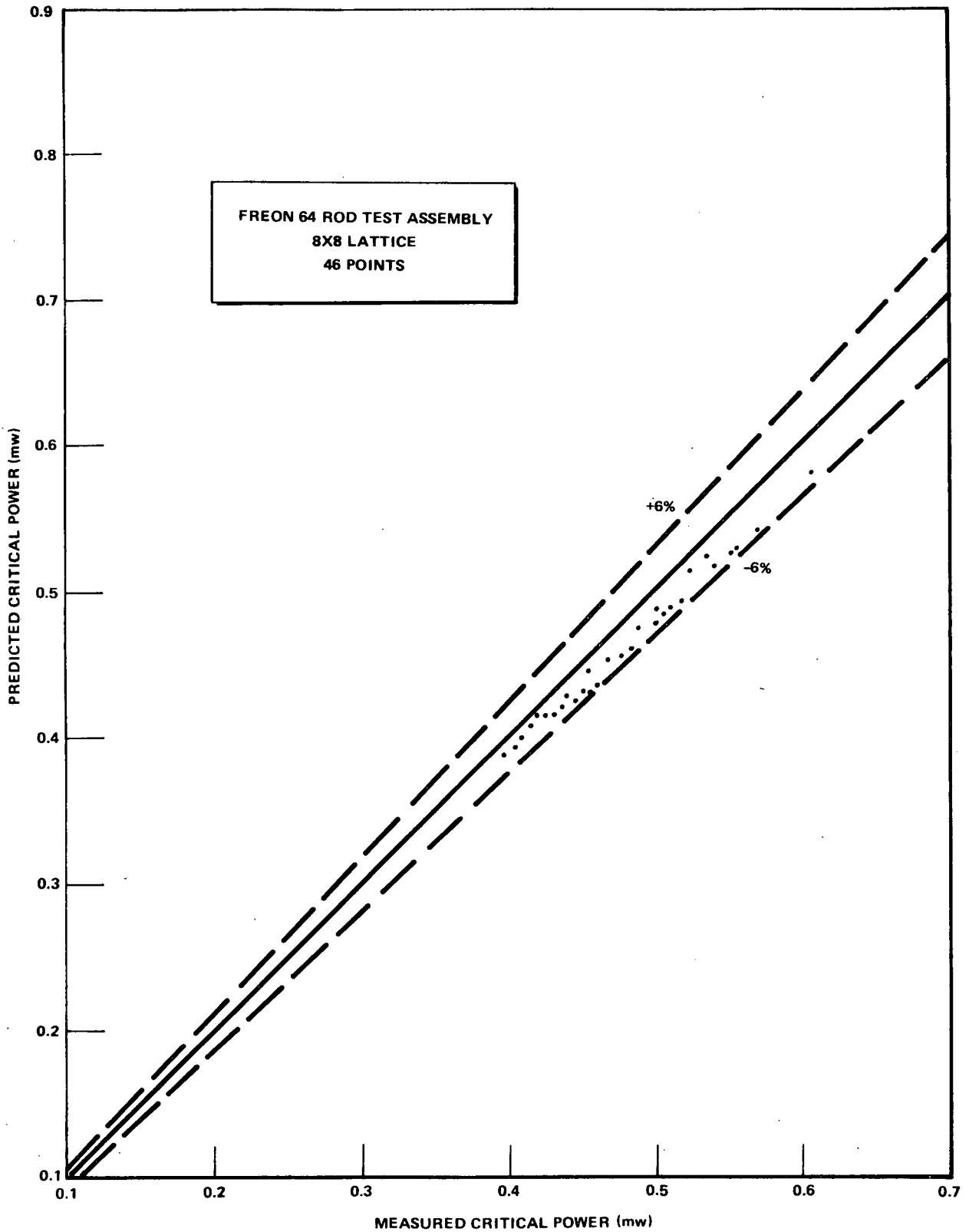


Figure 5-13. Freon 64-Rod Test Assembly, 8 X 8 Lattice, 46 Points

1.14

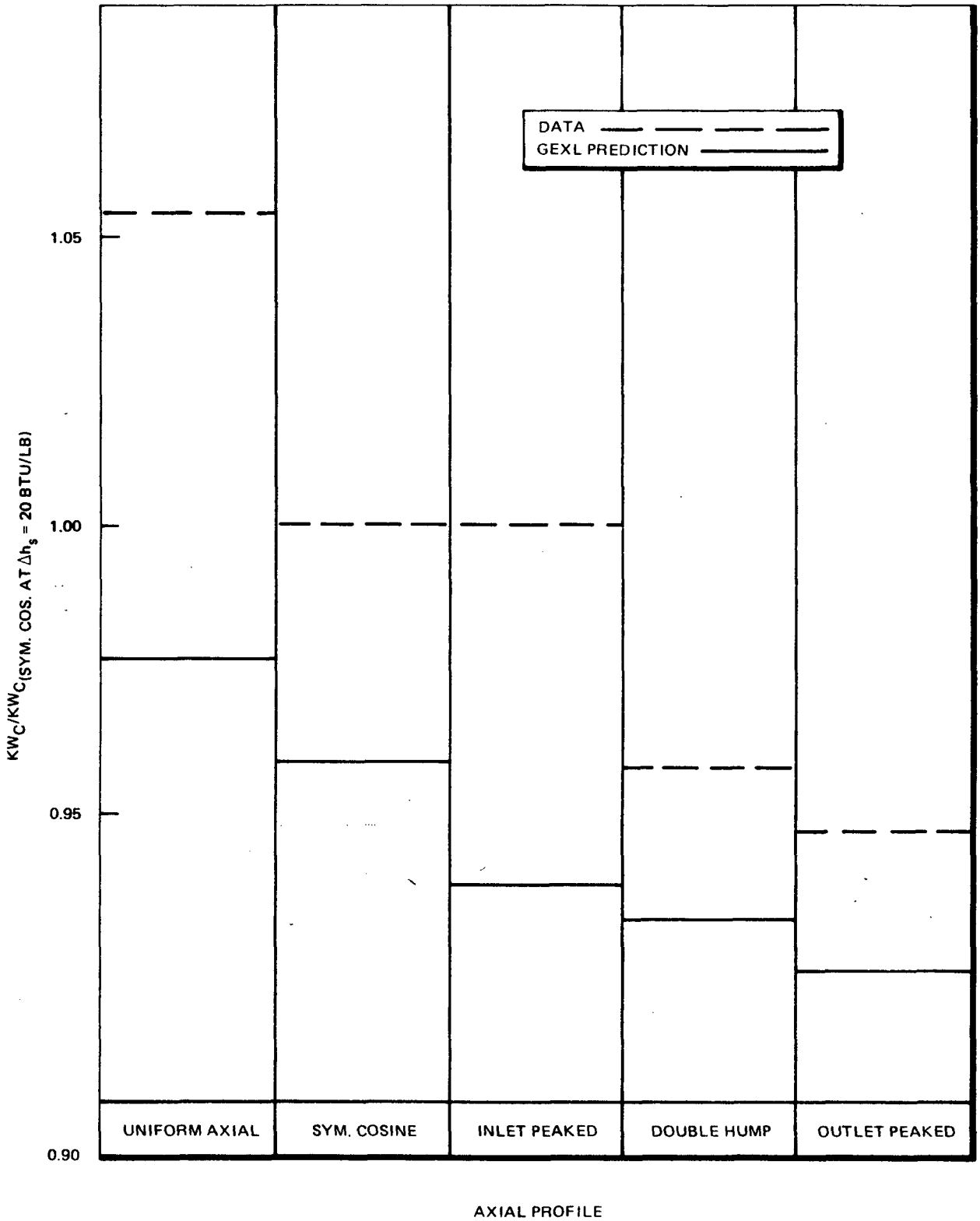


Figure 5-14. Predicted and Measured Critical Powers (Normalized with Respect to Measured Value for Symmetrical Cosine Axial Profile at  $\Delta h_s = 20$  Btu/lb) vs. Inlet Subcooling, Various Axial Profiles, 1.23/1.26 3-Rod Corner Peaking, 1000 psia,  $G = 1 \times 10^6$  lb/h-ft<sup>2</sup>



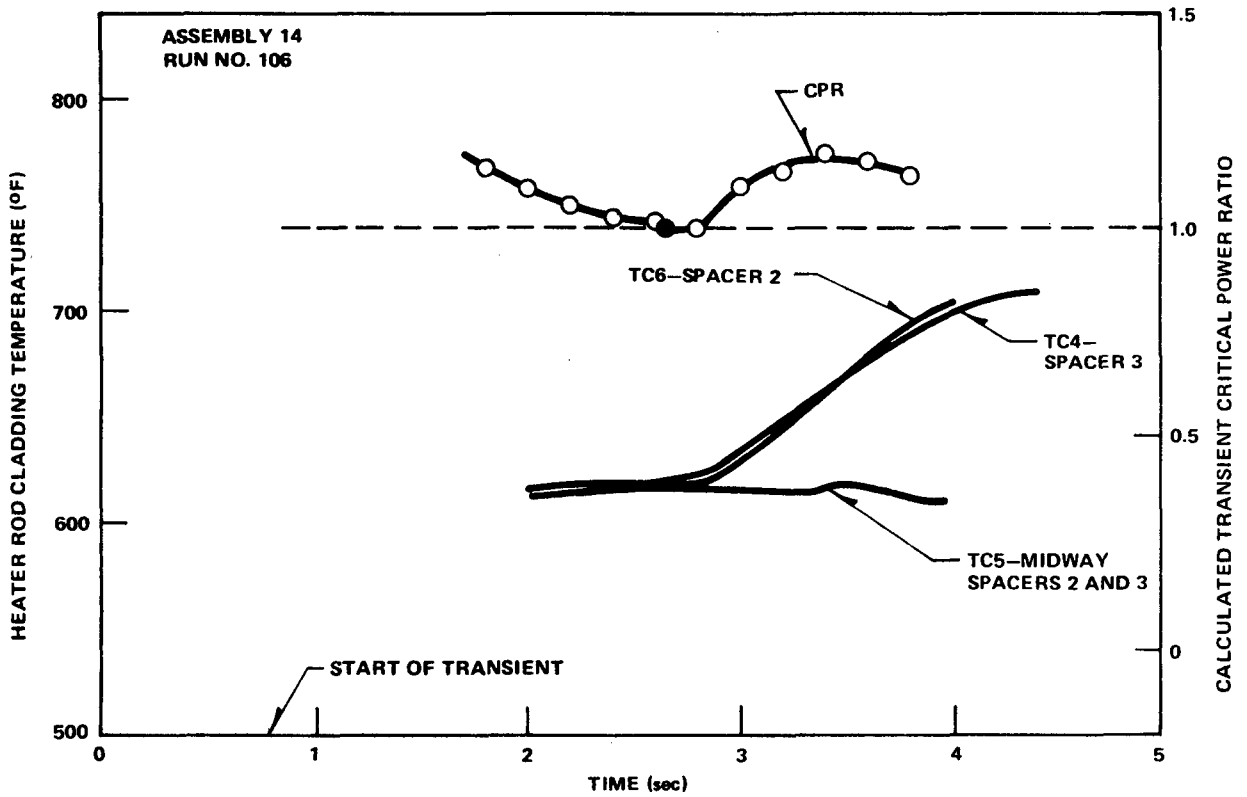


Figure 5-15. Calculated Transient Critical Power Ratio and Measured Heater Rod Cladding Temperature Vs Time

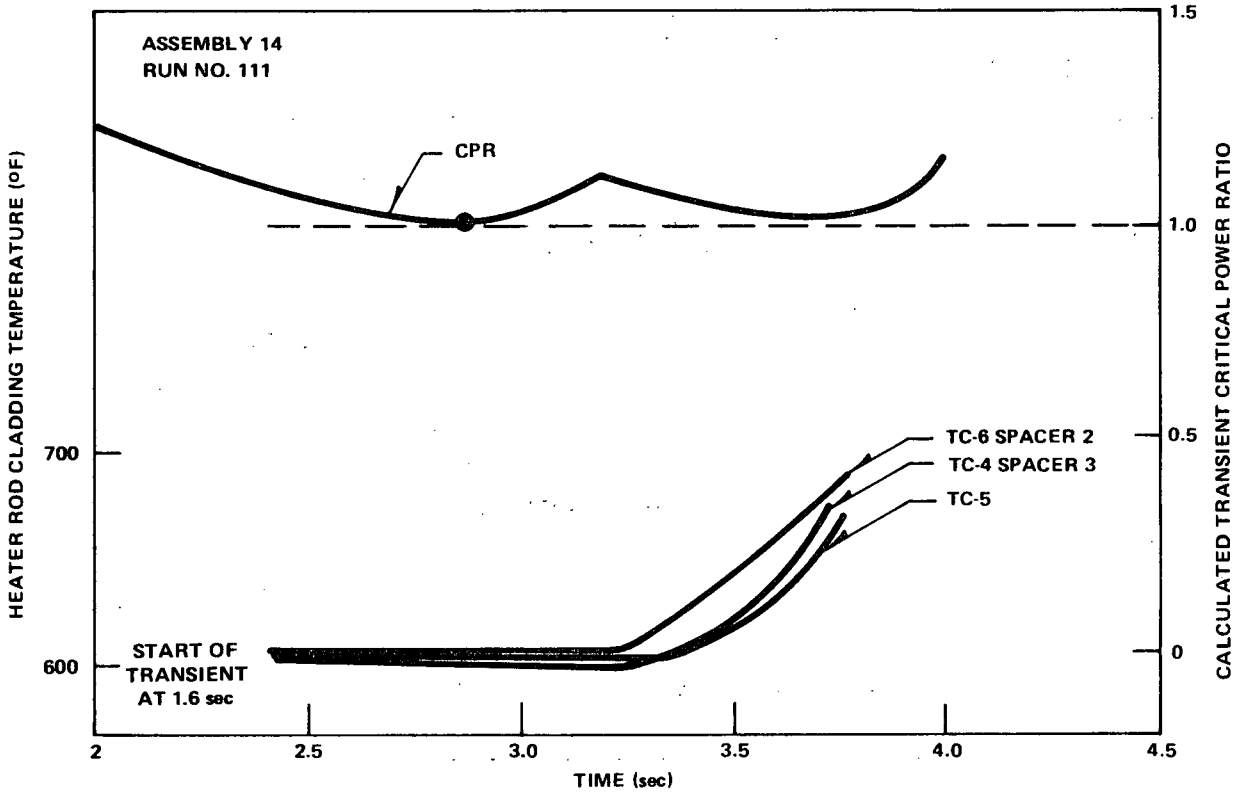


Figure 5-16. Calculated Transient Critical Power Ratio and Measured Heater Rod Cladding Temperature Vs Time

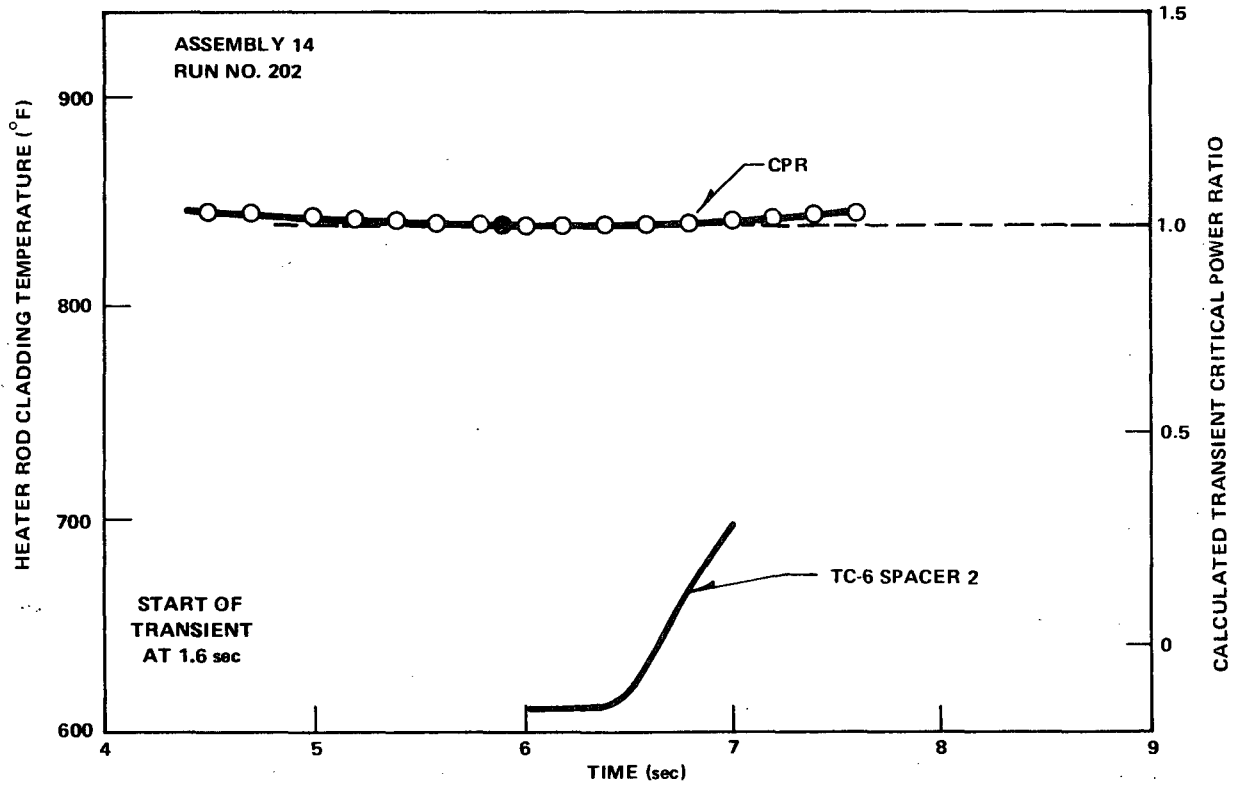


Figure 5-17. Calculated Transient Critical Power Ratio and Measured Heater Rod Cladding Temperature Vs Time

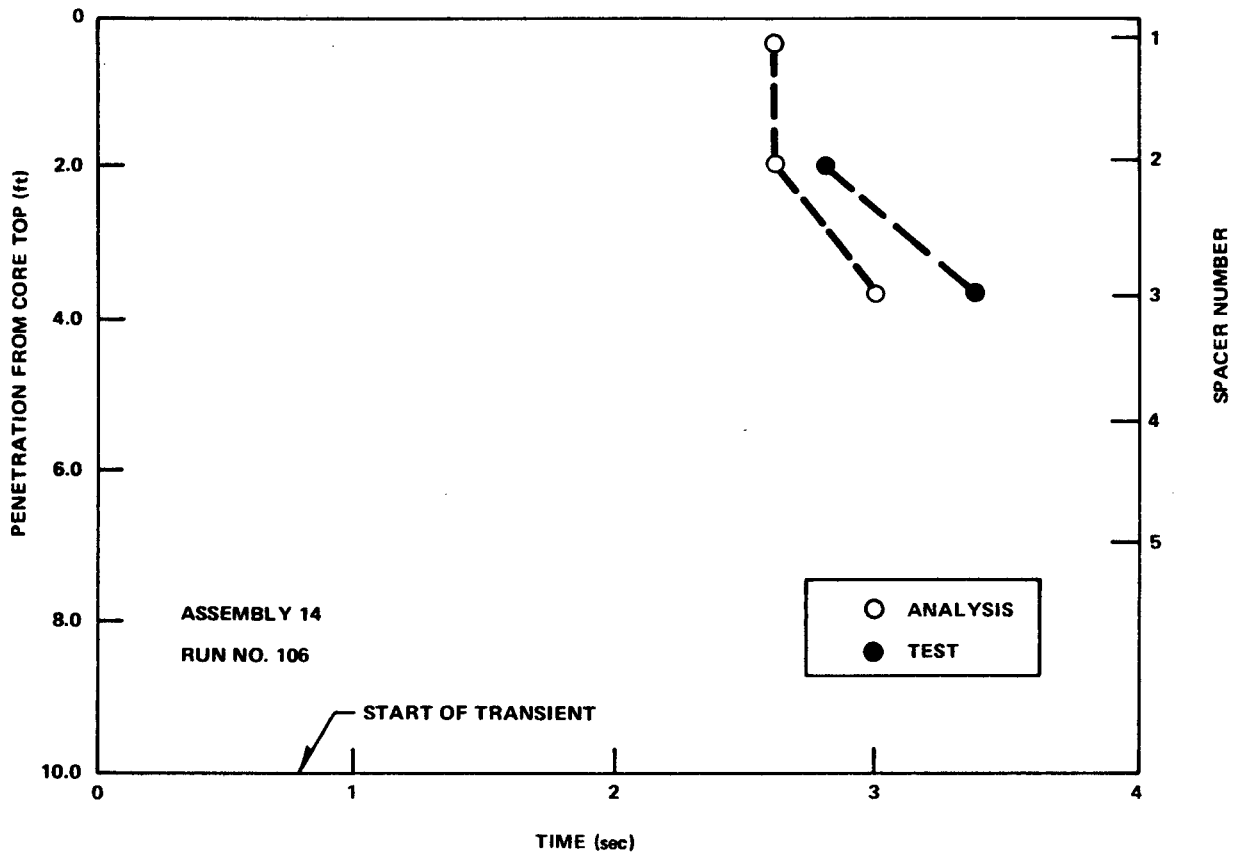


Figure 5-18. Axial Penetration of Boiling Transition Vs Time

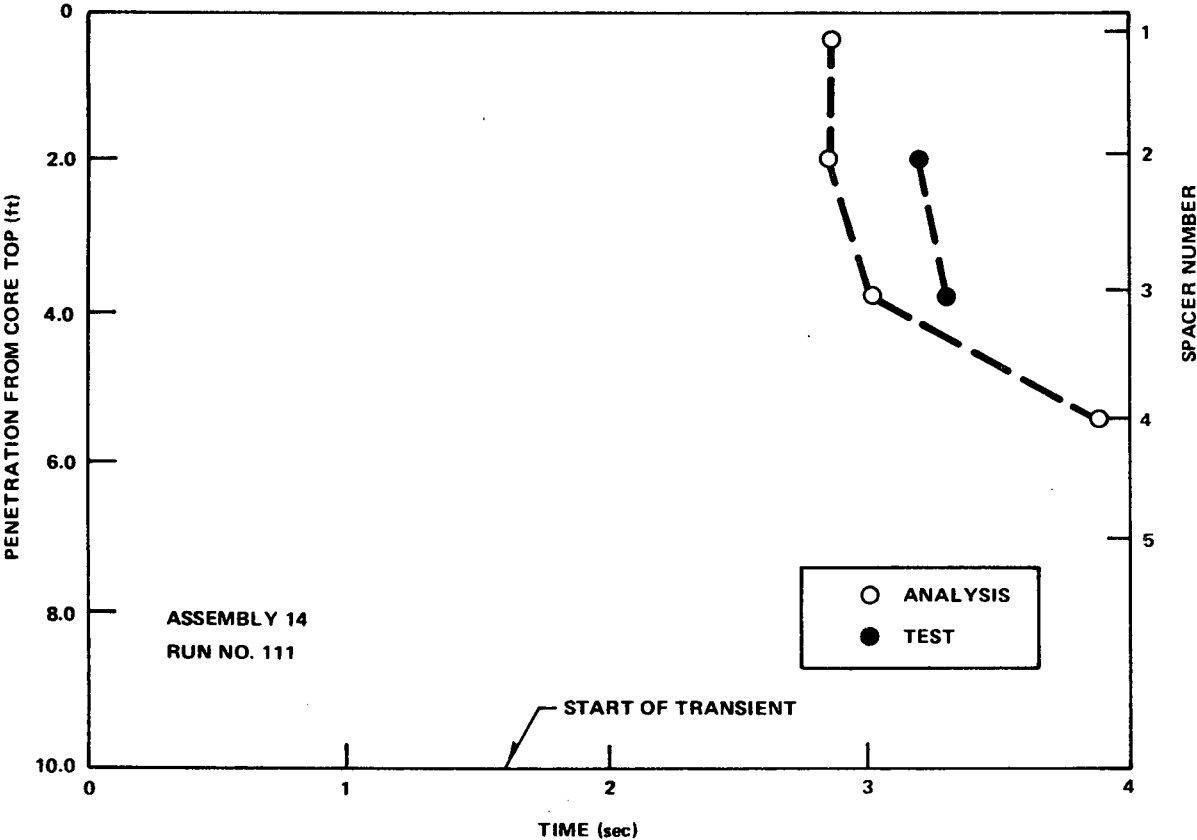


Figure 5-19. Axial Penetration of Boiling Transition Vs Time

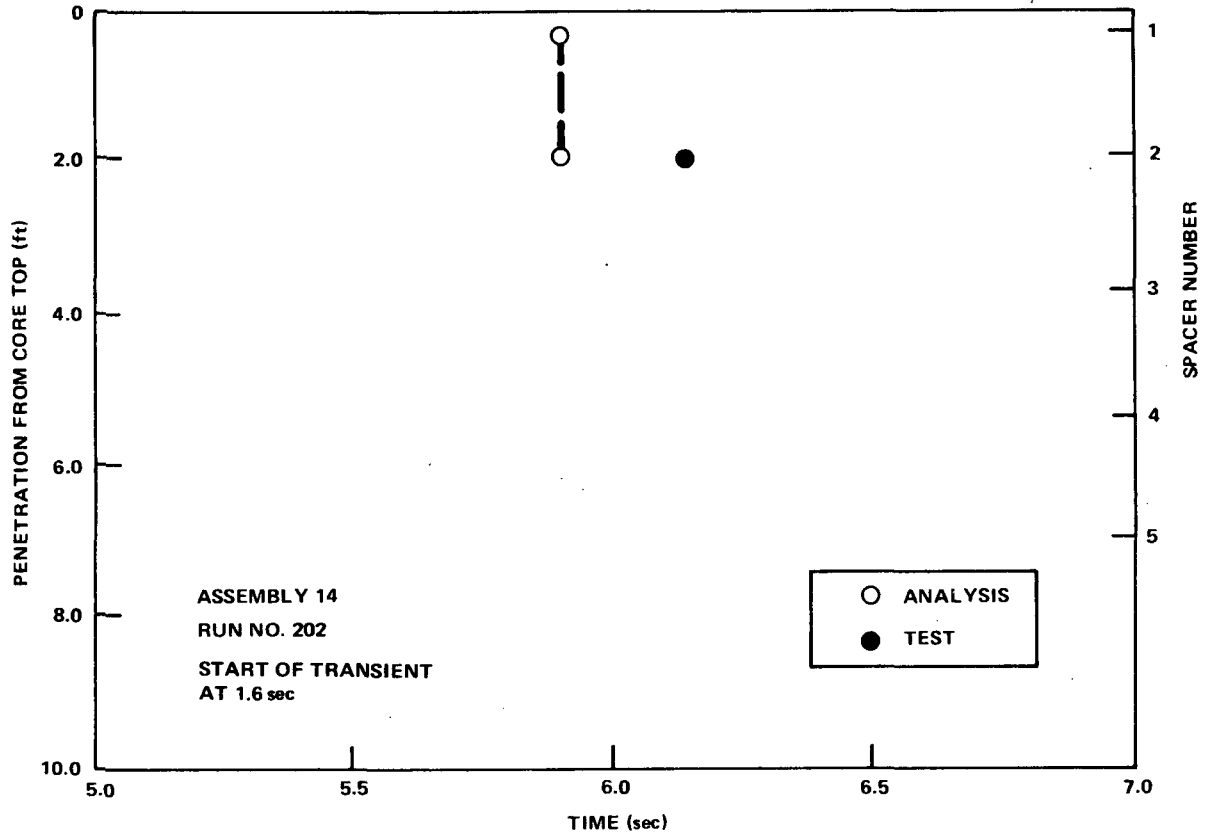


Figure 5-20. Axial Penetration of Boiling Transition Vs Time

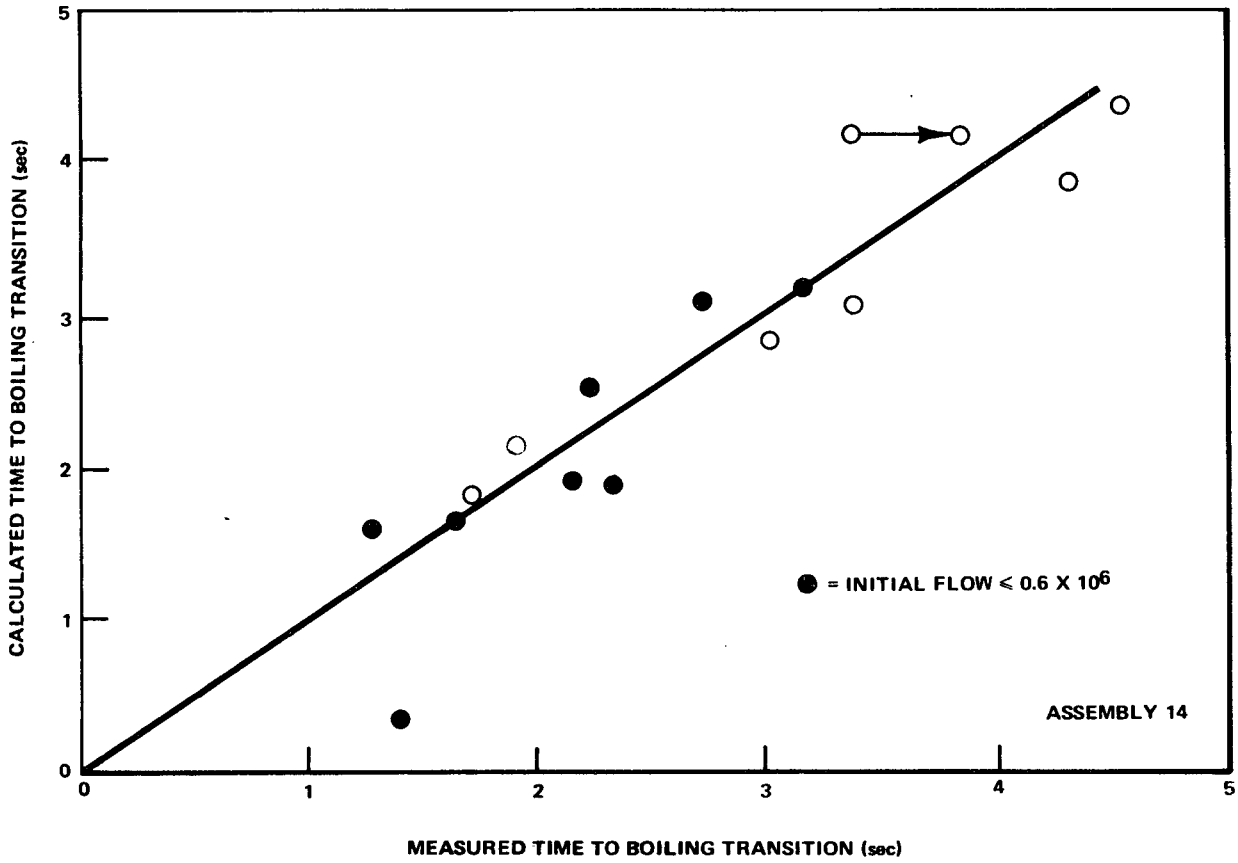


Figure 5-21. Calculated Time versus Measured Time to Initial Boiling Transition

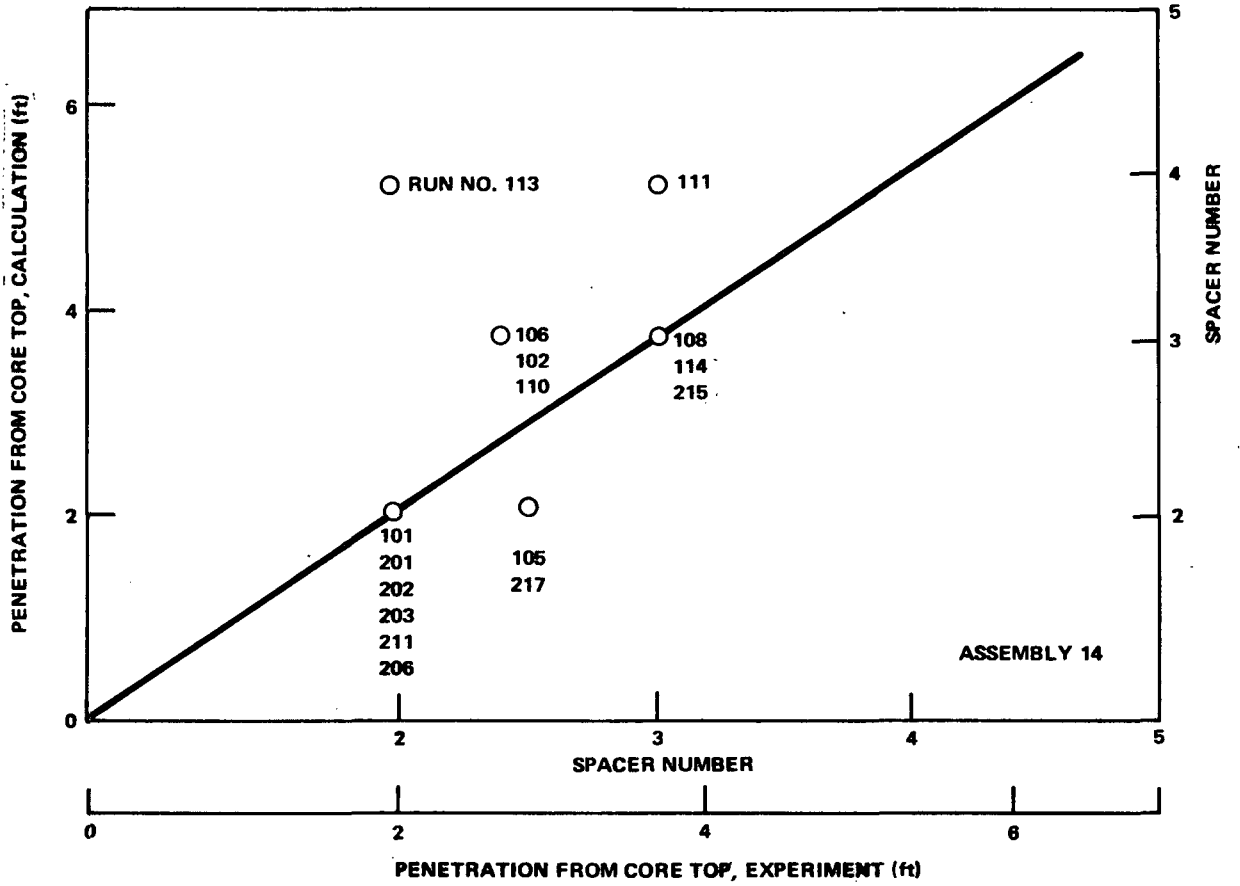


Figure 5-22. Boiling Transition Axial Penetration Calculated Vs Measured



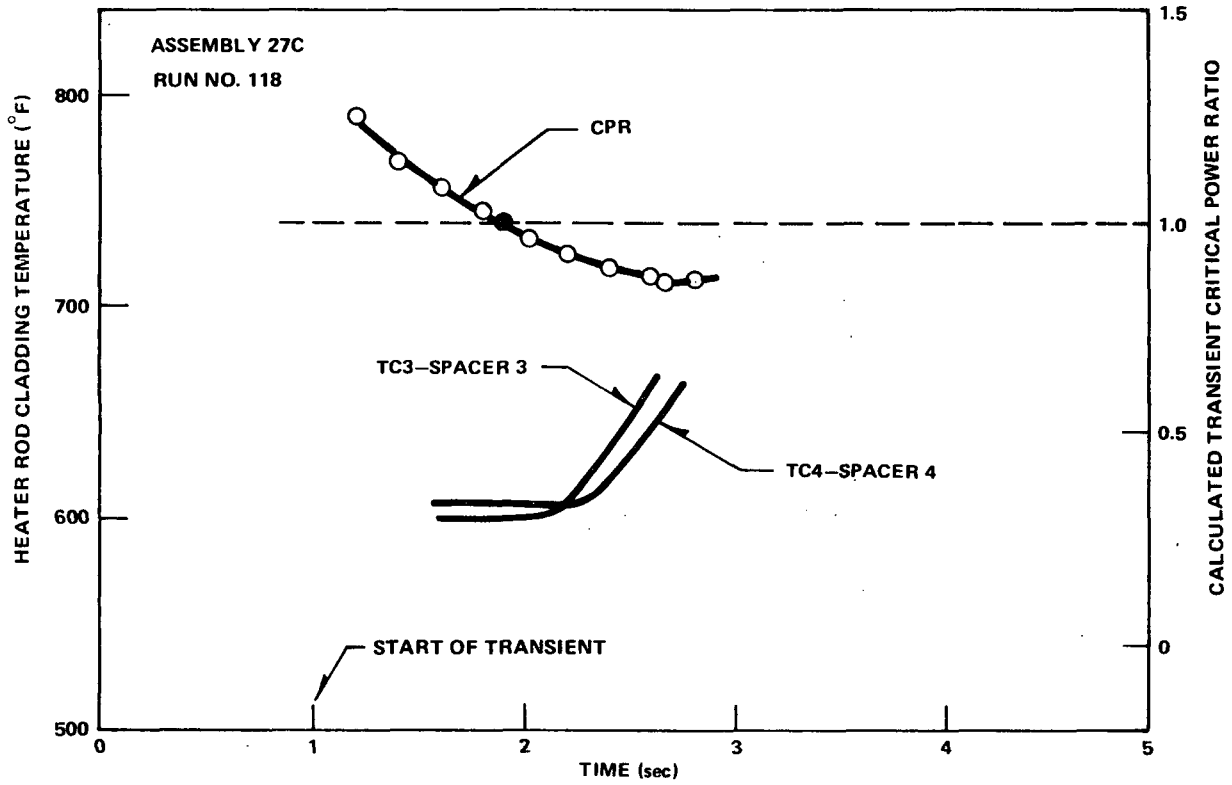


Figure 5-23. Calculated Transient Critical Power Ratio and Measured Heater Rod Cladding Temperature Vs Time

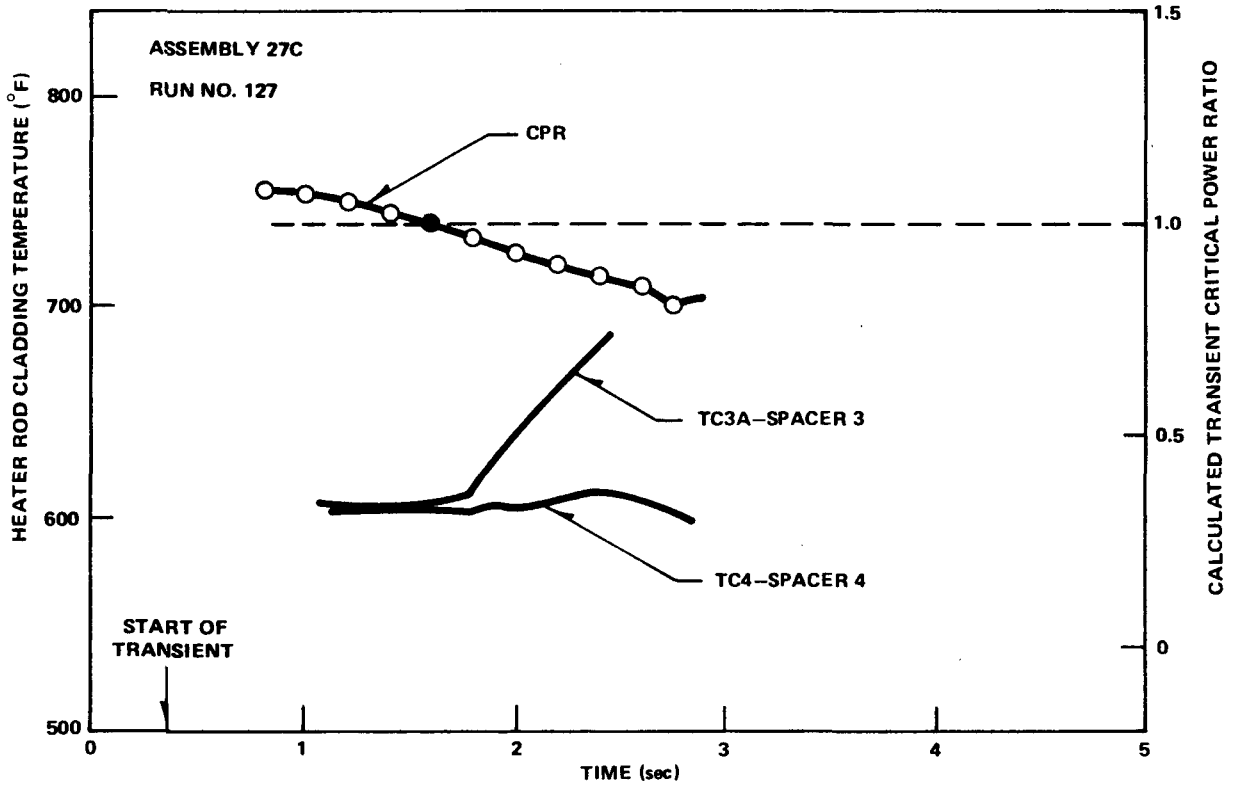


Figure 5-24. Calculated Transient Critical Power Ratio and Measured Heater Rod Cladding Temperature Vs Time

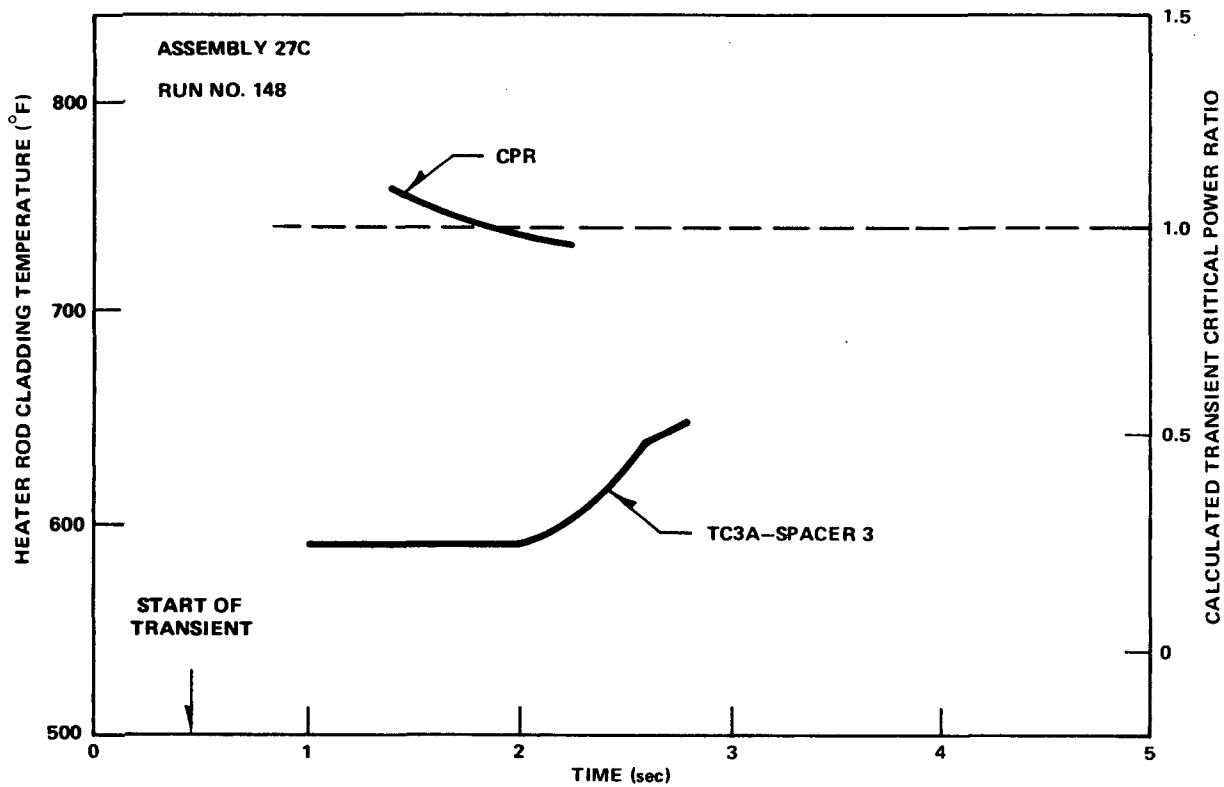


Figure 5-25. Calculated Minimum Critical Power Ratio and Measured Heater Rod Cladding Temperature Vs Time

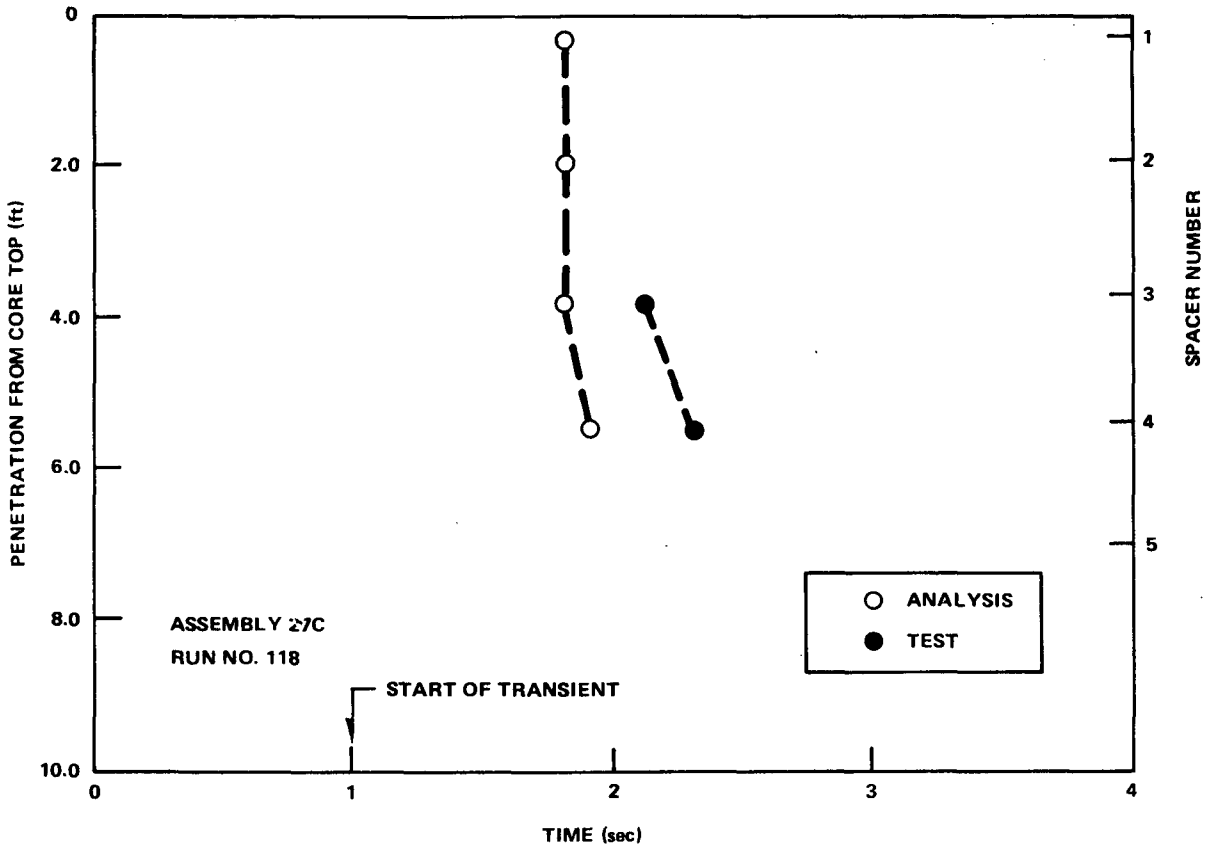


Figure 5-26. Axial Penetration of Boiling Transition Vs Time

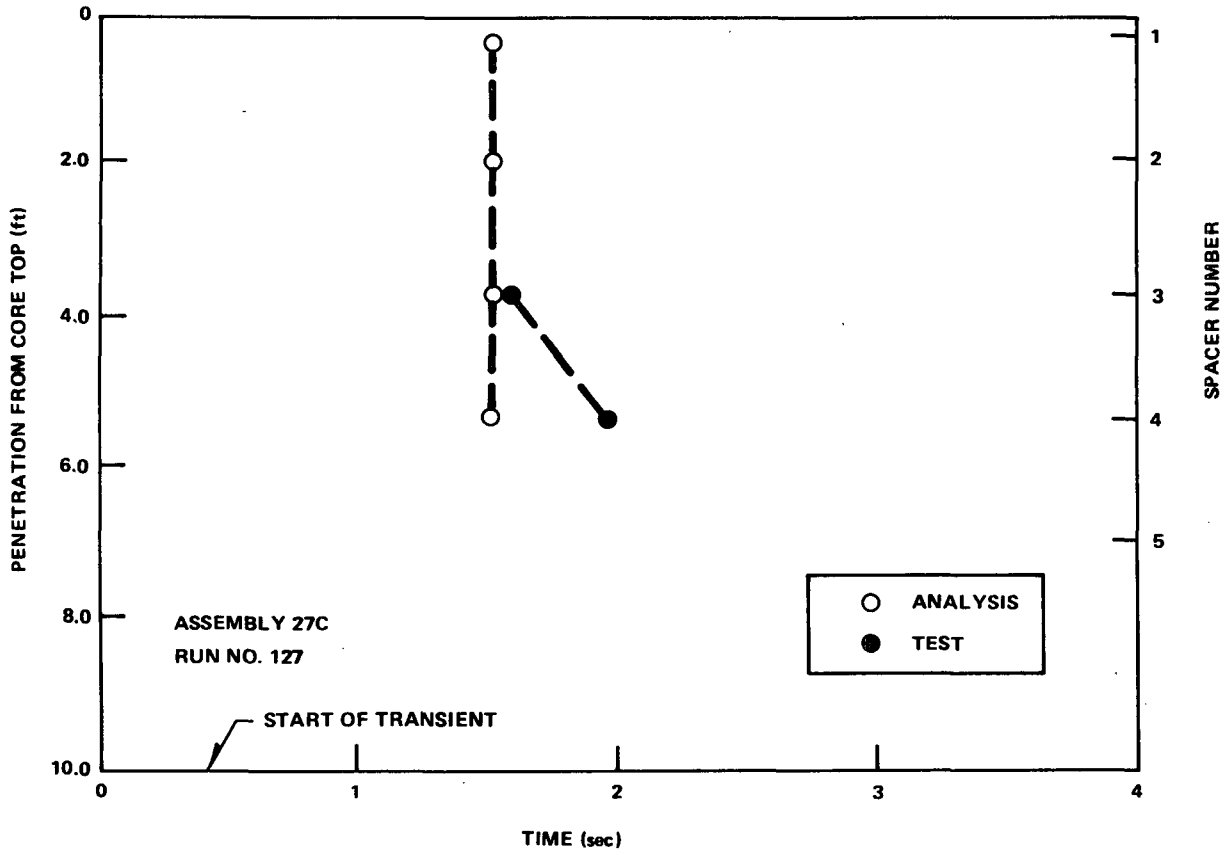


Figure 5-27. Axial Penetration of Boiling Transition Vs Time

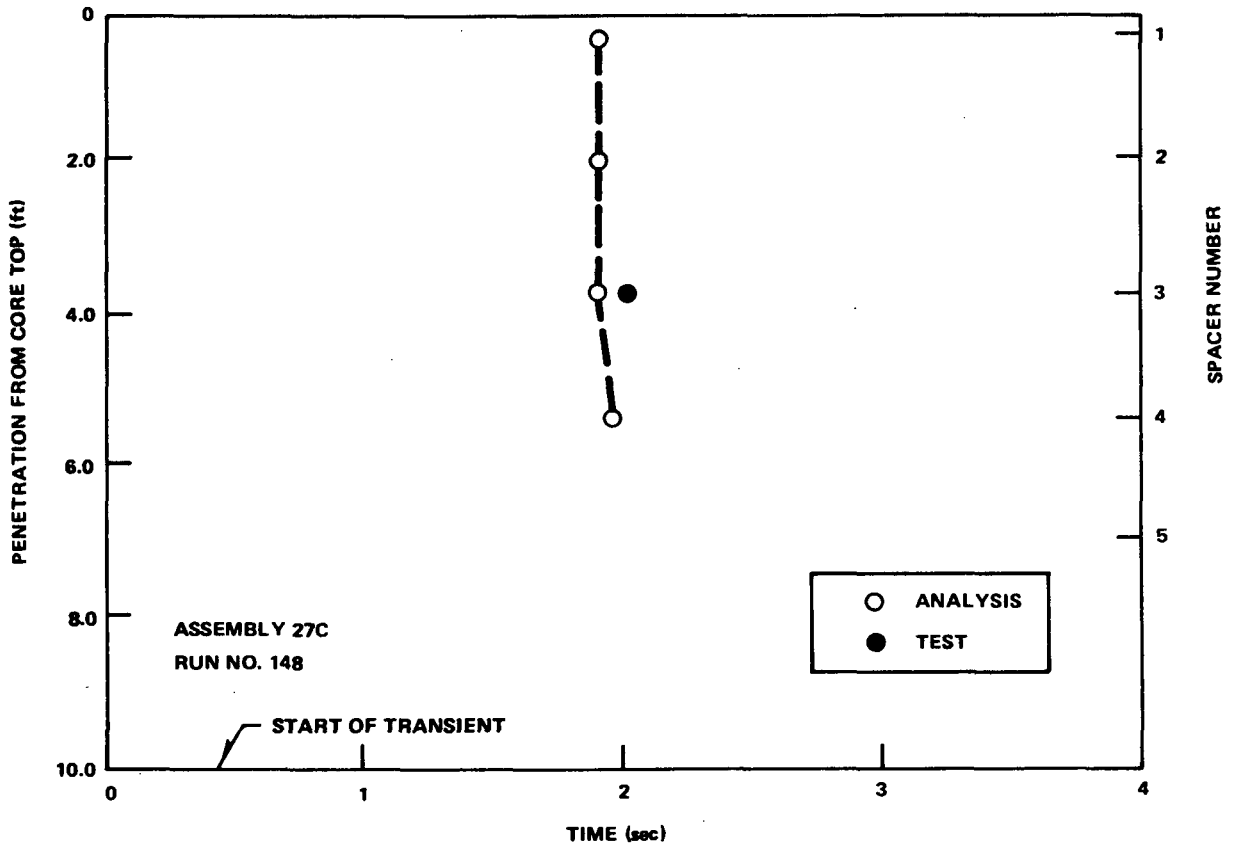


Figure 5-28. Axial Penetration of Boiling Transition Vs Time

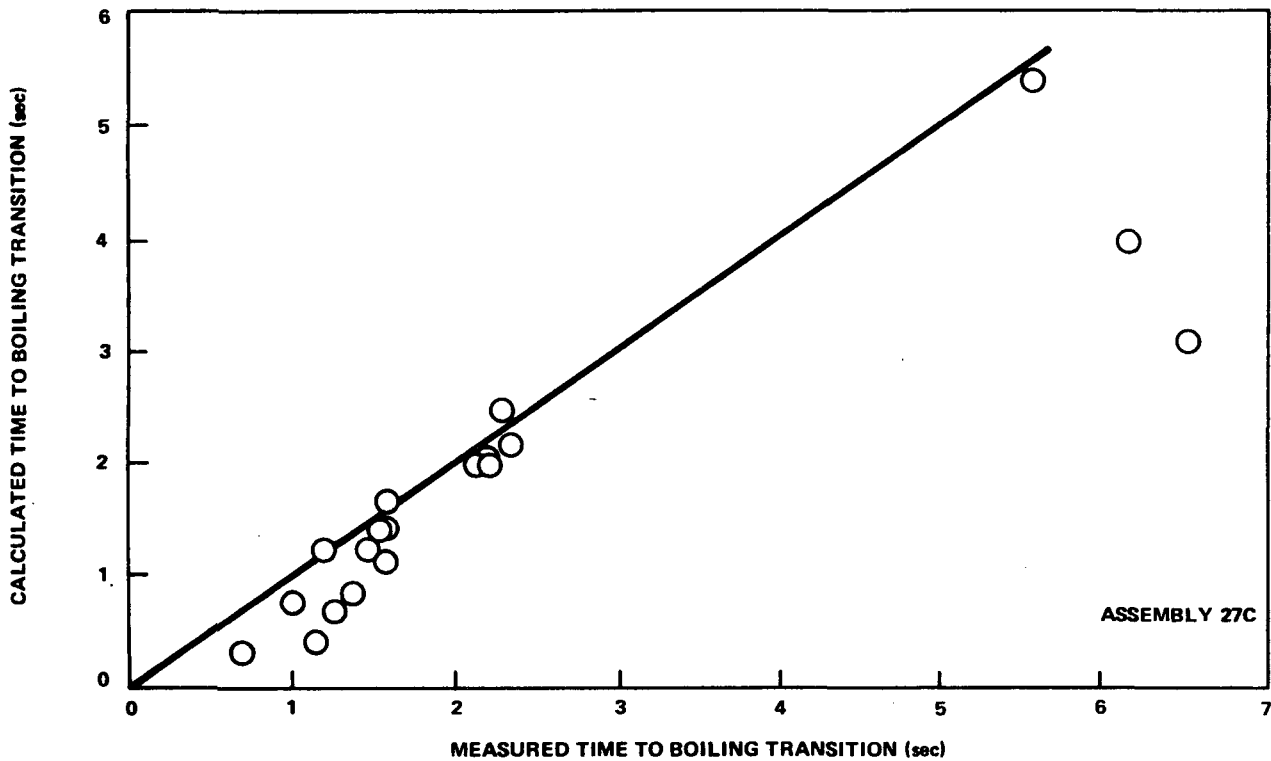


Figure 5-29. Calculated Time Vs Measured Time to Initial Boiling Transition

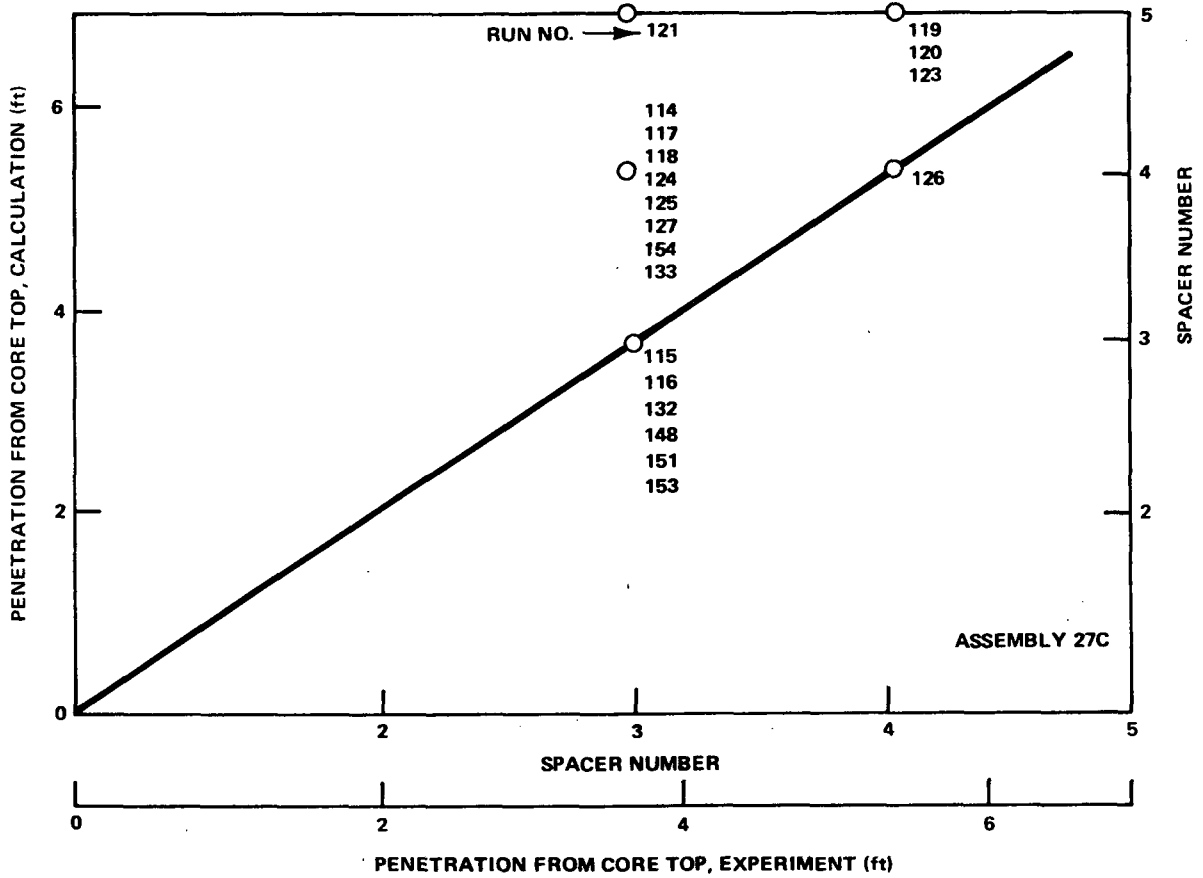


Figure 5-30. Boiling Transition Axial Penetration – Calculated Versus Measured



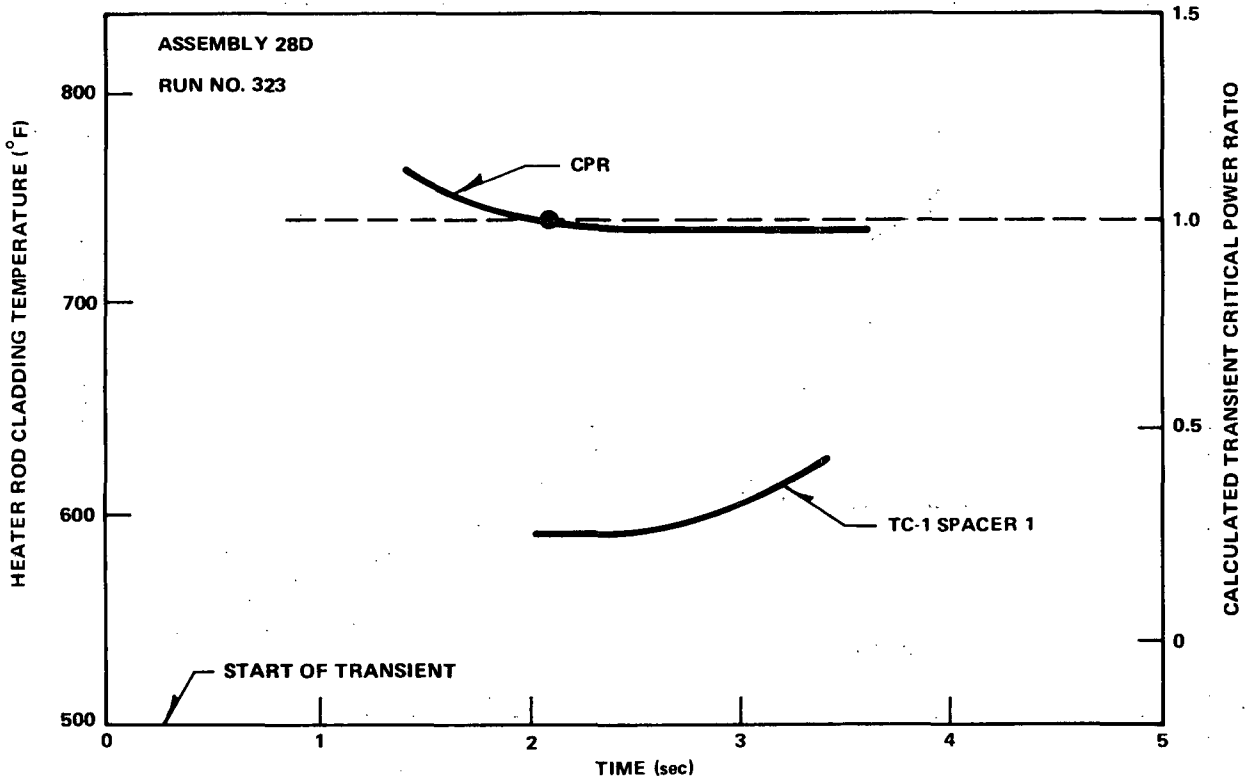


Figure 5-31. Calculated Transient Critical Power Ratio and Measured Heater Rod Cladding Temperature Vs Time

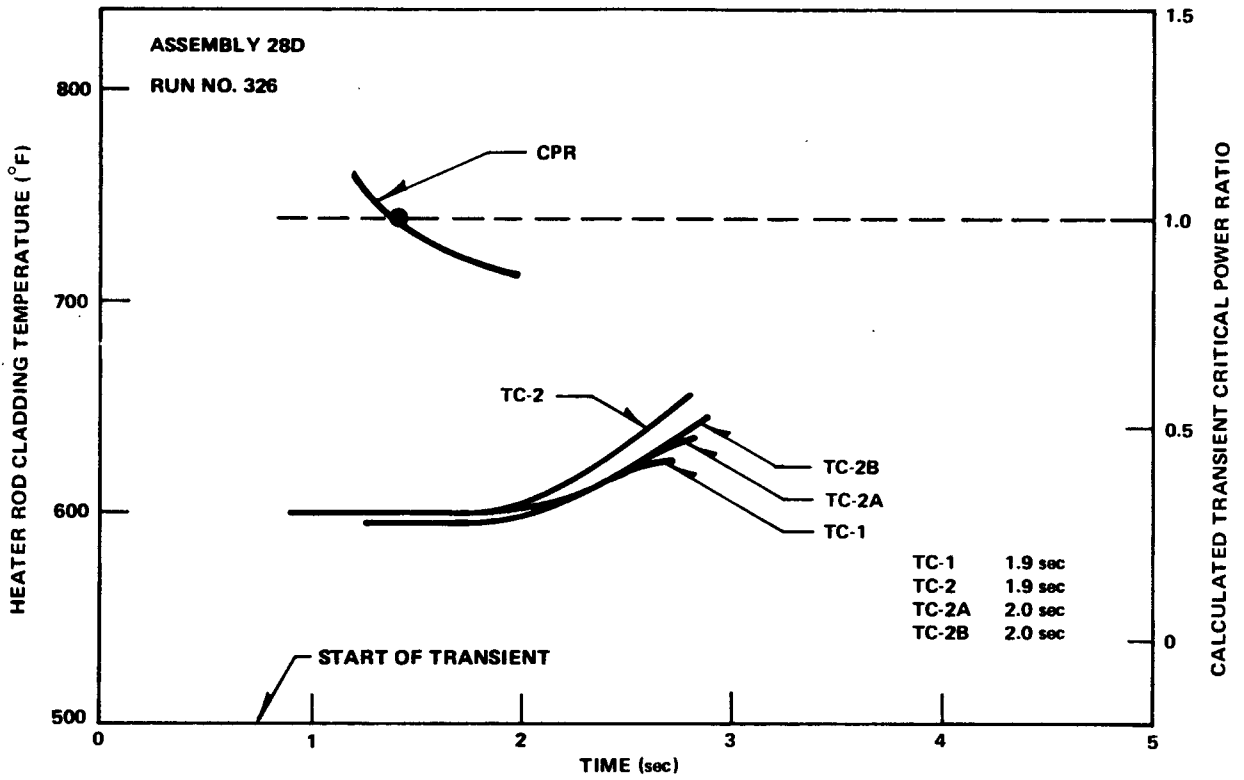


Figure 5-32. Calculated Transient Critical Power Ratio and Measured Heater Rod Cladding Temperature Vs Time

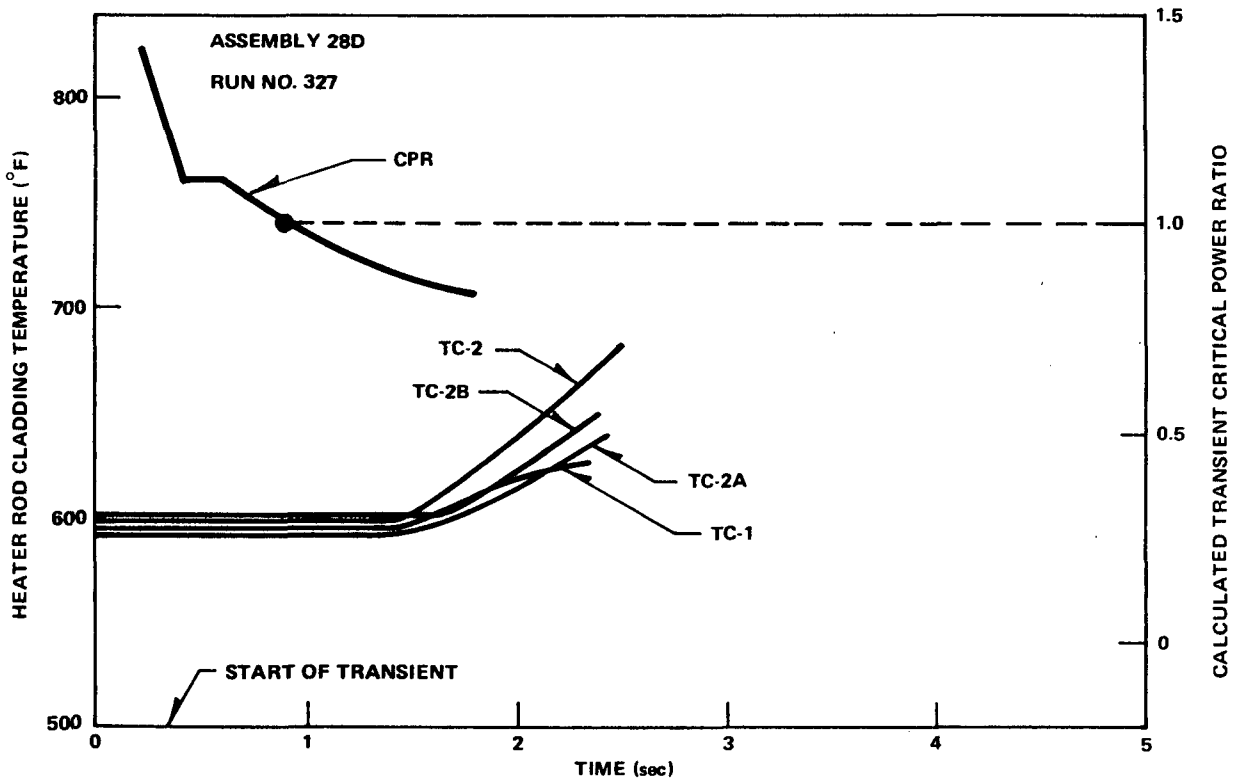


Figure 5-33. Calculated Transient Critical Power Ratio and Measured Heater Rod Cladding Temperature Vs Time

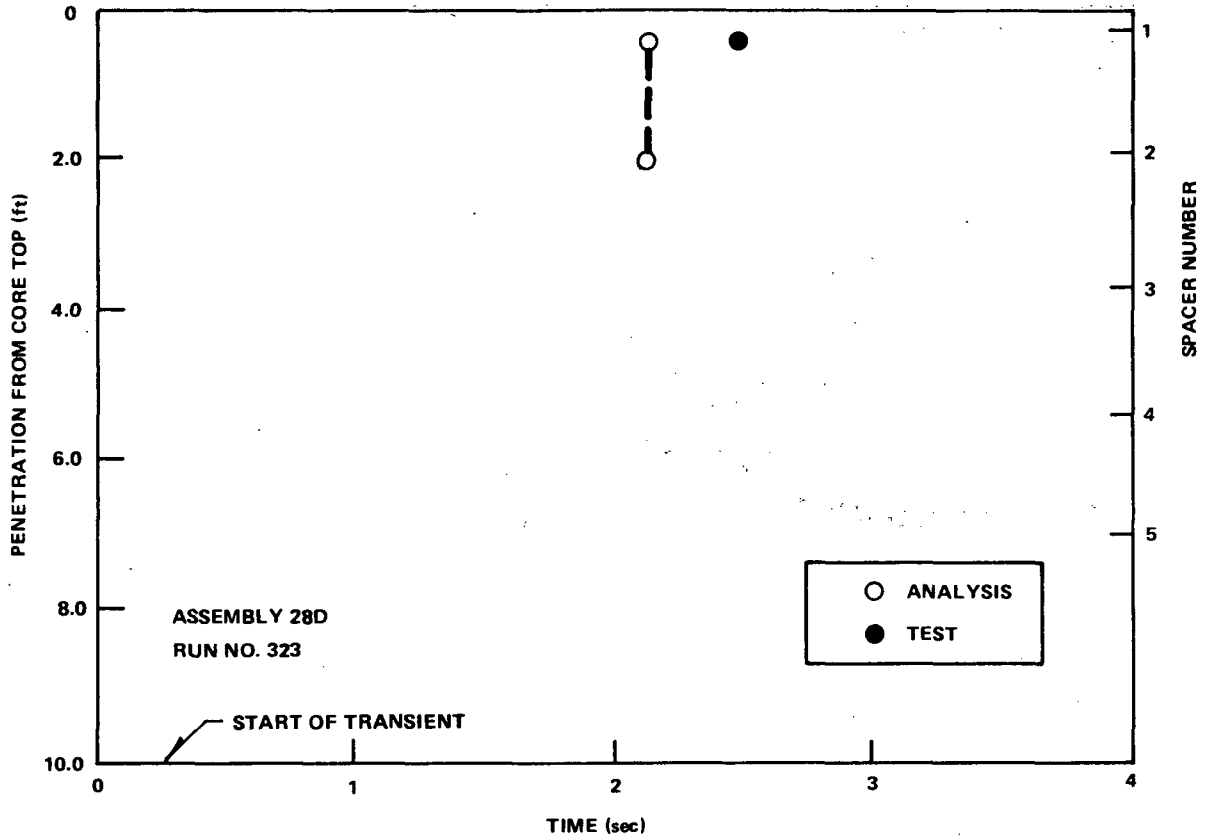


Figure 5-34. Axial Penetration of Boiling Transition Vs Time

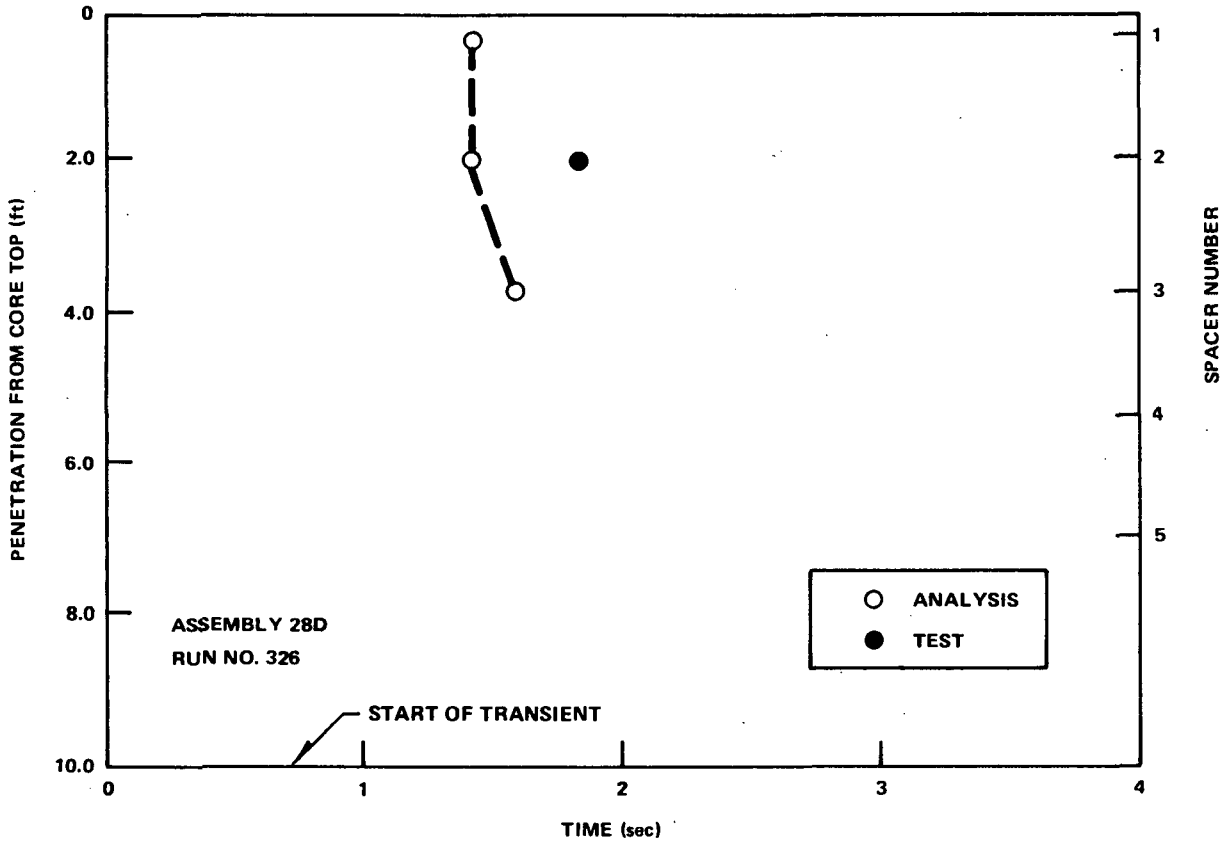


Figure 5-35. Axial Penetration of Boiling Transition Vs Time

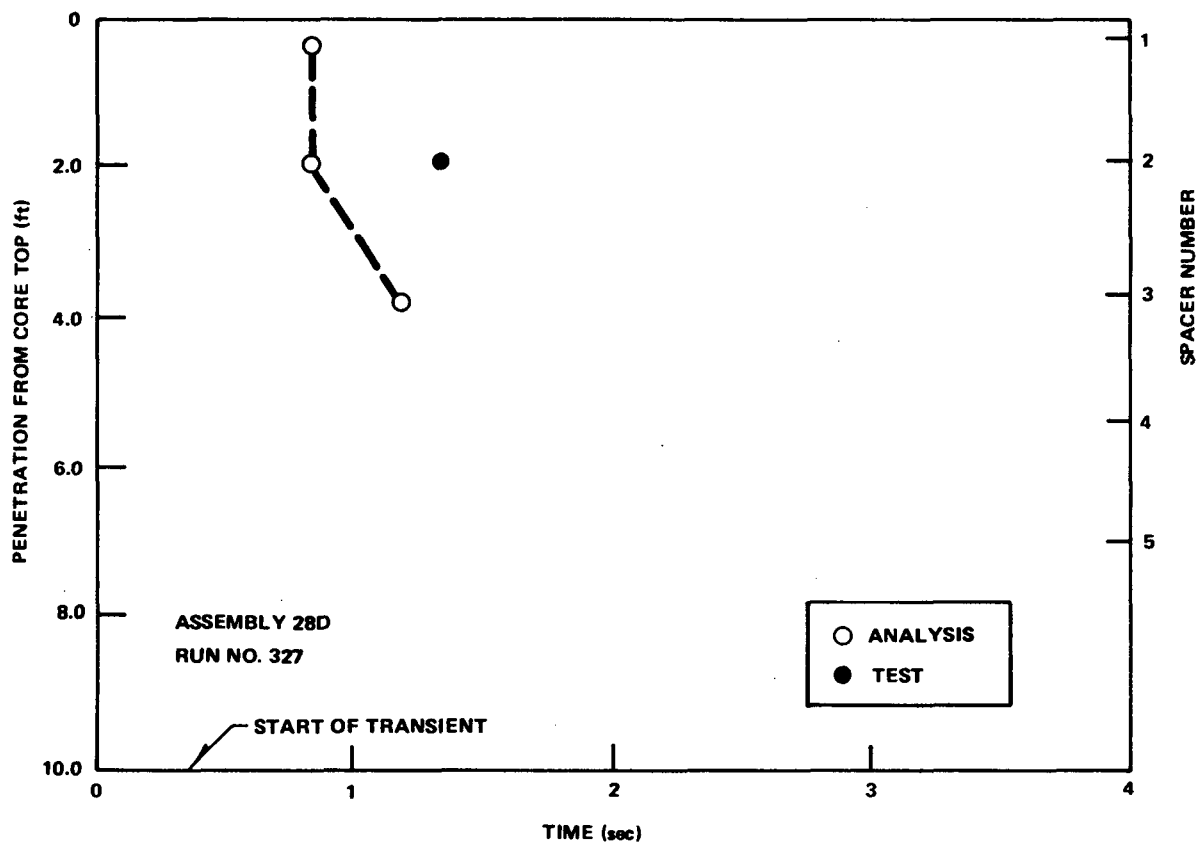


Figure 5-36. Axial Penetration of Boiling Transition Vs Time

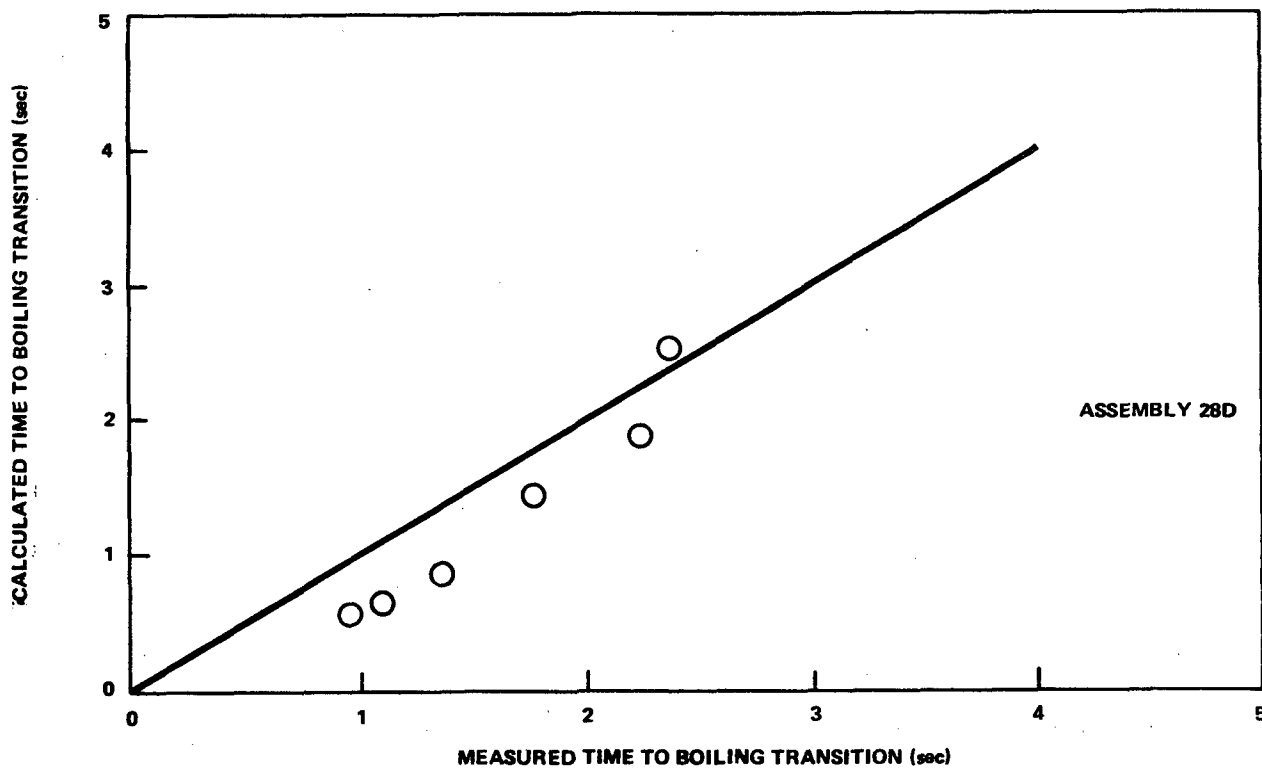


Figure 5-37. Calculated Time Vs Measured Time to Initial Boiling Transition

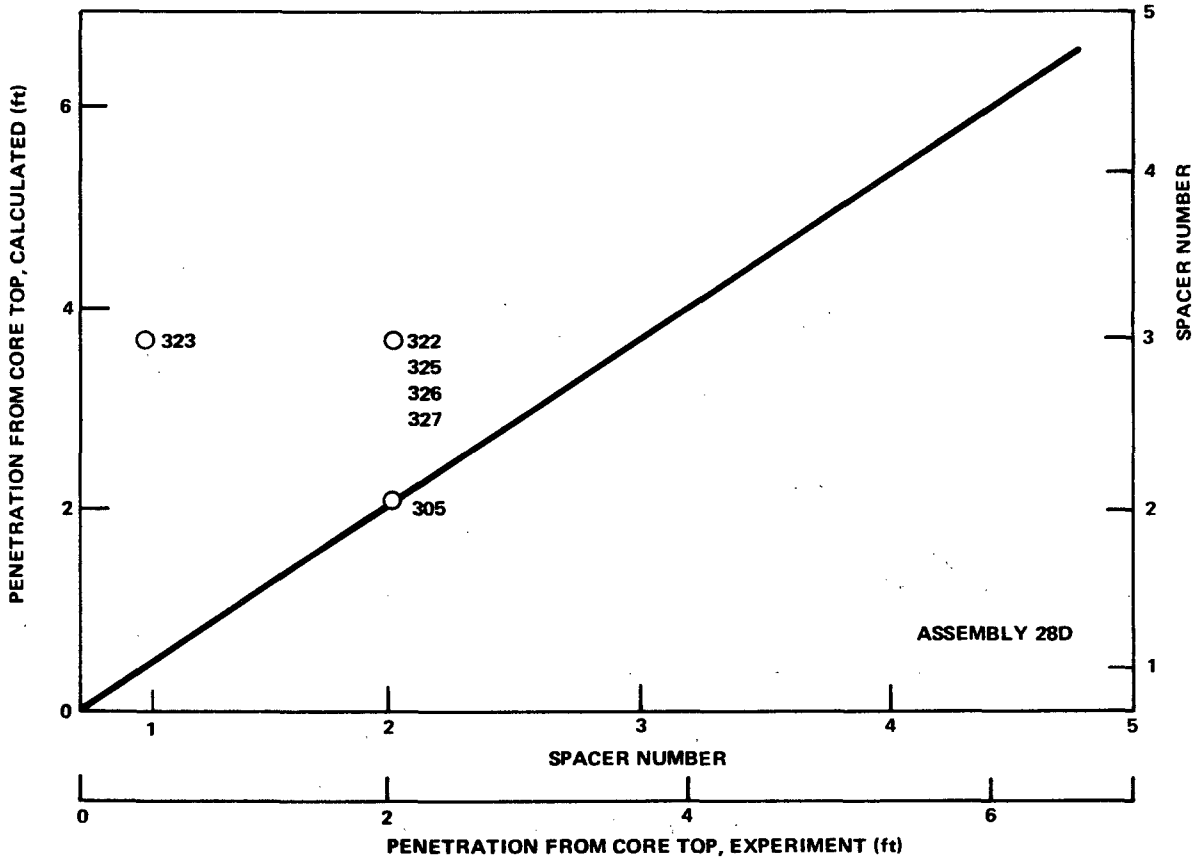


Figure 5-38. Boiling Transition Axial Penetration Calculated Vs Measured



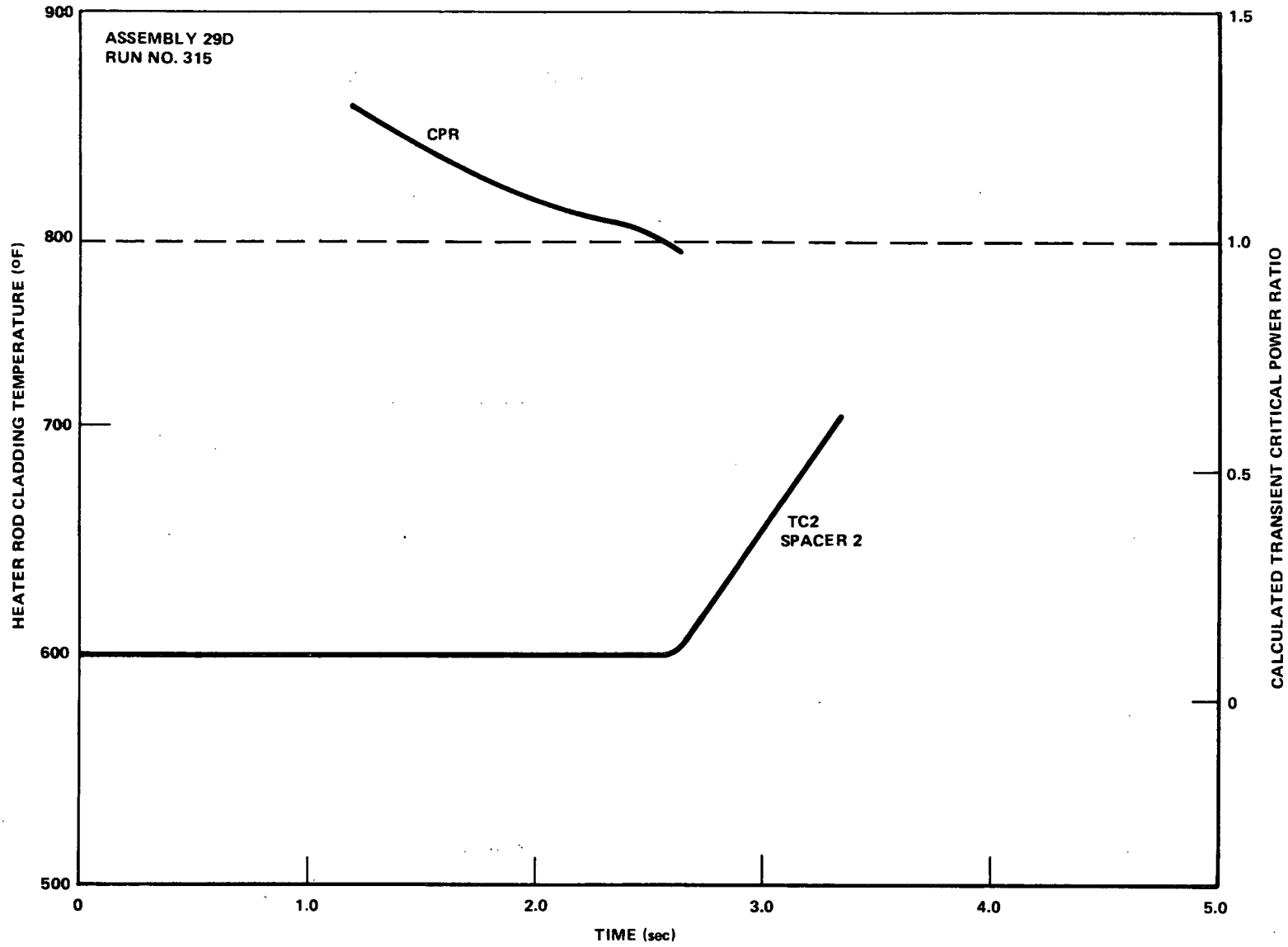


Figure 5-39. Calculated Transient Critical Power Ratio and Measured Heater Rod Cladding Temperature Vs Time

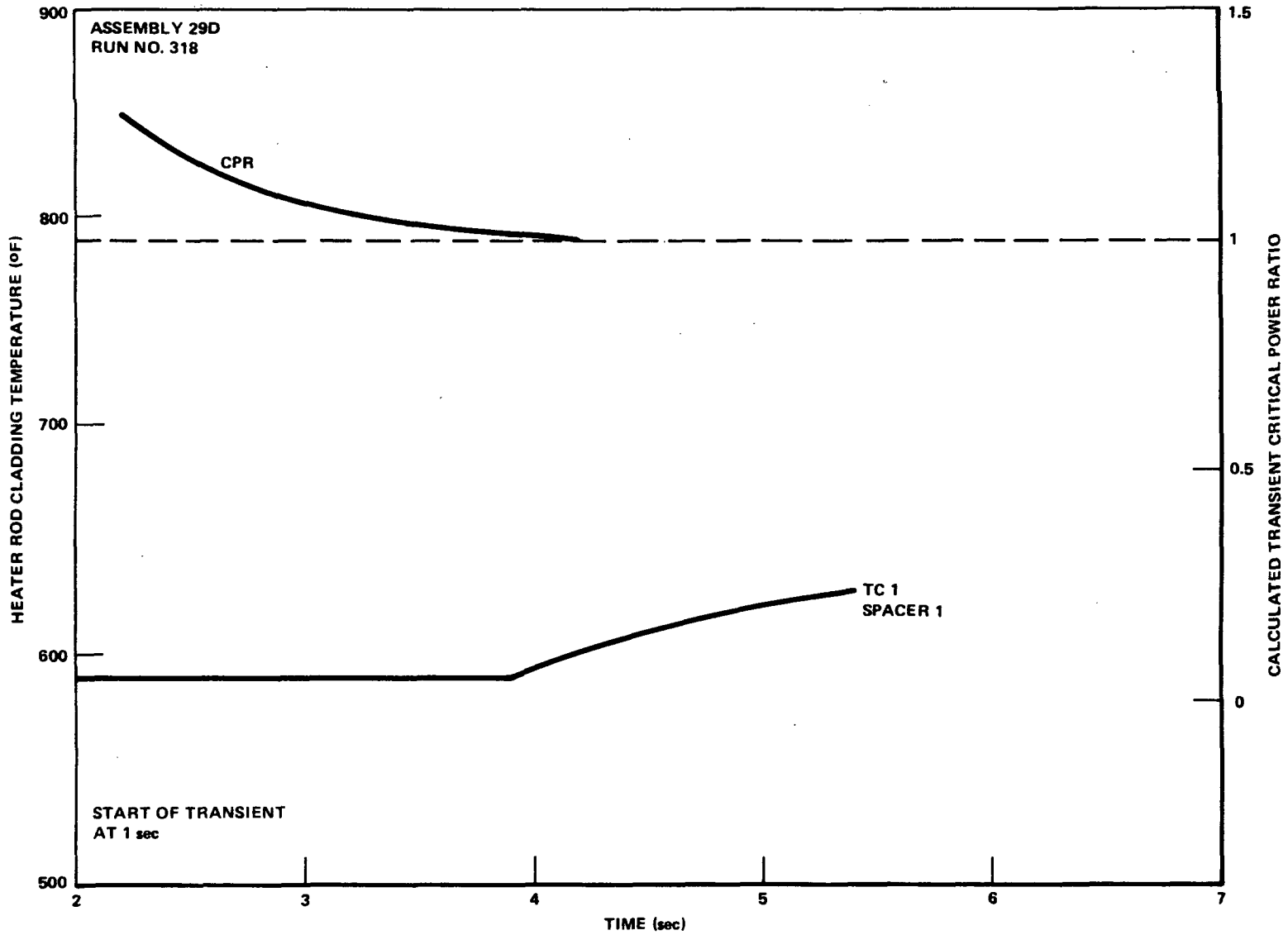


Figure 5-40. Calculated Transient Critical Power Ratio and Measured Heater Rod Cladding Temperature Vs Time

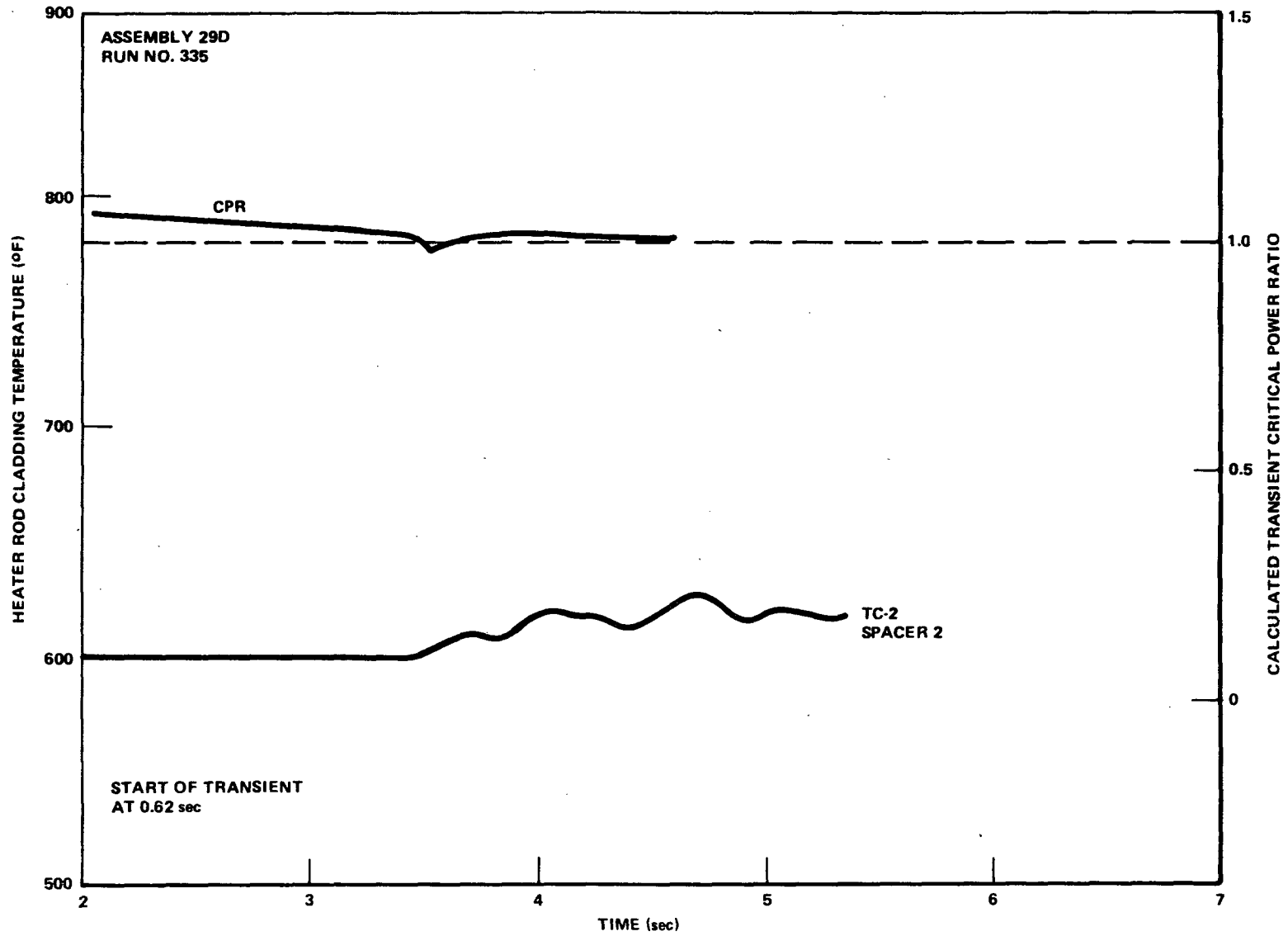


Figure 5-41. Calculated Transient Critical Power Ratio and Measured Heater Rod Cladding Temperature Vs Time

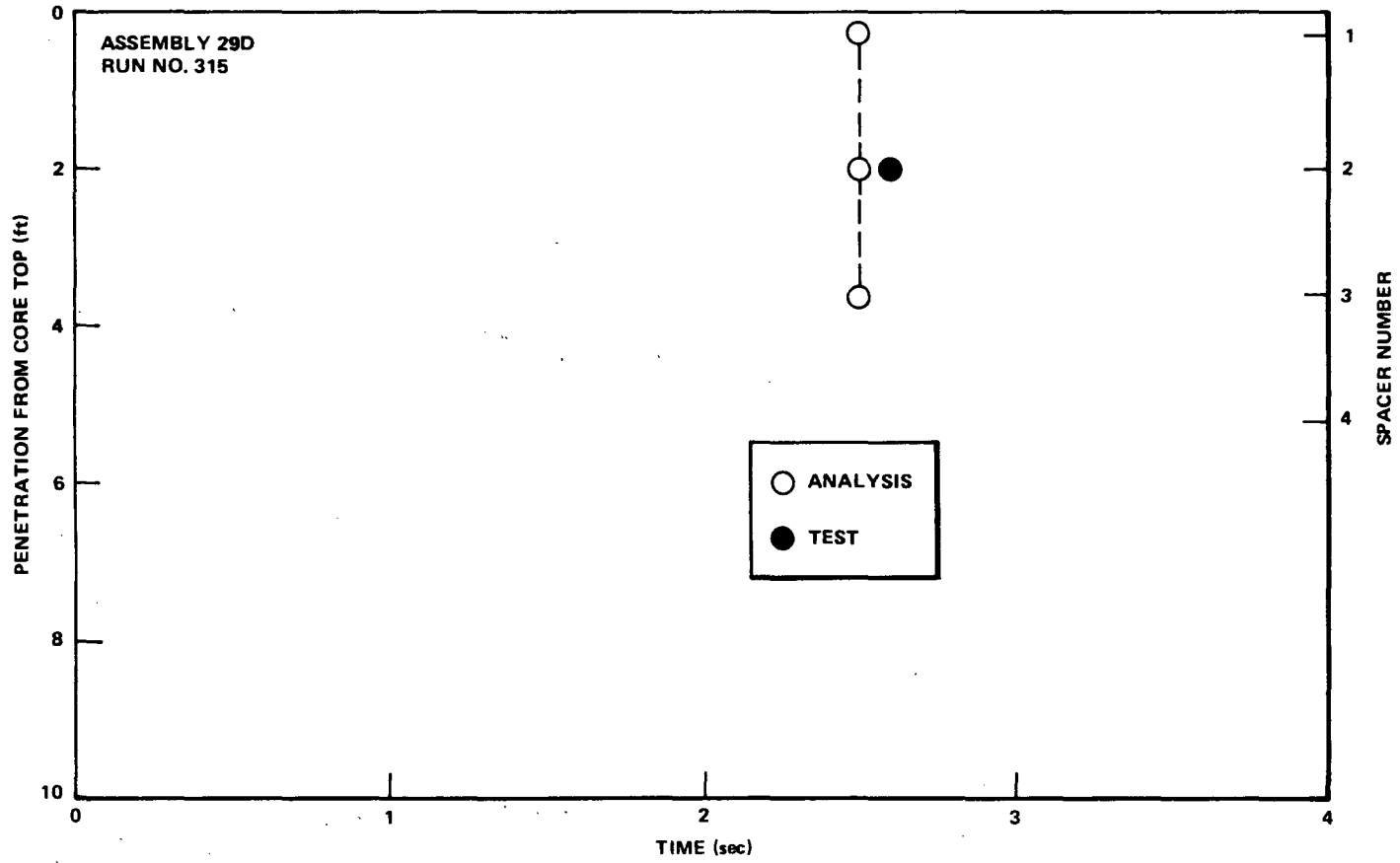


Figure 5-42. Axial Penetration of Boiling Transition Versus Time

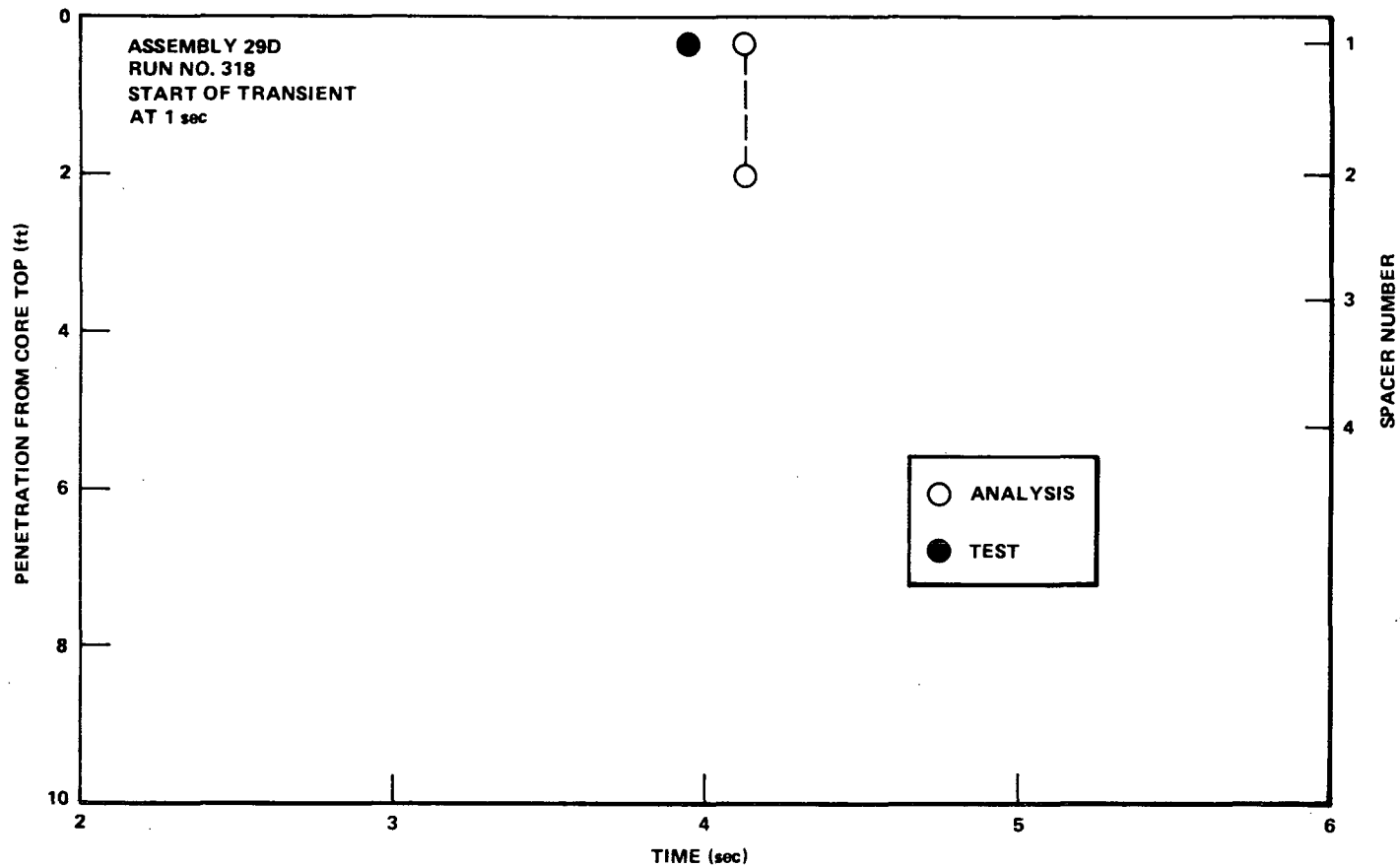


Figure 5-43. Axial Penetration of Boiling Transition Versus Time

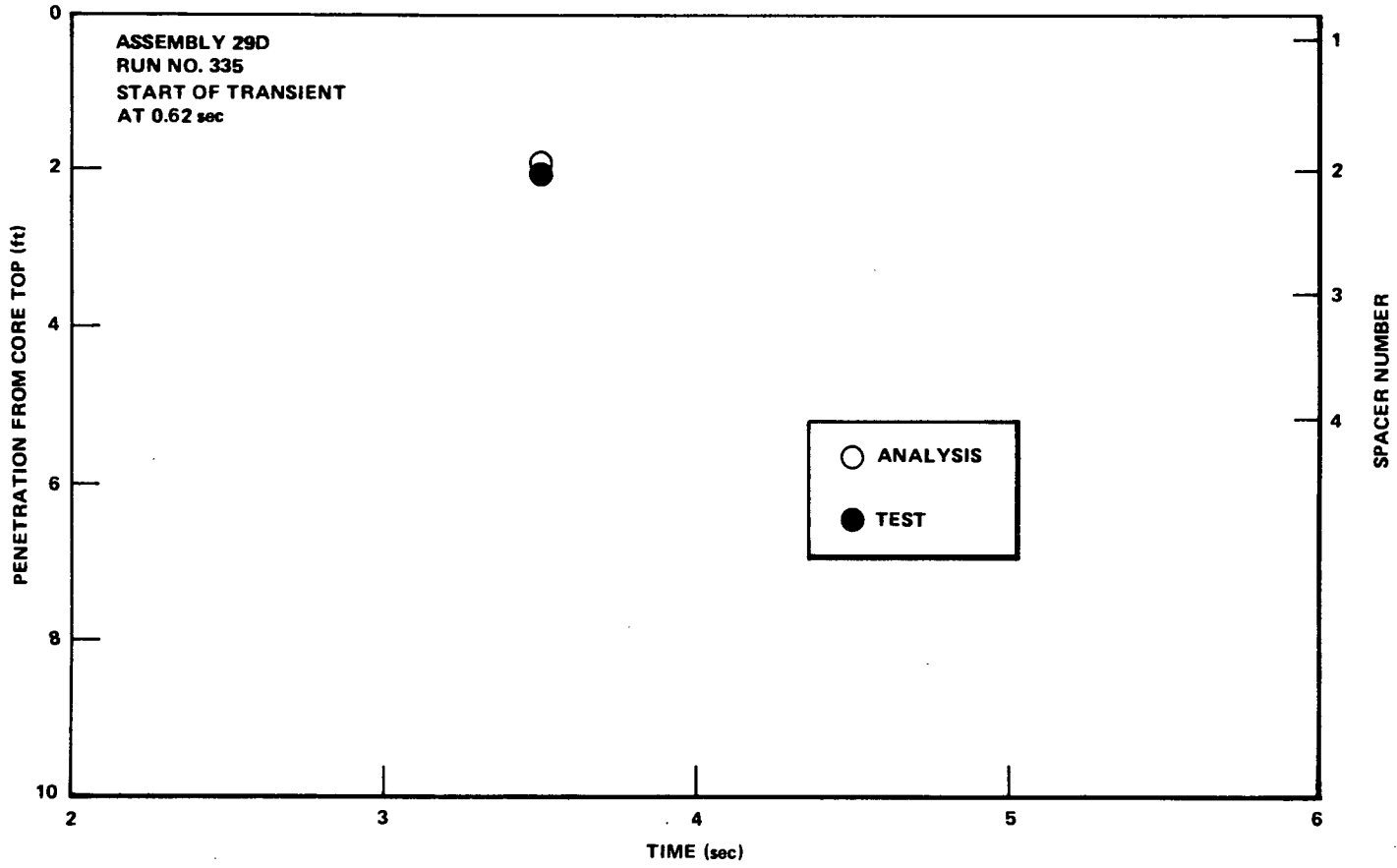


Figure 5-44. Axial Penetration of Boiling Transition Versus Time

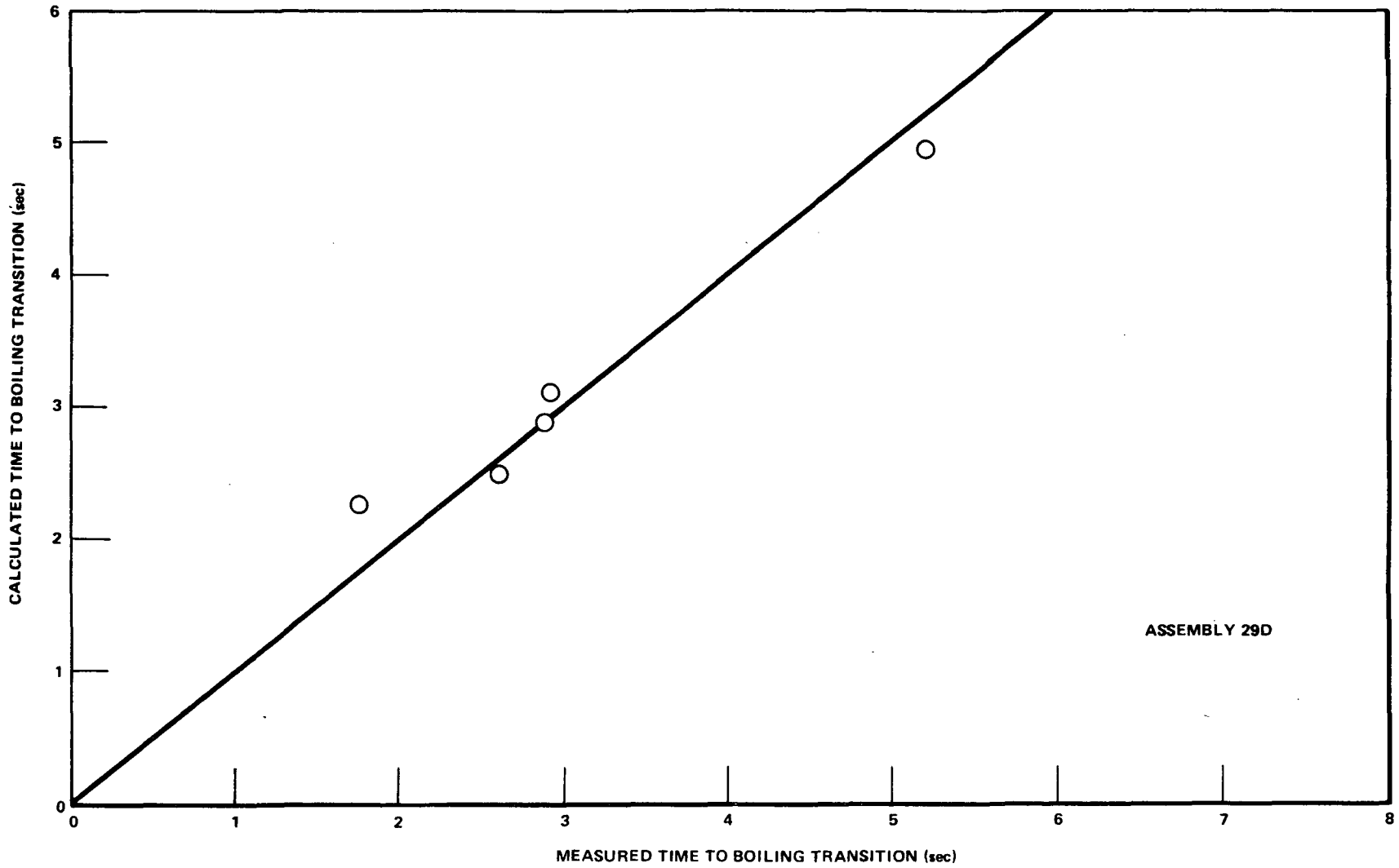


Figure 5-45. Calculated Time Vs Measured Time to Initial Boiling Transition

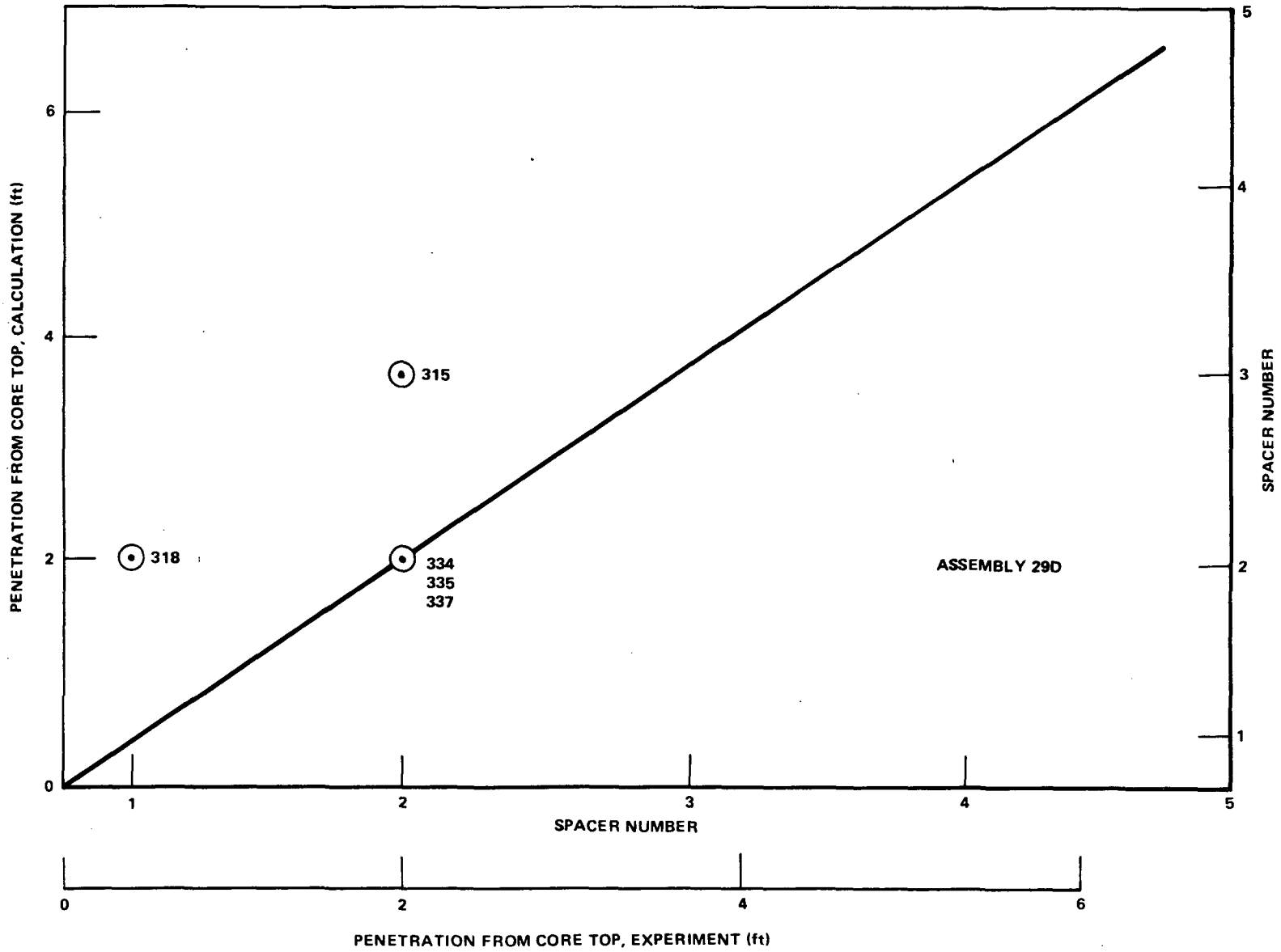


Figure 5-46. Boiling Transition Axial Penetration, Calculated Vs Measured



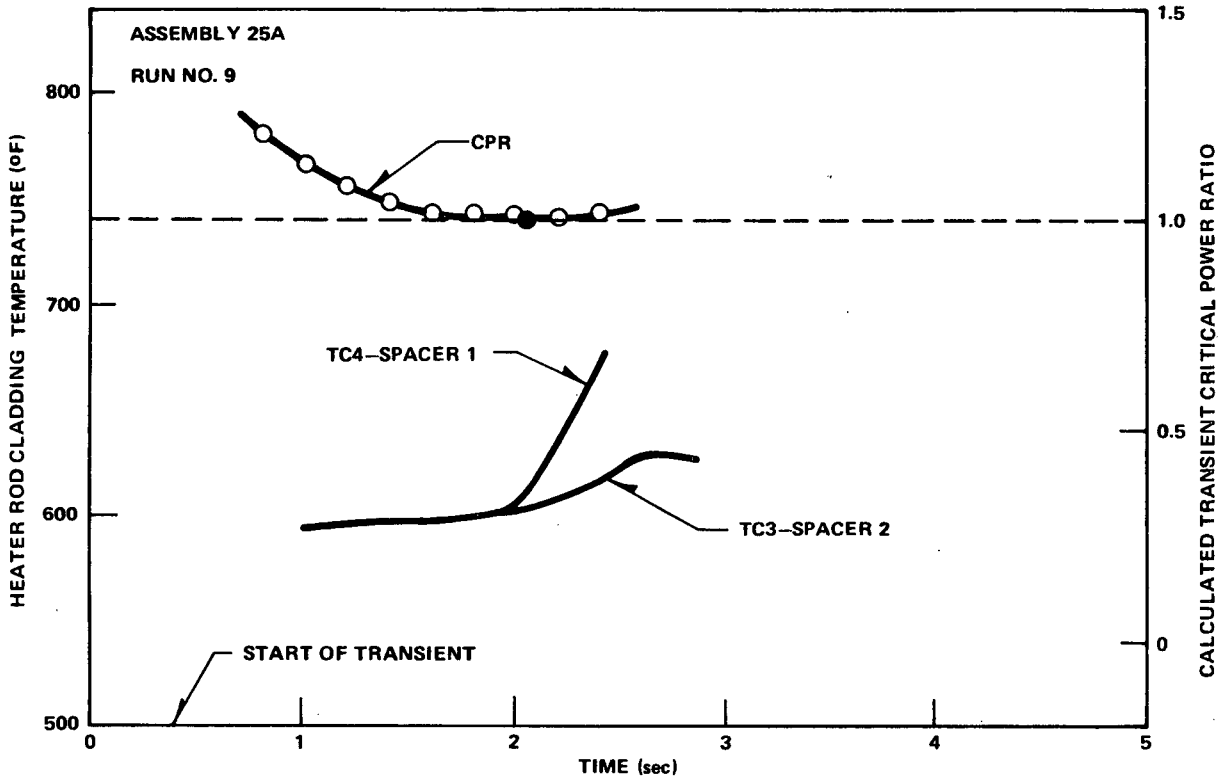


Figure 5-47. Calculated Transient Critical Power Ratio and Measured Heater Rod Cladding Temperature Vs Time

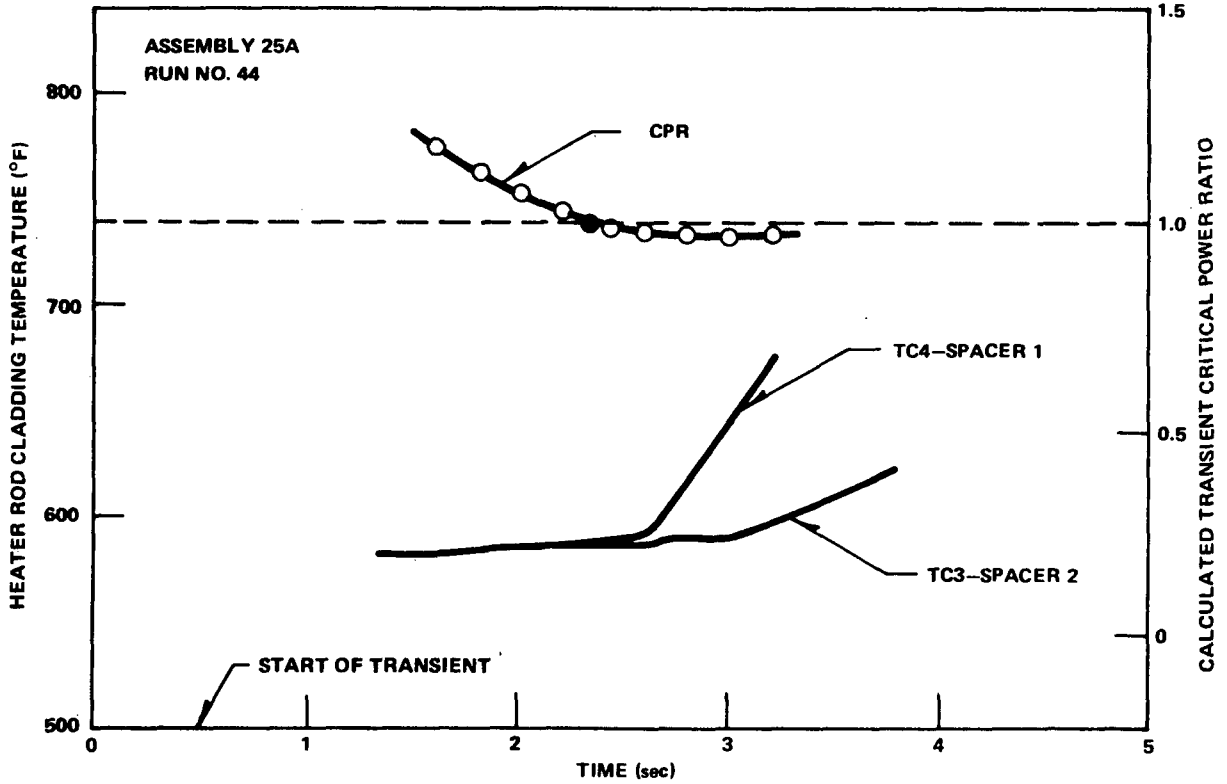


Figure 5-48. Calculated Transient Critical Power Ratio and Measured Heater Rod Cladding Temperature Vs Time

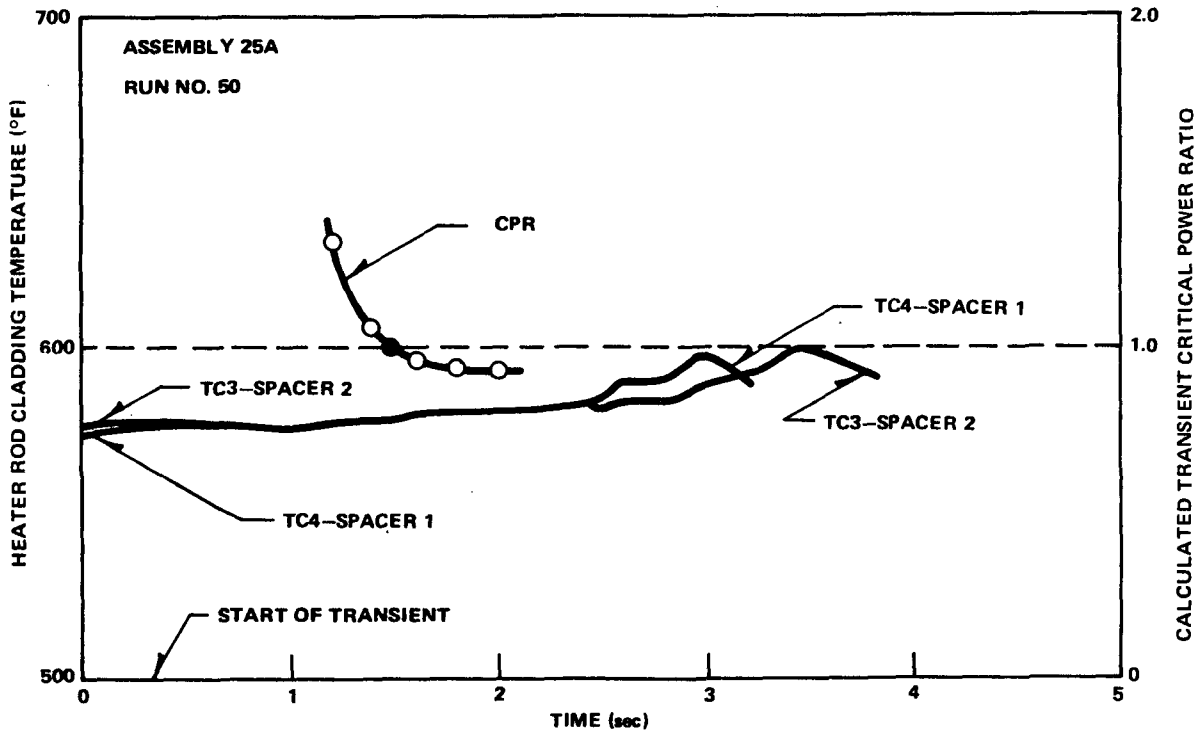


Figure 5-49. Calculated Transient Critical Power Ratio and Measured Heater Rod Cladding Temperature Vs Time

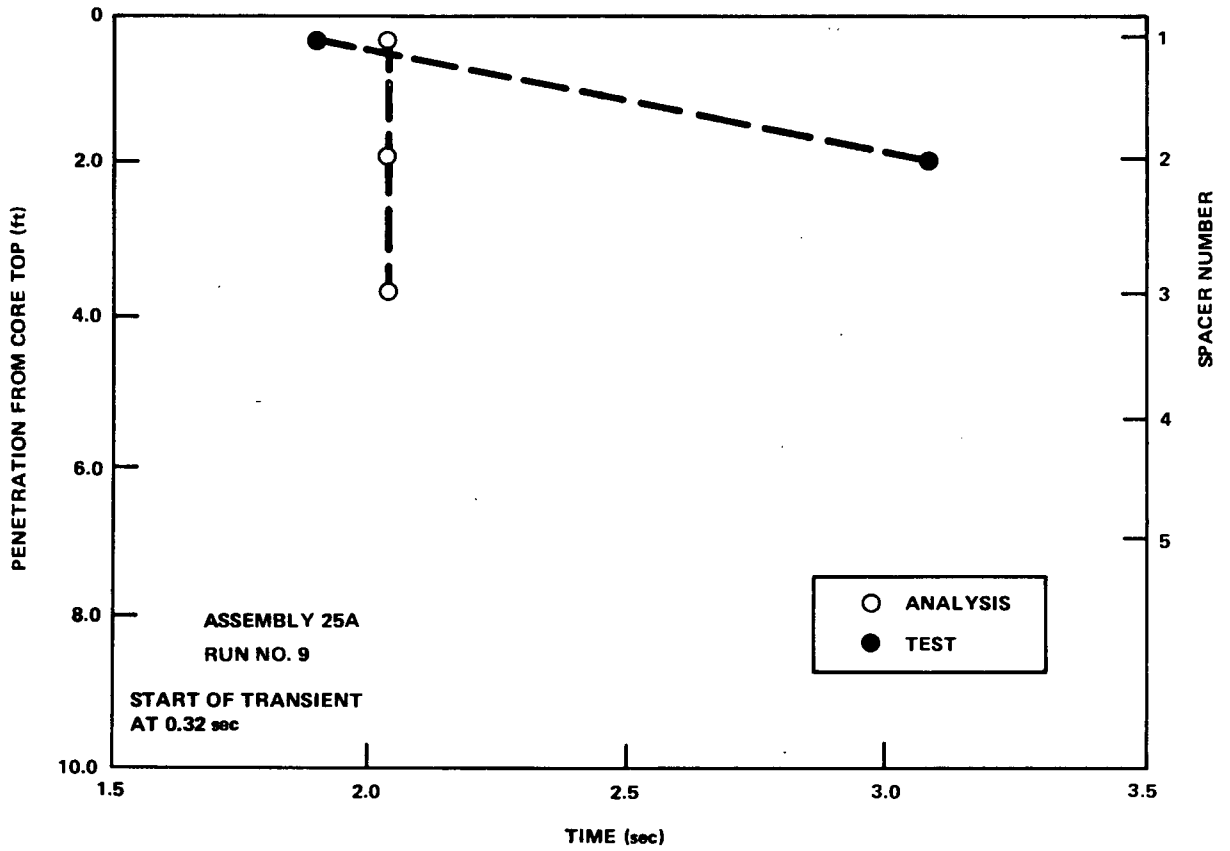


Figure 5-50. Axial Penetration of Boiling Transition Vs Time

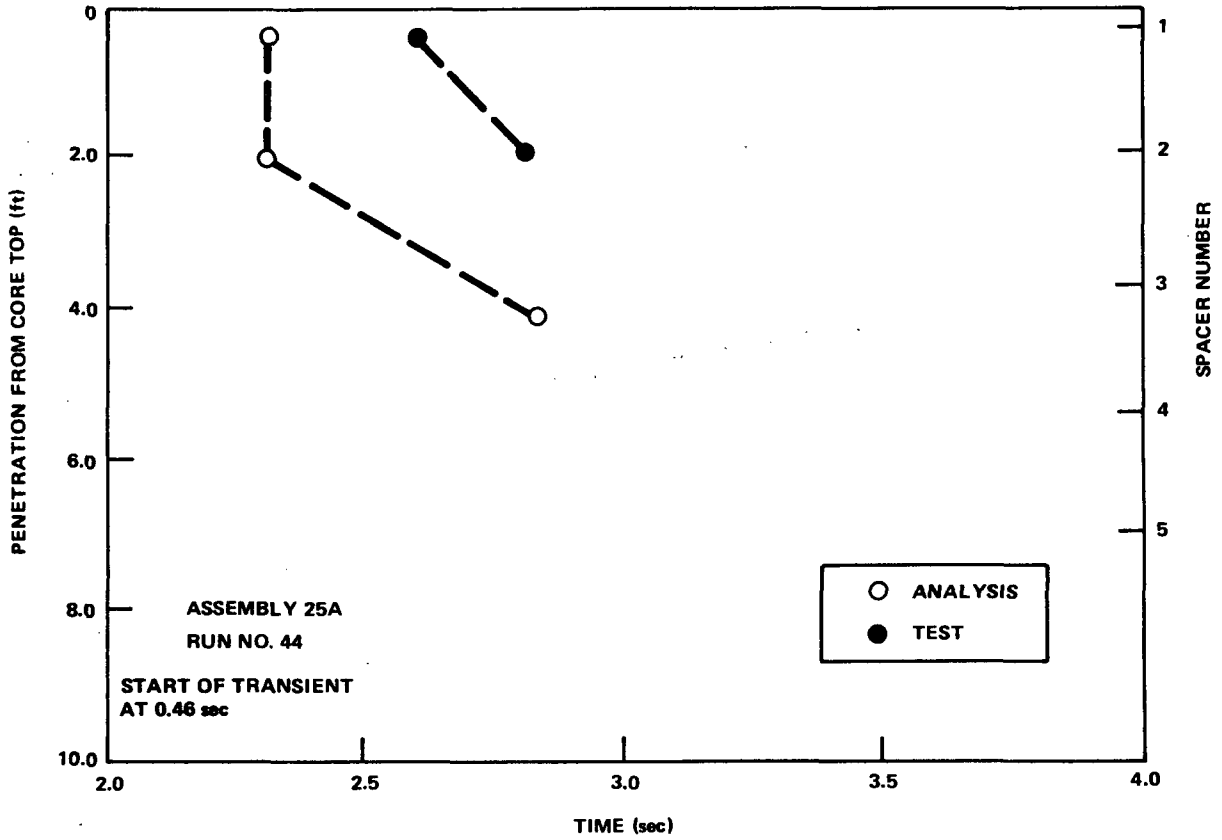


Figure 5-51. Axial Penetration of Boiling Transition Vs Time

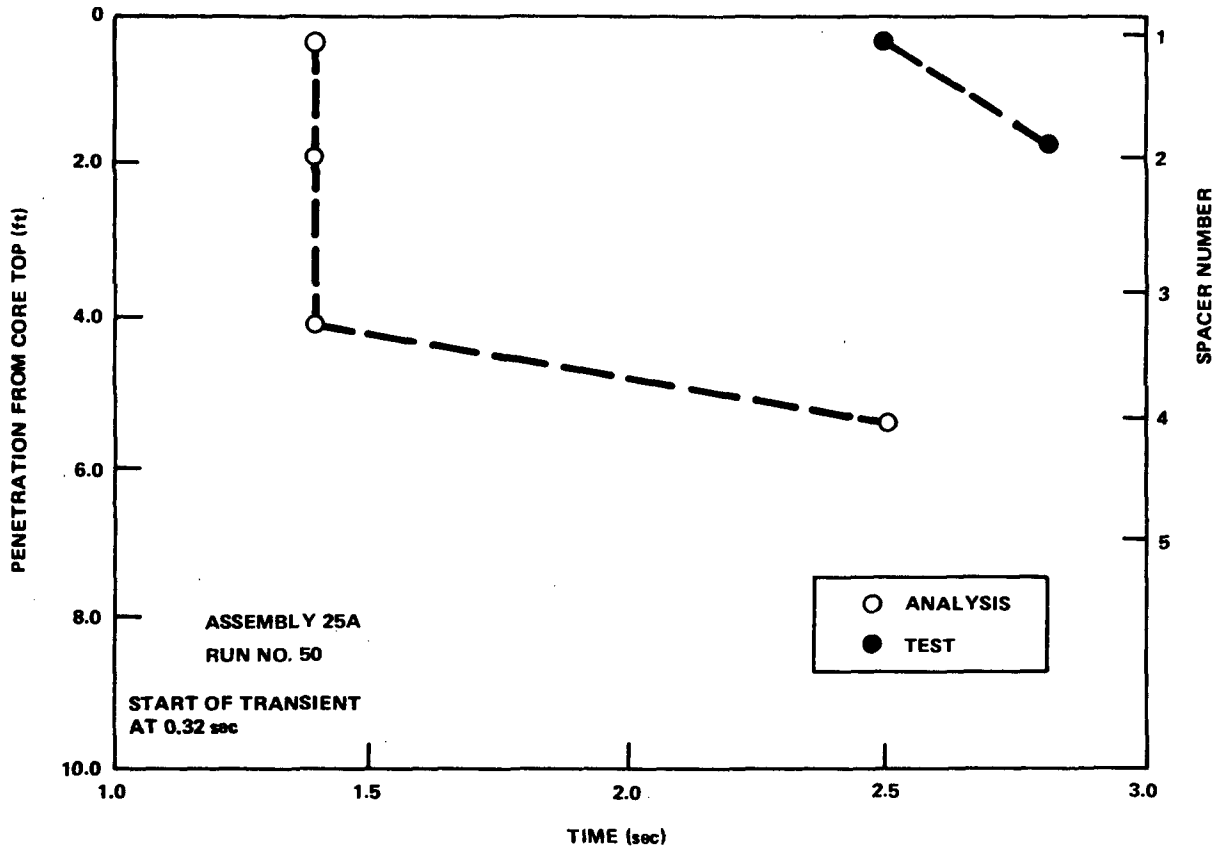


Figure 5-52. Axial Penetration of Boiling Transition Versus Time

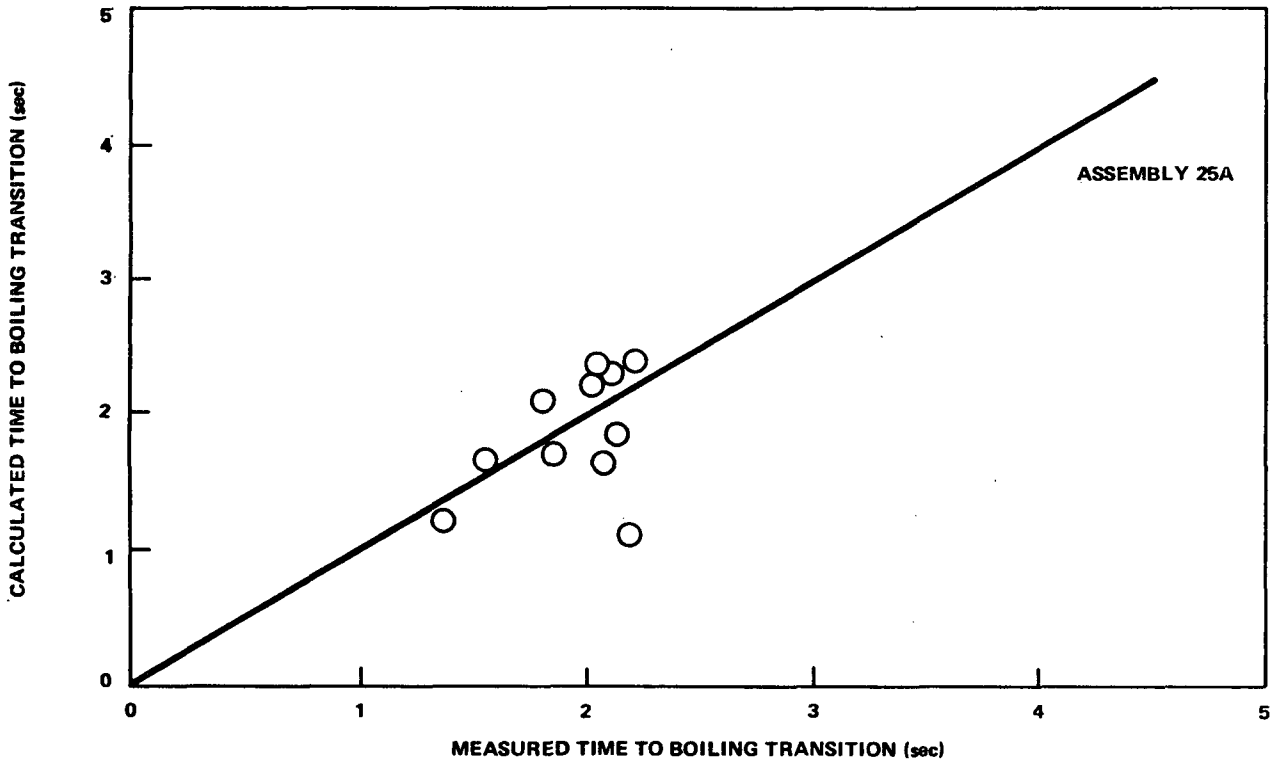


Figure 5-53. Calculated Time Vs Measured Time to Initial Boiling Transition

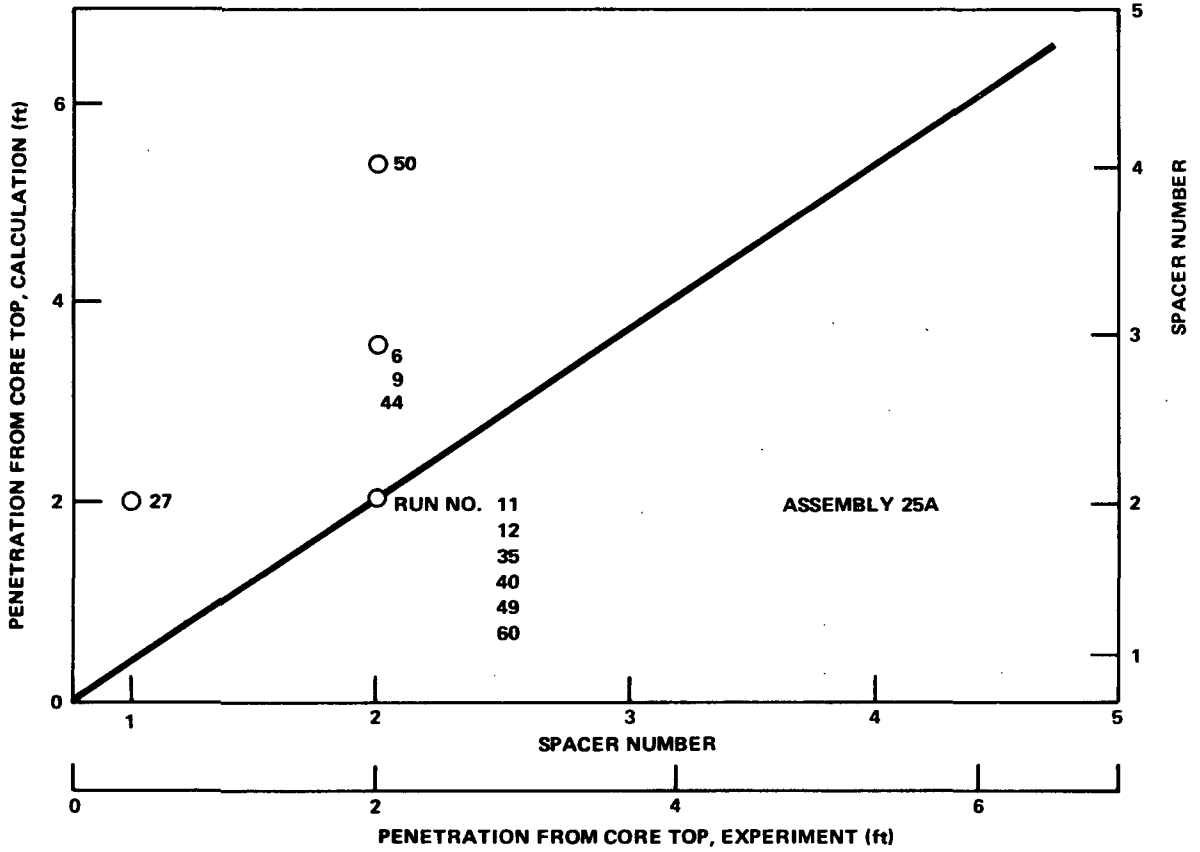


Figure 5-54. Boiling Transition Axial Penetration Calculated Vs Measured



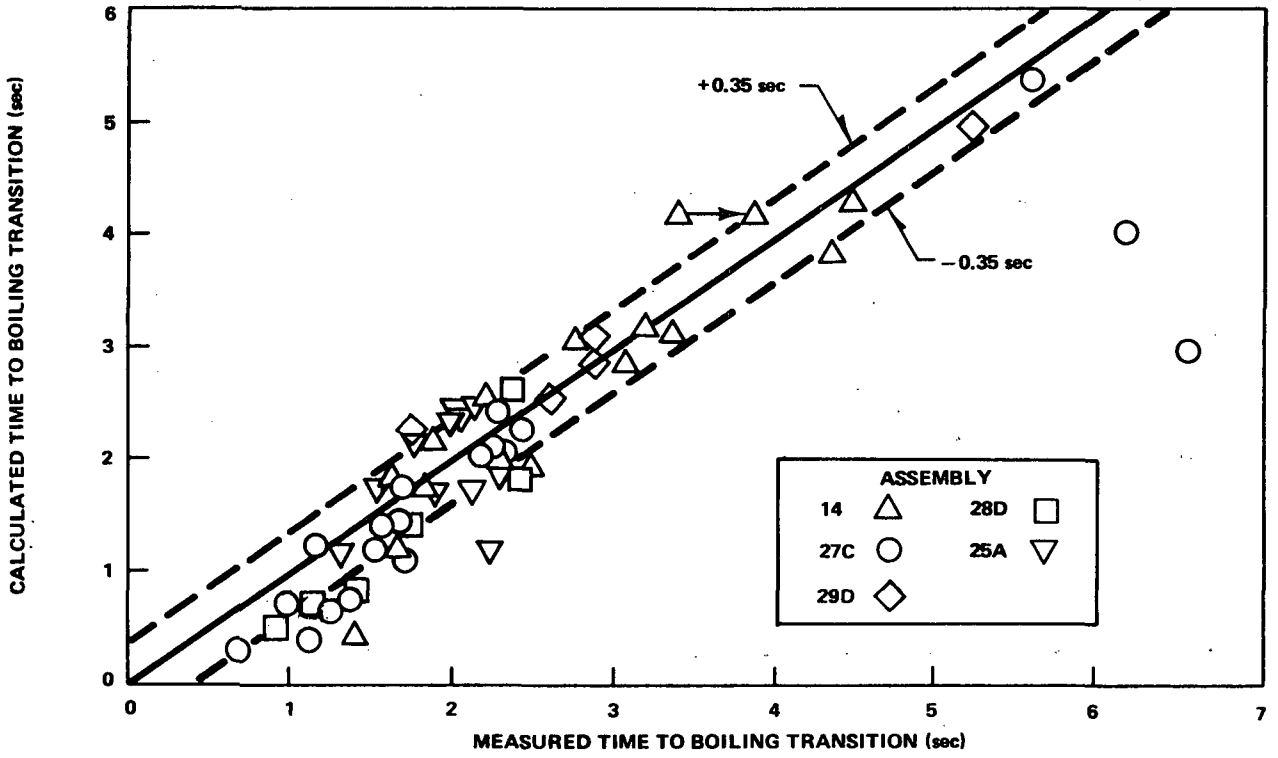


Figure 5-55. Calculated Time versus Measured Time to Initial Boiling Transition

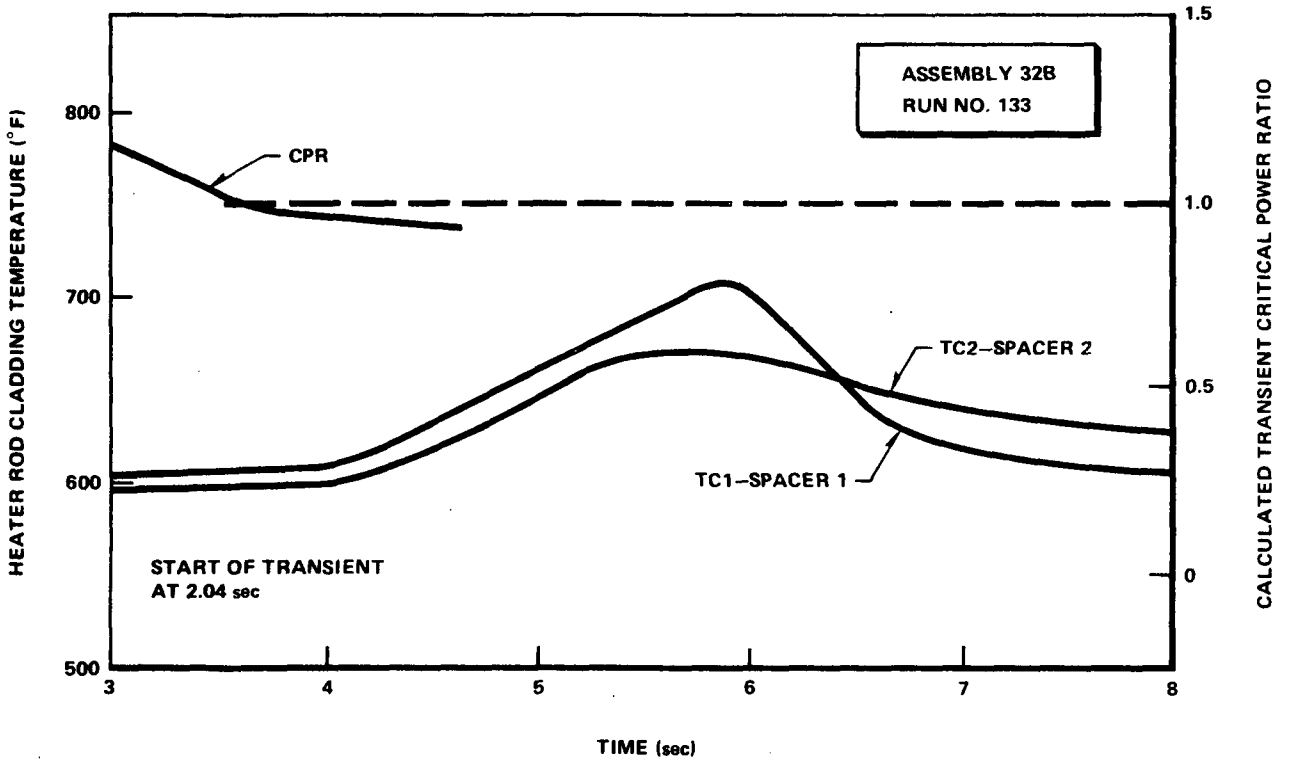


Figure 5-56. Calculated Transient Critical Power Ratio and Measured Heater Rod Cladding Temperature Vs Time

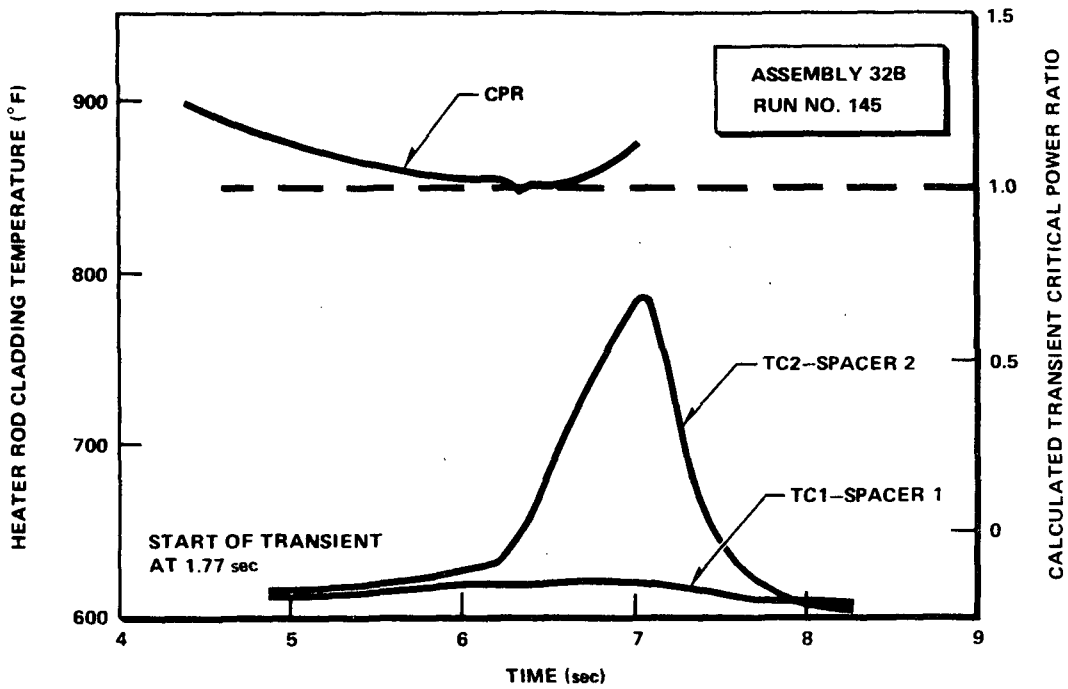


Figure 5-57. Calculated Transient Critical Power Ratio and Measured Heater Rod Cladding Temperature Vs Time

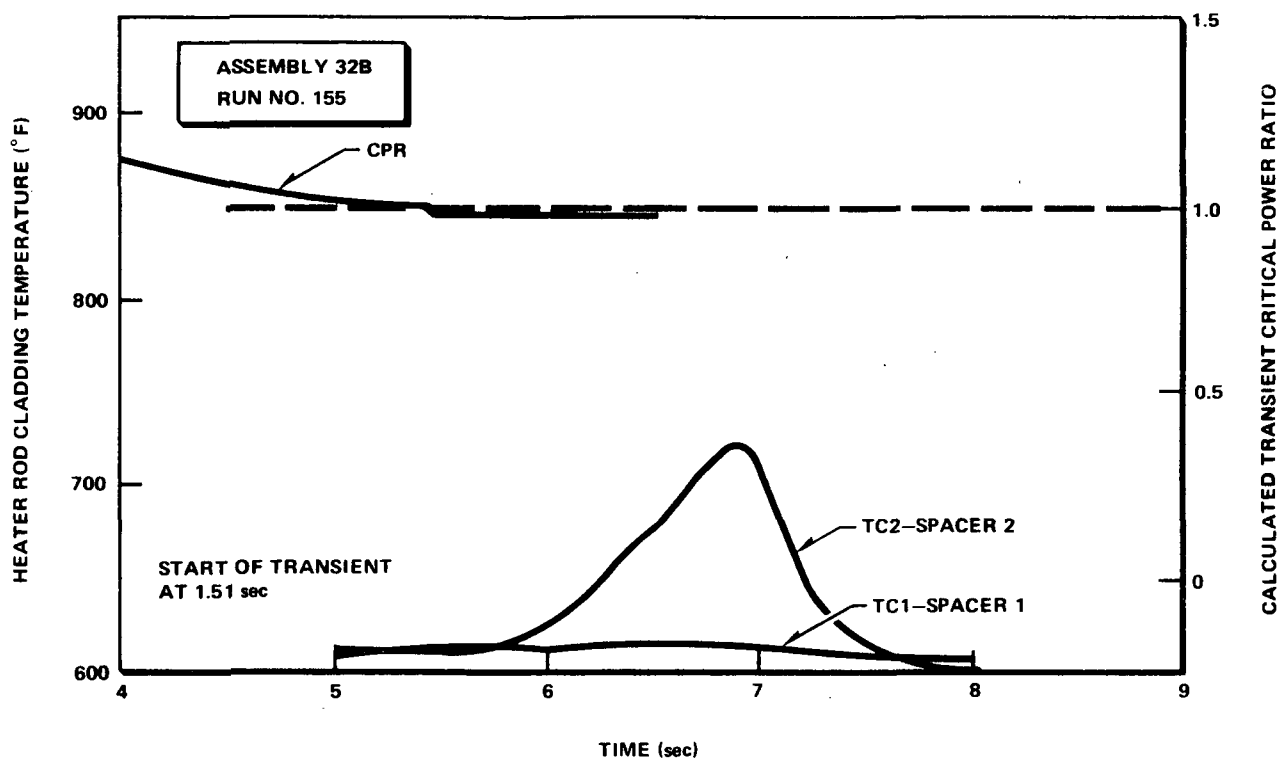


Figure 5-58. Calculated Transient Critical Power Ratio and Measured Heater Rod Cladding Temperature Vs Time

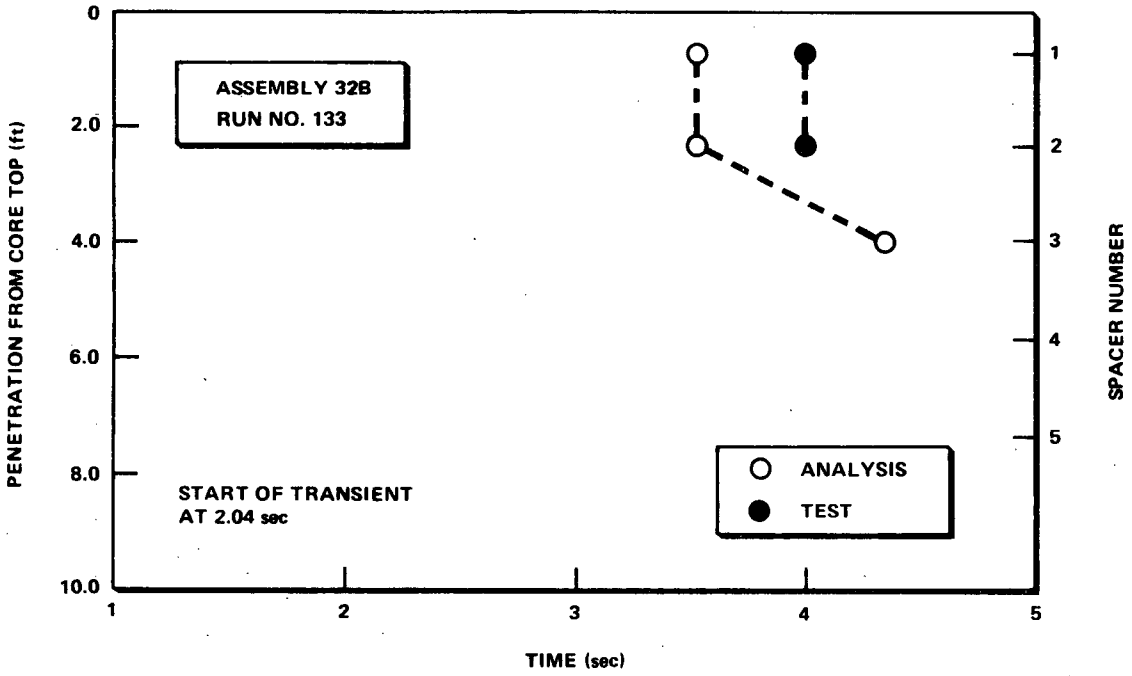


Figure 5-59. Axial Penetration of Boiling Transition Vs Time

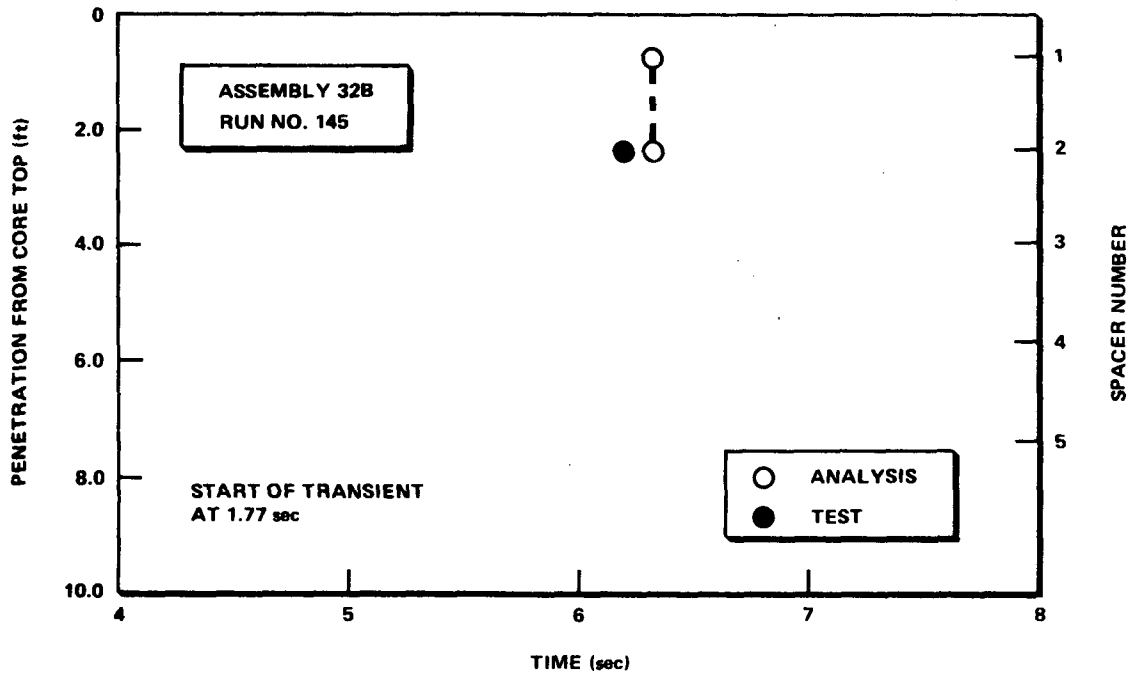


Figure 5-60. Axial Penetration of Boiling Transition Vs Time

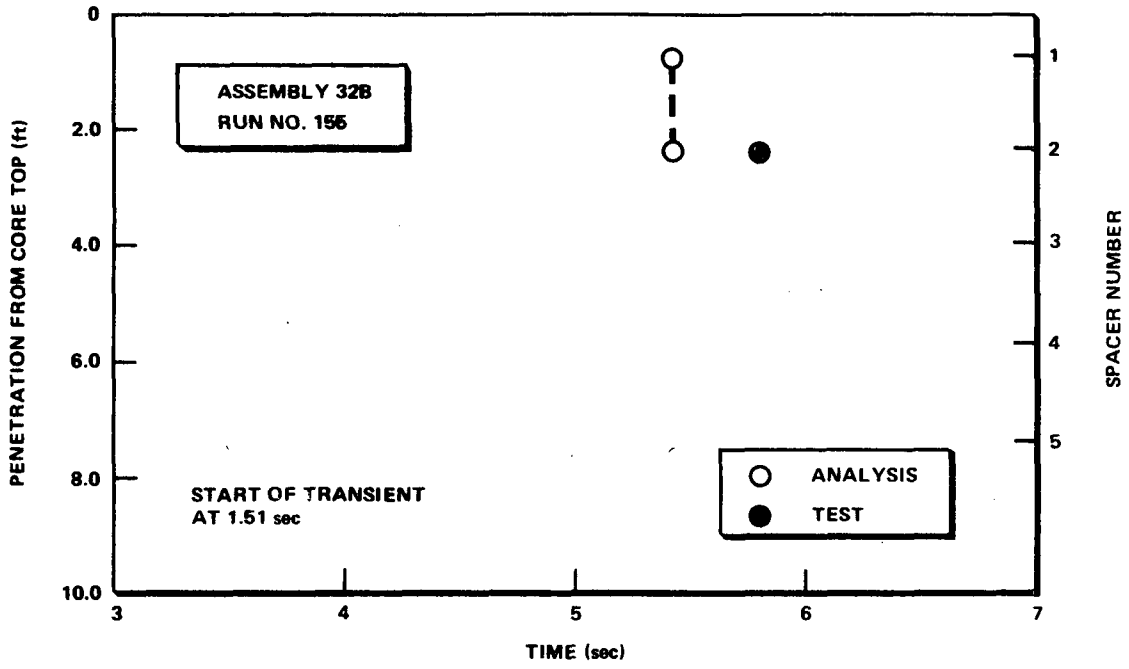


Figure 5-61. Axial Penetration of Boiling Transition Vs Time

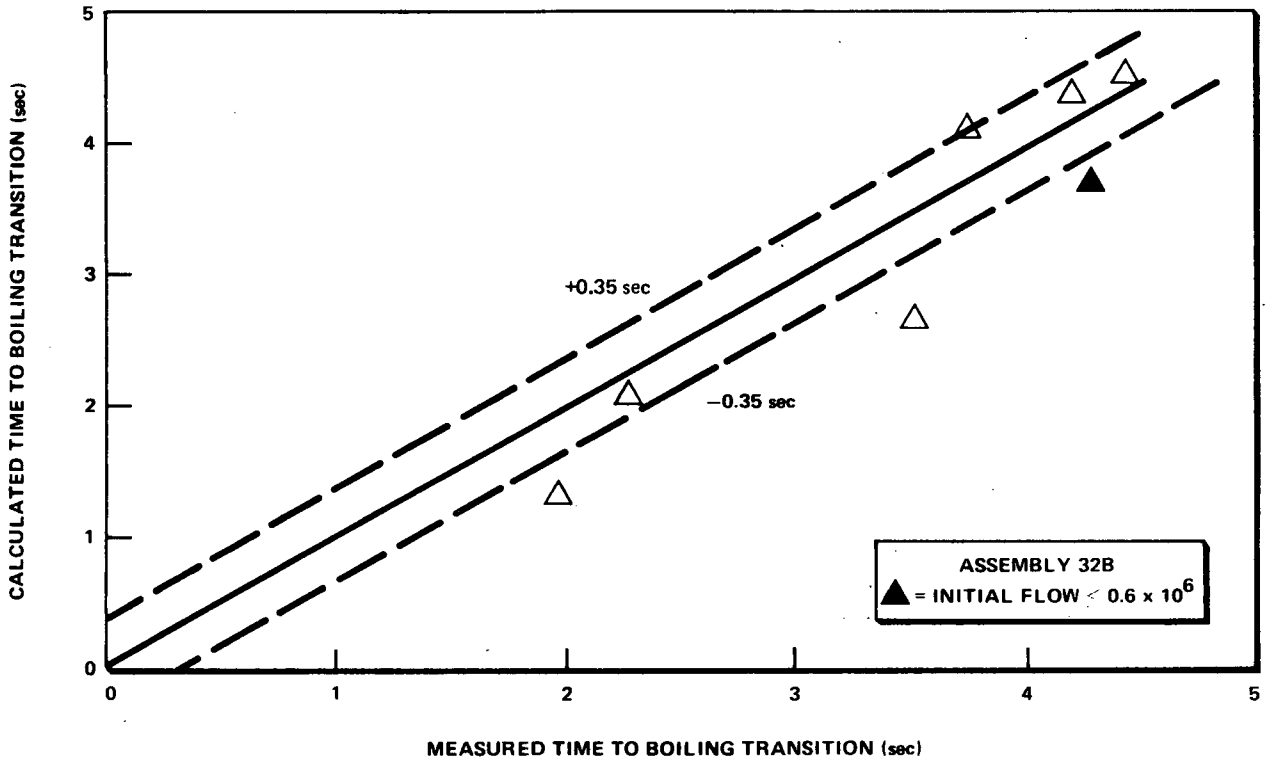


Figure 5-62. Calculated Time Vs Measured Time to Initial Boiling Transition



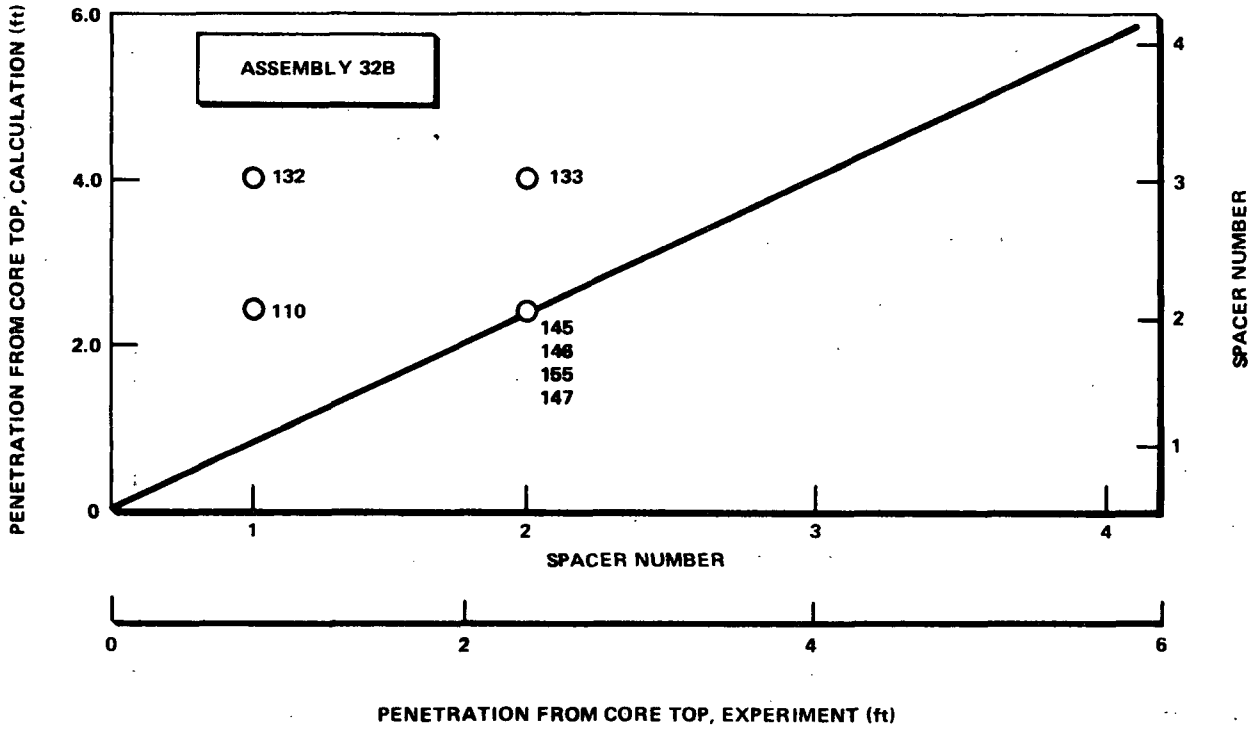


Figure 5-63. Boiling Transition Axial Penetration Calculated Vs Measured

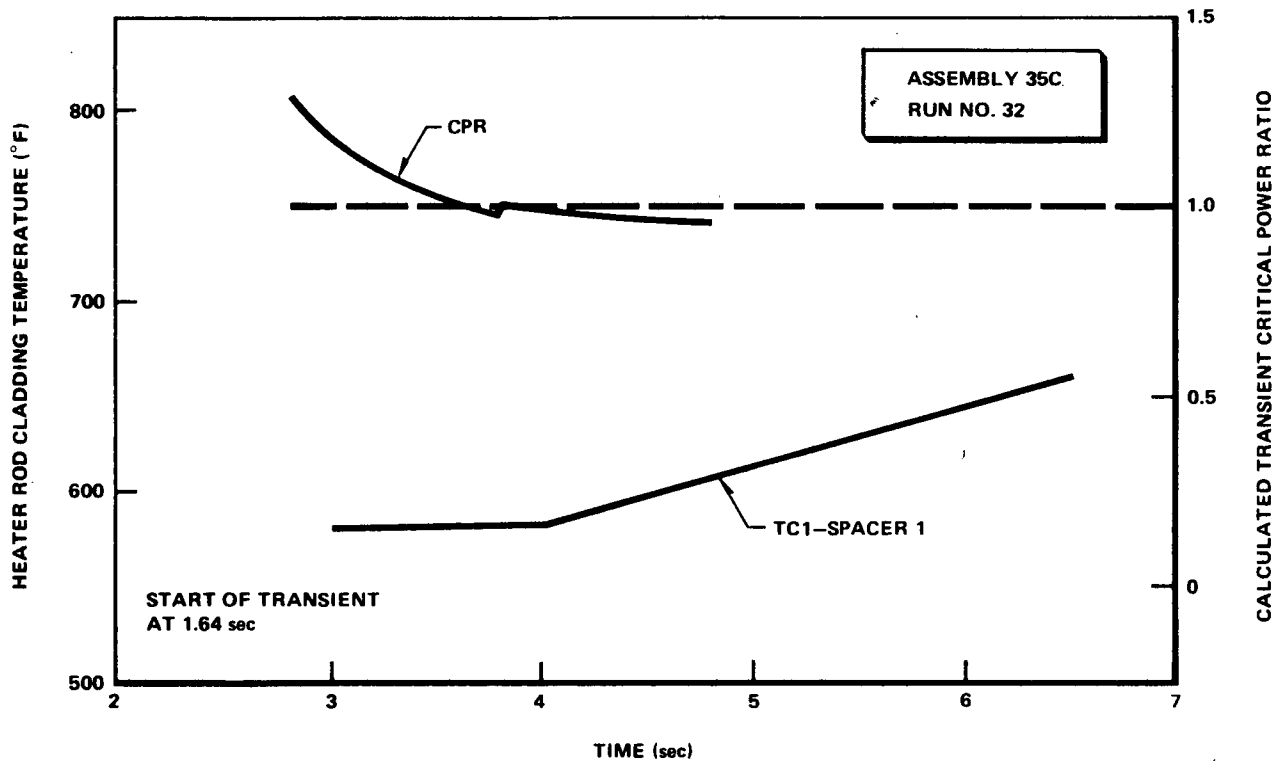


Figure 5-64. Calculated Transient Critical Power Ratio and Measured Heater Rod Cladding Temperature Vs Time

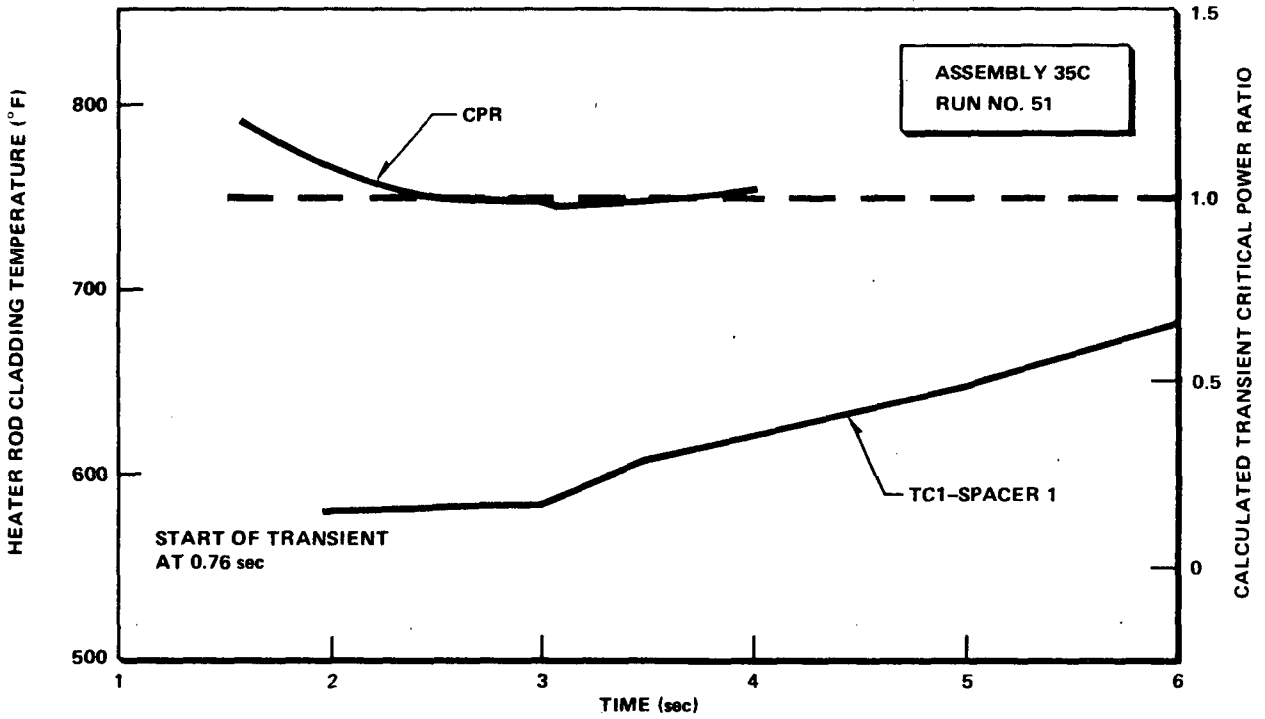


Figure 5-65. Calculated Transient Critical Power Ratio and Measured Heater Rod Cladding Temperature Vs Time

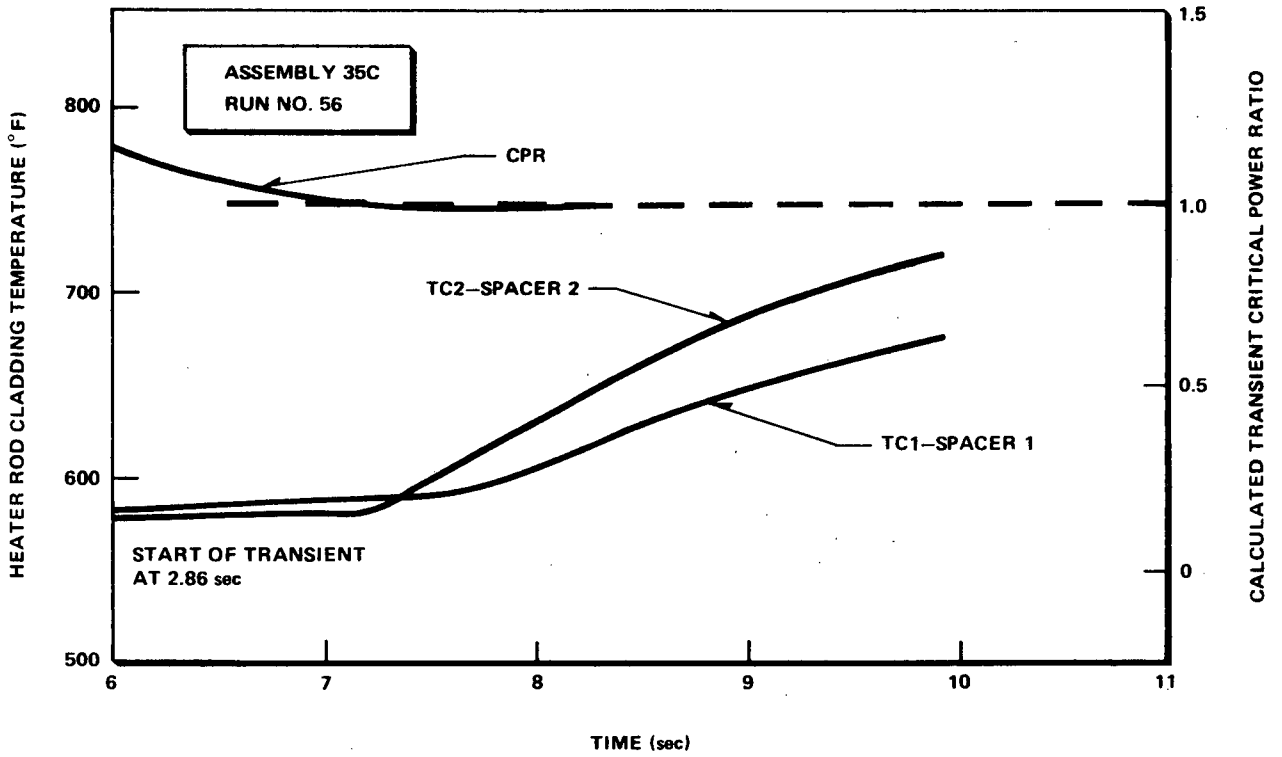


Figure 5-66. Calculated Transient Critical Power Ratio and Measured Heater Rod Cladding Temperature Vs Time

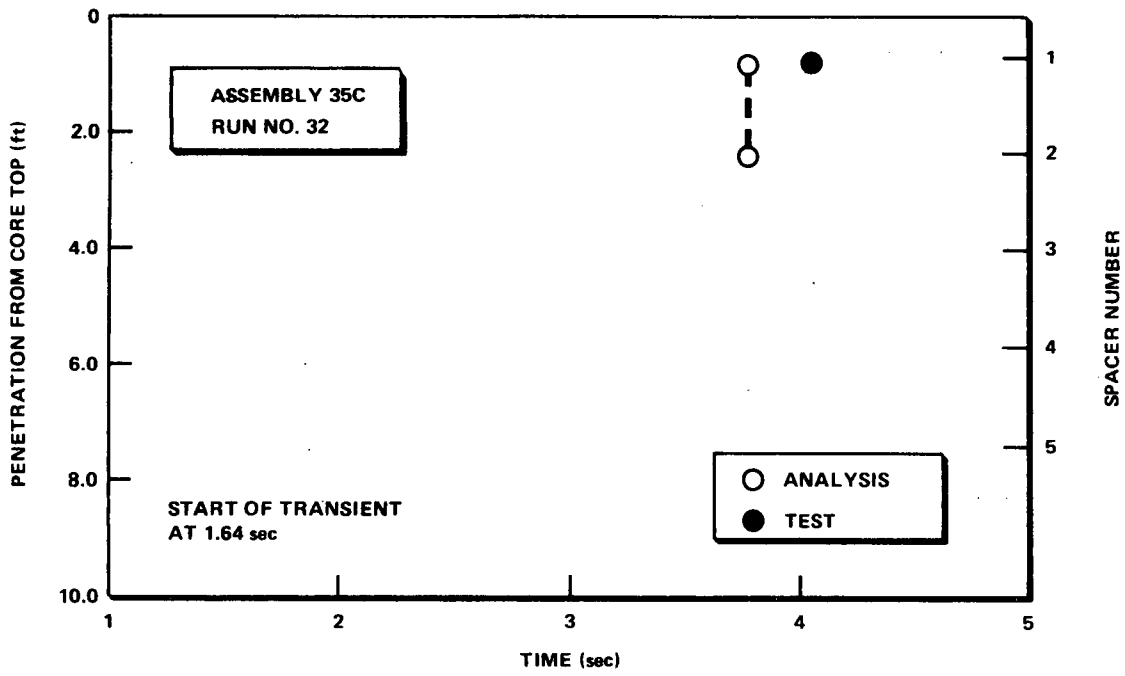


Figure 5-67. Axial Penetration of Boiling Transition Vs Time

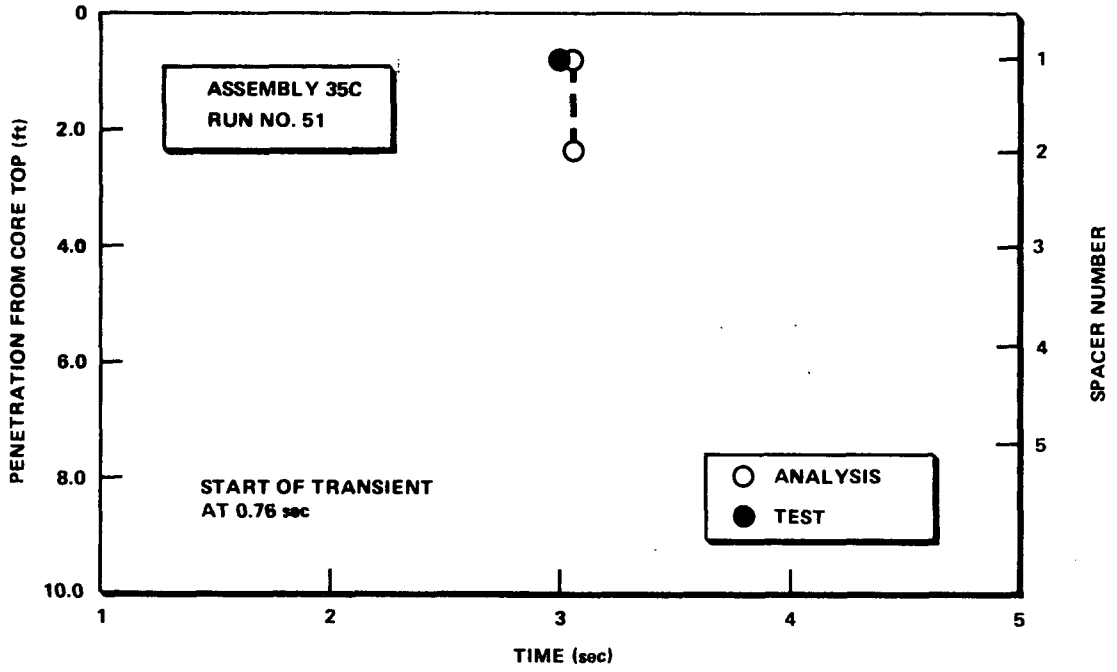


Figure 5-68. Axial Penetration of Boiling Transition Vs Time

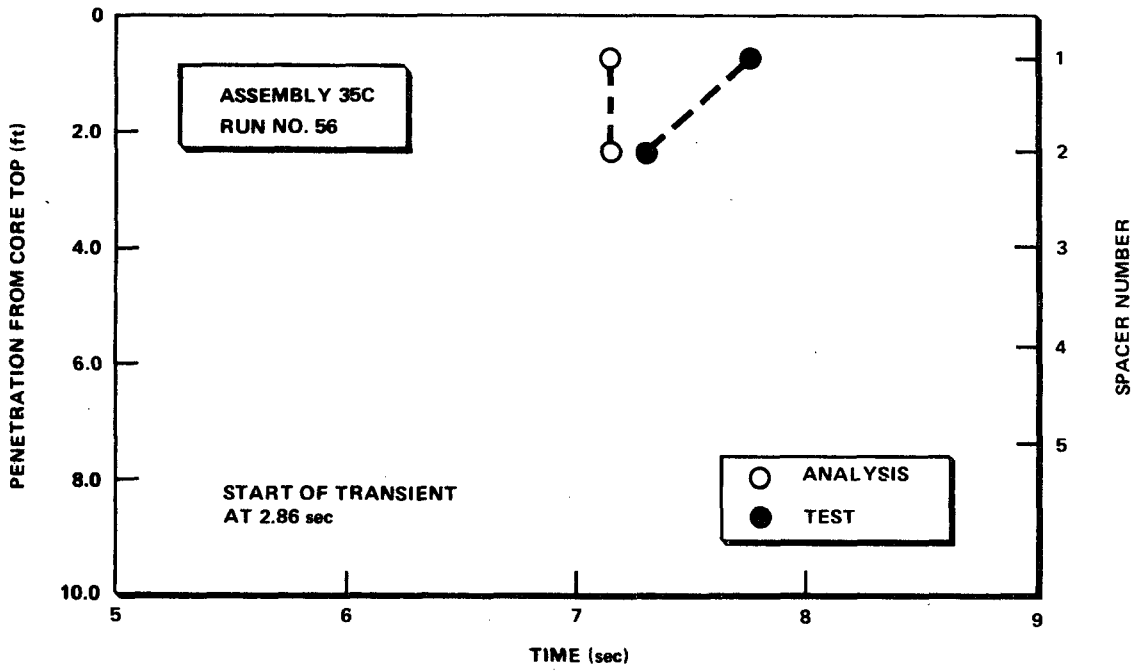


Figure 5-69. Axial Penetration of Boiling Transition Vs Time

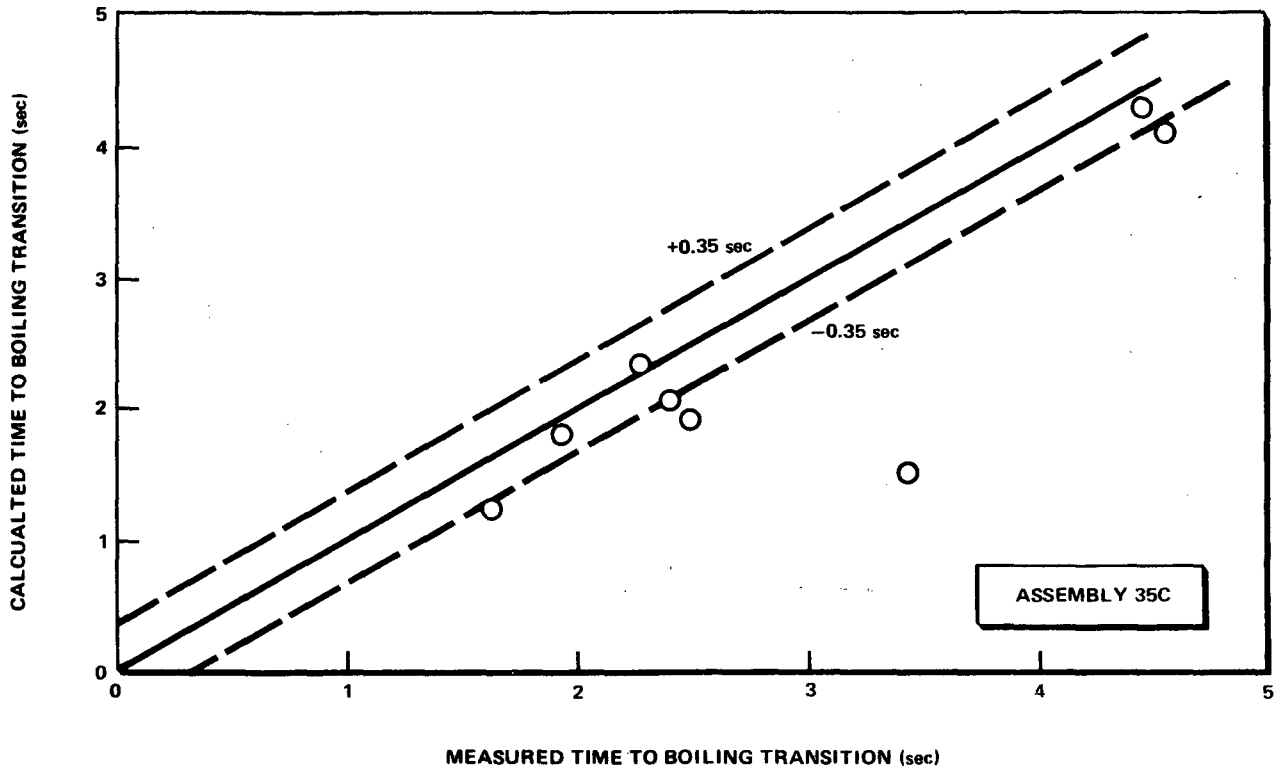


Figure 5-70. Calculated Time Vs Measured Time to Initial Boiling Transition



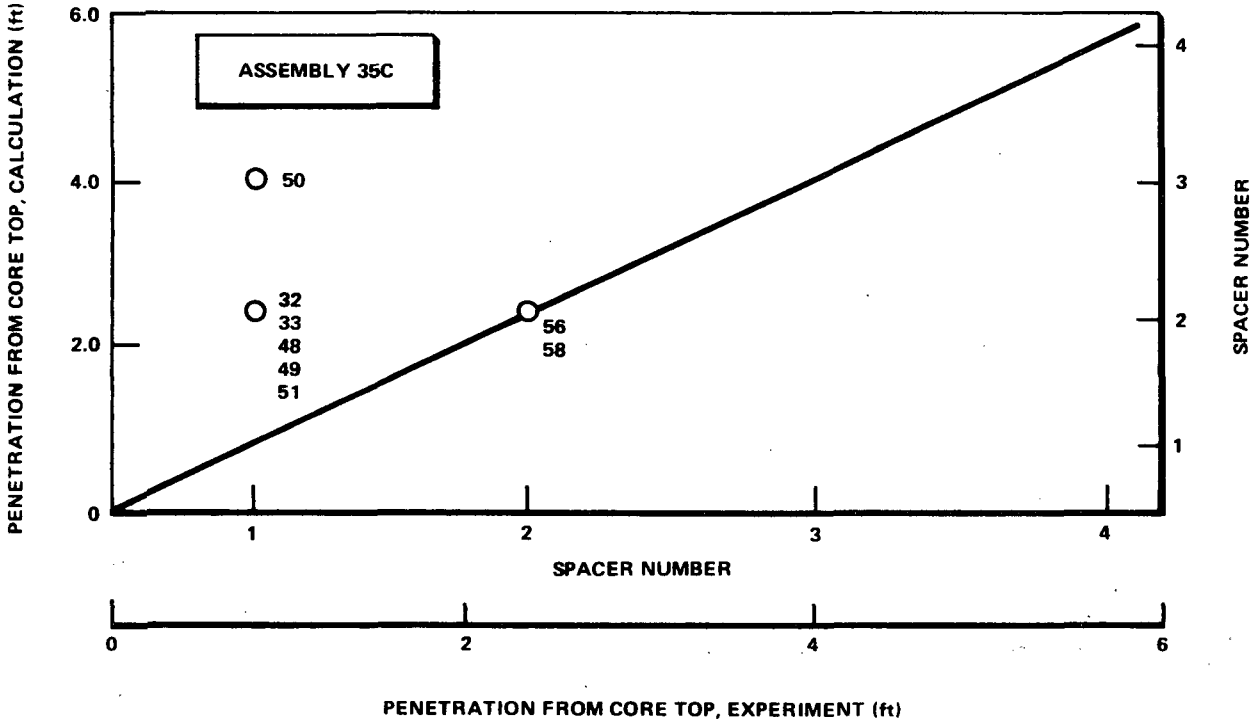


Figure 5-71. Boiling Transition Axial Penetration Calculated Vs Measured

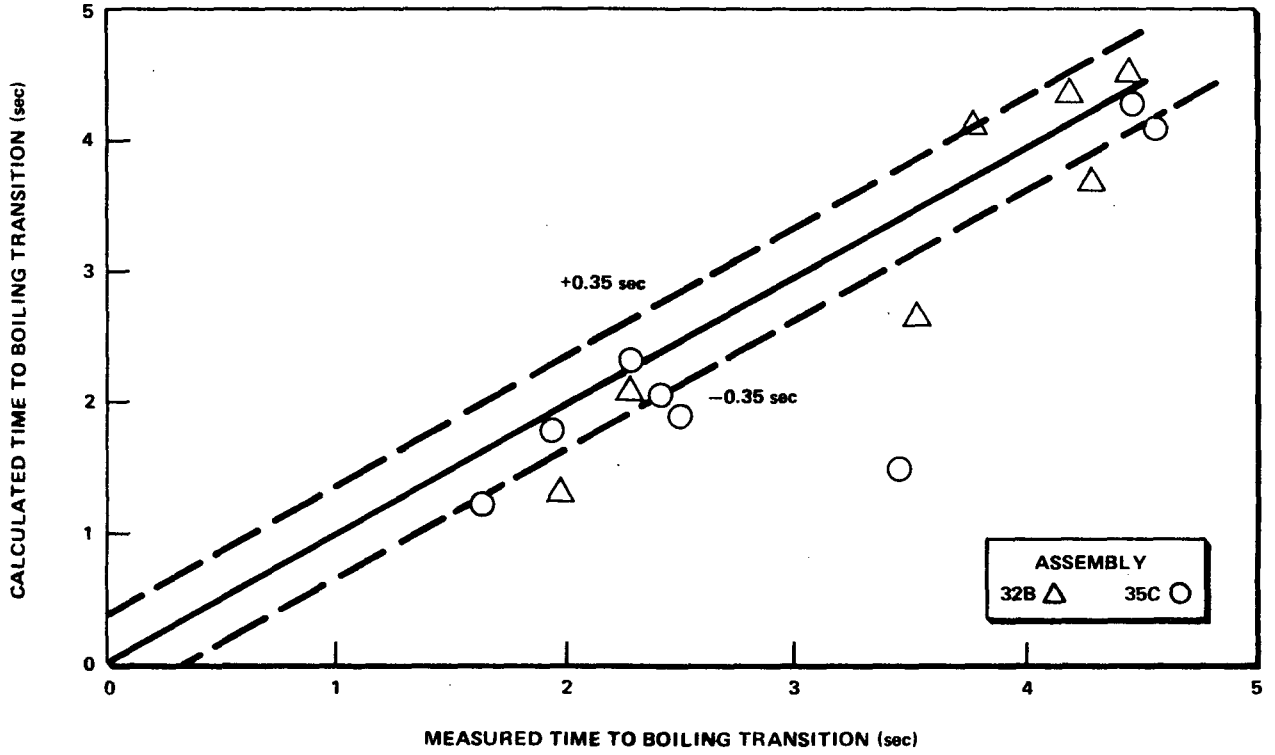


Figure 5-72. Calculated Time Vs Measured Time to Initial Boiling Transition

## 6. APPLICATION TO BWR DESIGN

### 6.1 INTRODUCTION

The availability of the full scale transition data and the new correlation capable of accurately predicting these data greatly improve the reliability of BWR thermal design. These advancements have led General Electric to make the following logical revisions in its design procedures and bases:

- (1) critical power ratio (CPR) is used rather than critical heat flux ratio (CHFR) as the new figure of merit for evaluating BWR thermal margin,
- (2) the best-fit correlation of the data is used rather than a limit line as the new design correlation; and
- (3) a statistical analysis of the core is the primary procedure for determination of design and operational thermal margin. Limits are stated in terms consistent with the form of the statistical result.

For the past several years, the design and operating limit for GE BWRs has been a minimum critical heat flux ratio (MCHFR) of 1.9 relative to the limits of APED 5286.<sup>1</sup> The value (1.9) was selected to provide margin to accommodate transients and uncertainties including those resulting from extrapolation of data from partial bundle heat transfer experiments to reactor conditions. For any of a special set of transients or disturbances caused by single operator error or single equipment malfunction, it was required that design analyses initialized at the steady-state operating limit (1.9) yield not less than 1.00 MCHFR during the transient. In addition, statistical analyses<sup>18</sup> were performed to verify that the combined effect of transients and uncertainties yielded an extremely low probability that any fuel rod would actually experience critical heat flux (i.e., a boiling transition).

The new heat transfer data, as described in earlier sections, include the effects of many more variables than was the case in Reference 1 and a much smaller uncertainty in predicting the conditions which lead to the onset of transition boiling (i.e., critical power). The heat transfer limits are based on full scale tests of electrically heated assemblies geometrically identical to reactor fuel, with thermal hydraulic conditions covering the same range as occurs in power reactors.

This improvement in understanding of the dependence of the boiling transition on fuel design characteristics leads to an increased confidence in the results of statistical analyses. Therefore, statistical analysis, with suitably conservative requirements, is the primary analytical basis for establishment of design and operating thermal margins. The position of a correlating line, best-fit or limit line is immaterial in these statistical studies because the actual position of the data is used.

Previous practice has been to quote thermal margin in terms of a critical heat flux ratio (CHFR). The form of the new correlation of the test data lends itself to the critical power ratio (CPR) which is not only more convenient for application, but also more descriptive of the relation between normal operating conditions and conditions which produce a boiling transition.

Several topics are discussed in this section: (1) description of the new figure of merit; (2) description of the statistical basis for establishing design and operating thermal limits including a numerical example; (3) recommendations for the Technical Specification; and (4) application of GEXL for steady-state, operational transients, and LOCA analyses. In this regard it should be emphasized that, except for the statistical studies, no new analytical models are introduced in the new design basis; only the introduction of a new correlation and a different figure of merit evaluated using the same analytical models previously used are involved.

### 6.2 CRITICAL POWER RATIO (CPR)

A primary design and operational objective is to maintain nucleate boiling and thus avoid a boiling transition. Therefore, BWR design and operational procedures are specified to maintain adequate margin to the onset of transition boiling. The GEXL correlation is an empirical representation of the conditions corresponding to the onset of transition boiling in the critical quality versus boiling length plane.

The figure of merit chosen for reactor design and operation is the critical power ratio (CPR). This is defined as the ratio of the bundle power which would produce equilibrium quality equal to but not exceeding the correlation value (critical quality), to the bundle power at the reactor condition of interest (i.e., the ratio of critical bundle power to operating bundle power). In this definition, the critical power is determined at the same mass flux\*, inlet temperature, and pressure which exist at the specified reactor condition. This ratio is evaluated as illustrated in Figure 6-1. Shown in the figure are bundle-average equilibrium steam quality distributions over the length of the bundle for critical and operating bundle powers and the corresponding GEXL correlation line. As seen in the figure, the critical power is that bundle power at which the heat balance curve becomes tangent to the correlation line.

The ratio of critical power to operating bundle power must be held above a prescribed value for all the fuel assemblies in the reactor core during normal steady-state operation. The reactor thermal margin is stated in terms of the minimum value of the critical power ratio, MCPR, corresponding to the most limiting fuel assembly in the core.

Critical power as a function of the significant variables divided by the prescribed MCPR is to be employed by the reactor operator as a limit on bundle power during normal steady state operation. The significant variables were identified in the ATLAS tests and include mass flux, subcooling, axial power peaking both in location and magnitude, and local (rod to rod) peaking.

In applying the GEXL correlation to plant operation, the parameter R, which characterizes the local peaking pattern, is expressed conservatively in terms of bundle-average exposure. Figure 6-2 gives an example for a typical single enrichment fuel assembly of a BWR-4 product line plant.

### 6.3 STATISTICAL BASIS FOR ESTABLISHING DESIGN AND OPERATIONAL THERMAL LIMITS

#### 6.3.1 Analytical Procedure

A statistical basis for selection of the appropriate design and operational thermal margin requires consideration of the probability that fuel rods will experience a boiling transition. Although the results of statistical analysis may be described in several conventional ways, the consideration of a finite probability that transition boiling events will occur is a necessity in developing a logical statistical basis for margin determination. Because the statistical model yields these finite probabilities, reasonable criteria must be established in the same terms. Construction of a statistical model representing the effects of uncertainties provides a useful tool for measuring the effects of variation in thermal margin. Application of a statistical model recognizes explicitly that there is a possibility, however small, that some combination of a transient and various uncertainties and tolerances may cause transition boiling to exist locally for some period of time, and quantifies that probability.

The steady state and transient minimum critical power ratios (MCPR) are derived from the single design basis requirement:

Transients caused by single operator error or equipment malfunction shall be limited such that, considering uncertainties in monitoring the core operating state, more than 99.9% of the fuel rods would be expected to avoid boiling transition.

The application of this requirement imposes a definite limit on the lowest allowable MCPR during particular transients which have been defined. A chosen MCPR limit is examined using the full-core statistical analysis technique presented in Appendix IV. This analysis simulates the limiting point in the transient and verifies that more than 99.9% of the rods in the core would be expected to avoid boiling transition. Although the statistical analysis is most frequently performed in simulation of transients in which power distribution is invariant, analyses are also performed for localized events such as rod withdrawal error.

The steady-state operating limit is derived from the lowest allowable transient MCPR limit by simple addition of the nominal change in MCPR associated with the transient (Figure 6-3).

\*See response to Question 1-17, Appendix VII, for further information.

It should be noted that the stated basis differs from that employed by other members of the nuclear industry in that by using GETAB, uncertainties in the reactor operating state are explicitly included in defining the required thermal margins. For example, the limit employed by other light-water nuclear steam suppliers is a minimum DNBR of 1.3 for transient events comparable to several of the BWR transients included in GETAB. The basis for this limit appears to be the statement that with 95% confidence a DNBR of 1.3 using the appropriate DNBR correlation will result in a 95% probability that the DNB does not occur. In this case, however, the only uncertainty included is the inherent variance of the DNB correlation prediction capability.<sup>20</sup>

Application of the same statistical technique to the GEXL correlation prediction capability discussed in subsection 5.2 would result in the statement, "with 95% confidence a CPR of 1.05 using the GEXL correlation will result in a 95% probability that a boiling transition does not occur." As will be shown, consideration of core operating state uncertainties as well as prediction capability uncertainty as required by GETAB produces a full core transient limit MCPR requirement of approximately 1.05. Thus, although GETAB can be shown to be directly comparable to the bases employed by other vendors it is believed that the thermal margin created can be best described by the use of analytical tools which treat the entire core and the uncertainties in monitoring core performance. Detailed analysis of only the limiting point in the core or studies not accounting for the interaction of process variables are far less significant.

In summary, statistical analysis yields the lowest allowable MCPR for transients. The addition of the transient effect yields the operating limit MCPR. The example which follows illustrates this process and includes additional statistical evaluations of the core at normal operating conditions.

**6.3.2 Numerical Example of Derivation of Transient and Operating Limits**

The Monte Carlo procedures described in Appendix IV have been employed in a general investigation of all classes of boiling water reactors. Resulting probabilities that essentially all of the fuel rods will not experience a boiling transition lie within a very narrow range. One such analysis is documented in detail here.

The reactor chosen for detailed discussion is a typical BWR-4. Analytically, the nominal initial condition is established by means of a three dimensional core analysis at rated power in which the control rod positions are adjusted to produce MCPR = 1.20. Reactor conditions representing the limiting point in severe transients are obtained by adjusting reactor power so that MCPR is equal successively to 1.15, 1.10, and 1.05.

For the example chosen for this illustration the tabulated results are:

<u>Statistical Results</u>	
<u>MCPR</u>	<u>Percent of Rods Expected to Avoid Boiling Transition</u>
1.20	99.9997
1.15	99.9978
1.10	99.974
1.05	99.905

The above results show that more than 99.9% of the fuel rods are expected to avoid boiling transition at MCPR = 1.05. If 1.05 is adopted as the limit for this type of transient, and if this is the most limiting of all transients, then the associated decrease in MCPR may be used to establish the rated power design and operating limit.

The following table presents the decrease in MCPR associated with each of the transients involving the full core.

Table 6-1  
TRANSIENT CHANGE IN MCPR

<u>Cause</u>	<u>ΔMCPR</u>
Load Rejection with Bypass	-0.07
Turbine Trip with Bypass	-0.07
Turbine Trip without Bypass	-0.14
Load Rejection without Bypass	-0.14
Inadvertent HPCI Activation	-0.10
Two-Pump Trip	0.0
Loss of 100° F Feedwater Heaters	-0.13

These cases cover all areas of plant transient behavior where significant reductions of the thermal margin could be expected. All other pressure disturbance events (single valve failures, MSIV closure, etc.) produce less severe transients than those listed. Core flow reduction transients show large thermal margins as demonstrated by the two-pump-trip case shown. The pump seizure, a related flow reduction situation, is discussed later in subsection 6.5.2. Transients in which flow and power increase are very mild from the thermal margin viewpoint. Abnormal operational transients involving cooler core inlet flow are bounded by the 100°F feedwater temperature change presented. In all these cases, existing reactor protection system settings were assumed (trip scrams from valve position switches, nonflow referenced APRM setpoint, etc.). Therefore, no changes in protection system requirements are needed to implement GETAB. All pertinent cases in which significant reductions in the thermal margin might be involved have therefore been considered in this evaluation.

The rod withdrawal error at full power is a highly localized event. Calculated change in MCPR is only -0.10, assuming that the withdrawal is blocked by the RBM. This event is obviously not controlling because other events which do affect the entire core produce larger changes. See Appendix VII, response to Question 3-4 for additional information.

The case of the misoriented fuel assembly accident is another highly localized event. The total expected number of rods in the core subject to boiling transition for this case is one rod. Additional detail is given in the answer to Question 3-4 (Appendix VII).

From these examples, it is obvious that the localized events do not lead to large numbers of rods experiencing boiling transition.

Considering the full-core transients in the table, the most limiting is the turbine trip without bypass. The statistical analysis showed a final MCPR as low as 1.05 is acceptable in terms of the basic requirement. Thus, a steady-state MCPR operating limit would be  $1.05 + 0.14 = 1.19$ . This analysis indicates that an operating MCPR  $> 1.19$  satisfies the basic requirement. Appendix V illustrates the influence of axial power shape and R-factor on these results.

The analysis was also performed on a higher power density BWR/6 core. The most limiting transient for this case was also found to be a generator load rejection without bypass, resulting in a  $0.14 \Delta$  MCPR. The statistical analysis established 1.07 as the minimum critical power ratio required to satisfy the design basis. Thus, the required steady-state MCPR operating limit for BWR/6 would be  $1.07 + 0.14 = 1.21$ .

As described in Appendix IV, each of the trials in the Monte Carlo procedure may be regarded as a possible reactor operating state. The collection of all trials is a sample of the population of all combinations of the variables, distributed about the nominal operating condition. Each trial leads to a sum of the probability contributions of all rods, called the expected number of rods subject to a boiling transition. It is so called because it is the sum of the product of a probability and "1" rod, for each rod. (Each such expected number of rods is not a mean value since the probabilities of rods subject to a boiling transition do not sum to 1.0; that is, they do not form a probability mass function, which is required for the expected number to be a mean.) Thus, a distribution of expected numbers of rods subject to a boiling

3-4

2-6

transition is formed, and it is the relationship between the arithmetic mean of this distribution and the nominal core minimum operating CPR which is used to set the minimum allowable critical power ratio corresponding to the criterion on page 6-3, which requires 99.9% of rods in the core to avoid boiling transition under the worst transient.

For a typical BWR-4 plant operating with its minimum CPR at 1.20 the expected number of rods subject to a boiling transition will have the following properties\*:

1. The mean expected number of rods subject to a boiling transition is 0.0807. For a plant having 27,440 fuel rods, this corresponds to a mean fraction of rods expected to avoid boiling transition of 99.99959%.
2. Based on the number and variability of the Monte Carlo trials made, 95% confidence limits on the mean expected number of rods subject to a boiling transition are approximately 0 to 0.176.
3. Analysis of the results of the Monte Carlo trials indicates that the expected numbers of rods subject to a boiling transition are approximately log-normally distributed as illustrated for one set of results in Figure 6-4. It is estimated by use of the log-normal distribution that 99.99% of rods will avoid boiling transition with 97.5% probability. (The assumption of log normality is necessary to this derivation.)

#### 6.4 TECHNICAL SPECIFICATIONS SAFETY LIMIT

Current practice is to apply a technical specification safety limit to total reactor power as a function of flow and pressure. The basis for calculation of this limit is the assumption of a particular power shape which initializes the core at the MCHFR operating limit at rated power and flow. For a given flow and pressure the safety limit is that total reactor power which would produce MCHFR = 1.0 with the assumed fixed power shape used to initialize the analysis.

An ideal safety limit would have the following characteristics:

- (1) for all possible modes of operation which do not violate the limit, the core integrity is preserved to the extent that health and safety of personnel are not compromised;
- (2) the performance characteristics to which the limits are applied should be capable of being monitored by process instrumentation requiring a minimum of data processing and interpretation; and
- (3) the limit should be appropriately conservative.

The introduction of the more accurate GEXL correlation provides an excellent opportunity for improvement in the safety limit formulation.

It is recommended that the safety limit be defined as follows:

"The existence of an instantaneous fuel assembly total time rate of energy deposition in the active coolant in excess of the critical value in more than one fuel assembly shall constitute violation of the fuel cladding safety limit."

Use of this limit would produce the following improvements relative to current practice.

- (1) It is conservative. Existence of greater than critical power in only one assembly would produce a boiling transition on only two to three fuel rods. In the event of an incident involving a calculated violation of the recommended safety limit, indications of cladding overheating could be used to confirm the violation. Imposition of limits below critical power levels would be unnecessarily conservative. If the safety limit were established below critical power, indications of cladding overheating would not be present following an incident, and the question of existence of a violation would be settled entirely on the basis of analysis. (See the response to Question 1-18, Appendix VII.)

\*See the response to Question 2-5d, Appendix VII.

- (2) Because the safety limit is expressed in the same terms used to characterize the mode of boiling heat transfer, it would not be possible for a particular combination of pressure, flow, and power shape to be predicted as causing a boiling transition without also being in violation of the safety limit.
- (3) With regard to ease of application, the new formulation of the limit does not materially differ from the old. In each case, power must be determined by processing directly measured quantities. The new formulation would require the additional step of application of a transverse peaking factor to determine maximum fuel assembly power. Note that the current procedure for adjusting the safety limit for conditions of high peaking factor is not necessary with the proposed formulation of the safety limit.

However, as required by NRC in the SER, the safety limit has been established at the full core transient limit.

## 6.5 PROCEDURES FOR DESIGN EVALUATIONS

### 6.5.1 Steady-State Thermal Margin Analysis

The methods and procedures employed in the evaluation of specific core designs are independent of the boiling transition correlation applied. These methods and procedures are fully described in GESSAR<sup>21</sup> and are only briefly described herein.

The steady-state thermal-hydraulic analysis of BWR cores is performed with a computer program which models the parallel flow channel core. The basic assumption in the program when performing hydraulic analyses is that the flow entering the core from the lower plenum will divide itself between the fuel assemblies in a manner such that each fuel assembly experiences the same total pressure drop. The pressure drop for a fuel channel, which determines the core flow distribution, is calculated as the sum of the individual pressure drop components. This includes the inlet orifice, the lower-tie-plate, the area change to the rodded assembly, the rodded friction loss (single and two-phase), spacer local loss (single and two-phase), the acceleration due to density change, elevation, the upper-tie-plate (single and two-phase) local loss, the unrodded channel friction loss, and the expansion loss into the upper plenum. The methods used in calculating these terms are based on test data and correlations in general use throughout the industry.

The designer specifies the core geometry, operating power and pressure levels, core inlet enthalpy, and power distributions within the core. The core flow is specified and the resulting core pressure drop, core flow distribution amongst the fuel assemblies, the leakage bypass flow and power, and the axial variation of quality, density, enthalpy within each assembly and critical power ratio for each channel type are calculated.

The calculated fluid properties (quality, enthalpy, and density) are averages for the in-channel coolant at each axial node position. This is consistent with the definition and assumptions of the GEXL correlation.

Consider an example corresponding to a typical BWR/4. The basic input parameters for this case are:

- (1) Core design thermal power: 2436 MWt
- (2) Design Power Distribution:
  - (a) Radial (Peak Bundle/Average Bundle): 1.4
  - (b) Axial (Peak of a Rod/Average of the Rod): 1.4
  - (c) Nonfuel power fraction: 0.04
  - (d) R: 1.065
  - (e) Average power density: 51.2 kW/1
- (3) Core Thermal-Hydraulic Parameters
  - (a) Total Flow:  $78.5 \times 10^6$  lb/hr
  - (b) Inlet Enthalpy: 523.7 Btu/lb
  - (c) Core Pressure: 1035 psia
- (4) Geometry: 560 bundles, 7 x 7 lattice, 144 inches active fuel length.



The results show that the core MCPR based on GEXL is 1.21, and for comparison the MCHFR based on Hench-Levy is 2.01. Thus, the core design satisfies the design thermal margin requirements of MCPR = 1.19 (as derived in subsection 6.3.2) for the most limiting expected power distribution in the core life.

Similarly, for a BWR/6

- (1) Core Design Thermal Power: 3833 MWt
- (2) Design Power Distribution:
  - (a) Radial (peak bundle/average bundle): 1.4
  - (b) Axial (peak of a rod/average of a rod): 1.4
  - (c) Nonfuel power fraction: 0.04
  - (d) R: 1.05
  - (e) Average power density: 56.0 kW/L
- (3) Core Thermal-Hydraulic Parameters
  - (a) Total flow:  $113.5 \times 10^6$  lb/hr
  - (b) Inlet enthalpy: 528.1 Btu/lb
  - (c) Core pressure: 1055 psia
- (4) Geometry: 784 bundles, 8 x 8 lattice, 148 inches active fuel length.

Applying GEXL to this case results in a steady-state MCPR of 1.22, which also satisfies the steady-state operating limit derived in Subsection 6.3.2.

### 6.5.2 Transient Analysis

The transient analysis procedures employed with GEXL are the same as those used with the Hench-Levy limit line. However, for completeness, a brief description of these procedures follows.

Abnormal operational transients are the result of single equipment failures or single operator errors. The predicted core dynamic behavior during such operational transients are determined using a computer simulated, analytical model of a generic BWR. All basic equations and assumptions of this model are presented in Reference 22. The report also contains extensive transient sensitivity studies for key transient safety events. Extensive comparison between BWR startup test data and the General Electric design process, which has utilized this basic model for several years, shows the conservatism of calculations performed for licensing purposes. Some of the significant features of this model are:

- (1) A point kinetic model is assumed with reactivity feedback from control rods (absorption), voids (moderation), and Doppler (capture) effects.
- (2) The fuel is represented by three four-node cylindrical elements, each enclosed in a cladding node. One of the cylindrical elements is used to represent core average power and fuel temperature conditions, providing the source of Doppler feedback. The other two are used to represent "hot spots" in the core, to simulate peak fuel center temperature and cladding temperature.
- (3) Four primary system pressure nodes are simulated. The nodes represent the core exit pressure, vessel dome pressure, steam line pressure, and turbine inlet pressure.
- (4) The active core void fraction is calculated from a relationship between core exit quality, inlet subcooling, and pressure. This relationship is generated from multinode core steady-state calculations. A second-order void dynamic model with the void "sweep time" calculated as a function of core flow and void conditions is also utilized.
- (5) Principal controller functions such as feedwater flow, recirculation flow, reactor water level, pressure, and load demand are represented together with their dominant nonlinear characteristics.
- (6) The ability to simulate necessary reactor protection system functions is provided.

These transient analyses procedures always include two types of conservatisms: (1) initial conditions and reactor characteristics are input to the model in a way that the course of the transient is more severely predicted; and (2) plant equipment is chosen so that adequate margins exist between any predicted variable and its limiting value from a safety viewpoint. Examples of these conservative inputs include:

- (1) A worst, usually maximum, power condition is assumed with thermally limited fuel conditions.
- (2) Minimum performance of all equipment is assumed. This is followed for valves (like safety-relief), inertia of a pump, control rod scram motion, or any other component involved in a transient.
- (3) Setpoints of devices expected to respond are assumed to be at the poorest edge of their specified error bands.
- (4) Conservative factors are applied to key inputs such as dynamic void reactivity and Doppler reactivity coefficients, or the reactivity worth of scram of the rods. In some cases, opposite factors are applied to different types of transients because a reversal of effect sometimes occurs. Recirculation reductions, for example, are run with less negative void reactivity feedback than the power-increase types of transients where highly negative void reactivity is more conservative.
- (5) Most severe initiation of each event is postulated, such as fastest closure of an MSIV.

22

The results of these analyses, as documented in licensing submittals as well as this topical report, also demonstrate significant margins held by BWR designs between the peak (or maximum) variables calculated by the preceding procedure and any safety limits. Most obvious are the margins in peak pressures for isolation type events. Covered in depth in this report are the margins that exist when thermal limits are evaluated using the following detailed procedure:

The following plant operating conditions and assumptions form the principal bases for which the core thermal margins are evaluated during abnormal operational transients.

- (1) The reactor core is operating at 100% of rated power and 100% core flow. These conditions result in minimum thermal margin and maximum linear heat generation rate.
- (2) The core is assumed to be operating at the design thermal limit for MCPR.
- (3) The steady-state operating power distribution is applied and is assumed to hold throughout the transient. Because cores are designed at steady-state to provide or exceed the minimum allowable steady-state critical power margin with the maximum allowable linear heat generation rate, some adjustment in the axial power distribution and radial power distribution might be necessary to put the core on LHGR and MCPR limits simultaneously.

The evaluation of a particular transient begins with predictions of the core dynamic behavior as determined from the aforementioned transient computer program. Calculated results are:

- (1) core flow vs. time;
- (2) core inlet enthalpy vs. time;
- (3) core pressure vs. time; and
- (4) energy generated within the fuel vs. time.

These results form the input for further analysis of the thermally limiting bundle with the single channel transient thermal hydraulic digital computer program described in Reference 14.\*

The principal result of this evaluation will be the transient value of MCPR which can then be compared to the limit derived as described in subsection 6.3.1.

As discussed in this section, the transient analysis is a bounding rather than a statistical analysis. The use of this conservative analysis approach in GETAB assures that the uncertainties associated with the transient are included in the transient  $\Delta$  MCPR used for derivation of the GETAB operating limits. (See response to Question 2-4, Appendix VII.)

In general, the results of transient analyses with the GEXL correlation are very similar to those obtained with the Hench-Levy correlation.\*\* It is notable, however, that whereas the worst transient on the Hench-Levy basis was the pump seizure, this event is no longer limiting. Instead, the worst transients with the GEXL correlation are the power increase transients such as the turbine trip without bypass transient as shown in Table 6-1. Because of the highly unlikely nature of this pump seizure event, it has been classified in the accident category by U.S. PWR vendors (the event is referred to as a "locked rotor accident" rather than pump seizure). The introduction of GETAB makes this a convenient time to reclassify this event to be consistent with the precedent set by the other vendors. Because the event is not limiting with GETAB, this reclassification will be incorporated in future BWR submittals.

\*See the response to Question 3-5, Appendix VII.

\*\*See the response to Question 3-1, Appendix VII.

### 6.5.3 Application to Loss of Coolant Accident (LOCA)

#### 6.5.3.1 Introduction

This section is devoted to a study of the LOCA analysis with the GEXL correlation and comparison of results to previous analysis. It will be shown that the peak cladding temperature is the same using the GEXL correlation as it is using the CHF correlation in the Interim Acceptance Criteria (IAC).

It is important to note at the outset that except for the substitution of the GEXL correlation, none of the standard LOCA calculational models previously approved for IAC LOCA analyses have been modified. Only the parameters which define the duration of nucleate boiling are different from past practice. The previous correlation used critical heat flux<sup>14</sup> (CHF), as a limit, whereas the new correlation (GEXL) is based on critical quality and boiling length as previously described in this report. The fundamental reason for applying either a CHF or a critical quality-boiling length correlation to the analysis of the LOCA is to determine the duration of the nucleate boiling heat transfer mechanism during the initial flow coastdown portion of the postulated LOCA blowdown. Per the Interim Acceptance Criteria models, the boiling heat transfer is examined throughout this time period.

#### 6.5.3.2 Selection of Initial Conditions

In order to establish an appropriately conservative initial condition to be used in LOCA analyses with the GEXL correlation, a parametric study was performed for the postulated DBA in a BWR/4 standard plant design with 7 x 7 fuel. Because the BWR/4 has larger recirculation lines than more recent BWR designs (i.e., BWR/5 and BWR/6), this study represents a more severe case than for the more recent designs. The local peaking factor, bundle mass flow rate, and maximum linear heat generation rate (LHGR) were varied to provide a wide range of input for the selection of the proper boundary conditions to use in a "worst case" analysis. The initial conditions of the cases investigated are given in Table 6-2 along with the calculated times to reach a calculated boiling transition condition in the bundle. The subsequent penetration of the boiling transition into the bundle is also included in the table.

The magnitude of the values used as input initial conditions for the four cases presented in Table 6-2 are representative limits. For the bundle mass flux a conservatively low value of  $1 \times 10^6$  lb/hr ft<sup>2</sup> was selected as compared to the more realistic design value of approximately  $1.1 \times 10^6$  lb/hr ft<sup>2</sup> for the highest powered bundle in the reactor core. Axial peaking factors of 1.5 and the design axial peaking factor of 1.4 were used in the study. For cases 2, 3, and 4 the bundle was assumed to be at a total power consistent with the maximum linear heat generation rate (LHGR) shown, the design axial peaking factor and the local peaking factor. For these three cases, a fuel design was postulated such that its calculated R gave an initial MCPR of 1.2, which is typical of the operating limit proposed in the previous section. For case 1, the highest value of R consistent with typical fuel designs was chosen and the bundle power was correspondingly reduced to produce an initial MCPR of 1.2.

Peak cladding temperature for the LOCA increases with greater LHGR and decreases with greater duration of nucleate boiling after the start of the LOCA. Therefore, a conservative core heatup analysis requires the selection of those parameters which result in the least amount of cooling for the highest powered fuel section. Inspection of the results presented in Table 6-2 for the four cases indicates that, although case 2 gives the earliest boiling transition, the LHGR of the axial node which experiences boiling transition is sufficiently low that it would not control peak cladding temperature. The case predicting the deepest penetration (i.e., case 3) is the controlling case. After the time of jet pump suction uncover (6.5 sec), the entire bundle is assumed to experience the boiling transition (per the IAC). The effect of bundle flow rate on the transient results is not significant; however, the table shows that use of  $1.0 \times 10^6$  lb/hr/ft<sup>2</sup> results in a slight conservatism. From all of these considerations it is clear that case 3 would result in the maximum peak cladding temperature, and thus the conditions for this case were used for the LOCA analysis.

#### 6.5.3.3 Evaluation of the Design Basis LOCA

In order to evaluate the overall effect of the new GEXL correlation on the LOCA, a core heatup calculation is first performed as described in Appendix D of Reference 14. As stated in subsection 6.5.3.2, the highest powered bundle in the reactor core is initialized to conservative limits consistent with the design peaking factors. For a postulated LOCA assuming the steady-state initial conditions given in subsection 6.5.3.2, a core heatup analysis was performed and compared to the corresponding analysis calculated using the previous CHF correlation. In order to

Table 6-2  
TYPICAL DBA – BWR/4 7 x 7 FUEL

Initial Conditions	Case			
	1	2	3	4
1. Bundle Power (MWt)	5	6	6	6
2. Bundle Mass Flux (lb/hr/ft <sup>2</sup> )	1 x 10 <sup>6</sup>	1 x 10 <sup>6</sup>	1 x 10 <sup>6</sup>	1.12 x 10 <sup>6</sup>
3. Axial Peaking (chopped cosine)	1.4	1.4	1.5	1.5
4. Maximum LHGR (kW/ft)	14.2	17.1	18.5	18.5
5. R (GEXL correlation)	1.12	1.06	1.046	1.056
6. Initial MCPR	1.2	1.2	1.2	1.2
<b>Results</b>				
1. First Indication of Boiling Transition				
(a) Time (sec)	1.3	0.8	1.1	1.2
(b) LHGR at location of critical condition (kW/ft)	9	10.9	11.1	11.1
2. At deepest penetration during flow coastdown period				
(a) Time (sec)	1.5	1.3	1.3	1.4
(b) LHGR at location of boiling transition (kW/ft)	11.7	14.1	14.9	14.9

understand the differences between these two analyses and to demonstrate that the key results of the LOCA analysis (i.e., peak cladding temperatures are not changed), the required input data for both the Hench-Levy and GEXL analyses are plotted and discussed.

The calculated reactor core pressure and calculated reactor core inlet flow versus time for the design basis LOCA are given in Figure 6-5 and 6-6. These parameters were obtained from the approved IAC evaluation models.

Using these calculated values of core pressure, core flow and core inlet enthalpy, the transient thermal-hydraulic code was used to calculate the MCHFR and the MCPR versus time for the case 3 conditions given in subsection 6.5.3.2. The results of these calculations are plotted in Figure 6-7. It is evident that the CHF correlation from Reference 14 predicts the continuation of nucleate boiling heat transfer to the start of flow period 2\* (i.e., the time of jet pump suction uncover). It is also evident that the duration of nucleate boiling for the lower-powered upper section of the reactor bundle is shorter with the use of the GEXL correlation.

However, it is important to note that the highest axial powered section of the bundle did not experience critical heat flux (MCHFR = 1) or boiling transition (MCPR = 1) before the start of period 2. Therefore, the axial plane of the bundle with the greatest LHGR is predicted by both correlations to have continued nucleate boiling throughout the entire flow coastdown period.

At the uppermost section of the bundle (spacers 2 and 3 from the top of the bundle), the LHGRs are, respectively, 60% and 81% of the peak LHGR. Since the difference in calculated time for these two axial nodes to reach the boiling transition is only 0.2 sec, the higher powered of these nodes was analyzed in the core heatup calculation to determine if it reaches a higher cladding temperature than the peak power node.

The boiling transition in the bundle does not occur simultaneously for all rods at a given axial plane. Most of the rods at the axial plane of boiling transition will remain in the nucleate boiling heat transfer regime, and the fuel channel

\*See Reference 14, p. C-2, Figure C-1.

will remain wetted by the flowing coolant in the bundle. At the onset of the boiling transition, the heat transfer mechanism would change from nucleate boiling with associated high heat transfer coefficients to transition boiling with somewhat lower heat transfer coefficients.

Eventually, the heat transfer mechanism on the nodes experiencing the boiling transition could reduce to film boiling heat transfer. The resulting heat transfer coefficients used in the core heatup calculation for both the Hench-Levy and GEXL correlations are shown in Figures 6-8 and 6-9.

The core heatup calculation was performed with the approved IAC evaluation model without modification. The results of the calculation for the highest powered axial node and the upper core node are given in Figure 6-10 and included in Table 6-3. As indicated in Figure 6-10, the calculated peak cladding temperature for the upper part of the core is 1970°F, as compared to the calculated peak cladding temperature of 2140°F at the peak LHGR location (midplane). The effect of axial power shape on these results is discussed in Appendix VI.

Because the highest-power axial section experiencing an early boiling transition does not closely approach the peak cladding temperature at the bundle midplane in this bounding calculation, it can be concluded that the peak cladding temperature as a result of a LOCA is not affected by adoption of the GEXL correlation in this sample case. This conclusion, it should be stressed, is not approximately true but strictly true, because the heat transfer mechanism in the axial plane experiencing the PCT is shown to be no different from that predicted with the Hench-Levy correlation in the approved IAC model.

The transient thermal-hydraulics code was also used to calculate MCHFR and MCPR versus time for a postulated design basis LOCA in a 251-BWR/6 with an 8 x 8 lattice. The results of these calculations are plotted in Figure 6-12. It is evident that both the CHF and the GEXL correlations predict the continuation of nucleate boiling heat transfer to the time of jet pump section uncovering when nucleate boiling is assumed to cease (per the IAC). In this sample case, and in accordance with the IAC, the calculated peak cladding temperature as a result of the DBA is not affected by adoption of the GEXL correlation.

**6.5.3.4 Evaluation of the Outside Steam Line Break**

In order to evaluate the effect of the new GEXL correlation on the overall analysis of the postulated break of the primary steam line outside the drywell, the transient thermal-hydraulic code was used to evaluate both the MCHFR and the MCPR, versus time for a typical BWR/4 nuclear power plant. The results of these calculations are plotted in Figure 6-11. Both the CHF correlation and the GEXL correlation predict the continuation of nucleate boiling heat transfer even beyond the time when the main steam line isolation valves close. Therefore, the new GEXL correlation does not change the previous results: there is no fuel rod cladding temperature increase before the isolation valves are closed.

**Table 6-3  
TYPICAL BWR/4 DESIGN BASIS LOCA  
(18.5 kW/ft PEAK LHGR)**

Thermal-Hydraulic Heat Transfer Model	Calculated Peak Cladding Temperatures	
	Core Midplane	Upper Core (see text)
1. Hench-Levy	2140°F	1790°F
2. GEXL	2140°F	1970°F

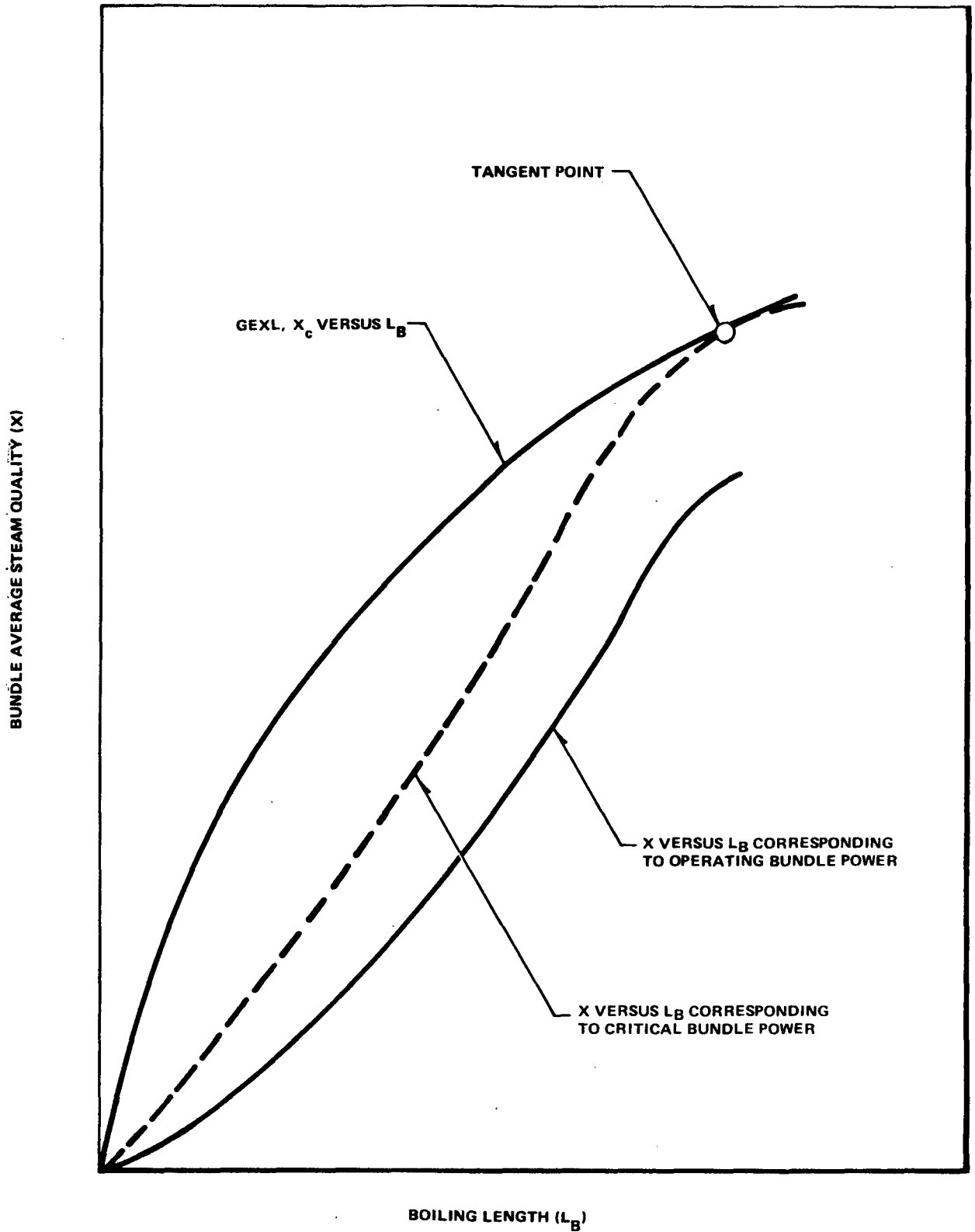


Figure 6-1. Graphical Illustration of CPR

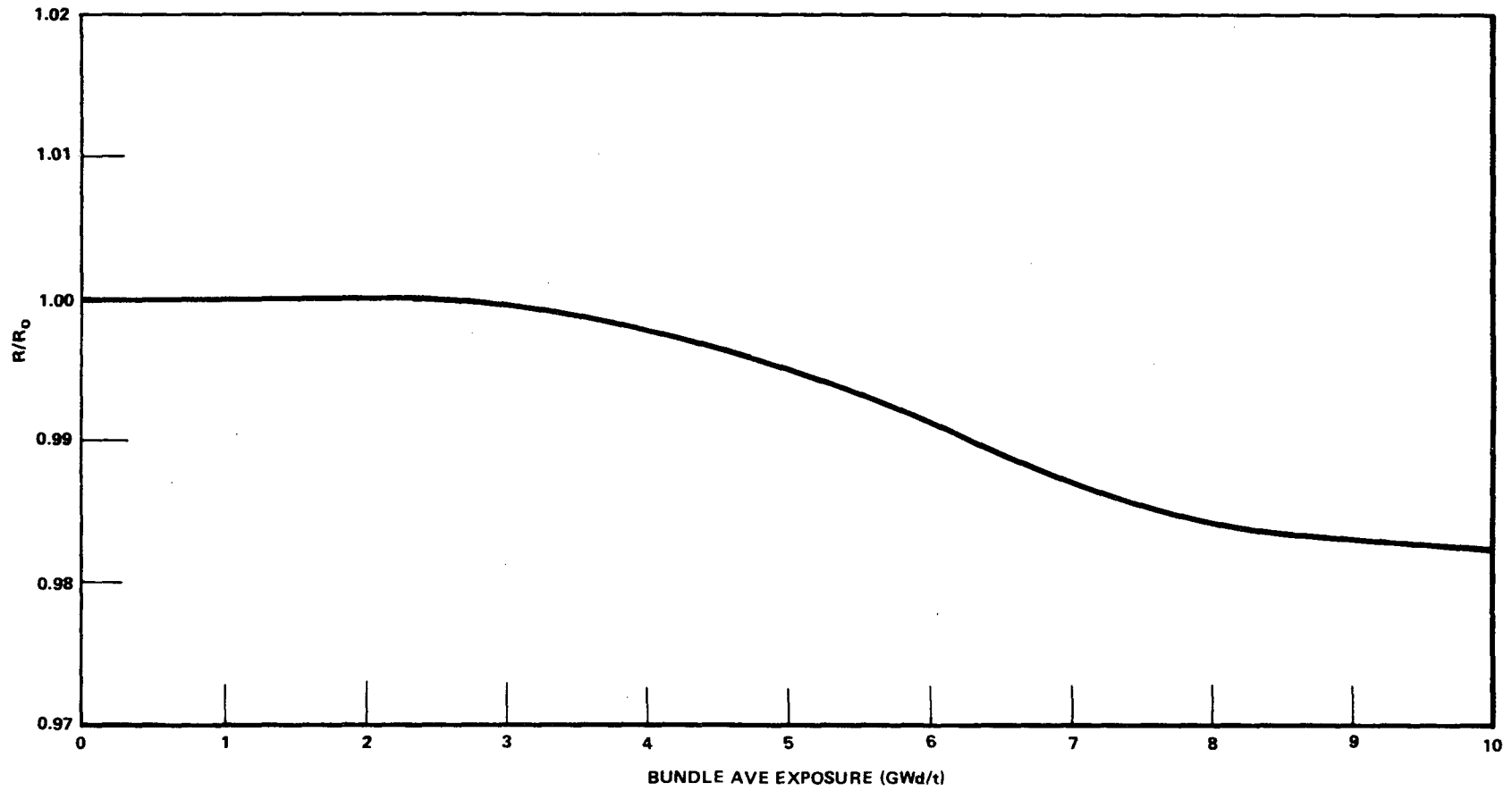


Figure 6-2. Normalized R Vs Bundle-Average Exposure, Typical Single Enrichment Assembly of BWR-4 Series



<u>M CPR</u>	<u>DESCRIPTION</u>
1.20 ←	STEADY-STATE OPERATING LIMIT DEFINES MARGIN FOR COMBINED EFFECTS OF TRANSIENTS AND UNCERTAINTIES
1.15	
1.10	
1.05 ←	TRANSIENT LIMIT FOR ABNORMAL FULL-CORE TRANSIENTS. RETAINS MARGIN FOR UNCERTAINTIES. LOCALIZED EVENTS BELOW THIS LEVEL ARE ALLOWABLE
1.00 ←	MEAN OF GEXL DATA BASE

Figure 6-3. Example of Critical Power Ratio Margins

Y = LOG OF NUMBER OF RODS EXPECTED TO EXPERIENCE BOILING TRANSITION

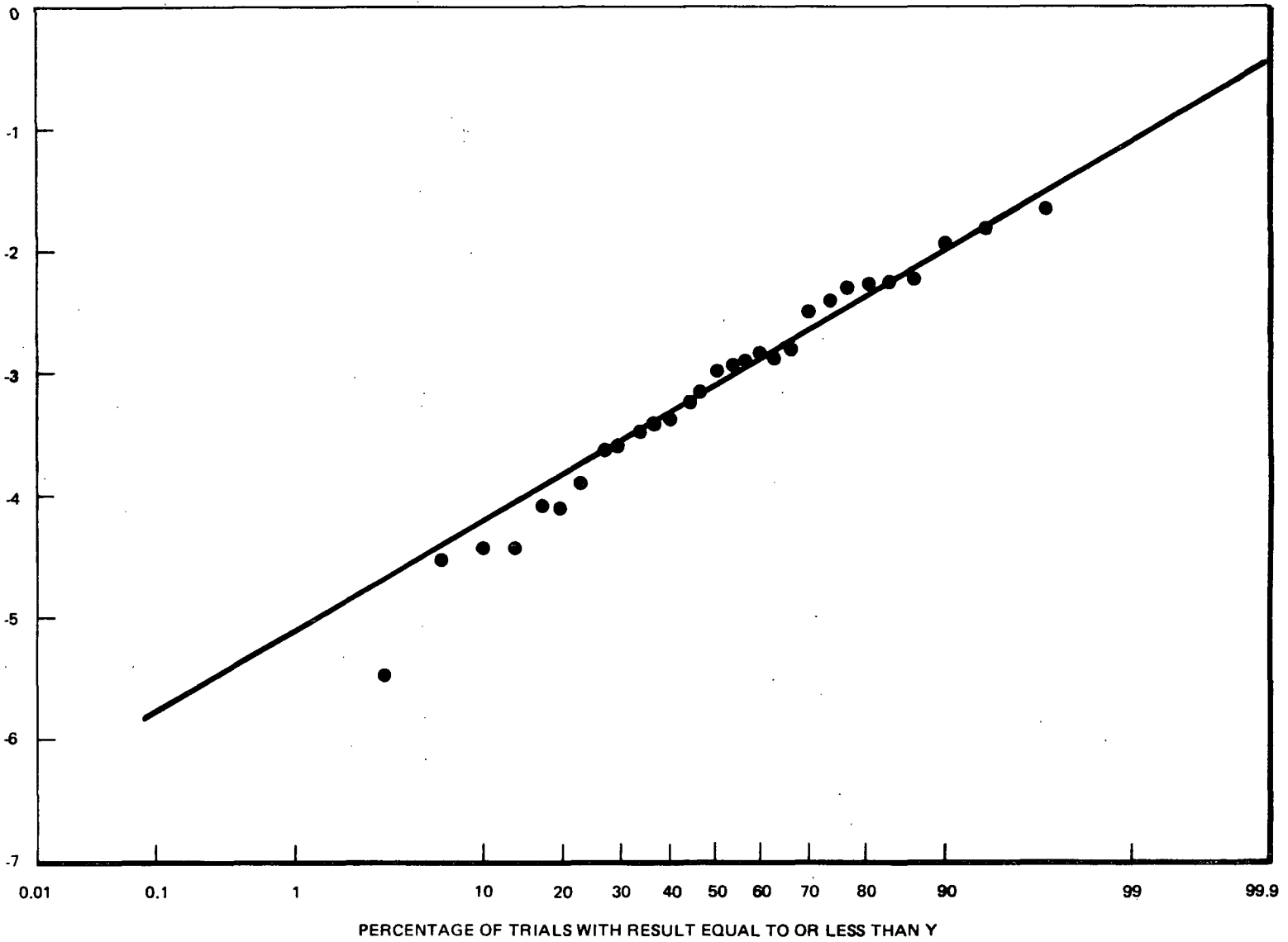


Figure 6-4. Typical Results of 30 Trials

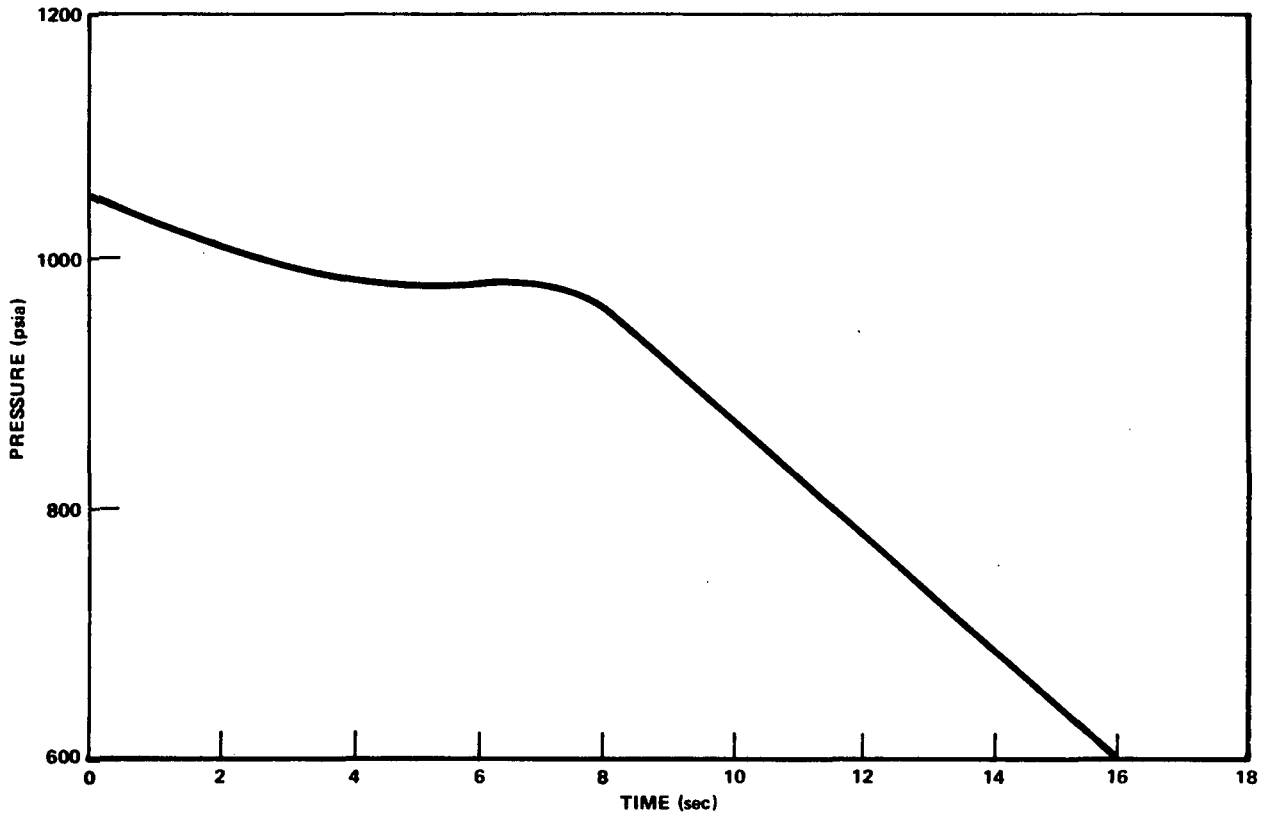


Figure 6-5. Core Pressure versus Time (DBA)

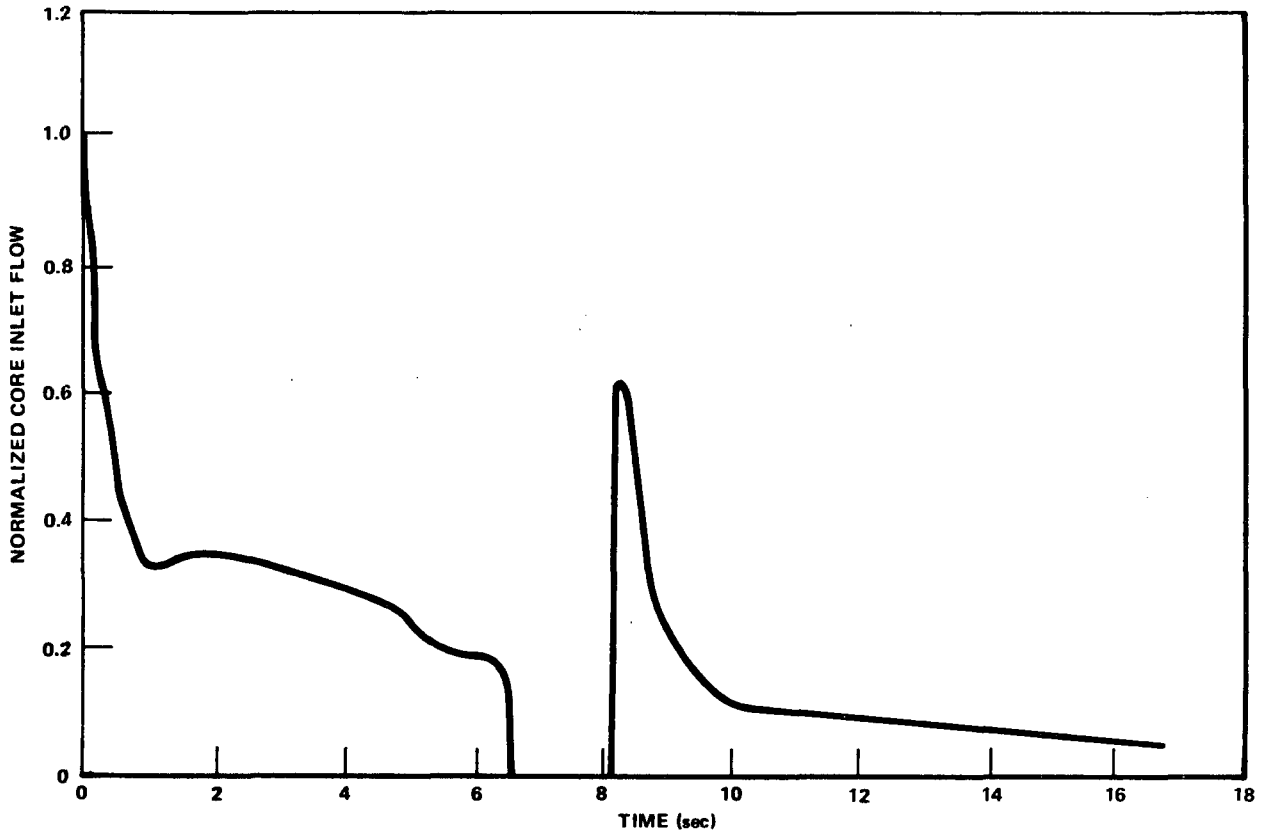


Figure 6-6. Normalized Core Inlet Flow versus Time (DBA)

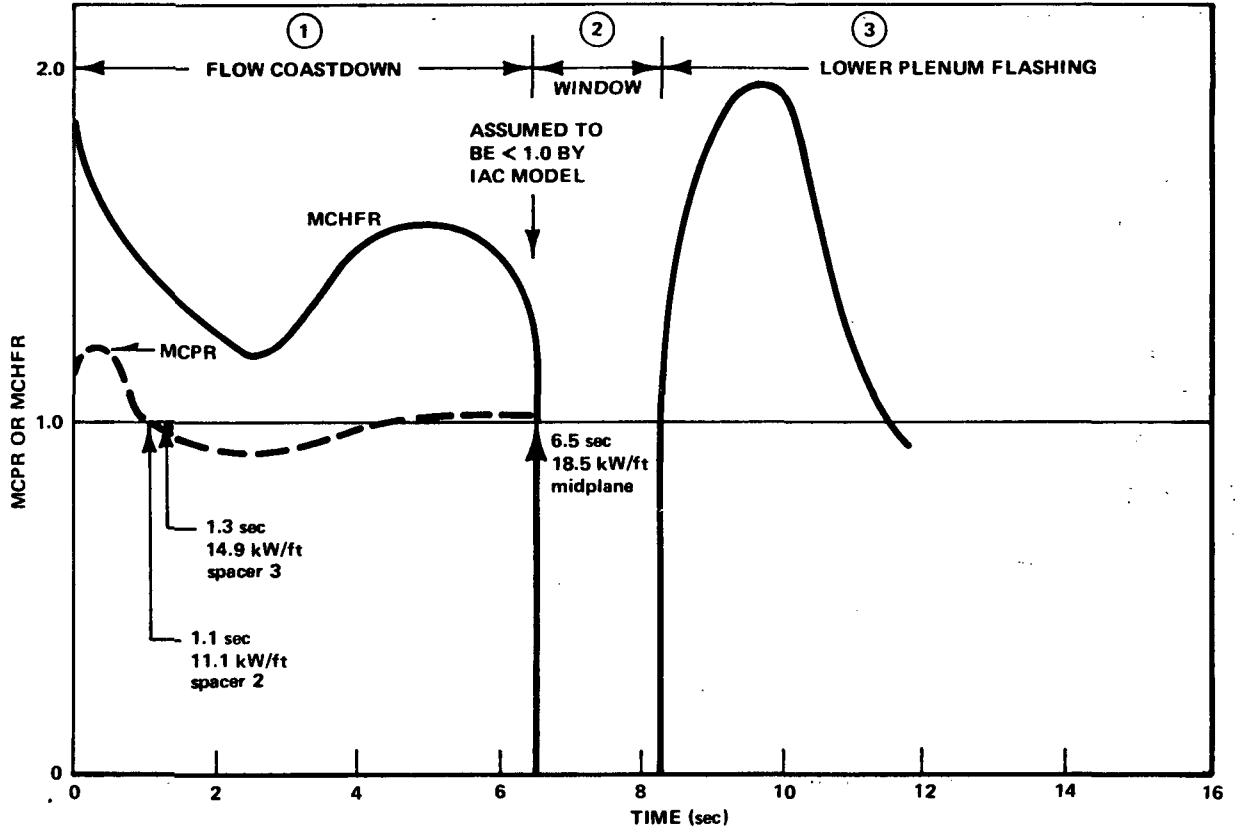


Figure 6-7. Minimum Critical Heat Flux Ratio and Minimum Critical Power Ratio versus Time (DBA)

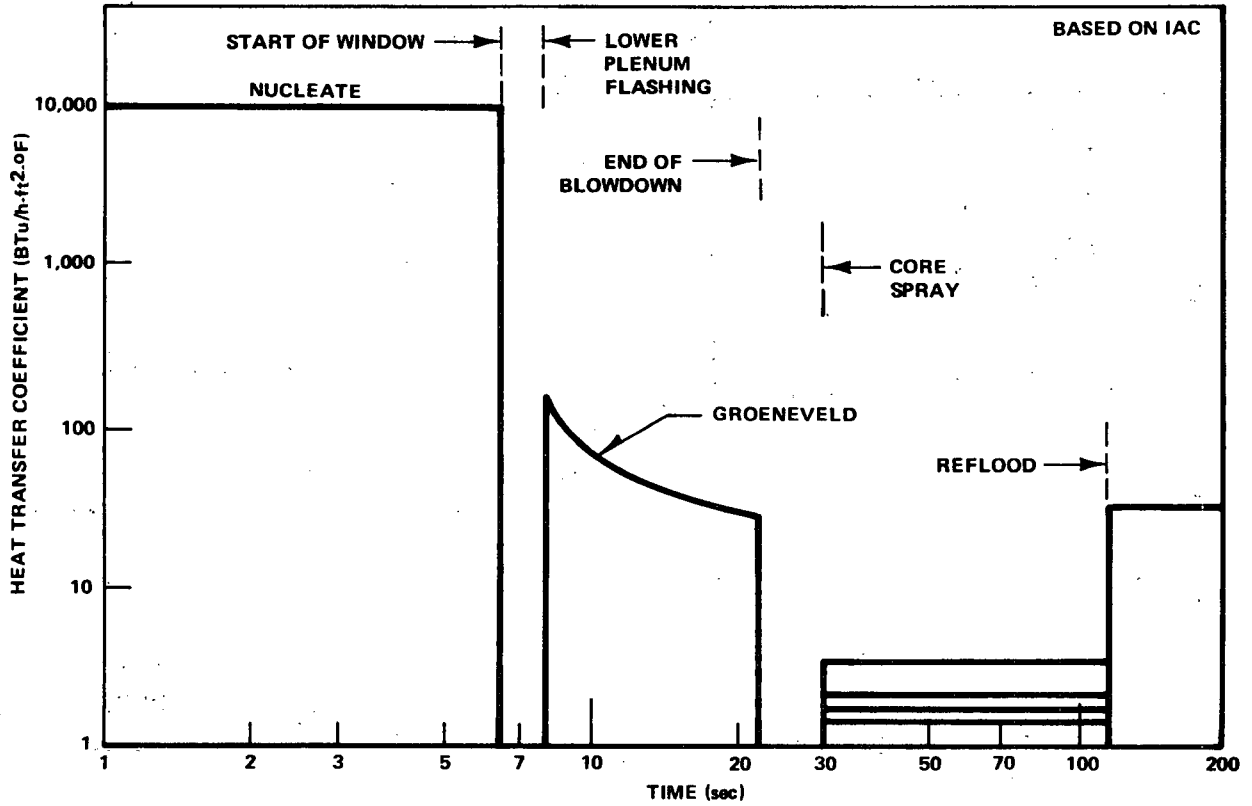


Figure 6-8. Heat Transfer Coefficient versus Time After Design Basis Accident (Hench-Levy)

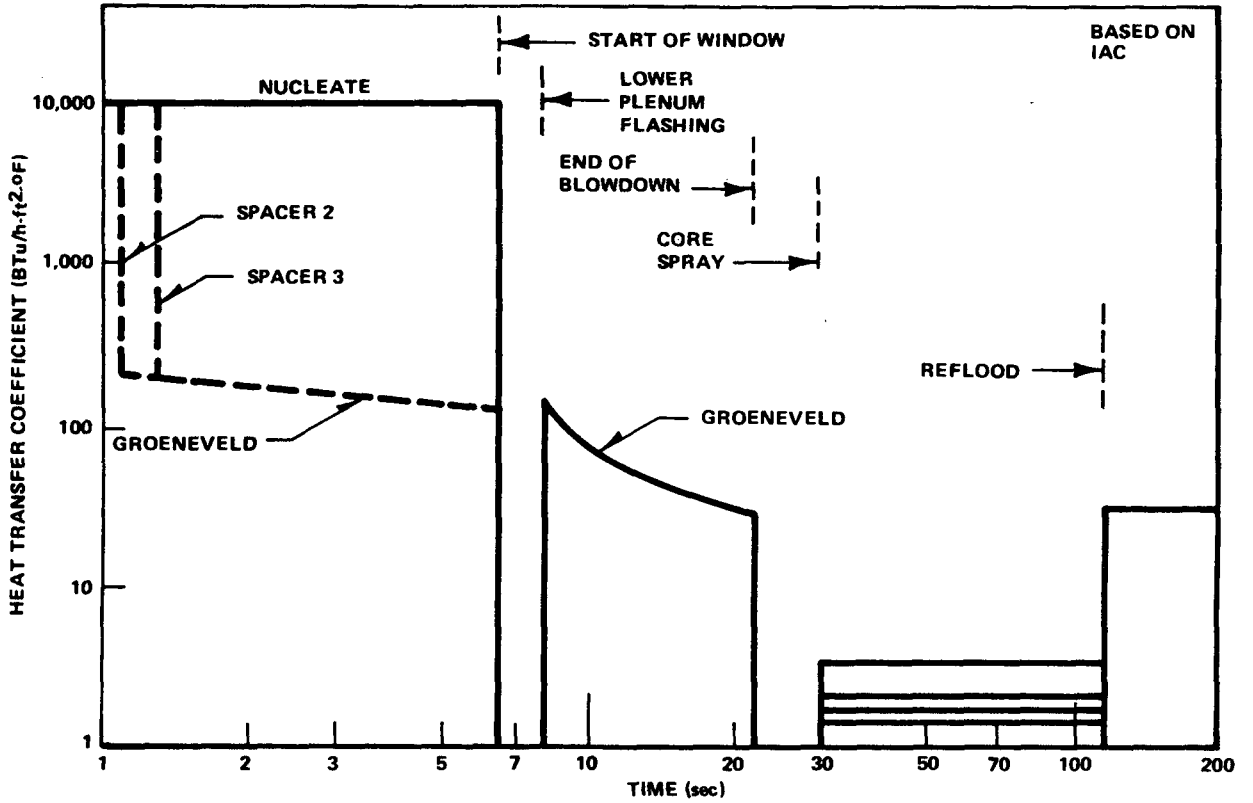


Figure 6-9. Heat Transfer Coefficient versus Time After Design Basis Accident (GEXL)

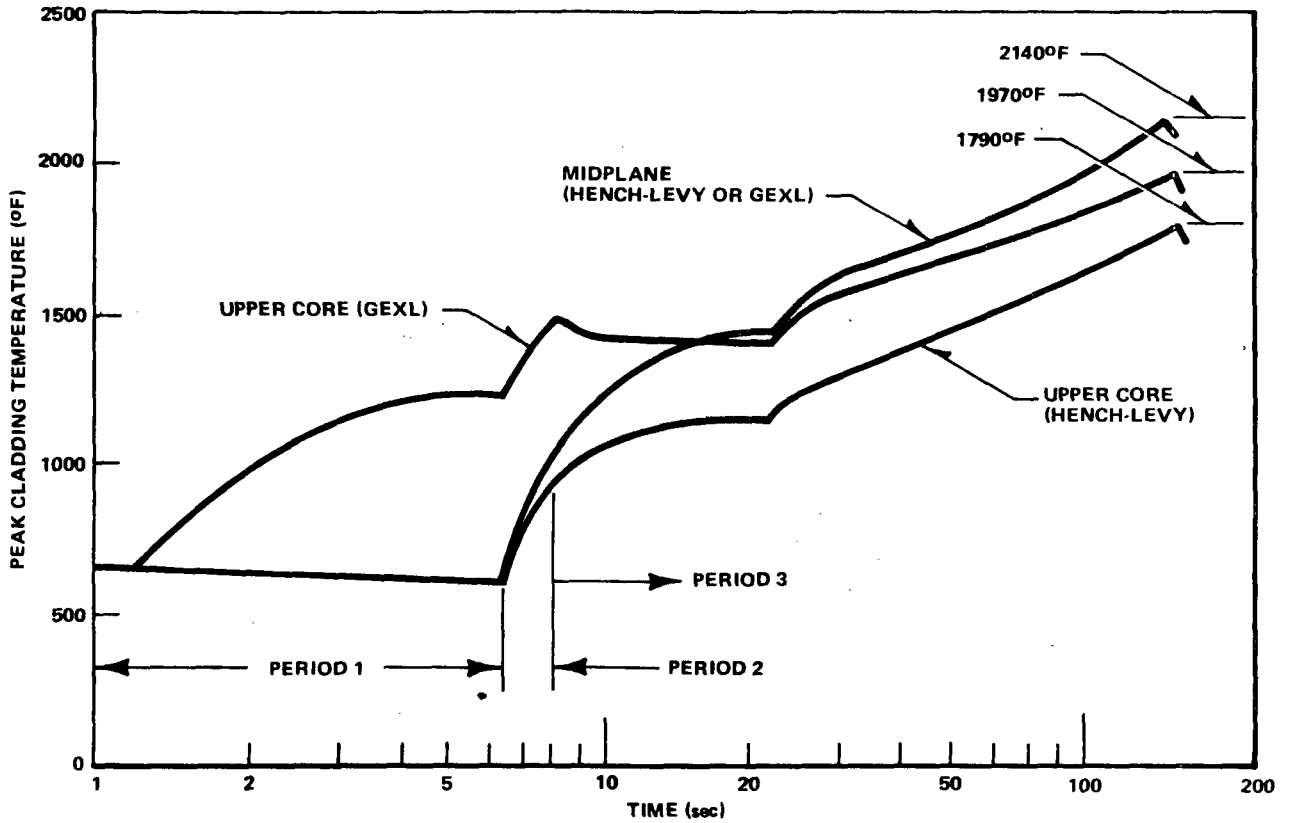


Figure 6-10. Peak Cladding Temperature Vs Time After Design Basis Accident (IAC Models)



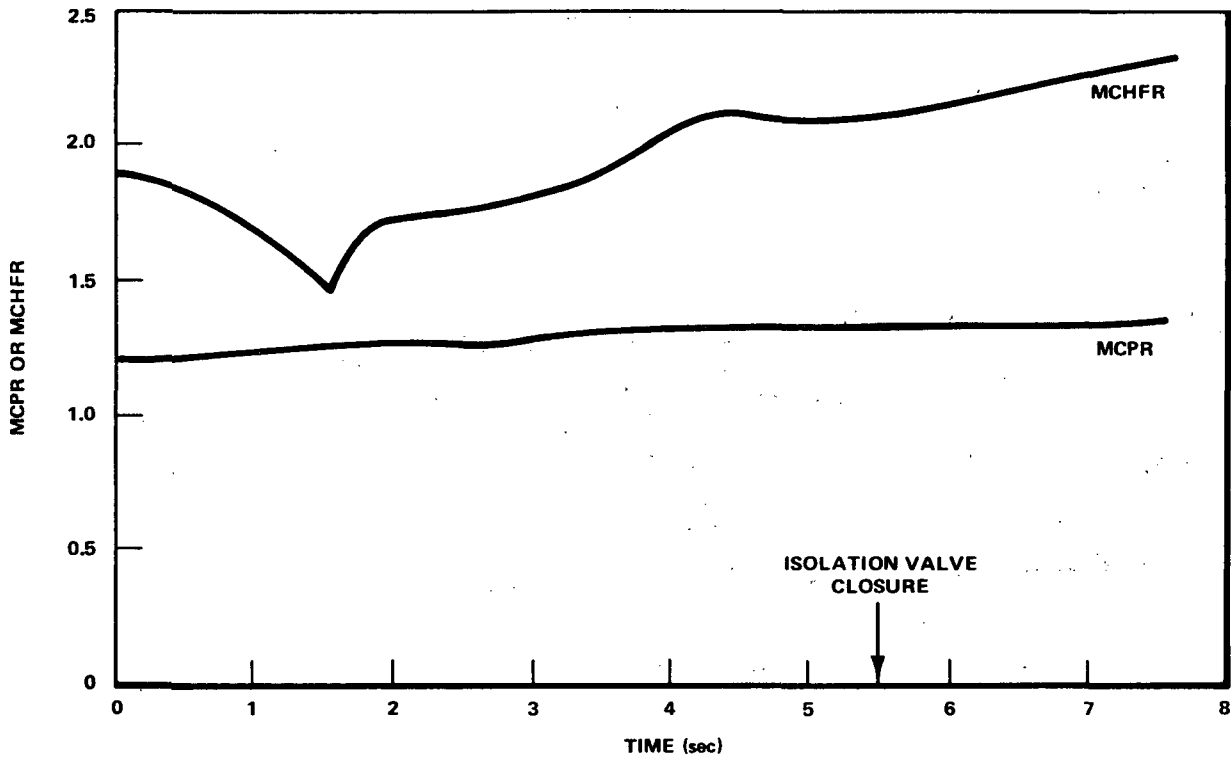


Figure 6-11. Minimum Critical Heat Flux Ratio and Minimum Critical Power Ratio Versus Time (Outside Steam Line Break) Typical BWR/4

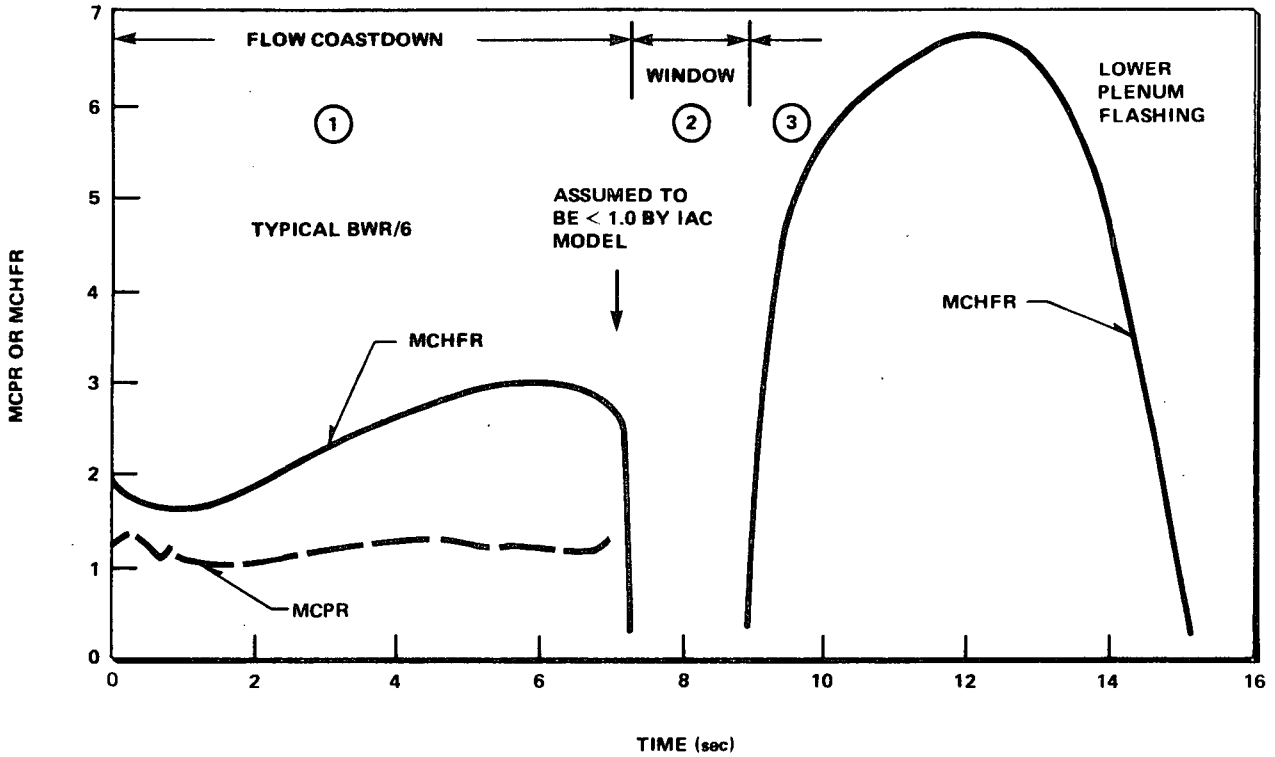


Figure 6-12. Minimum Critical Heat Flux Ratio and Minimum Critical Power Ratio Vs Time (DBA)

Figure 6-12. Minimum Critical Heat Flux Ratio and Minimum Critical Power Ratio versus Time (DBA)

## REFERENCES

1. J. M. Healzer, J. E. Hench, E. Janssen and S. Levy, *Design Basis for Critical Heat Flux Condition in Boiling Water Reactors* September 1966 (APED-5286).
2. S. Milioti, "A Survey of Burnout Correlations as Applied to Water-cooled Nuclear Reactors," M. E. Thesis, Pennsylvania State University, Dept. of Nuclear Engineering, September 1964.
3. G. C. Clerici, S. Garriba, R. Sala and A. Tozzi, "A Catalog of Burnout Correlations for Forced Convection in the Quality Region," EUR 3300.e, EURAEC Report No. 1729, prepared by ARS, Milano, Italy, 1966.
4. L. S. Tong, "Boiling Crisis and Critical Heat Flux," TID-25887, August 1972.
5. L. S. Tong, N. B. Currin, P. S. Larsen and O. G. Smith, "Influence of Axially Nonuniform Heat Flux on DNB," AIChE Preprint 17, Eighth National Heat Transfer Conference, Los Angeles, 1965.
6. O. G. Smith, L. S. Tong, and W. M. Rohrer, "Burnout in Steam-Water Flow with Axially Nonuniform Heat Flux," ASME Paper 65:WA/HT-33, 1965.
7. S. Bertoletti, G. P. Gaspari, C. Lombardi, G. Peterlongo, M. Silvestri and F. A. Tacconi, "Heat Transfer Crisis with Steam-Water Mixtures," *Energia Nucleare*, Vol. 12, No. 3, March 1965.
8. "Nonuniform Heat Generation Experimental Program," Final Report EURAEC 1846 (BAW-3238-13), April 1967.
9. B. S. Shiralkar, *Analysis of Nonuniform Flux CHF Data in Simple Geometries* April 1972 (NEDM-13279).
10. R. K. F. Keeys, J. C. Ralph, D. N. Roberts, *Post Burnout Heat Transfer in High Pressure Steam-Water Mixtures in a Tube with Cosine Heat Flux Distribution*, 1971 (AERE-R6411).
11. G. P. Gaspari, R. Granzini, A. Hassid, "Dryout Onset in Flow Stoppage, Depressurization, and Power Surge Transients," CISE paper presented at CREST Special Meeting on Emergency Core Cooling for Light Water Reactors, Munich, October 18-20, 1972.
12. E. Janssen and S. Levy, *Burnout Limit Curves for Boiling Water Reactors*, April 1962 (APED-3892).
13. R. T. Lahey, Jr., J. E. Hench, E. E. Polomik, *Critical Heat Flux During Transient Conditions of Pressure and Flow in a Single-Rod and Nine-Rod Bundle*, November 1970 (NEDE-10241).
14. B. C. Slifer, *Loss-of-Coolant Accident and Emergency Core Cooling Models for General Electric Boiling Water Reactors*, April 1971 (NEDO-10329).
15. B. S. Shiralkar, E. E. Polomik, R. T. Lahey, Jr., J. M. Gonzalez, D. W. Radcliffe, L. E. Schnebly, *Transient Critical Heat Flux - Experimental Results*, AEC R&D Report, September 1972, (GEAP-13295).
16. *Deficient Cooling - Eleventh Quarterly Progress Report, January 1 - March 31, 1972*, April 1972 (GEAP-10221-11).
17. *Deficient Cooling - 12th Quarterly Progress Report, April 1 - June 30, 1972*, July 1972, (GEAP-10221-12).
18. Vermont Yankee FSAR, Appendix H. Docket 50-271.
19. RESAR-3, Amendment 3, Chapter 4, April 1973.

20. L. S. Tong, "Prediction of Departure From Nucleate Boiling for an Axially Non-Uniform Heat Flux Distribution." *Journal of Nuclear Energy*, 21, pp 241 to 248, 1967.
21. General Electric Standard Safety Analysis Report, Docket No. STN 50-447.
22. R. B. Linford, *Analytical Methods of Plant Transient Evaluations for the GE BWR*, February 1973 (NEDO-10802).
22. R. B. Linford, *Analytical Methods of Plant Transient Evaluations for the GE BWR*, February 1973 (NEDO-10802).
23. R. T. Lahey, Jr., E. E. Polonick, and G. E. Dix, "The Effect of Reduced Clearance and Rod Bow on Critical Power in Simulated Nuclear Reactor Rod Bundles," Paper No. 5 presented at International Reactor Heat Transfer Meeting, Karlsruhe, Germany, 1973.
24. J. F. Carew, "Process Computer Performance Evaluation Accuracy," June 1974, (NEDO-20340).
25. J. F. Carew, "Process Computer Performance Evaluation Accuracy – Amendment 1," December 1974 (NEDO-20340-1).

1-7

3-8

**APPENDIX I**  
**RELATIONSHIPS FOR MAPPING ERROR BAND FROM  $X_C-L_B$  PLANE TO**  
 **$KW_c-\Delta h_s$  PLANE**

$$\text{Let } F(Z) = \left\{ \begin{array}{l} \text{fraction of total} \\ \text{power in length } z \end{array} \right\} = \frac{1}{L} \int_0^z \psi \, dz;$$

where:

$z_0$  = nonboiling length;

$z_c$  = distance to onset of boiling transition; and

$$L_B = \left\{ \begin{array}{l} \text{boiling length to onset} \\ \text{of boiling transition} \end{array} \right\} = (z_c - z_0)$$

From heat balance considerations:

$$F(z_0) = \frac{GA\Delta h_s}{3413 \cdot kW}$$

$$X = \frac{(3413)(kW)[F(z_c)]}{GAh_{fg}} - \frac{\Delta h_s}{h_{fg}}$$

It has been shown experimentally that  $z_c$  tends to be constant for a given axial heat flux profile and mass flux. Forming the total differentials, with  $z_c = \text{constant}$  and noting that  $\Delta G = 0$ ,  $\Delta P = 0$ , and  $\Delta(\Delta h_s) = 0$ :

$$\Delta X = \left( \frac{\partial X_c}{\partial kW} \right) (\Delta kW_c) = \left( \frac{3413}{GAh_{fg}} \right) \cdot [F(z_c)] (\Delta kW_c) \quad (I-1)$$

$$\Delta L_B = \left( \frac{\partial L_B}{\partial kW} \right) (\Delta kW_c) = \left( - \frac{\partial z_0}{\partial kW} \right) (\Delta kW_c)$$

For a chopped cosine profile,

$$\psi = 1.386 \sin \left[ \left( \frac{Z + 11.5}{167.0} \right) \pi \right]$$

and

$$F(Z_0) = 0.5116 \left[ \cos \frac{11.5\pi}{167.0} - \cos \left( \frac{Z_0 + 11.5}{167.0} \right) \pi \right] = \frac{GA\Delta h_s}{3413 \cdot kW}$$

$$\frac{\partial z_0}{\partial kW} = \frac{GA\Delta h_s \cdot L}{3413 (kW)^2} \frac{1}{1.386 \sin \left[ \left( \frac{Z_0 + 11.5}{167.0} \right) \pi \right]} = - \frac{GA\Delta h_s \cdot L}{3413 (kW)^2 \psi_0}$$

Therefore,

$$\Delta L_B = \frac{GA\Delta h_s L}{3413(kW)^2 \psi_o} (\Delta kW) \quad (I-2)$$

Equations I-1 and I-2 give the trajectory in the  $X_C$  vs  $L_B$  plane corresponding to changes in  $KW_c$  at a given subcooling. The error band in the  $X_C$  vs  $L_B$  plane, however, is given by,

$$\delta X_c = \Delta X_c - \left( \frac{dX_c}{dL_B} \right) (\Delta L_B) \quad (I-3)$$

where the derivative  $\frac{dX_c}{dL_B}$  comes

from the correlation \*

Combining Equations I-1, I-2, and I-3,

$$\Delta kW_c = \frac{\delta X_c}{\left( \frac{3413}{GAh_{fg}} \right) [F(Z_c)] - \left( \frac{dX_c}{dL_B} \right) \left( \frac{GA\Delta h_s L}{3413(kW)^2 \psi_o} \right)}$$

where

$\delta X_c$  = half width of error band in  $X_C - L_B$  plane.

$\Delta kW_c$  = half width of error band in  $kW_c - \Delta h_s$  plane.

---

\*The CISE correlation,<sup>7</sup> for example, yields,

$$\frac{dX_c}{dL_B} = \frac{ab}{(b + L_B)^2}$$

and

$$\delta X_c = \Delta X_c - \frac{ab}{(b + L_B)^2} \cdot \Delta L_B$$

**Appendix II**  
**TABLES OF CRITICAL POWER TEST CONDITIONS**  
**AND PREDICTION CAPABILITIES**

Table II-1  
NINE-ROD CRITICAL POWER TEST CONDITIONS, 1.7 MP LOOP

Year	Test Assembly No.	No. of Rods	Rod Diameter (in.)	Rod/Rod Clearance (in.)	Rod/Wall Clearance (in.)	Heated Length (in.)	Axial Profile	Type Spacer	Local Peaking	Special Features	Pressure (psia)	Mass Flux (mlb/hr-ft <sup>2</sup> )	Subcool (Btu/lb)	Runs Per Assembly
1967	1	9	0.570	0.183	0.135	72	Unif.	(Pin)	U	(Norm)	600/1400	0.25/1.25	10/250	120
	2			↓	0.060					Various	1000	0.50/0.75		15
	3			0.108	0.135					R/R and R/W Clearances		0.50/1.25		41
	4			↓	0.210							0.50/0.75		13
1968	1			↓	0.175			'67-PL		(Norm)	1000/1400	0.25/1.25		69
1969	4			↓	0.168			'65-PL		(Norm)	800/1000	0.25/1.00	10/400	34
	1									EHL	600/1400	0.25/1.50		144
	2									3 1/2" Before end channel,		0.25/1.25		115
	2A									1000 various arrangements of top spacers		1.0		6
1970	3											0.25/1.25		35
			0.563	↓	0.174					(Norm)	800/1000	0.25/1.00	10/350	63
					0.138					R/W = 0.030 in corner				38
										R/W = 0.060 in Corner				36
1971										0.138/0.075 Corner Rod Bow 0.060/0.030 Corner Rod Bow				28
														23
													TOTAL	780

Note: 1967 and 1968 data are listed in CDTM No. 68-11 and 69-2. 1969 through 1971 data are listed in GEAP-10347 and 10221-10.

II-2

NEDO-10958-A



Table II-2  
SIXTEEN-ROD CRITICAL POWER TEST CONDITIONS, COLUMBIA UNIVERSITY

Year	Test Assembly No.	No. of Rods	Rod Diameter (in.)	Rod/Rod Clearance (in.)	Rod/Wall Clearance (in.)	Heated Length (in.)	Axial Profile	Type Spacer	Local Peaking	Special Features	Pressure (psia)	Mass Flux (mlb/hr-ft <sup>2</sup> )	Subcool (Btu/lb)	Runs Per Assembly
1967	1	16	0.563	0.175	0.133	72	Unif.	(Pin)	U		600/1250	0.25/1.25	20/250	54
	2							'65-PL	U	Last Spacer 4" before EHL	↓	↓		48
	3							↓	↓		↓	↓		
	4							(Pin)	1.25		1000	0.50/1.25		26
									INT.		↓	↓		26
	5							'65-PL	↓		↓	0.75		4
1968	6				0.138			'67-PL	U		1000/1400	0.25/1.25		42
	7					48		↓	↓		1000	0.50/1.25		22
	8					72			1.22-1		↓	0.10/1.25		38
	9								1.22		↓	↓		44
	10								1.61-3		↓	↓		30
1969	11							"A"	U		1000/1400	0.25/1.25		59
	12							↓	1.27-3		↓	↓		55
	13							(Pin)	U	(Duplicate CU No. 1) Stiff Springs	1000	↓		59
	14							'67-PL	1.28-3		↓	↓		34
	15								U	(Duplicate CU No. 6)	1000/1400	↓		63
	16							Modified "A"	↓		↓	↓		65
	16A							↓	↓		↓	↓		44
1970	17							Canti-lever	1.19-3		1000/2250	↓		76
	18							↓	1.23		↓	1.0/3.0		72
									INT.				TOTAL	861

- Notes: (1) Channel liner of asbestos phenolic, assembly no. 1-5; of ceramic, all subsequent assemblies.  
 (2) Last spacer 1/2 in. past EHL except for pin type and test assembly no. 2 as noted.  
 (3) Peaking on corner rod unless otherwise noted. See Appendix II for peaking patterns.  
 (4) All data w/'65-PL and '67-PL spacers listed in Appendix III.

Table II-3  
SIXTEEN- AND FORTY-NINE ROD CRITICAL POWER TEST CONDITIONS, ATLAS LOOP

Year	Test Assembly No.	No. of Rods	Rod Diameter (in.)	Rod/Rod Clearance (in.)	Rod/Wall Clearance (in.)	Heated Length (in.)	Axial Profile	Type Spacer	Local Peaking	Special Features	Pressure (psia)	Mass Flux (mlb/hr-ft <sup>2</sup> )	Subcool (Btu/lb)	Runs Per Assembly
1971	1	16	0.563	0.175	0.133	72	Unif.	'67-PL	U	(Duplicate CU No. 15)	600/1400	0.50/1.25	20/200	83
	2	↓	↓	↓	↓	144	Sym cos	↓	1.24-3	↓	↓	0.25/1.25	↓	52
	3	↓	↓	↓	↓	↓	↓	↓	↓	(Duplicate ATLAS No. 2)	800/1200	0.50/1.25	↓	71
	4	↓	↓	↓	↓	↓	↓	↓	U	↓	↓	0.25/1.50	↓	113
1972	5	↓	↓	↓	↓	↓	↓	↓	1.16-3	↓	600/1400	0.50/1.50	↓	67
	8	↓	↓	↓	↓	↓	↓	↓	1.23-1	↓	800/1400	0.25/1.25	↓	49
	9	↓	↓	↓	↓	72	Unif.	↓	1.30-3	↓	1000	0.50/0.75	↓	4
	10	↓	↓	↓	↓	144	Sym cos	↓	1.27	Reduced R/R Interior	↓	0.25/1.25	↓	41
	11	↓	↓	↓	↓	↓	↓	↓	1.27	↓	1000/1400	↓	↓	50
	13	↓	↓	↓	↓	↓	↓	↓	1.42-1	↓	↓	↓	↓	43
	14	↓	↓	↓	↓	↓	↓	↓	U	↓	800/1000	0.25/1.00	↓	50
	15	↓	↓	↓	↓	↓	↓	↓	↓	Bowed Rod 0.060 R/W Hot Corner	↓	↓	↓	40
	16	↓	↓	↓	↓	↓	↓	↓	↓	↓	↓	↓	↓	42
	17	↓	↓	↓	↓	↓	↓	↓	1.47	↓	800/1400	0.25/1.25	↓	59
	18	49	↓	↓	0.144	↓	↓	↓	1.38-1	↓	1000	0.025/1.25	10/100	43
	19B	↓	↓	↓	↓	↓	↓	↓	1.23-1	1 Cold Rod	800/1300	0.025/1.25	↓	72
	19C	↓	↓	↓	↓	↓	↓	↓	1.21-1	↓	1000	0.50/1.25	↓	21
	19D	↓	↓	↓	↓	↓	↓	↓	↓	↓	800/1200	0.50/1.25	↓	27
	20A	16	0.494	0.146	0.151	148	Sym cos	Model 1	1.27-3	8X8 Lattice	1000	0.10/1.25	10/200	46
	20B	↓	↓	↓	↓	↓	↓	↓	1.27-1	↓	↓	0.17/1.25	↓	32
	21A	↓	↓	↓	↓	↓	↓	↓	1.19	1 Cold Rod	↓	0.25/1.25	↓	33
	21B	↓	↓	↓	↓	↓	↓	↓	1.11	↓	↓	↓	↓	36
	21C	↓	↓	↓	↓	↓	↓	↓	INT.	↓	↓	↓	↓	↓
		↓	↓	↓	↓	↓	↓	↓	U	↓	800/1200	↓	↓	43

Table II-3 (Continued)

Year	Test Assembly No.	No. of Rods	Rod Diameter (in.)	Rod/Rod Clearance (in.)	Rod/Wall Clearance (in.)	Heated Length (in.)	Axial Profile	Type Spacer	Local Peaking	Special Features	Pressure (psia)	Mass Flux (mlb/hr-ft <sup>2</sup> )	Subcool (Btu/lb)	Runs Per Assembly						
1972	21D	16	0.494	0.146	0.151	148	Sym cos	Model 1	1.12-3		800/1200	0.25/1.25	10/200	45						
	22A							Model 2	1.27-3		1000	0.25/1.25		31						
	22B								1.12-3		1000/1400			47						
	22C								U		1000	0.50/1.25		19						
1973	23A	16	0.494	0.146	0.151	148	Sym cos	Model 1	1.27-3		1000/1400	0.25/1.25		46						
	23B								U					50						
	23C								1.11		1000			26						
	24A							49	0.563	0.175	0.144	144	'67-PL	1.20		800/1400	0.025/1.25	10/100	108	
	24B													1.23-1	(Max R/W Hot Corner)	1000/1400			254	
	25A															800/1400	0.50/1.25		132	
	25B														1 Cold Rod Next to Corner				99	
	26A							16	0.563	0.175	0.133	144	Sym cos	'67-PL	1.22-1	Indirect Heaters	1000	0.50/1.00	25/168	11
	26B														1.23-3			0.25/1.25	21/176	76
	27A												Inlet Peak		U				16/120	132
	27B														1.15-3				14/130	165
	27C														1.25-3				9/134	173
	27D														1.43-1			0.50/1.00	15/161	100
	28A												Double Hump		U		800/1400	0.25/1.25	14/137	172
	28B														1.13-3		1000		17/146	124
	28C														1.43-1			0.50/1.25	16/152	107
	28D														1.26-3		800/1400	0.25/1.25	16/156	171
	29A												Outlet Peak		U		1000		18/154	122
29B								1.15-3				16/165	152							
29C								1.43-1				17/160	158							
29D								1.23-3				13/159	174							
30A						Unif.		1.24-3				17/155	146							
30B								1.40-1				17/164	150							

Table II-3 (Continued)

Year	Test Assembly No.	No. of Rods	Rod Diameter (in.)	Rod/Rod Clearance (in.)	Rod/Wall Clearance (in.)	Heated Length (in.)	Axial Profile	Type Spacer	Local Peaking	Special Features	Pressure (psia)	Mass Flux (mlb/hr-ft <sup>2</sup> )	Subcool (Btu/lb)	Runs Per Assembly			
1973	30C	16	0.563	0.175	0.133	144	Unif.	'67 PL	U		1000	0.25/1.25	22/199	158			
									1.12-3			23/164	183				
									1.26-3			23/144	36				
									1.26-3	(Duplicate ATLAS Nos. 3, 26B)	1000	0.5/1.25	17/158	30			
	31B								1.24-3			0.25/1.25	13/150	156			
	32A	64	0.494	0.146	0.152	148	Sym cos	Model 1	1.22-3	Reload Pattern	1000/1400	0.75/1.25	13/122	63			
	32B								1.22-3		800/1400	0.025/1.25	4/123	170			
	32C								1.59-3	Controlled Pattern	1000/1400	0.25/1.25	7/135	121			
	33								1.12-5	BWR/6 Pattern	800/1400	0.025/1.25	7/118	164			
	34C								Model 3	1.15		1000		9/121	88		
	34D								INT	1.15				4/122	87		
	34E								INT	1.16				5/120	57		
	34F								INT	1.15				5/134	76		
	34G								INT	1.15				3/126	94		
	34H								1.12-5					6/123	80		
	34J								1.12-5					5/111	52		
	35A								1.58-5					5/101	29		
	35B								1.23-5					6/145	79		
	35C								1.13-5					16/1400	0.05/1.25	13/150	184

6014

- Notes:
- (1) Axial profiles are shown in Appendix II.
  - (2) Peaking on corner rod unless otherwise noted. See Appendix II for peaking patterns.
  - (3) All data listed in Appendix III.

9-11

NEDO-10958-A

**Table II-4**  
**ONE, SIXTEEN, FORTY-FIVE, AND SIXTY-FOUR ROD CRITICAL POWER TEST CONDITIONS, FREON LOOP**

Test Assembly No.	No. of Rods	Rod Diameter (in.)	Rod/Rod Clearance (in.)	Rod/Wall Clearance (in.)	Heated Length (in.)	Axial Profile	Type Spacer	Local Peaking	Special Features	Pressure (psia)	Mass Flux (mlb/hr-ft <sup>2</sup> )	Subcool (Btu/lb)	Runs Per Assembly			
1	1	0.563	—	0.156	144	Cos	—	—	Annulus	123	0.29/0.66	2/20	15			
2	↓	↓	↓	↓	89	U + 1/2	↓	↓	↓	↓	↓	↓	20			
3	↓	↓	↓	↓	72	1/2 Cos	↓	↓	↓	↓	↓	↓	16			
4	↓	↓	↓	↓	144	Cos	↓	↓	↓	↓	↓	↓	16			
5	↓	↓	↓	↓	↓	Unif.	↓	↓	↓	↓	↓	↓	16			
6	↓	↓	↓	↓	↓	Cos	↓	↓	↓	↓	↓	↓	16			
7	↓	↓	↓	↓	72	Unif.	↓	↓	↓	↓	↓	↓	16			
8	↓	↓	↓	↓	↓	Cos	↓	↓	↓	↓	↓	↓	19			
9	↓	↓	↓	↓	↓	Inlet Peak	↓	↓	↓	↓	↓	↓	12			
10	↓	↓	↓	↓	144	Outlet Peak	↓	↓	↓	↓	↓	↓	12			
												One Rod Total Runs =	158			
000	16	0.563	0.176	0.132	72.5	Unif.	(Pin)	U	Last Spacer at various axial positions	123	0.29/0.82	2/20	66			
100	↓	↓	↓	↓	↓	↓	'67-PL	↓		at various axial positions	↓	↓	↓	65		
200	↓	↓	↓	↓	↓	↓	A	↓	Various Development Spacer configurations	↓	0.31/1.25	↓	42			
300	↓	↓	↓	↓	↓	↓	A	↓		Various Development Spacer configurations	↓	0.48/1.25	↓	23		
700	↓	↓	↓	↓	↓	↓	A'	↓		Various Development Spacer configurations	↓	0.45/0.82	↓	41		
800	↓	↓	↓	↓	↓	↓	A'	↓		Various Development Spacer configurations	↓	0.47/0.80	↓	21		
900	↓	↓	↓	↓	↓	↓	A''	↓		Various Development Spacer configurations	↓	0.31/0.70	↓	15		
1000	↓	↓	↓	↓	↓	↓	A''	↓		Various Development Spacer configurations	↓	0.30/0.81	↓	62		
1100	↓	↓	↓	↓	↓	↓	A''	↓		Various Development Spacer configurations	↓	0.30/0.80	↓	28		
1200	↓	↓	↓	↓	↓	↓	AIV	↓		Various Development Spacer configurations	↓	0.30/0.80	↓	30		
1400	↓	↓	↓	↓	↓	↓	AIV	Various		Various Development Spacer configurations	↓	0.62/0.90	2/20	78		
1500	↓	↓	↓	↓	↓	↓	A <sup>v</sup>	1.24 INT			Various Development Spacer configurations	↓	0.79/0.81	↓	33	
1600	↓	↓	↓	↓	↓	↓	A <sup>v</sup>	1.26-3	Various Development Spacer configurations	↓	0.49/0.81	↓	23			
1700	↓	↓	↓	↓	↓	↓	A <sup>v</sup>	1.26-3		Various Development Spacer configurations	↓	0.79/0.81	↓	17		
1800	↓	↓	↓	↓	↓	↓	A <sup>v</sup>	1.26-3,U			Various Development Spacer configurations	↓	0.49/0.81	↓	16	
1900	↓	↓	↓	↓	↓	↓	A <sup>x</sup>	1.26-3,U				Various Development Spacer configurations	↓	0.49/0.81	↓	24
2000	↓	↓	↓	↓	↓	↓	A <sup>x</sup>	1.26-3					Various Development Spacer configurations	↓	0.79/0.81	↓

Note: Peaking on corner rod unless otherwise noted.

Table II-4 (Continued)

Test Assembly No.	No. of Rods	Rod Diameter (in.)	Heated Length (in.)	Axial Profile	Type Spacer	Local Peaking	Special Features	Pressure (psia)	Mass Flux (mlb/hr-ft <sup>2</sup> )	Runs Per Assembly		
2200	16	0.563	72.5	Unif.	'67-PL	U	Stiff Spring	123 & 149	0.33/0.73	41		
2300					Dev.	Various	Stiff Spring	123 & 178	0.39/0.79	91		
2400					Dev.	Various	1 Finger Scoop	123	0.49/0.79	56		
2500							2 Finger Scoop		0.49/0.79	45		
3000							Flow Diverter		0.34/0.79	35		
3100							Reduced Spacing			34		
3200							Open Corner			76		
3300							'67-PL	U	Stiff Spring	123, 151, & 158	0.39/0.90	93
3400												77
3500							Dev.	1.24	Cant. Open Corner	123	0.33/0.79	80
4100							Dev.	1.24	Cant. Open Corner	123	0.33/0.79	26
4200							Dev.	U	Corner (Modified)			23
4300							Dev.	1.207				24
4400							Dev.	1.24CP		123	0.33/0.79	27
4500								1.207CD	Offset			27
4600								U	Cant. Corner Spacer			27
4700								1.207CD		151	0.36/0.88	28
4800								1.207CD		180	0.40/1.15	48
4900								1.23IP		123	0.50/1.5	41
5000								1.23IP		269	1.48/2.45	25
5100										308	1.5/2.5	22
5200										151	1.25/1.5	10
5300						180	0.84/1.68	17				
5400						224	1.4/1.7	13				
5500					1.207CP	269	1.5/1.7	12				
5700					1.189CP	123	0.33/.79	24				
5800						308	1.2/1.8	19				
5900						180	0.42/.84	18				
6000						151	0.37/.70	13				
6100						269	2.0	6				
6200						123	0.33/0.79	24				

Table II-4 (Continued)

Test Assembly No.	No. of Rods	Rod Diameter (in.)	Heated Length (in.)	Axial Profile	Type Spacer	Local Peaking	Special Features	Pressure (psia)	Mass Flux (mlb/hr-ft <sup>2</sup> )	Runs Per Assembly
1A	16	0.563	140.9	Cos	'67-PL	1.24	3-Rod Cor. Pk	123	0.31/0.73	31
1B	↓	↓	↓	↓	↓	1.17	↓	↓	↓	23
1C	↓	↓	↓	↓	↓	1.09	↓	↓	0.45/0.73	18
1D	↓	↓	↓	↓	↓	Unif.	—	↓	0.31/0.73	24
1E	↓	↓	↓	↓	↓	1.24	Mod Spacing	↓	↓	24
1F	↓	↓	↓	↓	↓	1.17	↓	↓	↓	24
1G	↓	↓	↓	↓	↓	1.09	↓	↓	0.45/0.73	20
1H	↓	↓	↓	↓	↓	Unif.	↓	↓	0.31/0.73	24
1I	↓	↓	↓	↓	Cant. O.C.S.	1.24	3-Rod Cor. Pk	↓	↓	24
1J	↓	↓	↓	↓	↓	1.17	↓	↓	↓	24
1K	↓	↓	↓	↓	↓	1.09	↓	↓	↓	24
1L	↓	↓	↓	↓	↓	Unif	—	↓	↓	23
1M	↓	↓	↓	↓	Single Fing. Scoop	1.24	3-Rod Cor. Pk	↓	0.31/0.71	30
1N	↓	↓	↓	↓	↓	Unif	—	↓	↓	24
1O	↓	↓	↓	↓	C.O.C.S.	1.24	Cor. Wall Scoop	↓	0.31/0.72	36
1P	↓	↓	↓	↓	↓	Unif.	↓	↓	↓	24
1Q	↓	↓	↓	↓	↓	—	Var. Local Pk	↓	0.46/0.73	36
1R	↓	↓	↓	↓	↓	1.24	Cor. Wall Scoops	↓	0.31/0.73	24
1S	↓	↓	↓	↓	↓	Unif	↓	↓	↓	24
1T	↓	↓	↓	↓	↓	—	Var. Local Pk	↓	0.46/0.73	54
2A	16	0.568	141.8	Peak Out	67-PL	Unif	—	123	0.31/0.73	24
2B	↓	↓	↓	↓	↓	1.07	3-Rod Cor Pk	↓	↓	24
2C	↓	↓	↓	↓	↓	1.17	↓	↓	↓	24
2D	↓	↓	↓	↓	↓	1.24	↓	↓	↓	30
2E	↓	↓	↓	↓	↓	1.23	Int. Pk	↓	↓	24
3A	16	0.563	143.4	Peak Inlet	67-PL	1.09	3-Rod Cor Pk	123	0.31/0.72	24
3B	↓	↓	↓	↓	↓	1.17	↓	↓	↓	30
3C	↓	↓	↓	↓	↓	1.24	↓	↓	↓	24
3D	↓	↓	↓	↓	↓	1.23	Int. Pk	↓	↓	30
3E	↓	↓	↓	↓	↓	Unif	↓	↓	↓	24

11-9

NEDO-10958-A

Table II-4 (Continued)

Test Assembly No.	No. of Rods	Rod Diameter (in.)	Heated Length (in.)	Axial Profile	Type Spacer	Local Peaking	Special Features	Pressure (psia)	Mass Flux (mlb/hr-ft <sup>2</sup> )	Runs Per Assembly			
7A	16	0.563	140.9	Cos	Min. Spacer	1.33	3-Rod Cor Pk	123	0.31/0.74	28			
7B						1.24				35			
7C						1.17				28			
7D						1.09				28			
7E						U				28			
7F						1.33	Int. Pk.			28			
7G						1.23				28			
7H						1.33	Side Pk			28			
7I						1.23				28			
7J						Min. Spacer w/Scoops	1.33			Side Pk	123	0.31/0.74	28
7K							1.33			Int. Pk.			28
7L							1.33			Cor. Pk			28
7M							1.17						28
7N						67-PL with Min. Spacers	1.23			Int. Pk.	123	0.31/0.74	24
7O							1.23			Side Pk			24
7P							U						24
7Q		1.24	Cor. Pk.			24							
7R		1.24				24							
9A	16	0.563	140.9	Cos	67-PL	1.23	Int. Pk.	123	0.31/0.74	24			
9B						1.33				24			
9C						1.23	Side Pk			24			
9D						1.33				24			
9E						U				0.34/0.80	28		
9F						1.27	Int. Pk			0.34/0.93	30		
9G						1.24	Cor. Pk Rod-16			0.34/0.83	30		
9H						1.24	Cor. Pk Rod-1			0.32/0.93	35		
9I						1.33	Cor. Pk.			0.31/0.74	28		
9J						1.24	2-Rod Cor Pk			0.34/0.93	35		
9K						1.15				0.34/0.93	35		

II-10

NEDO-10958-A



Table II-4 (Continued)

Test Assembly No.	No. of Rods	Rod Diameter (in.)	Heated Length (in.)	Axial Profile	Type Spacer	Local Peaking	Special Features	Pressure (psia)	Mass Flux (mlb/hr-ft <sup>2</sup> )	Runs Per Assembly
10A	16	0.563	140.75	Cos	67-PL	1.24	3-Rod Cor Pk	123	0.34/0.93	35
10B						U	—		0.34/1.17	35
10C						1.24	2-Rod Cor Pk		0.34/1.17	36
10D						1.09	Rod No. 1		0.34/1.17	48
10E							Rod No. 4		0.34/0.92	35
10F							Rod No. 16			35
10G							Rod No. 16			35
10H							Rod No. 4 .030 BOW			35
10I							Rod No. 1 .060 BOW			35
10J							Rod No. 16			35
							R-W .090			
10K							Rod No. 4			42
							.030 BOW R-W .090			
10L							Rod No. 1			35
							.060 BOW R-W .090			
10M							Rod No. 16 R-W .060			35
10N							Rod No. 4			35
							.030 BOW R-W .060			
10O							Rod No. 1 R-W .060			35
10P							Rod No. 16			35
							Chan. Bulge			
10Q							Rod No. 4, 0.030			35
							Bow & Chan Bulge			
10R							Rod No. 1			35
10S							Rod No. 16			35
11A	16	0.494	148.06	Cos	Model 1	1.24	2-Rod Cor. Pk	123	0.34/0.92	35
11B						1.09				35
11C						U	—			35
11D						1.24	3-Rod Cor. Pk			35
11E						1.15				35
11F						—	Various Int Pk		0.5/0.79	24

Table II-4 (Continued)

Test Assembly No.	No. of Rods	Rod Diameter (in.)	Heated Length (in.)	Axial Profile	Type Spacer	Local Peaking	Special Features	Pressure (psia)	Mass Flux (mlb/hr-ft <sup>2</sup> )	Runs Per Assembly
11H	↓	0.494	148.23	Cos	Model 2	1.24	3-Rod Cor Pk	123	0.34/0.92	35
11I						1.27				
11J						1.12	0.21/1.06		41	
11K						U	0.21/1.33		18	
11L						1.24	0.34/1.92		35	
11M						U	1		35	
11N						1.24	0.5/0.79		28	
									16-Rod Total Runs	4503
4A	↓	0.563	71.35	Unif	67-PL	U	3-Rod Cor Pk	123	0.30/0.78	40
4B						1.27				
4C						1.17	25			
4D						1.09	0.50/0.78		11	
4E						1.27			0.30/0.78	24
4F						1.17	0.50/0.78		12	
4G						U	0.33/0.78		12	
4H						1.17	Various Typical Reactor Peakings		24	
4I						1.22			24	
4J						1.24			24	
4K						1.21			23	
4L						1.21			24	
4M						1.20			24	
4N						--			Various Peakings	16
5A	↓	0.563	141.2	Cos	67-PL	1.22	Typical Reactor Patterns	123	0.31/0.74	29
5B						1.24				
5C						1.22	1 Cold Rod		26	
5D						1.24			34	
5E						1.26	29			
5F						U	Typical Reactor Patterns.		27	
5G						1.10			27	
5H						1.70			27	
5I						1.10	9 cold rods		26	

II-12

NEDO-10958-A

Table II-4 (Continued)

Test Assembly No.	No. of Rods	Rod Diameter (in.)	Heated Length (in.)	Axial Profile	Type Spacer	Local Peaking	Special Features	Pressure (psia)	Mass Flux (mlb/hr-ft <sup>2</sup> )	Runs Per Assembly
5J	49	0.563	141.2	Cos	67-PL	—	Var. Int. Pk	123	0.32/0.60	14
5K	↓	↓	↓	↓	↓	1.10	Typ Reactor Patterns ↓ Rctr Pk ↓ Cor. Pk ↓ Int. Pk ↓ Side Pk ↓ Middle Peak ↓ Cor Pk ↓ Cor. Pk	1 Cold Rod 1 Rod Remvd ↓ 123 ↓ 179 269 123 ↓ 123 ↓ 123 ↓ 123	0.31/0.74	27
5L	↓	↓	↓	↓	1.10	24				
5M	↓	↓	↓	↓	1.36	27				
6A	49	0.563	141.2	Cos	67-PL	1.22			33	
6B	↓	↓	↓	↓	↓	U	33	0.31/0.73	33	
6C	↓	↓	↓	↓	↓	1.50	39	0.31/0.87	39	
6D	↓	↓	↓	↓	↓	1.22	33	↓	33	
6E	↓	↓	↓	↓	↓	1.17	33	↓	33	
6F	↓	↓	↓	↓	↓	1.09	33	↓	33	
6G	↓	↓	↓	↓	↓	1.22	34	179	0.36/1.01	34
6H	↓	↓	↓	↓	↓	1.22	40	269	0.41/1.11	40
6I	↓	↓	↓	↓	↓	1.33	32	123	0.31/0.87	32
6J	↓	↓	↓	↓	↓	1.33	36	↓	36	
6K	↓	↓	↓	↓	↓	1.23	35	↓	35	
6L	↓	↓	↓	↓	↓	1.13	34	↓	34	
6M	↓	↓	↓	↓	↓	1.13	32	↓	32	
6N	↓	↓	↓	↓	↓	1.23	35	↓	35	
6O	↓	↓	↓	↓	↓	1.33	35	↓	35	
6P	↓	↓	↓	↓	↓	1.13	32	↓	32	
6Q	↓	↓	↓	↓	↓	1.23	34	↓	34	
6R	↓	↓	↓	↓	↓	1.33	35	↓	35	
6S	↓	↓	↓	↓	↓	1.70	34	↓	34	
6T	↓	↓	↓	↓	↓	2.0	34	↓	34	
8A	49	0.563	144.0	Outlet Peak	67-PL	1.50	Cor. Pk	123	0.32/0.88	35
8B	↓	↓	↓	↓	↓	1.33	↓	↓	0.32/1.03	35
8C	↓	↓	↓	↓	↓	1.22	↓	↓	0.32/0.88	70
8D	↓	↓	↓	↓	↓	1.17	↓	↓	0.32/0.88	34
8E	↓	↓	↓	↓	↓	1.09	↓	↓	0.32/0.88	34
8F	↓	↓	↓	↓	↓	U	—	↓	0.32/0.88	32
8G	↓	↓	↓	↓	↓	1.22	Rctr. Pk	↓	0.32/0.74	28
8H	↓	↓	↓	↓	↓	1.23	Center Pk	↓	0.32/0.88	35

Table II-4 (Continued)

Test Assembly No.	No. of Rods	Rod Diameter (in.)	Heated Length (in.)	Axial Profile	Type Spacer	Local Peaking	Special Features	Pressure (psia)	Mass Flux (mlb/hr-ft <sup>2</sup> )	Runs Per Assembly
8I	49	0.563	144.0	Outlet Peak	67-PL	1.23	Middle Pk	123	0.32/0.88	35
8J	↓	↓	↓	↓	↓	1.23	Side Pk	↓		35
								49-Rod Total Runs		1713
12A	64	0.494	149	Cos	Model 1	1.61	1-H <sub>2</sub> O Rod	123	0.33/0.77	24
12B	↓	↓	↓	↓	↓	1.235	1-H <sub>2</sub> O Rod	↓	0.33/1.06	35
12C	↓	↓	↓	↓	↓	1.16	1-H <sub>2</sub> O Rod	↓	0.33/0.77	24
12D	↓	↓	↓	↓	↓	1.14	Int. Pk -2-H <sub>2</sub> O Rods	↓	0.33/0.77	24
12E	↓	↓	↓	↓	↓	U	-	↓	0.33/1.06	46
12F	↓	↓	↓	↓	↓	-	Var. Local Peaking	↓	0.48/0.77	40
								64-Rod Total Runs		193

Table II-5  
TRANSIENT TEST CONDITIONS

Atlas Assembly Number	Run Nos.	Type of Transient	Nominal Pressure (psia)	$G_{Initial}/G_{Final}$ ( $10^6$ lb/hr-ft <sup>2</sup> )	$\tau$ (sec)	Initial Power (kw)	Inlet Temp. (°F)
3 (16-Rod)	102-120	Const. Power Flow Decay	1000	0.83/0.4	0.4-2.3	1200-2225	500
19D (49-Rod)	101-104	Flow & Power Decay	1000	1.0/0.3	6.0-8.0	5800-6000	510
	105-109	LOCA Simul.		1.0/0.4/0/0.4	$\tau_1/\tau_2/\tau_3$ 6/0/1-6/0/2	4000-4300	
	110-117	Const. Power Flow Decay		1.0/0.5	0.4-4.0	5000-5350	
	118	Flow Ramp Power Ramp		0.5/1.0	3	4800	
	119-121	Const. Flow Power Ramp		1.0	—	5400	
	122-127	Const. Power Flow on/off/ on		1.0/0/1.0	0.3-0.5	5050	
25A (49-Rod)	1-62	Flow & Power Decay	1000- 1050	1.25/0.63-0.9/0.32	0.6-1.25	4000-6325	510- 530
27C (16-Rod, Inlet Peak)	100-127	Const. Power Flow Decay	1000	0.86/0.4	0.4-2.0	1150-2225	500
	128-134	Flow & Power Decay		1.0/0.25	0.4 $\tau_1/\tau_2/\tau_3$	1050-1400	525
	135-146	LOCA Simul.		1.0/0.3/0/0.3	6/0/3	1000-1330	
	147-155	Const. Power Flow Decay		1.0/0.5	0.7-4.0	1700-1760	
	156-161	LOCA Simul.		1.0/0.3/0/0.3	$\tau_1/\tau_2/\tau_3$ 0.3/6/2	1080/1200	
28D (16-Rod, Double Hump)	300-306	Flow & Power Decay	1000	1.0/0.25	0.33 $\tau_1/\tau_2/\tau_3$	1050-1320	525
	307-318	LOCA Simul.		1.0/0.3/0/0.3	0.3/4/2- 0.3/6/3	950-1200	
	319-327	Const. Power Flow Decay		1.0/0.5	0.33-1.7	1500-2000	
29D (16-Rod, Outlet Peak)	311-318	Flow & Power Decay	1000	1.0/0.25	0.5 $\tau_1/\tau_2/\tau_3$	1000-1310	530
	319-332	LOCA Simul.		1.0/0.3/0/0.3	0.5/6/2- 0.5/6/3	1000-1340	
	333-338	Const. Power Flow Decay		1.0/0.5	0.5	1500-1800	
14	100-114 254-258	Const. Power Flow Decay	1000	1.0/0.5, 0.6/0.3 1.0/0.54	0.4-3.0 2.5-5.0	1490-2220 2100-2600	520

Table II-5 (Continued)

Atlas Assembly Number	Run Nos.	Type of Transient	Nominal Pressure (psia)	$\frac{G_{Initial}}{G_{Final}}$ ( $10^6$ lb/hr-ft <sup>2</sup> )	$\tau$ (sec)	Initial Power (kw)	Inlet Temp. (°F)
32B	117-150 171-188	Flow on/off/ on	1000	1.0/0/1.0, 0.5/0/0.5, 0.25/ 0/0.25	1.4-60.0 0.6-1.8	180-1260 1260-1670	520 520
	196-219	Flow & Power Decay	1000	1.0/0.38, 0.6/0.33	1.4-8.3	1770-2830	520
	220-222 232-253	LOCA Simulation	1000	1.0/0.3/0/0.3, 1.0/0.4/0/0.4, 1.0/0.5/0/0.5	$\tau_1/\tau_2/\tau_3$ 5/0/1-4, 8/0/1-3	1410-2050	520
	223-231	Power and Flow Ramp	1000	0.5/1.0	3.8	1340-2060	520
	101-110	Flow and Power Decay	1000	1.0/0.25	0.5	3600-4480	510
	111-115	LOCA	1000	1.0/0.3/0/0.3	0.5/6/2	3080-3595	515
	116-117	LOCA	1000	1.0/0.3/0/0.3	0.5/6/3	3350-3445	515
	118-121	LOCA	1000	1.0/0.3/0/0.3	0.5/5/2	3190-3370	515
	123-133	Constant Power Flow Decay	1000	1.0/0.5	0.5	5260-6000	515
	134-147	Constant Flow Power Ramp	1000	1.0	—	3112-4600	520
35C	148-157	Power and Flow Ramp	1000	0.5/1.0	0.5	2870-4050	520
	20-33	Flow and Power Decay	1000	1.0/0.25	0.4	4200-5190	525
	34-43	LOCA	1000	1.0/0.3/0/0.3	0.3/6/2	3800-4410	525
	44	LOCA	1000	1.0/0.3/0/0.3	0.3/6/3	4000	525
	45	LOCA	1000	1.0/0.3/0/0.3	0.3/6/2.5	4100	525
	46-47	LOCA	1000	1.0/0.3/0/0.3	0.3/6/1.5	4500-4550	525
	48-51	Constant Power Flow Decay	1000	1.0/0.5	0.4	6500-6650	525
	52-60	Constant Flow Power Ramp	1000	1.0	—	4500-4850	525

Table II-6  
ASSEMBLY 14

Run No.	Initial Conditions			Experimental					Prediction				Runs with MCPR > 1.0		Run No.
				Measured Initial Indication		Measured Final Indication			Predicted Initial Condition		Predicted Final Condition				
	G/10 <sup>6</sup> lb/hr-ft <sup>2</sup>	Subcooling Btu/lb	CPR	Measured Time to Onset of Boiling (sec)*	Observed Location	Measured Time to Onset of Boiling (sec)	Observed Location		Calculated Time to Onset of Boiling (sec)	Calculated Location	Calculated Time to Onset of Boiling (sec)	Calculated Location	Calc MCPR	Time (sec)	
					Spacer No.		Distance from Top (in.)	Spacer No.		Spacer No.		Spacer No.			
101	0.95	30	1.32	4.32	2				3.86	2					101
102	0.96	31	1.25	1.78	2	1.88	34		1.74	2	2.08	3	1.015	2.48	102
104	0.96	32	1.32	2.16	2										104
105	0.96	31	1.26	1.9	2	2.6	34		2.1	2					105
106	0.6	33	1.45	2.14	2	2.74	34		1.96	3					106
108	0.6	30	1.29	1.4	2	1.7		3	0.32	2	1.16	3			108
110	0.59	32	1.45	3.38	2	3.58	34		3.08	2	3.22	3			110
111	0.6	32	1.29	1.64	2	1.7		3	1.25	2	2.27	4			111
112	0.6	32	1.55	4.78	2								1.036	5.64	112
113	0.6	31	1.44	3.18	2				3.2	2	4.16	4			113
114	0.6	31	1.29	2.3	2	2.95		3	1.89	2	2.09	3			114
201	1	28	1.045	3.64	2								1.017	4.18	201
202	1	29	1.029	4.52	2				4.27	2					202
203	1	29	1.009	3.4	2				4.14	2					203
206	1	29	1.16	3.04	2				2.88	2					206
207	1	29	1.19	3.96	2								1.005	4.5	207
208	1	31	1.4	2.34	2								1.016	2.71	208
211	0.6	28	1.06	2.72	2				3.06	2					211
215	0.6	30	1.14	2.2	2				2.49	2					215
216	0.6	30	1.17	2.72	2								0.024	2.8	216
217	0.6	30	1.22	1.72	2	2.23	34		1.7	2					217
218	0.6	28	1.28	2.64	2								1.046	2.6	218

\* Reported in Reference 16.

Table II-7  
ASSEMBLY 27C

Run No.	Initial Conditions			Experimental				Prediction				Runs with MCPR > 1.0		Run No.
				Measured Initial Indication		Measured Final Indication		Predicted Initial Condition		Predicted Final Condition				
				Measured Time to Onset of Transition Boiling (sec)*	Observed Location	Measured Time to Onset of Transition Boiling (sec)	Observed Location	Calculated Time to Onset of Transition Boiling (sec)	Calculated Location	Calculated Time to Onset of Transition Boiling (sec)	Calculated Location			
					Spacer No.		Spacer No.		Spacer No.		Spacer No.			
114	0.88	61	1.28	2.2	3			2.0	4	2.32	3,4	0	0	114
115	0.89	59	1.25	2.16				2.08	3					115
116	0.89	57	1.22	2.32				2.46	3					116
117	0.85	56	1.19	5.6				5.42	4					117
118	0.85	60	1.13	1.3				0.82	3	0.86	4			118
119	0.85	59	1.08	1		2	4	0.74	3,4	1.24	5			119
120	0.85	60	1.06	1.2		2	4	0.72	3	1.28	5			120
121	0.84	61	1.04	1.1				0.44	3	1.12	5			121
123	0.85	61	1.02	0.72		1.4	4	0.36	3	0.8	5			123
124	0.86	63	1.15	1.68				1.72	4					124
125	0.85	58	1.08	1.2				1.22	3	1.26	4			125
126	0.85	62	1.08	1.52		2.4	4	1.24	4					126
127	0.86	63	1.06	1.64				1.2	4					127
132	1.0	26	1.47	2.08				2.02	3	2.16	4			132
133	1.02	32	1.48	2.4				2.14	3	2.38	4			133
148	1.02	29	1.22	1.56				1.44	3					148
151	1.02	30	1.22	1.6				1.46	3					151
153	1.02	31	1.20	6.2				4.0	3					153
154	0.865	29	1.16	6.6				3.02	4					154

11-18

NEDO-10958-A



Table II-8  
ASSEMBLY 28D

Run No.	Initial Conditions			Experimental				Prediction				Runs with MCPR > 1.0		Run No.
				Measured Initial Indication		Measured Final Indication		Predicted Initial Condition		Predicted Final Condition				
	G/10 <sup>6</sup> lb/hr-ft <sup>2</sup>	Subcooling Btu/lb	CPR	Measured Time to Onset of Boiling (sec)*	Observed Location	Measured Time to Onset of Boiling (sec)	Observed Location	Calculated Time to Onset of Boiling (sec)	Calculated Location	Calculated Time to Onset of Boiling (sec)	Calculated Location	Calc MCPR	Time (sec)	
					Spacer No.		Spacer No.		Spacer No.		Spacer No.			
305	1	28	1.502	2.4	2	2.8	1	2.54	2			0	0	305
322	1	27	1.244	1.74	2	2.5	1	1.44	2	2.36	3			322
323	1	29	1.268	2.26	1			1.84	3					323
325	1	28	1.118	1.36	2	2.3	1	0.88	2	1.02	3			325
326	1	27	1.062	1.08	2	2.1	1	0.7	2	1.12	3			326
327	1	27	1.061	0.96	2	1.4	1	0.52	2	0.78	3			327

II-19

NEDO-10958-A

Table II-9  
BUNDLE 29D

Run No.	Initial Conditions			Experimental		Prediction	
				Measured Initial Indication		Predicted Initial Condition	
				Measured Time to Onset of Transition Boiling (sec)*	Observed Location	Calculated Time to Onset of Transition Boiling (sec)	Calculated Location
					Spacer No.		Spacer No.
315	0.98	22	1.52	2.6	2	2.5	3
318	1.0	27	1.5	2.9	1	3.1	3
334	1.0	28	1.3	5.2	2	4.94	2
335	1.0	28	1.28	2.88	2	2.88	2
337	1.02	29	1.21	1.75	2	2.24	2

Table II-10  
ASSEMBLY 25A

Run No.	Initial Conditions			Experimental				Prediction				Runs with MCPR > 1.0		Run No.
				Measured Initial Indication		Measured Final Indication		Predicted Initial Condition		Predicted Final Condition				
	G/10 <sup>6</sup> lb/hr-ft <sup>2</sup>	Subcooling Btu/lb	CPR	Measured Time to Onset of Boiling (sec)*	Observed Location	Measured Time to Onset of Boiling (sec)	Observed Location	Calculated Time to Onset of Boiling (sec)	Calculated Location	Calculated Time to Onset of Boiling (sec)	Calculated Location	Calc MCPR	Time (sec)	
					Spacer No.		Spacer No.		Spacer No.		Spacer No.			
6	1.25	45	1.12	1.36	1	1.56	2	1.18	2	1.22	3			6
9	1.28	50	1.16	1.58	1	2.78	2	1.7	3					9
11	1.22	44	1.14	1.78	1,2			2.1	2	2.3	3			11
12	1.25	26	1.1	2.06	1,2			1.68	2					12
17	1.2	25	1.2	1.4	1	1.7	2					1.006	1.92	17
26	1.26	34	1.13	2	1							1.009	2.22	26
27	1.24	33	1.11	1.84	1			1.76	2					27
35	1.24	28	1.3	2.02	1	2.22	2	2.24	2					35
36	1.23	43	1.32	2.14	1	2.54	2					1.006	2.36	36
38	1.27	44	1.32	2.24	1	2.34	2					1.016	2.76	38
40	1.26	46	1.3	2.12	1	2.32	2	2.34	2					40
43	1.04	45	1.43	1.94	1	2.44	2					1.004	2.06	43
44	1.05	45	1.41	2.14	1	2.34	2	1.86	2	2.36	3			44
49	0.99	25	1.48	2.04	1	2.34	2	2.36	2					49
50	1.01	25	1.51	2.18	1	2.48	2	1.12	3	2.12	4			50
60	0.93	47	1.44	2.16	1	2.16	2	2.48	2					60
61	0.93	46	1.46	2.04	1	2.34	2					1.0025	2.58	61

Table II-11  
ASSEMBLY 32B

Run No.	Initial Conditions			Experimental				Prediction				Runs with MCPP > 1.0		Run No.
				Measured Initial Indication		Measured Final Indication		Predicted Initial Condition		Predicted Final Condition				
	G/10 <sup>6</sup> lb/hr-ft <sup>2</sup>	Subcooling Btu/lb	CPR	Measured Time to Onset of Boiling (sec)*	Observed Location	Measured Time to Onset of Boiling (sec)	Observed Location	Calculated Time to Onset of Boiling (sec)	Calculated Location	Calculated Time to Onset of Boiling (sec)	Calculated Location	Calc MCPP	Time (sec)	
					Spacer No.		Spacer No.		Spacer No.		Spacer No.			
110	1.01	39	1.74	3.5	1			2.86	2					110
132	1.03	34	1.28	2.26	1			2.08	2	2.88	3			132
133	0.99	34	1.27	1.96	1	1.96	2	1.48	2	2.3	3			133
145	1.0	34	1.79	4.43	2			4.55	2					145
146	0.98	35	1.74	4.23	2			4.5	2					146
147	0.98	34	1.66	3.76	2			4.12	2					147
155	0.5	34	1.39	4.29	2			3.91	2					155

II-22

NEDO-10958-A

Table II-12  
ASSEMBLY 35C

Run No.	Initial Conditions			Experimental				Prediction				Runs with MCPR > 1.0		Run No.
				Measured Initial Indication		Measured Final Indication		Predicted Initial Condition		Predicted Final Condition				
	G/10 <sup>6</sup> lb/hr-ft <sup>2</sup>	Subcooling Btu/lb	CPR	Measured Time to Onset of Transition Boiling (sec)*	Observed Location	Measured Time to Onset of Transition Boiling (sec)	Observed Location	Calculated Time to Onset of Transition Boiling (sec)	Calculated Location	Calculated Time to Onset of Transition Boiling (sec)	Calculated Location	Calc MCPR	Time (sec)	
				Spacer No.	Spacer No.	Spacer No.	Spacer No.	-Spacer No.						
32	1.01	33	1.65	2.41	1			2.12	2					32
33	1	32	1.62	2.47	1			1.98	2					33
48	0.98	35	1.3	3.4	1			1.52	2					48
49	1.01	39	1.3	1.92	1			1.8	2					49
50	0.93	32	1.26	1.6	1			1.24	2	3.98	3			50
51	1.01	48	1.32	2.24	1			2.3	2					51
55	0.98	31	1.78	4.84	2							1.005	4.36	55
56	1.0	38	1.81	4.44	2	4.89	1	4.28	2					56
57	1.02	40	1.82	4.96	2							1.009	4.48	57
58	1.02	35	1.78	4.58	2			4.12	2					58
59	1.01	50	1.84	4.44	2							1.004	4.5	59
60	1.02	48	1.82	4.46	2	5.01	1					1.003	4.32	60

11-23/11-24

NEDO-10958-A

**APPENDIX III**  
**AXIAL PROFILES AND LOCAL PEAKING PATTERNS**

**COLUMBIA TESTS\***

**PEAKING PATTERNS COLUMBIA 16-ROD TESTS**

1.00	1.00	1.00	1.00	0.75	1.00	1.00	0.75
1.00	1.00	1.00	1.00	1.00	1.25	1.25	1.00
1.00	1.00	1.00	1.00	1.00	1.25	1.25	1.00
1.00	1.00	1.00	1.00	0.75	1.00	1.00	0.75

**CUTA NOS.\* 1, 2, 3, 6, 7, 11, 13, 15,  
16, 16A**

**CUTA NOS. 4, 5**

1.22	1.11	1.11	0.94	0.94	0.94	1.11	0.94
1.11	0.94	0.94	0.94	0.94	1.22	0.94	1.11
1.11	0.94	0.94	0.94	1.11	0.94	0.94	0.94
0.94	0.94	0.94	0.94	0.94	1.11	0.94	0.94

**CUTA NO. 8**

**CUTA NO. 9**

1.61	1.61	1.12	0.95	1.27	1.27	1.08	0.90
1.61	1.22	0.95	0.65	1.27	1.08	0.90	0.90
1.12	0.95	0.66	0.65	1.08	0.90	0.90	0.90
0.95	0.65	0.65	0.65	0.90	0.90	0.90	0.90

**CUTA NO. 10**

**CUTA NO. 12**

\*CUTA = Columbia University Test Assembly

**PEAKING PATTERNS COLUMBIA 16-ROD TESTS**

1.28	1.28	1.09	0.89	1.22	1.22	1.09	0.92
1.28	1.09	0.89	0.89	1.22	1.09	0.92	0.92
1.09	0.89	0.89	0.89	1.09	0.92	0.92	0.92
0.89	0.89	0.89	0.89	0.92	0.92	0.92	0.92

**CUTA NO. 14**

**CUTA NO. 17**

0.92	0.92	0.92	0.92
0.92	1.23	1.23	0.92
0.92	1.23	1.23	0.92
0.92	0.92	0.92	0.92

**CUTA NO. 18**

\*Axial profile was uniform for all Columbia Tests.

## ATLAS TESTS

Note: Axial flux shapes for 7 x 7 lattice bundles given on Figure II-1. Axial flux shape for all 8 x 8 lattice bundles given by:

$$\psi = 1.387 \sin \left[ \left( \frac{z + 11.8}{171.6} \right) \pi \right]$$

Note: Values for rod peaking shown here for 16-rod and 49-rod assemblies are based on average rod power for all the rods in the array, including "cold" rods. Values for 64-rod assemblies are based on average rod power for the heated rods only.



PEAKING PATTERNS ATLAS TESTS

1.24	1.24	1.05	0.92	0.99	1.01	1.00	1.00
1.24	1.05	0.92	0.92	1.01	1.00	1.01	1.01
1.05	0.92	0.92	0.92	1.02	1.01	0.98	1.01
0.90	0.92	0.92	0.89	0.99	1.01	0.98	0.99

ATA\* NO. 2/3

ATA NO. 4

1.16	1.16	0.97	0.97	1.23	1.06	1.05	1.05
1.16	0.98	0.97	0.96	1.05	1.24	0.90	0.91
0.96	0.96	0.95	0.97	1.05	0.90	0.93	0.90
0.95	0.95	0.97	0.98	1.05	0.90	0.90	0.88

ATA NO. 5

ATA NO. 8

1.30	1.30	1.10	0.88
1.30	1.10	0.88	0.87
1.11	0.88	0.88	0.88
0.88	0.88	0.88	0.88

ATA NO. 9

0.89	0.94	0.91	0.91	1.42	1.20	1.05	1.02
0.93	1.26	1.27	0.89	1.21	1.21	1.03	1.03
0.91	1.27	1.26	0.91	1.05	1.03	0.57	0.57
0.91	0.91	0.91	0.91	1.02	1.02	0.57	1.00

ATA NO. 10, 11

ATA NO. 13

1.02	1.00	1.00	0.99	0.62	1.05	1.08	0.61
1.01	1.00	1.00	1.01	1.05	1.46	1.03	1.05
0.99	1.01	1.00	1.00	1.05	1.06	1.47	1.06
1.01	1.00	0.99	1.00	0.62	1.07	1.04	0.62

ATA NO. 14

ATA NO. 17

1.22	1.06	1.06	1.07	1.23	1.23	1.07	0.93
1.05	1.24	0.90	0.92	1.25	1.06	0.91	0.92
1.04	0.91	0.92	0.91	1.05	0.92	0.93	0.92
1.07	0.91	0.91	0.81	0.92	0.92	0.92	0.82

ATA NO. 26A

ATA NO. 26B

\*ATA = Atlas Test Assembly

## PEAKING PATTERNS ATLAS TESTS (Continued)

1.00	1.00	1.00	1.00	1.15	1.15	0.97	0.96
1.00	1.00	1.01	1.01	1.14	0.97	0.97	0.97
1.00	1.01	1.00	0.99	0.97	0.97	0.96	0.96
1.00	1.01	0.99	1.00	0.96	0.97	0.96	0.97

## ATA NO. 27A

1.25	1.26	1.08	0.90
1.25	1.08	0.91	0.91
1.07	0.91	0.90	0.89
0.90	0.91	0.90	0.90

## ATA NO. 27B

1.43	1.22	1.05	0.88
1.21	1.23	1.89	0.89
1.04	1.88	0.88	0.87
0.88	0.89	0.88	0.89

## ATA NO. 27C

1.01	1.00	1.00	1.00
1.01	1.01	1.00	0.99
1.00	1.00	1.00	0.99
1.00	1.00	0.99	1.00

## ATA NO. 27D

1.13	1.13	0.97	0.97
1.14	0.98	0.97	0.96
0.97	0.97	0.97	0.96
0.97	0.97	0.96	0.97

## ATA NO. 28A

1.43	1.23	1.03	0.88
1.23	1.23	0.89	0.88
1.03	0.89	0.89	0.88
0.89	0.88	0.88	0.89

## ATA NO. 28B

1.26	1.26	1.06	0.91
1.26	1.06	0.91	0.90
1.06	0.91	0.91	0.90
0.91	0.90	0.90	0.91

## ATA NO. 28C

1.01	1.00	0.99	1.01
1.00	1.01	1.00	1.00
0.99	1.00	1.00	0.99
1.01	1.00	0.99	1.01

## ATA NO. 28D

1.15	1.14	0.96	0.98
1.14	0.98	0.96	0.96
0.96	0.96	0.97	0.96
0.98	0.96	0.96	0.98

## ATA NO. 29A

1.43	1.21	1.05	0.89
1.21	1.21	0.88	0.88
1.05	0.88	0.89	0.88
0.89	0.88	0.88	0.89

## ATA NO. 29B

1.23	1.24	1.07	0.92
1.24	1.07	0.90	0.90
1.07	0.90	0.91	0.90
0.92	0.90	0.90	0.92

## ATA NO. 29C

## ATA NO. 29D

PEAKING PATTERNS ATLAS TESTS (Continued)

1.24	1.25	1.03	0.93	1.40	1.23	0.92	0.92
1.23	1.04	0.91	0.91	1.22	1.23	0.91	0.90
1.03	0.91	0.92	0.89	0.92	0.91	0.91	0.89
0.95	0.90	0.92	0.93	0.94	0.89	0.91	0.92

ATA NO. 30A

1.02	0.98	1.01	1.01
0.98	0.99	1.01	1.00
0.98	1.02	1.01	0.98
1.02	0.98	0.98	1.02

ATA NO. 30B

1.12	1.11	0.99	0.99
1.11	1.00	0.97	0.98
0.96	0.96	0.99	0.96
0.99	0.96	0.96	0.96

ATA NO. 30C

1.26	1.26	1.04	0.92
1.25	1.05	0.91	0.92
1.04	0.90	0.93	0.90
0.92	0.90	0.90	0.90

ATA NO. 30D

ATA NO. 30E

PEAKING PATTERNS ATLAS TESTS (7 x 7, 16 ROD)

1.26	1.26	1.07	0.91	1.24	1.26	1.07	0.92
1.25	1.07	0.92	0.90	1.25	1.07	0.92	0.90
1.06	0.91	0.91	0.90	1.07	0.91	0.91	0.90
0.92	0.90	0.89	0.88	0.93	0.90	0.90	0.88

ATA NO. 31A

ATA NO. 31B

PEAKING PATTERNS ATLAS TEST (7 x 7, 49 ROD)

1.38	1.19	1.08	0.99	0.90	0.89	0.89
1.19	1.19	1.02	0.93	0.91	0.93	0.90
1.04	1.02	1.02	0.92	0.93	0.93	0.92
1.02	0.92	0.92	0.92	0.93	0.92	0.92
0.95	0.94	0.92	0.92	1.01	1.01	1.03
0.94	0.94	0.95	0.94	1.01	1.17	1.17
0.94	0.94	0.95	1.00	1.04	1.17	1.36

ATA NO. 18

PEAKING PATTERNS ATLAS TESTS (7 x 7, 49 ROD) (Continued)

1.23	1.20	1.17	1.18	0.95	1.03	1.02
1.05	1.21	1.17	1.10	1.03	0.96	0.96
1.18	0.90	0.90	0.91	0.94	0.96	0.94
1.18	0.93	0.90	0.97	0.93	0.96	0.96
1.18	0.94	0.93	0	0.93	1.02	1.00
0.94	1.03	0.94	0.94	0.92	1.04	1.04
1.03	0.94	1.18	1.04	1.17	0.96	1.06

ATA NO. 19B

1.21	1.18	1.16	1.16	0.94	1.01	1.00
1.03	1.19	1.16	1.08	1.01	0.94	0.94
1.16	0.89	0.88	0.90	0.92	0.94	0.92
1.16	0.91	0.89	0.95	0.91	0.94	0.94
1.16	0.92	0.91	0.89	0.91	1.00	0.98
0.92	1.01	0.92	0.92	0.90	1.02	1.02
1.01	0.92	1.18	1.02	1.16	0.94	1.04

ATA NO. 19C

1.21	1.18	1.16	1.16	0.94	1.01	1.00
1.19	1.03	0.90	0.91	1.01	0.94	0.94
1.16	0.89	0.88	0.90	0.92	0.94	1.16
1.16	0.91	0.89	0.98	0.91	0.94	0.92
0.94	1.01	0.91	0.89	1.08	0.92	1.16
1.00	0.94	0.92	0.92	0.92	1.02	1.02
1.01	0.95	1.18	0.92	1.16	1.02	1.04

ATA NO. 19D

1.01	0.92	0.98	1.17	0.93	1.16	1.00
1.03	1.02	1.16	1.07	1.01	0.93	0.94
1.17	0.88	0.88	0.89	0.92	0.94	1.16
0.93	0.91	0.88	0.94	0.91	0.94	1.19
1.17	0.92	0.81	0.89	0.91	1.00	1.22
0.92	1.01	0.92	0.91	0.90	1.02	1.20
1.01	0.92	1.15	1.02	1.16	0.94	1.04

ATA NO. 24A

**PEAKING PATTERNS ATLAS TESTS (7 x 7, 49 ROD) (Continued)**

1.23	1.22	1.19	1.20	0.96	1.04	1.03
1.05	1.23	1.19	1.10	1.04	0.96	0.97
1.20	0.91	0.91	0.92	0.95	0.96	0.95
1.20	0.93	0.90	0.97	0.93	0.96	0.96
1.20	0.94	0.94	0	0.94	1.03	1.01
0.94	1.04	0.98	0.94	0.92	0.94	1.05
1.04	0.94	1.19	1.04	0.92	0.96	1.07

**ATA NO. 24B**

1.23	1.23	1.20	1.20	0.96	1.04	1.03
1.05	1.22	1.19	1.10	1.04	0.96	0.92
1.21	0.91	0.91	0.92	0.95	0.97	0.95
1.20	0.93	0.90	0.97	0.93	0.96	0.96
1.20	0.94	0.94	0	0.94	1.03	1.01
0.94	1.04	0.94	0.94	0.93	0.94	1.05
1.04	0.94	1.19	1.04	0.92	0.96	1.07

**ATA NO. 25A**

1.23	1.23	1.20	1.19	0.96	1.04	1.03
1.05	0	1.19	1.10	1.04	0.96	0.92
1.21	0.91	0.91	0.92	0.95	0.97	0.95
1.20	0.93	0.90	0.97	0.93	0.96	0.96
1.20	0.94	0.94	1.22	0.94	1.03	1.01
0.94	1.04	0.94	0.94	0.93	0.94	1.05
1.04	0.94	1.19	1.04	0.92	0.96	1.07

**ATA NO. 25B**

**PEAKING PATTERNS ATLAS TESTS (8 x 8, 16 ROD)**

1.27	1.28	1.05	0.91	1.27	1.01	1.05	1.04
1.27	1.04	0.90	0.91	1.04	1.28	0.90	0.91
1.02	0.90	0.90	0.92	1.03	0.91	0.90	0.92
0.91	0.91	0.90	0.90	1.03	0.91	0.91	0.90

**ATA NO. 20A**

**ATA NO. 20B**

PEAKING PATTERNS ATLAS TESTS (8 x 8, 16 ROD) (Continued)

1.05	1.04	1.03	1.04	0.97	0.96	0.96	0.97
1.04	1.19	1.16	1.04	0.97	1.11	1.08	0.97
1.03	1.18	0	1.05	0.96	1.10	1.10	0.98
1.04	1.05	1.04	1.04	0.97	0.97	0.97	0.97

ATA NO. 21A

1.00	1.00	0.99	1.00
1.00	1.00	1.00	1.00
0.99	1.01	1.00	1.01
1.00	1.00	1.00	1.00

ATA NO. 21B

1.12	1.12	0.96	0.97
1.11	0.98	0.97	0.98
0.96	0.98	0.98	0.99
0.97	0.98	0.97	0.97

ATA NO. 21C

1.27	1.28	1.04	0.91
1.28	1.03	0.90	0.91
1.03	0.90	0.90	0.91
0.91	0.91	0.90	0.91

ATA NO. 21D

1.12	1.11	0.98	0.98
1.11	0.98	0.97	0.98
0.98	0.97	0.97	0.98
0.98	0.98	0.97	0.97

ATA NO. 22A

1.01	1.01	1.00	1.00
1.01	1.00	0.99	1.00
1.00	1.00	0.99	1.00
1.00	1.00	0.99	1.00

ATA NO. 22B

1.27	1.26	1.03	0.91
1.28	1.05	0.90	0.92
1.01	0.91	0.92	0.91
0.91	0.91	0.90	0.92

ATA NO. 22C

0.99	0.98	1.00	1.01
1.00	0.99	1.03	1.00
1.00	1.03	0.99	1.00
1.00	0.99	0.99	1.00

ATA NO. 23A

0.96	0.96	0.97	0.98
0.97	1.11	1.08	0.98
0.98	1.08	1.10	0.97
0.97	0.96	0.96	0.98

ATA NO. 23B

ATA NO. 23C

**PEAKING PATTERNS ATLAS TESTS (8 x 8, 64 ROD)**

1.22	1.22	1.23	1.10	1.10	1.10	1.22	1.21
1.22	1.05	1.09	1.10	1.03	1.05	1.10	1.02
1.22	1.09	0.58	0.88	0.89	0.87	0.58	1.24
1.10	1.10	0.88	0.88	0.89	0.88	0.89	0.92
1.10	1.04	0.89	0.88	0	0.88	0.89	1.02
1.10	1.04	0.90	0.88	0.88	0.98	0.88	0.99
1.21	1.10	0.58	0.89	0.89	0.88	0.58	1.09
1.21	1.03	1.25	0.91	1.02	1.00	1.09	1.01

**ATA NO. 32A**

1.22	1.22	1.23	1.09	1.09	1.09	1.21	1.20
1.22	1.05	1.09	1.09	1.03	1.04	1.09	1.02
1.22	1.09	0.58	0.88	0.89	0.87	0.58	1.24
1.09	1.09	0.88	0.88	0.88	0.88	0.89	0.91
1.09	1.03	0.89	0.88	0	0.88	0.89	1.02
1.09	1.04	0.89	0.88	0.88	1.00	0.88	0.98
1.21	1.09	0.58	0.89	0.89	1.09	0.58	1.09
1.21	1.03	1.24	0.91	1.01	1.00	1.09	0.98

**ATA NO. 32B**

1.59	1.58	1.60	1.43	1.43	1.14	0.77	0.77
1.59	1.43	1.42	1.28	1.16	1.14	0.75	0.76
1.59	1.42	1.42	1.14	1.16	0.77	0.75	0.76
1.43	1.28	1.15	0	1.15	0.76	0.76	0.76
1.42	1.16	1.16	1.15	0.76	0.76	0.76	0.76
1.14	1.14	0.77	0.76	0.76	0.76	0.76	0.76
0.77	0.75	0.75	0.76	0.76	0.76	0.75	0.76
0.77	0.76	0.76	0.76	0.76	0.76	0.75	0.75

**ATA NO. 32C**

1.12	1.13	1.13	1.07	1.06	1.12	1.07	1.06
1.13	1.04	1.06	1.03	0.91	0.91	0.60	1.06
1.13	1.06	1.06	0.93	0.90	0.60	1.05	1.13
1.07	1.03	0.93	0	0.90	1.05	0.90	0.91
1.06	0.91	0.89	0.90	1.02	0.90	1.04	1.06
1.12	0.91	0.60	1.04	0.90	1.08	1.06	1.12
1.07	0.60	1.05	0.91	1.02	1.06	0.91	1.12
1.06	1.0	1.13	0.90	1.05	1.12	1.12	1.09

**ATA NO. 33A**

PEAKING PATTERNS ATLAS TESTS (8 x 8, 64 ROD) (Continued)

1.12	1.13	1.08	0.94	1.07	1.07	1.13	1.07
1.13	0.94	0.60	1.15	1.13	0.60	0.92	1.13
1.08	0.60	1.02	1.13	1.15	1.01	0.60	1.05
1.08	1.03	1.14	0.92	0.90	1.14	0.91	1.14
1.07	1.14	0.91	0.90	1.06	0.91	1.13	1.06
1.07	0.60	1.14	1.05	0.91	1.12	0.60	1.07
1.13	1.07	0.60	1.13	1.14	0.60	0.91	1.12
1.06	1.13	1.07	0.90	1.06	1.06	1.13	1.08

ATA NO. 34C

1.12	1.13	1.08	0.94	1.07	1.07	1.13	1.07
1.13	0.94	0.60	0.92	0.90	0.60	0.92	1.13
1.08	0.60	1.14	0.90	1.06	1.14	0.60	1.05
1.08	1.03	1.02	1.15	1.13	1.01	0.91	1.14
1.07	1.14	0.91	1.13	1.15	0.91	1.13	1.06
1.07	0.60	1.14	1.05	0.91	1.12	0.60	1.07
1.13	1.07	0.60	1.13	1.14	0.60	0.91	1.12
1.06	1.13	1.07	0.90	1.06	1.06	1.13	1.08

ATA NO. 34D

1.12	1.13	1.09	0.94	1.07	1.08	1.13	1.07
1.13	0.94	0.60	0.92	0.91	0.60	0.92	1.13
1.08	0.60	1.14	0.91	1.06	1.14	0.60	1.05
1.08	1.03	1.02	1.16	1.13	1.01	0.91	1.14
1.07	1.14	0.91	1.14	0.00	0.91	1.14	1.06
1.08	0.60	1.14	1.05	0.91	1.13	0.60	1.07
1.14	1.07	0.60	1.14	1.14	0.60	0.92	1.13
1.06	1.13	1.07	0.90	1.06	1.07	1.13	1.09

ATA NO. 34E

1.12	1.08	1.15	1.13	1.07	1.07	1.13	1.07
1.13	0.94	1.13	1.15	0.90	0.60	0.92	1.13
1.08	0.60	0.94	0.90	1.06	1.14	0.60	1.05
1.13	1.03	1.02	1.14	0.60	1.01	0.91	1.14
1.07	1.14	0.91	0.92	1.08	0.91	1.13	1.06
1.07	0.60	1.14	1.05	0.91	1.12	0.60	1.07
1.13	1.07	0.60	1.13	1.14	0.60	0.91	1.12
1.06	1.13	1.07	0.90	1.06	1.06	1.13	1.08

ATA NO. 34F



PEAKING PATTERNS ATLAS TESTS (8 x 8, 64 ROD) (Continued)

1.12	1.13	1.06	0.94	1.05	1.07	1.13	1.07
1.13	0.94	0.60	1.15	1.13	0.60	0.92	1.13
1.08	0.60	1.02	1.13	1.15	1.01	0.60	1.07
1.08	1.07	1.14	0.90	0.90	1.14	0.91	1.14
1.03	1.14	0.91	0.92	1.08	0.91	1.13	1.06
1.13	0.60	1.14	1.05	0.91	1.12	0.60	1.07
1.13	1.07	0.60	1.13	1.14	0.60	0.91	1.12
1.06	1.13	1.07	0.90	1.06	1.06	1.13	1.08

ATA NO. 34G

1.12	1.13	1.13	1.07	1.04	1.13	1.06	1.06
1.13	1.06	1.06	1.03	0.91	0.90	0.60	1.06
1.13	1.07	1.01	0.93	0.90	0.60	1.06	1.13
1.08	1.01	0.93	0.00	0.90	1.02	0.91	0.90
1.03	0.91	0.90	0.91	1.08	0.91	1.06	1.06
1.13	0.91	0.60	1.03	0.91	1.04	1.06	1.12
1.05	0.60	1.05	0.91	1.07	1.06	0.91	1.12
1.06	1.06	1.13	0.90	1.06	1.13	1.12	1.08

ATA NO. 34H

1.12	1.13	1.13	1.07	1.04	1.13	1.06	1.06
1.13	1.06	1.04	1.03	0.91	0.90	0.60	1.06
1.13	1.08	1.01	0.93	0.90	0.60	1.06	1.13
1.08	1.01	0.93	0.00	0.90	1.02	0.91	0.90
1.03	0.91	0.90	0.91	1.07	0.91	1.06	1.06
1.13	0.91	0.60	1.03	0.91	1.06	1.06	1.12
1.05	0.60	1.05	0.91	1.07	1.06	0.91	1.12
1.06	1.06	1.13	0.90	1.06	1.13	1.12	1.08

ATA NO. 34I

1.58	1.57	1.59	1.42	1.31	1.14	0.76	0.76
1.57	1.45	1.42	1.29	1.15	1.14	0.75	0.76
1.58	1.44	1.43	1.17	1.14	0.75	0.75	0.76
1.42	1.27	1.17	0.00	1.13	0.76	0.76	0.76
1.29	1.15	1.14	1.15	0.76	0.76	0.76	0.75
1.14	1.15	0.75	0.76	0.76	0.76	0.75	0.75
0.76	0.75	0.76	0.76	0.76	0.75	1.15	0.75
0.76	0.76	0.76	0.76	0.75	0.76	0.75	0.76

ATA NO. 35A

## PEAKING PATTERNS ATLAS TESTS (8 x 8, 64 ROD) (Continued)

1.23	1.22	1.22	1.11	1.02	1.11	1.25	1.23
1.23	1.06	1.11	1.10	1.04	1.04	1.10	1.04
1.22	1.11	0.59	0.91	0.88	0.89	0.58	1.25
1.11	1.10	0.91	0.89	0.88	0.89	0.89	0.89
1.01	1.02	0.88	0.90	0.00	0.89	0.89	1.00
1.11	0.99	0.88	0.88	0.88	1.03	0.59	1.04
1.25	1.10	0.59	0.88	0.88	0.59	0.89	1.11
1.24	1.05	1.23	0.87	1.04	1.04	1.10	1.04

## ATA NO. 35B

1.13	1.13	1.13	1.06	1.04	1.13	1.06	1.06
1.13	1.08	1.07	1.06	0.91	0.91	0.61	1.06
1.13	1.06	1.06	0.93	0.90	0.61	1.04	1.13
1.08	1.08	0.93	0.00	0.90	1.07	0.91	0.91
1.03	0.91	0.90	0.91	1.07	0.91	1.06	1.03
1.13	0.91	0.60	1.06	0.90	1.06	1.02	1.12
1.03	0.60	1.03	0.90	1.05	1.01	0.91	1.13
1.01	1.07	1.12	0.89	1.06	1.13	1.12	1.06

## ATA NO. 35C

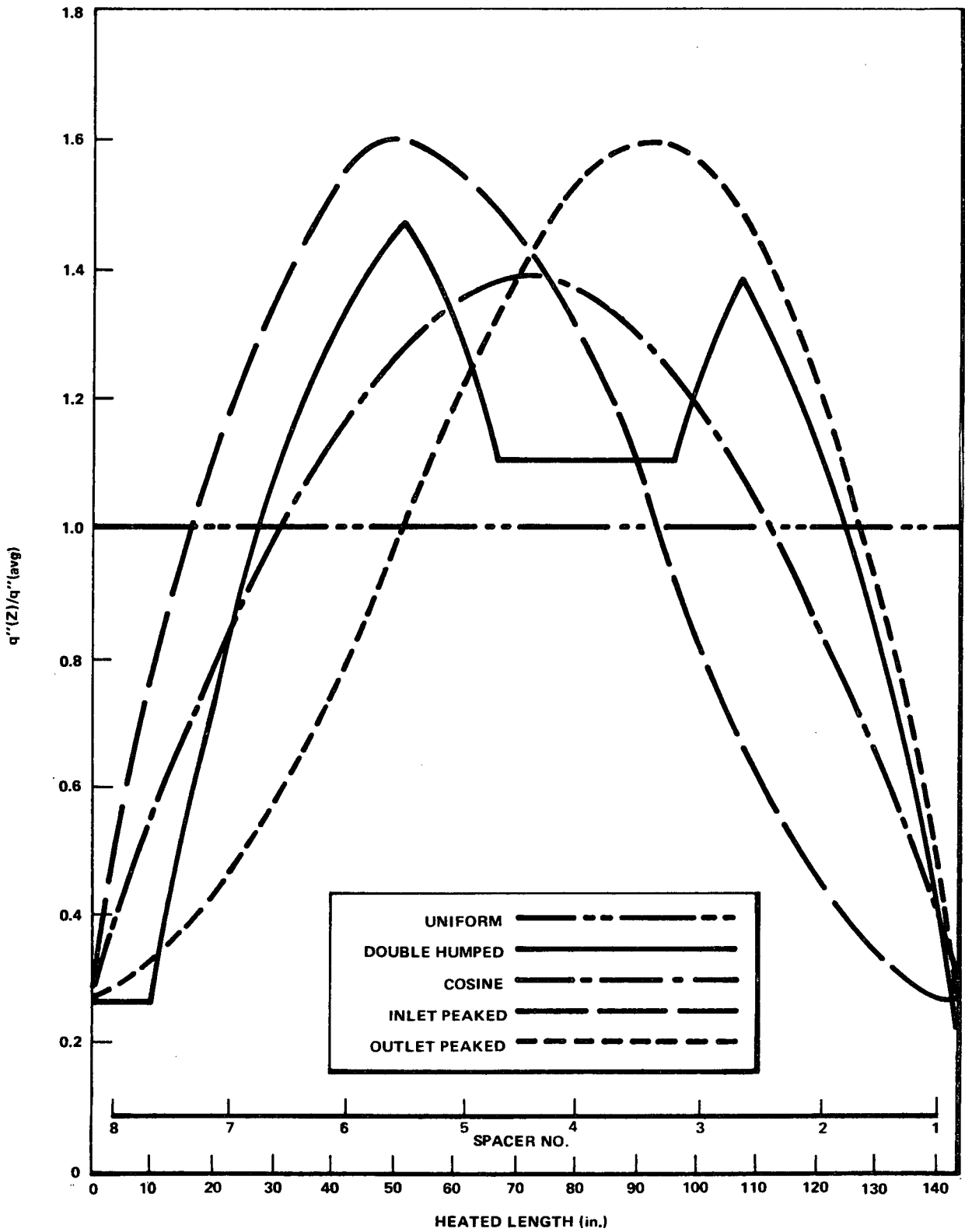


Figure III-1. Axial Flux Shapes for 7 X 7 Lattice

## APPENDIX IV STATISTICAL ROD BOILING TRANSITION ANALYSIS

### IV-1. INTRODUCTION

The subject of this section is the calculation of the number of rods which might experience boiling transition resulting from various operational transients and from steady-state operation at a given minimum critical power ratio (MCPR). A model of the BWR core that incorporates uncertainty effects of manufacturing tolerances, uncertainty in measurement of core operating parameters, calculational uncertainties, and statistical uncertainty associated with the GEXL correlation is used to calculate the probability of a boiling transition occurring and the number of rods which might possibly experience a boiling transition as a function of the nominal MCPR. The model is similar to that reported in recent FSAR submits (Reference 18) with the exception that the GEXL correlation is used as the predictor of boiling transition conditions and input uncertainties have been revised to be consistent with current expectation. The technique employed is to impose statistical uncertainties on an analytical representation of the core and evaluate the probability of avoiding boiling transition.

### IV-2. DEFINITIONS AND OBJECTIVES

The predictor of critical bundle power is the GEXL correlation. The uncertainty in the correlation is characterized by a normal distribution with standard deviation ( $\sigma$ ) constant over the range of independent variables of the correlation. A large number of critical power tests, with variation in the independent variables (pressure, boiling length, mass flux, R and thermal diameter) were performed. The observed dependent variable (ECPR) was found to approximate a normal distribution. Thus, for a bundle operating at critical power, as predicted by the GEXL, there is a 0.5 probability of the occurrence of a boiling transition. In a group of N rods each operating at the mean of the data, 0.5N or the rods are expected to experience a boiling transition.

### IV-3. ANALYTICAL PROCEDURES

#### IV-3-1. Selection of Significant Input Uncertainties

Critical power ratio (CPR) is not measured directly and neither are all the variables that determine CPR. These variables are mass flux, quality, pressure, boiling length, and local peaking pattern. Quality is determined by total power distribution, inlet subcooling, and pressure, but direct measurement is not made in the case of power level, and measurement of relative fission rate is performed at only a limited number of points. A similar situation exists with respect to the other variables which, by definition, directly determine CPR.

Sensitivity analyses\* of the input measurements have permitted elimination of those variables that do not contribute significantly to the uncertainty in the variable of primary interest. The variables that significantly affect the uncertainty in critical power ratio include measurement uncertainty in the core operating parameters, uncertainty due to the effects of manufacturing tolerances, and uncertainty in calculated parameters used by the model.

#### IV-3-2. Critical Power Data

The critical power data can be represented statistically. This approach recognizes that the experiments which yield critical power data are affected to some extent by manufacturing tolerances and uncertainties in the instruments which monitor the test facility. In addition it is an indication of the ability of the GEXL correlation to predict critical power over the range of the independent variables ( $R, G; P, L_B$ ). For this analysis GEXL is the best analytical representation of the data; observed values are very nearly normally distributed about the values predicted by GEXL with a standard deviation,  $\sigma$ .

#### IV-3-3. Application of the GEXL Correlation to the Statistical Model

The probability of a rod experiencing a boiling transition is evaluated from the value of the CPR for the given bundle. The probability for each rod is calculated and then summed over all rods in the bundle to form the total proba-

\*See responses to Questions 3-2 and 3-7 for details of these analyses.

bility of a boiling transition for that given bundle. The R factor variation in the bundle is used to calculate the rod by rod R factor, which is used in GEXL to predict the critical power ratio of each individual rod and ultimately the probability of a boiling transition.

**IV-3.4. Input Uncertainties**

The validity of the results of these studies depends on the validity of the input uncertainty values. These are presented in summary form in Table IV-1 and discussed briefly in the text which follows the table. Greater detail is given in the response to Question 3-8 in Appendix VII.

**Table IV-1  
DESCRIPTION OF UNCERTAINTIES**

Quantity	Standard Deviation* (% of Point)	Comment
Feedwater Flow	1.76	This is the largest component of total reactor power uncertainty.
Feedwater Temperature	0.76 } 0.50 }	These are the other significant parameters in core power determination.
Reactor Pressure		
Core Inlet Temperature	0.2 } 2.5 }	Affect quality and boiling length. Flow is not measured directly, but is calculated from jet pump $\Delta P$ . The listed uncertainty in core flow corresponds to 11.2% standard deviation in each individual jet pump flow.
Core Total Flow		
Channel Flow Area	3.0	This accounts for manufacturing and service induced variations in the free flow area within the channel.
Friction Factor Multiplier	10.0	Accounts for uncertainty in the correlation representing two phase pressure losses.
Channel Friction Factor Multiplier	5.0	Represents variation in the pressure loss characteristics of individual channels. Flow area and pressure loss variations affect the core flow distribution, influencing the quality and boiling length in individual channels.
TIP Readings	6.3	These sets of data are the base from which gross power distribution is determined. The assigned uncertainties include all electrical and geometrical components plus a contribution from the analytical extrapolation from the chamber location to the adjacent fuel assembly segment. Also included are uncertainties contributed by the LPRM system. LPRM readings are used to correct the power distribution calculations for changes which have occurred since the last TIP survey. The assigned uncertainty affects power distribution in the same manner as the base TIP reading uncertainty.
R Factor	1.5	This is the last of the three power distribution related uncertainties. It is a function of the uncertainty in local fuel rod power and is discussed in detail in the text.
Critical Power	3.6	Uncertainty in the GEXL correlation expressed in terms of critical power per Section 5.2:

\*Use of generic values is explained in the response to Question 3-3, Appendix VII.

38

#### IV-3-4-1. Justification of Assigned Uncertainty Values

Several of the quantities listed in Table IV-1 have a controlling influence on the calculated number of rods expected to experience boiling transition. These are feedwater flow, core total flow, TIP and LPRM readings, R, and the GEXL correlation. The uncertainty in the correlation has been discussed at length in the section describing its development. It is appropriate to present the sources of the other more significant values here.

#### IV-3-4-2. Friction Factor Multiplier

The ATLAS test facility has also been employed to determine two-phase friction multipliers. The data covered the normal operating ranges of flow, quality, and pressure, exhibiting a standard deviation of 8%. A more conservative value of 10% is used in the core analysis. An additional channel-to-channel friction multiplier standard deviation of 5% is employed to simulate the effects of non-uniform crud buildup. This is based on sensitivity studies relating hot channel flow variation to the various parameters affecting flow distribution.

#### IV-3-4-3. Core Total Flow

A detailed study of each component of the core flow measurement system using either specification tolerances or experience-based variations has given a standard deviation of 1.6%. During initial system testing, a field calibration is required. This final step introduces an additional uncertainty, leading to a final estimated standard deviation of 2.5% applicable to a typical rated flow monitoring situation.

#### IV-3-4-4. Feedwater Temperature

The standard deviation of the feedwater temperature measurement has been calculated to be 0.75%. The evaluation included consideration of sensor accuracy, junction imperfections, and radiation and temperature lifetime effects.

#### IV-3-4-5. Channel Flow Area

The 3% standard deviation applied to channel flow area is derived from manufacturing tolerances on the mechanical components which define the flow path, and it also includes consideration of non-uniform crud accumulation. Thus, the basis is mostly analytical, but also includes a limit amount of reactor crud accumulation data.

#### IV-3-4-6. Feedwater Flow

The feedwater flow uncertainty is composed of uncertainties from the flow element itself, the transmitter, and the conditioning and converting operation required for input to the process computer. For most reactors currently in operation, the system provided has a combined standard deviation of 1.6% based on a detailed analysis of the individual pieces of equipment and/or specification values. Most of the current projects which are under construction have an improved system expected to yield a combined standard deviation of 0.8%.

Experience has shown that installation and service conditions can sometimes lead to a loss of accuracy. Programs have been established to recalibrate any measurement systems which seem to have deteriorated.

The statistical analyses reported here employ a 1.6% standard deviation except for BWR-6, for which 0.8% is assumed.

#### IV-3-4-7. Local Peaking Parameters, R

As indicated in the discussion of the GEXL correlation, the parameter which expresses the effect of local peaking is defined for each fuel rod as a function of a linear combination of the square roots of relative rod powers of four to nine fuel rods in the region of interest. Therefore, the uncertainty in R is a function of the uncertainty in the local relative rod powers,  $r_i$ .

An exact derivation of  $\sigma_R$  requires knowledge of the relation, if any, between the four to nine  $r_i$  values involved. The  $r_i$  are actually weakly correlated through the neutron transport and fission mechanism. If this correlation is ignored

and the  $r_i$ 's are assumed independent, then it can be shown that  $\sigma_R = \sigma_r/3$ . A more conservative relation can be derived if it is assumed that all  $r_i$  are equal. This leads to  $\sigma_R = (\sigma_r)(0.5)$ . Because the refinement afforded by the more elaborate derivation is not required for these analyses, the current work employs the conservative upper limit relation  $\sigma_R = 0.5 \sigma_r$ .

The preceding discussion related uncertainty in R to uncertainty in  $r_i$ . The latter is a function of manufacturing variations as well as calculational uncertainty. For small changes,  $r_i$  may be written as a linear function of the variables and consequently

$$\sigma_{r_i}^2 = \sum_{j=1}^n \sigma_{x_j}^2$$

is an appropriate procedure for estimating the uncertainty in a given local relative rod power. The components of this uncertainty defined by the manufacturing process are presented in Table IV-2.

Table IV-2  
MANUFACTURING INDUCED UNCERTAINTIES

Characteristic	Standard Deviation	Effect on Local Relative Power ( $\Delta r_i/r_i$ )
Enrichment	0.015 wt% U-235	0.007
Fuel Density	0.11 g/cm <sup>3</sup>	0.011
Pellet Diameter	0.0005 in.	0.002
Fuel Rod Position in Assembly*	not defined	0.005

\*Lateral movement permitted by spacer.

Detailed lattice analyses performed in the normal design process lead to a specification of individual fuel rod enrichments. These calculations also yield relative fuel rod powers. Uncertainty in the calculated rod relative powers has been determined to correspond to a standard deviation of 2.6%. This uncertainty when combined with those associated with the allowable manufacturing variations yields a total standard deviation slightly less than 3% for a given individual relative rod power,  $r_i$ . Therefore, half of this value, 1.5%, is the standard deviation assigned to R for these statistical analyses.

#### IV-3-4-8. Traveling In-Core Probe (TIP) Readings

The TIP readings contain the majority of the information on gross power distribution. In practice, LPRM readings are used to extrapolate from a base set of TIP data to correct for minor changes in power or control rod configuration. For convenience in the statistical analysis, the uncertainty associated with this extrapolation was combined with the basic TIP uncertainty; and the analysis did not use LPRM inputs.

The TIP signal uncertainty arises from both the geometric mislocation of the TIP detector with respect to the neighboring fuel channels and the random neutron, electronic and boiling noise in the reactor. The random noise component of the signal has been determined by traversing a common instrument tube with the detector and recording the variance in the signal. The resulting random noise uncertainty (all values are with respect to a 6-inch segment) was found to be 1.2%. The geometrical component has been determined by comparing the random deviation from unity of the ratio of symmetrically located TIP signals (which should have identical readings during symmetric operation). This random deviation is the statistical superposition of the TIP geometrical and random noise uncertainties. The geometrical uncertainty, determined by statistically subtracting the known random noise component from the total deviation, was determined to be 2.3%. The geometrical and random noise TIP uncertainties combine to give an overall TIP uncertainty of 2.6%.

The local power range instruments are used in the core performance evaluation to update the base TIP axial flux profiles after a small power change ( $\leq 15\%$  of rated). The LPRM instrument signal uncertainty arises from the axial interpolation of the signals, random signal noise, system non-linearity and instrument sensitivity decay. LPRM-geometrical uncertainties are normalized out of the power evaluation. Estimates of these individual component uncertainties have been made based on the instrument design, a 15% (of rated) change in power and the maximum period between LPRM calibrations—30 days—and lead to an overall LPRM signal uncertainty of 3.4%. This LPRM uncertainty when combined with the base TIP uncertainty of 2.6% yields a resultant 4.3% uncertainty in the LPRM-extrapolated TIP signals.

In addition to the instrument related uncertainties, there is an uncertainty associated with the calculated relation between an instrument reading and the power of the adjacent segment of fuel assembly. This is estimated based on gamma scan data from operating reactors to be a standard deviation of 4.6%.

The combined standard deviation assigned to TIP readings for this analysis is 6.3% including estimated TIP, LPRM, and calculational contributions.

See references 24 and 25 for additional information on the TIP uncertainty.

#### IV-3-5. Reactor Model

The statistical analyses employ a generalized model of the core. Power density, flow per assembly, fuel assembly geometry, fuel assembly loading pattern, and subcooling are all matched to typical plants of the appropriate class. The core is represented analytically by a computer code that is equivalent to the process computer treatment. This code takes as input LPRM and TIP data as well as flow and heat balance information and produces a CPR map of the core. In the cases analyzed here, the input data were taken from design code calculations rather than from the plant instrumentation that will be used when the plant is operating.

The power distribution calculated using conventional control rod sequencing usually does not yield core MCPR values approaching limits. The control rod pattern is modified if required to achieve limiting conditions of MCPR and peak linear heat generation. After the base case has been developed, the fluxes at the instrument locations are used to generate simulated input to the process computer, represented here by the separate computer code mentioned earlier.

To achieve core MCPR ratios representative of the operational transients, the core thermal power is adjusted to achieve the MCPR characteristic of the transient of interest. To calculate the mixed enrichment loading cores, the power level, bundle flows and R factors of both the high and low enrichment bundles are used in the reactor model separately, and the resulting numbers of rods are combined linearly according to the fraction of the core associated with each fuel assembly type.

#### IV-3-6. The Calculational Process

The computer code which represents the process computer function may be regarded as a mathematical operator that transforms plant data into CPR for every bundle in the core. For purposes of the statistical analysis, this operator is driven by a Monte Carlo control program which imposes random variations on the inputs according to assigned frequency distributions, and in each trial, recalculates the CPR for every bundle in the core\*. In this step, the GEXL correlation is treated as an input subject to variation according to the assigned frequency distribution described earlier.

The Monte Carlo analysis process can be broken into several parts. These steps can best be explained by referring to the flow chart in Figure IV-4.

The process starts by performing a nominal reactor state calculation. Traveling In-core Probe (TIP) readings are generated analytically by simulating the traversing of the core with a U235 detector head which measures at different core elevations the average thermal neutron flux in a four bundle cell. The tip readings along with the total reactor power are then used by the model to calculate the detailed power distribution in the core.

\*See the response to Question 2-1, Appendix VII.



The next step utilizes other plant operating information such as core flow dome pressure, core coolant inlet temperature, channel flow areas, and friction multipliers to calculate the flow and void distributions. Using the previously calculated power distribution, iteration with respect to flow and void distributions is performed until the feedback effects of voiding are reflected in the flow. At this point in the calculation, the flow, void and power distributions are known for each bundle in the core.

R-factors—the weighted fuel pin power factors employed in GEXL—are then input to the model for each fuel assembly. This information along with the flow, void, and quality distributions is used in the GEXL correlation to calculate the critical power ratio for each fuel rod in the core.

The probability that a Boiling Transition event (B.T.) occurs in a fuel assembly ( $P_B$ ) can then be calculated using the individual values of CPR corresponding to each fuel pin in that lattice. A sample of how probabilities are calculated using a GEXL calculated critical power ratio (CPR) is shown in Figure IV-5. For example, if the uncertainty ( $\sigma_{CPR}$  = one standard deviation) between the GEXL predictions and the ATLAS test data were 4%, the probability of a rod experiencing boiling transition would be as illustrated by the cross-hatched area in Figure IV-5 found in normal probability table. Since the distribution is assumed to be normal, a probability of 0.1587 is calculated for this example for a rod with a GEXL predicted CPR of 1.04. The total bundle probability of B.T. is then calculated using the individual fuel pin probabilities ( $P_n$ ) as shown in the following relation:

$$1 - P_B = \prod_{n=1}^{N_{rod}} (1 - P_n)$$

where:

$P_B$  = prob. B.T. in a bundle

$P_n$  = prob. B.T. for a fuel rod

$N_{rod}$  = number of fuel rods in a bundle

The probability ( $P_C$ ) of boiling transition occurring anywhere in the active core region can be calculated in the same manner as bundle probabilities by substituting  $P_C$  for  $P_B$  and  $P_B$  for  $P_n$  in the above formulation with  $N$  equal to the total number of assemblies in the core. With a calculated value of  $P_C$ , the Monte Carlo procedure then either selects or rejects bundles depending on whether they will contribute significantly to the overall probability of B.T. in the Monte Carlo trials. For instance, the GEXL correlation and subsequent probability calculations during the Monte Carlo trials will only be performed on fuel bundles with nominal case probabilities ( $P_B$ )  $\geq P_C \times 10^{-9}$ . Therefore, any fuel bundle with very low probabilities of B.T. (i.e.,  $P_B < P_C \times 10^{-9}$ ) for the nominal case will always be insignificant during the Monte Carlo process when compared to bundles with higher probabilities of B.T.

With the nominal case run and fuel assembly selections made, possible reactor operating states can be calculated by random Monte Carlo selection from distributions of all operating parameters. For instance, there exists a calculated uncertainty ( $1\sigma$ ) associated with all TIP readings. It is assumed that the nominal value of the TIP reading is the mean and that the corresponding uncertainty is one standard deviation of a normal distribution. With this assumption a new TIP value can be selected randomly from its normal distribution in each Monte Carlo trial. For each trial, this random selection is performed once for each TIP reading, each R-factor, each bundle cross sectional flow area, core flow, core power, core coolant inlet temperature, core pressure, and for each bundle friction multiplier. After all of these operating parameters have been randomly selected from their respective normal distributions, the power, flow, void, and quality distributions are calculated in the exact same manner as the previous nominal case.

Again the GEXL correlation is used to calculate critical power ratios (CPR). However, instead of being applied to all the fuel rods in the core, the CPR's are only calculated for those rods contained in bundles considered significant in the nominal case calculation. Usually this reduced core calculation includes approximately one-third of the core's fuel rods.

As in the nominal case, the probability of a fuel rod experiencing boiling transition can be calculated as shown in Figure IV-5. Fuel rod probabilities of boiling transition ( $P_N$ ) are calculated for the same portion of the core (i.e., for the reduced core) as were the CPR's. The number of rods expected to experience boiling transition is then equal to the summation of all the fuel rod probabilities ( $P_N$ ).

The Monte Carlo program then proceeds to the next trial. As before, the values of the input operating parameters are randomly selected from their respective normal distributions. All calculations are performed as in the previous Monte Carlo trial with a resultant number of rods expected to experience boiling transition as the end product of the trial.

Minimum allowable critical power ratio is set to correspond to the criterion of 99.9% rods expected to avoid boiling transition by interpolation among the means of several distributions each formed from 49 Monte Carlo Trials at a nominal MCPR.

The Monte Carlo process can be repeated an arbitrary number of times: each trial produces a new value for the number of rods which might possibly experience a boiling transition event. After a reasonable number of trials (~20), the results of the process begin to assume their own statistical distribution and after about 30 trials, the means and standard deviations characterizing the output results are well defined. Based on these results GE has selected 49 trials for the statistical analysis. Although the number of trials appears small compared to the tens of thousands of histories used in nuclear physics Monte Carlo analysis, a single trial here may involve study of as many as 8000 individual rod candidates for boiling transition.

#### IV-4. EFFECT OF POWER DISTRIBUTION ON STATISTICAL ROD BOILING TRANSITION ANALYSIS

The first step in the statistical analysis procedure is an analytical construction of an initial condition of the reactor. This step employs a three dimensional BWR simulator code for which power, flow, and control rod patterns are inputs. The control rod pattern is adjusted to maintain  $k_{eff} = 1.00$  and achieve the desired power distribution. Power distribution constraints include maximum linear heat generation and core MCPR limits.

For a given reactor at a particular exposure there is a variety of rod patterns which produce  $k_{eff} = 1.0$  and satisfy local power and MCPR constraints. For conservatism, the statistical analyses of the core are performed for only those operating states yielding MCPR equal to the limit, unless this involves an unreasonable power distribution or gross violation of kW/ft limits.

The value of MCPR for a fuel assembly is a function of flow, R, axial power shape and sub-cooling. For a specific case, the fuel assembly design and exposure are known, leading to a specific rod-to-rod power distribution; and, consequently, a specific R value. The plant parameters determine inlet sub-cooling and flow. Therefore, imposition of the requirement that MCPR equal a particular limit leads to a set of total-assembly-power, axial-shape combinations for the limiting assembly.

For a fixed MCPR, the corresponding assembly power is not very sensitive to axial shape. The results of the statistical analysis, fractions of the rods in the assembly expected to experience boiling transition, have not been found sensitive to axial shape provided that MCPR is fixed.

Selection of a base rod pattern and power distribution proceeds on the basis that at least one assembly have a particular power output giving a particular MCPR. The reactor average assembly power is fixed at the rated value. In terms of gross peaking factors, the base case is now well constrained. For any reasonable axial shape, the desired peak to average assembly power is known. The remaining area of flexibility is the location of the highest and near-highest powered assemblies.

The collection of power distributions, all of which satisfy the basic requirement for an initial condition, yield a range of numbers of rods expected to experience boiling transition. The characteristic having the greatest influence has been found to be the transverse location of maximum power density. With symmetrical control rod patterns, existence of a high power annular region at the maximum possible radius from the core axis produces a larger number of rods

expected to experience boiling transition than a case with maximum power closer to the core axis. A higher power zone of maximum radius will contain a larger number of assemblies and fuel rods at peak power than a zone of smaller radius. Thus, the dependence on radial location of the peak is primarily geometrical.

The objective in establishing the initial condition power distribution is to satisfy total power and local limits and to maximize the calculated number of rods expected to experience boiling transition. Therefore, the rod patterns chosen are those which maximize the assembly powers in an annular zone of maximum radius. Displacement of the zone to an even larger radius is precluded by a combination of neutron leakage and an absence of possible control rod position changes that could continue to satisfy the other constraints. Various histograms are employed to provide a measure of the degree to which the power distribution satisfies this statistical analysis requirement during the process of selecting an initial condition. As a result, the quoted values of numbers of rods expected to experience boiling transition are determined conservatively considering the range of possible initial power distribution.

The detailed power distribution employed in the BWR/5 analysis for 63 active rod fuel assemblies is presented as an example in Figure IV-2, Table IV-3, and Figure IV-3. Figure IV-2 shows the fuel assembly relative power on a quarter-core map. Axial distributions are presented in Table IV-3 for the transverse locations indicated in Figure IV-2. Finally, Figure IV-3 gives the histogram of assembly relative powers. Each point represents the number of assemblies operating in the relative power interval equal to the abscissa value. The distribution is quite obviously skewed to the high powered side. The median assembly relative power for this case is 1.15. Transverse asymmetries would reduce the number of assemblies approaching limits. Therefore, an assumption of quadrant symmetry in this analysis is conservative.

**Table IV-3**  
**AXIAL POWER DISTRIBUTIONS**  
**(NODE POWER/ASSEMBLY AVERAGE NODE POWER)**

Axial Node	Location (Figure IV-2)		
	A	B	C
(top) 24	0.22	0.38	0.22
23	0.41	0.73	0.41
22	0.58	1.02	0.59
21	0.72	1.26	0.73
20	0.83	1.43	0.84
19	0.92	1.52	0.92
18	0.99	1.19	0.97
17	1.04	0.96	1.02
16	1.08	0.96	1.06
15	1.12	1.00	1.11
14	1.16	1.02	1.16
13	1.20	1.05	1.21
12	1.22	1.08	1.25
11	1.24	1.09	1.28
10	1.22	1.07	1.27
9	1.14	0.96	1.17
8	1.12	0.94	1.15
7	1.13	0.95	1.16
6	1.16	0.96	1.20
5	1.22	1.01	1.26
4	1.34	1.10	1.37
3	1.30	1.02	1.25
2	1.03	0.79	0.95
(bottom) 1	0.57	0.44	0.52

*Figure IV-1 has been deleted.*

See Responses to Questions 1-18 and 3-8e, Appendix VII.

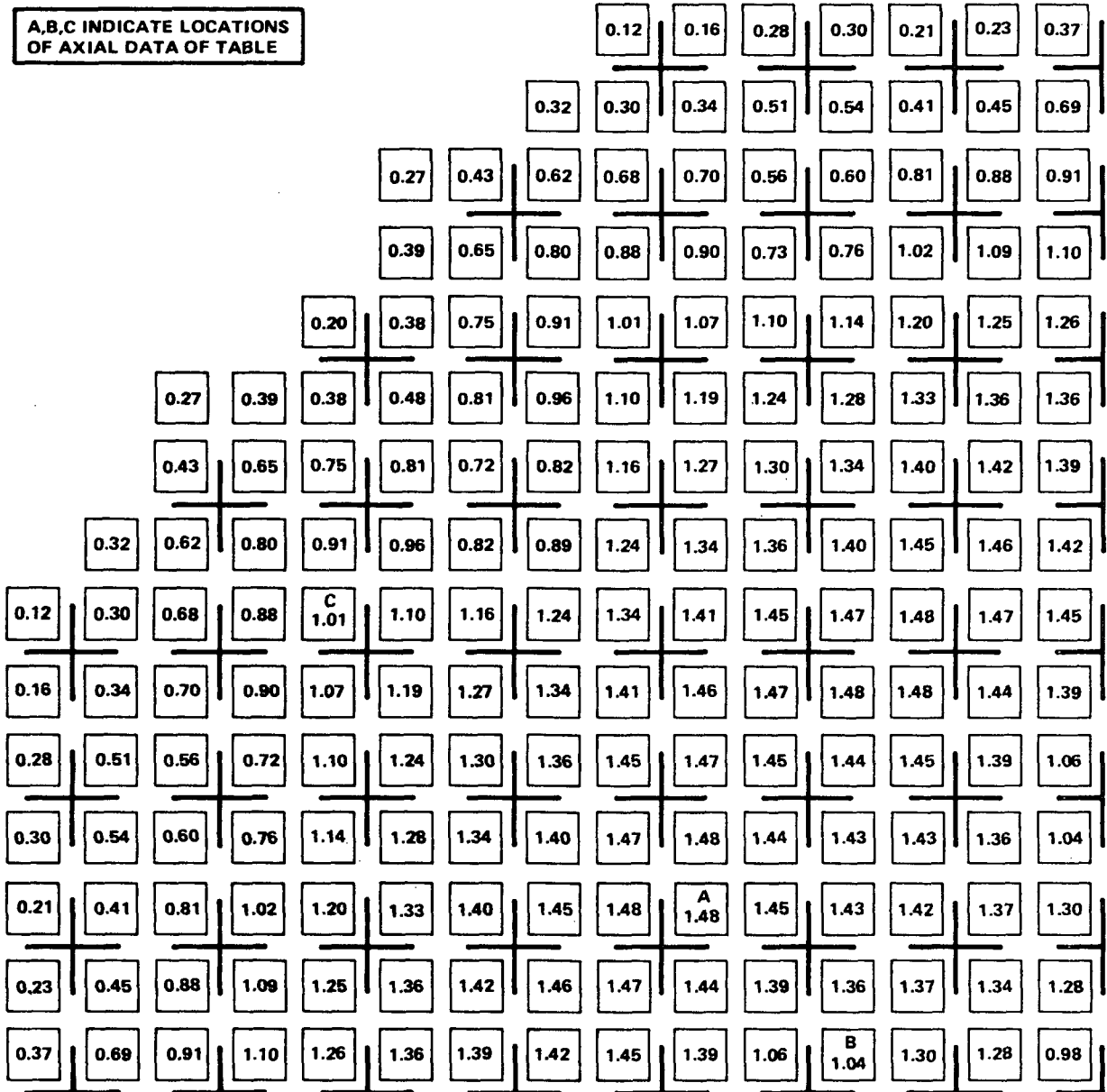


Figure IV-2. Fuel Assembly Relative Powers (One Quadrant of a 764 Assembly Core)

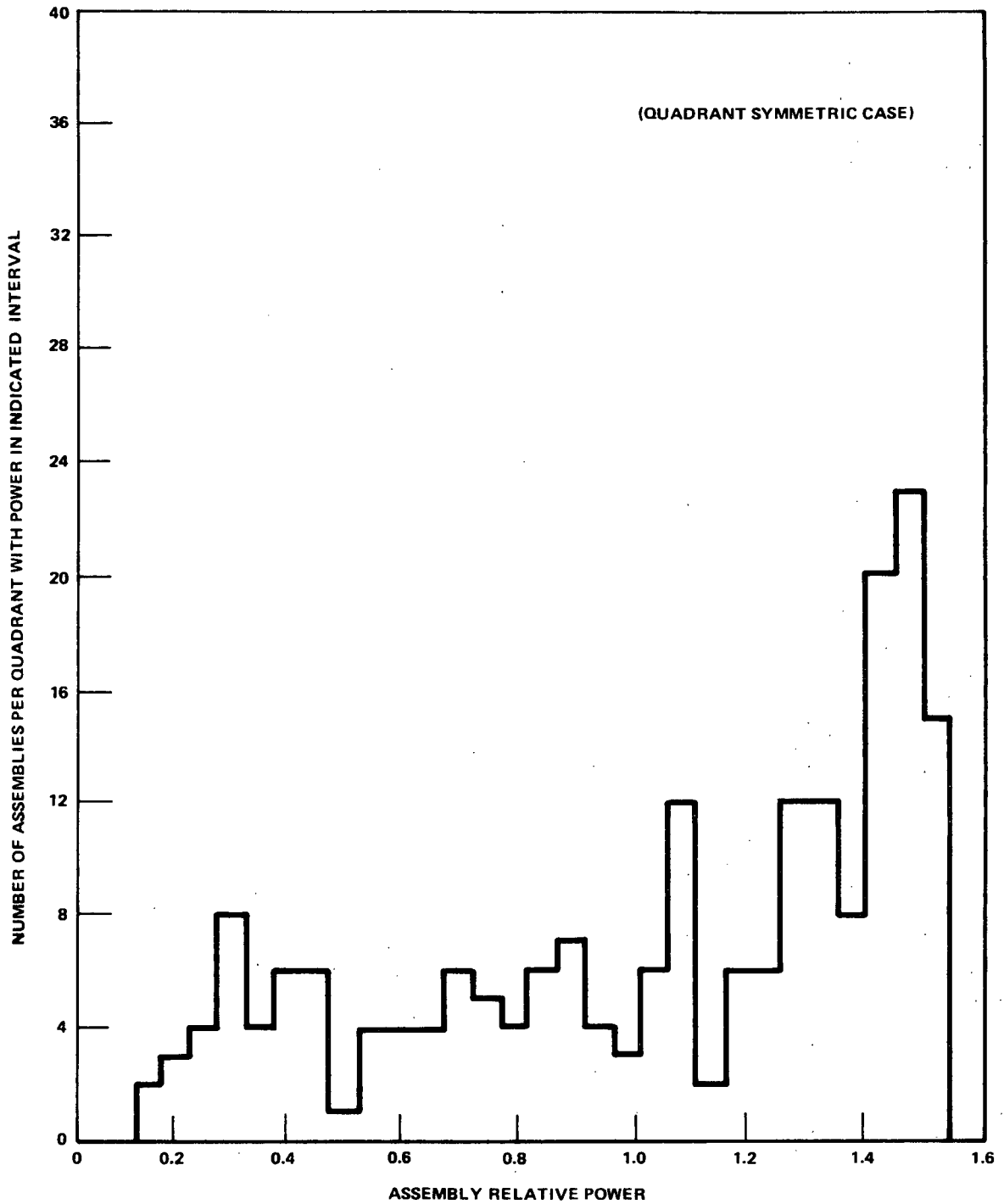


Figure IV-3. Frequency of Assembly Relative Powers

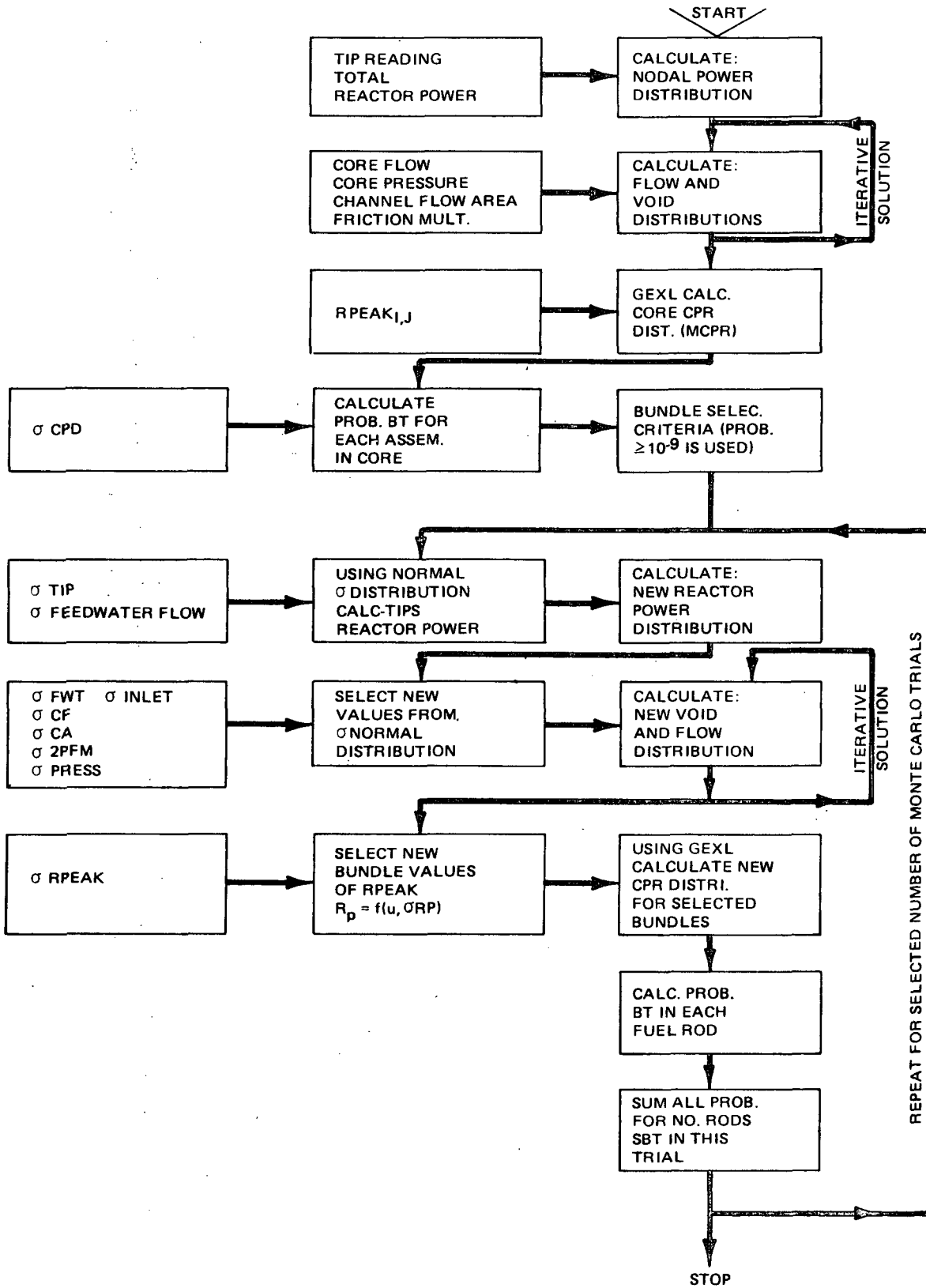


Figure IV-4. Monte Carlo Flow Chart

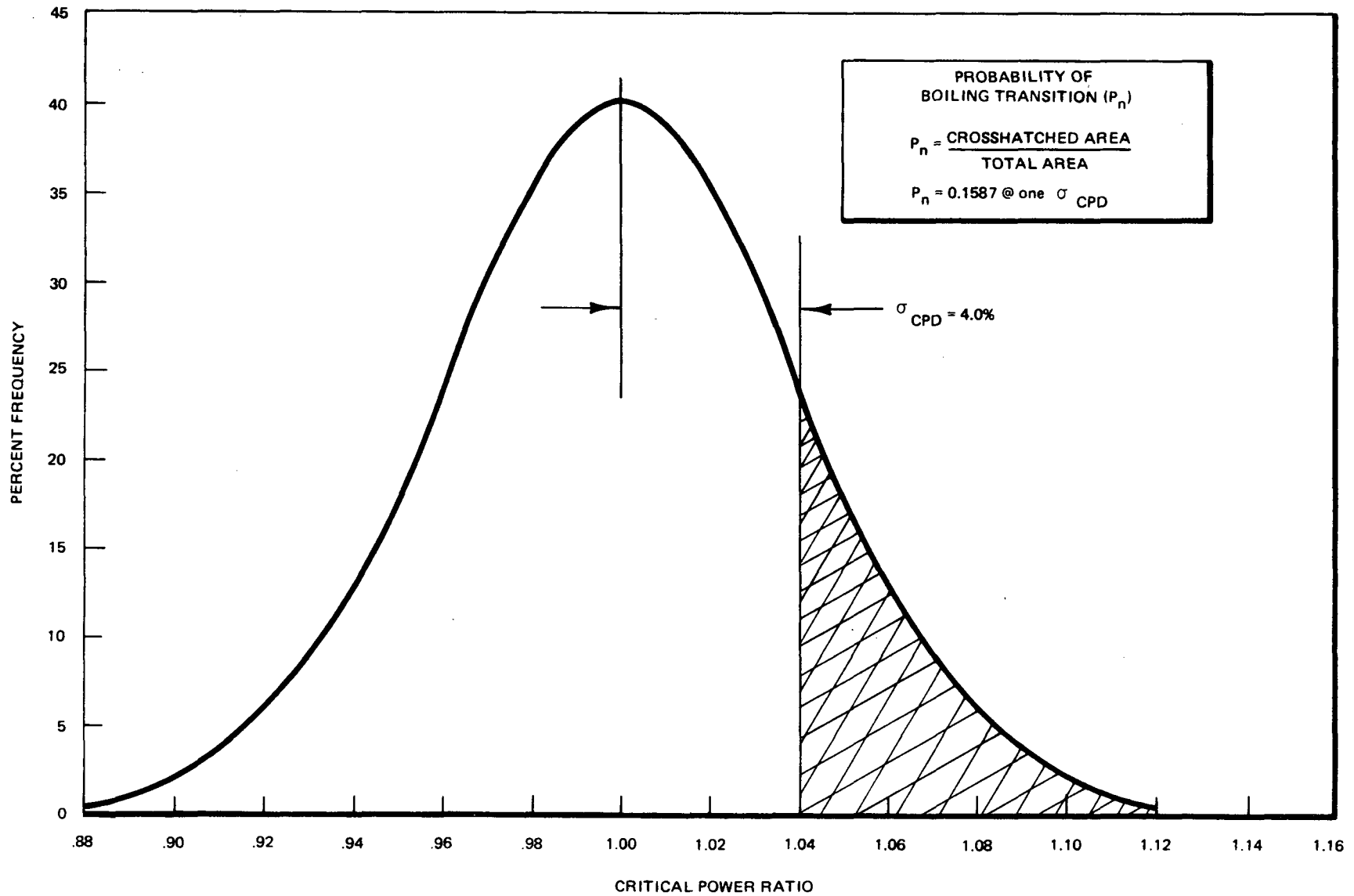


Figure IV-5. Normal Distribution of Atlas Test Data about GEXL predicted CPR of 1.0



## APPENDIX V. EFFECTS OF AXIAL SHAPE AND R FACTOR ON MCPR REQUIREMENT

The steady-state MCPR requirement for the thermally limiting bundle is derived from the transient margin losses due to single operator error, or equipment malfunction as defined in subsection 6.3.3. Because there are an infinite number of possible axial power distributions and R factors through an exposure cycle, it is obviously not feasible to perform these evaluations for each and every one. The approach taken in GETAB is to perform the transient analyses using appropriately conservative design values of axial power distribution (peaked at the core midplane) and R factor (highest value at the beginning of cycle) to reasonably bound expected operating conditions. In order to illustrate that this approach is indeed appropriate, the MCPR requirement for a typical BWR/4 was derived for several different axial shapes and for R factor variation over the entire range expected through the operating cycle.

In these evaluations, the full core transient producing the largest  $\Delta$ MCPR was the turbine trip without bypass and the transient limit MCPR required to satisfy the design basis was 1.04.

Figure V-1 shows the derived MCPR requirement as a function of location of the axial peak. As shown, with bottom peaked axials, the required MCPR decreases substantially as the axial is peaked lower in the core. For axials peaked in the middle and upper portions of the core, the required MCPR is essentially independent of peak location. Further, the bottom peaked axial is most frequently encountered in actual operation and the outlet peaked axial only occurs in controlled bundles, which, of necessity, have low transverse power factors and hence will never be limiting in actual operation.

The required MCPR was found to increase approximately 1% as the R factor is reduced from beginning of cycle to end of cycle. However, the end of cycle condition is associated with fully withdrawn control blades and axial peaking typically well below the core midplane. Therefore, from Figure V-1 the weak effect of lower R-factor is more than compensated by the low position of the axial peak at end of cycle.

Similar analyses were performed to evaluate the effect of magnitude of axial peaking. The results showed that for peaking factors less than 1.4, required MCPR decreases. The required MCPR increases less than 1% for an axial peak to average of 1.5. However, the higher axial peak to average values do not occur in combination with a high radial peaking factor, except for bottom peaked axials. Therefore, the required MCPR for peak to average values larger than 1.4 would again be no higher than the value derived with the design axial shape.

Thus, it is concluded that the midplane peaked axial shape together with the beginning of cycle R factor is an appropriately conservative representation of the entire operating cycle for use in calculating the transient  $\Delta$ MCPR inputs to GETAB.

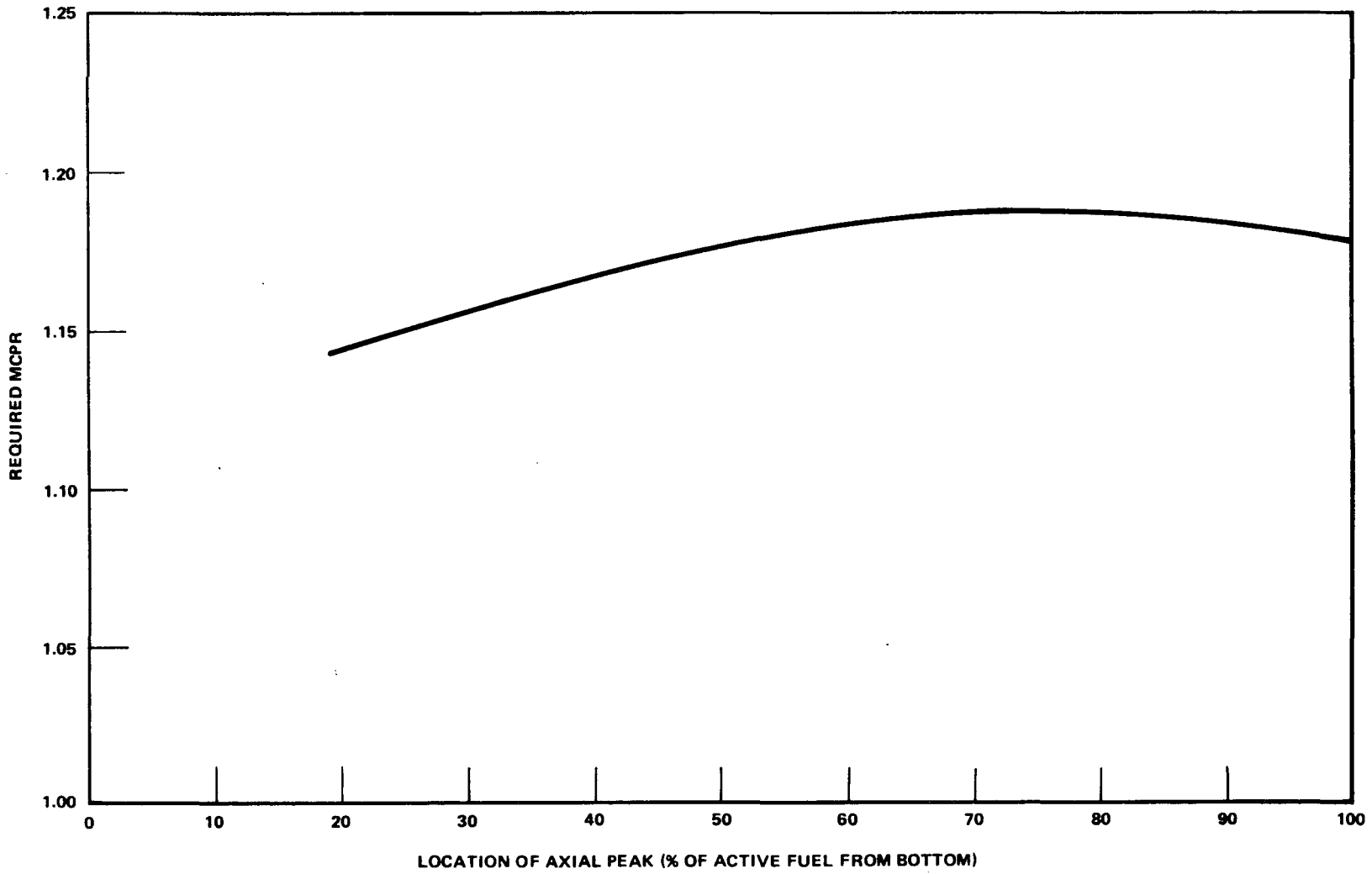


Figure V-1. Effects of Axial Peak Location on Required MCPR Design P/A = 1.4  
(Transient Limit MCPR = 1.04)

## APPENDIX VI EFFECT OF AXIAL POWER SHAPE AND R FACTOR ON LOCA ANALYSIS

### VI-1. BASE CASE

To evaluate the effect of the axial power shape on the design basis loss-of-coolant accident using the GEXL correlation, a core heatup calculation was first performed as described in Appendix D of Reference 14. The case investigated in Section 6 of this report was for a (251) BWR/4. The (218) BWR/4 was selected to be used in this parametric analysis to demonstrate the use of the GEXL correlation on a different size BWR and thereby provide a base analysis on a plant with a shorter time to jet pump uncover than the (251) BWR/4. The initial conditions selected for this base case are given in Table VI-1. Here, as in Section 6, R was chosen arbitrarily to set the initial MCPR at 1.2 at the design maximum bundle power.

**Table VI-1  
TYPICAL DESIGN BASIS ACCIDENT – BWR/4 (7 x 7 FUEL)**

#### Initial Conditions

1. Bundle Power (MWt at Design Radial = 1.4)	6.0
2. Bundle Mass Flux (lb/hr-ft <sup>2</sup> )	1 x 10 <sup>6</sup>
3. Axial Peaking (Chopped Cosine), Design	1.46
4. MAPLHGR* (kW/ft)	14.6
5. R Factor	1.052
6. Initial Steady-State MCPR	1.2

\*MAPLHGR = Maximum (Bundle) Average Planar Linear Heat Generation Rate

The important results from this base case analysis are the calculated times to reach a boiling transition (i.e., MCPR ≤ 1.0) in the bundle. These results are plotted on Figure VI-1 and listed in Table VI-2.

**Table VI-2  
CALCULATED BOILING TRANSITION (BASE CASE) – DESIGN BASIS ACCIDENT**

1. First Indication of Boiling Transition	
(a) Time (sec)	1.0
(b) APLHGR at location of critical condition (kW/ft)	8.6
2. Deepest Penetration During Flow Coastdown Period	
(a) Time (sec)	1.1
(b) APLHGR at location of boiling transition (kW/ft)	11.9

It is important to note that the highest axial powered section of the bundle (i.e., the midplane) did not experience boiling transition before jet pump uncover. Therefore, the axial plane of the bundle with the highest planar average power is predicted to have continued nucleate boiling heat transfer throughout the entire flow "coastdown" period.

At the upper sections of the bundle where boiling transition was predicted (spacers 2 and 3 from the top of the bundle), the APLHGR values\* were, respectively, 57% and 79% of the maximum axial value. Because the difference in calculated time for these two axial nodes to reach the boiling transition is only 0.1 sec, the third spacer node was analyzed in the core heatup calculation to determine if it reached a higher cladding temperature than the highest-powered axial node.

---

\*APLHGR = (Bundle) Average Planar Linear Heat Generation Rate

The core heatup calculation was performed with the approved IAC evaluation model. The results of the calculation for the highest-powered axial node and the third spacer node are shown in Figure VI-2. The calculated peak cladding temperature at the third spacer node is 1920°F, as compared to the calculated peak cladding temperature of 2160°F at the highest-powered node. Therefore, even though a lower power node experienced boiling transition first, the highest power (midplane) axial node remains the controlling location for the determination of peak cladding temperature. This midplane node is the one normally analyzed in a LOCA analysis.

**VI-2. EFFECT OF AXIAL PEAK LOCATION AND MAGNITUDE**

To ascertain the effect of the axial power shape location on the PCT, a range of axial power shapes was selected and used in the analysis. These power shapes included peaking at 2.5 ft to 8 ft from the bottom of the active fuel. Axial peaking above the 8-ft elevation need not be considered for LOCA analysis because it could only be experienced if a control blade were almost completely inserted. Such a bundle would be at considerably lower power levels and therefore would not provide a limiting condition for LOCA analysis. Axial peaking below the 2.5-ft elevation need not be considered because such a low axial peak is unlikely to occur in a BWR under normal operating conditions. The maximum axial peaking factors used in the analysis were 1.2, 1.4, and 1.5, a representative range for BWRs. The axial power shape for these three peaking factors is shown on Figures VI-3A, 3B, and 3C. The assumptions given in Table VI-3 were used in this portion of the parametric study.

**Table VI-3  
AXIAL POWER SHAPE INVESTIGATION PARAMETRIC ANALYSIS  
—DESIGN BASIS ACCIDENT— BWR/4 (7 x 7 FUEL)**

**Initial Conditions**

1. Bundle Power (MWt)	5.1 to 5.6*
2. Bundle Mass Flux (lb/hr-ft <sup>2</sup> )	1 x 10 <sup>6</sup>
3. Axial Peaking	12 different shapes (see Figures VI-3a, b, c)
4. Maximum LHGR	varied } depending on bundle power
5. MAPLHGR	
6. R	1.098
7. Initial MCPR	1.2

\*Power is selected such that initial CPR = 1.2.

The effect of the R value on the transient is presented in subsection VI-3. In this analysis, the maximum R value for the fuel type considered was used, and the bundle power was varied to yield initial MCPR of 1.2. This analysis is therefore representative of the actual operating conditions in the reactor under steady-state MCPR limits. The results of the axial power shape study are given in Table VI-4. The following conclusions can be drawn from the information presented in Table VI-4:

- (1) The bundle power required to give an initial MCPR of 1.2 is relatively insensitive to either the axial power shape or the magnitude of the peak.
- (2) The APLHGR at the location of maximum penetration of boiling transition is relatively insensitive to the axial power shape and magnitude of the axial peaking factor.
- (3) The time of onset of transition boiling at the location of maximum penetration is relatively insensitive to the axial power shape and magnitude of the axial peaking factor.
- (4) Boiling transition at the highest-powered axial location did not occur during the flow coastdown time in any of the cases.

Table VI-4  
**RESULTS – PARAMETRIC ANALYSIS**  
 $R = 1.098, * G = 1 \times 10^6 \text{ lb/h ft}^2$

Axial Peak	Location of Axial Peak (ft. from BAF)	Bundle Power to Give MCPR = 1.2 (MWt)	MAPLHGR (kW/ft)	Maximum Penetration of Boiling Transition Spacer No. from TAF	Distance from BAF for Maximum Penetration (ft)	Time of Maximum Penetration (sec)	APLHGR at Plane of Maximum Penetration (kW/ft)
1.5	8	5.14	12.8	2	9.9	1.2	10.3
1.5	6	5.22	13	3	8.2	1.1	10.4
1.5	4.5	5.35	13.4	4	6.55	1.0	11.1
1.5	2.5	5.46	13.6	5	4.85	1.1	10.8
1.4	8	5.24	12.2	2	9.9	1.2	10.2
1.4	6	5.31	12.4	3	8.2	1.1	10.2
1.4	4.5	5.43	12.7	4	6.55	1.2	10.8
1.4	2.5	5.54	13	4	6.55	1.0	9
1.2	8	5.38	10.8	2	9.9	1.0	10
1.2	6	5.4	10.8	3	8.2	1.3	9.8
1.2	4.5	5.46	10.9	3	8.2	1.0	9.1
1.2	2.5	5.43	10.9	3	8.2	1.0	8.6
1.464	6.0	6.0	14.6	3	8.2	1.1	11.9

\*Base Case  $R = 1.052$

It can therefore be concluded that the peak cladding temperature of the highest-powered axial position is significantly higher than that at the location of deepest boiling transition penetration as discussed in Section 6. These results confirm that the calculated peak cladding temperature is not affected by the use of GEXL in the analysis, regardless of the axial power shape or the magnitude of the axial peaking factor.

### VI-3. EFFECT OF R FACTOR ON PCT

The effect of the R factor on PCT was investigated with a variety of axial power shapes with an axial peaking factor of 1.5. The results of the investigation are shown in Table VI-5. In this analysis, R was varied arbitrarily, using values representative of BOC and EOC conditions, to investigate the sensitivity of the analysis to this parameter. As in the previous section, the bundle power was selected to produce initial MCPR = 1.2 in each case.

The following conclusions can be drawn from the information presented in Table VI-5:

- (1) The maximum penetration of boiling transition with a given axial power shape is extremely insensitive to the R factor.
- (2) The power fraction at the position of maximum penetration of the boiling transition is approximately 80% of the peak value.
- (3) Boiling transition was not experienced at the highest-powered axial location.

To complete this sensitivity analysis, a parametric study was conducted to determine the allowable power fraction at an upper node such that the cladding temperature of the upper node would not exceed the calculated peak cladding temperature. The results of this study are presented in Table VI-6.

**Table VI-5  
EFFECT OF R FACTOR (AXIAL PEAK = 1.5\*)**

R Factor	Location of Axial Peak Feet from BAF (ft)	Bundle Power to Give MCPR = 1.2 (MWt)	MAPLHGR (kW/ft)	Maximum Penetration of Boiling Transition Spacer Number from TAF	Distance from BAF for Maximum Penetration (ft)	Time of Maximum Penetration (sec)	APLHGR at Location of Maximum Penetration (kW/ft)	At Maximum Penetration Power Fraction of Rated (%)
1.098	8	5.14	12.8	2	9.9	1.2	10.3	80
1.048	8	5.96	14.9	2	9.9	1.0	11.9	80
1.098	6	5.22	13.3	3	8.2	1.1	10.4	80
1.048	6	6.01	15.03	3	8.2	1.0	12	80
1.098	4.5	5.35	13.4	4	6.55	1.0	11.1	82.5
1.048	4.5	6.13	15.34	4	6.55	1.0	12.7	82.5
1.098	2.5	5.46	13.6	5	4.85	1.1	10.8	79.3
1.048	2.5	6.13	15.34	5	4.85	1.2	12.2	79.3
1.052	6	6*	14.6	3	8.2	1.1	11.9	79

\*Base case Axial Peaking = 1.46

VI-4

NEDO-10958-A

**Table VI-6  
PARAMETRIC STUDY – UPPER NODE APLHGR  
(DESIGN BASIS ACCIDENT – BWR/4 – 7X7 FUEL)**

	Peak Node		Upper Node (3rd Spacer)		
	MAPLHGR (kW/ft)	Peak Cladding Temperature (°F)	APLHGR (kW/ft)	Peak Cladding Temperature <sup>a</sup> (°F)	Power Fraction of Peak <sup>b</sup> (%)
Base case . . . . .	14.6	2160	11.9	1920	79
Study . . . . .			12.7	2020	87
			13.2	2090	90
			13.7	2160	94

a Boiling transition was assumed to occur at 1.1 sec.  
b Percent of MAPLHGR = 14.6 kW/ft

The results of this study indicate that with an APLHGR of 87% of the maximum value, the calculated upper node peak cladding temperature would be 2020°F, which is below the 2160°F calculated at the peak location. Furthermore, the upper node in boiling transition could have an APLHGR as high as 94% of the peak and not exceed the previously calculated peak cladding temperature at the highest-powered axial plane.

**VI-4. CONCLUSIONS**

The results of this analysis indicate that the peak cladding temperature for the design basis loss-of-coolant accident is not affected by the magnitude or location of the axial power peak or the R value. Therefore, by using the GEXL correlation and the design axial power shape together with a consistent R factor, the thermal hydraulic performance evaluation of the fuel bundles during the postulated design basis LOCA is appropriately conservative.

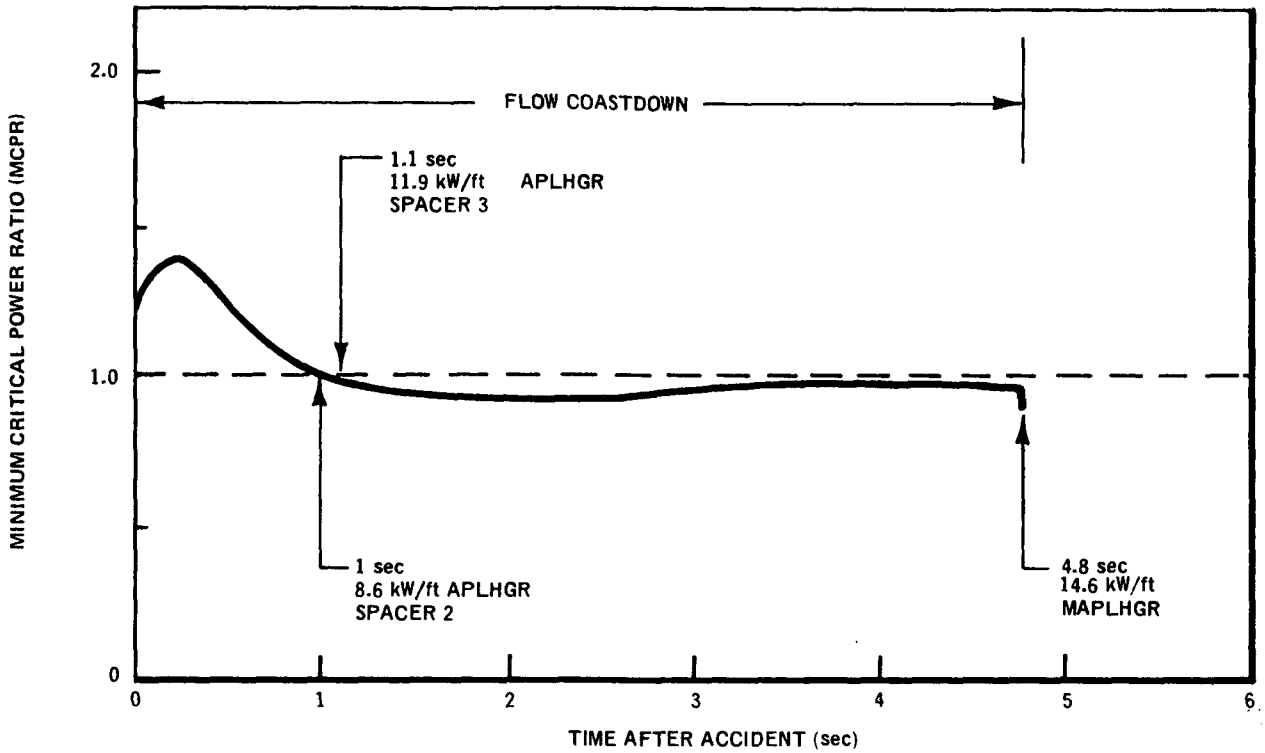


Figure VI-1. Minimum Critical Power Ratio Versus Time (DBA)

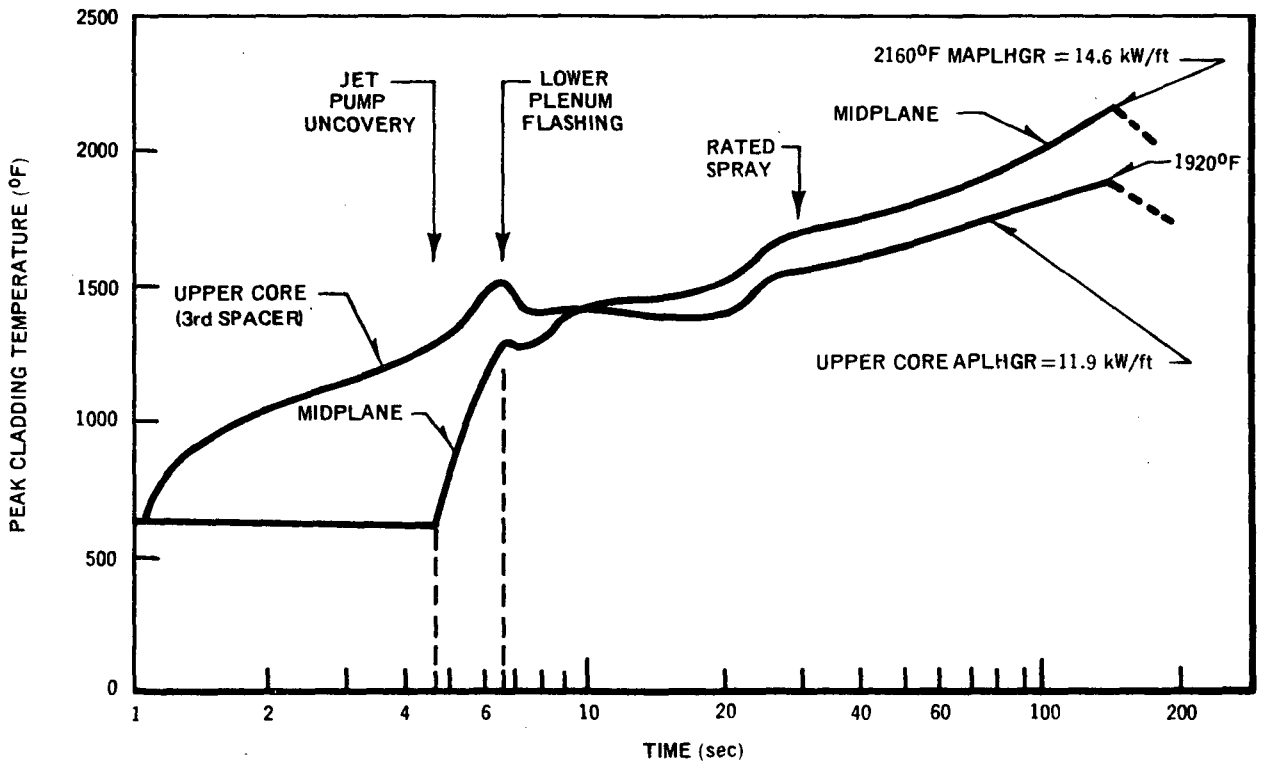


Figure VI-2. Peak Cladding Temperature Versus Time After Design Basis Accident - BWR/4 (7 x 7 Fuel)



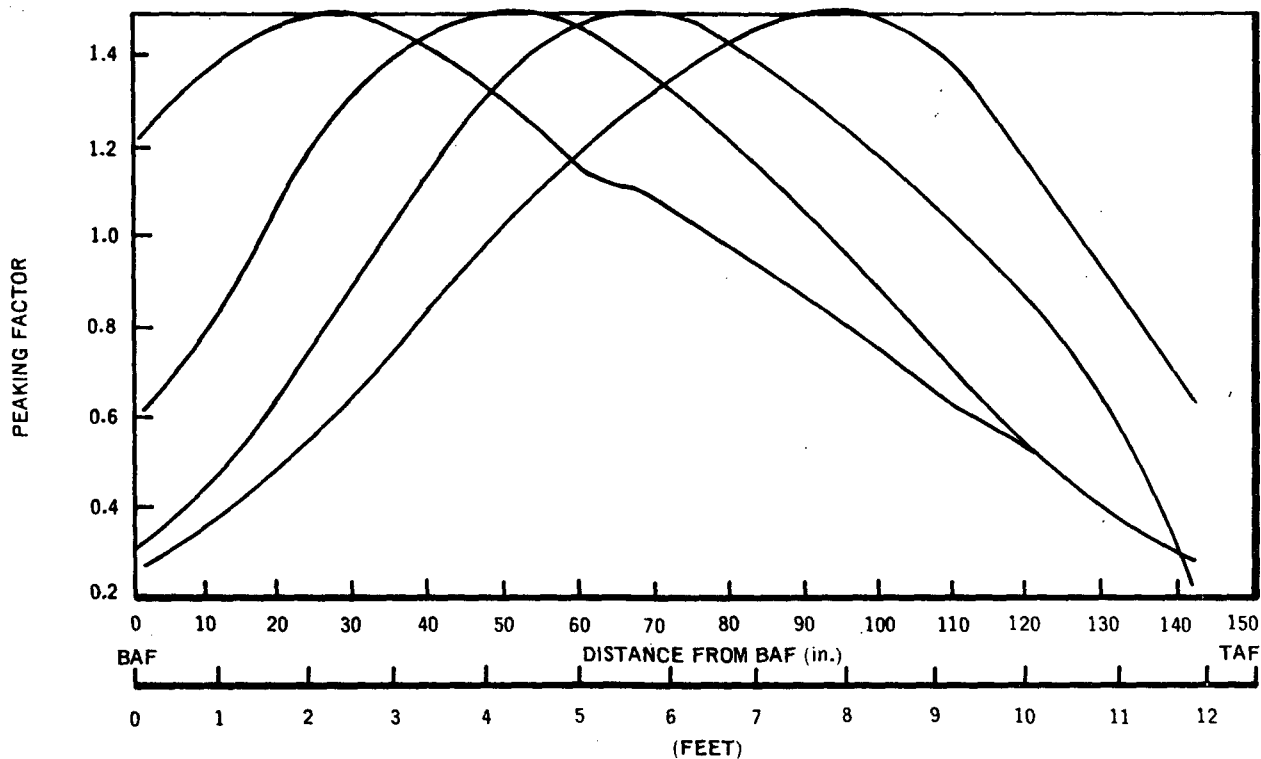


Figure VI-3a. Axial Power Shape

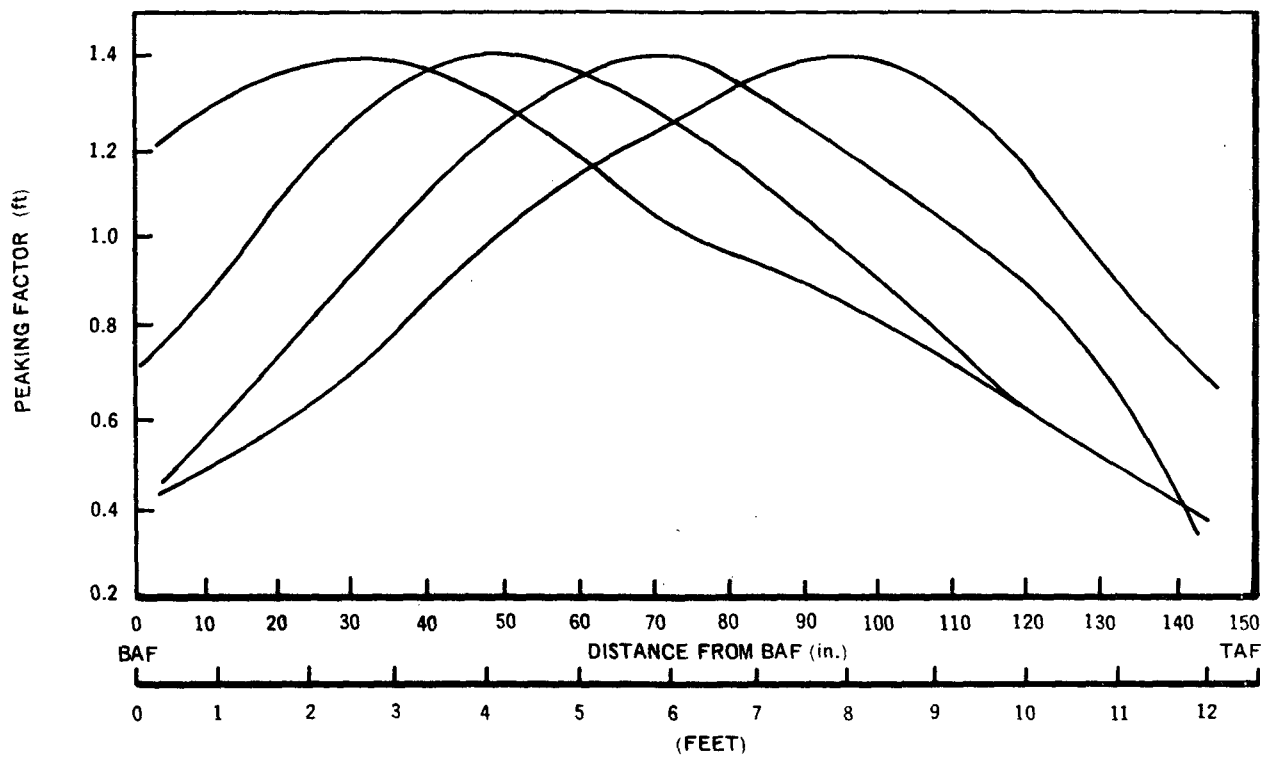


Figure VI-3b. Axial Power Shape

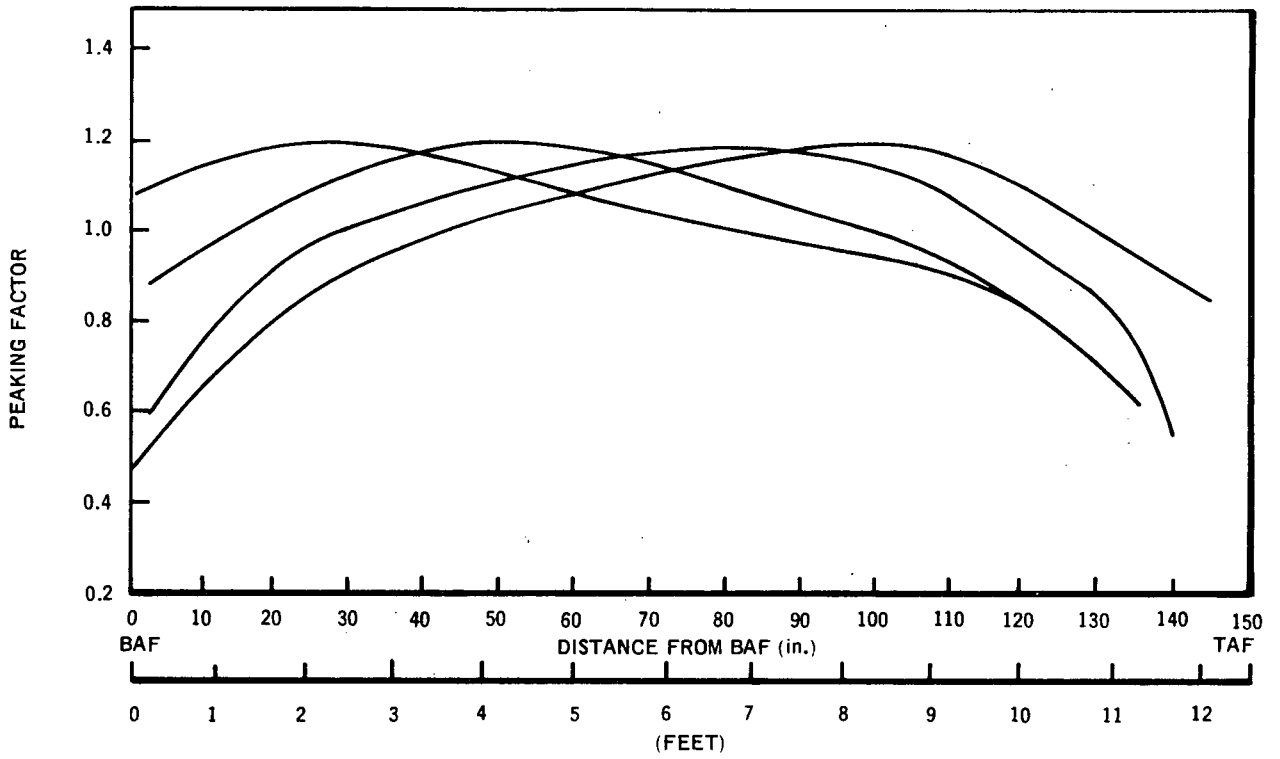


Figure VI-3c. Axial Power Shape

## APPENDIX VII NRC QUESTIONS

This appendix contains the three rounds of NRC questions on this topical report and NEDE 10958. All responses are documented in this appendix or in NEDE-10958.

### 1. ROUND 1 QUESTIONS

#### Question 1-1:

Page 3-3 – The form of the GEXL correlation ( $X_C$  vs  $L_B$ ) is attributed to work performed at CISE (Italy) and is described in Reference 7. However, comparison of the CISE correlation and GEXL shows significant differences in the definition of important parameters such as quality, critical power, and boiling length.

According to GE, the CISE correlation is:

$$X_C = \frac{\hat{W}}{GA h_{fg}} = \frac{a L_B}{L_B + b}$$

where

$X_C$  = critical steam quality

$\hat{W}$  = power input over boiling length at critical conditions

$L_B$  = boiling length (from saturated liquid to critical quality)

$G$  = mass velocity

$A$  = flow cross sectional area

$h_{fg}$  = heat of vaporization

$a, b$  = empirical factors

From Reference 7, the CISE correlation actually is:

$$\Delta X_S = X_o = \frac{\hat{W}_S}{\Gamma H_{gl}} = \frac{a L_S}{L_S + b}$$

where

$\Delta X_S$  = change in steam quality over saturation length,  $L_S$

$X_o$  = outlet steam quality (at end of heated length)  
( $\Delta X_S = X_o$  when steam quality is zero at start of  $L_S$ )

$\hat{W}_S$  = power input over saturation length at critical conditions

$L_S$  = saturation length (length over which steam quality is greater than zero)

$\Gamma$  = mass flow rate

$H_{gl}$  = heat of vaporization

a,b = empirical factors

Note that, in the CISE correlation,  $X_O$  is the outlet steam quality whereas, in GEXL (the GE version of CISE),  $X_C$  is the critical quality ( $X_O \geq X_C$ ). Similarly,  $L_S$  is the total boiling length (CISE), whereas in GEXL,  $L_B$  is the boiling length up to critical quality ( $L_S \geq L_B$ ).  $\hat{W}_S$  is the power applied to the total boiling length ( $L_S$ ) at critical conditions (CISE), whereas in GEXL,  $\hat{W}$  is the power applied to  $L_B$  at critical conditions ( $\hat{W}_S \geq \hat{W}$ ). Only in the case where critical conditions occur at the end of the heated section will GEXL and CISE correlations coincide. However, this is unlikely as, in GE tests, boiling transition occurs ahead of spacers which are located 10 to 30 inches before the end of the heated length.

Discuss the differences between CISE and GEXL and the effect on the present boiling transition work. Are these differences the reason for requiring the quality correction in GEXL in order to use the correlation as a boiling transition location predictor?

**Response:**

**Page 3-3.** The workers at CISE are credited with originally suggesting a correlation in the  $X_C - L_B$  plane. The reference given (Reference 7 in the document) is the first comprehensive paper, authored by the CISE workers and published in English, which advocates this type of correlation. We felt it was appropriate to use this paper as the reference. At the time the paper was written the CISE people still apparently believed that dryout (i.e., the boiling crisis for annular regional flow) should first occur at the exit end. This belief quickly changed, however, and the following year one of the original authors\* wrote a paper in which he clearly defined the boiling length in the correlation as "the tube length along which positive quality is developed up to the burnout point." A CISE paper presented as recently as June, 1972\*\* reiterates this position.

The general form of the correlation

$$X_C = f(L_B, G, P, \text{etc.})$$

is the same for both CISE and GEXL. The details of the formulation differ, which is not surprising inasmuch as neither is claimed to have complete generality, and each is based on an entirely different set of data. It is interesting to note, however, that both tend to predict a location for the boiling transition which is downstream of where it is normally first observed. It has been noted in the GETAB proprietary supplement that, because the GEXL correlation was optimized to give the best prediction of critical power, it predicts the boiling transition location slightly downstream of the true location. It is apparent, upon referring to Silvestri's 1966 paper (in which he uses the CISE correlation to examine some British data), that the CISE correlation also tends to predict the boiling transition location slightly downstream of the true location. We have noted this ourselves in using the CISE correlation to examine some of our Freon annulus data. This generic characteristic of  $X_C - L_B$  correlations is the reason that an empirical critical quality modifier was developed to allow accurate location prediction with GEXL.

**Question 1-2:**

**Page 3-4** — In the transformation of data from the  $X_C - L_B$  plane to the critical power-subcooling plane an assumed error band of  $\pm 0.01$  becomes  $\pm 0.013$  at low subcoolings and  $\pm 0.018$  at high subcoolings. In view of this, please check the statement that "... the error in the  $X_C - L_B$  plane is not magnified when predicting critical power at a given subcooling." Why are Freon data used as an example, rather than water data?

\* M. Silvestri, "On the burnout equation and location of burnout points," *Energia Nucleare*, v. 13, u. 3, Sept 1966.

\*\*G. P. Gaspari, R. Granzini, A. Hassid, C. Medich, "Heat Transfer Crisis (Dryout) in Rapid Depressurization Transients," Paper presented at the European Two-Phase Flow Group Meeting, C.S.N. Casaccia, June 6-8, 1972.

Response:

Page 3-4 (also Figure 3-8,\* page 3-12, and Appendix I, p. I-1 and I-2) – We felt it important to show that a small error in the  $X_C - L_B$  plane would not be magnified into a much larger error in the Critical Power - Subcooling plane. To do this we set out to show that the relative error in  $X_C$  was of the same order as the relative error in Critical Power ( $KW_C$ ). It is not really important whether Freon or water is used for illustrative purposes. In the original document we used Freon. In the following supporting presentation we will use water.

The relative error in  $X_C$  is  $SX_C/X_C$ . The relative error in  $KW_C$  is  $\Delta KW_C/KW_C$ . The relative error in  $KW_C$  can also be expressed as,

$$\frac{\Delta KW_C}{KW_C} = \frac{\Delta KW_C \cdot 3413}{GAh_{fg} \left( X_e + \frac{\Delta h_s}{h_{fg}} \right)}$$

$X_C$  is less than  $X_e + \Delta h_s/h_{fg}$ , but it is of the same order of magnitude (i.e.,  $\Delta h_s$  is normally small and the node where  $X = X_C$  is near the exit end). It follows that,

$$\frac{\Delta KW_C}{KW_C} < \frac{\Delta KW_C \cdot 3413}{GAh_{fg} X_C} \tag{1}$$

but it is of the same order.

It will be shown that  $\Delta KW_C \cdot 3413/GAh_{fg}X_C$  is of the same order as  $SX_C/X_C$ , and thus demonstrate that the relative error in  $KW_C$  is of the same order as the relative error in  $X_C$ .

Referring to equation I-3 in Appendix I

$$\Delta KW_C = \frac{SX_C}{\left\{ \frac{F(Z_C)}{GAh_{fg}/3413} - \left( \frac{dX_C}{dL_B} \right) \cdot \frac{GAh_{fg}}{3413} \cdot \frac{\frac{\Delta h_s}{h_{fg}} L}{(KW_C)^2 \psi_o} \right\}} \tag{2}$$

Multiplying both sides by  $(GAh_{fg}X_C/3413)^{-1}$ ,

$$\frac{\Delta KW_C \cdot 3413}{GAh_{fg}X_C} = \frac{SX_C/X_C}{\left\{ F(Z_C) - \left( \frac{dX_C}{dL_B} \right) \cdot \left( \frac{GAh_{fg}}{3413} \right)^2 \cdot \frac{\frac{\Delta h_s}{h_{fg}} L}{(KW_C)^2 \psi_o} \right\}} \tag{2}$$

\*The expression  $KW_C/GAh_{fg}$  shown in Figure 3-8 should be shown as  $\Delta KW_C/(GAh_{fg}/3413)$  to represent error and to be consistent with the units used in this document.

(Note: Figure 3-8 now reflects the revised expression.)

ATLAS Test Assembly Number 14 and the GEXL correlation were used to evaluate the terms in the denominator on the right of Equation (2). For Test Assembly Number 14,  $A = 0.0357 \text{ ft}^2$ ,  $D_Q = 0.728 \text{ inch}$ , and  $L = 144 \text{ inches}$ . Let

$$D \triangleq F(Z_C) - \left( \frac{dX_C}{dL_B} \right) \cdot \left( \frac{GAh_{fg}}{3413} \right)^2 \frac{\frac{\Delta h_s}{h_{fg}} L}{(KW_C)^2 \psi_o} \quad (3)$$

and consider, for example, the following four runs:

Run No.	Press (psia)	Mass Flux ( $10^6 \text{ lb/h-ft}^2$ )	Subcooling (Btu/lb)	$KW_C$	$F(Z_C)$	$\left( \frac{dX_C}{dL_B} \right)$ (inch $^{-1}$ )	$\psi_o$	D	$\frac{1}{D}$
6	993	0.499	23.4	1990	0.8685	$1.41 \times 10^{-3}$	0.7013	0.8382	1.19
9	1001	1.000	25.1	2929	0.8685	$1.47 \times 10^{-3}$	1.0995	0.8285	1.21
25	1003	1.007	83.9	3203	0.8685	$1.67 \times 10^{-3}$	1.2471	0.7547	1.33
27	998	0.496	83.7	2264	0.8685	$1.81 \times 10^{-3}$	1.1042	0.8011	1.25

It is readily seen, upon combining Equations (2) and (3), that  $\Delta KW_C \cdot 3413/GAh_{fg}X_C$  varies from 1.19  $SX_C/X_C$  to 1.33  $SX_C/X_C$ , and hence is of the same order as  $SX_C/X_C$ .

For  $SX_C = 0.01$ , the foregoing statement reduces to

$$0.0119 < \frac{\Delta KW_C}{GAh_{fg}/3413} < 0.0133$$

which corresponds to  $\pm 0.012$  and  $\pm 0.018$  given in the Freon example, Figure 3-8.

Thus it is clear that errors in the  $X_C - L_B$  plane continue at the same order of magnitude when mapped into the Critical Power-Subcooling plane, that is, they are not significantly magnified. (See Section 3.2.3.)

**Question 1-3:**

**Figures 3-2 and 3-3** – No reference given for the data.

**Response:**

**Figures 3-2 and 3-3** – The reference for the data shown on these two figures is Reference 8, given on page 3-3.

**Question 1-4:**

Why were some of the points in Figure 3-4 omitted from the plot in Figure 3-5?

**Response:**

**Figure 3-5** – Fewer points for a given profile are plotted in Figure 3-5 than appear in Figure 3-4. Figure 3-5 has been replotted (see Figure 3-5, dated February 1974, attached) to show the missing points. These points were omitted from the original plot to minimize crowding.

(Note: The originally attached figure has been incorporated into the main portion of this report.)

**Question 1-5:**

**Figure 3-6** – Identify the fluid used and pressure level.

**Response:**

**Figure 3-6** – This shows data from Reference 10, AERE-R6411, authored by R. K. F. Keeys, et al. The title identifies the fluid as "... High Pressure Steam-Water ..." The tests were run at a pressure of  $6.9 \times 10^6$  N/m<sup>2</sup> (1000 psia). (See Figure 3-6.)

**Question 1-6:**

**Page 4-2** – It is stated that, "bundle/channel clearance is minimum in the corner where the highest powered rods are located. As a result, the boiling transition tends to occur earlier, making the test data conservative for corner rod peaking."

The above procedure may be valid for a rod bundle geometry such as the 7x7 where the corner channel is apparently the "hot" channel. However, for the 8x8, in which the corner and interior channels appear to be equally "hot," minimizing of the corner channel clearance introduces an artificial effect. Discuss this aspect.

**Response:**

**Page 4-2** – Bundle/channel clearance variations have a significant effect upon the size of the corner subchannel. This explains the boiling transition sensitivity to this clearance for corner rod limited bundles. Since it is possible for the highest powered corner to sit tightly against the channel in an operating reactor, this most limiting corner condition was used for all tests.

Variations in the channel clearance are expected to have a very small effect upon the conditions in interior regions. Therefore, as Question 1-6 suggests, for interior rod limited bundles the clearance is neither conservative nor nonconservative.

(Note: This response has been incorporated into Section 4.4.)

**Question 1-7:**

**Page 4.2** – For corner peaking, the 8x8 critical power/mass flow is greater than the 7x7. With side or interior peaking, the 7x7 critical power/mass flow is about 10% greater than with corner peaking. With interior peaking, the critical power/mass flow for the 8x8 is equal to, or less than, that with corner peaking. This significantly different behavior implies that the rod bundle geometry of the 7x7 is different from the 8x8. Discuss the geometric differences between the 7x7 and 8x8 bundles and subchannels and provide the basis for such differences. Discuss the extent of rod bowing and the potential effect on critical power.

**Response:**

**Page 4-2** — Two significant factors determining the critical power performance of rod bundles are the spacer design and the clearance distributions. For the 7x7 design, the combination of the spacer design and the corner subchannel dimensions result in significantly less margin for the corner rod than for the remainder of the bundle. In the 8x8 design, the rod-to-rod spacing is less than that of the 7x7 design. This difference in the lattice geometry causes a different flow distribution within the 8x8 bundle compared to the 7x7 with less flow going into the interior subchannels. This flow redistribution makes the interior subchannel tend to be more limiting than that of the 7x7.

The better critical power performance of the 8x8 bundle is attributable to lower heat flux due to larger heated rod surface area in the 8x8 bundle.

The effects of rod bowing for the severe case of the limiting corner rod bowed toward the channel wall has been investigated experimentally.\* The results indicated negligible effect of the bow, even for extreme cases. Rod bowing in the interior of the bundle would have less effect upon the local subchannel areas than for the corner condition that was tested. Therefore, interior rod bowing is also expected to have a negligible effect on critical power. (Note: This paragraph is incorporated into Section 4.5).

**Question 1-8:**

How does the difference in rod spacers used in test bundles and actual fuel assemblies affect critical power? Discuss this effect for both 7x7 and 8x8.

**Response:**

The only differences in rod spacers (both 7x7 and 8x8) used in test bundles and actual fuel assemblies are the backup supports added to the spring members to maintain proper clearances under the electromagnetic forces of the tests.

Earlier studies\*\* have demonstrated that for the film dryout phenomenon characteristic of the onset of transition boiling which occurs in the range of applicability of the GEXL correlation, contact of an obstruction with the surface encourages earlier dryout. This is a hydrodynamic effect and results from the "scrubbing" action of an upstream vortex that is set up in the stagnation region directly ahead of the obstruction. The effect is more severe for larger and/or more blunt objects.

Since the test modifications to the spacer springs result in slightly more restrictive objects in contact with the rods, it should be expected that dryout will occur slightly earlier. The resultant test data have slightly lower values for critical power than would be the case in an actual reactor fuel assembly.

**Question 1-9:**

If boiling transition were to occur at a position other than at a thermocouple location, what would be the effect on bundle power and the GEXL correlation?

**Response:**

Both ATLAS water and Freon tests have consistently shown that boiling transition originates within 3/4 inch of the leading edge of our spacers. The boiling transition then spreads slowly upstream as power is increased. For example, during the testing of Assembly 31, a 7x7 lattice 16-rod bundle, boiling transition was found to originate on corner rod

\*R. T. Lahey, Jr., E. E. Polonick, and G. E. Dix, "The Effect of Reduced Clearance and Rod Bow on Critical Power in Simulated Nuclear Reactor Rod Bundles," Paper No. 5 presented at International Reactor Heat Transfer Meeting, Karlsruhe, Germany, 1973.

\*\*B. S. Shiralkar and R. T. Lahey, "The Effect of Obstacles on a Liquid Film," Transactions of ASME, Jour. Ht. Trans, Vol 95, No. 4, Nov. 1973.



NEDO-10958-A

just upstream of the second spacer. On one run, additional bundle power was applied until TC1-2A experienced a 300°F temperature rise. TC1-2B, 2-7/16 inches upstream of the second spacer, had only about a 150°F temperature rise while TC1-2C, 4-7/8 inches upstream of the second spacer saw practically no temperature rise at all.

These results agree with the theory that boiling transition should originate just upstream of a spacer due to:

The effect of a flow obstruction on decreasing the margin to boiling transition just upstream of an obstruction, (see response to Question 1-8),

Decreasing turbulence downstream of the preceding spacer which minimizes margin to boiling transition just upstream of a spacer.

Therefore, any boiling transition observed other than just upstream of a spacer (in a bundle with reasonably well axial heat flux profile) would be non-conservative. The GEXL correlation includes only data which do not suffer from this defect.

Question 1-10:

1-4 – An analysis should be given explaining why GEXL doesn't correlate the loose corner rod clearance data as well as it does the rest of the data. Was the actual (loose) corner clearance used in the prediction of critical power?

Response:

Increased clearance in the "hot" corner for Test Assembly 24B resulted in more effective cooling for the limiting condition hence in higher critical power. These high 24B data points were *not* used in developing the correlation. Corner clearance does not enter into the prediction of critical power since the correlation is purposely biased to the most minimum clearance conditions.

Question 1-11:

A flow deviation of 2.5% is listed as being the result of an 11.2% deviation in jet pump ΔP. Since the flow is the square root of ΔP why isn't the flow deviation equal to 5.4%?

Response: Table IV-1 has been corrected in Addendum 1 to read:

Standard deviation uncertainty in core flow corresponds to 11.2% standard deviation in each individual jet pump flow."

Since total core flow is equal to the sum of the flows from 20 jet pumps, with each individual pump flow having a standard deviation of 11.2% it can be shown that the uncertainty in total core flow is given by

$$\frac{0.112}{\sqrt{20}} = 0.025.$$

The following sentence from page 5-3 of the draft of September 13 was omitted from page 5-2: "Figure 21b compares measured critical power for ATLAS Test Assembly Number 1, which is a duplicate of one of the University Test assemblies (CU Test assembly – Number 15)." Since this was intended to serve as the

important link between the Columbia and ATLAS loops, please explain the omission of the comparison. In Table 11-1 CU Test Assembly Number 15 is reported to be duplicate of CU Number 6. Why were the data from the latter assembly not also compared with the ATLAS-1 data? Please provide the comparisons of CU-6 and CU-15 with ATLAS-1.

**Response:**

Page 5-2 -- Figure 21b, present in an early draft, was omitted from the final version of the GETAB document. Instead Figure 4-2 (page 4-6) was added to give a direct comparison between ATLAS Test Assembly No. 1 and CU (Columbia Test Assembly No. 15) data. We have prepared a new plot of Figure 4-2, dated February 1974, in which we have added data for CU Test Assembly Number 6. CU Test Assembly Number 15 was intended to be a duplicate of CU Number 6 except that in Assembly Number 15 the springs in the spacers were made stiffer to better resist electromagnetic forces. Inspection of the updated version of Figure 4-2 shows that the ATLAS data are in good agreement with the Columbia data except for CU No. 6 data at  $G/10^6 = 0.5 \text{ lb/hr ft}^2$ . The latter lie from 7% to 13% above CU No. 15 and ATLAS No. 1 data. Otherwise the ATLAS data lie generally within about 3% of the CU data, for both assemblies.

(Note: Figure 4-2 originally submitted with this response has been incorporated in the main portion of the text. Section 4.4 has been revised to reflect this.)

**Question 1-13:**

Page 5-2 -- "The GEXL correlation was optimized for the ATLAS data." On page 3-4 of NEDO-10958, six Columbia test assemblies are listed among those which supplied the data base for GEXL. Please explain this contradiction.

**Response:**

Page 5-2 -- In its initial formulation, the GEXL correlation was based on ATLAS data. The terms in this formulation are the terms which appear in Equations 3-2, 3-3, and 3-4, and in Equation 3-5 except for the last term,  $F$ . For the 7x7 GEXL,  $F = F_1$  is length dependent. All the terms which appear in the expression for  $F_1$ , except the last, were based on Columbia data. The last term was based on the 4- and 9-rod data which were the basis for the Hench-Lee line.

Inclusion of the length dependent terms has increased the generality of the correlation, but has also made it somewhat more complex.

The sentence in question on page 5-2 should read, "The GEXL correlation was optimized initially for ATLAS data, and was subsequently optimized for the Columbia data and for early GE data."

(Note: The above sentence has been incorporated into the main portion of this report.)

**Question 1-14:**

Page 5-2 -- The sentence referring to Figures 5-7 and 5-8 says the distributions of these histograms are "normal." Was a test for normality applied and with what results?

It is stated the "certain scaled Freon data have been successfully correlated using GEXL." Does this the GEXL correlation of water data accurately predicted the Freon data? If it means what it says, how did GEXL compare with the "water GEXL?" What is implied by "certain?"

It is stated that GEXL "correctly predicts the effects of . . . axial profile on critical power." This is a prediction of trends. However, examination of Figure 5-14 shows that the trends ( $kw_c/kw_c$  (sym. cos.) for sym. cos., inlet peak, at constant  $\Delta h$ ) are not predicted. Please comment.

**Response:**

**1-14a** Figures 5-7 and 5-8 are unimodal, nearly symmetrical, and have decreasing probabilities at greater distances from their means. The modest nonsymmetry present is in the conservative tail. Thus the normal distribution was selected as the single best choice to characterize these distributions. (Note: This is incorporated into Section 5.2.)

**1-14b** The statement is made on page 5-2 of the document that "certain scaled Freon data have been successfully correlated using GEXL." The adjective "certain" is intended to identify the data with the "certain Freon data (i.e., those taken from 16-rod, 49-rod, and 64-rod bundles, at the modeling pressure of 123 psia, mass fluxes from  $0.3 \times 10^6$  to  $1.1 \times 10^6$  lb/hr-ft<sup>2</sup>, and uniform local peaking . . ." described on page 4-3. The adjective "scaled" indicates that the mass flux has been divided by an appropriate modeling factor,  $K - G_F/G_{WG}^*$  and the critical power scaled by the mass flux and latent heat.

The Freon data thus described were correlated by the standard GEXL correlation via the use of this modeling factor. There is no "Freon GEXL" per se. However, other Freon data could be predicted using GEXL in combination with the modeling factor, provided only that the local peaking was uniform and that the geometry corresponded to either the 7x7 or the 8x8 lattice geometry as tested in ATLAS.

**1-14c** The original Figure 5-14 was intended to show both measured and predicted trends in critical power with axial flux shape. To better display the trend, and compare predicted with measured, we should limit the comparison to a subcooling typical of BWR operation. Figure 5-14, dated February 1974, is a cross plot of the original figure, at 20 Btu/lb subcooling. The result is a bar chart which clearly shows the trend in critical power with axial flux shape. Although the predicted values are 2% to 7-1/2% below the measured at this particular subcooling, the trend in predicted values is almost identical to the measured.

(Note: The Figure 5-14 originally attached is incorporated into the main portion of this report.)

**Question 1-15:**

**Page 5-9** — Is there any significance to the group of data scattered below the -6% line?

**Response:**

**Page 5-9** — Low points on a plot like this means that the prediction for those points is conservative, i.e., the predicted critical power lies below the measured critical power. The eleven lowest points, percentage wise, belong to test Assembly numbers 30A and 30E. These are both 7x7 16-rod assemblies with uniform axial profile and 1.24/1.26-3 rod corner peaking. The 30A data came in so high that Assembly 30E was assembled and tested as a check. The eleven data points in question are comprised of six points for Assembly 30A and five points for Assembly 30E. All eleven are at flows of  $G/10^6 = 1.0$  or 1.25, subcooling in the range 23 to 51 Btu/lb, and all are in the range of 10% to 15% above prediction. For reasons which have not yet been established, these data are higher than expected.

**Question 1-16:**

**Page 5-11** — This figure has been changed from the draft version (Figure 24 on page 5-22) with a smaller resulting scatter. Please explain.

**Response:**

**Page 5-11, figure 5-5** — The figure shows predicted critical power plotted versus measured critical power for ATLAS 8x8 lattice 16-rod test assemblies. In a draft of the document which was submitted earlier to the AEC, the corresponding figure showed more scatter than appears in Figure 5-5. This earlier figure had been prepared using an earlier, less accurate, version of the GEXL correlation for 8x8 lattice. Figure 5-5 shows the correct predictions.

\*This factor is given in Figure 3-29 of the proprietary supplement.

3  
08**Question 1-17:**

**Page 6-2** — When applying GEXL to a CPR calculation, the third sentence on the page states that the mass flux is assumed to remain constant as the power is increased from the nominal value to the critical value. Since normally the flow would decrease in this situation, the resulting CPR is not quite accurately calculated. Why is the critical power not evaluated at the somewhat reduced flow so as to accurately calculate the CPR?

**Response:**

The CPR as used in GETAB represents the margin inherent in the *bundle* operating power not in the *core* operating power. The definition incorporating constant mass flux is consistent with that used experimentally.

It is true that as core power increases, the flow through the hot channel decreases. However, such flow reduction is included in the analyses of the transient events. Thus, if the event under consideration is a total core power increase and the operating MCPR for the limiting bundle in the core is 1.20 a boiling transition would be predicted when the core power reaches a value somewhat less than 120% of the initial value.

If the CPR were defined on the basis of total core power, the core power ratio would be dependent upon core power shape. Therefore use of the core power ratio as a criteria to be met during plant operation would not guarantee that the limiting bundle in a given core operating state always has adequate thermal margin.

The choice of a particular figure of merit is also one of convenience. The ATLAS data show that the boiling transition is a critical bundle power phenomenon and hence, the CPR is a physically meaningful parameter which is very convenient for application.

It should also be emphasized that reactor operation will be governed by the bundle critical power ratio, not by a core power ratio. Thus a consistent margin definition is employed in the experiments, in the design and analyses and in operation.

**Question 1-18:**

**Page 6-5** — Why would "the existence of greater than critical power in only one assembly produce a boiling transition on only two or three fuel rods?" Regarding the use of "indications of cladding overheating" to establish a violation, the existence of such indications are often difficult to ascertain and once they are clearly visible, the cladding is often defected or nearly defected. Therefore, this method is not reliable to determine clad overheating.

**Response:**

The existence of greater than critical power in only one assembly results in boiling transition on only the limiting rod(s) in the assembly (i.e., the rod(s) with the highest R-factor). The ATLAS test data show that the occurrence of boiling transition on one or more rods will not propagate to other adjacent rods. That is, when boiling transition first occurs it occurs on the rod with the highest R-factor. The ATLAS data show that the boiling transition will not propagate to other rods unless power is increased sufficiently so that the boiling transition occurs on the lower R-factor rods also. Because the R-factors within a bundle are distributed as illustrated in Figure IV-1\* only a few rods would be involved at the critical power level. Stated differently, in order to involve many rods in boiling transition more than one assembly must exceed critical power.

It is true that overheating as result of boiling transition is difficult to detect by examination of the rods. The extent of cladding temperature increase would be expected to be minimal and very long periods of sustained operation beyond boiling transition would likely be required to develop readily visible indications. However, there is a much lower probability that physical evidence would exist if limits are established below critical power.

\*Figure IV-1 was subsequently deleted (see response to Question 3-8e) and is, therefore, included with this response.

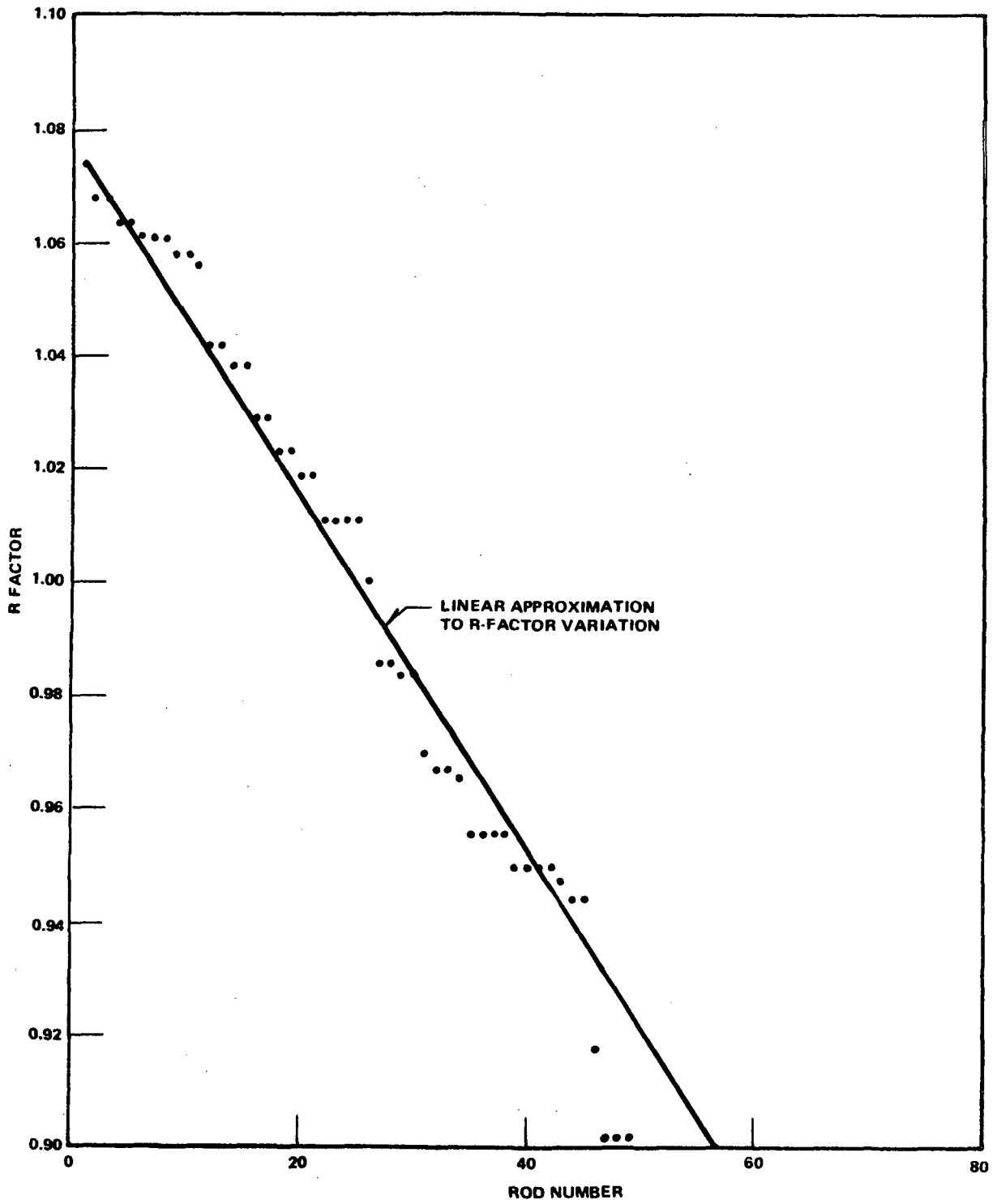


Figure IV-1. Variation of R Factor for A Bundle (7 X 7)

The following Round 1 Questions were in reference to the General Electric Company Licensing Topical Report NEDE 10958, "General Electric BWR Thermal Analysis Basis (GETAB): Data, Correlation and Design Application." Answers to these questions can be found in that report.

**1-19 Figure 3-3** – Please discuss the discrepancies between data and GEXL shown in Figures 3-3 to Figure 3-13.

**1-20 Page 3-1** –It is stated that, "GEXL predicts the boiling transition location slightly downstream of the true location. The reason given for this is that the GEXL correlation was synthesized for the prediction of critical power. Accordingly, a quality correction (reduction), determined empirically, has to be applied to GEXL in order to use GEXL as a locator predictor. Please explain this and the method used to predict the transient location predictor and the subsequent penetration distance.

Doesn't the need for the quality correction stem from the fact that GEXL assumes that the total bundle power goes only into two regions (overcoming inlet subcooling and vaporizing liquid to critical quality) whereas a third region (power required to increase critical quality to outlet quality) actually exists?

**1-21 Appendix II** – Pages II-3 and II-4 are missing.

**1-22 Nomenclature P. xi/xii** – Momentum density; in the first term,  $(-\alpha)$  should be  $(1-\alpha)$ .

**1-23 Page 4-7, Equation 4-19** – Is  $L_B/D_H$  an exponent of B or a coefficient of B?

**1-24 Page 3-6** – Extensive comparisons of GEXL predictions and data are shown. However, in many instances, the compared data are identical to data used to develop GEXL and thus do not constitute addition verification of GEXL. The comparisons shown in the following figures are of this nature: Figures 3-11, 3-14, 3-15, 3-16, 3-17 (3 of 4 data sets); Figures 3-25 through 28 for  $G > 0.1 \times 10^6$  lb/hr sq ft. This should be clarified in text.

**1-25 Figure 2-7** – Why are the lower points favored for drawing the 8x8 curve? For corner peaking less than 1.25, it appears that a more representative curve would be higher than that shown.

## 2. ROUND 2 QUESTIONS

### Question 2-1:

The GEXL correlation exhibits small, but definite, systematic errors, as noted below. In GETAB, a large space of possible reactor operating states is randomly sampled by a Monte Carlo technique. If it were certain that GEXL contained no systematic error, then it would be possible to assume that the statistical information derived from a relatively small number of Monte Carlo samples was a valid measure of the space. That is, the assumption of independence of parameters, as required in the Monte Carlo technique, would be valid. But, since GEXL contains systematic error, we are concerned that the space of operating states could contain conditions whose existence and character would not be predicted by and could not be extrapolated from a small number of random samples taken from the space. Considering the examples of systematic GEXL errors listed below, demonstrate that the GETAB/Monte Carlo methodology provides an adequate statistical measure of the entire space of possible operating states.

- a. Figure 4-21 of NEDE-10958, Supplement 1 shows systematic error with respect to corner peaking in 64 rod bundles.
- b. Figures 3-20 to 3-23 of the same document show systematic error with respect to axial power profile.
- c. Page 5-3, same document, last paragraph of Section 5-2, shows error with respect to geometry variations in the test bundles (whether or not this is systematic error cannot be determined since no data plots were provided to support the conclusions drawn about this error source).
- d. The ATLAS experimental procedure precludes the observation of subsequent boiling transition (e.g., on neighboring rods) following the initial boiling transition. Since the Monte Carlo method assumes independence of boiling transition on one rod from boiling transition on all other rods in arriving at an estimate of the total number of boiling transitions in the core, the experimental procedure presents a possible, as yet unexplored, source of systematic error.
- e. Figure 4-2 of NEDO-10958 shows systematic error between the Columbia and ATLAS tests.

### Response:

A general discussion of the issues raised in this question will be presented before turning to the specific illustrations cited in 1a to 1e. (Note: Specific answers to Question 2.1a through e either directly pertain to NEDE 10958 or contain information which is proprietary and are, therefore, presented in NEDE 10958.)

GEXL predictions, when compared to experimental results, exhibit two types of mean difference between observed and predicted critical power values. First, there are overall mean differences, found separately for the 7x7 and 8x8 lattices, given in the table on page 5-2 of NEDO-10958, and in Tables 5-3 and 5-6 of NEDE-10958. These differences will be discussed in response to question 3. Second, there are mean differences (i.e., systematic differences) for particular bundle operating states which are shown in Tables 5-4 and 5-7 of NEDE-10958 for exhaustive combinations of ranges of mass flux and inlet subcooling, and in Table 5-5 for axial flux shapes. Many of these systematic mean differences differ significantly\* from the grand mean difference, for the lattice. This discussion will consider these systematic differences.

The way in which systematic mean differences affect setting the minimum allowable critical power ratio for a plant (the Monte Carlo procedure) is in their contributions to the overall statistics of experimental mean and standard deviation. This relationship reflects a correct practice if the distribution of operating states in plant operation is approximately the same as the combinations of test conditions in the experiments; or, a conservative practice if the predominating operating states in plant operation are those having mean differences which are less than the grand mean

\*"Significantly", in response to question 1, means statistically, at the 5% level.

difference for the lattice. The latter is the case with respect to axial flux shape, since inlet peaked and cosine shape bundles predominate among those making largest contributions to expected number of rods subject to a boiling transition, and these shapes have mean differences less than or equal to the grand mean difference, as can be seen in Table 5-5 of NEDE-10958. However, because only cosine axial shapes have been tested in the 8x8 lattice, the standard deviation for the 8x8 lattice has been increased for use in the Monte Carlo analyses from 0.0280 to 0.0342, which is the square root of the sum of the variances of the 8x8 experiment results, and of the means of the axial shapes in the 7x7 testing. It should be emphasized that this adjustment is being made to place the 8x8 statistics on the same basis as the 7x7 and that the net effect is conservative as described in question 1b.

A similar relationship for mean difference is true for combinations of mass flux and inlet subcooling. The most common operating combination is cell 4, having mean differences either less than or not significantly greater than the grand mean for the lattice. The plant operating state for bundle size, however, involves only 49- or 64-rod bundles, whereas the experimental work included 16-rod bundles as well. For the 7x7 lattice, the 49-rod mean difference exceeded the overall mean difference for the symmetrical cosine axial flux shape by +0.0005; this difference was not significant, so no adjustment in grand mean was called for for that lattice. However, that difference was +0.0026 for the 64-rod bundles in the 8x8 lattice. As this difference was statistically significantly different from the grand mean, it was added to the grand mean for setting minimum allowable critical power ratio for plants using this lattice (i.e., calculation of expected number of rods subject to a boiling transition for the 8x8 lattice was done using a grand mean of 0.9874 rather than 0.9848). Such mean differences have also been searched for with respect to particular ranges of the other operating variables, and operating local peaking patterns, without finding other significant differences.

Setting a plant minimum allowable critical power ratio is done by choosing from uncertainty distributions for the plant measurements by Monte Carlo, and using an upper-tail probability value from the distribution of experimental critical power ratios, rather than entering this distribution by Monte Carlo. This procedure leads to a much more precise value for mean expected number of rods subject to a boiling transition for a given number of trials. The uncertainty distributions for the plant measurements may be sampled with no dependence of the sample from one upon that of another for all pairs of measurements, since any errors in those measurements appear to be independent, without exception. This is also true between all operating measurements and values from the distribution of critical power ratios from experiment. There is no implication that, once an operating state is chosen, an experimental critical power ratio value should be chosen from any particular part of that distribution. This is true because the overall distribution of experimental critical power ratio values is used, and the question of correspondence of proportion of operating states in plant operation to operating states in experiments and treatment of mean differences under selected operating states, were addressed above. Use of upper tail probabilities in the distribution of experimental critical power ratios is equivalent to assuming that the conditions for onset of a boiling transition are no more likely to be found in one portion of the distribution of experimental critical power ratios than in another, for any plant operating state.

It may be noted that, in general, the Monte Carlo procedure may be used even when the choice of some variable(s) depends on the choice of some previous variable(s) — that is, in which the error values of some pairs of variables are not independent — but such dependencies were not required in this application.

The ability of the Monte Carlo procedure to reflect the full range of possible error values of each operating variable is in no way impaired by any of the foregoing. Indeed, special precautions were taken against introducing systematic error by the Monte Carlo procedure itself.

#### Question 2-2:

It is not clear in NEDO-10958 and NEDE-10958, Supplement 1 exactly how the GEXL correlation was obtained. Thus, we are uncertain that the GEXL correlation has been statistically optimized. Respond to the following questions in this regard:

- a. In NEDO-10958, on page 3-2, equation 3-4 (the CISE form) expresses the critical quality as a ratio of two linear functions of boiling length. However, it is indicated there, that a quadratic correlation may be preferable. In performing regression analyses to derive GEXL, what functions were posed as possible correlating functions; e.g., linear or quadratic? How was the optimum form determined and what statistical tests were used in that determination?



- b. In NEDE-10958, Supplement 1, Appendix III the method for calculating R is given. Weighting factors for three types of variously located rods were assumed to be 1/4, 1/8, and 1. Describe the relationship of these weighting factors to subchannel fluid mechanics analyses. What assurance is there that these weighting factors were optimized and are not the source of systematic error in GEXL?

**Response:**

**2-2a** – In the development of the GEXL correlation, much use was made of graphical displays of data in the Quality – Boiling Length plane. The general form was established early and refinements were made as more data were generated, thus better defining the effect of certain parameters. The correlation was tested by (1) graphical comparison with data in the Critical Power – Subcooling plane, and (2) by numerical comparison of predicted critical power with measured critical power at each data point. The ratio of predicted to measured was evaluated, and the mean and standard deviation determined for each test assembly and flow condition. These tests of the correlation provided guidance during the latter stages of its development.

No regression analysis was used in the development of the GEXL 7x7 correlation. However, a regression analysis was used in the development of the GEXL 8x8. The coefficients were optimized using appropriately weighted data to best represent all the parameters of interest. The resulting correlation was tested as described above.

(Note: This response is incorporated into Section 5.1.)

**2-2b** – This response contains proprietary information and is, therefore, documented in NEDE-10958.

**Question 2-3**

The ratio of predicted (GEXL) to measured critical power has mean values less than one for both the 7x7 and the 8x8 data. Focusing on the 7x7 data; the mean is 0.9885, and the standard deviation is 0.036 for 2700 data points (Pages 5-4 and 5-5 of NEDE-10958, Supplement 1). The ideal value for the ratio is 1.0. With the implicit normal distribution assumption of GEXL/GETAB, a mean of 0.9885 indicates that about 62 percent of the 2700 measured 7x7 CPRs were below one. Thus, at a one percent significance level one could reject the hypothesis that GEXL provides an unbiased estimate of actual critical power. As in Question 2-1 above, we are concerned that because of the normality and independence requirements for Monte Carlo analysis, the GEXL correlation with attendant systematic error (bias) is not a best estimate representation of the ATLAS data. Please address these concerns.

**Response:**

The table on page 5-2 of NEDO-10958, and Tables 5-3 and 5-6 of NEDE-10958, reveal grand mean differences of the GEXL algorithm for the 7x7 and 8x8 lattices. These grand mean differences arise from the procedures used to estimate the coefficients in the prediction equation. Resulting critical power predictions by themselves are not unbiased; indeed, they are slightly conservative. However, because the mean differences found (except as noted for bundle size in response to Question 2-1) are used as the means of the distributions of experimental critical power ratios in the applications to plant operation, there will be no bias in the minimum allowable critical power ratios set in fulfillment of the thermal design criterion relative to critical power ratios which will be computed in plant operation. Normality is discussed in response to Question 2-5c, independence in response to Question 2-1.

**Question 2-4:**

In Sections 6.3.2 and 6.5.2 of NEDO-10950 there are tabulated the effects on MCPR for various transients. These sections do not contain definitive statements regarding the uncertainty of the transient analyses. Provide the statistical basis for combining the uncertainties in GEXL with uncertainties in the plant transient analyses.

**Response:**

The transient analysis is a bounding analysis rather than a statistical analysis as presented for the rest of the GETAB approach. The bounding nature of the transient analysis is obtained by choosing the most severe condition (e.g., worst tolerance) in the specification of hardware performance and design parameters and in addition applying conservative

factors to the void, Doppler and scram reactivity for input to the transient computation. This yields a doubly conservative analysis of dynamic events at any given power level. In addition to the above conservatisms in the dynamic calculations, all transients are analyzed from the turbine-generator design power level rather than rated at the initial condition which further maximizes the effects of transient response.

The effects of varying the important parameters in the nuclear model are presented in Section 3 NEDO-10802 "Analytical Methods of Plant Transient Evaluations for the General Electric Boiling Water Reactor". One of the transients considered is the turbine trip event which is one of the most severe from both the system pressurization and thermal margin point of view. While this does not provide any proof of the bounding nature of the transient analysis, it does demonstrate that void and Doppler coefficients, scram reactivity and core initial power are on the whole the most sensitive input parameters to the transient computation.

In Section 4 of NEDO-10802, the calculation of transient effects are compared with plant startup measurements. These comparisons show that in two of the three presented cases of turbine trip events the peak heat flux computed is higher than that measured at the actual plant during startup. In the other instance, a mild, full-bypass Tarapur event the peak heat flux of the nominal calculated case is within 2% of the startup results. If the power level were increased to T-G design and the conservative multipliers applied to the reactivity inputs as actually is done during design and safety analyses, the peak heat flux would increase by more than 10% which is well above that measured during the Tarapur startup tests. This demonstrates the bounding nature of the standard General Electric transient analysis procedure from both a computational and plant comparison basis.

Evaluation and review of dynamic models for the BWR is continuing. This evaluation will of course continue to occur as both specific and generic licensing discussions take place. Therefore, the conservative nature of the transient analysis will continue to be applied on a plant by plant basis as appropriate during the licensing process. The use of this analysis approach assures that uncertainties associated with the transient are conservatively included in the transient  $\Delta$  MCPR used for derivation of the GETAB operating limits.

#### Question 2-5:

There are several statistical inaccuracies in NEDO-10958 which should be corrected.

- a. Page 6-4. It is not generally true that "the antilogarithm of the mean logarithm" is equal to the average number, as implied by the last paragraph. Correct or qualify these statements to elucidate what is true for the GETAB application.
- b. Page IV-1, last sentence of second paragraph. When the probability of boiling transition is 0.5 per rod, the number of rods in a set of size N which "might possibly experience a boiling transition" is not 0.5N, but N. GE's statements imply that 0.5N is the maximum number of failures. It is instead the expected number.
- c. The GEXL/GETAB documents contain many references to the normality of the distribution of ATLAS data. What tests were applied to the data to make the judgment that the distribution was normal rather than for example, Cauchy? On what basis was the Poisson distribution ruled out for describing uncertainty in the predicted number of boiling transitions. Isn't the Poisson distribution traditionally preferred over the normal distribution when discrete integer numbers are involved?
- d. Page 6-5 and Figure 6-4 do not agree. On Figure 6-4 the mean number of rods experiencing a boiling transition, with 95 percent probability, is not 0.00303 to 0.0304, but is closer to 0.5. Correct or explain numbered statement (4) on page 6-5.
- e. Figure 6-4 alludes to 30 trials, yet only 23 points appear. Why?
- f. Define precisely all the steps required to complete a Monte Carlo "trial".

**Response:**

**2-5a** – This question is addressed in the reply to Question 2-6.

**2-5b** – The sentence in question will be changed to read: In a group of N rods each operating at the mean of the data, 0.5 N rods are expected to experience boiling transition. (Note: This change has been incorporated into this report.)

**2-5c** – A frequency distribution in which probabilities may be readily computed is needed to represent the distributions of experimental critical power ratios for use in setting the minimum allowable critical power ratio for a plant. (Use of this distribution is illustrated in the reply to question 5f). No distribution can be chosen on theoretical grounds (even the Cauchy, as we have the distribution of inverse residual ratios, rather than ratios of two independent normally distributed random variables), so an empirical choice is called for. Because the experimental critical power ratios can be well represented by the normal distribution – as indicated initially on normal probability plots – and because of its convenience in computing probabilities, and adjusting shape and width by the mean and variance, this distribution was chosen. By the usual Chi-squared test, the sample distributions were found to not differ significantly from normal distributions having the tabled means and standard deviations, following combining intervals in pairs in the sample distributions to reduce excessive frequency fluctuations between intervals from fine division, and following the rule of combining (end) intervals as necessary to assure no interval has a theoretical frequency of less than five.

On possible use of the Poisson distribution, while it is true that its variable may take on only integer values, it does not follow that this distribution will satisfactorily describe the frequency properties of integers arising under any circumstances. The Poisson distribution does have widespread application, but it applies theoretically only to "Poisson processes", ones in which events per unit time or space are being described, and—as it has but a single parameter—it is not flexible for making empirical applications. It was found to be not adequate for describing uncertainty in the predicted number of boiling transitions.

**2-5d** – Item (4) on Page 6-5 states that the true mean number of rods experiencing a boiling transition lies in the range 0.00303 to 0.0304 with 95% probability. This statement illustrates the confidence level placed on the mean number of rods experiencing boiling transition. That is, with a probability of 95% the interval 0.00303 to 0.0304 contains the true mean number of rods experiencing boiling transition. The 95% probability point in the distribution of individuals corresponds to approximately 0.5.

(Note: Item (4) on page 6-5 was deleted in the response to Question 3-6.)

**2-5e** – The missing points were inadvertently deleted. The corrected figure is attached. Note that the axis is cumulative and does not reach 100%. Therefore only 29 points appear.

(Note: The originally attached revised Figure 6-4 has been incorporated into the main portion of this report.)

**2-5f** – The Monte Carlo analysis process can be broken into several parts. These steps can best be explained by referring to the flow chart in Figure 1.

The process starts by performing a nominal reactor state calculation. Traveling In-core Probe (TIP) readings are generated analytically by simulating the traversing of the core with a U235 detector head which measures at different core elevations the average thermal neutron flux in a four bundle cell. The tip readings along with the total reactor power are then used by the model to calculate the detailed power distribution in the core.

The next step utilizes other plant operating information such as core flow dome pressure, core coolant inlet temperature, channel flow areas, and friction multipliers to calculate the flow and void distributions. Using the previously calculated power distribution, iteration with respect to flow and void distributions is performed until the feedback effects of voiding are reflected in the flow. At this point in the calculation, the flow, void and power distributions are known for each bundle in the core.

R-factors—the weighted fuel pin power factors employed in GEXL—are then input to the model for each fuel assembly. This information along with the flow, void, and quality distributions is used in the GEXL correlation to calculate the critical power ratio for each fuel rod in the core.

The probability that a Boiling Transition event (BT) occurs in a fuel assembly (PB) can then be calculated using the individual values of CPR corresponding to each fuel pin in that lattice. A sample of how probabilities are calculated using a GEXL calculated critical power ratio (CPR) is shown in Figure 2. For example, if the uncertainty ( $\sigma_{CPD}$  = one standard deviation) between the GEXL predictions and the ATLAS test data were 4%, the probability of a rod experiencing boiling transition would be as illustrated by the cross-hatched area in Figure 2 found in normal probability table. Since the distribution is assumed to be normal, a probability of 0.1587 is calculated for this example for a rod with a GEXL predicted CPR of 1.04. The total bundle probability of B.T. is then calculated using the individual fuel pin probabilities (PN) as shown in the following relation:

$$1 - P_B = \prod_{n=1}^{N_{ROD}} (1 - P_n)$$

where:

- PB = prob. B.T. in a bundle
- PN = prob. B.T. for a fuel rod
- NROD = number of fuel rods in a bundle

The probability ( $P_C$ ) of boiling transition occurring anywhere in the active core region can be calculated in the same manner as bundle probabilities by substituting  $P_C$  for PB and PB for PN in the above formulation with N equal to the total number of assemblies in the core. With a calculated value of  $P_C$ , the Monte Carlo procedure then either selects or rejects bundles depending on whether they will contribute significantly to the overall probability of B.T. in the Monte Carlo trials. For instance, the GEXL correlation and subsequent probability calculations during the Monte Carlo trials will only be performed on fuel bundles with nominal case probabilities ( $P_B$ )  $\geq P_C \times 10^{-9}$ . Therefore, any fuel bundle with very low probabilities of B.T. (i.e.,  $P_B < P_C \times 10^{-9}$ ) for the nominal case will always be insignificant during the Monte Carlo process when compared to bundles with higher probabilities of B.T.

With the nominal case run and fuel assembly selections made, possible reactor operating states can be calculated by random Monte Carlo selection from distributions of all operating parameters. For instance, there exists a calculated uncertainty ( $1\sigma$ ) associated with all tip readings. It is assumed that the nominal value of the tip reading is the mean and that the corresponding uncertainty is one standard deviation of a normal distribution. With this assumption a new tip value can be selected randomly from its normal distribution in each Monte Carlo trial. For each trial, this random selection is performed once for each tip reading, each R-factor, each bundle cross sectional flow area, core flow, core power, core coolant inlet temperature, core pressure, and for each bundle friction multiplier. After all of these operating parameters have been randomly selected from their respective normal distributions, the power, flow, void, and quality distributions are calculated in the exact same manner as the previous nominal case.

Again the GEXL correlation is used to calculate critical power ratios (CPR). However, instead of being applied to all the fuel rods in the core, the CPR's are only calculated for those rods contained in bundles considered significant in the nominal case calculation. Usually this reduced core calculation includes approximately one-third of the core's fuel rods.

As in the nominal case, the probability of a fuel rod experiencing boiling transition can be calculated as shown in Figure 2. Fuel rod probabilities of boiling transition (PN) are calculated for the same portion of the core (i.e., for the reduced core) as were the CPR's. The number of rods expected to experience boiling transition is then equal to the summation of all the fuel rod probabilities (PN).

The Monte Carlo program then proceeds to the next trial. As before, the values of the input operating parameters are randomly selected from their respective normal distributions. All calculations are performed as in the previous Monte Carlo trial with a resultant number of rods expected to experience boiling transition as the end product of the trial.

Minimum allowable critical power ratio is set to correspond to the criterion of 99.9% rods expected to avoid boiling transition by interpolation among the means of several distributions each formed from 30 Monte Carlo Trials at a nominal MCPR.

(Note: This response has been incorporated into Appendix IV-3-6. Figures 1 and 2 were incorporated as Figures IV-4 and IV-5 respectively.)

#### QUESTION 2-6:

It is our position that it is improper to use a log-normal distribution to describe the results of the Monte Carlo procedure (page 6-4 of NEDO-10959). Use of the log normal distribution gives an unjustifiably low estimate of the uncertainty; that is, the log-normal distribution yields the geometric average rather than the arithmetic average of the results and shrinks the attendant uncertainty interval. We see no basis in physics to justify the log-normal distribution. Rather, since the total probability of boiling transition is computed as the sum of probability of transition on 8000 individual rods (page IV-5 and IV-6), we would expect the distribution to be normal as is characteristic of sums of independent normal factors. By contrast, the log normal distribution is characteristic of products of independent normal factors. Provide justification for the log normal distribution. It is not sufficient to say that it fits the results, because it also gives a distorted view of the results. The use of geometric means (i.e., the computation of mean number of failures by taking the logarithm, averaging logarithms, and then taking the antilog of the mean) is unjustified and unacceptable. The arithmetic mean should be used.

#### Response:

The antilog of the mean logarithm of the results of the Monte Carlo trials was initially employed as the statistical indicator of the number of rods subject to boiling transition on the basis that the distribution of trial results was found empirically to be approximately log normal, and the antilog of the mean logarithm would be a reliable estimator of the median of the original distribution. Thus, the objective was to choose an indicator which was unaffected by the skewness of the distribution, even though of course it was not the "expected value" in the statistical sense.

A study has been performed to determine the effects of employing the arithmetic mean rather than the antilog of the mean logarithm. The results show that in order to satisfy the 99.9% design basis the minimum allowable transient MCPR would increase from 1.04 to 1.05 for the typical BWR/4 case and from 1.05 to 1.07 for the typical BWR/6 case, i.e., a substantial increase. These results also include the minor effect of the adjustments to the data statistics reported in answers to Question 2-1. Providing the allowance for transient  $\Delta$ MCPR results in the required operating MCPR increasing to 1.19 for BWR/4 and to 1.24 for BWR/6.

Although these increased margins are considered unnecessary, they can be accommodated within the operating margins available in BWR design. As required by Question 2-6, the GETAB process will be modified to utilize the arithmetic mean rather than the antilog of the mean logarithm. The final revision to the GETAB document will incorporate the necessary text revisions.

With respect to justification for the log normal distribution, the change to the use of arithmetic mean eliminates any dependency on log normality for a statistically significant indicator; i.e., the form of the results of the Monte Carlo trials is no longer important and the fact that the results have been observed to be approximately log normal does not enter into the derivation of operating limits.

(Note: Section 6.3.2 has been revised to reflect this response.)

**Question 2-7:**

In the statistical analysis you apparently assume that the rods with lower R values than the maximum in the hot bundle can be related to boiling transition by using the correlation based on the experimental results for rods with the highest R value. It appears that no tests were made to demonstrate the validity of this assumption. This limitation to testing apparently was made to prevent damage to the rods with highest R value. Please justify the assumption.

**Response:**

See the proprietary response to Question 2-1d.

**Question 2-8:**

It appears that for some reactor conditions and power patterns the shapes of the  $X_C$  and  $L_B$  curves from the heat balance and the critical power correlation can be very close in the neighborhood of the point of boiling transition. This means that small errors in either curve can have a large effect on the point of intersection or tangency. Although these errors should not affect critical power appreciably, there could be a large change in location. Furthermore, the boiling transition location is, due to the method of detection and location used in ATLAS, limited to that of the region immediate upstream of a spacer grid. Discuss how the above factors affect the accuracy of the location predictor.

**Response:**

The answer to this question contains proprietary information and is, therefore, given in NEDE 10958,-PA.

**Question 2-9:**

Since the number of thermocouples used in the final tests to determine the presence of boiling transition were quite limited, discuss the previous test results used to determine the adequacy of the final thermocouple arrangement. As inadequate location sensing could give a higher critical power, justify the assumption that the final choice of thermocouples was sufficient to locate the onset of boiling transition in the bundle for the various power patterns tested.

**Response:**

In the critical power testing of full scale bundles, the proper location of thermocouples to detect the first onset of boiling transition has been of central concern to us. For each test assembly some prior knowledge is necessary in order to predict, first, the proper axial location, next the limiting rod(s) and finally, the limiting sub-channel(s).

Concerning the proper axial location, it has been well established by tests run at Columbia\* and by tests run in Freon\*\* with thermocouples located at various positions before, after, and at intermediate positions between spacers, that the preferred axial location for the first boiling transition is just ahead of the first, second, or third spacer from the end of the heated length. This is true for inlet peaked, cosine, and outlet peaked axial profiles, and for a wide spectrum of local peakings. It has been confirmed by tests run in the ATLAS Loop.\*\*\*

Concerning the identity of the limiting rod(s) and subchannel(s) some initial assumptions must be made, based on the peaking pattern and on past experience with the particular geometry. A great deal of experience has been generated using the Freon Loop. As many as 100 thermocouples were used to instrument each 16-rod assembly, 200 thermocouples to instrument each 49-rod assembly, and as many as 250 thermocouples were used to instrument each 64-rod

\*E. Janssen, F. A. Schraub, R. B. Nixon, B. Natznor, and J. F. Casterline, "16-Rod Critical Heat Flux Investigation, Steam-Water at 600 to 1250 psia," Two-Phase Flow Symposium, ASME Winter Annual Meeting, Los Angeles, November 18, 1969.

\*\*J. C. Rawlings and G. F. Dix, "Clean Geometry and '67 P.L. Spacer Evaluation," NEDM-13076 February 1970 (Class III); also G. F. Dix and R. B. Nixon, "Non-Uniform Axial Critical Flux Performance, Freon Multirod Data - '67 P.L. Spacers," NEDE 13225 August 1971 (Class III).

\*\*\*"Deficient Cooling, 12th Quarterly Progress Report," GEAP-10221-12, July 1972. (Ref. 17.) See also response to AEC Question No. 1-9, in first round of questions on GETAB.

assembly. Only 100 thermocouples could be scanned during each run, and therefore, many runs were repeated with a different set of 100 thermocouples connected to the indicating/recording instruments. The Freon experience provided a useful guide in selecting locations for the ATLAS thermocouples.

In turn, experience has been generated using the ATLAS Loop. Early in the ATLAS sequence as many as 56 thermocouples were used to instrument a 16-rod assembly. With the advent of the increased ATLAS power supply as many as 44 thermocouples were used to instrument a 64-rod assembly. Our present practice is to install 20 or more thermocouples in each 49-rod and 64-rod assembly. These thermocouples are located just ahead of the last three spacers in each ATLAS assembly, on the several rods which experience has proven to be most limiting, on the side facing the corner subchannel or (particularly if a side or interior rod) the subchannel whose area is most restricted by the spacer configuration. Other selected rods and subchannels are also monitored. Repeat tests, with some of the thermocouples moved to other positions, are in generally good agreement with the original tests. Each ATLAS test assembly is carefully inspected after removal from the Loop. There has been no evidence (such as by rod overheating in some uninstrumented location) of earlier boiling transition than was observed in any of the tests reported in NEDO-10958.

The answers to the following Round 2 Questions contain Proprietary Information and are, therefore, given in NEDE-10958.

**2-10** Discuss what tests have been run to determine the location and magnitude of electrically induced rod and grid vibrations, in ATLAS, on boiling transition and the significance of the effect with respect to application of ATLAS results to reactor conditions.

**2-11** Define what is meant by separated flow model in the assumptions in the model.

**2-12** Which correlations are used to estimate turbulent mixing?

**2-13** Justify the use of Levy's void distribution to rod bundles.

**2-14** What are the formulations and basis for the following:

$(W_{1-2})_{CF}$  = the mass flow due to flow diversion or crossflow

$(W_{1-2})_{Mix}$  = the mass flow due to turbulent mixing

$(W_{1-2})_{VD}$  = the mass flow due to void drift?

**2-15** Describe the formulations and basis of the two phase flow multiplier for friction pressure drop.

**2-16 a.** Describe  $h^*$  enthalpy of the diversion crossflow.

b. Is  $h^*$  compatible with the void drift model?

c. Should the void drift model define  $h^*$ ?

**2-17** Define the formulations for  $q_{mix}$  and  $q_{VD}$ .

**2-18** Where are the comparisons between the G.E. subchannel data presented to justify the statement that "the predictions were found to be quite good and the ability of the code to predict conditions with these small spacings support its usefulness in analyzing BWRs with various design geometric characteristics?"

### 3. ROUND 3 QUESTIONS

#### Question 3-1:

The relative severity of various transients appears to vary depending on which criteria, MCPR or MCHFR, are used. For example, the calculated change in MCPR following a two-pump trip transient is less than 0.01, which indicates that this transient is inconsequential. However, the calculated change in MCHFR is 0.7, which indicates that this two-pump trip transient is the most severe. Explain this change in relative severity. If the differences are due to difference in calculation, explain the differences and present the results of calculations of changes in both MCPR and MCHFR.

#### Response:

The apparent relative severity of transients does vary depending on which thermal criterion is used. The heat flux-quality plane (MCHFR) reflects sensitivity to flow decay type transients because the Hench-Levy correlation is insensitive to changes in flow. In the critical quality-boiling length plane (GEXL-MCPR), the critical quality is affected by flow decay. These results are demonstrated in Figures 3.1-1 and 3.1-2 for a typical two-pump trip transient on an 8x8 core. The initial conditions for the transient were:

1. Bundle mass flux = 1.07 Mlb/hr-ft<sup>2</sup>
2. MCHFR = 1.90
3. MCPR = 1.28
4. Core Pressure = 1035 psia
5. Inlet subcooling = 22.3 Btu/lb

At 2.55 seconds into the transient, the critical heat flux ratio reaches a minimum. The pertinent hydraulic conditions at this time are:

1. Bundle mass flux = 0.75 Mlb/hr-ft<sup>2</sup>
2. MCHFR = 1.46
3. MCPR = 1.33
4. Core pressure = 1028 psia
5. Inlet subcooling = 21.2 Btu/lb

These figures show that for the transient analyzed MCHFR decreased by 0.44 while MCPR increased by 0.05. These differences are due only to the correlations. The calculation methods and procedures remained unchanged.

(Note: Figure 3.1-2 is Proprietary and is, therefore, documented in NEDE-10958.)

#### Question 3-2:

Provide the results of the analysis of the sensitivity of the critical power ratio to each of the variables listed on Table IV-1 of NEDO 10958.

#### Response:

The sensitivity of the critical power ratio to each parameter listed on Table IV-1 of NEDO-10958 was studied. A typical BWR/4 plant operating at a steady state MCPR = 1.20 was chosen for this study. The % change in CPR was calculated by changing the nominal values of the parameters one at a time by the amount corresponding to the one sigma value of uncertainty. The results are given in Table 3.2-1, showing the most sensitive parameter first, followed by the less sensitive ones.

The TIP uncertainty is applied separately to each axial node in a fuel assembly. Therefore, a variation of 1 $\sigma$  (6.3%) may produce bundle power changes from 0.0 to as much as  $\pm 6.3\%$ . A similar variation in CPR would occur. Because such variation exists the effect of TIP uncertainty was determined by performing 1 Monte Carlo trial and examining the variation in individual bundle TIP readings and the corresponding change in CPR. As expected, a range of results was obtained and presented in Figure 3.2-1.



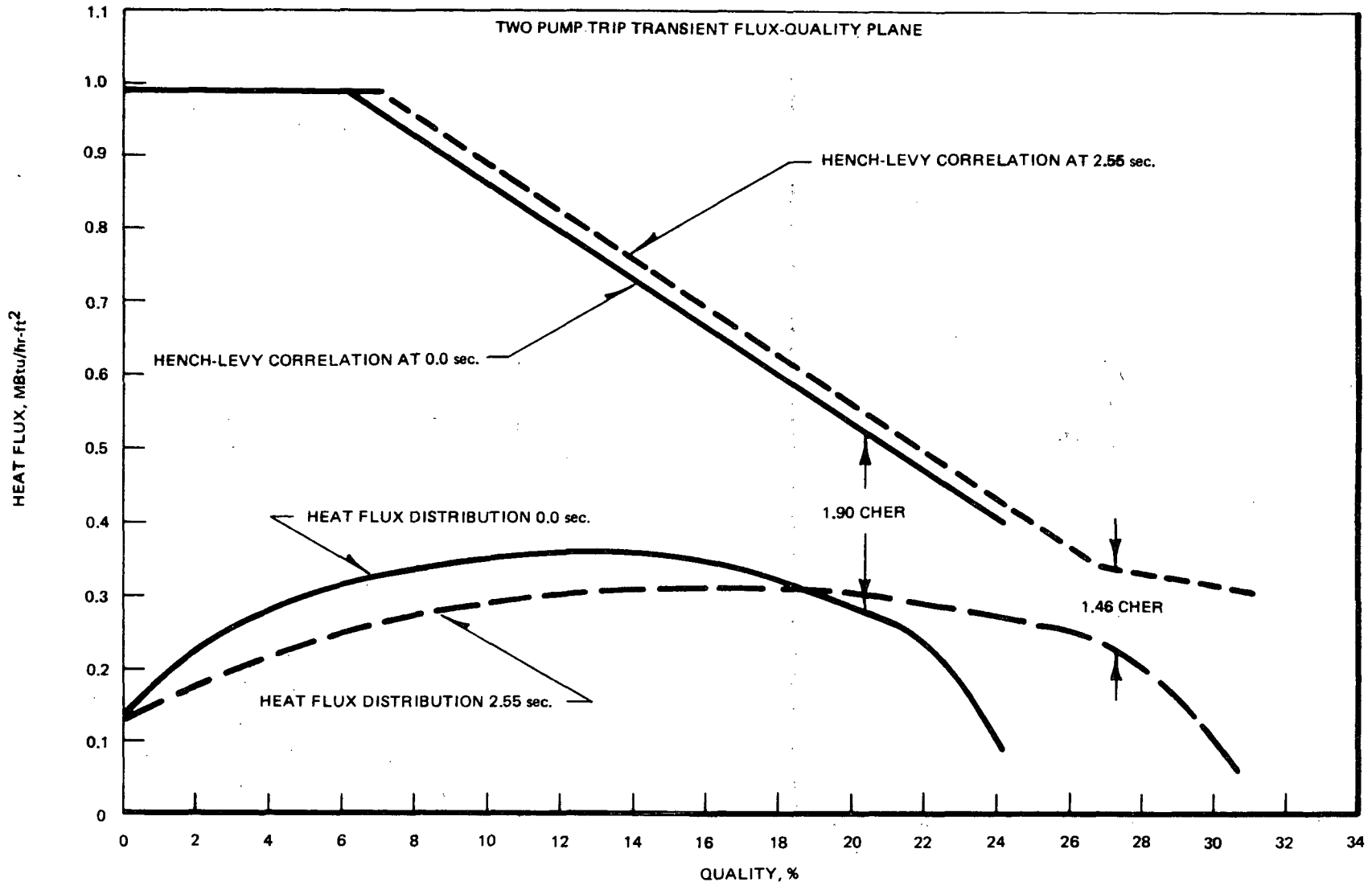


Figure 3.1-1

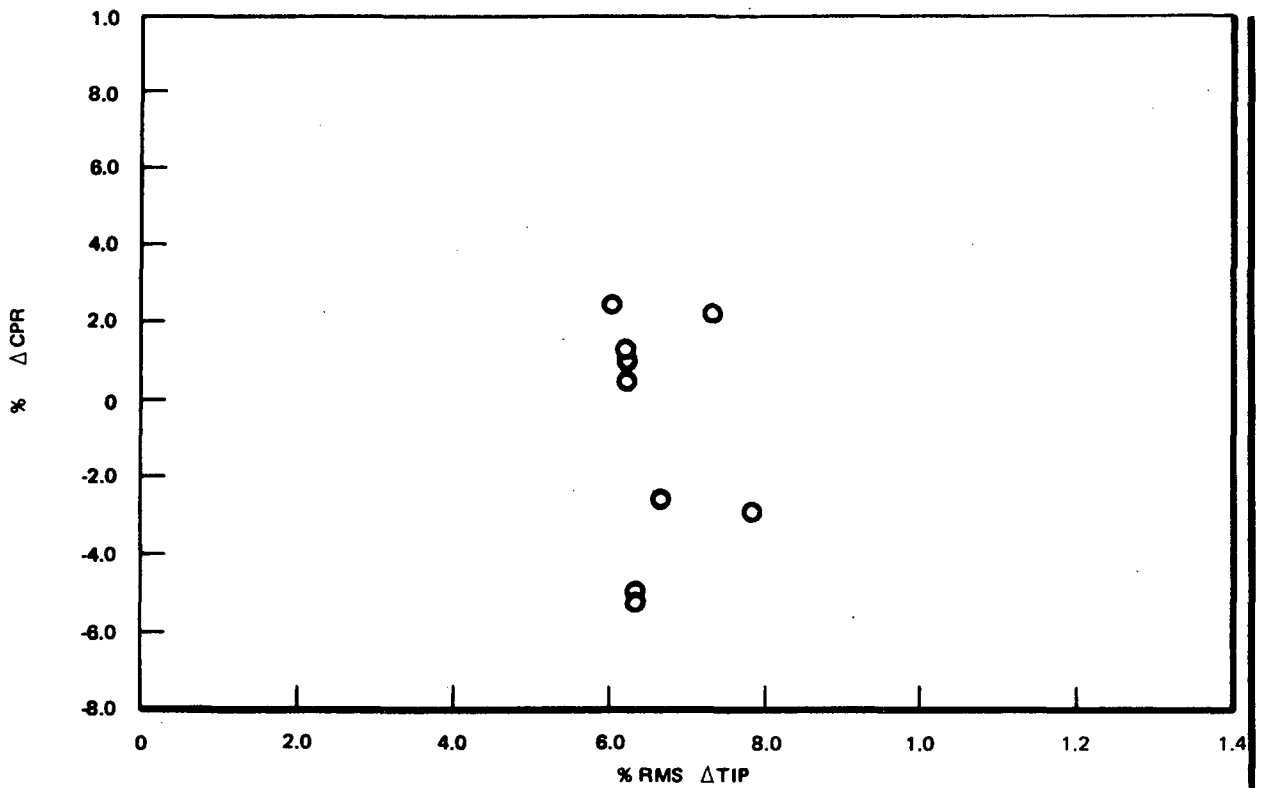


Figure 3.2-1

Table 3.2-1

Parameter	Standard Deviation ln %	% Change in CPR
R-factor	1.5	4.40
Feedwater flow	1.76	1.70
Core Flow	2.5	0.90
Inlet temperature	0.2	0.50
Channel flow area	3.0	0.40
Friction factor multiplier	10.0	0.30
Reactor pressure	0.5	0.12
Feedwater temperature	0.76	0.0255

**Question 3-3:**

Justify the use of one value of uncertainty in each variable as representative of the uncertainty in the variables for all types of GE reactors. For example, cores with bypass flow holes in the lower core support plate would be expected to have a smaller uncertainty in the TIP readings than cores which do not have these holes.

**Response:**

In order to minimize the number of GETAB limits and boiling transition evaluations, and when not overly conservative with regard to operating limits, single uncertainty values have been chosen. In general, these values are the actual estimated uncertainties for one class of plants and are conservative estimates for other plants. However, when there is a substantial difference in an uncertainty value for a certain class of plants, (resulting from a specific system improvement, e.g.) it is intended that these plants be analyzed separately.

With regards to bypass flow, it should be noted that both plants with and without bypass holds were designed to 10% leakage flow.

**Question 3-4:**

Describe the statistical simulation of highly localized events, such as a rod withdrawal error or a misoriented assembly. For a range of calculated MCPR, provide the number of rods in a) worst assembly, and b) in each adjacent assembly which would be expected to experience boiling transition.

**Response:**

**A. Misoriented Fuel Assembly**

The case of the misoriented fuel assembly was simulated for the statistical analysis in the following ways:

1. Core power distribution — the same as used for full core transient simulation.
2. Operating condition — 100% rated core power and flow.
3. Location — Limiting MCPR location in the core under normal condition (without misorientation).
4. Bundle power — Maximum value corresponding to the required MCPR for steady state operation (without misorientation).

The misorientation of a bundle has a negligible effect on the surrounding bundles. Thus, in this simulation, the only change in operating state from the nominal is that the local peaking characteristic is adjusted for the one misoriented assembly. The statistical analysis for a typical BWR/4 indicates that the misoriented assembly applied with a steady state operating limit MCPR = 1.19 results in MCPR = 1.04 and  $\Delta$ MCPR = 0.15. This yields the total expected number of rods in the core subject to boiling transition to be 1.0 rod. Since MCPR of all the other assemblies in the core is 1.19 or greater, no other assemblies contribute significantly to the expected number of rods subject to boiling transition.

The following table summarizes the results obtained for the range of MCPR of the misoriented bundle:

Normal MCPR	Misoriented MCPR	$\Delta$ MCPR	Exp. No. of Rod S.B.T.
1.19	1.034	0.156	1.1
1.19	1.011	0.179	1.8
1.19	0.996	0.194	2.4

The range of values was calculated by assuming various changes in local power distribution (R-factor).

(Note: Because a misoriented fuel assembly can occur only as a result of two operator errors, this event is classified as an accident.)

**B. Rod Withdrawal Error at Power**

The statistical analysis for the rod withdrawal error at power was performed at the reactor condition corresponding to the rod withdrawn to the Rod Block Monitor set point. The core power and the distribution at the reactor condition were obtained by the procedure described in detail in GESSAR Section 15. For a typical BWR/4 case, this condition corresponds to:

- 1) RBM point – 5 feet withdrawal of a control blade located at the center of the core.
- 2) Core power – 102.4% of rated.

The thermally limiting bundle is assumed to be initially on the steady state MCPR limit of 1.19, (for a fuel assembly in the immediate vicinity of the center of the core where the control blade is to be withdrawn). The analysis shows that this bundle is still limiting at the terminal point of the withdrawal, resulting in MCPR = 1.09 and  $\Delta$ MCPR = -0.10. This yields the expected number of rods subject to boiling transition in this bundle to be 0.6 rods. The total number of rods subject to B.T. in the core for this event is 4 rods, and is contributed by some 40 fuel assemblies (MCPR range 1.09 to 1.15) in the vicinity of the center of the core.

To provide an indication of the sensitivity of the rod withdrawal calculation, the results of the analysis for 4, 5 and 6 ft rod withdrawal cases are given in the following table:

Amount Withdrawn (ft)	Limiting MCPR	$\Delta$ MCPR	ENRSBT*	
			Limiting Bundle	Total in the core
4	1.10	-0.09	0.4	3.0
5	1.09	-0.10	0.6	4.0
6	1.03	-0.16	0.8	11.7

\*ENRSBT – Expected number of rods subject to boiling transition.

From these examples it is obvious that the localized events do not lead to large numbers of rods experiencing boiling transition.

**Question 3-5:**

Identify the specific portions of reference 14 which provide a description of the computer program used to calculate the MCPR or change in MCPR following transients.

Since the boiling length is not required in the Hensch-Levy correlation and the calculation of boiling length is not provided in reference 14, provide a description of the calculation of boiling length used in reference 14. Describe the method used to calculate CPR.

**Response:**

Appendix C of reference 14 provides a description of the thermal hydraulic model used to calculate CPR following transients. Although Reference 14 does not discuss the calculation of a boiling length (because it was not required for the Hench-Levy correlation) the addition of a boiling length calculation to the model in no way affects the basic thermal-hydraulic calculations required to be performed whether Hench-Levy or GEXL is applied as a measure of thermal margin. The additional calculations performed with the GEXL correlation are described in detail in documentation of the Appendix K ECCS models. Specifically, "10CFR50, Appendix K Section II, SCAT Code Documentation, Revision 2."

**Question 3-6:**

"Revise the table on page 6-3 titled, "Statistical Result" and the statistical statements made on the top of page 6-5 to reflect the modification to the use of a log-normal distribution."

**Response:**

The use of the arithmetic mean for statistical analyses yields the following.

**Statistical Results**

MCPR	Percent of Rods Expected to Avoid Boiling Transition
1.20	99.9997
1.15	99.9978
1.10	99.974
1.05	99.905

(The following material replaces the last two paragraphs on page 6-4, as well as all at the top of page 6-5 above "6.4 Technical Specifications Safety Limit.")

As described in Appendix IV, each of the trials in the Monte Carlo procedure may be regarded as a possible reactor operating state. The collection of all trials is a sample of the population of all combinations of the variables, distributed about the nominal operating condition. Each trial leads to a sum of the probability contributions of all rods, called the expected number of rods subject to a boiling transition. It is so called because it is the sum of the product of a probability and "1" rod, for each rod. (Each such expected number of rods is not a mean value since the probabilities of rods subject to a boiling transition do not sum to 1.0; that is, they do not form a probability mass function, which is required for the expected number to be a mean.) Thus, a distribution of expected numbers of rods subject to a boiling transition is formed, and it is the relationship between the arithmetic mean of this distribution and the nominal core minimum operating CPR which is used to set the minimum allowable critical power ratio corresponding to the criterion on page 6-3, which requires 99.9% of rods in the core to avoid boiling transition under the worst transient.

For a typical BWR-4 plant operating with its minimum CPR at 1.20 the expected number of rods subject to a boiling transition will have the following properties:

1. The mean expected number of rods subject to a boiling transition is 0.0807. For a plant having 27,440 fuel rods, this corresponds to a mean fraction of rods expected to avoid boiling transition of 99.99959%.
2. Based on the number and variability of the Monte Carlo trials made, 95% confidence limits on the mean expected number of rods subject to a boiling transition are approximately 0 to 0.176.

3. Analysis of the results of the Monte Carlo trials indicates that the expected numbers of rods subject to a boiling transition are approximately log-normally distributed as illustrated for one set of results in Figure 6-4. It is estimated by use of the log-normal distribution that 99.99% of rods will avoid boiling transition with 97.5% probability. (The assumption of log normality is necessary to this derivation).

(Note: This material has been incorporated as indicated above.)

**Question 3-7:**

List the variables which have been eliminated from consideration because they do not contribute significantly to the uncertainty of CPR. Present the results of the sensitivity analyses which form the basis for the elimination of each variable not considered. Discuss all excluded variables including the core inlet flow and temperature distributions between fuel assemblies, fuel assembly orifice area, core bypass flow, fuel rod diameter, bowing and location, "water-rod" flow, process computer calculations.

**Response:**

In general, in the analysis of each measurement and calculational system all identified sources of uncertainty have been allowed to make their contribution, however small. These effects are included in the quoted system uncertainty. In Table 3.7-1 a list of insignificant variables, their uncertainty and their effect on the total nodal power uncertainty, is presented. These variables have been included, although they contribute essentially zero percent increase in uncertainty.

The identified variables are discussed below:

*Core Inlet Flow Distribution.* The core inlet flow distribution is calculated by the process computer and not measured. The uncertainties in the model parameters which introduce errors into the calculated flow distribution (e.g., channel friction factors and flow areas) have been evaluated and are incorporated into the statistical analysis.

The core thermalhydraulic calculation in the process computer is performed with a condition of uniform pressure distribution in the reactor lower plenum. The uniformity of the pressure distribution has been verified experimentally for both one- and two-recirculation-pump operation by tests conducted in Monticello and Quad Cities 1 plants. Thus, no uncertainty associated with the inlet pressure distribution need be included in the statistical analysis. The detailed test results are provided in the following two licensing topical reports:

1. Kim, H. T., "Core Flow Distribution in a Modern Boiling Water Reactor as Measured in Monticello," NEDO-10299, January, 1971.
2. Kim, H. T. and Smith, H. S., "Core Flow Distribution in a General Electric Boiling Water Reactor as Measured in Quad Cities Unit 1," NEDO-10722, December, 1972.

*Core Inlet Temperature Distribution.* The temperature distribution used in the analysis is based on uniform mixing. No sources of temperature maldistribution have been identified in the present design and none have been included in the analysis. In addition, a temperature "Tilt" would introduce a systematic bias which could be either eliminated from the design or evaluated and incorporated into the analysis as a bias not as a random variation. It should be noted that the effect of temperature maldistribution would be to reduce the uniformity of core radial power distribution which in turn results in lower required MCPR.

*Core Bypass Flow.* The core bypass flow uncertainty is regarded as included in the total core flow uncertainty of 2.5%. No additional allowance need be made because core bypass flow is only 10% of total core flow and a very conservative allowance has been made for total core flow uncertainty.

TABLE 3.7-1

Variable	Estimated (1- $\sigma$ ) Uncertainty (%)	Percent Increase in Total Nodal Power Uncertainty
1. Temperature drop of cleaning system coolant	5.0	0.01
2. Control rod drive flow	3.0	0.001
3. Cleanup system flow	3.0	0.0001
4. Recirc pump power	5.0	0.0001
5. Control rod drive inlet temperature	5.0	0.00001
6. Leakage power fraction	5.0	0.010
7. Fraction of core power deposited in the active channel flow by non-convection mechanisms	5.0	0.010

*Process Computer Calculations.* The uncertainties due to process computer miscalculation have been incorporated in the effective TIP error.

*Fuel Assembly Orifice Area.* The uncertainty in the fuel assembly orifice area is that due to the manufacturing tolerance which is  $\pm 0.002$  inch ( $3\sigma$  level) on the diameter. At the  $1\sigma$  level, the orifice diameter uncertainty is  $\pm 0.00067$  inch which yields an orifice loss coefficient uncertainty of 0.21%. The resulting pressure drop uncertainty is 0.02 psi which amounts to less than 0.1% of the total bundle pressure drop. Although this uncertainty is insignificant, it is included in the bundle  $\Delta P$  uncertainty (see question 3-8).

*Fuel Rod Diameter.* The thermal-hydraulic effect of this uncertainty is accounted for in the friction factor and channel flow area uncertainties. The effect on the pin power is small and is present in the  $\gamma$ -scan experiments and accounted for in the local peaking factor uncertainty of 2.6%.

*Bowing and Location.* The effect of rod location in the fuel assembly has been included in the uncertainty in R-factor.

ATLAS tests (16 rod and 64 rod assemblies) conducted for evaluation of the effects of rod bowing on critical power performance show that the rod bowing effect is indeed small. The 16-rod test was conducted with a corner rod bowing toward the channel corner to a minimum clearance of 0.06 inch. The 64-rod test, with 4 rods in the critical interior region, bowed to a minimum clearance of 0.06 inch between each rod. The results of the 16-rod test were presented to an International Meeting on Reactor Heat transfer held at the Kernforschungszentrum Karlsruhe, October 9-11, 1973 by R. T. Lahey, Jr., et al. under the title of "The Effect of Reduced Clearance and Rod Bow on Critical Power in Simulated Nuclear Reactor Rod Bundles."

*"Water-Rod" Flow.* The water-rod flow is 0.5% of the bundle flow and consequently the uncertainty in this variable is negligible.

#### Question 3-8:

In Section IV-3-4 the justification of assigned uncertainty value is incomplete and the following information is required:

- List the components which contribute to the uncertainty in each variable.

- b. Provide the uncertainty of each of these components. Explain how the uncertainty of each component was determined. Justify the values of uncertainty selected. Describe the measurement systems which contribute to the total uncertainty, including the type, range, and accuracy of the sensors, transmitters and signal conditions.
- c. Provide the value of the contribution to the total uncertainty of each variable due to each component. Explain how the contribution to the total uncertainty was calculated.
- d. What portion of the total uncertainty of each variable is an allowance for deterioration in the accuracy of measurement systems during service. Describe the programs which have been established to recalibrate these systems.

**Response:**

Since the publication of the topical report in November, 1973, additional work has been performed to demonstrate the adequacy of the assigned uncertainty values. This work has resulted in minor modifications to some of the values presented in Table IV-1. However, these modifications tend to compensate for each other and are so slight that re-evaluation using all of the new uncertainties resulted in no discernable change to the results of the statistical analyses. (The revised table IV-1 is shown below. Note: This table has been incorporated into Appendix IV.)

Specific answers to questions a, b, c, and d are contained in the following discussion for each of the variables in the revised Table IV-1. Further explanation will be provided in the Process Computer Accuracy Topical Report NEDO 20340 scheduled for submittal to the AEC in July, 1974. (References 24 and 25)

**TABLE IV-1 (Revised)  
DESCRIPTION OF UNCERTAINTIES**

Variable	Standard Deviation % of Point
Feedwater Flow	1.76
Feedwater Temperature	0.76
Reactor Pressure	0.5
Core Inlet Temperature	0.2
Total Core Flow	2.5
Channel Flow Area	3.0
Friction Factor Multiplier	10.0
Channel Friction Multiplier	5.0
TIP Readings	6.3
R-Factor	1.5
Critical Power	3.6

**FEEDWATER FLOW MEASUREMENT**

The attached table lists the error sources which contribute to the total feedwater flow measurement system uncertainty. The first column of numbers shows the estimated or calculated values for the uncertainty contribution of each error source. The uncertainty values for the equipment (items 1, 5, 7, 8, 12) are specified in purchase specification documents. Uncertainty values for items 2 and 4 were obtained from vendor test data. The uncertainty values for the other error sources have been estimated based on industry experience.



The feedwater flow measurement system is shown schematically in Figure 8-1. As can be seen from this figure, it is a temperature compensated system which utilizes a throat tapped feedwater nozzle as the primary element. The flow measuring section consists of a flow straightening section upstream of the nozzle and an additional section downstream of the nozzle. The entire assembly is calibrated before installation in the plant. After the signal from the flow transmitter has been electronically compensated for density effects, the signal is sent to a square rooter to make it proportional to flow and then to the process computer where it is utilized in the calculation of core thermal power.

The contribution of each error source to the total uncertainty of the flow measurement system is shown in the last column of the attached table. Each component contribution was determined by relating the individual uncertainties to the total calculated uncertainty using the equation shown in Table 3.8-1.

Allowance for deterioration of the measurement system is inclusive in the estimated uncertainties, but it has not been determined as a separate item. The various electronic devices are calibrated periodically and a special radio-chemistry test can be performed to recalibrate the flow nozzle.

**FEEDWATER TEMPERATURE MEASUREMENT**

The feedwater temperature measurement system consists of an RTD element and a transmitter with the signal going directly to the process computer. The uncertainty values used for the feedwater flow temperature compensating system are also used for this system (Table 3.8-1, items #4, 5, 6, 7). The total temperature uncertainty is found by use of the following equation:

$$\text{Total Uncertainty} = \left[ \frac{1}{\text{No. of feedwater lines}} (\text{Random Uncertainties})^2 + (\text{Biased Uncertainties})^2 \right]^{1/2}$$

$$\text{Total Uncertainty} = \left\{ \frac{1}{2} [(\#5)^2 + (\#6)^2 + (\#7)^2] + (\#4)^2 \right\}^{1/2}$$

$$= \left\{ \frac{1}{2} [(0.19)^2 + (1.0)^2 + (0.25)^2] + (0.15)^2 \right\}^{1/2}$$

$$= \pm 0.76\%$$

**PRESSURE MEASUREMENT SYSTEM**

The pressure measurement system uses a bourdon tube type force balance transmitter which converts pressure to a milliamp D.C. signal. This signal is transmitted to the control room panel where a resistor in the panel converts the milliamp signal to a millivolt signal for the process computer.

These sources of uncertainty in the pressure measurement system, the estimated uncertainty of each, and the contribution of each are shown in the following table.

Error Source	Estimated Input Uncertainty (%)	Contribution to System Uncertainty
1. Transmitter accuracy	0.47	0.972
2. Resistor accuracy	0.08	0.028

$$\text{Total Pressure Uncertainty} = [(\#1)^2 + (\#2)^2]^{1/2}$$

$$\text{Total Pressure Uncertainty} = [(0.47)^2 + (0.08)^2]^{1/2}$$

$$\text{Total Pressure Uncertainty} = \pm 0.48\%$$

The total pressure uncertainty of 0.48% can be maintained by monthly calibration of the pressure transmitter. The estimated input uncertainties are calculated from manufacturers test data and are quite conservative. Later model BWR/4, 5 and 6 reactors have improved systems which can provide a system accuracy of about  $\pm 0.3\%$  over a six month calibration period.

*Core Inlet Subcooling.* The core inlet subcooling is calculated in the process computer (PC) using the relation

$$\Delta h_o = \frac{W_{FW}}{W_T} (H_F - H_{FW}) - F_{CU} H_{FG} + \frac{W_{CR}}{W_T} (H_F - H_{CR}) + \frac{Q_{CU}}{W_T} - \frac{Q_p}{W_T} C \quad (8-1)$$

where

$W_{FW}$  = Feedwater Flow

$W_T$  = Total Core Flow

$W_{CR}$  = Control Rod Drive System Flow

$H_F$  = Saturated Liquid Enthalpy

$H_{FW}$  = Feedwater Enthalpy

$H_{FG}$  = Difference between Saturated Steam and Liquid Enthalpy

$F_{CU}$  = Steam Carryunder Fraction

$Q_{CU}$  = Heat Loss in Cleanup System

$Q_p$  = Recirc Pump Power

$C$  = 3.413 MBUT/hr-MW

The relative effect of the uncertainties in these variables on the subcooling,  $\Delta h_o$ , has been determined. Based on the uncertainties listed in Table 3.8-2 the relative contributions to the total uncertainty in  $\Delta h_o$  is: core pressure - 4%, core flow - 59%, feedwater flow - 22%, feedwater temperature - 11%, and steam carry-under fraction - 3%. The remaining variables contribute less than 1% to the total core inlet subcooling uncertainty. The total uncertainty in the core inlet temperature due to all these component uncertainties has been determined to be less than 0.2%.

## CORE FLOW MEASUREMENT UNCERTAINTY

### Summary:

The results of statistical studies establish that the core flow measurement system is capable of a 1 sigma accuracy of 2.0% of rated core flow after calibration. The uncertainty is summarized as follows:

$$\begin{aligned} \sigma^2_{\text{core flow}} &= (1.93\%)^2_{\text{systematic}} + (0.58\%)^2_{\text{rand}} \\ &= (2.02\%)^2 \end{aligned}$$

Due to the nature of the system, the accuracy will be maintained below the 2.5% used in the statistical analyses by routine checking of the instrumentation and periodic in-reactor recalibration of the system if necessary.

**Description of System:**

On a typical jet pump BWR, the total core flow passes through 20 jet pump diffusers. Each diffuser is instrumented such that flow through each jet pump can be measured. The core flow measurement system instrumentation is shown in Figure 3.8-2.

All of the jet pumps are provided with a single diffuser tap and associated diffuser-to-plenum (single-tap)  $\Delta P$  instrumentation. In addition, four of the jet pumps are provided with another diffuser tap and associated diffuser-to-diffuser (double tap)  $\Delta P$  instrumentation. The double-tap diffusers are calibrated prior to installation, and calibration constants (KCALIBs) are developed which relate the diffuser flow to double-tap  $\Delta P$ . The single-tap instrumentation KCALIB will be calculated using the double tapped jet pump flows (found from the double tap instrumentation) and the associated single-tap  $\Delta P$  for those pumps. This KCALIB will then be used to calibrate all the single-tap instrumentation so that the loop flow indicators and core flow recorder read correctly.

**Contributions to Uncertainty:**

Figure 3.8-3 provides a schematic representation of the potential error sources in the jet pump core flow measurement system.

Flow through each double-tap jet pump is measured using the following formula:

$$W_{DT} = \sqrt{\frac{\Delta P_{DT} \rho C}{K_{DT}}} = \text{also } \sqrt{\frac{\Delta P_{ST} \rho C}{K_{ST}}} \tag{1}$$

where:

$W_{DT}$  = flow through the double-tap jet pump

$\Delta P_{DT}$  = double tap differential pressure

$\Delta P_{ST}$  = single tap differential pressure

$K_{DT}$  = double tapped calibration coefficient (KCALIB) dependent on M ratio\* and weakly on pump drive flow

$K_{ST}$  = single tapped KCALIB determined from in-reactor calibration

$\rho$  = density

C = constant

The average  $K_{ST}$  for the 4 double-tap jet pumps is then calculated and applied to all 20 jet pumps. During in-reactor calibration of the single tap KCALIB, random uncertainty will arise from  $\Delta P$  measurement and random uncertainty of the double-tap calibration coefficients. During the calibration systematic uncertainties arise in the double-tap calibration coefficients, drive flow measurement, jet pump sampling uncertainty and density measurement.

Considering these factors, it can be shown that the uncertainty on the flow through a single-tap jet pump can be expressed as:

$$\sigma^2 W_{ST} = \frac{1}{4} (\sigma^2 \Delta P)_{RAND} + \frac{1}{4} \left( \sigma_{\rho}^2 + \sigma^2 K_{DT} + \sigma^2_{df} + \sigma^2_{sampling} + \frac{1}{2} \sigma^2_{\Delta P} \right)_{SYS} \tag{8-2}$$

\* M ratio =  $\frac{\text{jet pump suction flow}}{\text{jet pump drive flow}}$

where:

- $\sigma^2_{W_{ST}}$  = variance in one single-tap jet pump flow
- $\sigma^2_{\Delta P}$  = variance in  $\Delta P$  measurement
- $\sigma^2_{\rho}$  = variance in density measurement
- $\sigma^2_{K_{DT}}$  = variance of the four double-tap jet pump calibration coefficients
- $\sigma^2_{df}$  = effect of uncertainty in M ratio (drive flow measurement) on the double-tap calibration coefficients
- $\sigma^2_{\text{sampling}}$  = variance of the means of a sample of 4 jet pump KCALIB's about the true jet pump population mean.

#### Variance in $\Delta P$ Measurement

$$\sigma^2_{\Delta P} = (2.0\%)^2$$

The  $\Delta P$  transmitters used in the system are commonly GE/MAC series 555 or comparable quality, with a rated accuracy of  $\pm 0.4\%$  of span (assumed to be  $2\sigma$  accuracy). At rated core flow, the reading will be  $\sim 44\%$  of span. Studies of reactor measurement variability show human reading variability of about 1.1% of transmitter output.

therefore:

$$\sigma^2_{\Delta P} = \left(\frac{0.2}{0.44}\%\right)^2 + (1.1)^2 = (1.2\%)^2$$

$\Delta P$  accuracy has been set at 2.0% for a conservative allowance for instrument degradation and human error.

#### Variance in Density ( $\rho$ ) Measurement

$$\sigma^2_{\rho} = (0.28\%)^2$$

this allows for a temperature variance of  $(2 \text{ } 1/2^\circ \text{ F})^2$ , which is easy to achieve and maintain.

#### Variance of the Four Double-Tap Jet Pump Calibration Coefficients

$$\sigma^2_{K_{DT}} = (3.05\%)^2$$

This variance combines the effects of the systematic and random uncertainties of the four double-tap jet pump calibration coefficients. The systematic uncertainty arises from the fact that all four jet pumps are calibrated in the same test facilities; the random uncertainty is from random calibration test uncertainty.

#### Effect of Uncertainty in M Ratio on Jet Pump Calibration Coefficients

$$\sigma^2_{df} = (1.40\%)^2$$

This term allows for uncertainty in M ratio and drive flow, which affect the double-tap calibration coefficients to a certain degree. The uncertainty in drive flow measurement is assumed to be 3.0%, and its effect is based on a conservative value of the sensitivity of the double-tap calibration coefficients to M ratio and drive flow.

**Variance in Jet Pump Sampling**

$$\sigma^2_{\text{sampling}} = \frac{1}{4} (\sigma_{\text{population}})^2 \frac{24-4}{24-1}$$

↙ number of calibrated jet pumps
↙ max. number of jet pumps in a plant

$$= 0.2174(2.6\%)^2$$

$$= (1.21\%)^2$$

$\sigma^2_{\text{population}} = (2.6\%)^2$  was derived from the variability of calibration test results of over 80 production jet pumps.

**Flow Uncertainty Calculation:**

The flow uncertainty for one jet pump is calculated as follows:

$$\sigma^2_{W_{ST}} = \frac{1}{4} (\sigma^2_{\Delta P})_{\text{RAND}} + \frac{1}{4} (\sigma^2_{\rho} + \sigma^2_{K_{DT}} + \sigma^2_{df} + \sigma^2_{\text{sampling}} + \frac{1}{2} \sigma^2_{\Delta P})_{\text{SYS}} \tag{8-2}$$

$$= \frac{1}{4} (2.0^2)_{\text{RAND}} + \frac{1}{4} (0.28^2 + 3.05^2 + 1.40^2 + 1.21^2 + \frac{1}{2} (2.0)^2)_{\text{SYS}}$$

$$= (1\%)^2_{\text{RAND}} + (1.93\%)^2_{\text{SYS}}$$

In the BWR/5 and BWR/6 plants in which the 20 jet pump flow signals are input to the process computer:

$$\sigma^2_{\text{core flow}} = \frac{1}{20} (1\%)^2_{\text{RAND}} + (1.93)$$

$$\sigma^2_{\text{core flow}} = \frac{1}{20} (1\%)^2_{\text{RAND}} + (1.93)^2_{\text{SYS}}$$

$$= (0.22\%)^2_{\text{RAND}} + (1.93)^2_{\text{SYS}}$$

$$\sigma^2_{\text{core flow}} = (1.94\%)^2$$

In earlier product lines, the flow signals from the jet pumps must pass through the square rooters and summers before being input to the process computer. The square rooters (typically GE/MAC type 565) and summers (typically GE/MAC type 563) have rated accuracies of  $\pm 0.5\%$  (assumed 2 sigma) of span. Summing the flow signals will reduce the random flow uncertainty, but at every stage, some additional uncertainty is added due to random instrument error. When this analysis is made:

$$\sigma^2_{\text{core flow}} = (0.58\%)^2_{\text{RAND}} + (1.93\%)^2_{\text{SYS}}$$

$$\sigma^2_{\text{core flow}} = (2.02\%)^2$$

**Maintenance of System Accuracy:**

Instrument accuracy is maintained by routine surveillance and periodic calibration checks of the instruments. Those systems with jet pump pressure transmitter signal input to the process computer will be easily maintained at the calibration level of uncertainty with only routine in-place checks of the pressure transmitters.

This flow measurement system measures pressure *rise* across the jet pump diffusers. Possible changes to the diffusers (such as degradation of surface finish) create increased pressure *drops*. The result will be measurement *under-prediction* of core flow, which is conservative.

**CHANNEL FLOW AREA UNCERTAINTY**

The channel flow area uncertainty used in the statistical analyses has been conservatively set at 3%. The use of this value is justified by evaluations of its components (manufacturing and service induced variations).

The manufacturing tolerance on channel width and depth is  $\pm 0.010$  inch ( $3\sigma$  level), resulting in a flow area change of  $0.133 \text{ in}^2$ . At the  $1\sigma$  level, the area uncertainty of  $0.133/3 \text{ in}^2 = 0.044 \text{ in}^2$ .

The manufacturing tolerance on the fuel rod diameter at the  $1\sigma$  level is 0.0025 inch, yielding a flow area uncertainty of  $0.124 \text{ in}^2$ .

The service induced variation is due to corrosion product deposition on fuel rods. For a 7x7 fuel assembly with 7.7 GWD/T exposure, the average corrosion product deposition has been recently measured as 5.22 mg per  $\text{cm}^2$  of surface area. Previous measurements indicated that the deposits have a density 1/3 that of iron, resulting in a calculated deposit thickness of 0.000779 inch. Assigning a 33% uncertainty to this value, results in a flow area uncertainty for an 8x8 assembly due to corrosion product deposition of  $0.0257 \text{ in}^2$ .

Combining these uncertainties results in a flow area uncertainty of  $0.1341 \text{ in}^2$  or 0.88%, which demonstrates that the 3% value used in the analyses is indeed conservative.

**FRICITION FACTOR MULTIPLIER**

The friction factor multiplier has been assigned a conservative uncertainty value (10%). This uncertainty was described in NEDO-10958 as representing only two-phase friction losses. This description is not appropriate because as used in the statistical model, it accounts for the uncertainty in correlating all of the bundle single and two-phase irreversible pressure losses. Pressure drop measurements on full scale assemblies (7x7 and 8x8) over a pressure range of 800 to 1400 psia demonstrate a prediction versus measured  $1\sigma$  uncertainty of less than 5.1%. Figure 3.8-4 is a typical comparison of prediction versus measured pressure drop.

**CHANNEL FRICTION FACTOR MULTIPLIER**

In addition to the friction factor multiplier uncertainty (10%), a channel-to-channel uncertainty of 5% is employed to simulate the effects of nonuniform corrosion product deposition. Changes in friction factors and local losses with variations in corrosion product deposition exhibit a linear relationship. Applying the 33% uncertainty in the corrosion product deposition thickness (see Channel Flow Area Uncertainty), to friction and local losses, results in an additional pressure drop uncertainty of 2.95% (1.89% due to friction and 2.26% due to local losses). The 5% value used in the statistical analyses is thus conservative because not only does it exceed the uncertainty due to corrosion product deposition, but it is applied in addition to the 10% conservative uncertainty in the Friction Factor Multiplier.

**TIP Readings**

See NEDO 20340 (References 24 and 25)

**R-Factor**

See NEDO 10958 and Question 3-8e.

**Critical Power**

See NEDO 10958 Section 5.2.

**Question 3-8e:**

In the determination of the uncertainty in the R-factor, explain why the listed components do not include Gd concentration, rod bowing and the uncertainty in the linear approximation of R shown in Figure IV-1. Justify the assumption that the local relative rod powers,  $r$ , are independent. Show how the expressions  $S_R = S_r/3$  and  $S_R = S_r/2$  are derived. Describe how the 2.6% uncertainty in the calculation of rod relative powers was determined.

**Response:**

The components of the uncertainty in R include both Gd concentration and rod bowing. Rod bowing is listed as the fourth entry in Table IV-2 with the clarifying footnote: "Lateral movement permitted by spacer." The gadolinia concentration variation contribution is negligible. Concentration changes of the order of 0.5 wt% would affect the high powered (non-gadolinia bearing) rods by approximately 0.1% or less in local peaking factors. Such effects are regarded as included in the calculational uncertainty, 2.6%. This value is a result of comparisons between calculated and measured rod relative powers, including some assemblies which employed gadolinia control augmentation. The comparisons also included assemblies adjacent to boron steel curtains in which the effects of variations in boron content and curtain position are somewhat larger than those associated with gadolinia concentration variations.

Examination of a wide variety of fuel designs has indicated that the linear approximation is generally conservative. Typical cases are shown in Figures 3.8-5 and 3.8-6. The example case presented in the topical report is atypical in that some of the actual R-factors for this case lie above the linear approximation. However, in order to assure that this portion of the calculation is never nonconservative the linear approximation will be adjusted as required to assure that the actual R-factor distribution is below the line employed in the statistical calculation.\* Thus, no uncertainty need be included for this portion of the calculation.

The derived uncertainty in R did not make use of an assumption of independence of the individual rod power factors. In fact, for conservatism, the strongest kind of dependence and correlation was used; i.e., it was assumed that the values of  $r_i$  employed in calculating a particular R were all equal. To clarify, consider the following derivations:

**Case 1**

$$R = \sum_{i=1}^n a_i \sqrt{r_i}$$

$$r_1 = r_2 = \dots = r_n \text{ assumption of dependence (equality)}$$

$$\text{Let } r_n = r \text{ and } \sum_{i=1}^n a_i = A$$

$$R = \sqrt{r} \sum_{i=1}^n a_i = A \sqrt{r}$$

$$\frac{\Delta R}{R} = \frac{1}{R} \frac{\partial R}{\partial r} \Delta r$$

$$\frac{\Delta R}{R} = \frac{1}{R} \frac{A}{2\sqrt{r}} \Delta r = \frac{1}{A\sqrt{r}} \cdot \frac{A}{2\sqrt{r}} \Delta r = \frac{1}{2} \frac{\Delta r}{r}$$

\*(Note: Therefore, Figure IV-1 and associated text have been deleted, see response for Question 1-18 for deleted figure.)

This illustrates the procedure resulting in the factor 1/2 which was employed in deriving the standard deviation of the R-factor. The same conclusions would have been reached had the  $r_i$  values been assumed proportional,  $r_i = c_i r$ , for example.

**Case 2**

This case illustrates the effect of the alternate limiting assumptions; i.e., that the  $r_i$  are completely independent.

$$R = \sum_{i=1}^n a_i \sqrt{r_i} \quad \text{as in Case 1}$$

$$\frac{\Delta R}{R} = \frac{1}{R} \left[ \sum_{i=1}^n \left( \frac{\partial R}{\partial r_i} \Delta r_i \right)^2 \right]^{1/2}, \quad \text{the conventional "statistical" combination approach}$$

$$\frac{\Delta R}{R} = \frac{1}{R} \left[ \sum_{i=1}^n \left( \frac{a_i}{2\sqrt{r_i}} \Delta r_i \right)^2 \right]^{1/2}$$

$$\frac{\Delta R}{R} = \frac{1}{R} \left[ \sum_{i=1}^n \left( \frac{a_i \sqrt{r_i}}{2} \frac{\Delta r_i}{r_i} \right)^2 \right]^{1/2} \quad \text{Assuming that } \frac{\Delta r_i}{r_i} = \text{a constant, } \frac{\Delta r}{r}$$

$$\frac{\Delta R}{R} = \frac{1}{2R} \left[ \sum_{i=1}^n (a_i \sqrt{r_i})^2 \right]^{1/2} \frac{\Delta r}{r}$$

or

$$\frac{\Delta R}{R} = \left[ \frac{\left( \sum_{i=1}^n (a_i \sqrt{r_i})^2 \right)^{1/2}}{\sum_{i=1}^n a_i \sqrt{r_i}} \right] \frac{1}{2} \frac{\Delta r}{r}$$

At this point, the similarity to the Case 1 result can be studied. In fact,  $\Delta R/R$  in this case differs from Case 1 only by the factor in brackets. From here on, the conclusion depends on the specific values of  $a_i$  and  $r_i$ . The reader is referred to the proprietary supplement for typical values. For the cases of interest,

$$0 < a_i \sqrt{r_i} < 1.0$$

$$\text{and } \sum_{i=1}^n a_i \sqrt{r_i} = R > 1$$



Consequently,

$$(a_i \sqrt{r_i})^2 < a_i \sqrt{r_i}$$

$$\sum_{i=1}^n (a_i \sqrt{r_i})^2 < \sum_{i=1}^n a_i \sqrt{r_i}$$

and

$$\left[ \sum_{i=1}^n (a_i \sqrt{r_i})^2 \right]^{1/2} < \sum_{i=1}^n a_i \sqrt{r_i}$$

Finally,

$$\frac{\Delta R}{R} = b \frac{\Delta r}{r}, \text{ where } b < \frac{1}{2}$$

In one example checked  $b \approx \frac{1}{3}$

However, the reader can appreciate the difficulty of generalizing this approach to incorporate the correct independence of the  $r_i$  to arrive at an appropriate value  $b < 1/2$ . Consequently, the approach has been abandoned and the more easily defended derivation of Case 1 was applied.

The final section of the question related to the determination of the 2.6% uncertainty in rod relative powers. This subject is presented in Section II.1.3.1, II.1.3.2, II.1.3.3, and II.1.3.4, of Appendix 4a of GESSAR. The referenced sections present detailed results of experiments with corresponding comparison to calculation. The value, 2.6% is presented at the end of Table 1 of II.1.3.4.

**Question 3-8f:**

In the determination of the uncertainty in the TIP reading, explain how the uncertainty in each component (random noise, geometrical LPRM and calculational) was determined. How is the 4.3% uncertainty in the LPRM-extrapolated TIP signal derived from the 2.6% uncertainty in the TIP signal and the 2.4% uncertainty in the LPRM signal?

**Response:**

*TIP Random Noise.* The random noise component of the TIP uncertainty has been determined by comparing TIP traces taken through the common TIP location during a period when the neutron flux was essentially constant. If  $t(i,j)$  represents the TIP signal recorded by the  $i$ -th detector at axial node  $j$ , then the statistical variation in the TIP signal is given by

$$\sigma^2 = \frac{1}{N} \sum_{i,j} \left( t(i,j) - \frac{1}{n} \sum_{i=1}^n t(i,j) \right)^2 \tag{2}$$

This expression has been evaluated for operating TIP data and found to be  $\approx 1.7\%$ .

The PC effective readings, for a typical 6-inch segment, are constructed by averaging the neighboring *point* TIP values since the point TIP noise is uncorrelated, this averaging procedure results in a reduction of the random TIP uncertainty. For pre-Brown's Ferry-1 plants the weighting coefficients are (1/6 2/3 3/6) and result in a reduction of  $1/\sqrt{2}$ . For BF-1 and later plants seven point values are averaged and a reduction of  $1/\sqrt{7}$  is realized. Consequently

the noise uncertainty in the early plants is  $\sim 1.2\%$  and  $\sim 0.65\%$  for post BF-1 plants. Since the uncertainty is small relative to other TIP related uncertainties its *net* effect is even smaller and the larger value of 1.2% is used.

*TIP Geometrical Uncertainty.* The TIP geometrical uncertainty has been determined by comparing TIP signals from symmetric core locations. These detector signals should be the same but because of random noise in the TIP signals and mislocation of the TIP detectors relative to their nominal design locations in the gap, the TIP signals will actually differ. Since the geometrical and random noise variation for the two TIPs are uncorrelated, the total statistical variation in the TIP ratio,  $T_1/T_2$ , may be written

$$\begin{aligned} \sigma^2_{T_1/T_2} &= \frac{\partial (T_1/T_2) \sigma (T_1)^2}{\partial T_1} + \frac{\partial (T_1/T_2) \sigma (T_2)^2}{\partial T_2} \\ &= \frac{T_1}{T_2} \frac{2}{T_1} \frac{\sigma_G(T_1)^2}{T_1^2} + \frac{\sigma_G(T_2)^2}{T_2^2} + \frac{\sigma_R(T_1)^2}{T_1^2} + \frac{\sigma_R(T_2)^2}{T_2^2} \end{aligned} \quad (3)$$

where the variation in signal  $i$ ,  $\sigma (T_i)$ , is the statistical superposition of the random noise,  $\sigma_R (T_i)$  and geometrical variation  $\sigma_G (T_i)$

$$\sigma (T_i)^2 = \sigma_R (T_i)^2 + \sigma_G (T_i)^2 \quad (4)$$

$T_i$  is the average of all detector  $i$  TIP signals at the axial node under consideration. The total TIP ratio variation,  $\sigma (T_1/T_2)$ , and the random variation,  $\sigma_R (T_i)$ , have been evaluated from operating TIP data. Assuming the geometrical variation is the same for both TIPs, equation (3) may be solved for the geometrical TIP uncertainty to yield

$$\sigma_G (T_i) = \sigma_G (T_2) = 2.3\%. \quad (5)$$

*Calculational TIP Uncertainty.* See NEDO 20340.

*LPRM-Update Uncertainty* The sources of uncertainty that enter into the LPRM-update of the base TIP profile are 1) the LPRM signal uncertainty and 2) the axial interpolation of the LPRM-TIP correction. The significant sources of detector error have been determined and in Table 3.8-3 estimates of these uncertainties and their bases are presented. These estimates are based on a *maximum* decay period equal to the typical 30 day calibration interval and a *maximum* power change of 15% (the PC demands a new TIP trade after a  $\sim 15\%$  local power change).

Since the LPRM is equipped with a high frequency filter, random noise uncertainty does not enter. These uncertainties combine to yield an overall detector uncertainty of 1.3%. The more conservative value of 3% was used.

The TIP-update or correction is determined at the 4 LPRM locations by the change in the LPRM. Since the initial LPRM reading is set proportional to the base TIP value the only additional uncertainty introduced at these locations is the detector uncertainty of  $\sim 3\%$ . At the axial locations between the LPRMs the TIP-update is determined by a 6th order axial interpolation. Based on the maximum 15% power change and an interpolation that is good to 10% ( $1 - \sigma$ ) the resulting additional error is 1.5%. Combining this with the 3.0% detector error results in a 3.4% combines with the base TIP of 2.6% to yield an overall LPRM-extrapolated TIP uncertainty of 4.3%.

#### Question 3-8g:

"Since some of the variables are correlated (e.g., flow, power and quality) justify the assumption that they are independent. If the variables are not independent how can the probability of boiling transition in a bundle or the core be determined from the probabilities of boiling transition of individual rods?"

**Response:**

The standard deviations shown in Table IV-1 of NEDO-10958 are those of normal distributions of true values of each variable about observed, measured or calculated values. These standard deviations are error values. Accordingly, as to whether a random value from one is independent of a random value from another, it must only be asked, "Does knowledge of the magnitude of error in variable 1 in a fuel rod improve the knowledge about the magnitude of error in variable 2 in that fuel rod?" If the answer is, "No," then errors in variable 1 are independent of errors in variable 2, and—in this context—that is a more exact statement of the more familiar, "Variable 1 is assumed to be independent of variable 2." Strictly speaking, that statement may not be true at all, due to a functional relationship between variables 1 and 2; it is the errors which we are concerned with.

All of the errors in Table IV-1 are independent with the exception of that for core inlet temperature which is a function of core flow, feedwater flow and feedwater temperature. The magnitude of uncertainty in core inlet temperature is derived from uncertainties in these variables as presented in the response to Question 3-8, parts a, b, c, d. Core inlet temperature (or subcooling,  $\Delta h_o$ ) enters the calculation of number of rods subject to boiling transition by its effect on bundle quality. Of the three variables affecting uncertainty in  $\Delta h_o$ , total core flow is dominant and appears with  $\Delta h_o$  in the expression for bundle quality. Therefore, concern for independence between the variables reduces to concern for independence between total core flow,  $W_T$ , and inlet temperature (or inlet subcooling,  $\Delta h_o$ ). It can be shown that

$$X = \frac{KQ}{h_{fg} W_T} - \frac{\Delta h_o}{h_{fg}} \quad (1)$$

where:  $Q$  = bundle power,

$h_{fg}$  = latent heat of vaporization,

$K$  = ratio of total core flow to bundle flow, and

$X$  = bundle quality.

Further from the reply to parts a, b, c, and d,  $\Delta h_o$  is inversely proportional to  $W_T$ . Therefore, in reality, reductions in core flow produce increases in quality which are always somewhat less than given by the change in the first term in equation 1. Because  $W_T$  and  $\Delta h_o$  are assumed to be independent in the Monte Carlo process, in this case only half of the trials which experience core flow reduction will experience the realistic behavior. The other half will experience quality increases somewhat larger than realistic, which of course, is conservative. Random increases in core flow in the Monte Carlo process obviously produce the reverse trend. However, the conservatism introduced in the trials with core flow reduction will obviously outweigh the non-conservatism in trials with core flow increase due to the dominant influence of the first term in equation 1). That is, the overpredictions of quality will occur for cases with high quality and the underpredictions will occur for cases with low quality. Ignoring the analysis momentarily, the effect is easily understood by simply recognizing that due to the functional relationship between the variables, greater variability is introduced into bundle quality by the assumption of independence than actually exists. Therefore, it can be concluded that the present method is conservative.

TABLE 3.8-1  
FEEDWATER FLOW MEASUREMENT SYSTEM ERROR SOURCES

Error Sources	Estimated Input Uncertainty (%)	Contribution to System Flow Uncertainty
1. Flow Element Calibration	1.0	0.086
2. Pressure Transmitter	0.3	0.004
3. Pressure Fluctuation	1.5	0.097
4. Thermocouple Calibration	0.15	0.002
5. Temperature Element	0.19	0.002
6. Temperature Fluctuation	1.0	0.043
7. mV/I Transmitter	0.25	0.003
8. Divider	0.25	0.003
9. Pressure Effect on Density	0.05	0.000
10. Manufacturing of Flow Element	0.41	0.029
11. Feedwater Line Differences	0.20	0.007
12. Square Rooter	0.47	0.038
13. Computer Summer	0.05	0.001
14. Human Error	2.0	0.687
		~ 1.000

Total System Flow Uncertainty =



$$\left[ \frac{1}{\text{No. of feedwater lines}} (\text{Random Uncertainties})^2 + (\text{Biased Uncertainties})^2 \right]^{1/2}$$

Total System Flow Uncertainty =

$$\left\{ \frac{1}{2} \left[ \frac{1}{4} (\text{No. } 2^2 + \text{No. } 3^2 + \text{No. } 5^2 + \text{No. } 6^2 + \text{No. } 7^2 + \text{No. } 8^2 + \text{No. } 9^2 + (\text{No. } 10)^2 + (\text{No. } 11)^2 + (\text{No. } 12)^2 + (\text{No. } 14)^2 \right] + \frac{1}{4} (\text{No. } 1)^2 + \frac{1}{4} (\text{No. } 4)^2 + (\text{No. } 13)^2 \right\}^{1/2} = \pm 1.71\%$$

where: Flow uncertainty =  $\left[ \frac{1}{4} (\Delta P \text{ uncertainty})^2 \right]^{1/2}$

**TABLE 3.8-2  
UNCERTAINTIES CONTRIBUTING TO CORE INLET TEMPERATURE UNCERTAINTY**

Variable	% Variable Uncertainty	Basis
$W_T$	2.5	In Text  Engineering Judgment 
$W_{FW}$	1.76	
Pressure	0.5	
$H_{FW}$	0.76	
$F_{CU}$	10.0	
$W_{CR}$	5.0	
$H_{CR}$	0.75	
$W_{CU}$	2.0	
$Q_p$	2.0	
$Q_{CU}$	1.0	

**TABLE 3.8-3  
LPRM DETECTOR UNCERTAINTIES**

Source	Uncertainty (%)	Basis
1. Detector and cable non-linearity	1.1	Chamber and cable non-linearity specs and a 15% power change. Typical of 5 cases analyzed.
2. Error in PC representation of detector sensitivity decay.	0.5	Detector sensitivity loss is $\leq 5\%$ during 30 day calibration period. 10% assumed miscalculation.
3. LPRM amplifier drift and non-linearity	0.4	LPRM amplifier spec.
<b>TOTAL</b>	<b>1.3</b>	

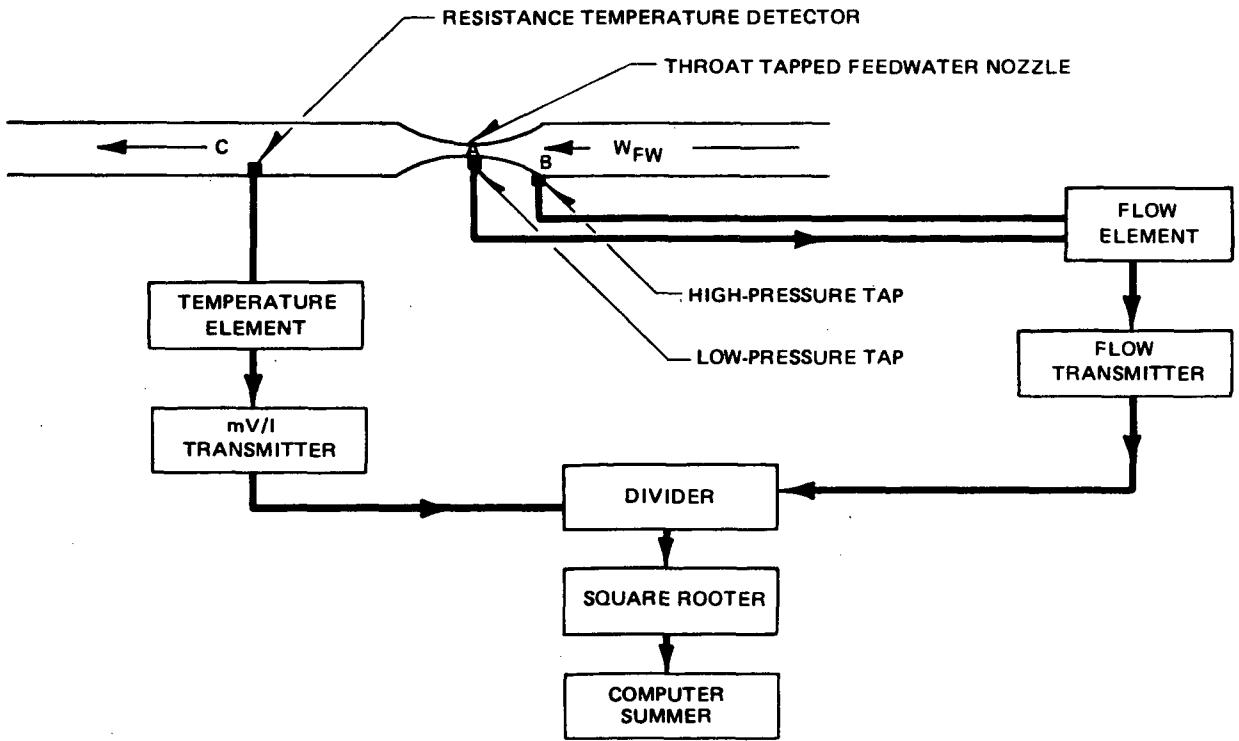
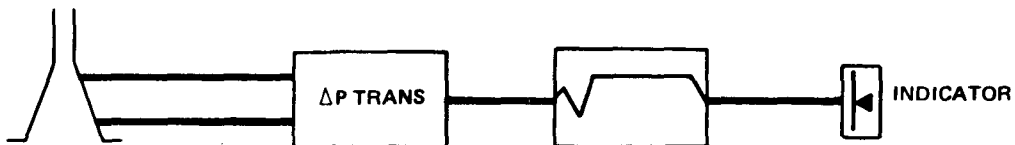


Figure 3.8-1 Feedwater Flow Measurement System

JET PUMP FLOW INSTRUMENTATION

A. DOUBLE TAP

TYPICAL OF JET PUMPS 1, 6, 11, AND 16



B. SINGLE TAP

[CORE FLOW MEASUREMENT SYSTEM]

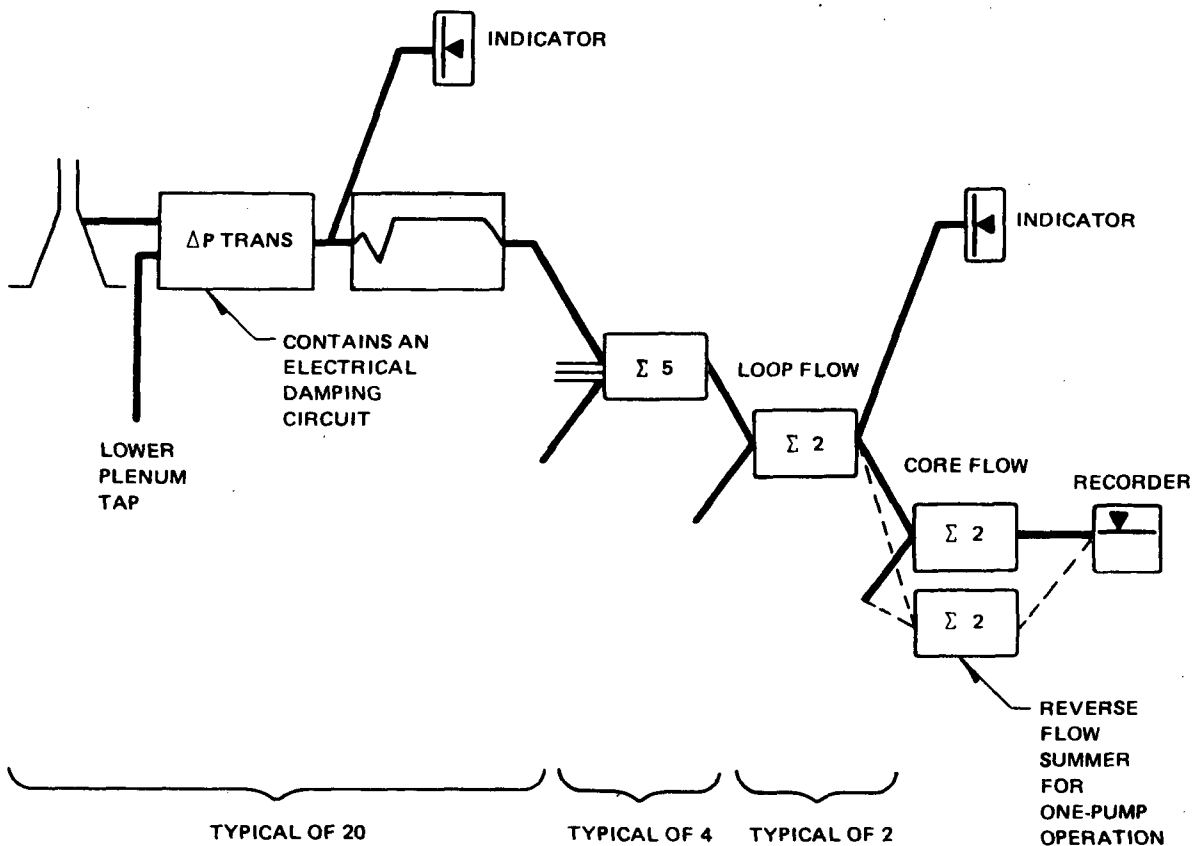


Figure 3.8-2 Recirculation System Flow Instrumentation

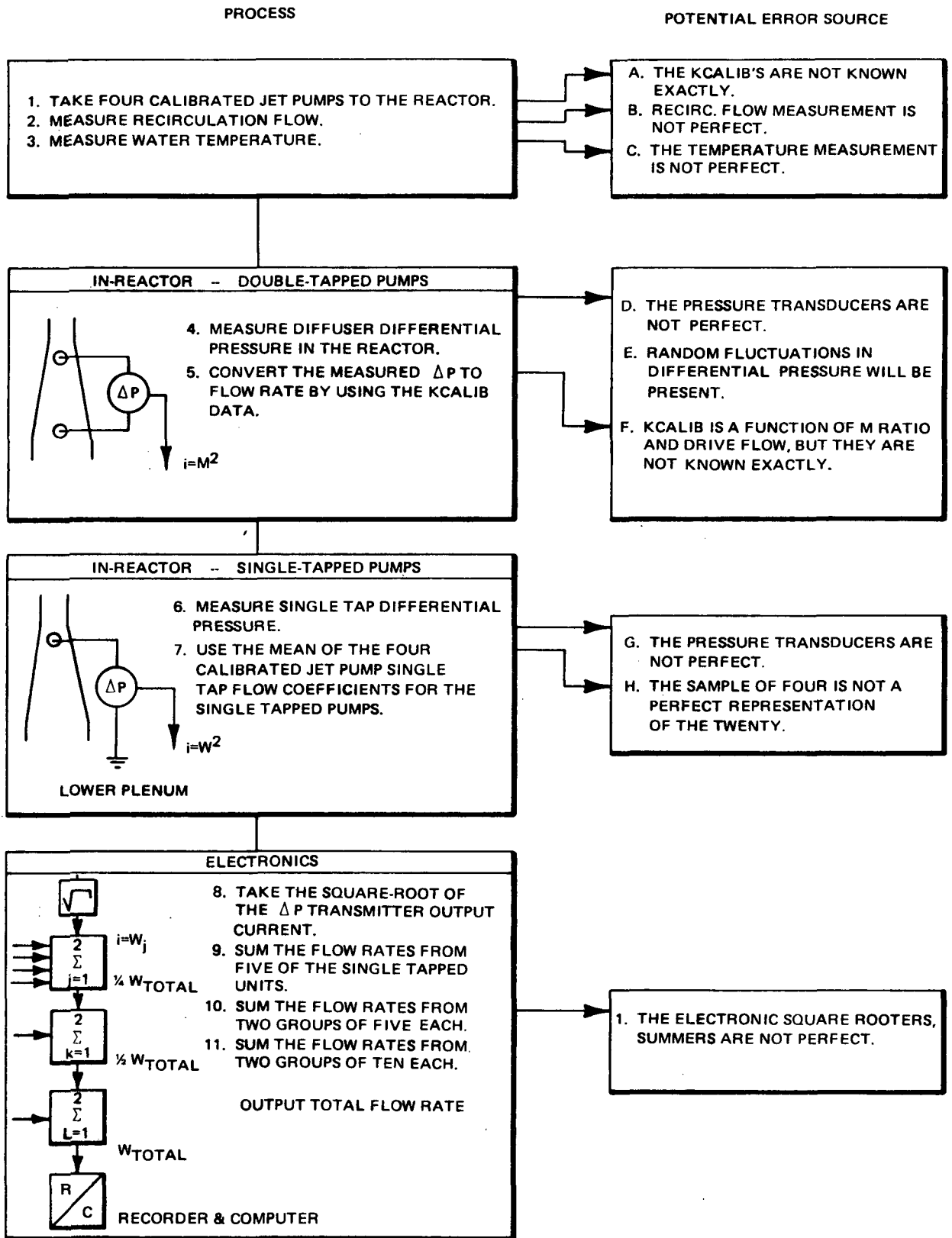


Figure 3.8-3 Schematic Representation of the Potential Error Sources in the Jet Pump Core Flow Measurement System



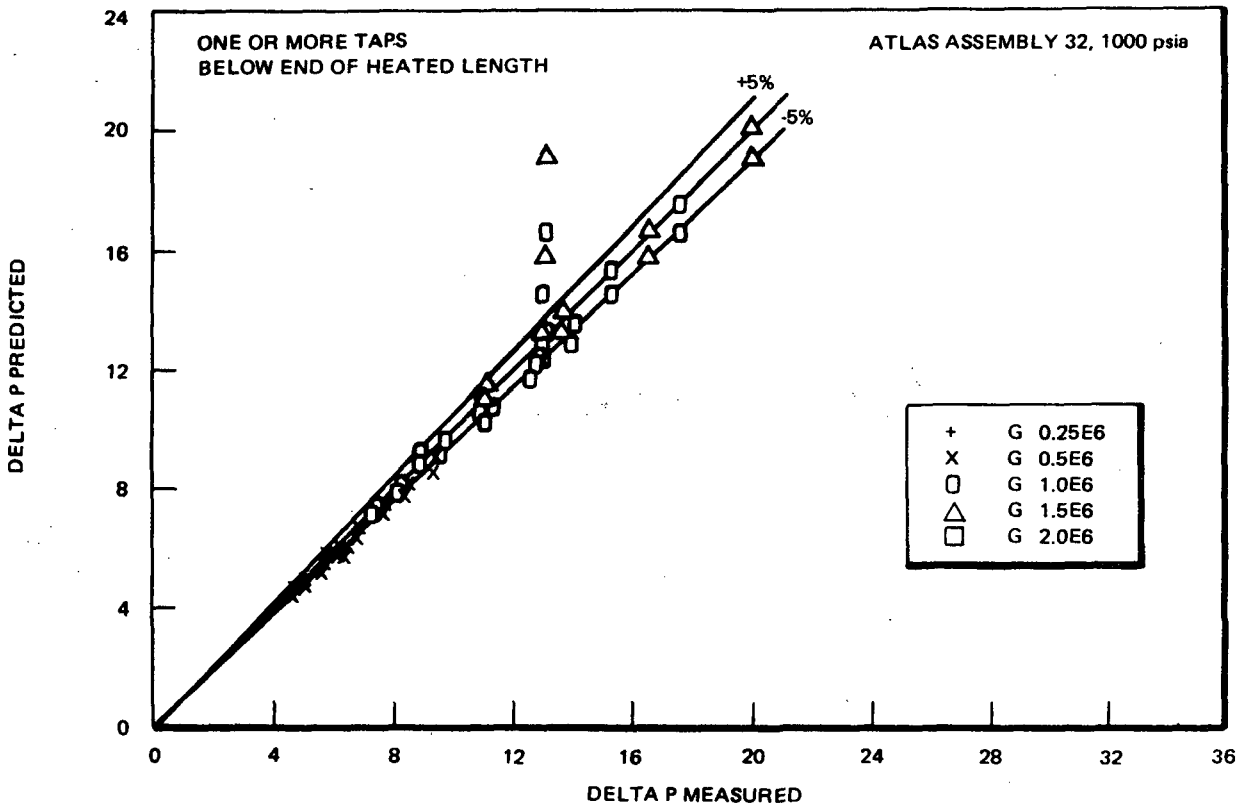


Figure 3.8-4 Predicted Versus Measured Pressure Drop, psi

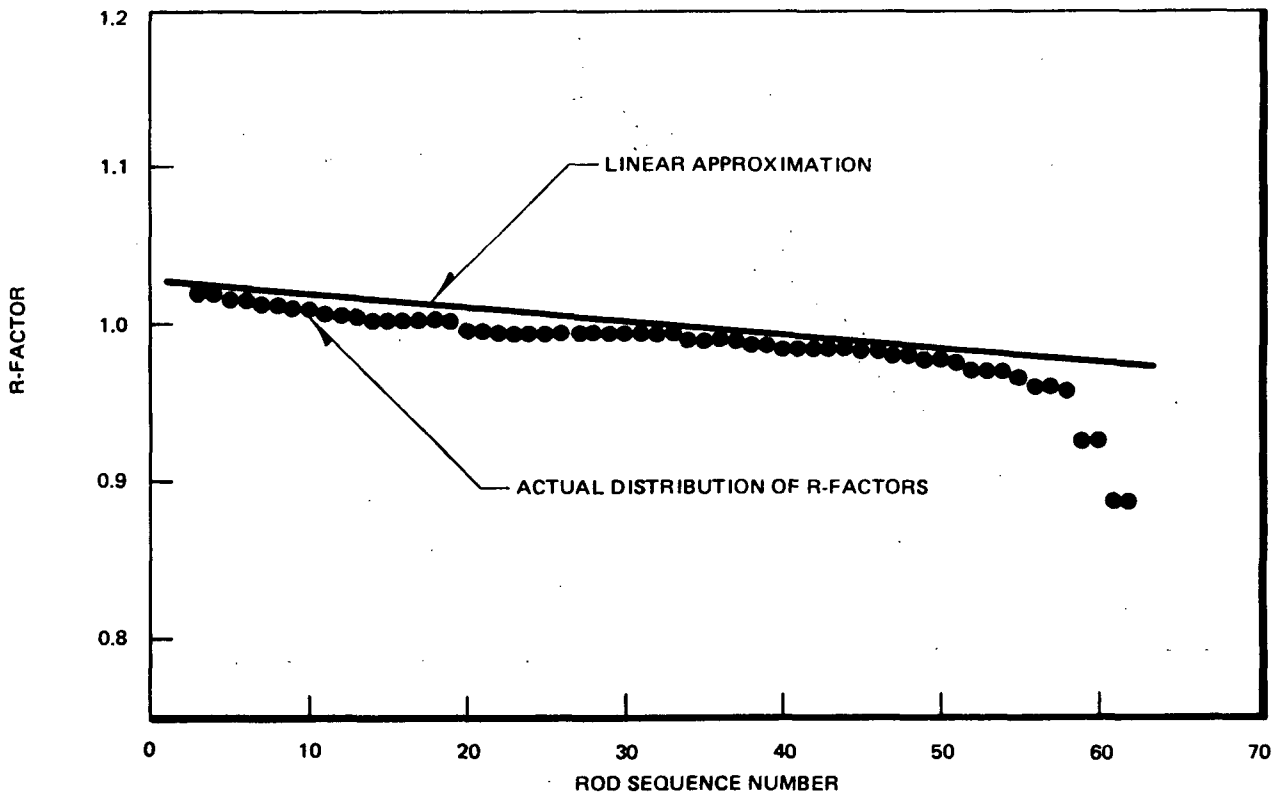


Figure 3.8-5 R Factor Distribution for a Typical BWR/6 Case

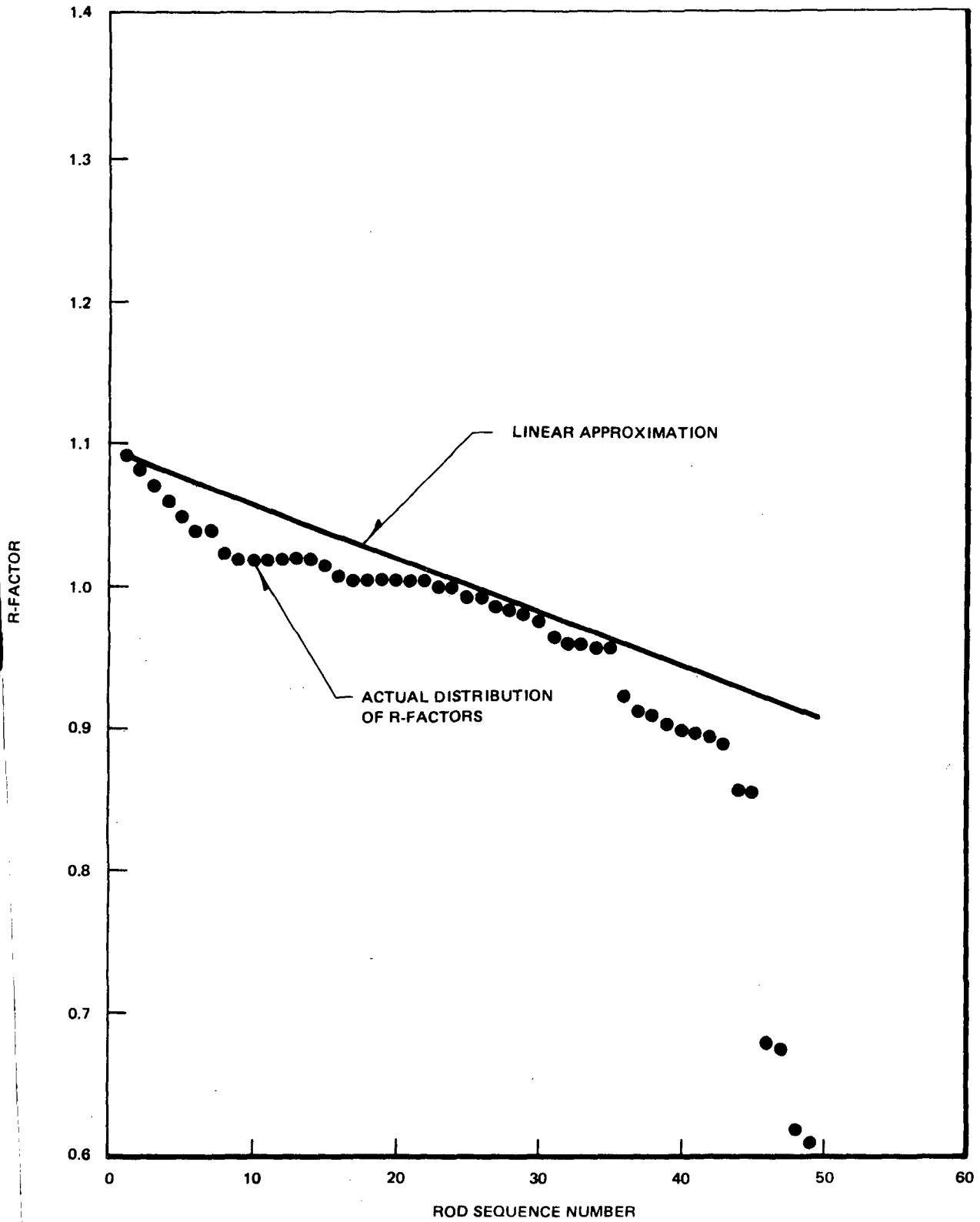


Figure 3.8-6 R Factor Distribution for a Typical BWR/6 Case

431-01-1283/10